

NASA CR-173, 119

JPL PUBLICATION 83-46

NASA-CR-173119
19830027790

Proceedings of the Workshop on Applications of Distributed System Theory to the Control of Large Space Structures

G. Rodriguez
Editor

LIBRARY COPY

JUL 24 1983

July 1, 1983

LANGLEY RESEARCH CENTER
LIBRARY NASA
HAMPTON, VIRGINIA



National Aeronautics and
Space Administration

Jet Propulsion Laboratory
California Institute of Technology
Pasadena, California

Langley Research Center
Hampton, Virginia



NF01445

JPL PUBLICATION 83-46

Proceedings of the Workshop on Applications of Distributed System Theory to the Control of Large Space Structures

G. Rodriguez
Editor

July 1, 1983

NASA

National Aeronautics and
Space Administration

Jet Propulsion Laboratory
California Institute of Technology
Pasadena, California

Langley Research Center
Hampton, Virginia

N83-36061 # ARW
N83-36096 #

This publication was prepared by the Jet Propulsion Laboratory, California Institute of Technology, under a contract with the National Aeronautics and Space Administration.

ABSTRACT

These proceedings report the results of a workshop on the applications of distributed system theory to the control of large space structures (LSS), which was held at the Jet Propulsion Laboratory, July 14-16, 1982. Co-sponsored by the Jet Propulsion Laboratory and Langley Research Center, this workshop responded to a rapidly growing interest within NASA in developing the control technology required to make possible the large, shuttle-based space systems planned for the 1980s and beyond. The scope of this workshop encompassed two mutually complementary themes, both of which involve the notion of a distributed system in some sense. One theme was the control theory for distributed parameter systems, in which the traditional emphasis is on developing basic control principles by means of distributed or continuum models. The other theme is that of distributed control for systems requiring spatially-distributed multipoint sensing and actuation -- whether described by lumped or continuum models. Papers considering both of these control theories were presented in the workshop sessions on modeling and control, control and stabilization, distributed control, control theory for distributed systems, and estimation and identification. The three discussion sessions held were devoted to the general topics of a summary of LSS control problems, LSS application of distributed system theory, and future research opportunities.

This Page Intentionally Left Blank

PREFACE

At the time this workshop was being formulated, I was the manager at NASA Headquarters responsible for a broad area of electronics and human factors research and technology that included space controls and guidance. In the fall of 1980, I suggested to Dr. G. Rodriguez of the NASA Jet Propulsion Laboratory and Dr. L. W. Taylor, Jr., of the NASA Langley Research Center that they should organize and conduct a workshop on this topic. My motivation and rationale are presented in the following paragraphs.

In reviewing the research supported by my office, it appeared that relatively little work was being done in the application of partial differential equation (PDE) control theory to the large space structure control problem. It is well known that certain large spacecraft configurations with rather uniform mass distribution can be most accurately modeled by a set of PDE's. Such equations, of course, are much more difficult to treat than ordinary differential equations that result from a finite-element model of a structure. For the most part, researchers who have used PDE models have made some approximations, either in the formulation or in the solution to obtain attractive control law designs.

Substantial theory existed at that time to treat control of PDE systems. For example, Professor A. V. Balakrishnan at UCLA had treated PDE control for aircraft flutter and had discussed the problem of large space structure control. It was not clear to me whether or not an exact PDE solution would be better than various approximate solutions when considering practical implementation constraints. However, it seemed most appropriate for the NASA organization responsible for advanced controls research to examine the state-of-the-art theories and applications and assess whether more research effort should be applied towards the PDE approach.

My suggestion for a workshop was to bring together the key researchers from both schools of thought and discuss the status, problems and potential and thus identify important research opportunities. The workshop that resulted, the workshop reported herein, had somewhat broader objectives but encompasses my original motivation. The main objectives of the workshop were:

- 1) To exchange ideas and explore the application of various control theories for distributed systems to large space structures; and
- 2) To identify the important unsolved problems of current interest leading to possible future collaborative NASA/university/industry efforts.

Here the term distributed systems was used in two ways: 1) to mean distributed parameter control theory leading to PDE control; and 2) to mean control for systems with spatially distributed multipoint sensors and actuators, whether modeled with finite elements or distributed parameters.

The workshop covered the topics of modeling and control, control and stabilization, control theory for distributed systems, and estimation and identification. There was a formal discussion period scheduled at the end of each of the first two days and a wrap-up panel discussion on the final day. The final wrap-up panel discussion focused on identifying future research opportunities

for NASA consideration. Technical synopses of these discussion periods, as well as a technical evaluation of the workshop, are included in this document.

One final note: the present NASA Administration has stated publicly that the permanent presence of man in space is NASA's current primary goal for the space program. This effort should result in the first U.S. large space station, followed by a series of other spacecraft, platforms, and satellites of very large dimensions. Many of the high-potential space applications, both civil and military, depend on having the technology to implement large space structures. The workshop addressed a very timely and important topic for the future exploitation of space.

H. A. Rediess
October, 1982

TABLE OF CONTENTS

SESSION I: MODELING AND CONTROL

Chairman: P.K.C. Wang, University of California, Los Angeles 1

MODELING AND CONTROL OF DISTRIBUTED STRUCTURES

L. Meirovitch 1

SPACE STRUCTURE VIBRATION MODES: HOW MANY EXIST? WHICH ONES ARE IMPORTANT?

Peter C. Hughes 31

CONTROL OF FLEXIBLE STRUCTURES: A SYSTEMATIC OVERVIEW OF THE PROBLEM

Richard Gran 49

INTRODUCTION AND SURVEY ON CONTINUUM MODELS FOR REPETITIVE LATTICE STRUCTURES

Larry S. Weisstein 63

MINIMUM INFORMATION MODELLING OF STRUCTURAL SYSTEMS WITH UNCERTAIN PARAMETERS

David C. Hyland 71

DISTRIBUTED SYSTEM MODELING OF A LARGE SPACE ANTENNA

M. Hamidi, G. Rodriguez, and D.B. Schaechter 89

SESSION II: CONTROL AND STABILIZATION

Chairman: R. R. Strunce, Charles Stark Draper Laboratory, Inc. 103

MODELING OF FLEXIBLE STRUCTURES FOR ACTIVE CONTROL

Arthur E. Bryson, Jr. 103

VIBRATION SUPPRESSION IN LARGE SPACE STRUCTURES

T.K. Caughey and C.J. Goh 119

CONTROL OF ANTENNA-FEED ATTITUDE AND REFLECTOR VIBRATIONS IN LARGE SPACEBORNE ANTENNAS BY MECHANICAL DECOUPLING AND MOVABLE DAMPERS

P.K.C. Wang, E.C. Hong, and J.S. Sarina 143

A CLOSED-LOOP PRINCIPAL COMPONENT ANALYSIS OF A TETRAHEDRAL TRUSS

Edmond A. Jonckheere 163

CONTROL OF LARGE SPACE ANTENNAS BASED ON ELECTROMAGNETIC-STRUCTURAL MODELS

Massih Hamidi and Farzin Manshadi 181

ACTIVE CONTROL OF SPACE STRUCTURES (ACOSS) MODEL 2	
Timothy C. Henderson	195
TRAVELLING WAVE EFFECTS IN LARGE SPACE STRUCTURES	
Andy von Flotow	211
DISTRIBUTED CONTROL OF LARGE SPACE ANTENNAS	
J.M. Cameron, M. Hamidi, Y.H. Lin, and S.J. Wang	225
<u>SESSION III: DISCUSSION--LSS CONTROL PROBLEMS</u>	
Moderator: R.R. Strunce, Charles Stark Draper Laboratory, Inc.	249
<u>SESSION IV: DISTRIBUTED CONTROL</u>	
Chairman: A.F. Tolivar, Jet Propulsion Laboratory	253
NUMBER AND PLACEMENT OF CONTROL SYSTEM SENSORS CONSIDERING POSSIBLE FAILURES	
Wallace E. Vander Velde and Craig R. Carignan	253
THE TOYSAT STRUCTURAL CONTROL EXPERIMENT	
J.A. Breakwell and G.J. Chambers	269
LARGE SPACE STRUCTURE MODEL REDUCTION AND CONTROL SYSTEM DESIGN BASED UPON ACTUATOR AND SENSOR INFLUENCE FUNCTIONS	
Y. Yam, J.H. Lang, T.L. Johnson, S. Shih, and D.H. Staelin	287
A DESIGN PROCEDURE FOR ACTIVE CONTROL OF BEAM VIBRATIONS	
Stephen L. Dickerson and George Jarocki	305
ON VIBRATION CONTROL OF TETHERED SATELLITE SYSTEMS	
D.M. Xu, A.K. Misra, and V.J. Modi	317
ORBITING CHAINS AND RINGS	
John V. Breakwell	329
HARDWARE VERIFICATION OF DISTRIBUTED/ADAPTIVE CONTROL	
Daniel B. Eldred and David B. Schaechter	337
<u>SESSION V: CONTROL THEORY FOR DISTRIBUTED SYSTEMS</u>	
Chairman: Lt. Col. D.C. Washburn, Kirtland Air Force Base	351
SOME REMARKS ON THE CURRENT STATUS OF THE CONTROL THEORY OF SINGLE SPACE DIMENSION HYPERBOLIC SYSTEMS	
D.L. Russell	351
APPROXIMATION IN CONTROL OF FLEXIBLE STRUCTURES, THEORY AND APPLICATION	
J.S. Gibson	383
SIMULTANEOUS CONTROL AND OPTIMIZATION FOR ELASTIC SYSTEMS	
Vadim Komkov	391

FIXED-ORDER DYNAMIC COMPENSATION THROUGH OPTIMAL PROJECTION David C. Hyland and Appasaheb N. Madiwale	409
STABLE FEEDBACK CONTROL OF DISTRIBUTED PARAMETER SYSTEMS: TIME AND FREQUENCY DOMAIN CONDITIONS Mark J. Balas	427
APPROXIMATION OF THE OPTIMAL COMPENSATOR FOR A LARGE SPACE STRUCTURE Michael K. Mackay	451
ANALYSIS OF STRUCTURAL PERTURBATIONS IN SYSTEMS VIA COST DECOMPOSITION METHODS Robert E. Skelton	465
FINITE DIFFERENCE NUMERICAL METHODS FOR BOUNDARY CONTROL PROBLEMS GOVERNED BY HYPERBOLIC PARTIAL DIFFERENTIAL EQUATIONS Goong Chen, Quan Zheng, Matthew Coleman, and Sunethra Weerakoon	477
<u>SESSION VI: DISCUSSION--LSS APPLICATIONS OF DISTRIBUTED SYSTEM THEORY</u> Moderator: R.S. Gran, Grumman Aerospace Corporation	497
<u>SESSION VII: ESTIMATION/IDENTIFICATION</u> Chairman: L.W. Taylor, Jr., Langley Research Center	505
ALGORITHMS FOR ESTIMATION IN DISTRIBUTED MODELS WITH APPLICATIONS TO LARGE SPACE STRUCTURES H.T. Banks	505
IDENTIFICATION OF LARGE FLEXIBLE STRUCTURES MASS/STIFFNESS AND DAMPING FROM ON-ORBIT EXPERIMENTS S.L. Hendricks, S. Rajaram, M.P. Kamat, and J.L. Junkins	511
JOINT STATE AND PARAMETER ESTIMATION N. Carmichael and M.D. Quinn	521
PARAMETER ESTIMATION IN TRUSS BEAMS USING TIMOSHENKO BEAM MODEL WITH DAMPING C.T. Sun and J.N. Juang	531
A FUNCTION SPACE APPROACH TO STATE AND MODEL ERROR ESTIMATION FOR ELLIPTIC SYSTEMS G. Rodriguez	547
STATE AND MODEL ERROR ESTIMATION FOR ELLIPTIC SYSTEMS: APPLICATIONS TO LARGE ANTENNA STATIC SHAPE DETERMINATION G. Rodriguez and R.E. Scheid, Jr.	575
<u>SESSION VIII: DISCUSSION--FUTURE RESEARCH OPPORTUNITIES</u> Moderator: H.A. Rediess, Milco International, Inc.	605
TECHNICAL EVALUATION REPORT OF THE WORKSHOP ON APPLICATIONS OF DIS- TRIBUTED SYSTEM THEORY TO THE CONTROL OF LARGE SPACE STRUCTURES	619

This Page Intentionally Left Blank

MODELING AND CONTROL OF DISTRIBUTED STRUCTURES*

L. Meirovitch

Department of Engineering Science and Mechanics
Virginia Polytechnic Institute and State University
Blacksburg, VA 24061

ABSTRACT

There appears to be some incongruity in the design of controls for structures. Structures are basically distributed-parameter systems, described by partial differential equations, and control theory is concerned almost exclusively with discrete (in space) systems, described by ordinary differential equations. The standard approach to solving this dilemma is to discretize the system in space, which precludes the use of distributed controls. A different approach, known as the independent modal-space control method, is designed to eliminate the incongruity by bringing about a closer correspondence between modeling and control theory. Indeed, the independent modal-space control method can treat distributed structures as well as discretized models and it permits design of both distributed and discrete-point controls.

INTRODUCTION

Structures are essentially distributed-parameter systems and their behavior is described by partial differential equations (Refs. 1,2). The difficulty in designing controls for distributed structures becomes immediately evident when it is recognized that the control theory is concerned for the most part with discrete systems, described by finite sets of simultaneous ordinary differential equations, and not with distributed systems. Through a modal expansion, it is possible to transform the partial differential equation governing the motion of a distributed structure into a set of simultaneous ordinary differential equations, but the set of equations is infinite, so that the question as to how to compute control gains for systems of infinite order remains. To circumvent this difficulty, an approach commonly used is to discretize the distributed structure, i.e., to represent it by a discrete model of finite order. This approach has several undesirable effects. In the first place, the control design tends to acquire all the characteristics of a discrete system. For example, distributed controls and distributed sensors must be ruled out immediately, as they do not fit in a finite-dimensional vector space formulation of modern control theory. Consistent with a discrete (-in-

*Supported in part by the NASA Cooperative Agreement NAG-1-225

space) theory, one must control structures by means of discrete-point actuators and sensors (see, for example, Refs. 3-7). Another drawback is that a discretized model is only an approximate model, so that if discretization of a distributed structure is not done with care, serious errors can be introduced, leading to an unstable system. From the above, we conclude that the choice of the mathematical model is dictated by limitations in the control theory and not by prudent structural modeling.

More often than not control of discrete (or discretized) systems represents one form or another of modal control (Refs. 8,9). The idea behind modal control is that one can control the structure by controlling its modes. In theory, one can control all the modeled modes of a discretized system with a single actuator and observe all these modes with a single sensor, provided the controllability and observability requirements are satisfied. In practice, problems can arise. Some of them relate to the control system performance and other to the computational algorithms for the control gains. Similar problems exist for multi input-multi output systems. In the case in which a discretized model is used to design controls for a distributed structure, one can encounter problems of control and observation spillover (Ref. 3). These problems can be attributed directly to the insistence on using discrete actuators and sensors to control a distributed structure.

It is standard practice in modal control to express the state of the system in terms of modal coordinates and velocities, in which case the formulation is in terms of the so-called modal equations of motion. In the case of open-loop controls the modal equations are decoupled. In feedback controls, however, the controls depend in general on all the controlled variables, so that the feedback controls recouple the modal equations of motion. We refer to this case as coupled controls. The approaches used in Refs. 3-7 belong basically in this category.

Another approach to modal control, known as the independent modal-space control method (Refs. 10-13), remains more faithful to the original structure. Indeed, the method can be used for distributed structures or for discretized models of distributed structures. The method consists of designing controls so that the modal equations of motion remain decoupled, thus reducing the control problem to the design of modal controls for a set of independent second-order modal equations. Then, the actual controls are synthesized from the modal controls via a simple transformation. Because the controls are designed for second-order systems only, the method permits a wider choice of control techniques and most of the problems associated with coupled controls disappear. It should be pointed out that, in the case of the independent modal-control method, if one chooses to work with a discretized model, then this choice is dictated by the inability of computing the entire infinity of modes of the structure and not by the inability of designing distributed controls. Of course, if all the modes of the structure are known, then no discretization is necessary. The independent modal-space control method is ideally suited for distributed controls, in which case no control spillover exists (Ref. 13). A similar statement can be made regarding observation spillover, provided one is able to measure (or estimate) the state at every point of the distributed structure.

This paper begins with the derivation of the equations of motion for distributed structures and follows with a discussion of proper modeling, with special emphasis on the case in which the eigenvalue problem can be solved only approximately. Some fine points concerning the nature of the approximate eigensolution of distributed structures are presented and their implications in model discretization are explored. Then, attention is given to various problems inherent in the control of distributed structures by means of discrete models. Finally, the independent modal-space control method is reexamined in the context of control of distributed structures.

EQUATIONS OF MOTION FOR THE STRUCTURE

The equations of motion for a distributed structure can be derived by means of the extended Hamilton principle (Ref. 1). This requires expressions for the kinetic energy, the potential energy and the virtual work. Denoting the displacement vector of any nominal point P in the structure by $\tilde{u}(P,t)$, the kinetic energy can be written as

$$T = \frac{1}{2} \int_D m \tilde{u}^T \dot{\tilde{u}} dD \quad (1)$$

where $m = m(P)$ is the mass density and D is the domain of extension of the structure. The potential energy can be written in the symbolic form

$$V = \frac{1}{2} [\tilde{u}, \tilde{u}] \quad (2)$$

where $[\tilde{u}, \tilde{u}]$ denotes an energy inner product (Ref. 2). Moreover, denoting the distributed force vector by $\tilde{f}(P,t)$, the virtual work has the expression

$$\delta W = \int_D \tilde{f}^T \delta \tilde{u} dD \quad (3)$$

where $\delta \tilde{u}$ is the virtual displacement vector. Note that in the case of feedback controls, the force vector \tilde{f} does not depend explicitly on the position P and time t but only implicitly through the state vector $[\tilde{u}^T \dot{\tilde{u}}^T]^T$.

The extended Hamilton principle has the form (Ref. 1)

$$\int_{t_1}^{t_2} (\delta L + \delta W) dt = 0, \quad \delta \tilde{u}(P,t) = 0, \quad t = t_1, t_2; \quad P \in D \quad (4)$$

where $L = T - V$ is the Lagrangian. Inserting Eqs. (1-3) into Eq. (4) and following the usual steps, we obtain the partial differential equation of motion for the structure

$$\underline{L}u + \underline{M}\ddot{u} = \underline{f}, \quad P \in D \quad (5)$$

where L is a differential operator matrix with entries of order $2p$ and M is a mass matrix. The displacement vector u is subject to the boundary conditions

$$B_i u = 0, \quad P \in S; \quad i=1,2,\dots,p \quad (6)$$

where B_i are differential operator matrices with entries of maximum order $2p-1$ and S is the set of points defining the boundary of D .

The relatively simple formulation (5-6) may be a little misleading. Indeed, in general a structure represents an assemblage of substructures acting together as a whole, so that the operator L may vary from one substructure to another and the operators B_i may vary from one boundary to another. It should be clear that control of a distributed-parameter system using Eqs. (5-6) directly is not possible, even for a structure of moderate complexity. This points to modal control as the only viable alternative. The idea behind modal control is that one can control a structure by controlling its modes. Before modal control can be implemented, it is necessary to compute the modes of the structure.

STRUCTURE DISCRETIZATION

As mentioned above, the problem defined by Eqs. (5-6) in general is too complex to permit closed-form solution. This applies not only to the control problem but also to the open-loop eigenvalue problem. Hence, we seek a solution for the modes of the structure by an approximate method, which requires the discretization of the structure. To this end, we use the finite element method, which can be regarded as a variant of the Rayleigh-Ritz method, at least in the case of structures.

Let us assume that the motion of the structure can be described in terms of n nodal coordinates $q_j(t)$ ($j = 1,2,\dots,n$). In general, the nodal coordinates consist of both translations and rotations. Introducing the n -vector $\underline{q}(t) = [q_1(t) \ q_2(t) \ \dots \ q_n(t)]^T$, the displacement vector $u(P,t)$ can be expressed in terms of the nodal coordinates by means of the linear transformation

$$\underline{u}(P,t) = L(P)\underline{q}(t) \quad (7)$$

where $L(P)$ is a matrix of interpolation functions (Ref. 2). Introducing Eq. (7) into Eqs. (1-2), we obtain the discretized kinetic energy and potential energy in the form

$$T = \frac{1}{2} \dot{\underline{q}}^T \underline{M} \dot{\underline{q}}, \quad V = \frac{1}{2} \underline{q}^T \underline{K} \underline{q} \quad (8a,b)$$

where

$$M = \int_D L^T(P) M L(P) dD(P), K = [L(P), L(P)] \quad (9a,b)$$

are $n \times n$ mass and stiffness matrices. Both M and K are symmetric. Moreover, M is positive definite and K is nonnegative, i.e., it can be either positive definite or positive semidefinite, the latter being the case when the structure admits rigid-body modes. In addition, inserting Eq. (7) into Eq. (3), we obtain the discretized virtual work

$$\delta W = \underline{Q}^T \delta \underline{q} \quad (10)$$

where

$$\underline{Q} = \int_D L^T(P) \underline{f}(P,t) dD(P) \quad (11)$$

is a nodal force vector and $\delta \underline{q}$ is the virtual nodal displacement vector.

The extended Hamilton principle remains in the form (4), except that the varied path is now subject to $\delta \underline{q} = 0$, $t = t_1, t_2$. It is not difficult to show that use of the principle, in conjunction with Eqs. (9) and (10), yields

$$\underline{M} \ddot{\underline{q}} + \underline{K} \underline{q} = \underline{Q} \quad (12)$$

which represents a set of simultaneous ordinary differential equations of motion. Hence, the effect of using the finite element method is to reduce a distributed structure with an infinite number of degrees of freedom to a discrete model with only n degrees of freedom. But, whereas Eq. (12) has the appearance of a discrete system it is in fact only a discretized system meant to represent a distributed structure. Hence, the process leading from Eq. (5) to Eq. (12) is a discretization and truncation process simultaneously. Indeed it should be very clear that a discretized model of a distributed structure is already a truncated model. The question remains to what extent the discretized model is representative of the actual distributed structure. We propose to examine this question in the next section.

THE NATURE OF THE DISCRETIZED MODEL

As pointed out above, the system described by Eq. (12) is not truly a discrete system but only a discretized and truncated model of a distributed structure. It is commonly believed that by increasing n the discretized model becomes a completely faithful representation of the distributed structure. It turns out that this is a mistaken belief, as we are about to show.

Let us consider the eigenvalue problem associated with Eq. (12) and write it in the form

$$K_{\underline{q}_r}^{(n)} = \lambda_r^{(n)} M_{\underline{q}_r}^{(n)}, \quad r=1,2,\dots, n \quad (13)$$

where $\lambda_r^{(n)}$ and $q_r^{(n)}$ ($r=1,2,\dots,n$) are eigenvalues and eigenvectors, respectively. The superscript (n) indicates that the eigenvalue problem (13) corresponds to a finite-dimensional model possessing n degrees of freedom. It is not difficult to show that all the eigenvalues are real and nonnegative. Next, let us consider a model possessing $n+1$ degrees of freedom and denote the associated eigenvalue problem by the superscript $(n+1)$, so that

$$K_{q_r}^{(n+1)} M_{q_r}^{(n+1)} = \lambda_r^{(n+1)} M_{q_r}^{(n+1)}, \quad r=1,2,\dots,n+1 \quad (14)$$

The question arises as to how the eigensolution of the n -degree-of-freedom model relates to the eigensolution of the $(n+1)$ -degree-of-freedom model. The answer is provided by the inclusion principle (Ref. 2). Assuming that the two sets of eigenvalues are arranged in ascending order of magnitude, $\lambda_1^{(n)} \leq \lambda_2^{(n)} \leq \dots \leq \lambda_n^{(n)}$ and $\lambda_1^{(n+1)} \leq \lambda_2^{(n+1)} \leq \dots \leq \lambda_{n+1}^{(n+1)}$, the inclusion principle states that the eigenvalues $\lambda_r^{(n+1)}$ ($r=1,2,\dots,n+1$) bracket the eigenvalues $\lambda_r^{(n)}$ ($r=1,2,\dots,n$), or

$$\lambda_1^{(n+1)} \leq \lambda_1^{(n)} \leq \lambda_2^{(n+1)} \leq \lambda_2^{(n)} \leq \dots \leq \lambda_n^{(n+1)} \leq \lambda_n^{(n)} \leq \lambda_{n+1}^{(n+1)} \quad (15)$$

The eigenvalues $\lambda_1^{(n)}$, $\lambda_2^{(n)}$, ..., $\lambda_n^{(n)}$, computed on the basis of the discretized model, are only approximations to the lowest n eigenvalues λ_1 , λ_2 , ..., λ_n of the actual structure. Hence, the question arises as to how the "computed eigenvalues" of the discretized model relate to the "actual eigenvalues" of the distributed structure. In this regard, it can be stated that (Ref. 2)

$$\lim_{n \rightarrow \infty} \lambda_r^{(n)} = \lambda_r, \quad r=1,2,\dots,n \quad (16)$$

Moreover, the computed eigenvalues approach the actual eigenvalues from above as n tends to infinity.

The fact that the computed eigenvalues approach the actual eigenvalues asymptotically as $n \rightarrow \infty$ is very reassuring, but in practice n is finite and not infinite. As it turns out, when n is finite the situation is not nearly as good. In particular, whereas the lower computed eigenvalues tend to be relatively good approximations to the actual eigenvalues, accuracy deteriorates as the mode number increases to the extent that the higher computed eigenvalues can be grossly in error, sometimes the error being of the order of several hundred percent. Paradoxically, this is true regardless how large n is. Indeed, by increasing n more computed eigenvalues tend to become accurate, but at the same time new computed eigenvalues are added at the upper end of the spectrum, and the new ones tend to be wildly in error. Hence, no discretized model can yield a totally accurate representation of a distributed structure. This fact must be taken into account in designing a control system, as the object is to control the structure itself and not the model.

MODAL EQUATIONS OF MOTION FOR CONTROL

In one form or another, virtually all approaches to the control of structures, whether distributed or discrete, are based on modal control. The idea is that if one controls the modes of a structure, then in essence one controls the structure. To design modal controls, it is convenient to transform the nodal equations of motion into modal equations of motion. This necessitates the structure eigenvalue and eigenfunctions, which in turn requires the solution of the eigenvalue problem for the structure.

More often than not, no closed-form solution of the eigenvalue problem exists, so that an approximate solution is frequently necessary. This approximate eigensolution is based on a discretized system, and is expressed in fact by Eq. (13). Hence, dropping the superscript (n), we denote the computed eigenvalues by λ_r and the computed eigenvectors by \underline{q}_r ($r=1,2,\dots,n$). The computed eigenvectors \underline{q}_r can be used to determine the computed eigenfunctions $\underline{\phi}(P)$ associated with the n lowest modes of vibration by writing

$$\underline{\phi}_r(P) = L(P)\underline{q}_r, \quad r=1,2,\dots,n \quad (17)$$

where $L(P)$ is the matrix of interpolation functions of Eq. (7).

Because the structure is self-adjoint, the eigenfunctions $\underline{\phi}_r(P)$ ($r=1,2,\dots,n$) are orthogonal. The orthogonality conditions can be demonstrated by recalling that the eigenvalue problem (13) is defined in terms of two real symmetric matrices, at least one of which is positive definite. The implication is that the eigenvectors \underline{q}_r ($r=1,2,\dots,n$) are orthogonal (Ref. 2). They can be normalized so as to satisfy

$$\underline{q}_s^T \underline{M} \underline{q}_r = \delta_{rs}, \quad \underline{q}_s^T \underline{K} \underline{q}_r = \lambda_r \delta_{rs} = \omega_r^2 \delta_{rs}, \quad r,s=1,2,\dots,n \quad (18a,b)$$

where ω_r are the computed natural frequencies. Then, considering Eqs. (9a) and (17) one can write

$$\int_D \underline{\phi}_s^T \underline{M} \underline{\phi}_r \, dD = \int_D \underline{q}_s^T L^T(P) \underline{M} L(P) \underline{q}_r \, dD = \underline{q}_s^T \underline{M} \underline{q}_r \quad (19)$$

so that, in view of Eq. (18a), the eigenfunctions satisfy the orthonormality relations

$$\int_D \underline{\phi}_s^T \underline{M} \underline{\phi}_r \, dD = \delta_{rs}, \quad r,s = 1,2,\dots,n \quad (20)$$

Moreover, Eqs. (9b) and (17) permit us to write

$$[\underline{\phi}_s, \underline{\phi}_r] = \underline{q}_s^T [L(P), L(P)] \underline{q}_r = \underline{q}_s^T \underline{K} \underline{q}_r \quad (21)$$

so that, in view of Eq. (18b), the eigenfunctions also satisfy the orthornormality relations

$$[\phi_{\sim s}, \phi_{\sim r}] = \lambda_r \delta_{rs}, \quad r, s=1, 2, \dots, n \quad (22)$$

Observing, however, that the operator L in Eq. (5) is related to the energy inner product by

$$\int_D \tilde{v}^T L \tilde{u} \, dD = [\tilde{v}, \tilde{u}] \quad (23)$$

it follows that the orthornormality relations (22) can be replaced by

$$\int_D \phi_{\sim s}^T L \phi_{\sim r} \, dD = \lambda_r \delta_{rs}, \quad r, s=1, 2, \dots, n \quad (24)$$

Note that the relation (23) is obtained via integrations by parts during which the boundary conditions (6) are used (Ref. 2).

From the computed eigenvalues λ_r and computed eigenfunctions $\phi_r(P)$ ($r=1, 2, \dots, n$) only a fraction can be expected to be accurate estimates of the true eigenvalues and eigenfunctions of the distributed structure. As a rule of thumb, less than one half of the computed ones are accurate. We consider the case in which we are interested in a discretized mathematical model with N degrees of freedom for control design, so that we must insist that at least N computed eigenvalues and eigenvectors are accurate. This implies that the algebraic eigenvalue problem to be solved must be of order $n \gg N$. Then, we wish to expand the displacement vector $\tilde{u}(P, t)$ into the series

$$\tilde{u}(P, t) = \sum_{r=1}^N \phi_{\sim r}(P) u_r(t) \quad (25)$$

where $u_r(t)$ are known as modal coordinates. Equation (25) is known as the expansion theorem (Ref. 2). Introducing the modal matrix

$$\Phi(P) = [\phi_{\sim 1}(P) \quad \phi_{\sim 2}(P) \quad \dots \quad \phi_{\sim N}(P)] \quad (26)$$

and the modal vector

$$\tilde{u}(t) = [u_1(t) \quad u_2(t) \quad \dots \quad u_N(t)]^T \quad (27)$$

Eq. (25) can be rewritten in the matrix form

$$\tilde{u}(P, t) = \Phi(P) \tilde{u}(t) \quad (28)$$

The modal matrix $\Phi(P)$ permits us to write all the orthonormality relations, Eqs. (20) and (24), in the compact form

$$\int_D \Phi^T M \Phi \, dD = I, \int_D \Phi^T L \Phi \, dD = \Lambda \quad (29a,b)$$

where I is the unit matrix of order N and

$$\Lambda = \text{diag} [\lambda_1 \lambda_2 \dots \lambda_N] = \text{diag} [\omega_1^2 \omega_2^2 \dots \omega_N^2] \quad (30)$$

is the diagonal matrix of eigenvalues, where Λ is also of order N . Introducing Eq. (28) into Eq. (5), multiplying by Φ^T , integrating over the domain D and considering Eqs. (29), we obtain the modal equations

$$\ddot{\underline{u}}(t) + \Lambda \underline{u}(t) = \underline{f}(t) \quad (31)$$

where

$$\underline{f}(t) = [f_1(t) \ f_2(t) \dots f_N(t)]^T = \int_D \Phi^T(P) \underline{f}(P,t) \, dD \quad (32)$$

is the N -dimensional modal control vector. Note that the components of the modal control vector have the explicit expressions

$$f_r(t) = \int_D \phi_r^T(P) \underline{f}(P,t) \, dD, \quad r = 1, 2, \dots, N \quad (33)$$

The control problem consists of designing a force vector $\underline{f}(P,t)$ so as to drive any undesirable disturbance to zero.

COUPLED MODAL CONTROL

Although the modal equations (31) have the appearance of a set of independent equations, they are in fact not independent. Indeed, the notation $\underline{f}(t)$ for the modal control vector is misleading, as for feedback control the vector \underline{f} depends only implicitly on time and it depends explicitly on the system state, or

$$\underline{f} = \underline{f}(\underline{u}(t), \dot{\underline{u}}(t)) \quad (34)$$

In the general case, the feedback control vector \underline{f} couples the modal equations of motion. We refer to this case as coupled modal control. In using a discrete system to design controls for a distributed system, the controls acquire discrete characteristics. As a result, it is impossible to design a distributed control vector $\underline{f}(P,t)$ to control a system in coupled form. Hence, in the case of coupled controls we must use discrete actuators.

In view of the above, we assume that the control is implemented by means

of M actuators acting at the discrete points $P=P_j$ ($j=1,2,\dots,M$). Discrete forces can be treated as distributed by writing

$$\tilde{f}(P,t) = \sum_{j=1}^M F_j(t) \delta(P-P_j) \quad (35)$$

where $\delta(P-P_j)$ are spatial Dirac delta functions and $F_j(t)$ are actuator force amplitude vectors. Introducing Eq. (35) into Eq. (32), we obtain the modal controls

$$\tilde{f}_r(t) = \sum_{j=1}^M \int_D \phi_r^T(P) F_j(t) \delta(P-P_j) dD = \sum_{j=1}^M \phi_r^T(P_j) F_j(t), \quad r=1,2,\dots \quad (36)$$

and we observe that the index r in Eqs. (36) has no upper limit, at least in theory. This implies that the actuator forces F_j ($j=1,2,\dots,M$) generate not only modal control forces f_r ($r=1,2,\dots,N$) acting on the modeled modes but also modal forces f_r ($r=N+1,N+2,\dots$) acting on the higher unmodeled modes. This fact is referred to as control spillover into the unmodeled modes. The assumption is that the number N of modeled modes is sufficiently large that control spillover into the unmodeled modes is insignificant.

Introducing the actual control vector

$$\tilde{F}(t) = [F_1^T(t) \ F_2^T(t) \ \dots \ F_M^T(t)]^T \quad (37)$$

and the modal participation matrix for the modeled modes

$$B_N = [\phi^T(P_1) \ \phi^T(P_2) \ \dots \ \phi^T(P_M)] \quad (38)$$

the modal control vector \tilde{f} can be written in terms of the actual control vector \tilde{F} in the form

$$\tilde{f}(t) = B\tilde{F}(t) \quad (39)$$

so that the modal equations, Eq. (31), become

$$\ddot{u}(t) + \Lambda u(t) = B\tilde{F}(t) \quad (40)$$

In the above formulation, it is assumed that there are N modeled modes. Yet, one may wish to control only a smaller number of these modes. Hence, we wish to distinguish between two classes of modeled modes, namely, controlled modes and uncontrolled modes, where the latter are referred to at times as residual modes. We denote the controlled and residual modes by the subscripts

C and R, respectively, and assume that there are N_C controlled modes and N_R residual modes, $N_C + N_R = N$. Hence, Eq. (40) can be written in the partitioned form

$$\begin{bmatrix} \ddot{\tilde{u}}_C \\ \ddot{\tilde{u}}_R \end{bmatrix} + \begin{bmatrix} \Lambda_C & | & 0 \\ \hline 0 & | & \Lambda_R \end{bmatrix} \begin{bmatrix} \tilde{u}_C \\ \tilde{u}_R \end{bmatrix} = \begin{bmatrix} B_C \\ B_R \end{bmatrix} \tilde{F} \quad (41)$$

where the notation is self-evident.

In modal control, the actual feedback control vector F is assumed to depend on the modal displacements and modal velocities corresponding to the controlled modes only, or

$$\tilde{F} = \tilde{F}(\tilde{u}_C, \dot{\tilde{u}}_C) \quad (42)$$

The force vector F can be determined by various techniques, such as pole allocation (Refs. 8,9) or optimal control (Refs. 14,15). We discuss these techniques later in this paper.

Although the actuators force vector F is designed so as to regulate the controlled modes only, in general these forces will excite the residual modes. Indeed, from Eq. (39), we can write

$$\tilde{f}_C = B_C \tilde{F}, \quad \tilde{f}_R = B_R \tilde{F} \quad (43a,b)$$

Equation (43b) shows clearly that there are modal forces acting on the residual modes, giving rise to so-called control spillover into the residual modes (Ref. 3). Some attempts have been made to suppress the residual modes (Ref. 5), but questions of implementation remain. Note that to eliminate this spillover, one must design \tilde{F} so that $\tilde{f}_R = 0$.

For linear controls, the actual controls are assumed to be proportional to the modal displacements and velocities, or

$$\tilde{F} = G_1 \dot{\tilde{u}}_C + G_2 \tilde{u}_C \quad (44)$$

where G_1 and G_2 are control gain matrices that can be determined by one of the methods mentioned above. This permits us to write the closed-loop modal equations in the form

$$\begin{bmatrix} \ddot{\tilde{u}}_C \\ \ddot{\tilde{u}}_R \end{bmatrix} + \begin{bmatrix} -B_C G_1 & | & 0 \\ \hline -B_R G_1 & | & 0 \end{bmatrix} \begin{bmatrix} \dot{\tilde{u}}_C \\ \dot{\tilde{u}}_R \end{bmatrix} + \begin{bmatrix} \Lambda_C - B_C G_2 & | & 0 \\ \hline -B_R G_2 & | & \Lambda_R \end{bmatrix} \begin{bmatrix} \tilde{u}_C \\ \tilde{u}_R \end{bmatrix} = \tilde{0} \quad (45)$$

It is clear from Eq. (45) the closed-loop poles of the controlled modes are determined by $-B_C G_1$ and $\Lambda_C - B_C G_2$ and the closed-loop poles of the residual modes are the same as the open-loop poles of the residual modes, so that the latter are not affected by the controls. It follows that control spillover into the residual modes cannot destabilize these modes. Although not specifically included here, the same conclusion is valid for the unmodeled modes.

CONTROL IMPLEMENTATION USING OBSERVERS

As pointed out by Eq. (42), or Eq. (44), to generate the actual feedback forces, one must know the modal displacements and velocities associated with the controlled modes at all times. Sensors, however, measure actual displacements and velocities, so that the question remains as to how to extract the modal displacements and velocities from actual measurements. It is customary to assume that sensors are discrete devices producing measurements at discrete points in the structure. Later in this paper, we will reexamine this assumption.

Let us consider the case in which K sensors measure displacements and velocities at the discrete points $P=P_i$ ($i=1,2,\dots,K$). Denoting the sensors signals by $\tilde{y}_i(t)$, we can write for displacements and velocity measurements

$$\tilde{y}_i(t) = \tilde{u}(P_i, t), \quad \dot{\tilde{y}}_i(t) = \dot{\tilde{u}}(P_i, t), \quad i=1,2,\dots,K \quad (46a,b)$$

respectively. Once again we propose to ignore the unmodeled modes on the grounds that their contribution to the overall motion is insignificant, so that the measurements are assumed to contain contributions from the controlled and residual modes only. Inserting Eq. (28) into Eqs. (47), we obtain

$$\tilde{y}_i(t) = \Phi(P_i) \tilde{u}(t), \quad \dot{\tilde{y}}_i(t) = \Phi(P_i) \dot{\tilde{u}}(t), \quad i=1,2,\dots,K \quad (47a,b)$$

where $\Phi(P_i)$ is the modal matrix evaluated at $P=P_i$, $\tilde{u}(t)$ is the modal displacement vector and $\dot{\tilde{u}}(t)$ is the modal velocity vector. Introducing the matrix

$$C = \begin{bmatrix} \Phi(P_1) \\ \Phi(P_2) \\ \dots \\ \Phi(P_K) \end{bmatrix} = [C_C \mid C_R] \quad (48)$$

where the partitioning is obvious, as well as the measurement vector

$$\tilde{y}(t) = [\tilde{y}_1^T(t) \quad \tilde{y}_2^T(t) \quad \dots \quad \tilde{y}_K^T(t)]^T \quad (49)$$

Eqs. (47) can be rewritten as

$$\underline{y}(t) = \underline{C}\underline{u}(t) = \underline{C}_C \underline{u}_C(t) + \underline{C}_R \underline{u}_R(t), \quad \dot{\underline{y}}(t) = \underline{C}\dot{\underline{u}}(t) = \underline{C}_C \dot{\underline{u}}_C(t) + \underline{C}_R \dot{\underline{u}}_R(t) \quad (50a,b)$$

For feedback control, we only need $\underline{u}_C(t)$ and $\dot{\underline{u}}_C(t)$, which can be extracted from measurements of actual displacements and velocities by means of an observer, or state estimator (Ref. 16). To this end, it is convenient to rewrite the equations of motion in state form. Hence, let us define the controlled and residual modal state vectors

$$\underline{v}_C = \begin{bmatrix} \dot{\underline{u}}_C^T \\ \underline{u}_C^T \end{bmatrix}^T, \quad \underline{v}_R = \begin{bmatrix} \dot{\underline{u}}_R^T \\ \underline{u}_R^T \end{bmatrix}^T \quad (51a,b)$$

the associated modal control vectors

$$\underline{V}_C = \begin{bmatrix} \underline{f}_C^T \\ \underline{0}^T \end{bmatrix}^T, \quad \underline{V}_R = \begin{bmatrix} \underline{f}_R^T \\ \underline{0}^T \end{bmatrix}^T \quad (52a,b)$$

the coefficient matrices

$$\underline{A}_C = \begin{bmatrix} \underline{0} & \underline{I} & -\underline{A}_C \\ \underline{I} & \underline{0} & \underline{0} \end{bmatrix}, \quad \underline{A}_R = \begin{bmatrix} \underline{0} & \underline{I} & -\underline{A}_R \\ \underline{I} & \underline{0} & \underline{0} \end{bmatrix} \quad (53a,b)$$

where \underline{I} are identity matrices of appropriate order, and

$$\underline{B}'_C = \begin{bmatrix} \underline{B}_C \\ \underline{0} \end{bmatrix}, \quad \underline{B}'_R = \begin{bmatrix} \underline{B}_R \\ \underline{0} \end{bmatrix} \quad (54a,b)$$

Then, Eq. (41) can be rewritten in the state form

$$\begin{aligned} \begin{bmatrix} \dot{\underline{v}}_C \\ \dot{\underline{v}}_R \end{bmatrix} &= \begin{bmatrix} \underline{A}_C & \underline{0} \\ \underline{0} & \underline{A}_R \end{bmatrix} \begin{bmatrix} \underline{v}_C \\ \underline{v}_R \end{bmatrix} + \begin{bmatrix} \underline{V}_C \\ \underline{V}_R \end{bmatrix} \\ &= \begin{bmatrix} \underline{A}_C & \underline{0} \\ \underline{0} & \underline{A}_R \end{bmatrix} \begin{bmatrix} \underline{v}_C \\ \underline{v}_R \end{bmatrix} + \begin{bmatrix} \underline{B}'_C \\ \underline{B}'_R \end{bmatrix} \underline{F} \end{aligned} \quad (55)$$

as indicated by Eq. (42), the actual control vector \underline{F} depends on the controlled state, or

$$\underline{F} = \underline{F}(\underline{v}_C) \quad (56)$$

For linear control, we obtain from Eq. (44)

$$\tilde{\mathbf{F}} = \mathbf{G}_{\tilde{\mathbf{C}}} \mathbf{v}_{\tilde{\mathbf{C}}} \quad (57)$$

where

$$\mathbf{G}_{\tilde{\mathbf{C}}} = [\mathbf{G}_1 \mid \mathbf{G}_2] \quad (58)$$

is the control gain matrix. The purpose of the observer is to extract the state vector $\mathbf{v}_{\tilde{\mathbf{C}}}$ from the system output, namely, the measurement vector \mathbf{y} . However, the output vector \mathbf{y} contains contributions not only from the controlled state $\mathbf{v}_{\tilde{\mathbf{C}}}$ but also from the residual state $\mathbf{v}_{\tilde{\mathbf{R}}}$, so that

$$\mathbf{y}(t) = \mathbf{C}'_{\tilde{\mathbf{C}}} \mathbf{v}_{\tilde{\mathbf{C}}} + \mathbf{C}'_{\tilde{\mathbf{R}}} \mathbf{v}_{\tilde{\mathbf{R}}} \quad (59)$$

where $\mathbf{C}'_{\tilde{\mathbf{C}}}$ and $\mathbf{C}'_{\tilde{\mathbf{R}}}$ are matrices representing combinations of $\mathbf{C}_{\tilde{\mathbf{C}}}$ and $\mathbf{C}_{\tilde{\mathbf{R}}}$, respectively, and null matrices, depending on the type of measurements used.

Observers are dynamical systems similar to the actual systems and receiving as input the output of the actual system. The observer eigenvalues are chosen so that the observer state approaches the state of the actual system asymptotically. The term actual system must be interpreted here as the discretized model and not the distributed system. Observers can be designed in various forms, but their main features are the same for all designs. We choose the observer in the form

$$\begin{bmatrix} \dot{\hat{\mathbf{v}}}_{\tilde{\mathbf{C}}}(t) \\ \dot{\hat{\mathbf{v}}}_{\tilde{\mathbf{R}}}(t) \end{bmatrix} = \begin{bmatrix} \mathbf{A}_{\tilde{\mathbf{C}}} & \vdots & 0 \\ 0 & \vdots & \mathbf{A}_{\tilde{\mathbf{R}}} \end{bmatrix} \begin{bmatrix} \hat{\mathbf{v}}_{\tilde{\mathbf{C}}}(t) \\ \hat{\mathbf{v}}_{\tilde{\mathbf{R}}}(t) \end{bmatrix} + \begin{bmatrix} \mathbf{B}'_{\tilde{\mathbf{C}}} \\ \mathbf{B}'_{\tilde{\mathbf{R}}} \end{bmatrix} \tilde{\mathbf{F}}(t) + \begin{bmatrix} \mathbf{K}_{\tilde{\mathbf{C}}} \\ \mathbf{K}_{\tilde{\mathbf{R}}} \end{bmatrix} [\mathbf{y}(t) - \hat{\mathbf{y}}(t)] \quad (60a)$$

$$\hat{\mathbf{y}}(t) = \mathbf{C}'_{\tilde{\mathbf{C}}} \hat{\mathbf{v}}_{\tilde{\mathbf{C}}}(t) + \mathbf{C}'_{\tilde{\mathbf{R}}} \hat{\mathbf{v}}_{\tilde{\mathbf{R}}}(t) \quad (60b)$$

where $\hat{\mathbf{v}}_{\tilde{\mathbf{C}}}$ and $\hat{\mathbf{v}}_{\tilde{\mathbf{R}}}$ are estimates of $\mathbf{v}_{\tilde{\mathbf{C}}}$ and $\mathbf{v}_{\tilde{\mathbf{R}}}$, respectively, $\mathbf{K}_{\tilde{\mathbf{C}}}$ and $\mathbf{K}_{\tilde{\mathbf{R}}}$ are observer gain matrices, chosen so that $\hat{\mathbf{v}}_{\tilde{\mathbf{C}}}$ approaches $\mathbf{v}_{\tilde{\mathbf{C}}}$ exponentially, and $\hat{\mathbf{y}}$ is the observer output. An observer of the type (60) is known as a Luenberger observer (Ref. 16). Equations (60) are similar to Eqs. (13) of Ref. 3, with the exception that here the residual modes are included in the observer dynamics and system output, whereas they are left out in Ref. 3. Excluding the residual modes from the observer dynamics and system output is equivalent to treating them as unmodeled. We examine the implications of this shortly.

In the feedback control vector $\tilde{\mathbf{F}}$ depends on the controlled state $\mathbf{v}_{\tilde{\mathbf{C}}}$. However, the observer produces the estimated state $\hat{\mathbf{v}}_{\tilde{\mathbf{C}}}$ and not the actual

Eqs. (47) can be rewritten as

$$\underline{y}(t) = \underline{C}\underline{u}(t) = \underline{C}_{\underline{C}}\underline{u}_{\underline{C}}(t) + \underline{C}_{\underline{R}}\underline{u}_{\underline{R}}(t), \quad \dot{\underline{y}}(t) = \underline{C}\dot{\underline{u}}(t) = \underline{C}_{\underline{C}}\dot{\underline{u}}_{\underline{C}}(t) + \underline{C}_{\underline{R}}\dot{\underline{u}}_{\underline{R}}(t) \quad (50a,b)$$

For feedback control, we only need $\underline{u}_{\underline{C}}(t)$ and $\dot{\underline{u}}_{\underline{C}}(t)$, which can be extracted from measurements of actual displacements and velocities by means of an observer, or state estimator (Ref. 16). To this end, it is convenient to rewrite the equations of motion in state form. Hence, let us define the controlled and residual modal state vectors

$$\underline{v}_{\underline{C}} = \begin{bmatrix} \dot{\underline{u}}_{\underline{C}}^T \\ \underline{u}_{\underline{C}}^T \end{bmatrix}^T, \quad \underline{v}_{\underline{R}} = \begin{bmatrix} \dot{\underline{u}}_{\underline{R}}^T \\ \underline{u}_{\underline{R}}^T \end{bmatrix}^T \quad (51a,b)$$

the associated modal control vectors

$$\underline{V}_{\underline{C}} = \begin{bmatrix} \underline{f}_{\underline{C}}^T \\ \underline{0}^T \end{bmatrix}^T, \quad \underline{V}_{\underline{R}} = \begin{bmatrix} \underline{f}_{\underline{R}}^T \\ \underline{0}^T \end{bmatrix}^T \quad (52a,b)$$

the coefficient matrices

$$\underline{A}_{\underline{C}} = \begin{bmatrix} \underline{0} & -\underline{\Lambda}_{\underline{C}} \\ \underline{I} & \underline{0} \end{bmatrix}, \quad \underline{A}_{\underline{R}} = \begin{bmatrix} \underline{0} & -\underline{\Lambda}_{\underline{R}} \\ \underline{I} & \underline{0} \end{bmatrix} \quad (53a,b)$$

where \underline{I} are identity matrices of appropriate order, and

$$\underline{B}'_{\underline{C}} = \begin{bmatrix} \underline{B}_{\underline{C}} \\ \underline{0} \end{bmatrix}, \quad \underline{B}'_{\underline{R}} = \begin{bmatrix} \underline{B}_{\underline{R}} \\ \underline{0} \end{bmatrix} \quad (54a,b)$$

Then, Eq. (41) can be rewritten in the state form

$$\begin{aligned} \begin{bmatrix} \dot{\underline{v}}_{\underline{C}} \\ \dot{\underline{v}}_{\underline{R}} \end{bmatrix} &= \begin{bmatrix} \underline{A}_{\underline{C}} & \underline{0} \\ \underline{0} & \underline{A}_{\underline{R}} \end{bmatrix} \begin{bmatrix} \underline{v}_{\underline{C}} \\ \underline{v}_{\underline{R}} \end{bmatrix} + \begin{bmatrix} \underline{V}_{\underline{C}} \\ \underline{V}_{\underline{R}} \end{bmatrix} \\ &= \begin{bmatrix} \underline{A}_{\underline{C}} & \underline{0} \\ \underline{0} & \underline{A}_{\underline{R}} \end{bmatrix} \begin{bmatrix} \underline{v}_{\underline{C}} \\ \underline{v}_{\underline{R}} \end{bmatrix} + \begin{bmatrix} \underline{B}'_{\underline{C}} \\ \underline{B}'_{\underline{R}} \end{bmatrix} \underline{F} \end{aligned} \quad (55)$$

as indicated by Eq. (42), the actual control vector \underline{F} depends on the controlled state, or

$$\underline{F} = \underline{F}(\underline{v}_{\underline{C}}) \quad (56)$$

For linear control, we obtain from Eq. (44)

$$\tilde{F} = G_{C\sim C} \tilde{v}_C \quad (57)$$

where

$$G_C = [G_1 \parallel G_2] \quad (58)$$

is the control gain matrix. The purpose of the observer is to extract the state vector \tilde{v}_C from the system output, namely, the measurement vector \tilde{y} . However, the \tilde{y} output vector contains contributions not only from the controlled state \tilde{v}_C but also from the residual state \tilde{v}_R , so that

$$\tilde{y}(t) = C'_{C\sim C} \tilde{v}_C + C'_{R\sim R} \tilde{v}_R \quad (59)$$

where $C'_{C\sim C}$ and $C'_{R\sim R}$ are matrices representing combinations of C_C and C_R , respectively, and null matrices, depending on the type of measurements used.

Observers are dynamical systems similar to the actual systems and receiving as input the output of the actual system. The observer eigenvalues are chosen so that the observer state approaches the state of the actual system asymptotically. The term actual system must be interpreted here as the discretized model and not the distributed system. Observers can be designed in various forms, but their main features are the same for all designs. We choose the observer in the form

$$\begin{bmatrix} \dot{\hat{v}}_C(t) \\ \dot{\hat{v}}_R(t) \end{bmatrix} = \begin{bmatrix} A_C & \vdots & 0 \\ 0 & \vdots & A_R \end{bmatrix} \begin{bmatrix} \hat{v}_C(t) \\ \hat{v}_R(t) \end{bmatrix} + \begin{bmatrix} B'_C \\ B'_R \end{bmatrix} F(t) + \begin{bmatrix} K_C \\ K_R \end{bmatrix} [\tilde{y}(t) - \hat{y}(t)] \quad (60a)$$

$$\hat{y}(t) = C'_{C\sim C} \hat{v}_C(t) + C'_{R\sim R} \hat{v}_R(t) \quad (60b)$$

where \hat{v}_C and \hat{v}_R are estimates of \tilde{v}_C and \tilde{v}_R , respectively, K_C and K_R are observer gain matrices, chosen so that \hat{v}_C approaches \tilde{v}_C exponentially, and \hat{y} is the observer output. An observer of the type (60) is known as a Luenberger observer (Ref. 16). Equations (60) are similar to Eqs. (13) of Ref. 3, with the exception that here the residual modes are included in the observer dynamics and system output, whereas they are left out in Ref. 3. Excluding the residual modes from the observer dynamics and system output is equivalent to treating them as unmodeled. We examine the implications of this shortly.

In the feedback control vector F depends on the controlled state \tilde{v}_C . However, the observer produces the estimated state \hat{v}_C and not the actual

observability matrix

$$\mathbf{O} = \begin{bmatrix} C_C^T & A_C^T C_C^T & (A_C^T)^2 C_C^T & \dots & (A_C^T)^{2N-1} C_C^T \end{bmatrix} \quad (68)$$

we can state the theorem: For the state v_C to be completely observable, it is necessary and sufficient that the matrix observability matrix \mathbf{O} be of rank $2N$ (Ref. 16). In the case under consideration, the observability matrix reduces to

$$\mathbf{O} = \begin{bmatrix} C_C^T & 0 & -\Lambda_C C_C^T & 0 & \dots & 0 \\ 0 & -\Lambda_C C_C^T & 0 & \Lambda_C^2 C_C^T & \dots & \Lambda_C^{N-1} C_C^T \end{bmatrix} \quad (69)$$

Hence, the state v_C is completely observable if no column of C_C is zero. Physically, this implies that lack of observability can occur only if all the sensors are located at the nodal points of a given mode. Clearly, the problem of observability disappears as the number of sensors increases.

MODAL FILTERS (IN SPACE)

As shown earlier, the purpose of a Luenberger observer is to generate an estimate \hat{v}_C of the modal state v_C from the system output. But a Luenberger observer is strictly a discrete system device, which does not consider the distributed nature of a structure. In particular, by writing the output in the form (50), no advantage is taken of the structure characteristics, as reflected in the orthogonality of modes. It turns out that, by taking advantage of the orthogonality of modes, the modal state can be estimated in a more direct way, thus obviating the need for a Luenberger observer. Or, by measuring displacements alone, one can use the same direct procedure to estimate the modal displacements and then use a Luenberger observer to estimate the modal velocities.

Equation (25), expanding the displacement vector $u(P,t)$ in a series of the structure eigenfunctions multiplied by modal coordinates, is only the first part of the expansion theorem. The second part of the expansion theorem relies on the orthonormality of modes, Eqs. (20), and permits the computation of the modal coordinates from the actual displacements, as follows:

$$u_r(t) = \int_D \Phi_r^T(P) M u(P,t) dD, \quad \dot{u}_r(t) = \int_D \Phi_r^T(P) M \dot{u}(P,t) dD, \quad r=1,2,\dots \quad (70a,b)$$

Equations (70) filter out the modal coordinates $u_r(t)$ and modal velocities $\dot{u}_r(t)$ ($r=1,2,\dots$) from measurements of the actual displacement vector $u(P,t)$ and actual velocity vector $\dot{u}(P,t)$ at every point P of the structure and for all times t . Hence, they can be regarded as (spatial) modal filters. It should be pointed out that in the case of distributed measurements, as postulated in Eqs. (70), observability is guaranteed by definition. Indeed,

observability is a concept peculiar to discrete sensors, particularly when their number is small.

In the case in which distributed measurements are not available, we must consider the problem of estimating $u_r(t)$ and $\dot{u}_r(t)$ ($r=1,2,\dots,N_C$) from discrete measurements. To this end, let us assume that there are K sensors capable of measuring displacements, velocities, angular displacements and angular velocities at the discrete points $P = P_i$ ($i=1,2,\dots,K$). Then, the question can be posed simply as to the number of measurements necessary to generate accurate estimates $\hat{u}(P,t)$ and $\hat{\dot{u}}(P,t)$ of $u(P,t)$ and $\dot{u}(P,t)$. This is not a new question, as the question has been asked frequently in the finite element method. In particular, the question is to the number of finite elements that must be used to approximate the displacement profile of a certain distributed structure, given a set of interpolation function and the values of the displacement function at the boundaries of the finite elements. Of course, the number depends on the type of functions to be approximated, the type of interpolation functions and the desired accuracy. In our case, we wish to generate approximate functions $\hat{u}(P,t)$ and $\hat{\dot{u}}(P,t)$ of sufficient accuracy to permit accurate estimates $\hat{u}_r(t)$ and $\hat{\dot{u}}_r(t)$ of the first N_C modal displacements $u_r(t)$ and modal velocities $\dot{u}_r(t)$. Hence, in the case of discrete measurements, the modal filters can be written in the form

$$\hat{u}_r(t) = \int_D \phi_r^T(P) M \hat{u}(P,t) dD, \quad \hat{\dot{u}}_r(t) = \int_D \phi_r^T(P) M \hat{\dot{u}}(P,t) dD, \quad r=1,2,\dots,N_C \quad (71a,b)$$

To illustrate the procedure, let us assume that the domain D is divided into $K-1$ elements D_i ($i=1,2,\dots,K-1$) and denote the displacement and velocity vectors in D_i by $\hat{u}_i(P,t)$ and $\hat{\dot{u}}_i(P,t)$. Moreover, denoting the vector of nodal displacement measurements at the boundaries of D_i by $\tilde{y}_i(t)$, where $\tilde{y}_i(t)$ includes translational and rotational coordinates, we can write

$$\hat{u}_i(P,t) = L^T(P) \tilde{y}_i(t), \quad \hat{\dot{u}}_i(P,t) = L^T(P) \dot{\tilde{y}}_i(t), \quad P \in D_i, \quad i=1,2,\dots,K-1 \quad (72a,b)$$

where $L(P)$ is a matrix of interpolation functions of the same type as that used in Eq. (7). Then, Eqs. (71) can be replaced by

$$\hat{u}_r(t) = \sum_{i=1}^{K-1} \int_{D_i} \phi_r^T(P) M \hat{u}_i(P,t) dD = \sum_{i=1}^{K-1} I_{ri}^T \tilde{y}_i(t), \quad r=1,2,\dots,N_C \quad (73a)$$

$$\hat{\dot{u}}_r(t) = \sum_{i=1}^{K-1} \int_{D_i} \phi_r^T(P) M \hat{\dot{u}}_i(P,t) dD = \sum_{i=1}^{K-1} I_{ri}^T \dot{\tilde{y}}_i(t), \quad r=1,2,\dots,N_C \quad (73b)$$

where

$$\mathbf{I}_{\sim r i}^T = \int_{D_i} \hat{\Phi}_{\sim r}^T(P) M L^T(P) dD \quad (74)$$

are integrals that can be computed off-line. Hence, the entire process of estimating modal coordinates and velocities has been reduced to a simple summation of vector products. These estimates can be produced almost instantaneously, as soon as the measurements become available.

It is perhaps appropriate to point out that the use of discrete measurements in conjunction with the interpolation scheme described above results in estimated measurements that must be regarded as distributed. Hence, observability of the first N_C modes is virtually guaranteed.

As mentioned earlier, if only one type of measurement is available, such as displacements only or velocities only, then one can use N_C independent second-order modal Luenberger observers to estimate the other type of variables needed to complete the estimate $\hat{\mathbf{v}}_C$ of the state \mathbf{v}_C .

A comparison between Luenberger observers and modal filters appears in order. Clearly, Luenberger observers must be used when only a limited number of sensors is available. In fact, Luenberger observers can be used in conjunction with a single sensor. Questions of observability arise, however, as the location of the single sensor can be critical. Then, there is the question of selecting observer gains, for which there are no good criteria. Moreover, convergence requires a little time, depending on the observer poles. By contrast, modal filters require a larger number of sensors, the number depending on the highest mode targeted for control, as the number must be such as to permit reasonably accurate finite element approximation to that mode. If the number of sensors presents no objections, modal filters are likely to be far superior to Luenberger observers, as they represent a concept that takes full advantage of the dynamic characteristics of the distributed structure. Indeed, modal filters screen out quite efficiently contaminations from the higher uncontrolled modes. The reason for this lies in the orthogonality property, so that higher modes are filtered out regardless whether they are known or not. Hence, clear advantages of modal filters are that they are virtually free of observation spillover and that the relatively large number of sensors used precludes questions of observability. Finally, modal filters involve only simple on-line operations, such as additions and multiplications, so that they provide virtual instantaneous estimation of the modal coordinates and velocities required for feedback.

INDEPENDENT MODAL-SPACE CONTROL (IMSC)

The independent modal-space control method is basically a method for controlling structures, or any other system admitting independent modes. It can be used for distributed systems, for discretized models of distributed systems, or for purely discrete systems (if indeed such systems do exist). When used for discretized models, it is for entirely different reasons than in the case of coupled controls. Indeed, in coupled controls a finite-dimensional model must be used because the control gain matrix must have finite dimensions. On

the other hand, the main consideration in choosing a discretized model in the IMSC is whether a closed-form eigensolution for the distributed structure exists or not. Moreover, in the IMSC method it is possible to design distributed controls, whereas in coupled controls it is not. It will prove convenient to divide the discussion of the IMSC method according to the type of actuators used.

i. Control by distributed actuators

Let us first assume that a closed-form eigensolution for the distributed structure exists, so that the entire infinity of modes is known, and rewrite Eqs. (31) as an infinite set of second-order differential equations of the form

$$\ddot{u}_r + \omega_r^2 u_r = f_r, \quad r=1,2,\dots \quad (75)$$

Note that in this case the entire infinity of modes is modeled, and there are no unmodeled modes.

In coupled controls, the modal feedback controls f_r depend in general on all the controlled modal coordinates and velocities, so that in such a case the feedback controls recouple the equations. Here, we wish to consider the case in which the feedback controls have the special form

$$f_r = f_r(u_r, \dot{u}_r), \quad r=1,2,\dots \quad (76)$$

Because the modal control for the r th mode depends only on the r th modal coordinate u_r and the r th modal velocity \dot{u}_r , Eqs. (75) become completely decoupled, i.e., they become both internally (plant-) and externally (controller-) decoupled. Hence, in this case Eqs. (75) represent an infinite set of independent modal equations. The essence of the independent modal-space control (IMSC) method is to design modal controls of the type (76). There is no restriction on the form of f_r , so that the modal controls f_r can be linear or nonlinear functions of the modal coordinate u_r and/or modal velocity \dot{u}_r . In coupled controls one designs the actual controls r directly. By contrast, in the IMSC method one designs first the modal controls and then synthesizes the actual controls from the modal controls. Indeed, in the case of distributed controls one can synthesize the actual control force $\tilde{f}(P,t)$ from the modal controls f_r by means of the formula

$$\tilde{f}(P,t) = \sum_{r=1}^{\infty} M(P)\Phi_r(P)f_r(t) \quad (77)$$

In using the IMSC method, one can control the entire infinity of modes or only a finite number of modes. If only N_C modes are to be controlled, then one can simply take $f_r \neq 0$ for $r=1,2,\dots,N_C$ and $f_r = 0$ for $r=N_C + 1, N_C + 2, \dots$. Clearly, because all modes are modeled, there are only two classes of modes, controlled and uncontrolled. Moreover, because $f_r = 0$ for $r = N_C + 1, N_C + 2, \dots$, there is no control spillover into the uncontrolled modes.

It must be pointed out that a system subject to distributed controls is completely controllable by definition. Indeed, controllability is strictly a discrete controls concept having no counterpart in distributed controls.

Next, let us consider the question of modal-space control implementation. In the case of linear controls, the modal controls can be taken as

$$f_r = G_{r1} \dot{u}_r + G_{r2} u_r, \quad r=1,2,\dots \quad (78)$$

where G_{r1} and G_{r2} ($r=1,2,\dots$) are modal gains, ordinarily taken as real negative scalars. In the case of nonlinear, on-off controls, the modal controls have the form

$$f_r = \{-k_r, \dot{u}_r > d_r; 0, |\dot{u}_r| < d_r; k_r, \dot{u}_r < -d_r\}, \quad r=1,2,\dots \quad (79)$$

where k_r is a control gain parameter and $2d_r$ is the magnitude of the deadband region. Then, the actual distributed controls are synthesized from the modal controls by inserting Eq. (78) or Eqs. (79) into Eq. (77). Note that in the case of on-off modal controls, if a finite number of modes are controlled, then the actual control of any point P is quantized, i.e., it has the form of a staircase in time.

The control of discretized structures by distributed actuators is very similar to the control of distributed structures. The only difference is that the modes corresponding to $r > N$ are not known with sufficient accuracy. In this case, it is not possible to control the entire infinity of modes. Hence, if only N_C modes are to be controlled, $N_C < N$, then the synthesis can be carried out simply by using the formula

$$\tilde{f}(P,t) = \sum_{r=1}^{N_C} M(P) \Phi_r(P) f_r(t) \quad (80)$$

But, as shown by Eq. (77), distributed controls can accommodate an infinity of modal coordinates and not just N_C . Taking $f_r = 0$ for $r = N_C + 1, N_C + 2, \dots$, formulas (77) and (80) become interchangeable, so that it does not matter whether the modes corresponding to $r > N$ are known or not. But, because distributed controls of the type (80) can be interpreted to mean that $f_r = 0$ for $r > N_C$, it can be concluded that once again control spillover into the uncontrolled modes does not exist. As in the case of distributed structures, in the case of discretized models controlled by distributed actuators controllability of the controlled modes is guaranteed.

ii. Control by discrete actuators

Distributed controls have many advantages over discrete controls. In many cases, however, distributed controls may not be feasible, so that one must consider control implementation by discrete actuators.

In the case of discrete actuators, only a finite number of modes can be controlled. Let us assume that N_C modes are to be controlled, which makes the infinity of remaining modes uncontrolled. The task is to be carried out by means of M discrete actuators. As shown earlier, discrete forces can be treated as distributed by using Eq. (35). Denoting the vector of controlled modes by u_C and the vector of modal control forces by f_C and using Eq. (43a), the modal equations for the controlled modes can be written in the form

$$\ddot{u}_C + \Lambda_C u_C = f_C = B_C F \quad (81)$$

where F is the M -vector of actuator forces. As pointed out earlier, in the IMSC method one designs first the modal control vector f_C and then synthesizes the actual control vector F from f_C . From the right side of Eq. (81), the synthesis amounts to writing

$$F = B_C^\dagger f_C \quad (82)$$

where B_C^\dagger is the pseudo-inverse of B_C . However, pseudo-inverses can be quite inaccurate. It is possible to avoid the use of pseudo-inverses by taking the dimension of F to be the same as the dimension of f_C , $M = N_C$, which implies that the number of actuators must be the same as the number of controlled modes. In this case, B_C is a square matrix, so that Eq. (82) reduces to

$$F = B_C^{-1} f_C \quad (83)$$

Note that the controllability of u_C is guaranteed when using IMSC, because one has always the freedom of placing the actuators in a way that B_C is nonsingular.

Next, let us examine the spillover problem. Denoting the infinite-dimensional vector of uncontrolled modes by u_U , the modal equations for the uncontrolled modes can be written as

$$\ddot{u}_U + \Lambda_U u_U = B_U F = B_U B_C^{-1} f_C \quad (84)$$

where the notation is obvious. Whereas f_C depends on u_C and \dot{u}_C , this does not imply coupling between the controlled and the uncontrolled modes. Indeed, as far as the uncontrolled modes are concerned, the vector f_C is a known function of time, so that Eq. (84) clearly indicates that control spillover into the uncontrolled modes does exist, but because the frequency components of f_C are entirely different from the natural frequencies of Λ_U , no instability due to resonance is possible. Because in IMSC one has the freedom of choosing the location of the actuators, spillover can be reduced by placing them so as not to excite critical modes. Moreover, because in IMSC control of modes are

designed independently for every mode, it is very easy to control any other mode that may be critical due to external factors, no matter how high the mode is. For example, one is able to control the first four modes and the twelfth mode, without controlling any intermediate mode or modes higher than the twelfth.

It should be pointed out that control spillover into the uncontrolled modes always exists when using discrete actuators, and this is true regardless of the method of control. The only way control spillover can be eliminated is through the use of distributed controls, and this is possible only in conjunction with IMSC and not with coupled controls. It must also be pointed out that the control spillover is not as serious a problem as it may seem. In the first place, for most realistic structures higher modes are extremely difficult to excite, as this requires large amounts of energy. In addition, all structures have a certain amount of inherent damping, which tends to attenuate higher modes at a higher rate than lower modes.

Control of discretized structures by discrete actuators is carried out in exactly the same manner as the control of distributed structures by discrete actuators discussed above. Indeed, as long as only N_c are to be controlled, and these modes are known accurately, it does not matter whether the remaining modes are known or not.

COMPUTATIONAL ALGORITHMS FOR CONTROL

When attempting to control structures by techniques of modern control, one must be struck by the fact that structures are basically distributed systems and modern control theory is concerned with discrete systems. To circumvent this problem, the standard approach has been to discretize the structure, which leads to a problem of a different kind. Complicated structures require discretized models of relatively high order and computational algorithms work well for low-order systems but experience serious difficulties for high-order systems. This is the situation in the case of coupled controls. Because the IMSC method reduces the control problem to a set of independent second-order systems, its advantages should become immediately obvious. Not only is the IMSC unlikely to experience computational difficulties with discretized systems, but it is also able to design controls for distributed structures, if all its modes are known.

There are two commonly used techniques for computing the control gains in the case of linear controls, namely, the pole allocation method and optimal controls. The methods are discussed in the following in the context of coupled controls and IMSC.

i. Pole allocation

In the pole allocation method, the closed-loop poles ρ_k ($k=1,2,\dots,2N_c$) of the controlled modes are selected in advance, and then the control gains are computed so that the coefficient matrix of the closed-loop system possesses eigenvalues equal to the selected poles. First, we concentrate on coupled

controls. The application is relatively simple for single inputs. In this case, the state equation for the controlled modes reduces to

$$\dot{\tilde{v}}_C = A_C \tilde{v}_C + \tilde{b}_C' F(t) \quad (85)$$

It is shown in Ref. 9 that the single input $F(t)$ can be expressed in the form

$$F(t) = \tilde{g}^T \tilde{v}_C(t) \quad (86)$$

where the gain vector \tilde{g} has the expression

$$\tilde{g} = \sum_{j=1}^{2N_C} \frac{\prod_{k=1}^{2N_C} (\rho_k - \lambda_j) v_{\tilde{j}}}{\tilde{v}_{\tilde{j}}^T \tilde{b}_{\tilde{j}}' \prod_{\substack{k=1 \\ k \neq j}}^{2N_C} (\lambda_k - \lambda_j)} \quad (87)$$

in which $v_{\tilde{j}}$ are the left eigenvectors of A_C and λ_j are the open-loop poles.

In the case of multi-input controls, one must solve a set of $2N_C$ nonlinear algebraic equations for the elements of the gain matrix G_C (Ref. 9). In addition to being nonlinear, the set of equations is undetermined, so that no unique solution exists. The undetermined equations can be augmented by additional equations, leading to special types of controllers, such as "minimum-gain modal controllers" and "prescribed-gain modal controllers" (Ref. 9). Both techniques are not feasible for large-order systems.

Another approach to computing gains for multi-input controllers is referred to as "dyadic control" and is due to Simon and Mitter (Ref. 8). The computational difficulties associated with the nonlinear equations are circumvented by considering a special class of systems characterized by a control gain matrix G_C in the form of an outer (dyadic) product of two vectors, one of which (denoted by h) is chosen arbitrarily, but in a way so as to ensure the controllability of the modes, and the other (a row vector) is determined as the feedback gain of a single-input system by using the closed-form solution of Ref. 8. The resulting gain matrix G_C has always rank one, as its rows are proportional to one another, from which it follows that the control inputs are proportional to one another. The required control law can be shown to have the form

$$\tilde{F}(t) = h \sum_{j=1}^{2N_C} \frac{\prod_{k=1}^{2N_C} (\rho_k - \lambda_j) v_{\tilde{j}}^T}{\tilde{v}_{\tilde{j}}^T \tilde{b}_{\tilde{j}}' \prod_{\substack{k=1 \\ k \neq j}}^{2N_C} (\lambda_k - \lambda_j)} \tilde{v}_C(t) \quad (88)$$

Hence, dyadic control does not represent a genuine multi-input control, as it restricts the freedom of designing the components of $F(t)$ as distinct functions of time. It can be concluded from the above that for the case of coupled controls, the pole allocation method is recommended only when a single actuator is used and a low number of modes is controlled.

In contrast to coupled controls, when the IMSC method is used computation of the modal controls for desired closed-loop poles is very easy. Denoting the closed-loop poles by

$$\rho_r = \alpha_r \pm i\beta_r, \quad r = 1, 2, \dots \quad (89)$$

and inserting the modal forces f_r as given by Eqs. (78) into Eqs. (75), it is not difficult to verify that the r modal controls corresponding to the poles defined by Eqs. (89) have the form

$$f_r = 2\alpha_r \dot{u}_r + (\omega_r^2 - \alpha_r^2 - \beta_r^2)u_r, \quad r = 1, 2, \dots \quad (90)$$

Then, the actual controls are obtained by inserting Eqs. (90) into Eq. (71) for distributed controls and into Eq. (82) for discrete controls.

ii. Linear optimal control

In the case of coupled controls, we consider the performance index

$$J = \int_0^t \tilde{v}_C^T Q \tilde{v}_C + \tilde{F}^T R \tilde{F} dt \quad (91)$$

where Q and R are weighting matrices. Minimization of J leads to the optimal control vector

$$\tilde{F}(t) = -R^{-1} B^T K(t) \tilde{v}_C(t) \quad (92)$$

where $K(t)$ is a $2N_C \times 2N_C$ symmetric matrix satisfying the matrix Riccati equation

$$\dot{K} = -KA_C - A_C^T KQ - KB^T R^{-1} B^T K \quad (93)$$

Because K is symmetric, the number of simultaneous nonlinear equations to be solved is $2N_C^2 + N_C$. For large N_C , computational difficulties arise.

In the steady-state case, $\dot{K} = 0$, we obtain the algebraic matrix Riccati equation. Through a series of linear transformations, the solution of the steady-state Riccati equation can be reduced to the eigensolution of a real general matrix (Ref. 17). Even though stable eigensolution algorithms for general matrices exist, such algorithms are likely to experience difficulties for relatively high-order matrices. It is estimated that the solution of the

matrix Riccati equation requires in excess of $600N_C^3$ multiplications for convergence. Hence, the computational time increases dramatically with the number of controlled modes.

In the transient case, the nonlinear Riccati equation can be transformed into a $4N_C \times 4N_C$ linear matrix equation, which must be integrated on-line. For large N_C , this requires ample computer capacity, so that an on-line process may not be possible.

In the case of the IMSC method, the performance index can be expressed as (Ref. 13)

$$J = \sum_{r=1}^{\infty} J_r \quad (94)$$

where J_r are independent modal performance indices of the form

$$J_r = \int_0^{t_f} (\mathbf{v}_r^T \mathbf{Q}_r \mathbf{v}_r + f_r^2 R_r / \omega_r^2) dt, \quad r = 1, 2, \dots \quad (95)$$

in which \mathbf{v}_r is the r th modal state, \mathbf{Q}_r is a 2×2 diagonal matrix and R_r is a scalar. To compute the control gains, one must solve now only a set of r independent 2×2 matrix Riccati equations. If only N_C modes are controlled by discrete actuators, then, the number of operations to determine the control forces is of the order $N_C^3/2$, which are required primarily to invert B_C for use in Eq. (83). Hence, the computational time required by IMSC is smaller by a factor of 1,200 compared with coupled controls. Of course, in the case of distributed controls by IMSC, no matrix inversion is necessary and the computational time reduces dramatically. Note that in practice one controls only a finite number of modes.

As a final item of interest, let us compute the closed-loop poles for optimal control designed by the IMSC method. From Ref. 13, we obtain the modal controls

$$f_r = \omega_r^2 (1 - \sqrt{1 + R_r^{-1}}) u_r - \omega_r [2(-1 + \sqrt{1 + R_r^{-1}}) + R_r^{-1}]^{1/2} u_r, \quad r = 1, 2, \dots \quad (96)$$

so that, comparing Eqs. (90) and (96) and considering Eq. (89), we conclude that the closed-loop poles are

$$\rho_r = -\frac{1}{2} \omega_r [2(-1 + \sqrt{1 + R_r^{-1}}) + R_r^{-1}]^{1/2} \pm i \frac{1}{2} \omega_r [2(1 + \sqrt{1 + R_r^{-1}}) - R_r^{-1}]^{1/2}, \quad r = 1, 2, \dots \quad (97)$$

From the above, it is evident that IMSC offers a wider choice of computational techniques than coupled controls, including nonlinear control. IMSC and coupled controls have been compared on the basis of computational effort and control energy and IMSC was found superior (Ref. 18). In addition, in

the case of IMSC the control energy is independent of the location of the actuators (Ref. 19). Finally, the IMSC was demonstrated to be robust with respect to changes in the system parameters (Ref. 20).

SUMMARY AND CONCLUSIONS

In designing controls for structures, one is faced with the dilemma that structures are basically distributed-parameter systems and the control theory is concerned almost exclusively with discrete systems. To overcome this impasse, the approach commonly used has been to represent a distributed structure by a discrete model, i.e., to discretize the structure. But, in discretizing a distributed structure, one must exercise extreme care, as no discretized model is capable of representing a distributed system with complete accuracy.

Virtually all methods used for the control of structure represent one form or another of modal control, whereby one attempts to control the motion of a structure by controlling its modes. To this end, it is customary to express the motion of the structure in terms of modal coordinates. In the case of open-loop control, the modal equations of motion are independent. In the case of feedback controls, the feedback forces depend in general on the controlled modal coordinates and velocities, the modal equations of motion are recoupled by the feedback controls, unless the feedback controls are designed so as to preserve the independence of the modal equations.

In implementing feedback controls, it is necessary to know the modal states for the modes to be controlled. These states can be estimated from the measured output of the structure by means of a Luenberger observer. In general, however, a Luenberger observer does not take advantage of the orthogonality property of the modes. If a sufficiently large number of sensors is used, the modal states can be estimated more directly by means of so-called modal filters. By contrast, the modal filters do take advantage of the orthogonality of modes. As a result, observation spillover is virtually eliminated.

In general, the feedback controls depend on all the controlled states, giving rise to coupled controls. In using coupled controls, one is limited to linear controls, as nonlinear controls are not feasible. One of the major problems in designing coupled feedback controls is the computation of the control gains. In the first place, all computational algorithms for the determination of the control gains lead to finite-dimensional control gain matrices. This implies the assumption that the actuators are discrete in nature, which precludes distributed controls. Secondly the computational algorithms encounter difficulties for control gain matrices of large dimensions, so that one is limited in the number of modes that can be controlled and in the number of actuators that can be used.

Another modal approach consists of designing controls independently for each mode and is known as the independent-modal-space control (IMSC) method. One of the advantages of IMSC is that it permits design of distributed controls, which eliminates control spillover completely. This makes it ideally suited for the control of flimsy structures, such as antenna membranes, for which discrete

actuators are likely to produce the difficulties mentioned above.

REFERENCES

1. Meirovitch, L., Analytical Methods in Vibrations, The Macmillan Co., New York, 1967.
2. Meirovitch, L., Computational Methods in Structural Dynamics, Sijthoff-Noordhoff Co., The Netherlands, 1980.
3. Balas, M. J., "Active Control of Flexible Systems," Journal of Optimization Theory and Applications, Vol. 25, No. 3, 1978, pp. 415-436.
4. Lin, J. G., Hegg, D. R., Lin, Y. H. and Keat, J. E., "Output Feedback Control of Large Space Structures: An Investigation of Four Design Methods," Proceedings of the Second VPI&SU/AIAA Symposium on Dynamics and Control of Large Flexible Spacecraft, Blacksburg, Va., 1979, pp. 1-18.
5. Sesak, J.R., Likins, P.W. and Coradetti, T., "Flexible Spacecraft Control by Model Error Sensitivity," Ref. 4, pp. 349-368.
6. Gran, R. and Rossi, M., "Closed-Loop Order Reduction for Large Structures Control," Ref. 4, pp. 443-458.
7. Strunce, R.R. and Henderson, T.C., "Application of Modern Modal Controller Design to a Large Space Structure," Ref. 4, pp. 661-676.
8. Simon, J.D. and Mitter, K., "A Theory of Modal Control," Information and Control, Vol. 13, 1968, pp. 316-353.
9. Porter, B. and Crossley, T.R., Modal Control-Theory and Applications, Taylor and Francis, Ltd., London, 1972.
10. Meirovitch, L., VanLandingham, H.F. and Oz, H., "Control of Spinning Flexible Spacecraft by Modal Synthesis," Acta Astronautica, Vol. 4, No. 9-10, 1977, pp. 984-1010.
11. Meirovitch, L. and Oz, H., "Modal-Space Control of Distributed Gyroscopic Systems," Journal of Guidance and Control, Vol. 3, No. 2, 1980, pp. 140-150.
12. Oz, H. and Meirovitch, L., "Optimal Modal-Space Control of Flexible Gyroscopic Systems", Journal of Guidance and Control, Vol. 3, No. 3, 1980, pp. 218-226.
13. Meirovitch, L. and Baruh, H., "Control of Self-Adjoint Distributed-Parameter Systems", Journal of Guidance and Control, Vol. 5, No. 1, 1982, pp. 60-66.
14. Kirk, D. E., Optimal Control Theory, Prentice-Hall, Inc., Englewood-Cliffs, NJ, 1970.

15. Kwakernaak, H. and Sivan, R., Linear Optimal Control Systems, Wiley-Interscience, New York, 1972.
16. Brogan, W.L., Modern Control Theory, QPI Publishers, Inc., New York, 1974.
17. Laub, A.J., "A Schur Method of Solving Algebraic Riccati Equations," IEEE Transactions on Automatic Control, Vol. AC-24, No. 6, 1979, pp. 913-921.
18. Meirovitch, L., Baruh, H. and Oz, H., "A Comparison of Control Techniques for Large Flexible Systems," Paper No. 81-195, AAS/AIAA Astrodynamics Specialist Conference, Lake Tahoe, Nevada, August 3-5, 1981.
19. Baruh, H. and Meirovitch, L., "On the Placement of Actuators in the Control of Distributed-Parameter Systems," Proceedings of the AIAA/ASME/ASCE/AHS 22nd SDM/Dynamics Specialists Conference, 1981, pp. 611-620.
20. Meirovitch, L. and Baruh, H., "Control Sensitivity of Distributed Systems to Changes in Parameters," Paper No. 82-0313, AIAA 20th Aerospace Sciences Conference, Orlando, FLA, January 11-13, 1982.

This Page Intentionally Left Blank

SPACE STRUCTURE VIBRATION MODES: HOW MANY EXIST? WHICH ONES ARE IMPORTANT?

Peter C. Hughes
University of Toronto
Toronto, Ontario, Canada M3H 5T6

AUTHOR'S PREFACE

To set the context of this paper, one or two prefatory remarks may be helpful.

Last summer, at the Third "Blacksburg" Conference on this subject, I was surprised to hear several speakers refer to the "fact" that "real" structures have "an infinite number of modes." These remarks were usually accompanied by the strong implication that any (mathematical) model of a structure that did not possess this essential characteristic was quite suspect, and that such models would therefore be difficult for sophisticated persons to tolerate. In fairness to the structural analysis community, I should hasten to add that this Infinite Modes Assertion was made chiefly by speakers who, whatever else their achievements, were not distinguished as structural analysts. If pressed to guess, I would suppose their backgrounds to be in controls and applied mathematics.

In any case, repeated references to the Infinite Modes Assertion at Blacksburg III prompted my recollection of a similar occasion just six years earlier where, at what some call the Zeroth Blacksburg Conference (organized by Prof. Peter Likins at UCLA), the kickoff panel session was titled "Primitive Methods." Not wishing to offend the members of that panel, Prof. Likins explained that in choosing this session title he was not implying that the panel members were themselves primitive. Instead, he said, he was using the word "primitive" in a narrow technical sense, to refer to methods based on "first principles." In essence, this meant the use of partial differential equations.

In spite of Prof. Likins' disclaimer, however, there remained the notion that if one's capability to analyse the dynamics of flexible space structures did not extend beyond PDE's, one was rather handicapped. That notion seemed sensible in 1975, and it seems even more sensible today. Unfortunately, this notion tends in practice to be inconsistent with the Infinite Modes Assertion (for reasons to be reviewed in this paper).

To return to Blacksburg III, I had the temerity during an end-of-conference panel session to question not only the importance of the Infinite Modes Assertion, but the Assertion itself. I would like to thank Dr. G. Rodriguez of JPL, who was present on that occasion, for the opportunity to expand on this theme at this workshop.

HOW MANY VIBRATION MODES DOES A REAL STRUCTURE HAVE?

A 'vibration mode' refers to a motion that is physically possible in the

absence of any external influence, and in which the elastic displacements $u(\underline{r}, t)$ at position \underline{r} and time t all move in unison: all displacements pass through zero simultaneously, and they all attain their maxima simultaneously. The concept of a 'vibration mode' is, in fact, a mathematical concept and can be stated most precisely and succinctly in mathematical form: if a distribution of elastic displacements of the form

$$u(\underline{r}, t) = \phi(\underline{r})\eta(t) \quad (1)$$

is autonomously possible, $\phi(\underline{r})$ is called the 'mode shape' and $\eta(t)$ shows the time dependence shared by the elastic displacements at all points in the structure. It is plain from (1) that the idea of 'mode shape' is a special case of the more general mathematical idea of 'separation of variables'.

Realization vs. Idealization

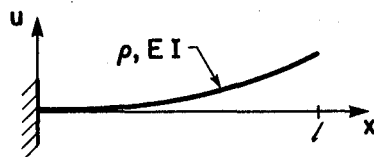
Much of the following argument rests on the important distinction between a 'real' (i.e., physical) structure and someone's mathematical model of that real structure. This distinction is, of course, essential on a philosophical level: whether dealing with high-energy particle physics, black holes, or flexible space structures, one is wise to discriminate between a symbolic representation of reality and reality itself. However, one hardly needs to evoke the Scientific Method to justify the distinction between the real structure and its mathematical representation. First, there is an almost unlimited quantity of experimental data on the dynamics of real structures; virtually none of this data agrees exactly with 'theory'. Second, if one returns to the fundamental assumptions that underlie 'theory', it is apparent that a large number of idealizations are made. These assumptions and idealizations are normally reasonable and defensible, but collectively they do constitute a well-documented case for distinguishing between the structure itself and its mathematical model.

Take, for example, what is arguably the simplest structure of all--the long, slender, uniform, cantilevered rod. This 'structure' is shown in Fig. 1a. (Its cousin, the 'two-rod satellite', accompanies it in Fig. 1b.) As is well known, the PDE and associated end conditions for the lateral displacements of the rod are

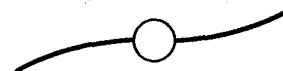
$$EIu'''' + \rho\ddot{u} = f(x, t) \quad (2)$$

$$u(0, t) = u'(0, t) = u''(l, t) = u'''(l, t) = 0$$

(A table of symbols is appended.)



(a) Long, Slender, Uniform Cantilevered Rod



(b) Simple Flexible Satellite

Fig. 1: The 'Simplest' Cases

Yet the following idealizations must be made to arrive at the Euler-Bernoulli equation (above) for this 'structure': (a) material continuum, (b) perfectly elastic material, (c) stress proportional to strain, (d) infinitesimally small deflections, (e) perfectly cantilevered root, (f) negligible rotational inertia, (g) negligible shear deflections. This list is undoubtedly incomplete but amply long enough already to demonstrate that properties of the PDE (2) will not likely be exactly the same as the corresponding properties of *actual* long slender uniform cantilevered rods. Experimental evidence tends to support this expectation; the model (2) is reasonable for many purposes if used intelligently, but (2) is not in any sense an *exact* representation of reality.

The Infinite Modes Assertion

There is no doubt that the PDE (2) has modes of the form (1), and that it has an infinite number of such modes. The question at issue is whether *real* rods also possess these properties. To state that a real structure has an infinite number of modes is, on reflection, to state an absurdity. How can a structure have more modes than it has molecules, or, for that matter, than there are molecules in the known universe? What does a frequency of $\omega = 10^{100}$ Hz mean? Does it mean, among other things, that particles in the structure move faster than the speed of light?

At this point the reader may retort, "Wait a minute. Let's not be extreme. When someone asserts that a structure has an infinite number of modes, all he really means is that the structure has a very large (but finite) number of modes." Not so, in the author's experience. The Infinite Modes Assertion is often made at technical meetings to an audience that includes individuals who are familiar with structural models that contain thousands of degrees of freedom (and therefore thousands of modes). To make the Assertion to such an audience clearly means that thousands of modes is not enough (in the Asserter's opinion); nothing less than infinity will do.

Yet it is clear that the Assertion is wrong, on the grounds of physical impossibility.

"All right," the reader may persist, "the Assertion is indeed made (in its strong form) and it is indeed wrong, but it is, after all, only a harmless misunderstanding". Again not so, in the author's opinion. Million-dollar R & D contract proposals on the dynamics and control of large space structures are currently under technical adjudication. If the adjudicators fall prey to a corollary of the Assertion--namely, that any methodology that does not use PDE's is faulty--they will tend to favor proposals that promise an infinite number of modes. In most cases, this viewpoint would be unwise and unjust.

How Many Modes Are There?

If a physical structure does not have an infinite number of modes, how many vibration modes *does* it have? The most precise (but not very helpful) answer is: "none". As an approximation, the mathematical concept of a 'mode' is still very useful, however. This is especially true for the lower modes. On the other hand, as one goes higher and higher in mode number (past the 100th mode,

say, or the 1000th) the mathematical idea of a 'mode' tends to become increasingly inappropriate until, somewhere well this side of infinity, it is wholly inappropriate.

To emphasize this idea, we introduce the following definition in connection with mode shapes as a set of basis functions:

Definition: The *absurd subspace* associated with a PDE idealization of a structure is the subspace spanned by all but the first billion modes.

All PDE structural models have an absurd subspace. This absurd subspace is a flaw in these models but not an important one (unless glorified by the Assertion).

It is a curious paradox that the greatest advantage of modal analysis--the analyst can expand the general motion of a complex structure approximately in terms of a few important submotions--is lost if an infinite number of modes is insisted upon.

THE FINITE ELEMENT METHOD

When one analyses structures *in general*, one is not bothered by the necessity of generating numerical information. For example, it may suffice to say that the small deflection $\underline{u}(\underline{r},t)$ is related to the excitation $\underline{f}(\underline{r},t)$ via an appropriate operator \underline{K} that is,

$$\underline{K}\underline{u} + \sigma \ddot{\underline{u}} = \underline{f}(\underline{r},t) \quad (3)$$

where σ is the mass density. \underline{K} is a symmetric, 3×3 , partial differential stiffness operator. Assuming that rigid displacements are prevented (as in Fig. 2), \underline{K} is positive definite. The mode shapes for Eq. (3) satisfy

$$\underline{K}\underline{\phi}_\alpha(\underline{r}) = \omega_\alpha^2 \sigma \underline{\phi}_\alpha(\underline{r}) \quad (4)$$

and the orthonormality conditions are

$$\int_E \underline{\phi}_\alpha(\underline{r}) \underline{\phi}_\beta(\underline{r}) dm = \delta_{\alpha\beta} \quad (5)$$

where $dm = \sigma(\underline{r})dV$. For a system that deserves to be called a 'structure', there will be an infinite number of eigenfunctions (mode shapes). However, as we have seen above, the real structure that Eq. (3) represents does not share this 'infinite-modes' characteristic.

The modal coefficients of momentum and angular momentum (about O) are defined as follows:

$$\underline{p}_\alpha = \int_E \underline{\phi}_\alpha dm ; \underline{h}_\alpha = \int_E \underline{r}^X \underline{\phi}_\alpha dm \quad (6)$$

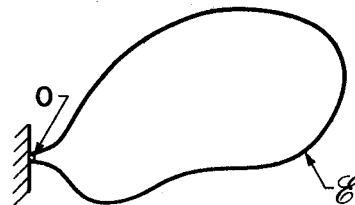


Fig. 2: General Elastic Structure

It can be shown (Ref. 1) that the modal

identities in the first column of Table 1 are satisfied by these coefficients. These modal identities and results like Eqs. (3), (4) and (5) for the generic structure of Fig. 2 are powerful in that they apply to all structures that satisfy the general assumptions that underlie Eq. (3).

The 'Mathematical Solution' Swindle

Operations like the integration $\int_E(\)dm$ in Eq. (5), or the Σ_1^∞ in Table 1 can be performed with the stroke of a pen. Engineers dealing with *specific* space structures require numerical data, not just elegant theoretical results.

The classical method for dealing with PDE's like Eq. (3) is to expand the solution in terms of a series of functions that are defined, named, examined, cataloged, and expounded upon. Usually these functions are not especially easy to calculate. Even worse is to define the solution of Eq. (3) in terms of a difficult integral. This "solution" (as the mathematicians call it) is in practical terms often just another mathematically equivalent way of stating the problem. The Knotkwit function, whose origins are traced in Appendix A, furnishes an example of the different meanings that may be attached to the word 'solution' by a mathematician and an engineer.

Even the functions sin, cos, sinh, cosh that make up the well-known solution for the vibration modes of the simple rod in Fig. 1a require some numerical sophistication to calculate efficiently. For most structures of practical interest, 'closed-form' solutions are not available and, even if they were, they would not likely be much help in numerical calculations.

The Ritz Method Revisited

Frustrated by their difficulties in formulating PDE's for complex structures, and their further difficulties in extracting numerical information from these PDE's once they have them, structural analysts began to chop up complicated structures (on paper) into small elements. Each of these elements could be analysed and numerical data of the required accuracy extracted relatively easily. Initially this approach rested for its justification on physical understanding, but applied mathematicians (e.g., Ref. 2) have since shown that, if properly used, this finite element method model (FEM model) is, in fact, an ingenious implementation of the much older method of Ritz. A FEM model therefore enjoys the same theoretical foundations as the Ritz method. In particular, the conditions for convergence are known. This convergence is to the so-called 'exact' solution, i.e., to the elusive solution of the PDE model that has the same modeling assumptions as the FEM.

This property of convergence is a highly desirable one and can often be used to advantage--in connection with the identities of Table 1, for example. But in our celebration of this convergence to the 'exact' solution we should not overlook the fact that the 'exact' solution is 'exact' only for the PDE model. It is not 'exact' at all for the actual structure because the PDE model is not exact for the actual structure.

This raises the following question: How can an 'error' of (say) 1% matter,

when the 'error' is with respect to an equation that is itself only valid to within (say) 10%? Yet it is this sort of error, no matter how small (and it can be made as small as desired by using sufficient finite elements), that seems to be the chief concern of the Infinite Mode Assertors. They do not trust the FEM model because it fails to predict the 'absurd subspace' (see earlier definition). In the author's opinion, however, this 'failure' is trivial and should, if anything, be counted as a point in the FEM model's favor because the absurd subspace doesn't exist physically anyway.

Unification

To this point in the discussion the FEM model and the PDE model have been treated as though they were competing alternatives. They are in an important sense *the same model*. The FEM model should be viewed as a numerical treatment of a corresponding PDE model. The finite element method must surely be one of the most spectacular success stories in the history of engineering analysis. FEM models circumvent the formulational and computational difficulties of their PDE counterpart models, while at the same time providing a numerical approximation to the latter that can be made arbitrarily accurate. If enough modeling elements are used, the error due to a finite number of coordinates can always be restricted to an 'absurd subspace'. The strength of the FEM model is that one can do numerical calculations for complicated structures; the weakness of the FEM model is that it can never be better than the associated PDE model to which it converges.

USES AND ABUSES OF LONG SLENDER RODS

A long, slender uniform cantilevered rod appears in Fig. 1 and its PDE model is given by Eq. (2). The attraction of this 'structure' is its simplicity and this makes it ideal as a learning tool. It provides a simple example for students being introduced to structural dynamics. For much the same reasons it is often cited to help in explaining new ideas to colleagues. Moreover, many satellites have rod-like appendages; in such cases the closed-form characteristics of cantilevered rods (summarized in Appendix B) have direct practical utility.

Nevertheless, because of its seductive simplicity, the slender rod structure tends to be focused upon rather more often than its limited range of application would warrant. In fact, the Infinite Modes Assertion is often a symptom of slender-rod overemphasis. If all the structures in the world were long slender rods, there certainly would be no need for the finite element method, at least not for structures. Slender rod enthusiasts often seem to imply that FEM models are really only undignified 'engineering approximations'. If such an enthusiast also wishes to ignore the crucial distinction between a physical structure and its PDE model, he has the right mind-set for accepting the Infinite Modes Assertion.

Modal Convergence

As a prelude to addressing the question 'Which modes are important?' we shall ourselves also use the long slender rod as a convenient starting point. Then, in the next section, a more realistic (and complicated) structure will be discussed. The notation and results in Appendix B will be taken for granted here.

The modal identities of Table 1 can be used as indicators of the error introduced into a structural model by modal truncation (i.e., error with respect to the 'exact' PDE representation, which is, as we have said repeatedly, not to be trusted too far itself). The modal parameters p_α and h_α are shown for the first few modes in Fig. 3. It is evident that they decrease nonotonically with mode number and that h_α decreases with α faster than p_α . These observations can be made also from Fig. 4, where the model error indices

$$\epsilon_1(N) = 1 - 2 \sum_{\alpha=1}^N \lambda_\alpha^{-2} \kappa_\alpha^2 \quad (7)$$

$$\epsilon_2(N) = 1 - 12 \sum_{\alpha=1}^N \lambda_\alpha^{-4} \quad (8)$$

have been introduced, corresponding respectively to the p_α and the h_α . With no modes, $\epsilon_1(0) = \epsilon_2(0) = 1$. For all the *theoretically* infinite number of modes, $\epsilon_1(\infty) = \epsilon_2(\infty) = 0$.

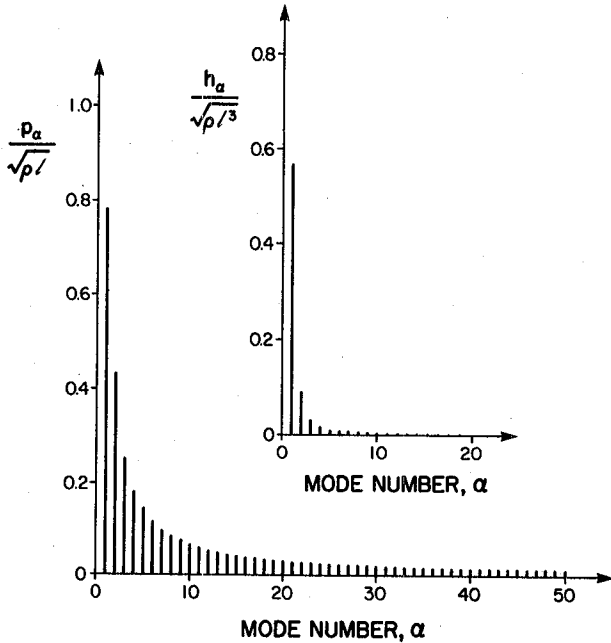


Fig. 3: Momentum Coefficients for Slender Rod

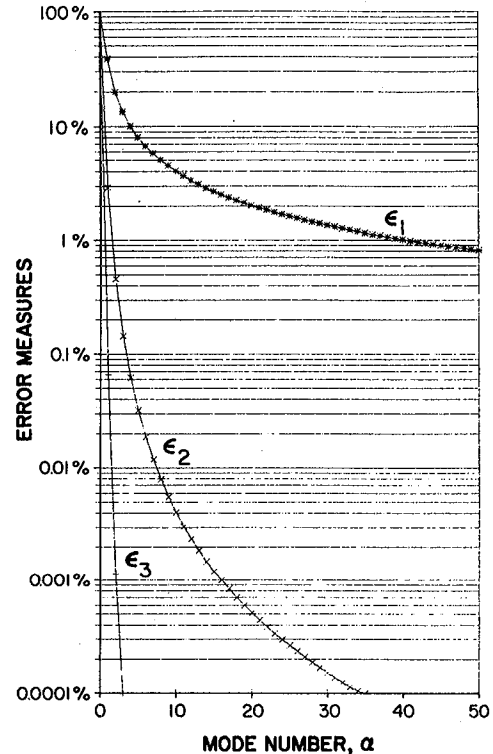


Fig. 4: Measures of Model Error

Also shown in Fig. 4 is the third measure of error,

$$\epsilon_3(N) = 1 - \frac{1680}{11} \sum_{\alpha=1}^N \lambda_{\alpha}^{-8} \quad (9)$$

(see last entry in Table 1). This error indicator takes both momentum coefficients and frequencies into account and is thus a more plausible measure of model error than ϵ_1 or ϵ_2 . The index ϵ_3 recognizes that, other things being equal ('other things' in this case being p_{α} and h_{α}), the low-frequency modes are more important than the high-frequency modes. If one wished to have a maximum of 1% model error, for example, as measured by ϵ_3 , only the 1st mode should be retained and the rest deleted.

LARGE DEPLOYABLE SPACE REFLECTOR

Long, slender, uniform, cantilevered rods can be carried only so far. They are useful in teaching certain basic lessons, but some of these lessons are not true for more general structures. Therefore we now consider a typical space structure of current interest--a large deployable space reflector. Shown in Fig. 5 is the wrap-rib antenna reflector developed by the Lockheed Missiles and Space Corporation (Ref. 3). A FEM model has been developed for this reflector by the Jet Propulsion Laboratory (Ref. 4) and a typical mode shape, taken from Ref. 4, is shown in Fig. 6.

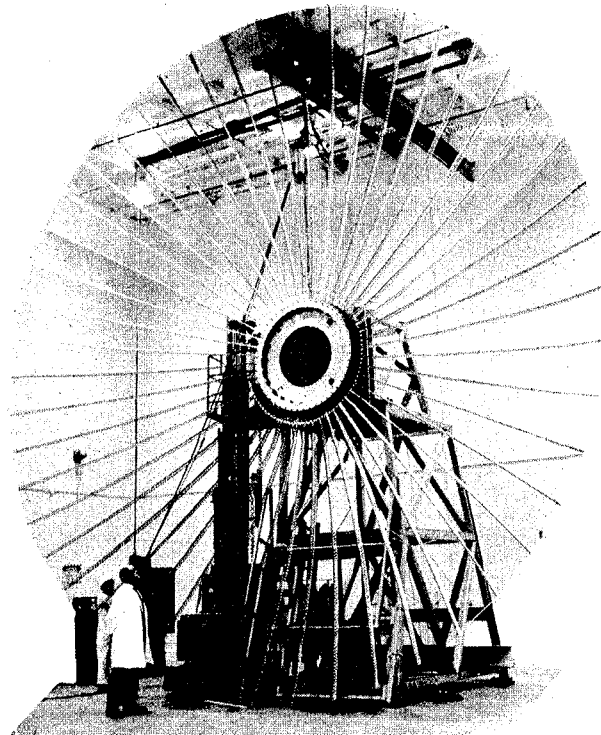


Fig. 5: Lockheed Wrap-Rib Reflector Used on ATS 6

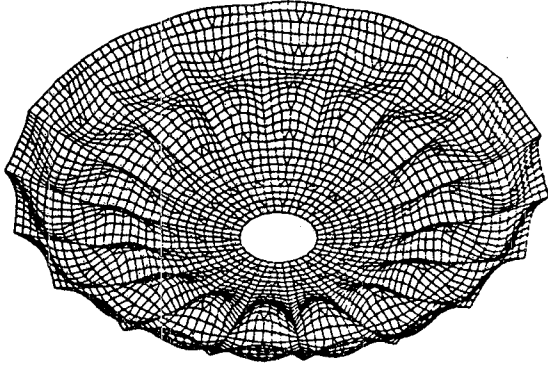


Fig. 6: Typical Wrap-Rib Mode Shape (from Ref. 4)

This model has several complexities that a simple rod does not have. The first is that a PDE model is very difficult and does not seem to have even been attempted. This leads to the use of a FEM model. The second complexity is three-dimensionality. For example, the modal momentum coefficients \underline{p}_α and the modal angular momentum coefficients \underline{h}_α are no longer scalars, but are 3×1 .

A Criterion for Mode Selection

A more subtle distinction between the wrap-rib reflector and the slender rod is that simple *modal truncation* becomes generalized to a process of *mode selection*. A glance back at Fig. 3 shows that for a slender rod the p_α and h_α decrease monotonically with α . In other words, whether we order the modes according to increasing frequency, or according to decreasing p_α , or according to decreasing h_α , the order of the modes is unchanged. This lesson, learned well for slender rods, must be unlearned for more complex structures. The question of which modes to keep is not simply a question of 'keeping the first N' and dropping the rest. There are several ideas available (Refs. 5,6) for mode selection, and the ones that rely solely on the structural dynamics are those that depend on ω_α , \underline{p}_α , and \underline{h}_α .

We can, for example, take the first three modal identities in Table 1. These three matrix identities correspond to 18 (independent) scalar identities. To create a single scalar indicator of how well these 18 identities are being satisfied, it is observed that they may be written as

$$\sum_{\alpha=1}^{\infty} \underline{M}_\alpha = \underline{M}_\infty \quad (10)$$

where the definitions

$$\underline{M}_\alpha = \begin{bmatrix} \underline{p}_\alpha \underline{p}_\alpha^T & \underline{p}_\alpha \underline{h}_\alpha^T \\ \underline{h}_\alpha \underline{p}_\alpha^T & \underline{h}_\alpha \underline{h}_\alpha^T \end{bmatrix}; \quad \underline{M}_\infty = \begin{bmatrix} \underline{m} \underline{1} & -\underline{c}^X \\ \underline{c}^X & \underline{J} \end{bmatrix} \quad (11)$$

have been introduced. Then the following scalar quantity is a measure of how well these identities are satisfied after the first N modes:

$$\epsilon_M(N) = \rho \left[\underline{1} - \underline{M}_{-\infty}^{-1/2} \left(\sum_{\alpha=1}^N \underline{M}_{-\alpha} \right) \underline{M}_{-\infty}^{-1/2} \right] \quad (12)$$

where $\rho[\cdot]$ stands for the spectral norm of $[\cdot]$. Note that $\underline{1}$ is here the 6×6 unit matrix, while in Eq. (11) $\underline{1}$ refers to the 3×3 unit matrix. (In other words, $\underline{1}$ always stands for a unit matrix of compatible size.)

The reasoning behind Eq. (12) is as follows: the \sum_1^N sum is normalized based on Eq. (10) in such a manner that symmetry is retained. The resulting matrix is compared to the ideal sum, $\underline{1}$. The cumulative sum in Eq. (12) is non-decreasing since $\underline{M}_{-\alpha}$ is positive semi-definite. The matrix difference in Eq. (12) must be positive definite for finite N. Thus its eigenvalues will be six real numbers between 0 and 1. The greatest of these six numbers is defined to be the error, $\epsilon_M(N)$.

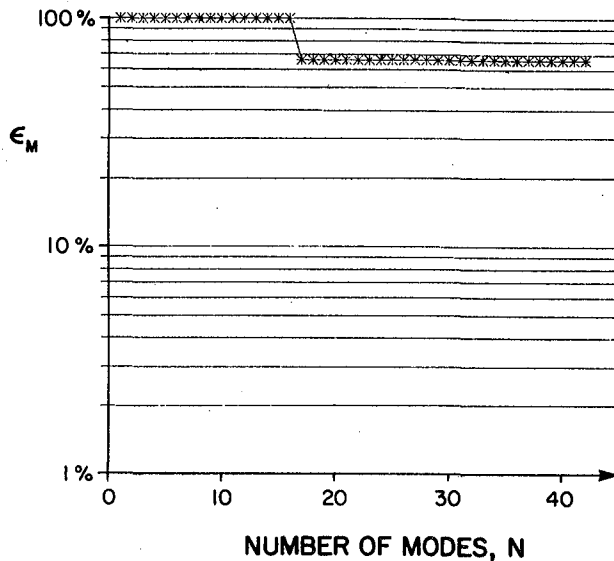


Fig. 7: Reduction of Model Error by First 42 Modes Using only Inertial Quantities in Error Measure, i.e., Using Eq. (12)

The error $\epsilon_M(N)$ is plotted in Fig. 7 for data typical of a wrap-rib reflector with 48 ribs and 44.4 m in diameter. Even after 42 modes, $\epsilon_M(42) = 0.66$. This slow convergence prompts the following comments.

- In the model used, some of the higher-wave-number modes have already been deleted. However, it is not expected that they would contribute materially to ϵ_M . (This is, in fact, why they were deleted.)
- Just because the $\epsilon_M(N)$ vs. N curve is 'flat' does not mean that intermediate modes are not making a positive contribution. This behavior just means that they are not contributing to reducing the maximum eigenvalue of the matrix in Eq. (12).
- A more detailed examination of the six eigenvalues of the matrix in Eq. (12) discloses that it is the $\sum_1^{\infty} \underline{p}_{-\alpha} \underline{p}_{-\alpha}^T = \underline{m}_1$ identity that is slow to con-

verge. This is in accordance with the slow convergence of p_α for the slender rod in Fig. 3. The so-called 'breathing' modes for the wrap-rib reflector are few and far between; yet it is these modes that must produce convergence in the (3,3) element of $\sum_{\alpha=1}^{\infty} p_\alpha p_\alpha^T = m\underline{1}$.

A Better Criterion for Mode Selection

Obviously the error criterion (12) is excessively harsh. It is counter-intuitive that a 42-mode model can have a 66% error. A goodly part of the problem is that the criterion (12) does not take the frequencies ω_α account. One of the messages in this paper is that frequency is not the only parameter of importance in modal selection. However, it would be extreme in the opposite direction to exclude the ω_α entirely, as Eq. (12) does. We therefore consider instead the last three modal identities in Table 1. These identities may be combined into the single 6x6 identity.

$$\sum_{\alpha=1}^{\infty} \underline{\underline{E}}_\alpha = \underline{\underline{E}}_\infty \quad (13)$$

where the definitions

$$\underline{\underline{E}}_\alpha = \omega_\alpha^{-2} \underline{\underline{M}}_\alpha \quad (14)$$

$$\underline{\underline{E}}_\infty = \int_E \int_E \begin{bmatrix} 1 \\ \underline{\underline{r}}^X \end{bmatrix} F(\underline{\underline{r}}, \underline{\underline{\xi}}) \begin{bmatrix} 1 \\ \underline{\underline{\xi}}^X \end{bmatrix}^T dm_r dm_\xi \quad (15)$$

have been used.

The modal identity (13) suggests the following model error indicator:

$$\epsilon_E(N) = \rho [1 - \underline{\underline{E}}_\infty^{-1/2} (\sum_{\alpha=1}^N \underline{\underline{E}}_\alpha) \underline{\underline{E}}_\infty^{-1/2}] \quad (16a)$$

This indicator is patterned after Eq. (12), and is plotted in Fig. 8. According to this indicator, if an error of only 2.5% were the most that could be tolerated in the model, the first 28 modes would have to be kept.

There is, however, a hidden premise in this last procedure, namely, *the premise that the modes must be selected in their natural order* (i.e., by increasing frequency). There is no basis for this premise or this procedure. Figure 3 shows that, for a slender rod, p_α and h_α decrease monotonically with α , as would $p_\alpha^2/\omega_\alpha^2$, $h_\alpha^2/\omega_\alpha^2$, etc. Thus, for a slender rod, all methods of ordering modes produce the same order--the 'natural' order. For more complex structures this is no longer true. The error indicator in Eq. (16a) can therefore be improved (i.e., fewer modes required for the same model accuracy) by taking the modes in the cumulative sum in a different order. Thus we replace Eq. (16a) by

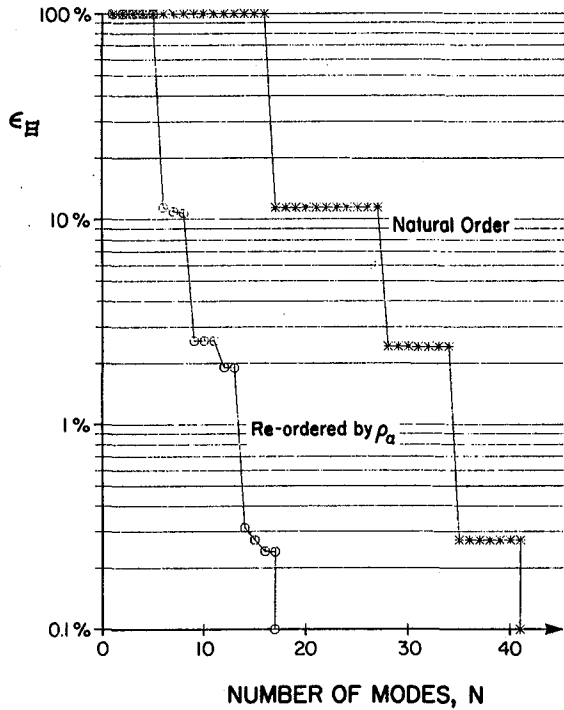


Fig. 8: Reduction of Model Error by First 42 Modes Using Eq. (16)

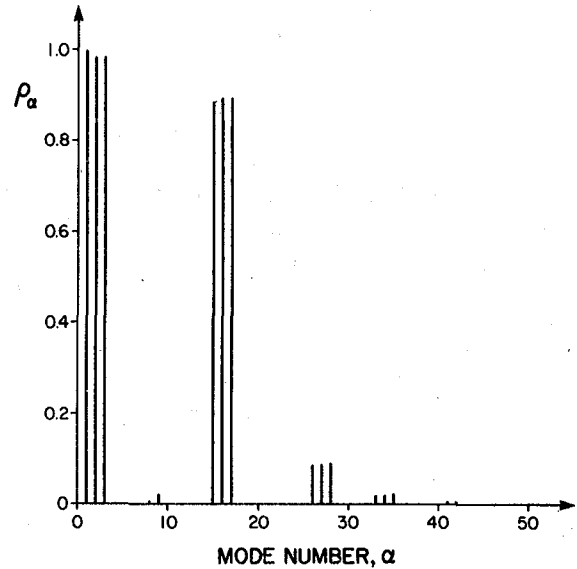


Fig. 9: Dynamical Significance of First 42 Modes as Measured by ρ_α

$$\epsilon_H(N) = \rho \left[1 - \frac{1}{\epsilon_\infty} \left(\sum_{\alpha=\alpha_1}^{\alpha_N} \frac{1}{\epsilon_\alpha} \right) \frac{1}{\epsilon_\infty} \right] \quad (16b)$$

where

$$\rho_{\alpha_1} > \rho_{\alpha_2} > \rho_{\alpha_3} > \dots \quad (17)$$

and ρ_α is defined by

$$\rho_\alpha = \rho \left[\frac{1}{\epsilon_\infty} \frac{1}{\epsilon_\alpha} \frac{1}{\epsilon_\infty} \right] \quad (18)$$

(Note, however, that the spectral radius operator does not commute in addition; that is

$$\epsilon_H(N) \neq 1 - \sum_{\alpha=\alpha_1}^{\alpha_N} \rho_\alpha$$

as might be assumed at first sight.)

As can be inferred from Fig. 9, ρ_α certainly does not decrease monotonically with α . This would suggest that the re-ordering of modes required by Eq. (16b) should be beneficial. The second plot in Fig. 8 shows that this is indeed

the case. In fact, only 9 modes are now needed to give as low as 2.5% error--a saving of 19 modes (and a reduction in system order by 38 state variables) over the previous un-re-ordered scheme. Evidently mode selection can be, for complex structures, far superior to simple modal truncation.

CONCLUDING REMARKS

In summary, the main points discussed in this paper are the following:

- (a) Neither a PDE model nor any other mathematical model of a structure is exact.
- (b) For complicated structures, PDE models are very difficult to formulate and very difficult to extract numerical information from.
- (c) Even when a PDE model does exist, the 'solution' in terms of 'known functions' may still require considerable effort to extract numerical information.
- (d) Viewed as a Ritz method, a FEM model is not in competition with the corresponding PDE model; it is, instead, a very powerful numerical method for solving the PDE model.
- (e) The idea of a 'mode' is, in essence, a mathematical one. It is highly unlikely that any real structure can vibrate *exactly* so that all its points move in unison; in other words, it is highly unlikely that any structure has any modes. As an approximation, however, the idea of a mode is an excellent one for many structures, especially for the 'lower modes'. The agreement between experiment and theory for the 'higher modes' tends to become weaker.
- (f) In this approximate sense, most structures have a very large number of modes. It is elementary to show, however, that no real structure has an infinite number of modes. The Infinite Modes Assertion is false.
- (g) The only utility of the Infinite Modes idea is within the purely mathematical domain. See, for example, the modal identities in Table 1.
- (h) The long, slender, uniform cantilevered rod has a simplicity that is at once helpful and dangerous. It is a reasonable structure on which to explain a new idea, or to test a new idea, but the validation or generalization of the idea must be carried out on structures of more realistic complexity.
- (i) Many 'error indices' can be defined as guidelines for structural modal order reduction. Simple modal truncation, although suggested by experience with slender rods, is naive. The proper process is mode selection, based on an appropriate error criterion.
- (j) The error criterion in Eq. (12) is unnecessarily pessimistic because it ignores frequency information. It is as naive as a 'frequencies-only' criterion, at the opposite extreme.
- (k) The error criterion in Eq. (16) is superior to Eq. (12), especially if the modes are selected according to the order specified by Eq. (17). This is

illustrated for a wrap-rib antenna reflector in Fig. 8.

REFERENCES

1. Hughes, P. C. "Modal Identities for Elastic Bodies, With Application to Vehicle Dynamics and Control", *Jour. Appl. Mech.*, Vol. 47, No. 1, March 1980, pp. 177 - 184.
2. Strang, G.
Fix, G. J. *An Analysis of the Finite Element Method*, Prentice-Hall, 1973
3. Woods, A. "Final Report for Study of Wrap-Rib Antenna Design", Lockheed Missiles and Space Company, Space Systems Division, Sunnyvale, California.
4. El-Raheb, M.
Wagner, P. "Static and Dynamic Characteristics of Large Deployable Space Reflectors", AIAA Paper 81-0503-PC, 22nd Structures, Structural Dynamics and Materials Conference, April 6 - 8, 1981.
5. Likins, P. W.
Ohkami, Y.
Wong, C. "Appendage Modal Coordinate Truncation Criteria in Hybrid Coordinate Dynamic Analysis", *Jour. Spacecraft and Rockets*, Vol. 15, Oct. 1976, pp 611 - 617.
6. Hughes, P. C.
Skelton, R. E. "Modal Truncation for Flexible Spacecraft," *J. Guid. and Control*, Vol. 4, No. 3, May - June 1981, pp. 291 - 297.

Acknowledgements

This paper was supported in part by the Natural Sciences and Engineering Research Council of Canada under Grant No. A4183, in part by the Industrial Research Funding program of the Canadian Department of Communications (through Dynacon Enterprises Ltd.), and in part by the Jet Propulsion Laboratory.

The numerical calculations were made by Dr. G. B. Sincarsin; the plots were computed by David MacLaren; and the figures were prepared by Ida Krauze.

Appendix A - The Origin of the Knotkwit Function

Some years ago, the eminent applied mathematician Professor Will Knotkwit encountered in his theoretical study of structures a certain PDE whose solution he could not express in closed form. Nor could he express the solution in terms of known functions. Eventually an important idea occurred to Prof. Knotkwit: he introduced a new function that was, by definition, the solution of his troublesome equation. He pro-

ceeded to write several papers on the interesting mathematical properties of the Knotkwit function (as it became known shortly before his retirement). Professor Knotkwit even lived to see his function referred to, by one of his former graduate students, as a 'known' function.

It is not likely that the Knotkwit function will ever be called an 'elementary' function. What is clear, how-

ever, is that any solution to a structural dynamics problem that can be written in terms of Knotkwit functions, or even that can be expressed as an integral whose integrand involves Knotkwit functions in a fairly simple manner,

will be called a 'closed-form' solution.

Thus, ultimately, Professor Knotkwit achieved his 'closed-form' solution in terms of 'known' functions.

Appendix B - Long Slender Rod Modes

The well-known solution to Eq. (2) is

$$u(x,t) = \sum_{\alpha=1}^{\infty} \phi_{\alpha}(x) \eta_{\alpha}(t) \quad (B1)$$

where

$$\ddot{\eta}_{\alpha} + \omega_{\alpha}^2 \eta_{\alpha} = \int_0^{\ell} \phi_{\alpha}(x) f(x,t) dx \quad (B2)$$

and

$$\phi_{\alpha} = (\rho \ell)^{-1/2} [(\cosh \lambda_{\alpha} \xi - \cos \lambda_{\alpha} \xi) - \kappa_{\alpha} (\sinh \lambda_{\alpha} \xi - \sin \lambda_{\alpha} \xi)] \quad (B3)$$

where

$$\lambda_{\alpha} = \frac{\rho \omega_{\alpha}^2 \ell^4}{EI}; \quad \xi = \frac{x}{\ell}; \quad \kappa_{\alpha} = \frac{S_{\alpha} - s_{\alpha}}{C_{\alpha} + c_{\alpha}} \quad (B4)$$

with $s_{\alpha} = \sin \lambda_{\alpha}$, $c_{\alpha} = \cos \lambda_{\alpha}$, $S_{\alpha} = \sinh \lambda_{\alpha}$, $C_{\alpha} = \cosh \lambda_{\alpha}$.

The natural frequencies are calculated by numerical solution of the transcendental equation

$$c_{\alpha} C_{\alpha} + 1 = 0 \quad (B5)$$

The mode shapes of Eq. (B3) can readily be shown (directly from the differential equation) to satisfy the orthogonality conditions

$$\int_0^{\ell} \phi_{\alpha}(x) \phi_{\beta}(x) dx = 0 \quad (\alpha \neq \beta) \quad (B6)$$

It is more onerous to show that Eq. (B3) satisfies the normality condition

$$\int_0^{\ell} \phi_{\alpha}^2 dm \equiv \rho \ell \int_0^1 \phi_{\alpha}^2 d\xi = 1 \quad (B7)$$

This latter fact is often omitted from textbook discussions.

In free vibration, the force and torque on the rod at O are (see Fig. 1a):

$$F(t) = \sum_{\alpha=1}^{\infty} p_{\alpha} \ddot{\eta}_{\alpha}; \quad G(t) = \sum_{\alpha=1}^{\infty} h_{\alpha} \ddot{\eta}_{\alpha} \quad (\text{B8})$$

where p_{α} and h_{α} are the coefficients given (in general) by Eq. (6). For our present simple 'structure',

$$p_{\alpha} = \int \phi_{\alpha} dm \equiv \rho \ell \int_0^1 \phi_{\alpha} d\xi = 2(\rho \ell)^{1/2} \kappa_{\alpha} / \lambda_{\alpha} \quad (\text{B9})$$

$$h_{\alpha} = \int x \phi_{\alpha} dm \equiv \rho \ell^2 \int_0^1 \xi \phi_{\alpha} d\xi = 2(\rho \ell^3)^{1/2} / \lambda_{\alpha}^2 \quad (\text{10})$$

Therefore the modal identities of the first column in Table 1, which assume the special form shown in the second column for a slender rod, imply the identities shown in the third column in Table 1. Note that the sums involve an infinitude of transcendental numbers.

Appendix C - Table of Symbols

<u>Roman</u>		<u>Greek</u>	
\underline{c}	first moment of inertia, $\int r dm$	α	modal index
\underline{EI}	flexural rigidity of a long slender rod	$\delta_{\alpha\beta}$	1 if $\alpha = \beta$; otherwise 0
$\underline{f(x,t)}$	force per unit length, at position x , at time t	η_{α}	modal coordinate associated with mode α
$\underline{F(r,\xi)}$	deflection at position r , due to unit force at position ξ	κ_{α}	see Eq. (B4) in Appendix B
$\underline{h_{\alpha}}$	modal angular momentum coefficient; see Eq. (6)	λ_{α}	see Eq. (B4) in Appendix B
\underline{J}	(second) moment-of-inertia matrix	ξ	x/ℓ for slender rod
\underline{K}	stiffness operator	$\underline{\xi}$	dummy position vector
$\underline{\ell}$	rod length	ρ	mass per unit length for slender rod
\underline{m}	mass	σ	mass density function
\underline{N}	number of modes retained	ϕ_{α}	mode shape for mode α
$\underline{p_{\alpha}}$	modal momentum coefficient; see Eq. (6)	ω_{α}	natural frequency for mode α
\underline{r}	position vector	<u>Special Symbols</u>	
\underline{t}	time	$\rho[]$	spectral radius
\underline{u}	small elastic displacement	$\underline{1}$	unit matrix (of appropri. size)
\underline{x}	distance along slender rod	$()'$	spatial derivative
		$(\dot{\ })$	temporal derivative

TABLE I: SUMMARY OF MODAL IDENTITIES

	'MOST GENERAL' CASE (Linear Elastic Body)	'LEAST GENERAL' CASE (Long, Slender, Uniform Cantilever Beam)	TRANSCENDENTAL IMPLICATIONS
p_α, h_α	$\sum_{\alpha=1}^{\infty} p_\alpha p_\alpha^T = m \underline{1}$ $\sum_{\alpha=1}^{\infty} h_\alpha p_\alpha^T = \underline{c}^X$ $\sum_{\alpha=1}^{\infty} h_\alpha h_\alpha^T = \underline{J}$	$\sum_{\alpha=1}^{\infty} p_\alpha^2 = \rho l$ $\sum_{\alpha=1}^{\infty} h_\alpha p_\alpha = \frac{\rho}{2} l^2$ $\sum_{\alpha=1}^{\infty} h_\alpha^2 = \frac{\rho}{3} l^3$	$\sum_{\alpha=1}^{\infty} \lambda_\alpha^{-2} \kappa_\alpha^2 = \frac{1}{4}$ $\sum_{\alpha=1}^{\infty} \lambda_\alpha^{-3} \kappa_\alpha = \frac{1}{8}$ $\sum_{\alpha=1}^{\infty} \lambda_\alpha^{-4} = \frac{1}{12}$
ω_α	$\sum_{\alpha=1}^{\infty} \omega_\alpha^{-2} = \text{trace} \int_E \underline{F}(\underline{r}, \underline{r}) d\mathbf{m}$	$\sum_{\alpha=1}^{\infty} \omega_\alpha^{-2} = \frac{\rho}{12EI} l^4$	$\sum_{\alpha=1}^{\infty} \lambda_\alpha^{-4} = \frac{1}{12}$
$\omega_\alpha, p_\alpha, h_\alpha$	$\sum_{\alpha=1}^{\infty} \omega_\alpha^{-2} p_\alpha p_\alpha^T = \int_E \int_E \underline{F}(\underline{r}, \underline{\xi}) d\mathbf{m}_r d\mathbf{m}_\xi$ $\sum_{\alpha=1}^{\infty} \omega_\alpha^{-2} h_\alpha p_\alpha^T = \int_E \int_E \underline{r}^X \underline{F}(\underline{r}, \underline{\xi}) d\mathbf{m}_r d\mathbf{m}_\xi$ $\sum_{\alpha=1}^{\infty} \omega_\alpha^{-2} h_\alpha h_\alpha^T = - \int_E \int_E \underline{r}^X \underline{F}(\underline{r}, \underline{\xi}) \underline{\xi}^X d\mathbf{m}_r d\mathbf{m}_\xi$	$\sum_{\alpha=1}^{\infty} \omega_\alpha^{-2} p_\alpha^2 = \frac{\rho^2}{20EI} l^5$ $\sum_{\alpha=1}^{\infty} \omega_\alpha^{-2} h_\alpha p_\alpha = \frac{13\rho^2}{360EI} l^6$ $\sum_{\alpha=1}^{\infty} \omega_\alpha^{-2} h_\alpha^2 = \frac{11\rho^2}{420EI} l^7$	$\sum_{\alpha=1}^{\infty} \lambda_\alpha^{-6} \kappa_\alpha^2 = \frac{1}{80}$ $\sum_{\alpha=1}^{\infty} \lambda_\alpha^{-7} \kappa_\alpha = \frac{13}{1440}$ $\sum_{\alpha=1}^{\infty} \lambda_\alpha^{-8} = \frac{11}{1680}$

This Page Intentionally Left Blank

CONTROL OF FLEXIBLE STRUCTURES: A SYSTEMATIC OVERVIEW OF THE PROBLEM

Richard Gran

Research and Development Center
Grumman Aerospace Corporation
Bethpage, NY 11714

ABSTRACT

In the theory of flexible structures control, there are two approaches that are usually advocated. The first is based on the theory of partial differential equations and the statement of the problem is : "If one does not use a continuum approach there will always be a problem that has been overlooked and any design will not work when implemented on a real system." In contrast the second approach is based on the tacit assumption that "finite is beautiful." This school contends that a finite model can always be made to approximate the original system to any desired level of accuracy. Following this strategem, the design is based on a finite dimensional model whose order is determined by a scientific method such as mode truncation, residue matching methods (based on the partial fraction expansion or the eigenvectors from the diagonalizing transformation) or using modal costs. These two schools are not irreconcilable.

The key to developing a reduced order model that subsumes the objections of the first school while providing the finite model required by the second school is the realization that no reduced model can be specified without first specifying the closed loop gains. A high gain system means a large control bandwidth; a large bandwidth means that many more flexible modes must be retained. On the other hand, the controller bandwidth is determined by the desired performance and the disturbances that will cause performance degradation. It is important to realize that no control is required if the system is not being disturbed. We are confronted with a tail chasing dog syndrome. We can't design the control until we have a model and we can't get a model until we've designed the control. This is the major argument used by the spokesmen of the distributed or p.d.e. school.

The compromise position advocated here is to design the system using finite methods and verify the design's robustness using results from the continuum school. Thus one should follow the recipe:

- o Determine the expected disturbances from both external and internal sources (including the measurement devices).
- o Determine the control bandwidth that will satisfy the desired specifications (i.e. reduce the disturbance amplitudes).
- o Truncate the structural model to include all frequencies up to some multiple of the control bandwidth.

- o Of the structural modes retained, additionally discard those that have low mode costs (i.e. that are not excited by the disturbances because they are either almost uncontrollable or are not observable through the performance measure used for evaluating the design.)
- o Carefully evaluate the potential interactions of the sensors and actuators at their locations to insure that unstably interacting modes are not discarded even though they don't contribute to the cost.
- o Design the controller, the compensation and the feedforward control using a reduced state feedback control design algorithm.
- o Verify that the bandwidth of the controller is that assumed at the start of the design process. If not - redesign the control.
- o Verify stability, robustness and performance of the final design.

This paper reviews each of these design steps. It is shown that without damping there is no finite model that can be used to design the control system. The definitions of stably and unstably interacting modes are given, and the design of reduced order control and compensator systems is described. The algorithm for the reduced order control that uses an explicit computation of the gradient and Hessian of the performance index is shown.

INTRODUCTION

There are many concepts in the control of distributed systems that are important for practical control design. However, no matter what one thinks of the continuum approach, at some step in the design process it must be discarded to allow the designer to use a finite controller. It is not possible to implement a continuum design nor is it possible to compute such a design for any practical structure. Thus the issue in the continuum vs. finite argument is not whether or not one must use a finite model, but when. It is possible to carry a linear design through to its Riccati p.d.e. form and then use a Galerkin method or other projection concept to develop a finite controller (see for example Gibson Ref. 1). The alternative is to use a finite model at the start. This is usually preferred by the control community whose task it is to design controllers for flexible structures because of the availability of structural analysis tools like NASTRAN.

To minimize the number of definitions we have to introduce, the notation used here follows that of Ref.2. The theoretical results discussed here are proved in Refs. 2 and 3, and the example that is described appears in an INTELSAT report (Ref. 4). The last step of the design process in which the spillover bounds are evaluated from the p.d.e. description of the system and the robustness is verified is not discussed here. These can be found in the papers by Balas (Refs.5 and 6) and Kosut (Ref.7).

FINITE DIMENSIONAL MODELS FOR STRUCTURAL CONTROL

The only reason that control is required in any system is that the disturbances cause the system to be perturbed away from some nominal value (position, velocity etc.) and this perturbation is large enough to cause the specifications to be exceeded. Therefore the starting point for any control design discussion must be the disturbances and the specifications. The specifications determine the performance index that is used to determine an optimal or suboptimal design. Typical performance measures include line of sight motion of a satellite, the line of sight motion of the optical axis of a telescope, or the pointing direction of an antenna. These can always be related to the small angle motions of a structure and through those motions to the displacements of the structure from some nominal position. Therefore the criteria for which disturbances are important is the contribution to the performance index of those disturbances that are expected. This is the message of the modal cost approach of Skelton. It is not necessary to use modal costs to determine the modes that should be retained if the design starts with a continuum approach. Therefore, the continuum model is used initially to develop a rough measure of the required bandwidth of the system subject to the disturbances as they are expected.

If the output of a sensor is denoted by y_j then, from Fig.1, the Laplace transform of the output is given by

$$y_j(s) = H_m^j(s) \sum_{k=1}^{\infty} \frac{\varphi_{\alpha k}^c \varphi_{\beta k}^m H_c^k(s) u_p(s) + \varphi_{\alpha k}^d \varphi_{\beta k}^m H_d^k(s) w_r(s)}{s^2 + 2\zeta_k \omega_k s + \omega_k^2} \quad (1)$$

where:

- $H_c(s)$ is the control actuator transfer function
 - $H_d(s)$ is the disturbance model transfer function
 - $H_m(s)$ is the measurement devices transfer function
 - $w(s)$ is the Laplace transform of the disturbance
 - $u(s)$ is the Laplace transform of the control input
- The remaining terms are defined in Fig. 1.

Using (1), the infinite dimensional system has been written as an infinite series whose individual terms represent the Laplace transform of the modes of the system. This is the resolvent of the semigroup of the system written as a sum. Since the operators are bounded, this series always converges and becomes the actual (transcendental) resolvent. Because it more closely resembles the approximate transfer functions that result from finite models, the form (1) is used here to develop the arguments that follow.

Using the form (1), it was shown in Ref. 2 that the transfer function of a finite approximation to (1) becomes asymptotically invariant as the number of modes increases. This result is useful because it says that if enough modes are retained then a finite model exists that will be arbitrarily close to the infinite dimensional system. The unfortunate aspect of this approximation is that the modes are sinusoidal, and the convergence of the inverse transform of

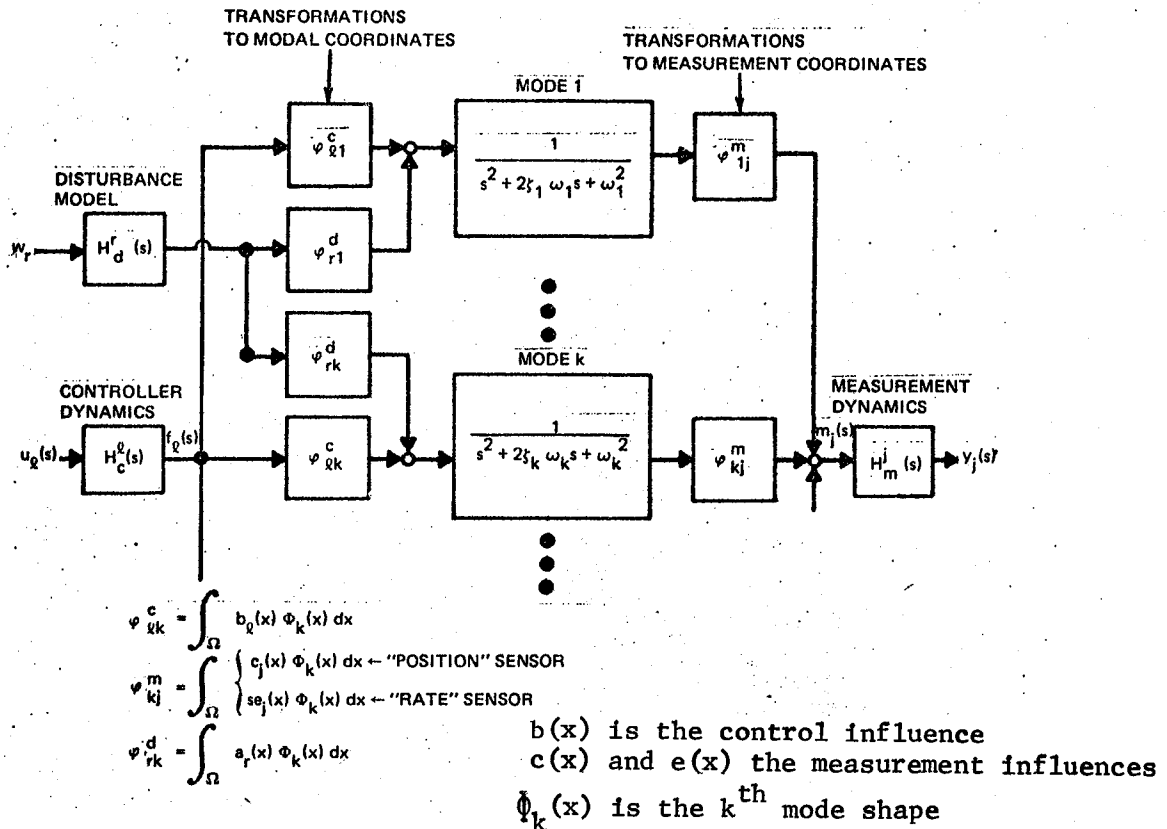


Figure 1
Block Diagram of Structural Dynamics Control Problem

the series that results from (1) is only in L_2 so we have a Gibbs phenomena effect. Thus the convergence is always poor at step type of discontinuities. This effect was noticed by Wie and Bryson (Ref. 8). Another consequence of this approximation is that a system whose transcendental transfer function is minimum phase can result in a finite approximation that is non-minimum phase. This result also is shown in Ref. 8 and its consequences are also discussed in Ref. 2 and Ref. 9.

Since a finite model can always be selected that approximates the continuum description to within an arbitrarily small error, the next question is how many modes must be kept. As was pointed out in the introduction, this question can only be answered based on the bandwidth of the controller. Thus if the control bandwidth is f_c , then the highest mode frequency that must be retained is $10^n f_c$, where the damping is 10^{-n} . This result is proved in Ref. 2 and can be loosely justified based on the magnitude of the resonance peaks that appear in the transfer function (1). At resonance, the amplitude of

the Bode plot magnitude is given by $1/(2\zeta_k\sqrt{1-\zeta_k^2})$, where the frequency of the mode is ω_k and the frequency at which the resonance occurs is $\omega_m = \pm\sqrt{1-2\zeta_k^2}\omega_k$. Thus on a log magnitude plot the amplitude in db of the resonance is $20 \log_{10} H(j\omega)$, which is $20n-6$ db at the resonance. Therefore, since only those modes that have an amplitude that exceeds 0 db can cause a loss of stability or performance, the criteria for discarding high frequency modes depends on the control bandwidth and the fact that for any well behaved control the closed loop response "rolls off" at least 20 db/decade after f_c . Thus the first frequency that guarantees that the resonance is always below the 0 db line is n decades away from f_c or $n/2$ decades away if the system rolls off at 40 db/decade (which usually happens for any system with actuators and sensors because of their dynamics).

STABLE AND UNSTABLE MODE INTERACTIONS

The question of which modes are to be retained is not completely answered by the criteria described above. There are many modes that should be discarded because they are not controllable, observable, or disturbable (when we say not, we should strictly speaking say weakly, because it is almost never true that a mode is completely unobservable or uncontrollable in practice). However there is a significant caveat that must be heeded when discarding modes. This is the rule that one never throws away a mode that is unstably interacting. The criteria for determining the stability of a mode is shown in Fig.2. The important point is that there is a phase shift between the measurement and control caused by the relative positions of the actuators and sensors. This phase shift is either 0° or 180° depending on whether the actuator and sensor are on opposite sides of a modes node. The best way of determining this is by using the pictures of the mode shapes, as is shown in Fig.2

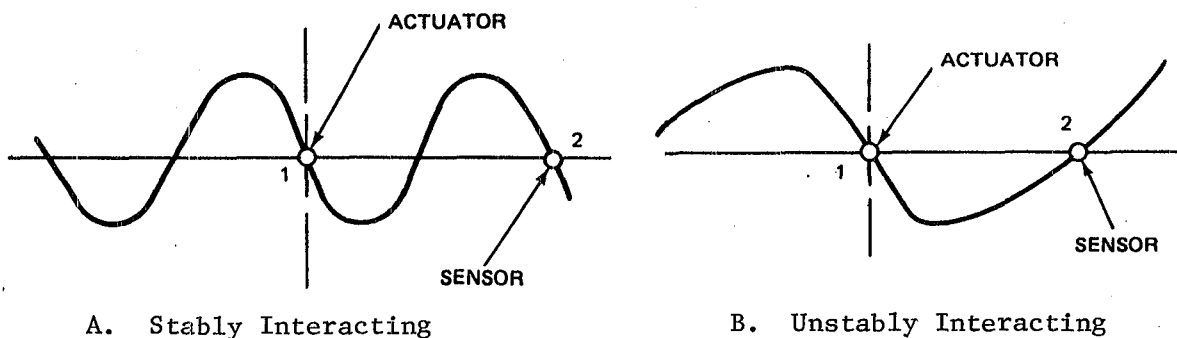


Figure 2
Mode Shapes for Stable and Unstable Interactions

The evaluation of which modes to discard based on mode costs can be done in a simple and straightforward graphical way by plotting the Laplace transform of the costs on a gain/phase plot for the disturbances expected. This plot gives a visualization of the levels of disturbance at any frequency and relates both the disturbance spectrum and the dynamics of the structure to the cost. An example of such a plot is shown in Fig. 3. This figure also shows the mode numbers that are causing significant motion and the pole zero order as one moves upward in frequency. Poles that occur before zeros near the $j\omega$ axis are unstably interacting and vice versa. Thus, a plot such as Fig. 3 can be used to truncate additional modes from the problem based on mode costs without a complicated calculation of the costs.

There are several issues that arise in the debate on control of large structures that are resolved by the definition of stable and unstable mode interactions. The main issue is the question of whether or not a design approach leads to spillover instability. Since the modes that interact stably can not be driven unstable by any gain change, any design result that shows no stability loss or good gain and phase margins when additional modes are added are probably adding only stably interacting modes. This is particularly true if the assumption is made that the actuators and sensors are collocated.

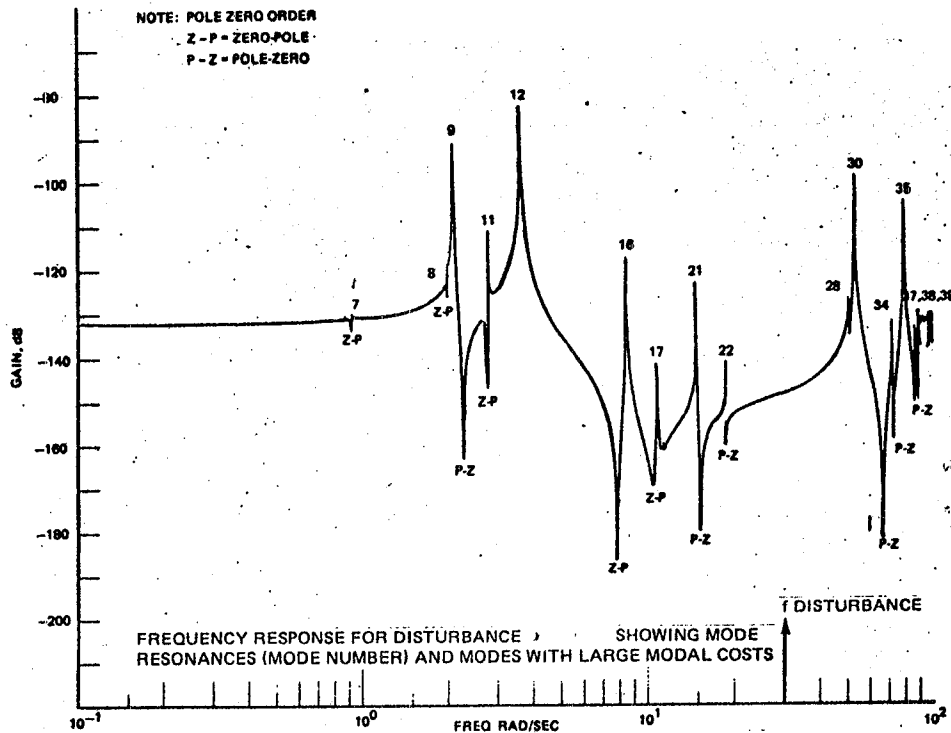


Figure 3
 Mode Costs for a Structure
 The mode cost for this design was L.O.S. motion, and the disturbance was a monochromatic sinusoid at the frequency shown.

The second issue that is clarified by the definition of stable and unstable modes is what happens when there are geometry changes. The only way that a controller can stabilize an unstably interacting mode is to introduce 180° of phase shift into the control loop at the frequency of the unstably interacting mode. Thus if one were to plot the frequency response of an observer or Kalman filter from any sensor to any actuator, those modes that interact unstably will be notched (i.e. there will be a deliberate 180° phase shift at the mode frequency). This has dire consequences when the geometry changes. Either the mode frequency change or the mode shape change can cause the phase shift to be introduced at the wrong frequency and the resulting design will be unstable since the 180° phase shift introduced to stabilize the original design is now at the wrong frequency in the geometrically different structure (because of the phase shift introduced by the controller in its attempt to stabilize the interaction we now have a control with gain >1 at a phase of 180°, which is unstable). The message is clear: if there are geometry changes and there are unstably interacting modes, some way must be developed to track the mode frequencies, i.e. adapt, or else the design will not work.

REDUCED STATE FEEDBACK CONTROL FOR LARGE STRUCTURES

In Ref. 2, a reduced state feedback control design algorithm developed by Rossi, Ref. 11 was briefly described. We have successfully used this algorithm to design a control system for a large structure using it to develop the feedback gains for a constrained configuration that connects the output of a particular sensor to a particular actuator. Simultaneously the algorithm derives the poles and zeros for compensators that are required by making these pole-zero locations gains that are also determined by the algorithm.

If the control system to be designed is structured as shown in Fig.4, then the optimal reduced state feedback algorithm is used to determine the feedback and feedforward gains that optimize the performance index:

$$J = \int_0^{\infty} z^T Q_z z + u^T R u \, dt \quad (2)$$

where:

- z is the output (which is not necessarily the sensor)
- u is the control
- Q_z is the weight on the output
- R is the weight on the control

The reduced state algorithm gives a solution that depends on the initial conditions since (2) is equivalent to $x_0^T P x_0$. The minimizing feedback gain is determined from a search. The algorithm for determining the minimum uses an explicit calculation of the gradient and Hessian tensors for J and the search is done in four steps. The first step is to compute the gradient and Hessian matrices and then to diagonalize the Hessian. Since the Hessian is symmetric, the diagonalization can be performed by an orthogonal transformation. Since in

general the Hessian will not be positive definite, the negative eigenvalues are arbitrarily changed in sign to make the step direction correspond to a locally quadratic curve fit. Thus if H_0 represents the Hessian matrix at the zeroth iteration, this step consists of forming the following matrices:

$$H_0 = [V_1 \ V_2] \begin{bmatrix} D_1 & 0 \\ 0 & -D_2 \end{bmatrix} \begin{bmatrix} V_1^T \\ V_2^T \end{bmatrix} \quad (3)$$

where:

$D_{1,2}$ are diagonal matrices

$V_{1,2}$ are the elements of the orthogonal transformation

$$\text{and } H^\dagger = [V_1 \ V_2] \begin{bmatrix} D_1 & 0 \\ 0 & D_2 \end{bmatrix} \begin{bmatrix} V_1^T \\ V_2^T \end{bmatrix} \quad (4)$$

The only difference between H_0 and H^\dagger is that the second matrix is now positive definite.

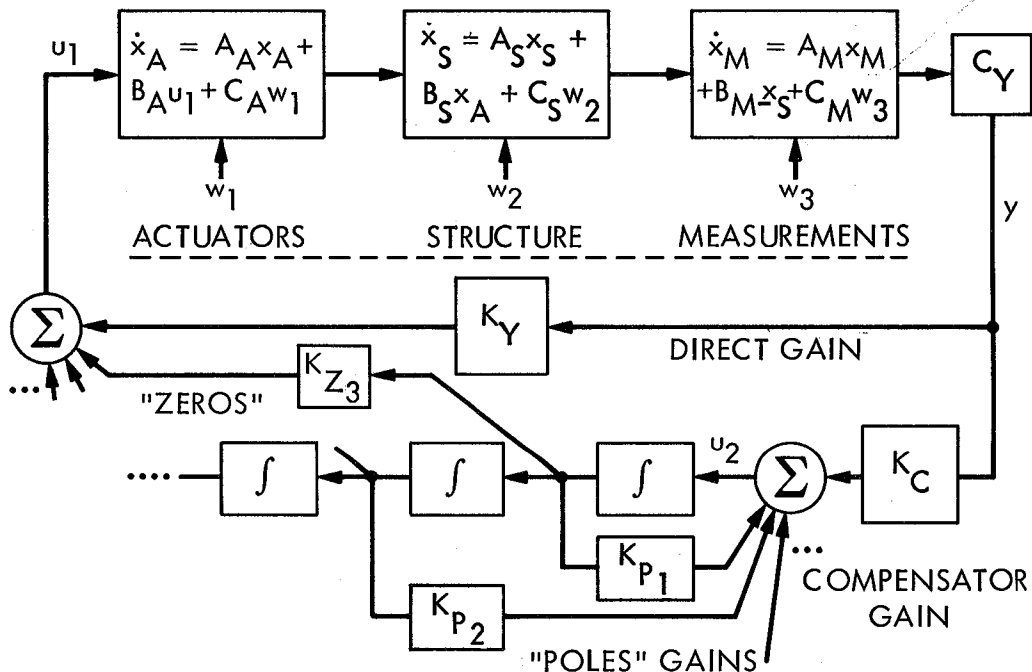


Figure 4

Block Diagram of the Reduced State Feedback Control Design
The control gains shown are selected to provide the lowest cost J for the configuration shown. Only the gains shown are derived by the algorithm giving both the feedback control and the compensator.

The second step in the algorithm is the determination of the step direction for the search. This is done by using the Taylor series for the cost as follows:

$$J(K_1) = J(K_0) + (K_1 - K_0)^T G + Q(K_0, K_1, H^\dagger) + \dots \quad (5)$$

where: Q is the quadratic term in the artificial Hessian H^\dagger
 K is the vector of gains that are being optimized
 G is the gradient (in this case a vector)

From (5) the step direction is given by $-[H^\dagger]^{-1}G$. Thus the third part of the algorithm is the determination of this step from the approximate Hessian. The fourth step before the process is repeated again is the determination of the step magnitude. This is accomplished using a one dimensional optimization so that $K_1 = K_0 + (a)s_0$, where s_0 is the step direction determined above and "a" is the parameter that is to be determined by the one dimensional search so that J is minimized. Many different heuristic algorithms have been used to determine "a". One of the important aspects of the algorithm is that its value is never permitted to cause the gains to result in an unstable solution. This is done by altering the one dimensional search if the step size is too big. Stability is tested as a by product of the gradient and Hessian calculations.

The most interesting aspect of the optimization algorithm is the fact that the gradient and Hessian are developed from the same equations. These are Lyapunov type equations and are therefore solved using the same algorithm. The gradient and Hessian matrices satisfy equations given in Refs. 10 and 11.

The overall algorithm flow is shown in Fig. 5. In practice we find that the solutions obtained from the reduced state feedback control designs are within one or two percent of the full state designs with orders of magnitude fewer gains. The important features of this design approach is that it allows one to incorporate the actuator dynamics and the sensor dynamics, the noises on both the sensor and the disturbances exciting the structure (even if they are correlated) and the specifications in terms of a pre-specified model. If the latter is used, the model states are included in the dynamic description of the system (in the A matrix, the B matrix and the measurement matrix) and are used to define the errors that are optimized in the performance index, but the feedback gains from the model states are not used. This becomes an implicit model following approach. The last feature that is important is the explicit incorporation of the compensator dynamics. Fig. 4 shows the way the compensator dynamics are included when it is desired to design a notch filter for removing the influence of an unstably interacting mode.

EXAMPLE

The spacecraft design shown in Fig. 6 is an example of a communication satellite with a large solar array, an antenna that deploys, and a requirement

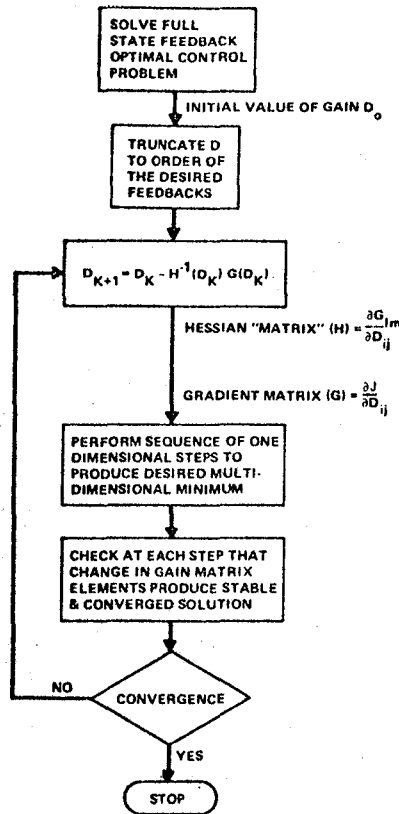


Figure 5
Constrained Optimal Control Algorithm Flow Chart

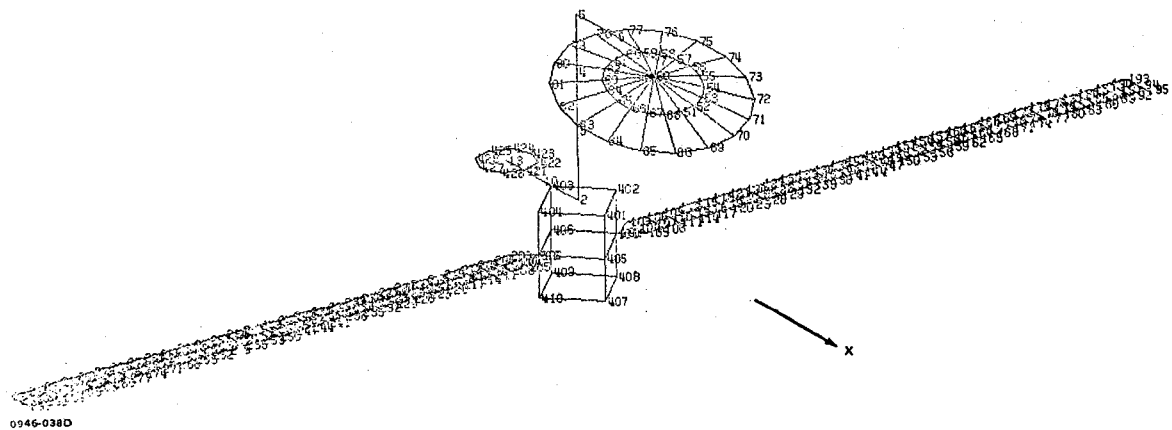
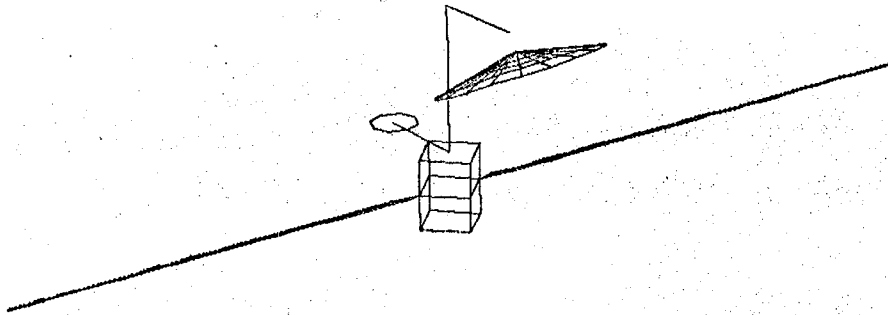


Figure 6
Illustrative Example: Communication Satellite Finite Element Model

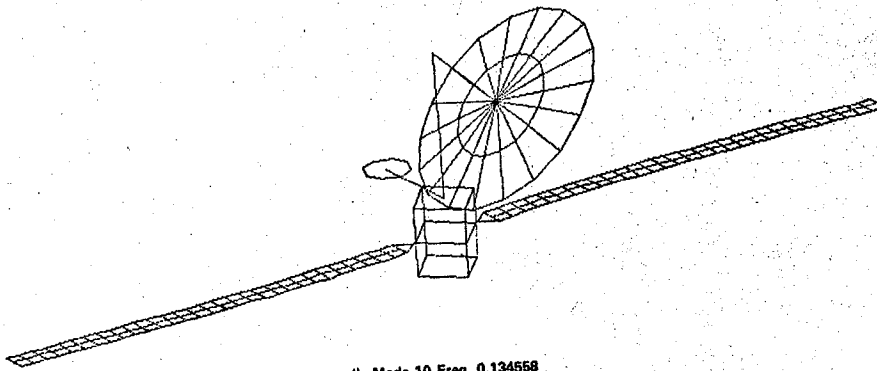
on the pointing of the antenna and the relative location of the antenna with respect to its feed. The finite element model shown has enough detail to allow the modes up to 3 Hz. to be accurately determined. Three Hertz is 20 times the highest frequency contained in the disturbances, which for the damping assumed in this model is sufficient to guarantee that the higher modes are unimportant. This model is the starting point for the design. The mode shapes are shown in Fig. 7, and of those the unstably interacting modes are indicated with an asterisk. These unstable interactions come about because there are two sets of three actuator - the first at the central or core mast which contains the "rigid body" actuators which are reaction wheels for the three axes of rotation. The second set of actuators are at the antenna mast attachment point. There is a two degree of freedom gimbal joint and a worm screw device to deflect the boom that carries the antenna relative to the mast. This last control provides control of the feed horn to antenna displacement. The sensors are three position and rate sensors at the central core plus three position and rate sensors at the antenna joint, and a displacement and rate sensor that gives the antenna position relative to the feed. Thus there are 14 measurements, and 6 actuators. After eliminating the modes with low mode costs that are stably interacting, the number that must be retained in any design including the rigid body modes is 13. The disturbance due to the solar array motion is modeled as a lightly damped second order system excited by white noise and each actuator and sensor is modeled as a first order system with an associated white noise disturbance (either a measurement or an excitation). The combined state dimension, with all of these dynamics, becomes 42. The control gains were selected to provide the smallest number of gains possible. Thus the individual actuators were given inputs from only those sensors that measure the variables in the same degree of freedom (i.e. the pitch reaction wheel used gains only on the pitch attitude and rate, etc.). The resulting gains are shown in Table I. The Table also shows the full state control cost, which was line of sight motion of the antenna, compared with the same cost from the reduced control design. As can be seen, the costs are within a few percent of each other, even though there are only 12 gains in the reduced state design compared with 598 in the full state design. Not only that, but the reduced state design has essentially the same response to the disturbances, the same closed loop bandwidth, and the same robustness as the original full state design.

Table I
Gains for the reduced state design

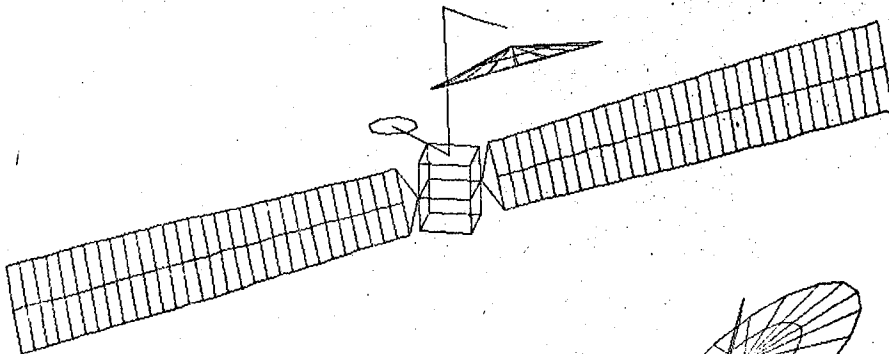
		Sensors (Pos. then Rate)					
		Rigid Body Sensors			Antenna		
		x	y	z	feed		
Rigid Body	x	-3E6	-2E7				
Rotation	y		6E6	-2E7			
Actuators	z	not used		-1E5	-2E5		
Antenna	x	3E4	5E4				
Actuators	y		7E5	4E6			
	z					6E2	4E6
Full state LOS error		6x10 ⁻³ rad.		Reduced state LOS error		35x10 ⁻³ rad.	



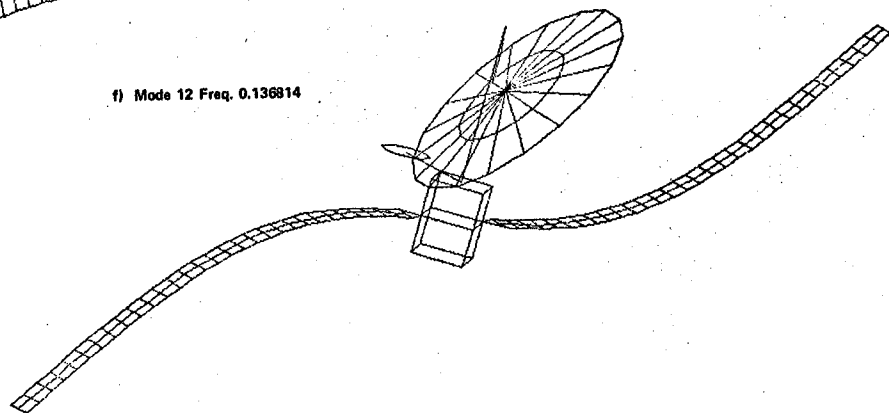
e) Mode 9 Freq. 0.132858



d) Mode 10 Freq. 0.134558



f) Mode 12 Freq. 0.136814



g) Mode 13 Freq. 0.179146

Figure 7
Mode Shapes for the Communication Satellite of Fig. 6 Showing Some
Modes That Have Unstable Interactions

CONCLUSIONS

The main point of this paper is that there exists a way of designing a control system using a finite model that accounts for the distributed nature of the control problem in a systematic way. This is accomplished by using a mode description of the system and from that description determining the number of modes that must be retained based on the performance and the disturbance descriptions. The design then uses a full order model that includes all of the dynamics: sensor, actuator, disturbance and flexible motion. The designs that result are simple, robust, perform well and have the added distinction of being easy to implement.

REFERENCES

1. Gibson, J.S., "The Riccati Integral Equations for Optimal Control Problems on Hilbert Spaces,"SIAM J. Contr. Opt., Vol 17 (4),July, 1979
2. Gran, R., "Finite-Dimensional Controllers for Hyperbolic Systems",Proc. of Third VPI&SU/AIAA Symposium on Dynamics and Control of Large Flexible Spacecraft, June, 1981.
3. Gran, R., "Qualitative Stability of Large Space Structures with Non-Colocated Actuators and Sensors",Proc. of 20th IEEE Conf. on Decision and Control, San Diego, CA, Dec. 1981.
4. Gran, R. and Proise, M., Final Report for INTELSAT Contract INTEL-064, in preparation.
5. Balas, M.J., "Trends in Large Space Structure Control Theory : Fondest Hopes Wildest Dreams," IEEE Trans. on A. C., Vol. AC-27 No. 3, June 1982.
6. Balas, M.J., and Meisner, T.L., "Spillover and Model Error Bounding Techniques for Large Scale Systems", Proc. Third VPI&SU/AIAA Symposium, *ibid*.
7. Kosut, R., "Stability and Robustness of Control Systems for Large Space Structures," Proc. Third VPI&SU/AIAA Symposium, *ibid*.
8. Wie, B., and Bryson, A., "Modeling and Control of Flexible Space Structures," Proc. Third VPI&SU/AIAA Symposium, *ibid*.
9. Gran, R. and Proise, M., "Flexible Spacecraft Attitude Control-Phase 2 Final Report for INTELSAT Contract INTEL-064," Research and Development Center Report RE-632, August, 1981.
10. Jameson, A., "Optimization of Linear Systems of Constrained Configuration," Int .J. of Cont., Vol. 11, No. 3, 1970.
11. Rossi, M., "Optimal Design of an Automatic Control System for Submerged Hydrofoil Boats," IEEE Conf on Eng. in Ocean Envs., Sept,1972.

This Page Intentionally Left Blank

INTRODUCTION AND SURVEY ON CONTINUUM MODELS FOR REPETITIVE LATTICE STRUCTURES

Larry S. Weisstein
Lockheed Missiles and Space Company
Sunnyvale, CA 94086

ABSTRACT

This paper is a brief introduction and modest survey to aid and familiarize researchers interested in the use of continuum modeling procedures applied towards large space structure technology. The use of such structural models for the distributed control of large flexible lattice structures offers a significant advantage over a numerical approach. Any references not identified in the bibliography can probably be obtained in individual articles. This survey was completed in the month of December 1981.

INTRODUCTION

A high degree of repetition enables a recurring bay or module to fully identify a structural system. If the module is composed of a moderate number of structural elements, an analytical description of the deformation response rather than a numerical one may be obtained. For example, domes, barrel vaults, and booms are typical repetitive lattices. They exhibit high stiffness, light weight, and allow for architectural freedom in providing large span areas with no intermediate supports.

A historical development of structural lattices is given in reference [1]. Domes are given as an example. In particular, it is shown that gradual changes in material strength and weight of lattice domes were paralleled by an increase in span areas and a decrease in rise to span ratios. The inevitable collapses which followed forced engineers to consider more scientific and systematic methods of analysis and design. As the number of joints and members continued to grow, a full exact analysis became impractical and simplifying assumptions were made. For instance, determinate truss systems with pin joints were easier to analyze than more efficient, indeterminate lattices composed of flexural members joined by rigid welds. Other designs may have ignored that the collapse load of a full structure due to buckling can be less than the load corresponding to the maximum stress of an individual member in the structure. Also, recursive procedures (known as relaxation techniques) introduced in the mid thirties could be carried out for only a few cycles by hand because of time and effort involved for many iterations required by an exact solution. It is the advent of the computer and computer methods of structural analysis that surmounted many of these early problems.

Currently, repetitive lattices are drawing attention for application in space. References [2,3] describe projects such as large antennae and space platforms for communication, satellite sensory recognition, solar collectors, and future manned space operation centers. These structures must be simple, light, portable, and of a highly regular design to facilitate automated production and assembly. The large sizes which are anticipated will also make space lattices very flexible. It is the flexing motion that will affect a satellite's orientation and performance; therefore, it is important to identify the static and dynamic behavior of space lattices for a variety of loading conditions. The large size of the problem can make full "direct" solutions more expensive than an approximate analytical approach which exploits the repetitive nature of the lattice. Analytical approaches are therefore very appealing.

REVIEW OF CURRENT METHODS OF ANALYSIS

Present techniques used to study space lattices fall into three categories [4,5]. These are 1) matrix methods, 2) discrete field techniques, and 3) continuum modeling. The first consists of numerically solving a set of algebraic equations in a direct manner. The other two, discrete field techniques and continuum modeling, are analytical approaches. Each have attractive features; however, recent studies indicate that the continuum modeling approach shows great promise.

Direct methods of structural analysis use matrix methods based on discrete-element idealization. Numerical methods such as the finite element technique or finite difference method belong to this category. In addition, matrix methods may be classified into displacement (stiffness) methods, force (or flexibility) methods, or a mixture of the two. An example of displacement and force methods is given in reference [6], mixed methods are treated in reference [7]. What all these methods have in common is the numerical solution of a set of simultaneous algebraic equations. Today, computer programs can quickly assemble and solve a system of linear equations as well as efficiently manage data within a limited core space. However, the preoccupation with handling data can be a major expense when the system of equations is too large to be stored in central core. Obviously, solving an analytical system described by a few equations is more preferable to solving a large system of equations numerically, especially if it has to be done more than once.

Discrete field techniques belong to one class of methods used to describe lattice structures or a pattern of elements analytically. The popularity for this approach is due to the fact that the discrete nature of the lattice is preserved in the governing equilibrium equations. Furthermore, exact closed form solutions may be obtained for simple configurations that include continuous-discrete systems of mixed dimensionality. In comparison with direct numerical methods, a discrete field analysis does not increase in problem size as the number of basic modules in the lattice is increased. There are two approaches to modeling a repetitive lattice by discrete field methods. One method models the structural system as a whole whereas the other describes the lattice by a typical component. These procedures are referred to as macro and micro methods respectively.

Macro methods are particularly well suited for problems where continuous structural systems interact with discrete elements such as ribbed plates. The model is in the form of summation equations for discrete systems or summation-integral equations for mixed discrete-continuous systems. The limitation is finding suitable kernel functions that satisfy the system boundary conditions. In references [8-10], the method is applied to the static and stability analysis of ribbed plates and discrete-core sandwich plates. In reference [11], studies are made of a ribbed hyperbolic cooling tower. By modeling the tower as a surface of revolution, a two dimensional axisymmetric problem is reduced to a one dimensional beamlike problem.

Micro methods apply primarily to lattice systems whose components are regularly arranged. The system model consists of difference equations which represent a recurrence relation (expressed in terms of difference operators) for a typical joint. The effectiveness of this method is demonstrated in references [12-16] for application in determining displacements and critical loads of one dimensional planar trusses. It is interesting to note that the author in ref. [13] found it easier to solve the analogous equivalent beam problem by converting finite difference equations into differential equations via truncated Taylor series rather than seek exact closed form solutions for the difference equations directly.

There are a number of publications that deal with the analysis of rotationally symmetric shell-type lattices. In ref. [8] simple truss members are used for a static analysis and static-stability studies by Gutkowski broaden the problem by inclusion of flexural-torsional members [17-19]. Early ad hoc attempts by Gutkowski to achieve a pure discrete field displacement method evolve into a clear and systematic variational formulation that uses a discrete-element idealization procedure in ref. [20]. By taking advantage of the rotational symmetry, an exact one dimensional beamlike description is obtained. The procedure also includes a dynamic analysis. A similar vibration study is made in ref. [21] in which ring elements are used for bracing. Investigation of the stability of a cylindrical lattice shell under axial compression is made in ref. [22]. The intent of the study was to validate the range of equivalent continuous shell models. A noteworthy point in the study includes the use of joints with varying rigidity which are modeled as rotational springs. Buckling studies which include member imperfections are made for shell and beamlike structures with periodic cross sections in ref. [23]. A dynamic stability problem for the same lattices is addressed in ref. [24]. With the exception of ref. [20], these works are confined to simply supported edge constraints.

The last group of methods consist of approximating a repetitive lattice by an equivalent continuum. The equivalence is designed so that the continuous model exhibits identical or similar response as the actual discrete lattice for equivalent applied loads or energies. The approximation assumes that distances between nodes are small compared to the structure's overall dimensions and therefore may be treated by differential operators. There are a number of reasons for using such an approach. One is the familiarity with differential operators and various class of methods for solving differential equations. Secondly, continuum theories of elasticity allow a rational equivalence based on qualitative decisions that reduce the dimensionality of the mathematical model and physically identify the nature of deformation (e.g. warping, bending, shear).

Another consideration are works by Dzieniszewski [25,26] who shows that optimization of lattices based on a continuous model allows a straightforward comparison of stiffnesses with lattices of different configurations.

Two things are noteworthy of a continuum model as the number of repeating modules are increased: one is that the accuracy of the response improves; and secondly, continuum models (like discrete field techniques) do not increase in problem size as the number of repeating modules are increased. However, the cost of approximating finite distances by infinitesimal ones isn't free, therefore the range of application for the continuum model must be well defined. Early continuum models were unreliable because there was no way of rationally assessing the approximation introduced. Basically, the methods range from intuitive approaches to more recent ones having a rational basis.

Intuitive methods postulate the result before the analysis is undertaken. By assuming the response of the lattice is approximated by that of classical plate or shell model a priori, existing differential equations and constitutive relations can be used for the study. The approach may be extended so that the analogous gridwork contributes to the continuum by averaging or uniformly distributing over some area the stiffness properties belonging to the families of parallel members or individual members within a repeating module. The stiffnesses for the overall effective continuum, determined by orthogonal transformation of each parallel set or individual members within a repeating module, are then equated with those of the existing plate or shell. A number of works apply this technique to bending and membrane problems of grid and shell-type lattices [22,27-31]. It should be noted that as the structure increased in complexity, intuitive methods can be misleading and highly impractical. (See for example ref. [32]).

A rational approach does exist. The method basically replaces discrete field variables with truncated Taylor series; furthermore, the local error introduced by truncation can be accounted for mathematically. (See for example refs. [34,35]). There are two approaches: one method converts governing difference equations into differential equations; the second replaces strain and kinetic energies based on discrete parameters with continuous field variables and their derivatives obtained from the Taylor series.

Converting finite difference equations into differential equations is studied in refs. [33-37] for single and double layered grids. In addition, one work by Bazant and Christiansen show by direct analogy that a lattice with rigid joints exhibits couple stresses and antisymmetric shear strains which is not characteristic of classical elasticity. This micropolar continuum theory presented by Eringen [44] is a generalization of elasticity theory for which classical methods of elasticity are a subset. Converting difference equations into differential equations works well for simple problems, however it is difficult to apply to more complicated configurations due to the complex nature of the resulting differential equations.

The energy equivalence method is a rational approach that transforms energies of a discrete lattice into a continuum representation. This method is practical and simple because variational formulations allow the differential equations, boundary conditions, and constitutive relations to be determined for complicated spatial configurations. The effectiveness of this method is

demonstrated in a variety of works. References [38,39] apply this to beam and platelike truss lattices for static, vibration and thermal analyses. References [36,40-42] consider beam and platelike lattices with rigid joints where a micropolar continuum is useful. Lastly, ref. [43] expands the range of application of continuum modeling to include buckling as well as vibration wavelengths of deformation on the order of the size of the repeating module as well as large (global) wavelengths of deformation. Analysis of a repetitive beamlike lattice which consists of thin-wall beam members with open cross sections for space application is also explored.

REFERENCES

1. Z.S. Makowski, "Space Structures: A Short Review of Their Development", Space Structures, R.M. Davies editor, Blackwell Scientific Publications Oxford and Edinburgh, 1966, chapter 1.
2. M.C. Card and W.J. Boyer, "Large Space Structures - Fantasies and Facts", AIAA Paper No. 80-0674-CP, presented at the AIAA/ASME/ASCE/AHS 21st Structures Structural Dynamics and Materials Conference, Seattle, Wash., May 12-14, 1980.
3. NASA Conference Publication 2168, Large Space Systems Technology - 1980, Vol. I - Systems Technology, Vol. II - Base Technology.
4. Lattice Structures: State-of-the-Art Report, J. Struct. Div. ASCE, Vol. 102, No. St11, Nov., 1976.
5. Bibliography on Lattice Structures, J. Struct. Div. ASCE, Vol. 98, No. St7, July, 1972.
6. J.S. Prezemieniecki, Theory of Matrix Structural Analysis, McGraw-Hill Book Company, 1968.
7. A.K. Noor, "Mixed Methods of Analysis", Structural Mechanics Software Series, The University of Virginia Press, Vol. 3, 1980, pp. 263-305.
8. D.L. Dean, Discrete Field Analysis of Structural Systems, Springer-Verlag, 1976.
9. D.L. Dean, Hota, V.S. Ganarao, "Macro Approach to Discrete Field Analysis", J. Engrg. Mech. Div. ASCE, Vol. 96, No. EM4, Aug. 1970.
10. R. Avent, "Micro and Macro Stability Analysis of Lattice Structures", anonymous
11. D.K. Roy, J.L. Hulsey, and P. Zia, "Analysis of Ribbed Hyperbolic Cooling Tower", Paper Presented at Canadian Society of Civil Engineers Annual Conference in Winnipeg, Canada, 1980.
12. C. Omid'varan, "Discrete Analysis of Latticed Columns", J. of Str. Div. ASCE, Vol. 94, No. St1, Jan. 1968.
13. J.D. Renton, "Behavior of Howe, Pratt, and Warren Trusses", J. Str. Div. ASCE, Vol. 95, No. St2, Feb. 1969.
14. D.L. Dean, "Behavior of Howe, Pratt, and Warren Trusses", J. Str. Div. ASCE, No. St9, Sep. 1969.
15. D.L. Dean and S. Tauber, "Solutions for One-Dimensional Structural Lattices", J. Engrg. Mech. Div. ASCE, Vol. 85, No. Em4, Oct. 1959.

16. D.L. Dean and F.R. Jetter, "Analysis for Truss Buckling", J. Str. Div. ASCE, Vol. 98, No. St8, Aug. 1972.
17. W. Gutkowski, "Statics and Stability of Prismatic Fram-Lattice Shells", Bullentin de L'Academie Polonaise des Sciences, Serie des Sciences Techniques, Vol. IX, No. 5, 1961.
18. Gutkowski, "The Stability of Lattice Struts", Zeit fur Ang. Math. Mech. 43, 6 (1963).
19. W. Gutkowski, "Cylindrical Grid Shells", Bullentin de L'Academie Polonaise des Sciences, Serie des Sciences Technique, Vol. XIII, No. 3, 1965.
20. W. Gutkowski, "Mechanical Problems of Elastic Lattice Structures", Progress in Aerospace Sciences, Vol. 15, Pergamon Press, 1974.
21. T. Wah, "vibration of Cylindrical Gridwork Shells", AIAA Journal, Vol. 3, No. 8, Aug. 1965.
22. S.E. Forman, "Buckling of Reticulated Shell Structures", Ph.D. Thesis, Havard University, Cambridge, Mass., June 1969.
23. M.S. Anderson, "Buckling of Periodic Lattice Structures", AIAA Paper No. 80-068], presented at the AIAA/ASME 21st Structures, Structural Dynamics and Materials Conference in Seattle, Wash., May 12-14, 1980.
24. M.S. Anderson, "vibration of Prestressed Periodic Lattice Structures", AIAA Paper No. 81-0620, presented at the AIAA Dynamics Specialists Conference in Atlanta, Georgia, April 9-10, 1981.
25. W. Dzieniszewski, "Optimization of Lattice Rod Structures", Archives of Mechanics, Vol. 23, issue 2, pp. 223-248, 1971.
26. W. Dzieniszewski, "Optimization of Elastic Lattice Structures Designs on a Prescribed Surface", Vol. 23, issue 5, pp. 663-680.
27. S. Timoshenko, Theory of Plates and Shells, p. 190, McGraw-Hill, New York, 1940.
28. D.T. Wright, "Membrane Forces and Buckling in Reticulated Shells", J. Struct. Div. ASCE, Vol. 91, No. St1, Feb. 1965.
29. E.F. Bernard, "A Study of the Relationship Between Lattice and Continuous Structures", Ph.D. Thesis, University of Illinois, Sept. 1965.
30. W.C. Schnobrich and B. Mohraz, "Analysis of Latticed Structures as Equivalent Continuum", anonymous.
31. A.H. Nayfeh and M.S. Hefzy, "Continuum Modeling of the Mechanical and Thermal Behavior of Discrete Large Structures", AIAA, 1980. (80-0679).

32. J.D. Renton, "On the Gridwork Analogy for Plates", J. Mech. Phys. Solids, 1965, Vol. 13, pp. 413-420, Pergamon Press Ltd.
33. E. Lightfoot, "A Grid Framework Analogy for Laterally Loaded Plates", Int. J. Mech. Sci., Pergamon Press Ltd., 1964, Vol. 6, pp. 201-208.
34. J.D. Renton, "The Related Behaviour of Plane Grids, Space Grids and Plates", Space Structures, R.M. Davies editor, Blackwell Scientific Publications, 1967, Chapter 3, pp. 19-32.
35. K. Heki and Y. Fujitani, "The Stress Analysis of Grids Under the Action of Bending and Shear", Space Structures, R.M. Davies editor, Blackwell Scientific Publications, 1967, Chapter 4, pp. 33-43.
36. Z.P. Bazant and M. Christensen, "Analogy Between Micropolar Continuum and Grid Frameworks Under Initial Stress", Int. J. Solids Structures, 1972, Vol. 8, pp. 327-346.
37. Z.P. Bazant and M. Christensen, "Continuous Approximation of Large Regular Frameworks and The Problem of a Substitute Frame", Amer. Concrete Inst., Special Publication No. SP-36, Detroit, 1973, Paper SP36-13.
38. A.K. Noor, M.S. Anderson, and W.H. Greene, "Continuum Models for Beam-and-Platelike Lattice Structures", AIAA Journal, Vol. 16, No. 12, Dec. 1978, pp. 1219-1228.
39. A.K. Noor and C.M. Anderson, "Analysis of Beam-Like Lattice Trusses", Computer Methods in Applied Mech. and Engrg., 1979, Vol. 20, pp. 53-70, North-Holland Publishing Company.
40. A.K. Noor and M.P. Nemeth, "Micropolar Beam Models for Lattice Grids with Rigid Joints", Computer Methods in Applied Mech. and Engrg., 1980, Vol. 21, pp. 249-263, North-Holland Publishing Company.
41. A.K. Noor and M.P. Nemeth, "Analysis of Spatial Beamlike Lattices with Rigid Joints", Computer Methods in Applied Mech. and Engrg., 1980, Vol. 24, pp. 35-59, North-Holland Publishing Company.
42. M.P. Nemeth, "Continuum Models for Repetitive Lattice Structures with Rigid Joints", M.S. Thesis, George Washington University Center at NASA Langley Research Center, 1979.
43. L.S. Weisstein, "Continuum Models for Repetitive Beamlike Lattice Structures", M.S. Thesis, George Washington University Center at NASA Langley Research Center, 1982.

MINIMUM INFORMATION MODELLING OF STRUCTURAL SYSTEMS WITH UNCERTAIN PARAMETERS*

David C. Hyland, Massachusetts Institute of Technology Lincoln Laboratory
Lexington, MA 02173

ABSTRACT

This paper reviews recent work wherein the design of active structural control is formulated as the mean-square optimal control of a linear mechanical system with stochastic parameters. In practice, a complete probabilistic description of model parameters can never be provided by empirical determinations, and a suitable design approach must accept very limited *a priori* data on parameter statistics. In consequence, we formulate the mean-square optimization problem using a complete probability assignment which is made to be consistent with available data but maximally unconstrained otherwise through use of a maximum entropy principle. The ramifications of this approach for both robustness and large dimensionality are illustrated by consideration of the full-state feedback regulation problem.

1. INTRODUCTION

Most techniques so far proposed for the design of active structural control - even those which purport to treat the problem of modelling error (see, for example, Refs. [1-3]) implicitly assume, at some stage, that all the maps of the linear system model are precisely known. A nominal or base-line design (often quadratically optimal) is then predicated upon this deterministic model. Unfortunately, such a design pertains to but a single point in a suitably defined system-parameter space, while, due to numerous sources of modelling error (especially in constructing large order structural models), the actual system is almost surely to be found at some other point in parameter space. This fact vitiates any claim to optimality for numerous current design approaches and necessitates much ad-hoc "hedging" about the nominal design in order to recover basic system properties that are lost in consequence of parameter uncertainties. This paper reviews a recently developed approach (that of minimum data/maximum entropy modelling) which directly incorporates the impact of modelling uncertainty in the design process by use of a stochastic model and seeks to achieve desirable system properties while accepting parameter uncertainties at their *a priori* levels.

To circumvent the deficiencies of current design schemes, it is first necessary to recognize that any model (even a large-order "verification" model) never encompasses the truth but, at best, is a mathematical statement of what and how much is known. Considered as such, a design model must not only specify nominal or expected values of the system parameters but must also contain an admission of prior ignorance regarding deviations from nominal values. This provides motivation for the quantification of prior ignorance by the representation of the structure as a linear system with random multiplicative parameters.

* This work is sponsored by the Department of the Air Force. The U.S. Government assumes no responsibility for the information presented.

At this point, it is tempting to adopt a minimum expected cost approach -i.e. assume the random parameters to be subject to some given probability law and then design a controller which is optimal on the average. Because of its simplicity and relative familiarity, we confine attention here to mean-square optimality, choosing the average of a quadratic functional over the parameter ensemble as the performance measure.

However, the problem is more subtle than is suggested by the minimum expected cost approach. In practice, one is never provided with a complete probability assignment based upon empirical determinations but must rely upon a highly limited set of available statistical data. Avoidance of ad hoc assumptions (and the invention of data which does not exist) requires that one induce a complete probability model for the parameters which is consistent with the data on hand but admits the greatest possible prior ignorance with regard to all other data. The prescription for doing this is quite straightforward: first define a measure of prior ignorance, the entropy, and then determine the probability assignment which maximizes entropy subject to the constraints imposed by available data.

Now this idea of a maximally unpresumptive stochastic design model may be carried still further, for we may discern a minimum set of a priori statistical data which is just sufficient to induce a well defined probability model. The maximum entropy approach to modelling and controller design consists in (1) acknowledging only the minimum data set as available (2) construction of the maximum entropy model induced by this data and (3) control design through quadratic optimization under the maximum entropy statistics. Note that this approach acknowledges only the minimum data on parameter statistics because this leads to a particularly tractable design model and entails the greatest design conservatism in that the model is maximally chaotic.

The minimum data/maximum entropy model accounts directly for a priori uncertainties without resort to ad hoc measures and provides a mechanism whereby the least possible prior information may be incorporated within the control design. As suggested by the specific results reviewed in the following sections, this approach can provide robustness levels comparable with modelled levels of uncertainty and, most importantly, its use has profound ramifications for the problem of large dimensionality in connection with the burden of design computations.

2. Stochastic Modelling and Mean-Square Optimization: General Features

In this and the following sections, the steps, outlined above, for construction of a maximally unpresumptive stochastic model are described more specifically. Actually, the following considerations constitute extension, originally given in Ref. [4], of various initial results, Refs., [5,6], pertaining to a very restricted class of parameter uncertainties. Although future developments for the treatment of general forms of uncertainty may be anticipated, we shall confine attention here to the results of Ref. [4], wherein parameter deviations of a skew-hermitian form were treated. Accordingly, consider the linear system:

$$\dot{x} = (\bar{A} + ia(t) - F)x + w, \quad x \in \mathcal{C}^n, t \in [t_0, t_1] \quad (1)$$

where x comprises the state of the plant together with that of any linear dynamic compensation that might be employed. \bar{A} denotes the nominal or expected value of the plant dynamics map, where

$$\bar{A} + \bar{A}^H < 0 \quad (2)$$

is assumed. $a(t)$ represents that portion of the system dynamics which is subject to modelling error and a priori uncertainty, where

$$a(t) = a^T(t) \in R^{n \times n} \quad (3)$$

To admit a sufficiently broad functional class for $a(t)$ (as it is represented in the design model) we additionally assume that $a(t)$ is a zero-mean stationary, random process which is separable, of bounded total power and is such that the integral increments:

$$a(t_1, t_2) \triangleq \int_{t_1}^{t_2} da(\tau) \quad (4)$$

possess moments of all orders for all finite $t_2 - t_1$.

The above assumptions regarding \bar{A} and $a(t)$ permit a reasonably tractable point of departure and, moreover render (1) applicable to structural systems conjoined with a variety of controller forms.

Further, $w(t)$ in (1) denotes white disturbance and/or observation noise of intensity V while F represents the effect of control action and is, in some degree, subject to design choice. With these provisions, we should like to incorporate parameter uncertainties (as embodied in $a(t)$) in the design formulation by use of an explicitly statistical model combined with a measure of performance defined on the parameter ensemble. As noted in section 1, we adopt, as the performance measure, the average of a quadratic functional

$$\bar{J} = \lim_{|t_1 - t_0| \rightarrow \infty} \frac{1}{|t_1 - t_0|} E \left[\int_{t_0}^{t_1} dt \ x^H R x \right] \quad R = R^H \geq 0 \quad (5)$$

where $E[.]$ denotes an average over both disturbance and parameter ensembles, the time invariant matrix R encompasses the desired penalty on the state and control inputs, and consideration is limited to the steady-state case wherein F is time invariant.

Here we note that the class of time invariant F which renders (5) finite and (1) second-mean stable is nonempty.

Under the above assumptions, it is desired to determine the unconstrained parameters of F so as to minimize \bar{J} . This problem may be simplified somewhat by a restatement in terms of the co-state matrix. Straightforward manipulations give:

$$\left. \begin{aligned}
\min_F \quad \bar{J} &= \text{tr} [\bar{P}V] \\
\bar{P} &= \bar{P}^H \underline{\Delta} E [P] \in \mathbb{C}^{n \times n} \\
0 &= (\bar{A} + \dot{a}(t) - F)^H P + P (\bar{A} + \dot{a}(t) - F) + R
\end{aligned} \right\} (6)$$

However, largely by virtue of the linearity of system (1), it can be shown that:

$$E[(\dot{a}(t))^H P + P \dot{a}(t)] = H[\bar{P}] \quad (7)$$

where $H[\cdot]$ is a linear mapping of the class of hermitian matrices onto itself. Thus, (6) may be recast in the form:

$$\begin{aligned}
\min_F \quad \bar{J} &= \text{tr}[\bar{P}V] \\
0 &= (\bar{A} - F)^H \bar{P} + \bar{P} (\bar{A} - F) + H[\bar{P}] + R
\end{aligned} \quad (8)$$

where, at least in principle, all requisite ensemble averages have been carried out and the problem is posed solely in terms of the expected cost matrix, \bar{P} . However, (see the explicit expressions (26) and (27) of Ref. [5]), the evaluation of $H[\cdot]$ demands a complete statistical model of $a(t_1, t_2)$, i.e., knowledge of the joint probability distributions of all orders of all countable sets of increments of the form (4). But, such a complete probability assignment is never actually available from empirical determinations. In practice, one is provided (or strives to obtain) a very limited and incomplete set of statistical data on the uncertain parameters. Typically, this available data may comprise estimates of the nominal or mean values of system parameters together with various simple measures of statistical deviation from the nominal values. In connection with available data, it is well to set forth certain ground rules at this point by recognizing that however little is known regarding uncertainties in system dynamics some pattern in a priori knowledge is almost always induced by the procedures used in the construction of the system model. In devising a particular model as the embodiment of physical law, the modelling analyst must not only estimate the nominal or expected values of system characteristics but must also identify those physical mechanisms with respect to which his analysis is prone to significant error. This last step is clearly necessary since, ultimately, the validity of the model must be checked over the possible range of variation of the uncertain effects. Within the context of linear systems, the poorly modelled effects may often be represented by uncertainties in parameters which enter linearly into the system dynamics. In other words, variations in the dynamics map from its nominal value due to errors in the modelling of a particular physical effect assume the form aB , where $B \in \mathbb{C}^{2n \times 2n}$ is a known matrix and a is an uncertain scalar. In total, uncertainty in the dynamics may be represented by:

$$a = \sum_{k,j} a_{kj} B_{kj} \quad (9)$$

where the a_{kj} are uncertain scalars.

In addition to identifying the "weak spots" in his system description, the modelling analyst must ultimately estimate bounds or statistical measures of the magnitudes of the a_{kj} . Such estimates are usually performed with reference to each a_{kj} separately, i.e., in a statistical context, the a priori data (which the analyst either presumes on the basis of modelling judgement or strives to determine empirically) comprises assigned numerical values of linear functionals of $p [a_{kj}]$ where $p [a_{kj}]$ denotes the probability density of a_{kj} . For very large order systems this is perhaps the only practicable approach, since the large number of uncertain parameters precludes any empirical determination of the joint statistics of several of the parameters, simultaneously.

Thus, we argue that in the process of constructing a model and assessing its accuracy, the analyst necessarily induces a set of "directions" (that is, the set of the deterministic matrices, B_{kj} , in (9)) which describes the geometric articulation of modelling uncertainties and a priori data. Under the stipulation that only marginal statistics of the a_{kj} separately are available, the B_{kj} may be said to specify the "a priori information pattern" arising from the model and constitute an essential element of available knowledge. Note that we retain for the $a_{kj}(t)$ all the assumptions mentioned above for $a(t)$.

Having discerned the a priori pattern of available information, one might ask if it is possible to avoid ad hoc assumptions regarding unavailable parameter statistical data by constructing a full probability model which is consistent with the data at hand but which presumes as little as possible with regard to unavailable data. Proceeding further: "Is there a set of statistical data which is just sufficient to induce any well-defined maximally unpresumptive stochastic model?" These are the basic modelling questions relating to the optimization problem (8), that we address.

3. The Minimum Data/Maximum Entropy Model

Now consider the problem of constructing a stochastic model of system (1) which replicates available data while admitting the maximum degree of prior ignorance regarding all other data. The successful principle enunciated by Jaynes [7,8] has immediate application here: the desired probability assignment is the one which, under the constraints imposed by available data, can be realized in the maximum number of ways or, equivalently, maximizes an appropriate measure of prior ignorance (the entropy).

We may introduce measures of information reposed in the statistics of parameter deviations in the following way. First, note that under the a priori pattern of (9), only increments of the form:

$$a_{kj} (t_1, t_2) \stackrel{\Delta}{=} \int_{t_1}^{t_2} da_{kj} (t)$$

enter the evaluation of $H[\cdot]$ and thus have a bearing upon the optimization problem. Next, define a division

$$\left[\left\{ t_0^{(kj)}, t_1^{(kj)}, \dots, t_{N_{kj}}^{(kj)} \right\}; (k,j) \in \eta \right] \triangleq J[\eta] \quad (10)$$

of the real line, where η is a set of ordered pairs $\{(k,j); k \leq j \leq n\}$ and denote the set of increments (over right semi-closed intervals):

$$a_{kj}(t_0^{(k,j)}, t_1^{(k,j)}), a_{kj}(t_1^{(k,j)}, t_2^{(k,j)}), \dots, a_{kj}(t_{N_{kj}-1}^{(k,j)}, t_{N_{kj}}^{(k,j)}) \quad (11)$$

by $\{a; J[\eta]\}$. Finally, let $P(\{a; J[\eta]\})$ denote the joint probability density of the increments (11). Then, a measure of statistical uncertainty associated with the increments (11) is given by the relative entropy of these increments:

$$H[P(\{a; J[\eta]\})] \triangleq -\int d\sigma P(\{a; J[\eta]\}) \ln P(\{a; J[\eta]\}) \quad (12)$$

where $d\sigma$ is the volume element in the sample space of (11). Although it is possible to define a measure of entropy for the stochastic system as a whole, the measures (12) defined directly on the $a_{kj}(t_1, t_2)$ will suffice for present purposes.

Of course we wish to work with distributions constrained by statistical data. Let \mathcal{D} denote the set of available data each element of which consists of the assignment of a numerical value to a particular linear functional of $P(\{a; J[\eta]\})$ in a manner consistent with the a priori pattern. Let $P(\{a; J[\eta]\}|\mathcal{D})$ denote the conditional density given the data set \mathcal{D} . Then the entropy of $\{a; J[\eta]\}$ in the presence of this data is simply $H[P(\{a; J[\eta]\}|\mathcal{D})]$ in accordance with definition (12).

With these notations we can state that the maximally unprejudiced probability assignment, $P_{\mathcal{D}}^*(\{a; J[\eta]\})$, under the constraints imposed by data \mathcal{D} is defined by:

$$H[P_{\mathcal{D}}^*(\{a; J[\eta]\})] = \sup_P H[P(\{a; J[\eta]\}|\mathcal{D})]; \quad \forall J[\eta] \quad (13)$$

and it is this probability assignment which avoids ad hoc restrictions on the available data.

But further, we note the functional dependence of $H[P^*(a; J[\eta])]$ upon \mathcal{D} . Clearly, distinct data sets generally induce distinct values of maximum entropy and this implies an ordering of prior data sets. Thus, it is natural to enquire whether or not there exists a "minimum data set", $\mathcal{D}^* \subset \mathcal{D}$, for which:

$$H[P_{\mathcal{D}^*}^*(\{a:J[\eta]\})] = \sup_{\mathcal{D}} [\sup_P H[P(\{a:J[\eta]\}) | \mathcal{D}]] \quad (14)$$

for all $J[\eta]$ and for all \mathcal{D} such that $H[P(\{a:J[\eta]\}) | \mathcal{D}]$ is bounded. If such a \mathcal{D}^* consistent with the a priori information can be found, then acknowledgement of only \mathcal{D}^* as available data leads to a probability assignment which is maximum entropy over all admissible selections of available data. The corresponding stochastic system model thus incorporates the minimum prior information.

Details concerning the resolution of the above questions are to be found in Ref. [4]. Here we merely state the results. For the system considered, the minimum data set, \mathcal{D}^* , may be said to comprise the nominal system maps, the matrices B_{kj} defining the prior information pattern and the so-called "uncertainty relaxation times", T_{kj} :

$$T_{kj} = \frac{1}{2} \int_0^{\infty} d\tau E[\cos a_{kj}(0, \tau)] \quad (15)$$

These time scales correspond to essential information on the scales of parameter deviations from nominal values. From the assumed properties of the $a_{kj}(t_1, t_2)$, it can be seen that the T_{kj} are real, non-negative and increase without bound as the limit of the deterministic dynamics map is approached. Thus we may say that the reciprocal relaxation times, $1/T_{kj}$ ($k, j = 1, \dots, n$), constitute fundamental, albeit unconventional, measures of parameter uncertainty consistent with the a priori information pattern.

The above data set is minimum in the following sense. If available data lacks any element of this set, there exists no maximum entropy probability assignment under which all the $a_{kj}(t_1, t_2)$ possess finite even-order moments for finite $|t_2 - t_1|$. Indeed in this circumstance, the entropy maximum problem is ill-posed in that available data imposes no bound upon $H[P_{\mathcal{D}}^*(\{a:J[\eta]\})]$. Thus, the B_{kj} and T_{kj} must be made available in order to construct a full probability model in a rational manner. On the other hand, for any $\mathcal{D} \supset \mathcal{D}^*$ and for all $J[\eta]$:

$$\sup_P H[P(\{a:J[\eta]\}) | \mathcal{D}] \leq \sup_P H[P(\{a:J[\eta]\}) | \mathcal{D}^*] \quad (16)$$

Thus, a truly "minimum information" model is obtained by acknowledging only the minimum data set, \mathcal{D}^* , as available. Taking this step also results in a design model which is eminently tractable in optimization computations. In fact, the assignment, $P_{\mathcal{D}^*}^*$, induced by \mathcal{D}^* yields a form of Stratonovich state dependent noise [9] for which system (1) has the Ito differential:

$$\left. \begin{aligned} dx(t) &= (\bar{A}_m - F) x(t)dt + \sum_{k,j} da_{kj}^*(0, t) B_{kj} x(t) + dW(t) \\ \bar{A}_m &\triangleq \bar{A} - \frac{1}{2} \sum_{k,j} \frac{1}{T_{kj}} B_{kj}^2 \end{aligned} \right\} \quad (17)$$

where the a_{kj}^* (0,t) are mutually independent Wiener processes with intensities, $1/T_{kj}$. Furthermore, under this minimum data/maximum entropy model, the operator $H_{kj}[\cdot]$ appearing in the optimization problem, (8), assumes the form:

$$\left. \begin{aligned} H[\bar{P}] &= \sum_{k,j} H_{kj}[\bar{P}] & \text{a.} \\ H_{kj}[\bar{P}] &= \frac{1}{2T_{kj}} [B_{kj}, [\bar{P}, B_{kj}]] & \text{b.} \end{aligned} \right\} (18)$$

where $[A,B]$ denotes the commutator:

$$[A,B] \triangleq AB - BA \quad (19)$$

As noted in Ref. [4], when the scale of a_{kj}^* (0,t) is taken to be large $H_{kj}[\bar{P}]$ represents the leading term in the asymptotic expansion of $H[\bar{P}]$ under the actual parameter statistics (as distinguished from the maximum entropy statistics). In other words, the minimum data/maximum entropy model manages to preserve various asymptotic properties of the expected cost, \bar{P} , for large levels of parameter uncertainty. Thus, the design consequences of very great uncertainties may be readily investigated.

Combining the above results, the mean-square optimization problem, (8), under the probability model (17) assumes the form:

$$\left. \begin{aligned} \min_{\bar{F}} : \bar{J} &= \bar{u}[\bar{P}\bar{V}] \\ 0 &= (\bar{A} - \bar{F})\bar{H}\bar{P} + \bar{P}(\bar{A} - \bar{F}) + \sum_{k,j} \frac{1}{2T_{kj}} [B_{kj}, [\bar{P}, B_{kj}]] + R \end{aligned} \right\} (20)$$

With this result, the minimum data, maximum entropy stochastic model, (17), may be directly applied to the mean-square optimal design of a variety of controller types (e.g., full state feedback regulation, dynamic compensation with output feedback, etc.). One such development for structural systems is described in the following sections.

4. Application to Structural Systems - The Mean-Square Optimal Full-State Feedback Regulation Problem

Now we illustrate the application of the above results to structural control. For simplicity, consideration is limited to flexible mechanical systems undergoing deformations in the linear range with no rigid body degrees of freedom and negligible gyroscopic effects. Generalizations to include rigid body and gyroscopic effects are straightforward and will not be addressed here.

To further fix ideas, we consider the case in which the mass distribution, internal damping and the sensor/actuator dynamics, locations and alignments are precisely known. While only the elastic operator of the structure is to be considered subject to a priori uncertainty, this uncertainty reflects some of the most important sources of structural modelling errors. The elastic operator em-

bodies detailed information on such properties as material characteristics, geometry, construction and structural joint conditions which, in absence of extensive testing, are difficult to ascertain with precision.

It is further supposed that the original distributed parameter equations for the structure are resolved in the basis of N (N finite but large) modal coordinates associated with a set of mode shapes for the nominal system (the structure with its nominal values of parameters). In this fixed modal basis (independent of parameter uncertainties), we may write the state-space equation in the eigen-basis of the nominal, open-loop plant as : (see Ref. [11] for a detailed derivation):

$$\dot{x} = \mu x + \beta u + w; \quad x \in \mathbb{C}^{2N} \quad (21)$$

where β is the control input map and w is a white disturbance of intensity $\psi \geq 0$. μ has the form:

$$\mu = \begin{bmatrix} i\Omega - \eta \bar{\Omega} & 0 \\ 0 & -i\Omega - \eta \bar{\Omega} \end{bmatrix} \quad (22)$$

where η and $\bar{\Omega}$ are diagonal matrices comprising, respectively, the modal damping ratios, $\eta_K; K=1, \dots, N$, and the nominal or expected values, $\bar{\omega}_K; K=1, \dots, N$, of the modal frequencies. Owing to uncertainty in the structural stiffness, Ω is symmetric and positive definite but not diagonal. However, the expected value of Ω is $\bar{\Omega}$ so that the off-diagonal elements of $\Omega - \bar{\Omega}$ are zero-mean random perturbations.

With regard to the control optimization formulation, we explicitly consider here only the very simplest controller form - i.e. full state feedback regulation:

$$u = -Kx \quad (23)$$

with the time-invariant gain, K , chosen to minimize:

$$J = E[x^H \sigma_1 x + u^T R_2 u] \quad \sigma_1 \geq 0, \quad R_2 > 0 \quad (24)$$

subject to (21). This restriction is made purely for illustrative purposes - a companion paper, [12], describes application of the maximum entropy approach to far less idealized controller forms.

Now, note that because an ensemble-independent functional basis is employed, β is deterministic and only Ω is subject to statistical variation. Moreover, from the above definitions, it is seen that $\mu - \bar{\mu}$, where:

$$\bar{\mu} = E[\mu] = \text{diag} \left[i\bar{\omega}_1 - \eta_1 \bar{\omega}_1, \dots, i\bar{\omega}_N - \eta_N \bar{\omega}_N, \right. \\ \left. -i\bar{\omega}_1 - \eta_1 \bar{\omega}_1, \dots, -i\bar{\omega}_N - \eta_N \bar{\omega}_N \right] \quad (25)$$

is a zero-mean skew-hermitian variation of the form appearing in (1). Thus, the maximum entropy modelling approach described in the preceding section can be

immediately applied here.

To illustrate most simply the qualitative ramifications of the maximum entropy stochastic modelling approach, we suppose here that in the vector basis of (21), all the elements of $\mu - \bar{\mu}$ are a priori subject to significant uncertainty. Thus, in conformity with the notation of (9) we write:

$$B_{kj} \triangleq \begin{cases} (e^{kj} + e^{jk}) (1 - \frac{1}{2} \delta_{kj}) \\ 0 : k > N, j < N \text{ or } k < N, j > N \end{cases} \quad (26)$$

where $e^{kj} \in \mathbb{R}^{2N \times 2N}$ is the matrix whose elements are zero except for the $(k, j)^{th}$ which is unity.

With this pattern of a priori information, non-trivial relaxation times may be given as:

$$T_{kj} = T_{jk} = \frac{1}{2} \int_0^{\infty} d\tau E[\cos[(\Omega_{kj} - \bar{\Omega}_{kj}) \tau]] \quad (27)$$

Acknowledging only $\bar{\mu}$, β , v , the B_{kj} and the T_{kj} as available data, there immediately results a maximum entropy model of the form (17). Of more immediate interest, however, is the counterpart of (20) in the present context. Defining:

$$\bar{\mu}_m \triangleq \bar{\mu} - \frac{1}{2} I$$

$$I = \begin{bmatrix} J & 0 \\ 0 & J \end{bmatrix}, \quad J \triangleq \text{diag} \left[\sum_{j=1}^N \frac{1}{T_{kj}} \right] \quad (28)$$

and denoting the expected cost matrix by $\bar{\rho}$, the optimization problem embodied in (21) - (24) under the minimum data/maximum entropy model of (21) (consistent with the prior pattern (26)) can be shown to assume the form:

$$\min_{\kappa} : J = \text{tr}[\bar{\rho} v] \quad (29)$$

with $\bar{\rho} \geq 0$ satisfying:

$$0 = (\bar{\mu}_m + \beta \kappa)^H \bar{\rho} + \bar{\rho} (\bar{\mu}_m - \beta \kappa) + D[\bar{\rho}] + \sigma_1 + \kappa^H R_2 \kappa \quad (30)$$

where

$$D[\bar{\rho}] \triangleq \sum_{j, k} \frac{1}{T_{kj}} [B_{kj} \bar{\rho} B_{kj} + B_{k+N, j+N} \bar{\rho} B_{k+N, j+N}] \geq 0$$

with B_{kj} as defined in (26).

We pause to note that when all the T_{kj}^{-1} approach zero (the limit of a deterministic plant) (30) reduces to the familiar Lyapunov equation.

Equations (29) - (31) now represent a rather tractable variational problem and we devote the remainder of this paper to a review of its properties.

Denoting $\beta R_2^{-1} \beta^H \geq 0$ by σ_2 , the main results on optimality and stability may be summarized as follows:

Theorem 1 Consider (29) - (31) with $\bar{\mu}, \bar{\mu}_m, \beta, \sigma_1, R_2$ and σ_2 as defined above. If $(\sigma_1^{-1/2}, \bar{\mu})$ is reconstructible, then

$$K = R_2^{-1} \beta^H \bar{\rho} \quad (32)$$

minimizes the performance index (29), where ρ is the unique positive definite solution of

$$0 = \bar{\mu}_m^H \bar{\rho} + \bar{\rho} \bar{\mu}_m + D[\bar{\rho}] + \sigma_1 - \bar{\rho} \sigma_2 \bar{\rho} \quad (33)$$

Moreover, with (32), the closed-loop system under the minimum data/maximum entropy statistics is second moment and almost surely exponentially stable for all $T_{k_j}^{-1} \geq 0$. (For a discussion of this and other stochastic concepts of stability see Ref. [13]).

Proof: See Theorems 1 and 2 of [11].

Thus, under reasonably mild restrictions, the stochastic design approach yields a well posed optimization problem and affords considerable assurance of closed-loop stochastic stability.

Equation (33), termed the "stochastic Riccati equation", is seen to be the central design equation for mean-square optimal regulation under the minimum data/maximum entropy model. Note that the familiar L Q gain relation, (32), is preserved and, in the deterministic limit ($T_{k_j}^{-1} \rightarrow 0, \forall k, j$), (33) reduces to the standard Riccati equation. Additional qualitative properties are noted in [5] and [14], moreover, Refs. [5] and [15] describe several numerical procedures for solution of (33), most of them displaying guaranteed linear or quadratic convergence. Ref. [15] gives illustrative numerical results which reveal dramatic qualitative differences between (33) and the standard Riccati equation - particularly at modest to high levels of parameter uncertainty. Such properties are the subject of the next section.

5. The Stochastic Riccati Equation - Asymptotic Properties for Large Uncertainties

Having determined that under the conditions of Theorem 1, a unique positive definite solution of (33) exists for all positive $T_{k_j}^{-1} : k, j = 1, \dots, N$, it is natural to inquire what behavior $\bar{\rho}$ attains for large uncertainties, i.e., for very small relaxation times.

Defining:

$$\{M\} \triangleq \text{diag } [M_{kk}] \quad (34)$$

for any square matrix, M, we first consider the case wherein there is very great uncertainty with regard to the open loop frequencies of (21) (T_{kk}^{-1} very large).

Theorem 2 Assume the conditions of Theorem 1 and introduce the positive scaling factor, σ , into T_{kk} :

$$T_{kk} = \sigma \tilde{T}_{kk} ; \forall k \quad (35)$$

Then, with $\bar{\rho}$ the positive definite solution of (33):

$$A. \quad \lim_{\sigma \downarrow 0} \bar{\rho} = \{\bar{\rho}^*\} = \begin{bmatrix} \{\hat{\rho}\} & 0 \\ 0 & \{\hat{\rho}\} \end{bmatrix} ; \{\hat{\rho}\} \in \mathcal{R}^{N \times N} \quad (36)$$

where $\{\hat{\rho}\}$ is the positive definite solution to:

$$0 = -2 \eta_k \bar{\omega}_k \hat{\rho}_{kk} + \sum_{l \neq k} \frac{1}{T_{kl}} (\hat{\rho}_{ll} - \hat{\rho}_{kk}) + \hat{\sigma}_{1kk} - \hat{\sigma}_{2kk} \hat{\rho}_{kk}^2 \quad (37)$$

; $k = 1, \dots, N$

and where

$$\{\hat{\sigma}_1\} \triangleq \{\sigma_1\} \quad \{\hat{\sigma}_2\} = \{\sigma_2\} \quad (38)$$

B. With $\bar{\rho} = \{\bar{\rho}^*\}$, u given by (32) is a rate feedback law under which system (21) is stable for all stable μ of the form (22) such that $\mu - \bar{\mu}$ is diagonal.

Proof: Theorem 3 of [11]. See also Theorem 16 of [5].

Thus, under very large levels of uncertainties in the open-loop frequencies, the solution of the stochastic Riccati equation automatically reduces to a relatively simple asymptotic form in which the expected cost matrix, $\bar{\rho}$, is diagonal in the eigen-basis of the nominal system dynamics map. This asymptotic solution gives rise to a rate feedback control law which is stable regardless of the values of open-loop frequencies and structural damping ratios. Thus, inclusion of a class of parameter uncertainties within the stochastic design model results in a mean-square optimal design which is robust in the presence of the modelled uncertainties. The above theorem show that frequency uncertainties may always

be modelled with sufficient conservatism that the control approaches an inherently robust law arbitrarily closely.

The asymptotic properties of the state covariance are entirely analogous to those of $\bar{\rho}$, and we may say that the principal effect of open-loop frequency uncertainties is to suppress cross-correlation among distinct structural modes. Additional effects arise when we consider the random intermodal coupling introduced by uncertainty in the off-diagonal elements of Ω in (22). These new characteristics are illustrated by the case in which all the relaxation times approach zero:

Theorem 3 Let $\bar{\rho}$ be the positive definite solution of (33) under the conditions of Theorem 1 and introduce the positive scaling factor, σ into T_{kj} :

$$T_{kj} = \sigma \tilde{T}_{kj}, \quad \tilde{T}_{kj} \in (0, \infty), \quad \forall k, j \quad (39)$$

Then:

$$A. \quad \lim_{\sigma \downarrow 0} \bar{\rho} = \hat{\hat{\rho}} I_{2N} \quad (40)$$

$\hat{\hat{\rho}}$ is the positive scalar:

$$\hat{\hat{\rho}} = [-\bar{\Delta} + (\bar{\Delta}^2 + \bar{\sigma}_1 \bar{\sigma}_2)^{1/2}] / \bar{\sigma}_2 \quad (41)$$

where

$$\bar{\Delta} \triangleq \frac{1}{N} \sum_{k=1}^N \eta_k \bar{\omega}_k \quad \bar{\sigma}_1 \triangleq \frac{1}{N} \sum_{k=1}^N \hat{\sigma}_{1kk} \quad \bar{\sigma}_2 \triangleq \frac{1}{N} \sum_{k=1}^N \hat{\sigma}_{2kk} \quad (42)$$

and where $\{\hat{\sigma}_1\}$ and $\{\hat{\sigma}_2\}$ are as defined in (38).

B. With $K = R_2^{-1} \beta^H \hat{\hat{\rho}}$ in (23), the control is a rate feedback law which is stable for all $\Omega \in \Omega_T \geq 0$ in (22).

Proof: Theorem 4 of [11].

Thus, in addition to the diagonalization of $\bar{\rho}$, large uncertainties in all the elements of the structural stiffness tend to suppress differences among the diagonal elements of $\bar{\rho}$. As can be seen from (40) and (41), the asymptotic solution no longer distinguishes the separate roles of individual modes. Indeed, we obtain a solution corresponding to undifferentiated chaos in which the asymptotic mean-square optimal control seeks to minimize a performance index characterized by an averaged (i.e., averaged over the modes of the system) state weighing, $\bar{\sigma}_1$, and input weighing, $\bar{\sigma}_2$, for a system possessing an average damping, $\bar{\Delta}$.

Part B shows, once again, that we may always choose the relaxation times sufficiently small that the control approaches an inherently robust form as closely as desired. In contrast to Theorem 2.B, however, we now have the assurance of stability in the face of uncertainties in all elements of Ω . Moreover, the asymptotic form of the control can actually be implemented. If one has rate sensors co-located with actuators: then

$$y = \beta^H x \quad (43)$$

and the asymptotic control of Theorem 3 may be written:

$$u = - \hat{\rho} R_2^{-1} \beta^H x = - \hat{\rho} R_2^{-1} y \quad (44)$$

Since $\hat{\rho} R_2^{-1} > 0$ this is precisely the direct rate output feedback law discussed by Balas [16] and is known to be stable in the face of uncertainties in all modal parameters.

In summary, the above results provide a new theoretical justification for the use of rate feedback in structural control and illustrate the general principle: In the presence of very great parameter uncertainty, the mean square optimal control within a minimum data/maximum entropy stochastic model is a control which is inherently energy dissipative.

6. Incoherence and Isotropy: Treatment of High Order Systems.

The specific results of the last section are mainly concerned with the case in which the relaxation times are all uniformly small. It is more typically the case, however, that certain groups of modes are rather well known while the remaining modes are endowed with highly uncertain parameters. To fix ideas, suppose that the open loop modes of (21) are arranged in order of increasing nominal modal frequencies. Furthermore to reflect a progressive degradation in the modelling accuracy for higher order modes assume that the quantities:

$$\zeta_k \triangleq \sum_{j=1}^N \frac{1}{T_{kj}}; \quad \zeta_{k+1} \geq \zeta_k \quad (45)$$

increase monotonically with k . Under these circumstances, various qualitative features in line with Theorem 17 of Ref. [5] are to be expected and will be stated here without proof.

Considering a design model of finite but arbitrarily large dimension under the above conditions, we have that given $\epsilon > 0$ there exists an $N_c(\epsilon)$ sufficiently large that:

$$\|\bar{\rho} - \tilde{\rho}\| < \epsilon \|\bar{\rho}\| \quad (46)$$

where $\bar{\rho}$ is the solution to (33) and

$$\bar{\rho} \triangleq \begin{bmatrix} \bar{\rho}_{c11} & 0 & | & \bar{\rho}_{c12} & 0 \\ 0 & \{\hat{\rho}_I\} & | & 0 & 0 \\ \hline \bar{\rho}_{c12} & 0 & | & \bar{\rho}_{c22} & 0 \\ 0 & 0 & | & & \{\hat{\rho}_I\} \end{bmatrix} \quad (47)$$

with $\rho_{c11}, \rho_{c12}, \rho_{c22}, \epsilon \in C^{N_c \times N_c}$ determined according to a $N_c \times N_c$ stochastic Riccati equation of the form (33) pertaining to the first N_c modes and $\{\hat{\rho}_I\}$ is of the asymptotic form (36). In brief, if modeled uncertainty levels increase with increasing modal order in accordance with (45), the resulting mean-square optimal control for the high order, very uncertain modes approaches the asymptotic rate feedback form of Theorem 2. Furthermore, if the $T_{kj}; k = j$ are sufficiently small, we may again assert (46) - (47) but with:

$$\{\hat{\rho}_I\} = \begin{bmatrix} \{\rho'_I\} & 0 \\ 0 & \hat{\rho}_{II} \end{bmatrix} \quad (48)$$

In other words, the control for very high order modes may approach the asymptotic form of Theorem 3.

Under the conditions stipulated above, the state covariance matrix, Q will approximately attain the forms analogous to (47) and (48) for ϵ sufficiently small. Modes of order greater than $N_c(\epsilon)$ are said to constitute the incoherent range* and are approximately mutually uncorrelated. Lower order modes which retain significant cross-correlation are termed "coherent" modes. Of course, with T_{kj} sufficiently small, modes may be found such that a result for Q analogous to (40) holds, and these modes comprise the isotropic* subrange. As noted in Ref. [11], the values of the relaxation times not only delineate these important qualitative regimes but also determine the rapidity with which the system approaches, from an arbitrary initial state, the special statistical states associated with (47) and (48). From this point of view alone, the relaxation times may be considered essential parameter statistical information.

* This terminology, introduced in earlier work [4-6], arose from analogies with wave propagation in random media.

Obviously, the above properties for \bar{p} and Q have important implications for the treatment of high-order systems. Supposing that the parameters associated with only a relatively few modes may be considered well known, a priori norm bounds (see Ref. [5]) may be used to determine an $N_c \ll N$ sufficiently large that the magnitudes of all elements in the error, $R_2^{-1} \beta^H (\bar{p} - \tilde{p})$, incurred in the approximation:

$$\kappa \approx R_2^{-1} \beta^H \tilde{p} \quad (49)$$

are as small as desired. Thus, to within a given approximation, the solution of (33) for N large may be obtained by solution of a reduced order ($N_c \times N_c$) stochastic Riccati equation together with solution of $N - N_c$ equations of the form (37) or evaluation of closed-form expressions (41), corresponding to the incoherent and isotropic ranges, respectively.

Since the solution of (37) or (41) requires little or no computational effort, the main task is the solution of the reduced order version of (33) for the coherent modes. In practice, it is likely that N_c will be modest ($\sim 10 - 20$) and thus the computational burden will not be excessive even for very high order design models. For uncertainties of a more restricted class than considered here, this possibility has already been demonstrated by specific numerical results for a variety of design examples.

7. Concluding Remarks

This paper has reviewed the basic ideas of the minimum data/maximum entropy modelling approach and displayed its application to structural systems having significant a priori uncertainty in the stiffness operator. To illustrate the design consequences of the resulting stochastic model, the problem of mean-square optimal, full-state feedback regulation was considered. Treatment of the less idealized problem of fixed-order dynamic compensator design under the maximum entropy approach is reserved for a companion paper.

For the stochastic Riccati equation arising from the regulator problem, sufficient conditions were given for existence and uniqueness of solutions. From the results of Section 4 one has assurance of stochastic stability for the closed-loop system. Moreover, by virtue of the asymptotic properties given in Section 5, uncertainty levels may always be modelled with sufficient conservatism to secure stability over the actual (as distinct from the minimum information) parameter ensemble.

Finally, the special structure of the stochastic Riccati equation gives rise to a qualitative distinction among coherent, incoherent and isotropic modes and consequently permits the use of very high order models in regulator design computations. These features have significant consequences for the problem of large dimensionality. In control design for large-order linear systems, the "curse of dimensionality" is manifested in the great mass of processing of fundamental data (of system models presuming complete information) required for the formulation of an optimal control policy. The results described above intimate the possibility

that by consistent use of design models incorporating limited system information, we may so arrange matters that the processing required for control policy formulation may be similarly limited.

References

1. M. G. Safonov and M. Athans, "Gain and Phase Margins for Multi-Loop LQG Regulators", IEEE Trans. Aut. Contr., AC-22, 1977, p.173.
2. J. C. Doyle and G. Stein, "Robustness With Observers", IEEE Trans. Autom. Contr., AC-24, 1979, pp.607-611.
3. R. E. Skelton and R. Yedavalli, "Modal Cost Analysis of Flexible Space Structures with Uncertain Modal Data", IEEE Confer. on Decision and Control, Albuquerque, N.M., Dec. 1980.
4. D. C. Hyland, "Minimum Information Stochastic Modelling of Linear Systems with a Class of Parameter Uncertainties", No. 9474, American Control Conference, June 1982.
5. D. C. Hyland, "Optimal Regulation of Structural Systems with Uncertain Parameters", MIT Lincoln Laboratory, TR-551, 2 Feb. 1981, DDC AD-A099111/7.
6. D. C. Hyland, "Active Control of Large Flexible Spacecraft: A New Design Approach Based on Minimum Information Modelling of Parameter Uncertainties", VPI & SU/AIAA Symposium, June 1981.
7. E. J. Jaynes, "New Engineering Applications of Information Theory", Proc. of the First Symp. on Engineering Application of Random Function Theory and Probability, J. E. Bogdanoff and F. Kozin, Eds. (Wiley, New York, 1963).
8. E. J. Jaynes, "Prior Probabilities", IEEE Trans. Systems Science Cybern., SEC-4, 227 (1968)
9. R. L. Stratonovich, "A New Form of Representation of Stochastic Intergrals and Equations", SIAM J. Contr. 4, 362 (1966).
10. D. C. Hyland, "Robust Spacecraft Control Design in the Presence of Sensor/Actuator Placement Errors", No. 82-1405, AIAA Astro-dynamics Conf., August 1982.

11. D. C. Hyland, "Maximum Entropy Stochastic Approach to Control Design for Uncertain Structural Systems", No. 9475, American Control Conference, June 1982.
12. D. C. Hyland, "Fixed-Order Dynamic Compensation Through Optimal Projection", This conference.
13. F. Kozin, "A Survey of Stability of Stochastic Systems", Automatica 5, 95 (1969).
14. D. C. Hyland, "Optimal Regulator Design Using Minimum Information Modelling of Parameter Uncertainties: Ramifications of the New Design Approach", VPI & SU/AIAA Symposium, June 1981.
15. D. C. Hyland and A. N. Madiwale, "Minimum Information Approach to Regulator Design: Numerical Methods and Illustrative Results, VPI & SU/AIAA Symposium, June 1981.
16. M. J. Balas, "Direct Velocity Feedback Control of Large Space Platforms", J. Guid, and Contr., Vol. 2, No. 3, 252-53 (May - June 1979).

DISTRIBUTED SYSTEM MODELING OF A LARGE SPACE ANTENNA

M. Hamidi, G. Rodriguez, and D.B. Schaechter
Jet Propulsion Laboratory
California Institute of Technology
Pasadena, CA 91109

ABSTRACT

A general approach for distributed parameter modeling of complex dynamical systems is described. The method consists of dividing the system in parts which can be modeled by simple partial differential equations and coupling the equations thus obtained by applying Hamilton's variational formalism to the entire system. The modeling of a large, offset-fed, wrap-rib antenna is presented to illustrate the approach. Although such models are perhaps not as precise as finite-element models, they can be useful for initial physical insight and parametric design.

INTRODUCTION

Large space structures are traditionally modeled utilizing the finite element method. This procedure results in matrix representations of very high dimensions ranging from a few hundred to a few tens of thousands. When used for control design, the high dimensionality of the model creates a gamut of almost insurmountable computational problems such as: the length of computing times, the high volume of core memory required, the numerical truncation and round off errors, and so forth. Furthermore, onboard computers used in space flights are only capable of accommodating models with dimensions of the order of ten or less. To use the finite element model, one has therefore to resort to order reduction and face all the problems thus created.

Another undesirable aspect of finite element modeling is that the system representations consist of a series of numbers which provide no insight to the physical behavior of the system. Parametric study is thus made almost impossible since, for each new value of each parameter, a new model of the system has to be computed.

A distributed parameter modeling, if feasible, would alleviate many of these difficulties. Indeed, a partial differential equation representation has a concise mathematical formulation, requires no order reduction, provides physical understanding of the system, and is very suitable for parametric studies. Moreover, control techniques based on partial differential equations have been previously developed and successfully applied to simple systems.

In this paper, we present a general approach for distributed parameter modeling of complex dynamical systems. It consists of first partitioning the system into a number of elements which can each be modeled by simple partial differential equations. Hamilton's variational formalism is then applied to the entire system. This results in coupling the equations describing each part into a set of equations representing the whole system. The following

section of this paper details the procedures. The application of the method to the modeling of a 55-m, offset-fed, wrap-rib antenna is described in the last section to illustrate the approach.

CONCEPT

A large space structure can be conceptually partitioned into an assembly of rigid and flexible bodies, as schematized in Fig. 1. It is indispensable that the partitioning be conceived as to lead to flexible bodies of simple structure such as strings, beams, membranes, and so forth.

The dynamical model for the structure is derived using the variational approach, i.e., by writing that for any virtual displacement from the system's trajectory

$$\delta \int_{t_1}^{t_2} (T-V)dt + \delta \int_{t_1}^{t_2} F.rdt = 0 \quad \forall t_1, t_2$$

where T and V are the kinetic and potential energies respectively and F.r indicates the work of the applied forces during the displacement.

The modeling task is therefore reduced to the computation of the different terms T, V, F.r and their respective variations.

Kinetic Energy

The kinetic energy is given by the expression

$$T = \sum_i \left(\frac{1}{2} \int_{\Omega_i} \rho \dot{R} \cdot \dot{R} d\Omega \right)$$

where R is the vector from the origin of the inertial reference frame to an arbitrary point of the system (cf. Fig. 1) and ρ the mass density at this point. Ω_i indicates the volume of the i^{th} body, and $(\dot{})$ the differentiation with respect to time. The summation is performed over all rigid and flexible bodies.

Performing the indicated integrations, one obtains an expression of the form

$$T = \frac{1}{2} \dot{x}_1^T M_1 \dot{x}_1 + \sum_{FB_i} \left(\frac{1}{2} \int_{FB_i} \dot{x}_{2i}^T M_{2i} \dot{x}_{2i} d\Omega_i \right)$$

The first term in this expression represents the sum of the kinetic energies due to the movement of the rigid bodies and to the rigid body motion of the flexible bodies. The second term characterizes the kinetic energy produced by the deformations of the flexible bodies. x_1 is a vector of continuous time functions: $x_1 \in C(R^n)$. x_{2i} are vectors of continuous functions of time and space on the flexible body i (FB_i): $x_{2i} \in L^2(FB_i)$. M_1 and M_{2i} are self-adjoint positive semidefinite matrices. The physical properties of the structure impose a set of geometric boundary conditions involving x_1 and x_{2i} .

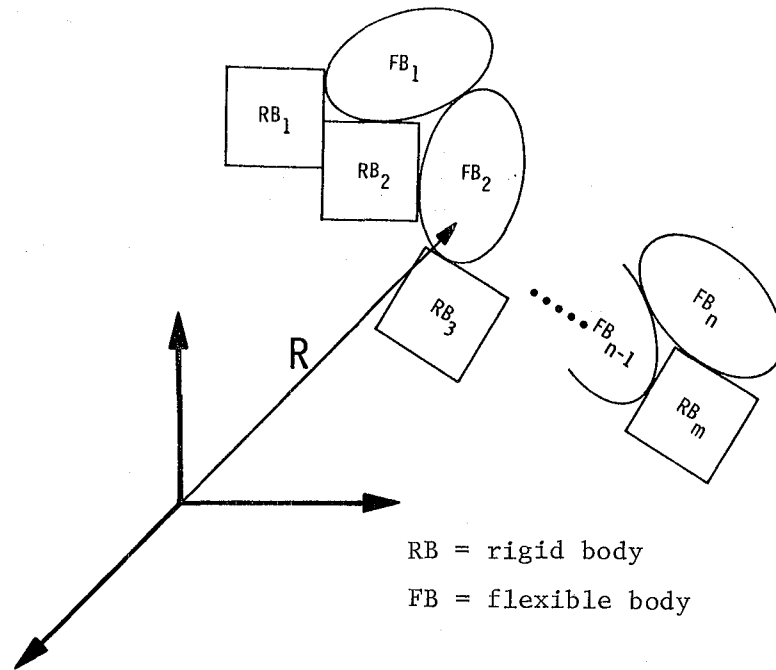


Figure 1. Conceptual Representation of a Large Space Structure

Defining the state space

$$s = C(\mathbb{R}^n) \times \prod_{i=1}^n L^2(\text{FB}_i)$$

and the proper scalar product \langle, \rangle on this space the kinetic energy can be written as

$$T = \frac{1}{2} \langle M\dot{x}, \dot{x} \rangle$$

where

$$x = (x_1^T \quad x_{21}^T \quad x_{22}^T \quad \dots \quad x_{2n}^T) \in s$$

and M is a self-adjoint, positive definite, linear mapping from s to s .

Potential Energy

The potential energy is stored in the distortions of the flexible bodies only. It is given by

$$V = \sum_{\text{FB}_i} \frac{1}{2} \int_{\text{FB}_i} K_i(x_{2i}, x_{2i}) d\Omega_i$$

where K_i are positive semidefinite quadratic forms. It is always possible (Riesz representation theorem) to reduce V to the form

$$V = \frac{1}{2} \langle Kx, x \rangle$$

where K is a self-adjoint positive semidefinite linear mapping from s to s .

Model

The kinetic and potential energies evaluated, the next step is to apply the variational principle. Let y be an arbitrary admissible state of the system such that $y(t_1) = y(t_2) = 0$, and let λy , $\lambda \in \mathbb{R}$, be a virtual displacement from the trajectory x . To the first approximation, for λ small, the variation of the time integral of the kinetic energy is given by

$$\delta \int_{t_1}^{t_2} T dt = \lambda \int_{t_1}^{t_2} \langle M\dot{x}, \dot{y} \rangle dt$$

or integrating by part

$$\delta \int_{t_1}^{t_2} T dt = - \lambda \int_{t_1}^{t_2} \langle M\ddot{x}, y \rangle dt$$

The kinetic energy leads to

$$\delta \int_{t_1}^{t_2} K dt = \lambda \int_{t_1}^{t_2} \langle Kx, y \rangle dt$$

and the virtual work to

$$\delta \int_{t_1}^{t_2} F \cdot r dt = \lambda \int_{t_1}^{t_2} \langle F, y \rangle dt$$

Thus, the equations of motion are given by

$$\int_{t_1}^{t_2} (\langle M\ddot{x}, y \rangle + \langle Kx, y \rangle - \langle F, y \rangle) dt = 0$$

or, since this equation must hold for all arbitrary times t_1 and t_2 and arbitrary vectors $y \in s$,

$$\langle M\ddot{x}, y \rangle + \langle Kx, y \rangle = \langle F, y \rangle$$

which can be written symbolically

$$M\ddot{x} + Kx = F$$

Note that M and K are matrices whose elements are scalars and functions of spatial variables, as well as operators with domain in FB_1s , the flexible bodies.

MODELING OF A 55-m WRAP-RIB ANTENNA

The modeling of a 55-m wrap-rib offset antenna will be presented in this section to illustrate the approach described in the previous section. The antenna, designed for the Land Mobile Satellite Service (LMSS) Project [Ref. 1] is schematized in Fig. 2. It consists of a massive spacecraft-feed

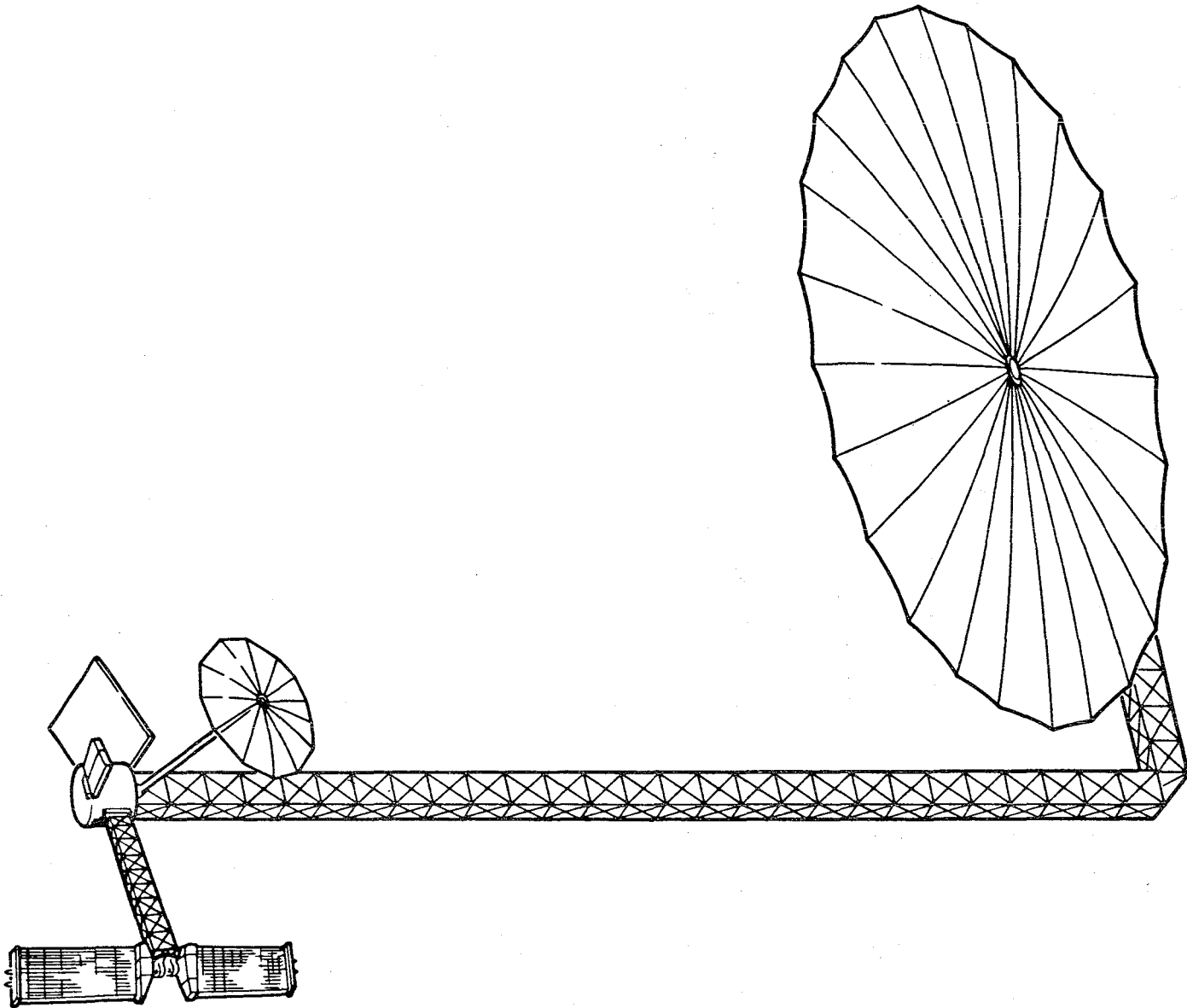


Figure 2. Schematic Diagram of the Antenna

assembly and a 55-m, deployable, wrap-rib, reflector dish connected by an L-shaped frame. The longer arm of the frame, which supports the spacecraft-feed assembly at its free end, has a length of 80 m and the shorter arm, which supports the dish, a length of 33.8 m. In the sequel, the short arm will be referred to as the upper boom and the long arm as the lower boom.

The following approximations and assumptions are made for the modeling:

- 1) The longitudinal distortions of the booms are neglected: only lateral flexures and torsion about the principal axis of the boom was considered.
- 2) The boom's masses are also neglected. Indeed, they constitute less than 3% of the total mass.
- 3) The dish is assumed planar and attached to the upper boom through a rigid and fixed hub.
- 4) The spacecraft-feed assembly is approximated by a rigid body whose center of gravity is placed at the extremity of the lower boom.

Kinetic Energy

Let m_0 and I_0 be the mass and inertia matrix of the spacecraft-feed assembly and m_1 the reflector-dish mass. It is easily established that, neglecting the booms' masses, the kinetic energy of the system is given by

$$T = \frac{1}{2} m \dot{R} \cdot \dot{R} + \frac{1}{2} \dot{\lambda}_0^T I_0 \dot{\lambda}_0 + \frac{1}{2} \int_{\Omega} \rho \dot{P} \cdot \dot{P} d\Omega$$

where

$$m = \frac{m_0 m_1}{m_0 + m_1} \text{ is the reduced mass of the system,}$$

R = the vector joining the spacecraft and dish mass centers (cf. Fig. 3),

λ_0 = the rotation vector of the spacecraft,

Ω = the domain of the dish,

ρ = the dish mass density, and

P = the vector from the dish mass center to an arbitrary element of the dish surface.

The value of the second term, in the expression for T , is directly given, but the other two terms have to be evaluated.

For the first term we need the vector R . Let us define two orthogonal coordinate systems as follows (cf. Fig. 3):

(g_1, g_2, g_3) with the origin at the elbow of the booms at rest; g_3 has the same direction and orientation as the vector r_0 joining the spacecraft's mass center to the elbow at rest, g_1 orthogonal to g_3 in the plane of the booms at rest and oriented such as to make the smallest angle with r_1 , vector coinciding with the upper boom at rest and

oriented towards the reflector's hub; g_2 is such as to form a direct system with g_1 and g_3 .

(g_4, g_5, g_6) with the origin at the reflector's center at rest; g_5 is the outward normal at the center of the dish, g_6 is along and in the same orientation as r_1 , and g_4 forms a direct system with g_5 and g_6 . Let u be the displacement of the lower boom's tip expressed in the (g_1, g_2, g_3) coordinate frame.

s is the displacement of the upper boom's tip expressed in the (g_4, g_5, g_6) coordinate frame.

h_0 is the vector from the dish point of attachment to the dish mass center in the undistorted configuration.

μ_0 is the translation of the mass center of the dish due to the dish distortion only.

Given these definitions and the assumption that the booms have no longitudinal distortion, the vector R is given by (cf. Fig. 3)

$$R = r_0 + r_1 + h_0 + \mu_0 + u_1 g_1 + u_2 g_2 + s_1 g_4 + s_2 g_5$$

A simple differentiation leads to

$$\begin{aligned} \dot{R} = & \dot{\lambda}_0 \times R + \dot{u}_1 g_1 + \dot{u}_2 g_2 + \dot{s}_1 g_4 + \dot{s}_2 g_5 + \dot{\mu}_0 + \dot{\gamma}_1 g_3 \times (h_0 + r_1) \\ & + \dot{\gamma}_2 g_6 \times h_0 \end{aligned}$$

where γ_1 is the rotation of the tip of the lower boom about g_3 and γ_2 the rotation of the tip of the upper boom about g_6 .

It remains to evaluate the last term, $\int_{\Omega} \rho \dot{P} \cdot \dot{P} d\Omega$. Let P_0 be the vector from the mass center of the dish to some arbitrary point in the undistorted configuration which corresponds to P after deformation, and let μ be the vector joining this point before deformation to its position after distortion (cf. Fig. 4). To the first approximation,

$$P - P_0 = \mu - \mu_0$$

which yields

$$\dot{P} = (\dot{\lambda}_0 + \dot{\gamma}_1 g_3 + \dot{\gamma}_2 g_6) \times P_0 + \dot{\mu} - \dot{\mu}_0$$

With these values of \dot{R} and \dot{P} , some simple but tedious algebraic manipulations lead to the following expression:

$$T = \frac{1}{2} \dot{x}^T M_1 \dot{x} + \frac{1}{2} \int_{\Omega} \rho \dot{\mu} \cdot \dot{\mu} d\Omega$$

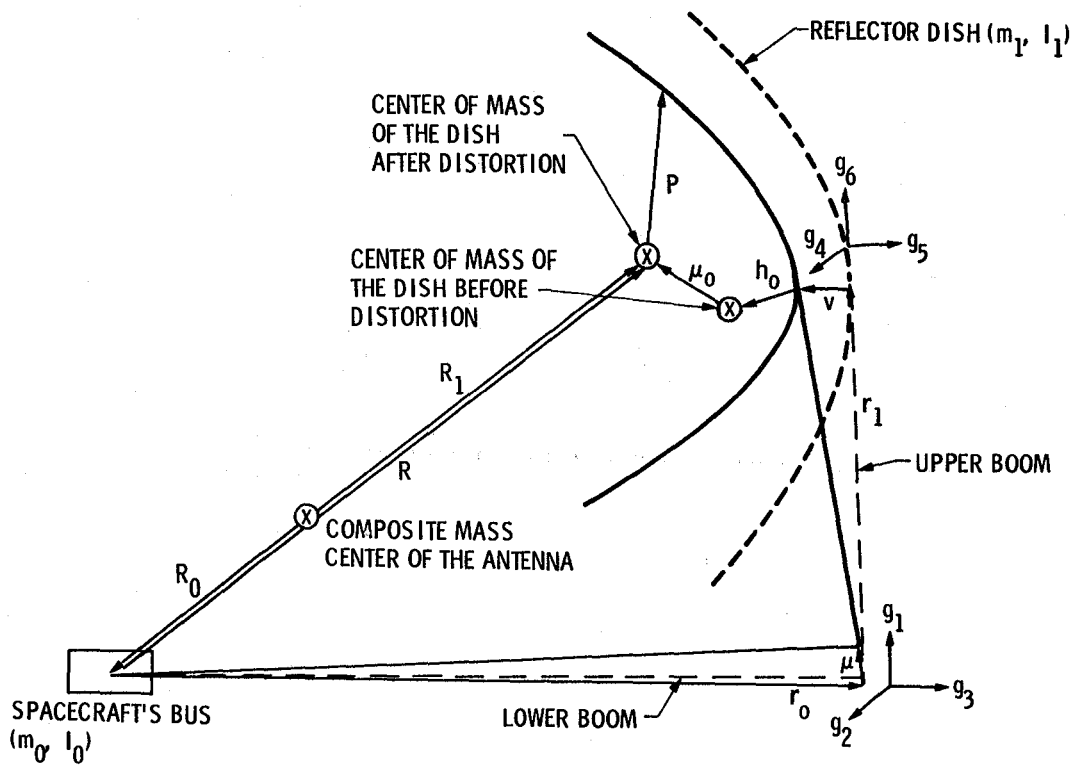


Figure 3. Diagram of Antenna after Deformation

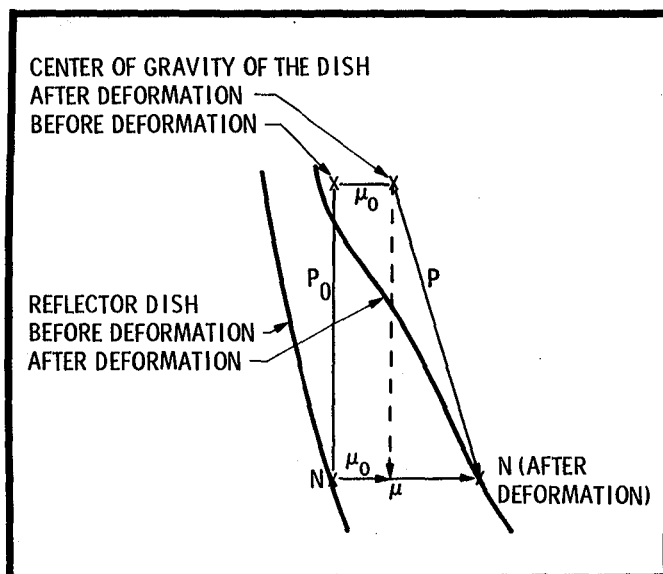


Figure 4. Schematic Representation of Dish Distortion

The state space vector x is given by

$$x = (\lambda_0^T \quad u_1 \quad u_2 \quad \gamma_1 \quad s_1 \quad s_2 \quad \gamma_2 \quad \mu_0^T \quad \psi_0^T)^T$$

With ψ_0 defined as

$$\psi_0 = I_1^{-1} \int_{\Omega} \rho P_0 x (\mu - \mu_0) d\Omega,$$

where

$$I_1 = \int_{\Omega} \rho [P_0^T P_0 E - P_0 P_0^T] d\Omega$$

is the inertia matrix of the dish in its undistorted state, and E the identity matrix.

The matrix M_1 is given by

$$M_1 = \begin{pmatrix} l_0 + l_1 + l_{00} & m \tilde{R} g_1 & m \tilde{R} g_2 & (l_1 + l_{10}) g_3 & m \tilde{R} g_4 & m \tilde{R} g_5 & (l_1 + l_{20}) g_6 & m \tilde{R} & l_1 \\ m g_1^T \tilde{R}^T & m & 0 & m g_1^T \tilde{r}_2^T g_3 & m g_1^T g_4 & m g_1^T g_5 & m g_1^T \tilde{h}_0^T g_6 & m g_1^T & 0 \\ m g_2^T \tilde{R}^T & 0 & m & m g_2^T \tilde{r}_2^T g_3 & m g_2^T g_4 & m g_2^T g_5 & m g_2^T \tilde{h}_0^T g_6 & m g_2^T & 0 \\ g_3^T (l_1 + l_{01}) & m g_3^T \tilde{r}_2^T g_1 & m g_3^T \tilde{r}_2^T g_2 & g_3^T (l_1 + l_{11}) g_3 & m g_3^T \tilde{r}_2^T g_4 & m g_3^T \tilde{r}_2^T g_5 & g_3^T (l_1 + l_{21}) g_6 & m g_3^T \tilde{r}_2 & g_3^T l_1 \\ m g_4^T \tilde{R}^T & m g_4^T g_1 & m g_4^T g_2 & m g_4^T \tilde{r}_2^T g_3 & m & 0 & m g_4^T \tilde{h}_0^T g_6 & m g_4^T & 0 \\ m g_5^T \tilde{R}^T & m g_5^T g_1 & m g_5^T g_2 & m g_5^T \tilde{r}_2^T g_3 & 0 & m & m g_5^T \tilde{h}_0^T g_6 & m g_5^T & 0 \\ g_6^T (l_1 + l_{02}) & m g_6^T \tilde{h}_0^T g_1 & m g_6^T \tilde{h}_0^T g_2 & g_6^T (l_1 + l_{12}) g_3 & m g_6^T \tilde{h}_0^T g_4 & m g_6^T \tilde{h}_0^T g_5 & g_6^T (l_1 + l_{22}) g_6 & m g_6^T \tilde{h}_0 & g_6^T l_1 \\ m \tilde{R}^T & m g_1 & m g_2 & m \tilde{r}_2^T g_3 & m g_4 & m g_5 & m \tilde{h}_0^T g_6 & (m - m_1) E & 0 \\ l_1 & 0 & 0 & l_1 g_3 & 0 & 0 & l_1 g_6 & 0 & 0 \end{pmatrix}$$

The dish is formed by N (forty-eight in our case) lenticular cross-sectional ribs attached to a central, circular, rigid, hub with equal angular spacing θ_0 (cf. Fig. 5). A pretensioned mass is stretched between the ribs. The dish can thus be divided in N identical sectors numbered from zero to $N-1$. Due to the nature of the material forming the mesh, the distortions of the dish surface are due mainly to the deformations of the ribs. The ribs are considered to be cantilevered at the hub. To compute the kinetic energy, the mass of the mesh is lumped on the ribs. For each sector, the kinetic energy is given by

$$T_n = \frac{1}{2} \left(\int_0^L \rho \dot{v}_n \cdot \dot{v}_n d\Omega + \int_0^L \rho \dot{w}_n \cdot \dot{w}_n d\Omega \right)$$

where v is the in-plane distortion, i.e., the projection of μ on the plane of the dish; w is the out-of-plane distortion, i.e., the projection of μ on the normal to the dish plane; and L is the length of the rib.

The kinetic energy can thus be expressed as

$$T = \frac{1}{2} \dot{x} M_1 \dot{x} + \frac{1}{2} \sum_{n=0}^{N-1} \int_{\Omega}^L \rho (\dot{v}_n \dot{v}_n + \dot{w}_n \dot{w}_n) d\Omega$$

Potential Energy

The potential energy of the system is the sum of the potential energies stored in the booms and in the dish.

If L_1 and L_2 are the lengths of the lower and upper boom respectively, and U_1 , U_2 , and Γ_1 are the bendings and the torsion along the lower boom, s_1 , s_2 are

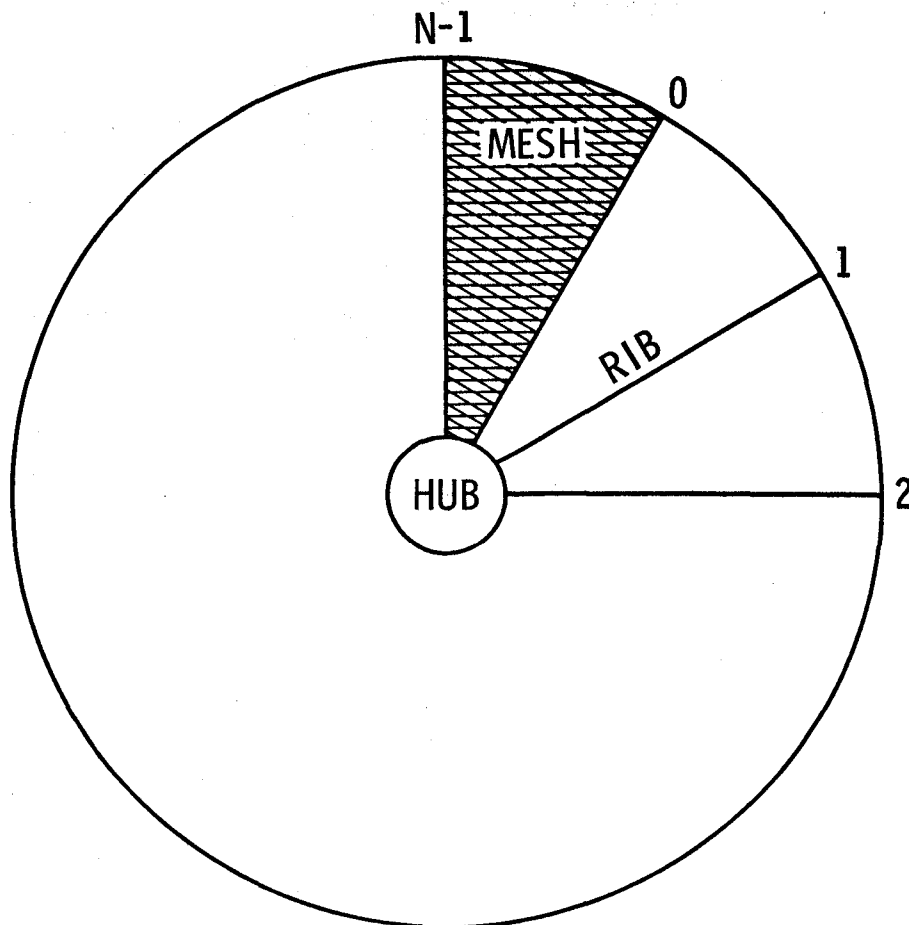


Figure 5. Schematic Diagram of the Reflector Dish

the bendings and the torsion along the upper boom, the potential energy stored in the booms is given by

$$\frac{1}{2} \int_0^L [E_1 I_1 \left(\frac{\partial^2 U_1(r,t)}{\partial r^2} + \frac{\partial^2 U_2(r,t)}{\partial r^2} \right) + G_1 J_1 \left(\frac{\partial \Gamma_1(r,t)}{\partial r} \right)^2] dr +$$

$$\frac{1}{2} \int_0^L [E_2 I_2 \left(\frac{\partial^2 S_1(r,t)}{\partial r^2} + \frac{\partial^2 S_2(r,t)}{\partial r^2} \right) + G_2 J_2 \left(\frac{\partial \Gamma_2(r,t)}{\partial r} \right)^2] dr$$

For each sector of the dish, neglecting the torsion of the ribs, the potential energy is the sum of the following components:

Bending energy of the rib:

In-Plane:

$$\frac{1}{2} \int_0^L EI_i \left(\frac{\partial^2 v_n(r,t)}{\partial r^2} \right)^2 dr$$

Out-of-Plane:

$$\frac{1}{2} \int_0^L EI_o \left(\frac{\partial^2 w_n(r,t)}{\partial r^2} \right)^2 dr$$

Mesh shear energy:

$$\frac{1}{2} \int_0^L \int_0^{\theta_o} E_{rc} \left(\frac{\partial v_n(r,t)}{\partial r} - \frac{v_n(r,t)}{r} \right)^2 r d\theta dr$$

Out-of-plane stiffness energy due to circumferential pretension:

$$\frac{1}{2} \int_0^L \frac{T_c}{r\theta_o} w_n^2(r,t) dr$$

In-plane stiffness energy due to mesh stretching:

$$\frac{1}{2} \int_0^L \frac{E_c}{r\theta_o} v_n^2(r,t) dr$$

Equations of Motion

The expressions obtained for the kinetic and potential energies lead to the following equations for the antenna:

$$M_{1x} \ddot{x} = \left(0 \frac{\partial^3 U_1}{\partial r^3} \Big|_{r=0} \quad \frac{\partial^3 U_2}{\partial r^3} \Big|_{r=0} \quad - \frac{\partial \Gamma_1}{\partial r} \Big|_{r=0} \quad \frac{\partial^3 S_1}{\partial r^3} \Big|_{r=0} \quad \frac{\partial^3 S_2}{\partial r^3} \Big|_{r=0} \quad - \frac{\partial \Gamma_2}{\partial r} \Big|_{r=0} \quad 0 \quad 0 \right)^T$$

$$\frac{\partial^4 U_i}{\partial r^4} = \frac{\partial^4 S_i}{\partial r^4} = \frac{\partial^2 \Gamma_i}{\partial r^2} = 0 \quad i = 1, 2$$

$$\rho \ddot{w} + \frac{\partial^2}{\partial x^2} EI_0 \frac{\partial^2}{\partial x^2} w = \frac{T_c}{x\theta_0} A_1 w$$

$$\rho \ddot{v} + \frac{\partial^2}{\partial x^2} EI_1 \frac{\partial^2}{\partial x^2} v = \frac{E_c}{x\theta_0} A_1 v + \frac{\theta_0}{2} E_{rc} \left[\frac{\partial}{\partial x} x \frac{\partial}{\partial x} A_2 v - \frac{A_2 v}{x} \right]$$

where

$$v = \begin{bmatrix} v_0 \\ v_1 \\ \vdots \\ \vdots \\ v_{N-1} \end{bmatrix}, \quad w = \begin{bmatrix} w_0 \\ \vdots \\ \vdots \\ v_{N-1} \end{bmatrix}$$

$$A_1 = \begin{bmatrix} -2 & 1 & & & & 1 \\ 1 & -2 & 1 & & & 0 \\ & & 1 & -2 & 1 & \\ & & & \cdot & \cdot & \cdot \\ & & & & \cdot & \cdot \\ & 0 & & & \cdot & 1 \\ 1 & & & & 1 & -2 \end{bmatrix}$$

$$A_2 = \begin{bmatrix} 2 & 1 & & & & \\ 1 & 2 & 1 & & & 0 \\ & & 1 & 2 & 1 & \\ & & & \cdot & \cdot & \cdot \\ & 0 & & \cdot & \cdot & \cdot \\ 1 & & & & \cdot & 1 \\ & & & & 1 & 2 \end{bmatrix}$$

Boundary Conditions:

$$\left. \frac{\partial^2 U_i}{\partial r^2} \right|_{r=L_1} = \left. \frac{\partial^3 U_i}{\partial r^3} \right|_{r=L_1} = 0 \quad \left. \frac{\partial^2 U_i}{\partial r^2} \right|_{r=0} = 0 \quad i = 1, 2$$

$$\left. \frac{\partial^2 S_i}{\partial r^2} \right|_{r=L_2} = \left. \frac{\partial^3 S_i}{\partial r^3} \right|_{r=L_2} = 0 \quad \left. \frac{\partial^2 S_i}{\partial r^2} \right|_{r=0} = 0 \quad i = 1, 2$$

$$\left. \frac{\partial \Gamma_1}{\partial r} \right|_{r=L_1} = \left. \frac{\partial \Gamma_2}{\partial r} \right|_{r=L_2} = 0$$

Remark:

The equations of the in- and out-of-plane motion of the ribs are given in a matrix form. They can be decoupled in a set of scalar equations by noticing that both matrices A_1 and A_2 have eigenvectors given by

$$\phi_n = \begin{bmatrix} \cos 0(n-1) \frac{2\pi}{N} + \sin 0(n-1) \frac{2\pi}{N} \\ \cos 1(n-1) \frac{2\pi}{N} + \sin 1(n-1) \frac{2\pi}{N} \\ \vdots \\ \cos (N-1)(n-1) \frac{2\pi}{N} + \sin (N-1)(n-1) \frac{2\pi}{N} \end{bmatrix}$$

corresponding to the eigenvalues

$$\lambda_{1n} = -4 \sin^2(n-1) \frac{\pi}{N}$$

and

$$\lambda_{2n} = 4 \cos^2(n-1) \frac{\pi}{N} \quad n = 1, \dots, N$$

for A_1 and A_2 respectively.

The decoupled equations can be written as

$$\begin{aligned} \rho p_n + \frac{\partial^2}{\partial x^2} EI_o \frac{\partial^2 p_n}{\partial x^2} &= \frac{T_c \lambda_{1n}}{x\theta_o} p_n \\ \rho q_n + \frac{\partial^2}{\partial x^2} EI_i \frac{\partial^2 q_n}{\partial x^2} &= \frac{E_c \lambda_{1n}}{x\theta_o} q_n + \frac{\theta_o}{2} E_{rc} \lambda_{2n} \left[\frac{\partial}{\partial x} \times \frac{\partial q_n}{\partial x} - \frac{q_n}{x} \right] \end{aligned}$$

Computation Results

In order to establish the accuracy of the model and its adequacy for simple and fast computations, the modal frequencies of the reflector dish were evaluated using a Ritz approximation scheme with assumed mode shapes of the form

$$\sum a_i \left(1 - \cos \frac{i\pi r}{L} \right).$$

The following table shows a comparison of the results to those obtained through finite element modeling [Ref. 2] (using 6624 modes).

Table 1. Comparison Between Continuum and Finite Element Models

Circumferential Wave Number	PDE		FE	
	0	1	0	1
1st out-of-plane	0.77276	0.772763	0.78971	0.78988
2nd out-of-plane	3.33615	3.33615	-	-
1st in-plane	0.175461	0.175877	0.18134	0.19082
2nd in-plane	0.726048	0.725721	0.70185	0.70423

The accuracy is quite satisfactory as it can be observed. As to the required computational effort, the difference with the finite element method is striking: the whole algorithm could be programmed on an intelligent terminal, and the computational cost was about 30 times less.

CONCLUSION

A general approach to partial differential equation modeling of large space structures was presented and its application to the modeling of a large, wrap-rib, offset-fed antenna was described.

The partial differential model thus obtained has all the expected traits of simplicity, conciseness, and suitability for parametric studies.

The model was used to evaluate the modal frequencies of the dish. For low frequencies the results are very close to those obtained from a finite-element model of very high dimension. The striking feature is that the required computational effort was more than an order of magnitude smaller.

ACKNOWLEDGEMENT

The research described in this paper was carried out at the Jet Propulsion Laboratory, California Institute of Technology, under contract with the National Aeronautics and Space Administration.

REFERENCES

1. F. Naderi, ed., "Land Mobile Satellite Service, A Conceptual System Design and Identification of the Critical Technology," JPL publication 82-19, Jet Propulsion Laboratory, February 1982.
2. M. El-Raheb and P. Wagner, "Static and Dynamic Characteristics of Large Deployable Space Reflectors," 1981 AIAA/ASME/ASCE/AHS 22nd Structures, Structural Dynamics and Materials Conference, April 6-8, 1981, Atlanta, GA, and AIAA 81-0503PC, April 9-10, 1981, Atlanta, GA.

MODELING OF FLEXIBLE STRUCTURES FOR ACTIVE CONTROL*

Arthur E. Bryson, Jr.
Stanford University
Stanford, CA 94305

ABSTRACT

If a flexible structure has a plane of symmetry, the equations of motion can be split into two uncoupled sets, one for symmetrical motions and one for anti-symmetric motions.

If there are m controls, it is often convenient to assign the linear combinations of controls that enter into the m lowest frequency modes and "new" controls.

As an example the feed-support structure of a spacecraft antenna is considered. It is modeled as a tetrahedron made up of flexible bars and connected to the spacecraft by six short flexible legs containing force actuators and displacement sensors. Due to the three-sided symmetry of this structure, both the symmetric and the anti-symmetric equations of motion can be decoupled into two subsystems. The resulting four subsystems are:

- (1) Pitch/fore-aft motions with four degrees of freedom (DOF), two controls, and one output (the fore-aft motion of the feed).
- (2) Vertical motions with three DOF, one control, and one output (the vertical motion of the feed).
- (3) Roll/lateral motions with four DOF, two controls, and one output (the lateral motions of the feed).
- (4) Yaw motion with one DOF, one control, and no output (the feed does not move during yaw motion).

Such a decomposition obviously simplifies the task of synthesizing active control logic for the structure.

INTRODUCTION

The example was suggested by the ACOSS (Active Stabilization of Space Structures) problem posed by the Draper Laboratory a few years ago (see Ref. 1 and Figure 1). The only difference in the data from that problem is that we have

* This research was supported under NASA Grant NAG-1-236 from the Langley Research Center, monitored by Ray Montgomery.

taken the three vertical bars of the tetrahedron to be identical. This results in four lateral modes that have identical frequencies to four longitudinal modes.

The ACOSS problem may be interpreted as the problem stated in the abstract if one assumes that the spacecraft mass is large compared to the feed-tower mass so that the spacecraft motions are negligible.

EQUATIONS OF MOTION

The structural model is oversimplified and was apparently only intended to be an example of a multi-input, multi-output system. The structure consists of twelve bars, six of which (10 meters long) form a regular tetrahedron with the feed at its apex (point 1). Two bars (each 2.828 meters long) connect each of the three joints at the base of the tetrahedron (points 2,3,4) to the antenna dish on the spacecraft. The cross-section area of the three base members is ten times the cross-section area of the vertical members and the legs. The mass of the structure is "lumped" at the four joints (equal mass at each joint).

Since there are two actuators applying forces at each of the three base joints, it is possible to create independent horizontal and vertical forces at each of these joints. Let (V_i, H_i) be the (vertical, horizontal) forces at joint i ($i=2$ to 4) as shown in Figure 2.

Let $k(i)$ be the values of $EA(i)/mL(i)$ (stiffness/mass) for the base members ($i=1$), the vertical members ($i=2$), and the legs ($i=3$), where E = Young's modulus, A = cross-section area of the member, L = length of member, and m = lumped mass at each joint. We have taken $m=2$, and

$$\begin{aligned} k(1) &= 50 && 1/\text{sec}^2, \\ k(2) &= 5 && 1/\text{sec}^2, \\ k(3) &= 17.6775 && 1/\text{sec}^2. \end{aligned}$$

Using the vectors $x = (x_1, y_1, z_1; x_2, y_2, z_2; x_3, y_3, z_3; x_4, y_4, z_4)'$, $f = (V_2, H_2; V_3, H_3; V_4, H_4)'$, the equations of motion may then be written as:

$$\ddot{x} = -K \cdot x + G \cdot f,$$

where

$$\begin{aligned} K &= 12 \text{ by } 12 \text{ matrix,} \\ G &= 12 \text{ by } 6 \text{ matrix.} \end{aligned}$$

The matrices K and G were calculated and are given in Appendix A.

DECOMPOSITION INTO SYMMETRIC AND ANTI-SYMMETRIC MOTIONS

Motions of the feed-tower can be decomposed into motions that are either symmetric or anti-symmetric with respect to the y - z plane of symmetry. The

decomposition can be performed by the following change of variables:

$$s = (y_1, z_1, (x_2 - x_3)/2, (y_2 + y_3)/2, (z_2 + z_3)/2, y_4, z_4),$$

$$a = (x_1, (x_2 + x_3)/2, (y_2 - y_3)/2, (z_2 - z_3)/2, x_4),$$

$$S = ((H_2 - H_3)/2, (V_2 + V_3)/2, V_4)$$

$$A = ((H_2 + H_3)/2, (V_2 - V_3)/2, H_4)$$

where (s,a) are vectors of (symmetric, anti-symmetric) joint displacements, and (S,A) are vectors of (symmetric, anti-symmetric) actuator forces. The equations of motion then split into two uncoupled sets:

$$\ddot{s} = -KS \cdot s + GS \cdot S,$$

and

$$\ddot{a} = -KA \cdot a + GA \cdot A.$$

The KS, KA, GS, GA matrices were calculated and are given in Appendix A.

DECOUPLING OF THE SYMMETRIC MOTIONS INTO PITCH/FORE-AFT AND VERTICAL MOTIONS

Using an eigenvalue/eigenvector computer code, the symmetric equations of motion were put into modal form (see Appendix B). The three modes of this system with the lowest frequencies correspond to quasi-rigid pitching, vertical translation, and fore-aft translation. Linearly-independent combinations of the symmetric actuator forces control each of these quasi-rigid modes, so we chose to regard these combinations as "new" symmetric controls. When this was done, a further decoupling appeared, in that two of the four higher-frequency (deformation) modes were controllable only by the new pitch and fore-aft controls (f_p, f_f), while the other two modes were controllable only by the new vertical control (f_v). Furthermore, f_p and f_f control only the fore-aft motions of the feed (y_1), while f_v controls only the vertical motion of the feed (z_1).

The modes that involve only fore-aft motions of the feed are shown in Figure 3. The pitch/fore-aft equations of motion in modal form are given in Figure 4. Figure 5 shows the combinations of the primary controls that form f_p and f_f .

The modes that involve only vertical motion of the feed are shown in Figure 6. The vertical equations of motion in modal form are given in Figure 7. Also shown in Figure 7 is the combination of primary controls that forms f_v (equal values of V_2, V_3, V_4).

DECOUPLING OF THE ANTI-SYMMETRIC MOTIONS INTO ROLL/LATERAL AND YAW MOTIONS

A similar procedure was followed for the anti-symmetric motions (see Appendix B). The three lowest frequency modes were quasi-rigid roll, lateral translation,

and yaw. Here the two higher frequency (deformation) modes were controllable only with the new roll/lateral actuator forces (f_r, f_l).

The modes that involve only roll/lateral motions of the feed are shown in Figure 8. The roll/lateral equations of motion in modal form are given in Figure 9. Figure 10 shows the combinations of the primary controls that form f_r and f_l .

The modes that involve only yaw motion of the feed are shown in Figure 11. The yaw equation of motion in modal form are given in Figure 12. Also shown in Figure 12 is the combination of primary controls that forms f_y (equal values of H_2, H_3, H_4).

The natural frequencies of the roll/lateral subsystem are identical to those of the pitch/fore-aft subsystem, which is not surprising in view of the symmetry of the structure.

SUMMARY

Figure 13 is a summary of the decoupling of the system into four subsystems. The 24th order system with six controls and three outputs has been decoupled into two 8th order subsystems with two controls and one output, a 6th order system with one control and one output, and a 2nd order system with one control and no output. This greatly simplifies the problem of synthesizing active control logic for the system.

REFERENCES

1. Henderson, T. and Strunce, R., ACOSS Problem #1, Draper Laboratory, 1979.

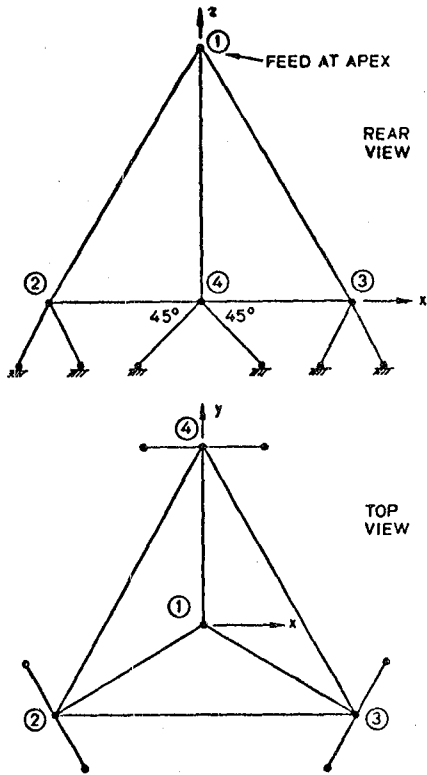


Figure 1. Antenna-Feed Tower

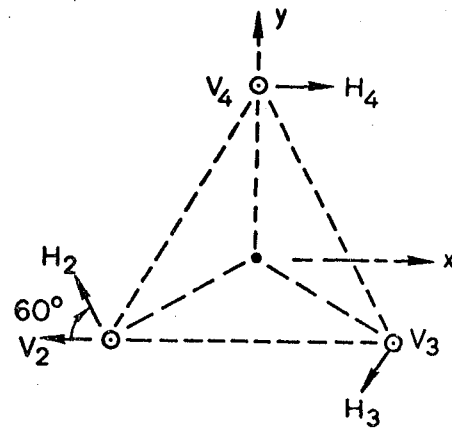


Figure 2. Control Forces

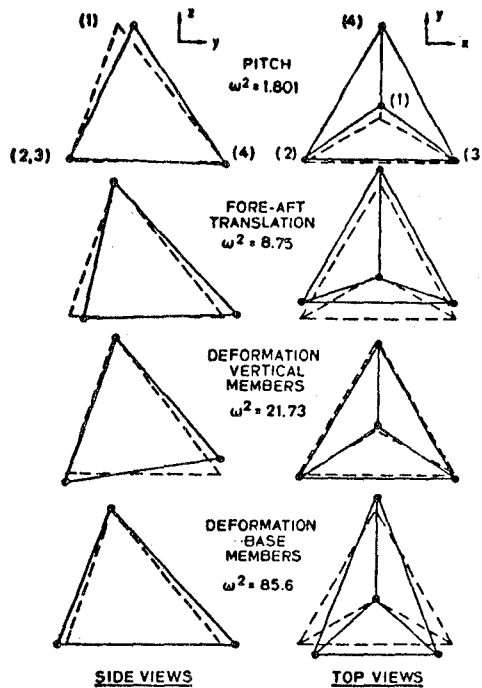


Figure 3. Modes that Involve Only Y Motions of Apex

$$\begin{bmatrix} \ddot{m}_1 \\ \ddot{m}_4 \\ \ddot{m}_7 \\ \ddot{m}_{10} \end{bmatrix} = \begin{bmatrix} -(1.342)^2 & 0 & 0 & 0 \\ 0 & -(2.957)^2 & 0 & 0 \\ 0 & 0 & -(4.662)^2 & 0 \\ 0 & 0 & 0 & -(9.251)^2 \end{bmatrix} \begin{bmatrix} m_1 \\ m_4 \\ m_7 \\ m_{10} \end{bmatrix} + \begin{bmatrix} .1907 & 0 \\ 0 & .6652 \\ -.9848 & .7914 \\ -.1320 & -.5788 \end{bmatrix} \begin{bmatrix} f_P \\ f_F \end{bmatrix}$$

Where

$$\begin{bmatrix} y_1 \\ x_2 \\ y_2 \\ z_2 \\ y_4 \\ z_4 \end{bmatrix} = \begin{bmatrix} 1 & -.2629 & .1979 & -.0317 \\ \hline .0165 & .0832 & .0057 & .9673 \\ .0997 & .8557 & -.1190 & -.6753 \\ .0534 & -.1214 & -.5000 & .0188 \\ \hline .1283 & 1 & -.1090 & 1 \\ -.1069 & .2424 & 1 & -.0376 \end{bmatrix} \begin{bmatrix} m_1 \\ m_4 \\ m_7 \\ m_{10} \end{bmatrix} \quad \begin{array}{l} x_1 = 0 \\ z_1 = 0 \\ x_3 = -x_2 \\ y_3 = y_2 \\ z_3 = z_2 \\ x_4 = 0 \end{array}$$

And

$$\begin{bmatrix} H_2 \\ V_2 \\ \bar{V}_4 \end{bmatrix} = \begin{bmatrix} .2602 & 1 \\ .5000 & -.4872 \\ \hline -1 & .9744 \end{bmatrix} \begin{bmatrix} f_P \\ f_F \end{bmatrix} \quad \begin{array}{l} H_3 = -H_2 \\ V_3 = V_2 \\ H_4 = 0 \end{array}$$

NOTE: (m_1, m_4) are Quasi-Rigid modes, (m_7, m_{10}) are Deformation modes.

Figure 4. Pitch/Fore-Aft Subsystem

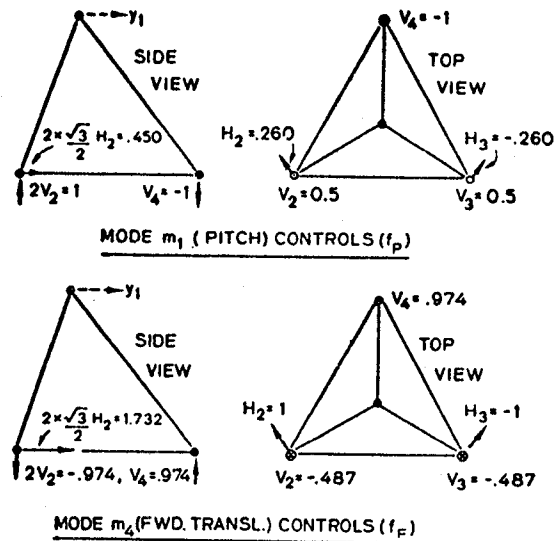


Figure 5. Pitch/Fore-Aft Controls

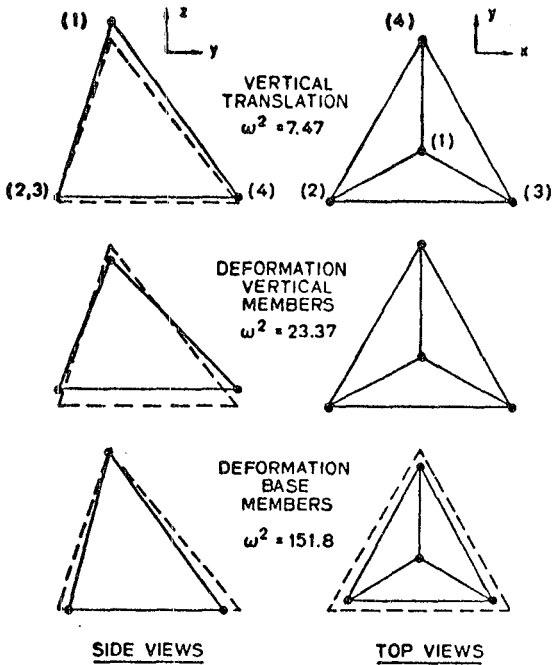


Figure 6. Modes Involving Only Z Motions of Apex

$$\begin{bmatrix} \ddot{m}_3 \\ \ddot{m}_9 \\ \ddot{m}_{12} \end{bmatrix} = \begin{bmatrix} -(2.734)^2 & 0 & 0 \\ 0 & -(4.835)^2 & 0 \\ 0 & 0 & -(12.322)^2 \end{bmatrix} \begin{bmatrix} m_3 \\ m_9 \\ m_{12} \end{bmatrix} + \begin{bmatrix} .6208 \\ .8476 \\ .0192 \end{bmatrix} \{f_V\}$$

Where m_3 is Quasi-Rigid, (m_9, m_{12}) are Deformation modes,

$$\begin{bmatrix} z_1 \\ x_2 \\ y_2 \\ z_2 \\ y_4 \\ z_4 \end{bmatrix} = \begin{bmatrix} 1 & -.7307 & .0512 \\ .0107 & -.0275 & -.8659 \\ .0064 & -.0160 & -.5000 \\ .2440 & .9994 & -.0193 \\ -.0120 & .0316 & 1 \\ .2440 & 1 & -.0193 \end{bmatrix} \begin{bmatrix} m_3 \\ m_9 \\ m_{12} \end{bmatrix} \quad \begin{array}{l} x_1 = 0 \\ y_1 = 0 \\ -x_3 = x_2 \\ y_3 = y_2 \\ z_3 = z_2 \\ x_4 = 0 \end{array}$$

And

$$\begin{bmatrix} V_2 \\ V_3 \\ V_4 \end{bmatrix} = \begin{bmatrix} 1 \\ 1 \\ 1 \end{bmatrix} \{f_V\} \quad \begin{array}{l} H_2 = 0 \\ H_3 = 0 \\ H_4 = 0 \end{array}$$

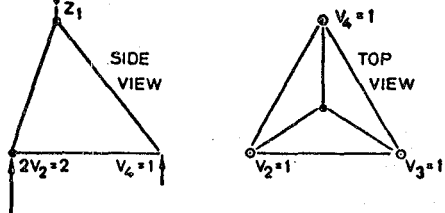


Figure 7. Vertical Subsystem

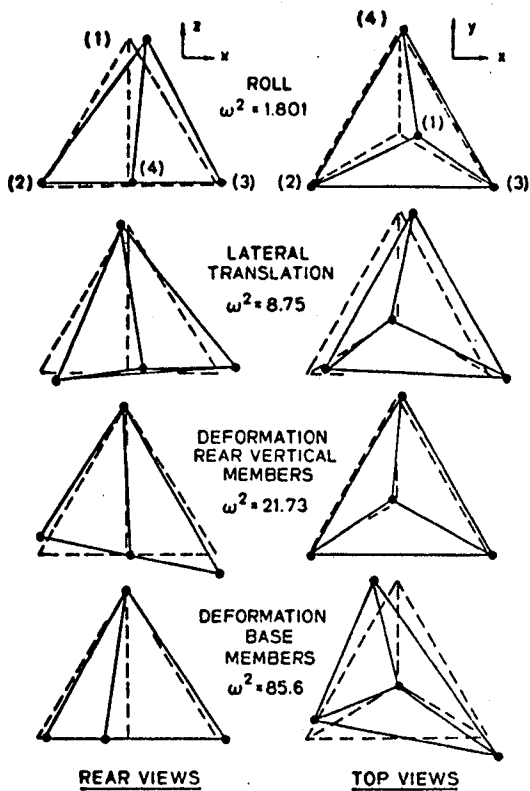


Figure 8. Modes that Involve Only X Motions of Apex

$$\begin{bmatrix} \ddot{m}_2 \\ \ddot{m}_5 \\ \ddot{m}_8 \\ \ddot{m}_{11} \end{bmatrix} = \begin{bmatrix} -(1.342)^2 & 0 & 0 & 0 \\ 0 & -(2.957)^2 & 0 & 0 \\ 0 & 0 & -(4.662)^2 & 0 \\ 0 & 0 & 0 & -(9.251)^2 \end{bmatrix} \begin{bmatrix} m_2 \\ m_5 \\ m_8 \\ m_{11} \end{bmatrix} + \begin{bmatrix} .2202 & 0 \\ 0 & .5482 \\ .9845 & -.5925 \\ .1880 & .6184 \end{bmatrix} \begin{bmatrix} f_R \\ f_L \end{bmatrix}$$

Where

$$\begin{bmatrix} x_1 \\ x_2 \\ y_2 \\ z_2 \\ x_4 \end{bmatrix} = \begin{bmatrix} 1 & -.2761 & -.2286 & .0256 \\ .1188 & 1 & .1300 & -.3579 \\ .0165 & .0874 & -.0068 & -.7840 \\ .0926 & -.2207 & 1 & -.0264 \\ .0901 & .8483 & .1409 & 1 \end{bmatrix} \begin{bmatrix} m_2 \\ m_5 \\ m_8 \\ m_{11} \end{bmatrix} \quad \begin{matrix} y_1 = 0 \\ z_1 = 0 \\ x_3 = x_2 \\ y_3 = -y_2 \\ z_3 = z_2 \\ y_4 = 0 \\ z_4 = 0 \end{matrix}$$

And

$$\begin{bmatrix} H_2 \\ V_2 \\ H_4 \end{bmatrix} = \begin{bmatrix} -.1735 & -.5000 \\ 1 & -.7299 \\ .3470 & 1 \end{bmatrix} \begin{bmatrix} f_R \\ f_L \end{bmatrix}$$

NOTE: (m_2, m_5) are Quasi-Rigid Modes, (m_8, m_{11}) are Deformation modes, and frequencies = frequencies of pitch/fore-aft subsystem.

Figure 9. Roll/Lateral Subsystem

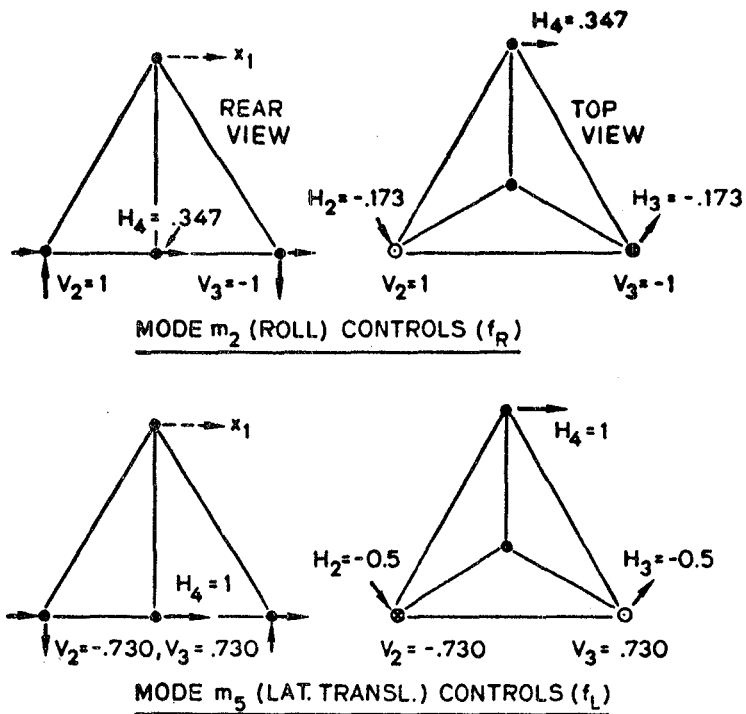


Figure 10. Roll/Lateral Controls

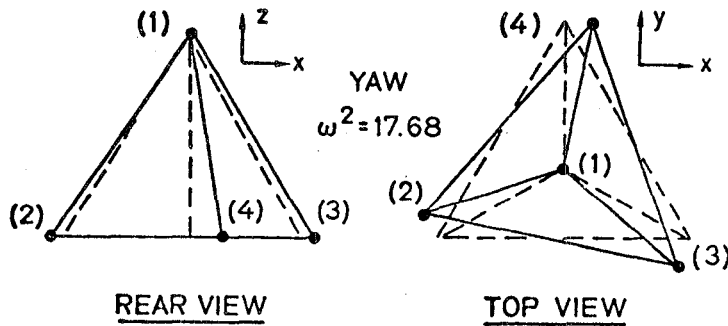


Figure 11. Anti-Symmetric Mode Involving no Motion of Apex

$$\ddot{m}_6 = -(4.204)^2 m_6 + .5773 f_Y$$

Where

$$\begin{bmatrix} x_2 \\ y_2 \\ x_4 \end{bmatrix} = \begin{bmatrix} -.5000 \\ .8660 \\ 1 \end{bmatrix} \begin{bmatrix} m_6 \end{bmatrix}$$

$$\begin{aligned} x_1 &= y_1 = z_1 = 0 \\ z_2 &= 0 \\ x_3 &= x_2 \\ y_3 &= -y_2 \\ z_3 &= z_2 \\ y_4 &= z_4 = 0 \end{aligned}$$

And

$$\begin{bmatrix} H_2 \\ H_3 \\ H_4 \end{bmatrix} = \begin{bmatrix} 1 \\ 1 \\ 1 \end{bmatrix} \begin{bmatrix} f_Y \end{bmatrix}$$

$$\begin{aligned} V_2 &= 0 \\ V_3 &= 0 \\ V_4 &= 0 \end{aligned}$$

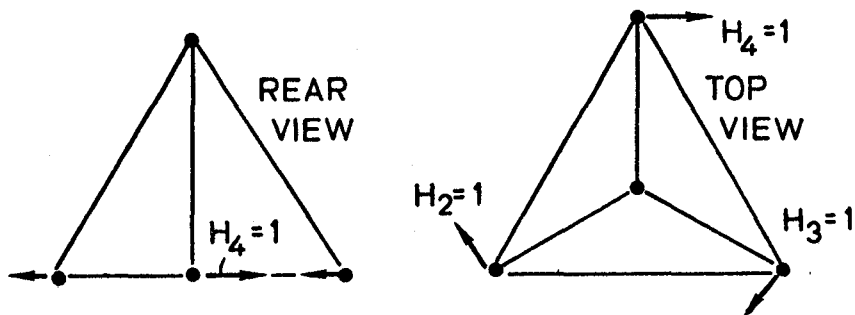


Figure 12. Yaw Subsystem

SUBSYS. MODES	PITCH/ FORE-AFT	ROLL/ LATERAL	VERTICAL	YAW
QUASI-RIGID	m_1, m_4	m_2, m_5	m_3	m_6
DEFORMATION	m_7, m_{10}	m_8, m_{11}	m_9, m_{12}	-
CONTROLS	f_P, f_F	f_R, f_L	f_V	f_Y
OUTPUTS	y_1	x_1	z_1	-

Figure 13. Summary of Uncoupled Subsystems

APPENDIX A. EQUATIONS OF MOTION

Let:

$$\begin{aligned} x(i,k) &= \text{kth component of the displacement vector of the } i\text{th joint,} \\ u(i,j,k) &= \text{kth component of nominal unit vector from } i\text{th to } j\text{th joint,} \\ f(i,k) &= \text{kth component of control force on } i\text{th joint} \\ k(i) &= E \cdot A(i) / m \cdot L(i), \\ &= \text{stiffness/mass,} \end{aligned}$$

where $i=1$ for base members, $i=2$ for vertical members, and $i=3$ for the legs, and

$$\begin{aligned} E &= \text{Young's modulus,} \\ A &= \text{cross-section area of bar,} \\ m &= \text{lumped mass at each joint,} \\ L &= \text{length of bar.} \end{aligned}$$

Then the equations of motion are:

$$\begin{aligned} \ddot{x}(1,k) &= -k(2) \cdot u(1,2,k) \cdot u(1,2,j) \cdot [x(1,j) - x(2,j)] \\ &\quad - k(2) \cdot u(1,3,k) \cdot u(1,3,j) \cdot [x(1,j) - x(3,j)] \\ &\quad - k(2) \cdot u(1,4,k) \cdot u(1,4,j) \cdot [x(1,j) - x(4,j)], \end{aligned}$$

$$\begin{aligned} \ddot{x}(2,k) &= -k(2) \cdot u(2,1,k) \cdot u(2,1,j) \cdot [x(2,j) - x(1,j)] \\ &\quad - k(1) \cdot u(2,3,k) \cdot u(2,3,j) \cdot [x(2,j) - x(3,j)] \\ &\quad - k(1) \cdot u(2,4,k) \cdot u(2,4,j) \cdot [x(2,j) - x(4,j)] \\ &\quad - k(3) \cdot u(2,5,k) \cdot u(2,5,j) \cdot x(2,j) \\ &\quad - k(3) \cdot u(2,6,k) \cdot u(2,6,j) \cdot x(2,j) \\ &\quad + f(2,k), \end{aligned}$$

$$\begin{aligned} \ddot{x}(3,k) &= -k(2) \cdot u(3,1,k) \cdot u(3,1,j) \cdot [x(3,j) - x(1,j)] \\ &\quad - k(1) \cdot u(3,2,k) \cdot u(3,2,j) \cdot [x(3,j) - x(2,j)] \\ &\quad - k(1) \cdot u(3,4,k) \cdot u(3,4,j) \cdot [x(3,j) - x(4,j)] \\ &\quad - k(3) \cdot u(3,7,k) \cdot u(3,7,j) \cdot x(3,j) \\ &\quad - k(3) \cdot u(3,8,k) \cdot u(3,8,j) \cdot x(3,j) \\ &\quad + f(3,k), \end{aligned}$$

$$\begin{aligned} \ddot{x}(4,k) &= -k(2) \cdot u(4,1,k) \cdot u(4,1,j) \cdot [x(4,j) - x(1,j)] \\ &\quad - k(1) \cdot u(4,2,k) \cdot u(4,2,j) \cdot [x(4,j) - x(2,j)] \\ &\quad - k(1) \cdot u(4,3,k) \cdot u(4,3,j) \cdot [x(4,j) - x(3,j)] \\ &\quad - k(3) \cdot u(4,9,k) \cdot u(4,9,j) \cdot x(4,j) \\ &\quad - k(3) \cdot u(4,10,k) \cdot u(4,10,j) \cdot x(4,j) \\ &\quad + f(4,k), \end{aligned}$$

where

$$\begin{aligned} f(2,1) &= -s \cdot H_2 / m, & f(2,2) &= c \cdot H_2 / m, & f(2,3) &= V_2 / m, \\ f(3,1) &= -s \cdot H_3 / m, & f(3,2) &= -c \cdot H_3 / m, & f(3,3) &= V_3 / m, \\ f(4,1) &= H_4 / m, & f(4,2) &= 0 & f(4,3) &= V_4 / m, \end{aligned}$$

and

$$s = \frac{1}{2}, \quad c = \frac{\sqrt{3}}{2}$$

We have taken $m=2$ and:

$$\begin{aligned} k(1) &= 50 & 1/\text{sec}^2 \\ k(2) &= 5 & 1/\text{sec}^2 \\ k(3) &= 17.6775 & 1/\text{sec}^2 \end{aligned}$$

A BASIC computer code, TETRA, was developed to calculate the terms in the equations above, and to find the terms in the symmetric and anti-symmetric equations of motion. It is listed in the following pages, followed by the output.

```

100 REM ***** TETRA **** 4/26/82 *****
110 REM * FINDS STIFFNESS MATRIX K, &
120 REM * CONTROL DISTRIBUTION MATRIX
 30 REM * G, FOR TETRAHEDRON ON LEGS,
140 REM * WHERE
150 REM *   XDOTDOT=-K*X+G*U.
160 REM *
170 REM * THEN FINDS K AND G FOR
180 REM * SYMMETRIC & ANTI-SYMMETRIC
190 REM * MOTIONS.
200 REM *****
210 REM
220 REM * READS DATA *
230 REM
240 DIMX(10,3),M(4,10,3),K(12,12):FORI=1TO10:FORJ=1TO3:READX(I,J):NEXTJ,I
250 READK1,K2,KL:DEFFNR(S)=INT(10000*S+.5)/10000
260 REM
270 REM * FINDS NOMINAL DISPLACEMENT VECTORS FROM FOUR TETRAHEDRON JOINTS
280 REM * TO EACH OTHER & ALONG LEGS *
290 REM
300 FORI=1TO4:FORJ=1TO10:FORK=1TO3:M(I,J,K)=X(I,K)-X(J,K):NEXTK,J,I
310 REM
320 REM * FINDS ELEMENTS OF STIFFNESS MATRIX *
330 REM
340 FORI=1TO3:FORJ=4TO6:K(I,J)=M(1,2,I)*M(1,2,J-3)*K2:NEXTJ,I
350 FORI=1TO3:FORJ=7TO9:K(I,J)=M(1,3,I)*M(1,3,J-6)*K2:NEXTJ,I
360 FORI=1TO3:FORJ=10TO12:K(I,J)=M(1,4,I)*M(1,4,J-9)*K2:NEXTJ,I
370 FORI=4TO6:FORJ=7TO9:K(I,J)=M(2,3,I-3)*M(2,3,J-6)*K1:NEXTJ,I
380 FORI=4TO6:FORJ=10TO12:K(I,J)=M(2,4,I-3)*M(2,4,J-9)*K1:NEXTJ,I
390 FORI=7TO9:FORJ=10TO12:K(I,J)=M(3,4,I-6)*M(3,4,J-9)*K1:NEXTJ,I
400 FORI=1TO3:FORJ=4TO12:K(J,I)=K(I,J):NEXTJ,I
410 FORI=4TO6:FORJ=7TO12:K(J,I)=K(I,J):NEXTJ,I
420 FORI=7TO9:FORJ=10TO12:K(J,I)=K(I,J):NEXTJ,I
430 FORI=1TO3:FORJ=1TO3:K(I,J)=-K(I,J+3)-K(I,J+6)-K(I,J+9):NEXTJ,I
440 FORI=4TO6:FORJ=4TO6:K(I,J)=-K(I,J-3)-K(I,J+3)-K(I,J+6):NEXTJ,I
450 FORI=4TO6:FORJ=4TO6:K(I,J)=K(I,J)-M(2,5,I-3)*M(2,5,J-3)*KL:NEXTJ,I
460 FORI=4TO6:FORJ=4TO6:K(I,J)=K(I,J)-M(2,6,I-3)*M(2,6,J-3)*KL:NEXTJ,I
470 FORI=7TO9:FORJ=7TO9:K(I,J)=-K(I,J-6)-K(I,J-3)-K(I,J+3):NEXTJ,I
480 FORI=7TO9:FORJ=7TO9:K(I,J)=K(I,J)-M(3,7,I-6)*M(3,7,J-6)*KL:NEXTJ,I
490 FORI=7TO9:FORJ=7TO9:K(I,J)=K(I,J)-M(3,8,I-6)*M(3,8,J-6)*KL:NEXTJ,I
500 FORI=10TO12:FORJ=10TO12:K(I,J)=-K(I,J-9)-K(I,J-6)-K(I,J-3):NEXTJ,I
510 FORI=10TO12:FORJ=10TO12:K(I,J)=K(I,J)-M(4,9,I-9)*M(4,9,J-9)*KL:NEXTJ,I
520 FORI=10TO12:FORJ=10TO12:K(I,J)=K(I,J)-M(4,10,I-9)*M(4,10,J-9)*KL:NEXTJ,I
530 PRINTTAB(10);"STIFFNESS/MASS MATRIX, UPPER LEFT QUADRANT"
540 FORI=1TO6:FORJ=1TO6:PRINTFNR(K(I,J)):NEXTJ:PRINT:NEXTI
550 PRINTTAB(10);"UPPER RIGHT QUADRANT":FORI=1TO6:PRINTTAB(10):FORJ=7TO12
560 PRINTFNR(K(I,J)):NEXTJ:PRINT:NEXTI
570 PRINTTAB(10);"LOWER RIGHT QUADRANT"
580 FORI=7TO12:PRINTTAB(10):FORJ=7TO12:PRINTFNR(K(I,J)):NEXTJ:PRINT:NEXTI
590 REM
600 REM * CALCULATES ANTI-SYMMETRIC, SYMMETRIC STIFFNESS MATRICES *
610 REM
620 DIMT(12,12),TI(12,12),L(12,12),L1(12,12):C=.5:T(1,1)=1:T(2,6)=1
630 T(3,7)=1:T(4,2)=1:T(4,8)=1:T(5,3)=1:T(5,9)=1:T(6,4)=1:T(6,10)=1:T(7,2)=1
 10 T(7,8)=-1:T(8,9)=1:T(8,3)=-1:T(9,10)=1:T(9,4)=-1:T(10,5)=1:T(11,11)=1
650 T(12,12)=1:TI(1,1)=1:TI(2,4)=C:TI(2,7)=C:TI(3,5)=C:TI(3,8)=-C:TI(4,6)=C
660 TI(4,9)=-C:TI(5,10)=1:TI(6,2)=1:TI(7,3)=1:TI(8,4)=C:TI(8,7)=-C:TI(9,5)=C
670 TI(9,8)=C:TI(10,6)=C:TI(10,9)=C:TI(11,11)=1:TI(12,12)=1
680 FORI=1TO12:FORJ=1TO12:FORK=1TO12:L1(I,J)=L1(I,J)+K(I,K)*T(K,J):NEXTK,J,I
690 FORI=1TO12:FORJ=1TO12:FORK=1TO12:L(I,J)=L(I,J)+TI(I,K)*L1(K,J):NEXTK,J,I
700 PRINTTAB(10);"ANTI-SYMMETRIC STIFFNESS/MASS MATRIX:"
710 FORI=1TO5:PRINTTAB(10):FORJ=1TO5:PRINTFNR(L(I,J)):NEXTJ:PRINT:NEXTI
720 GOTO750
 30 PRINTTAB(10);"CROSS-COUPLING MATRIX:"
740 FORI=1TO5:PRINTTAB(10):FORJ=6TO12:PRINTFNR(L(I,J)):NEXTJ:PRINT:NEXTI
750 PRINTTAB(10);"SYMMETRIC STIFFNESS/MASS MATRIX:"

```

```

760 FORI=6TO12:PRINTTAB(10);:FORJ=6TO12:PRINTFNR(L(I,J));:NEXTJ:PRINT:NEXTI
770 GOTO830
780 PRINTTAB(10);"CROSS-COUPLING MATRIX:"
790 FORI=6TO12:PRINTTAB(10);:FORJ=1TO5:PRINTFNR(L(I,J));:NEXTJ:PRINT:NEXTI
800 REM
810 REM * COMPUTES GA & GS *
820 REM
830 DIMG(12,6),G1(12,6)
840 G(4,1)=-.25:G(5,1)=.43301:G(6,2)=.5:G(7,3)=-.25:G(8,3)=-.43301:G(9,4)=.5
850 G(10,5)=.5:G(12,6)=.5
860 FORI=1TO12:FORJ=1TO6:FORK=1TO12:G1(I,J)=G1(I,J)+TI(I,K)*G(K,J):NEXTK,J,I
870 PRINTTAB(10):PRINT"ANTI-SYMMETRIC CONTROL DISTRIBUTION MATRIX GA(I,J), IS:"
880 FORI=1TO5:PRINTTAB(10);:FORJ=1TO6:PRINTFNR(G1(I,J));:NEXTJ:PRINT:NEXTI
890 PRINTTAB(10):PRINT"SYMMETRIC CONTROL DISTRIBUTION MATRIX GS(I,J), IS:"
900 FORI=6TO12:PRINTTAB(10);:FORJ=1TO6:PRINTFNR(G1(I,J));:NEXTJ:PRINT:NEXTI
910 END
920 REM
930 REM * TETRA *
940 REM
950 REM * ACROSS TETRAHEDRON; X=(X1,Y1,Z1,X2,Y2,Z2,X3,Y3,Z3,X4,Y4,Z4)
960 REM * U=(H2,V2,H3,V3,H4,V4); 4/26/82 *
970 REM
980 REM * ENTER DATA HERE *
990 REM
1000 REM * ENTER X,Y,Z COORDINATES OF JOINTS 1 THRU 10 *
1010 DATA 0,0,10.165,-5,-2.887,2,5,-2.887,2,0,5.7735,2,-6,-1.1547,0
1020 DATA -4,-4.6188,0.4,-4.6188,0.6,-1.1547,0,2,5.7735,0,-2,5.7735,0
1030 REM * ENTER STIFFNESS/MASS FOR HEAVY MEMBERS, LIGHT MEMBERS, & LEGS *
1040 DATA .5,.05,2.2097
READY.

```

STIFFNESS/MASS MATRIX, UPPER LEFT QUADRANT

-2.5 0 0 1.25 .7218 2.0413
 0 -2.5001 -2E-04 .7218 .4167 1.1786
 0 -2E-04 -10.0001 2.0413 1.1786 3.3334
 1.25 .7218 2.0413 -68.1694 -14.7184 -2.0413
 .7218 .4167 1.1786 -14.7184 -51.1771 -1.1764
 2.0413 1.1786 3.3334 -2.0413 -1.1764 -21.011

UPPER RIGHT QUADRANT

1.25 -.7218 -2.0413 0 0 0
 -.7218 .4167 1.1786 0 1.6667 -2.357
 -2.0413 1.1786 3.3334 0 -2.357 3.3334
 50 0 0 12.5 21.6513 0
 0 0 0 21.6513 37.5021 0
 0 0 0 0 0 0

LOWER RIGHT QUADRANT

-68.1694 14.7184 2.0413 12.5 -21.6513 0
 14.7184 -51.1771 -1.1764 -21.6513 37.5021 0
 2.0413 -1.1764 -21.011 0 0 0
 12.5 -21.6513 0 -42.6776 0 0
 -21.6513 37.5021 0 0 -76.6709 2.357
 0 0 0 0 2.357 -21.011

ANTI-SYMMETRIC STIFFNESS/MASS MATRIX:

-2.5 2.5 1.4435 4.0825 0
 1.25 -18.1694 -14.7184 -2.0413 12.5
 .7218 -14.7184 -51.1771 -1.1764 21.6513
 2.0413 -2.0413 -1.1764 -21.011 0
 0 25 43.3025 0 -42.6776

SYMMETRIC STIFFNESS/MASS MATRIX:

-2.5001 -2E-04 1.4435 .8335 2.3572 1.6667 -2.357
 -2E-04 -10.0001 4.0825 2.3572 6.6667 -2.357 3.3334
 .7218 2.0413 -118.1694 -14.7184 -2.0413 21.6513 0
 .4167 1.1786 -14.7184 -51.1771 -1.1764 37.5021 0
 1.1786 3.3334 -2.0413 -1.1764 -21.011 0 0
 1.6667 -2.357 43.3025 75.0043 0 -76.6709 2.357
 -2.357 3.3334 0 0 0 2.357 -21.011

ANTI-SYMMETRIC CONTROL DISTRIBUTION MATRIX GA(I,J), IS:

0 0 0 0 0 0
 -.125 0 -.125 0 0 0
 .2165 0 .2165 0 0 0
 0 .25 0 -.25 0 0
 0 0 0 0 .5 0

SYMMETRIC CONTROL DISTRIBUTION MATRIX GS(I,J), IS:

0 0 0 0 0 0
 0 0 0 0 0 0
 -.125 0 .125 0 0 0
 .2165 0 -.2165 0 0 0
 0 .25 0 .25 0 0
 0 0 0 0 0 0
 0 0 0 0 0 .5

APPENDIX B. MODAL FORMS

An eigenvalue/eigenvector code was used to find the natural frequencies and mode shapes from the symmetric and anti-symmetric equations of motion determined in Appendix A. The results are shown below and on the next page.

Tetrahedron Lateral

x=(x1,x2,y2,z2,x4);u=(h2,v2,h4)
Units sec: 4/26/82

Dynamics Matrix F, is:

- 2.500 + 2.500 + 1.443 + 4.082 + .000
+ 1.250 -18.169 -14.718 - 2.041 +12.500
+ .721 -14.718 -51.177 - 1.176 +21.651
+ 2.041 - 2.041 - 1.176 -21.011 + .000
+ .000 +25.000 +43.302 + .000 -42.677

Control Distribution Matrix, G, is:

+ .000 + .000 + .000
- .250 + .000 + .000
+ .433 + .000 + .000
+ .000 + .500 + .000
+ .000 + .000 + .500

Eigenvalues are:

Real	Imaginary	Mode
- 85.5753 +	.0000	11
- 21.7350 +	.0000	8
- 17.6775 +	.0000	6
- 8.7462 +	.0000	5
- 1.8009 +	.0000	2

Eigenvector Matrix, T, is:

+ .0256 - .2286 - .0001 - .2761 +1.0000
- .3579 + .1300 - .4998 +1.0000 + .1188
- .7840 - .0068 + .8659 + .0874 + .0165
- .0264 +1.0000 + .0004 - .2207 + .0926
+1.0000 + .1409 +1.0000 + .8483 + .0901

The Modal Controllability Matrix, Inv(T)*G, is:

- .2010 - .0106 + .2010
- .0336 + .4748 + .0334
+ .3333 + .0001 + .1667
- .1458 - .0759 + .1458
- .0427 + .0878 + .0427

y₁ = 0
z₁ = 0
x₃ = x₂
y₃ = -y₂
z₃ = -z₂
y₄ = 0
z₄ = 0

H₃ = H₂
V₃ = -V₂
V₄ = 0

Tetrahedron Longitudinal

$x=(y1,z1,x2,y2,z2,y4,z4);u=(h2,v2,y4)$

Units sec: 4/26/82

Dynamics Matrix F, is:

- 2.500	- .000	+ 1.443	+ .833	+ 2.357	+ 1.666	- 2.357	
- .000	-10.000	+ 4.082	+ 2.357	+ 6.666	- 2.357	+ 3.333	
+ .721	+ 2.041	-**.**	-14.718	- 2.041	+21.651	+ .000	(-118.1694)
+ .416	+ 1.178	-14.718	-51.177	- 1.176	+37.502	+ .000	
+ 1.178	+ 3.333	- 2.041	- 1.176	-21.011	+ .000	+ .000	
+ 1.666	- 2.357	+43.302	+75.004	+ .000	-76.670	+ 2.357	
- 2.357	+ 3.333	+ .000	+ .000	+ .000	+ 2.357	-21.011	

Control Distribution Matrix, G, is:

+ .000	+ .000	+ .000
+ .000	+ .000	+ .000
- .250	+ .000	+ .000
+ .433	+ .000	+ .000
+ .000	+ .500	+ .000
+ .000	+ .000	+ .000
+ .000	+ .000	+ .500

$$x_1 = 0$$

$$x_3 = -x_2$$

$$y_3 = y_2$$

$$z_3 = z_2$$

Eigenvalues are:

Real	Imaginary	Mode
-151.8372	+ .0000	12
- 85.5752	+ .0000	10
- 23.3728	+ .0000	9
- 21.7345	+ .0000	7
- 8.7467	+ .0000	4
- 7.4719	+ .0000	3
- 1.8008	+ .0000	1

$$x_4 = 0$$

$$H_3 = -H_2$$

$$V_3 = V_2$$

$$H_4 = 0$$

Eigenvector Matrix, T, is:

+ .0000	- .0317	+ .0000	+ .1980	- .2629	- .0000	+1.0000
+ .0512	- .0000	- .7309	+ .0000	- .0007	+1.0000	- .0000
- .8659	+ .9673	- .0275	+ .0057	+ .0832	+ .0107	+ .0165
- .5000	- .6753	- .0159	- .1190	+ .8557	+ .0064	+ .0997
- .0193	+ .0188	+ .9998	- .5001	- .1214	+ .2440	+ .0534
+1.0000	+1.0000	+ .0316	- .1091	+1.0000	- .0120	+ .1283
- .0193	- .0376	+1.0000	+1.0000	+ .2425	+ .2441	- .1069

The Modal Controllability Matrix, Inv(T)*G, is:

- .0000	- .0064	- .0032
- .2821	+ .0049	- .0049
- .0000	+ .2826	+ .1413
- .0670	- .3165	+ .3165
+ .2653	- .0460	+ .0460
+ .0002	+ .2069	+ .1035
+ .0741	+ .0507	- .0507

VIBRATION SUPPRESSION IN LARGE SPACE STRUCTURES

T.K. Caughey* and C.J. Goh**
California Institute of Technology
Pasadena, CA 91109

I. INTRODUCTION

The need of active control of large space structures is well-known hence needs no reiteration here. The highly complex and interactive nature of the problem gives rise to numerous difficulties which have been well documented by BALAS (Ref. 1). Due to the inherently high order of the structure and the fact that only a finite number of sensors and actuators is available, the use of modern optimal control theory for vibration suppression purposes seems unjustified as it inevitably encounters the problem of control and observation spillover. More specifically, active control of low frequency modes by such techniques causes intermediate or high frequency modes to become unstable, as demonstrated both in theory and in experiment (see Refs. 2 and 3). Sophisticated compensation techniques can be used to overcome this problem but nevertheless lead to further complication. Another much simpler technique is the use of collocated velocity (rate) feedback control (see Refs. 4 and 5) which guarantee that all modes remain stable. Spillover still exists in this case but rather than being detrimental, can stabilize the uncontrolled and unmodelled modes. However, there still remains a crucial problem, unfortunately ignored by most researchers in this field, namely the interaction of actuator dynamics with the structure. It is thus the central objective of this paper to point out that actuator dynamics, if not properly treated, may give rise to instability. We shall also suggest a couple of ways to overcome this. The analysis will be carried out in the context of collocated feedback control though it can be carried out in terms of optimal control just as well. In the present paper, we shall present only a brief summary of the concepts and theory involved; interested readers may like to refer to Refs. 6 and 7 for further details.

II. NATURE OF THE PROBLEM

A large but finite order (N) vibrating system with collocated rate feedback control can be modelled by a second order equation:

$$\ddot{M}x + D\dot{x} + Kx = -S^T C S \dot{x}$$

*Professor of Applied Mechanics

**Graduate Student

[M is the inertia matrix including the inertia of the sensors and actuators]

where the sensor/actuator (S/A) location matrix S is defined by

$$(S)_{ij} = \begin{cases} 1 & \text{if S/A pair } i \text{ is located at element } j \\ 0 & \text{otherwise} \end{cases} \quad (2)$$

Applying the appropriate orthogonal transformation

$$x = \Phi \xi \quad (3)$$

such that $\Phi^T M \Phi = I$, $\Phi^T D \Phi = \mathcal{D}$, $\Phi^T K \Phi = \Omega$, where \mathcal{D} is in general non-diagonal but diagonally dominant and Ω is diagonal with the square of the modal frequency down the diagonal. Eqn. (1) is reduced to

$$\ddot{\xi} + \mathcal{D} \dot{\xi} + \Omega \xi = -\Phi^T S^T C S \Phi \dot{\xi} = -B \dot{\xi} \quad (4)$$

Thus, the addition of feedback simply modifies the closed loop damping matrix to

$$\tilde{\mathcal{D}} = \mathcal{D} + B \quad (5)$$

It is easy to prove that (see Refs. 6 and 4) if $\tilde{\mathcal{D}}$ and Ω are positive definite matrix, then the system is stable. Furthermore, if the elements of $\tilde{\mathcal{D}}$ are relatively small compared to Ω , then the dynamical behavior of the coupled system is basically dominated by the diagonal elements of $\tilde{\mathcal{D}}$. This can be shown easily using perturbation theory. If we rewrite $\tilde{\mathcal{D}}$ as:

$$\tilde{\mathcal{D}} = \epsilon \tilde{\mathcal{D}}^* \quad (6)$$

where $\tilde{\mathcal{D}}^*$ is of the same order of magnitude as Ω and ϵ is a representative small parameter, then the eigen values of the close loop system is given as the zeroes of

$$\det \begin{bmatrix} (s^2 + \epsilon \tilde{d}_{11}^* s + \omega_1^2) & \epsilon \tilde{d}_{12}^* & \epsilon \tilde{d}_{13}^* & \cdots & \epsilon \tilde{d}_{1N}^* \\ \epsilon \tilde{d}_{21}^* & (s^2 + \epsilon \tilde{d}_{22}^* s + \omega_2^2) & \epsilon \tilde{d}_{23}^* & \cdots & \epsilon \tilde{d}_{2N}^* \\ \vdots & \vdots & \ddots & \ddots & \vdots \\ \epsilon \tilde{d}_{N1}^* & \epsilon \tilde{d}_{N2}^* & \cdots & \cdots & (s^2 + \epsilon \tilde{d}_{NN}^* s + \omega_N^2) \end{bmatrix} = 0$$

$$\text{or } \prod_{i=1}^N (s^2 + \tilde{d}_{ii} s + \omega_i^2) + O(\epsilon^2) = 0 \quad (7)$$

where lower case letters denote elements of corresponding upper case matrix. Hence to 1st order accuracy, the system decoupled into N scalar vibrating system with damping dictated by the diagonal term \tilde{d}_{ij} . Subsequently if N_A S/A pairs are available, we can approximately assign the closed loop poles arbitrarily. One way of doing such is to decide on what the closed loop damping of the first N_A modes are, which is equivalent to prescribing the first N_A diagonal elements of the modal gain matrix B . Thus if we choose the first $N_A \times N_A$ top left corner block of B as

$$B_{11} = \begin{bmatrix} b_1 & & & & \\ & b_2 & & & \\ & & \ddots & & \\ & & & \ddots & \\ 0 & & & & b_{N_A} \end{bmatrix}, \quad b_i > 0 \quad (8)$$

then the gain matrix C can be computed uniquely as

$$C = (\Phi_1^T S^T)^{-1} B_{11} (S \Phi_1)^{-1} \quad (9)$$

$$\text{where } \Phi = N \begin{bmatrix} \Phi_1 & \vdots & \Phi_2 \end{bmatrix} \quad (10)$$

and C is positive definite by virtue of the positive definiteness of B_{11} , the modal gain matrix B must therefore be positive-semi-definite also, and it takes the form

$$B = \Phi^T S^T C S \Phi = \left[\begin{array}{c|c} \begin{array}{c} b_1 \\ \vdots \\ b_{N_A} \end{array} & B_{11} (S\Phi_1)^{-1} (S\Phi_2) \\ \hline (S\Phi_2)^T (S\Phi_1)^{-T} B_{11} & (S\Phi_2)^T (S\Phi_1)^{-T} B_{11} (S\Phi_1)^{-1} (S\Phi_2) \end{array} \right] \quad (11)$$

Note in passing that controllability and observability of the system are equivalent in this case by virtue of the colocation, and is identical to the invertibility of the matrix $(S\Phi_1)$. This is easily achieved by placing the S/A pairs away from the nodes of the controlled modes. In the space structure K is only positive semi-definite. However, if $y^T(D+B)y$ is positive definite for any vector y orthogonal to N_K . $(D+B)Z=0$ for $Z \in N_K$, then the vibrational modes are Liapunov asymptotic stable.

We have in essence furnished a brief review of the theory of collocated rate feedback control. Further details will be found in ref. 5. We shall concern ourselves more with the interaction of actuator dynamics. In practice, the actuators inevitably possess inertia hence cannot be regarded as memoryless devices. This leads to a finite actuator bandwidth. BALAS [ref. 8] argues that by ignoring the fast modes, the actuator dynamics can be ignored if it is sufficiently fast. This argument is questionable since firstly, omittance of fast modes is not justifiable and secondly, no matter how fast the actuator dynamics are, they cannot be faster than all the system modes whose bandwidth eventually become infinite. This is one of the many fallacies which arises in flexible spacecraft control to date, in that we are using finite resources to control an infinite dimensional system and hence ignorance or truncation of the infinite dimensionality is never justifiable.

With the presence of actuator dynamics, eqn. (1) is modified to be:

$$M\ddot{x} + D\dot{x} + Kx = -S^T C z \quad (12)$$

$$I_{N_A} [\ddot{z} + \beta_a \dot{z} + \omega_a^2 z] = \omega_a^2 S \dot{x} \quad (13)$$

Applying the appropriate canonical transformation and letting

$$z = S\Phi \eta \quad , \quad (14)$$

eqns. (12) and (13) are equivalent to

$$\ddot{\xi} + \mathcal{D}\dot{\xi} + \Omega\xi = -B\eta = -\Phi^T S^T C S \Phi \eta \quad (15)$$

$$I_N[\ddot{\eta} + \beta_a \dot{\eta} + \omega_a^2 \eta] = \omega_a^2 \dot{\xi} \quad (16)$$

As before, if the damping matrices \mathcal{D} and \mathcal{B} are relatively small, we can regard, to first order accuracy, the coupled system as N decoupled scalar system. This is a useful concept which will enable us to investigate instability via classical control technique. A typical reduced scalar system is governed by

$$\ddot{\xi}_i + \beta_i \dot{\xi}_i + \omega_i^2 \xi_i = -b_i \eta_i \quad (17)$$

$$\ddot{\eta}_i + \beta_a \dot{\eta}_i + \omega_a^2 (\eta_i - \dot{\xi}_i) = 0 \quad (18)$$

For notational convenience we shall discard the index i from ξ_i and η_i . Henceforth the symbols ξ and η are regarded as scalar quantities until otherwise specified. By taking Laplace Transform, the combined system-actuator dynamics can be shown easily to be governed by the characteristic equation:

$$(s^2 + \beta_i s + \omega_i^2)(s^2 + \beta_a s + \omega_a^2) + b_i \omega_a^2 s = 0 \quad (19)$$

Using conventional Nyquist diagram methods, it can be shown that, for stability, the scalar gain b_i has to be upper and lower bounded by

$$\gamma_L < b_i < \gamma_U \quad (20)$$

where

$$\begin{aligned} \gamma_U = & 4\zeta_n \zeta_a (\zeta_n \omega_i + \zeta_a \omega_a) \left(\frac{\omega_i}{\omega_a}\right) + (\zeta_a \omega_a - \zeta_n \omega_i) \left[1 - \left(\frac{\omega_i}{\omega_a}\right)^2\right] \\ & + (\zeta_n \omega_i + \zeta_a \omega_a) \sqrt{\left[1 - \left(\frac{\omega_i}{\omega_a}\right)^2\right]^2 + 16 \zeta_n^2 \zeta_a^2 \left(\frac{\omega_i}{\omega_a}\right)^2 + 8 \zeta_n \zeta_a \left(\frac{\omega_i}{\omega_a}\right) \left[1 + \left(\frac{\omega_i}{\omega_a}\right)^2\right]} \quad (21) \end{aligned}$$

$$\begin{aligned} \gamma_L = & 4\zeta_n \zeta_a (\zeta_n \omega_i + \zeta_a \omega_a) \left(\frac{\omega_i}{\omega_a}\right) + (\zeta_a \omega_a - \zeta_n \omega_i) \left[1 - \left(\frac{\omega_i}{\omega_a}\right)^2\right] \\ & - (\zeta_n \omega_i + \zeta_a \omega_a) \sqrt{\left[1 - \left(\frac{\omega_i}{\omega_a}\right)^2\right]^2 + 16 \zeta_n^2 \zeta_a^2 \left(\frac{\omega_i}{\omega_a}\right)^2 + 8 \zeta_n \zeta_a \left(\frac{\omega_i}{\omega_a}\right) \left[1 + \left(\frac{\omega_i}{\omega_a}\right)^2\right]} \quad (22) \end{aligned}$$

These are fairly messy expressions but nevertheless can be slightly simplified if terms in $O(\zeta_n^2)$ are neglected. A typical plot of these bounds as a function of ω_i with $\zeta_a, \zeta_n, \omega_a$ as fixed parameters is shown in Fig. 1. For non-trivial ζ_n , the shaded area defines the stable region, i.e., for any frequency mode of frequency ω_i^* to be stable, the gain (positive or negative) is required to be bounded by

$$\gamma_L(\omega_i^*) < b_i(\omega_i^*) < \gamma_U(\omega_i^*) \quad , \quad (23)$$

For trivial ζ_n , the stability boundaries are shown by broken lines, part of which coincides with the ω_i axis. They also partition the stability region [for a system of non-trivial ζ_n] into four sectors. We shall defer the significance of these sectors till later but as ζ_n decreases, the stability region shrinks correspondingly. It is now easy to see why instability can occur. Suppose in the process of designing the gain matrix C , large values of scalar gain b_i 's occur on the diagonal of B , so much so that it lies outside the stability boundary, then the corresponding mode will result in instability. Such large b_i can result in several ways, e.g., the prescribed damping is too high, the matrix $(S\Phi_1)$ is near singular due to a poor choice of S/A location, or simply because the natural damping is so low that the stability region is not large enough to accommodate even reasonably small gain. One has to bear in mind that this argument is only accurate to first order since coupling terms have been ignored, nevertheless it works pretty well even in actual simulation. It is also obvious from Fig. 1 that those modes whose frequencies are around ω_a to roughly $2\omega_a$ are most vulnerable to instability as the stability boundary (γ_U) is relatively low in this range [we shall call it the "critical frequency range" henceforth]. For zero ζ_n and positive gain, it is also true that all modes with frequency greater than ω_a are unconditionally unstable. Fortunately actual ζ_n occurring in space is not zero even though it may be very small indeed. The smaller ζ_n is, the larger is the critical frequency range and the more likely instability is to occur. In any case the resulting closed loop damping of all higher modes will be lower than their natural damping. This can be explained, qualitatively in terms of root locus diagram but instead we shall provide a more quantitative analysis.

Suppose we equate the characteristic equation (19) to the closed form expression

$$(s^2 + \beta_p s + \omega_p^2)(s^2 + \beta_q s + \omega_q^2) = 0 \quad (24)$$

If we expand both eqns. (19) and (24) and equate coefficients in powers of s , four algebraic equations will result which enable us to solve for the four unknown $\gamma, \beta_p, \omega_p, \omega_q$ with β_p prescribed a-priorily. After some algebra it can be shown that the gain corresponding to a prescribed damping β_p is

$$\gamma = \frac{-B \pm \sqrt{B^2 - 4AC}}{2A} \quad , \quad B^2 - 4AC > 0 \quad (25)$$

where

$$A = \omega_a^4 \quad (26)$$

$$B = -\omega_a^2(\beta_p G_1 + \beta_q G_1 - 2G_2) \quad (27)$$

$$C = (\beta_p G_1 - G_2)(\beta_q G_1 - G_2) + (\beta_p - \beta_q)^2 \omega_i^2 \omega_a^2 \quad (28)$$

$$\beta_q = \beta_i + \beta_a - \beta_p \quad (29)$$

$$G_1 = \omega_i^2 + \omega_a^2 + \beta_i \beta_a - \beta_p \beta_q \quad (30)$$

$$G_2 = \beta_i \omega_a^2 + \beta_a \omega_i^2 \quad (31)$$

Since ω_p is expected to be close to ω_i for sufficiently low gain, the damping β_p can be related to the prescribed damping ratio ζ_p approximately by

$$\beta_p = 2 \zeta_p \omega_i \quad (32)$$

The locus of γ vs ω_1 for fixed ζ_p are plotted in Fig. 2. For $\zeta_p = 0\%$, the locus coincide with the stability boundaries. For $\zeta_p = \zeta_n$, the locus coincide with the stability boundary for $\zeta_n = 0$ and within each of the 4 sectors divided by this locus

In Sector I, $\gamma > 0$, $\zeta_p > 0$

In Sector II, $\gamma > 0$, $\zeta_p < 0$

In Sector III, $\gamma < 0$, $\zeta_p < 0$

In Sector IV, $\gamma < 0$, $\zeta_p > 0$

We also see that as ω_1 gets closer to ω_a , the maximum attainable damping gets smaller. Furthermore for $\omega_1 > \omega_a$, less than natural damping will always result if positive gain is used. Even if negative gain is used, very high gain is required just to achieve reasonable low damping.

Now that sufficient physical insight to the problem has been gathered, we shall consider ways of overcoming these difficulties.

III. RATE FEEDBACK WITH LEAD COMPENSATION

Lead compensation has been used extensively in classical control theory to increase the phase margin of marginally stable system, but is usually applicable for single-input-single-output system whereby scalar transfer junction is realizable. In our multi-dimensional case, however, scalar lead compensation is generalized to vector lead compensation, again by involving the argument that the N^{th} order coupled system can be approximated by N decoupled scalar systems. There is no rigorous theoretical justification to such but we only know that it works fairly well in actual simulation.

The concept of lead compensation as applied to scalar system is well-known hence needs no elaboration here. In particular it works very well in this case because of the highly resonant nature of the system (due to small ζ_n). The increase in gain by compensation only leads to very small change of n cross-over frequency but the corresponding increase in phase is substantially high enough to reverse the phase margin of critical modes from negative to positive. A very detailed discussion of this can be found in [6] by means of Bode's diagram argument. We shall only generalize the scalar argument into the multivariate case. With the inclusion of a vector lead compensation network, the combined dynamics are modified to

$$I_N \ddot{\xi} + D \dot{\xi} + \Omega \xi = - \Phi^T S^T C \eta \quad \xi \in R^N \quad (33)$$

$$I_{N_A} [\ddot{\eta} + \beta_a \dot{\eta} + \omega_a^2 \eta] = I_{N_A} \omega_a^2 \dot{\rho} \quad \eta, \rho \in R^{N_A} \quad (34)$$

$$I_{N_A} [T_1 \dot{\rho} + \rho] = T_2 (S \Phi \dot{\xi}) + (S \Phi \xi) \quad T_1, T_2 \in R, T_1 < T_2 \quad (35)$$

Conceivably, T_1 and T_2 can be generalized to be positive definite matrices for perhaps better performance but for the moment we shall assume them to be scalars. The choice of T_1 and T_2 is a debatable art, the complete behavior of eqns. (33) - (35) is extremely complicated; the best we can do is to guess by scalar inference. Intuitively, we would like the increase in phase shift to start from $\omega_1 = \omega_a$, hence T_2 is chosen to be around $T_2 = \frac{T_1}{\omega_a}$. The choice of T_1

is related to the size of the increase in phase shift, the larger T_1 is the more the increase. If T_1 is too small, then the increase in gain will be too high but if T_1 is too large, the increase in phase shift will not be sufficient to create positive phase margin for the critical modes. As a good rule of thumb, the ratio $\frac{T_2}{T_1}$ is chosen to be between 5 and 10.

In section V we shall demonstrate by simulation the feasibility of this technique.

IV. POSITIVE POSITION FEEDBACK WITH TUNING FILTERS

As before, we shall look at the concept of positive position feedback from the scalar point of view. Here again regard ξ and η as scalar representing the states of the system and the actuator respectively, as described by

$$\ddot{\xi} + \beta_i \dot{\xi} + \omega_i^2 (\xi - b_i \eta) = 0 \quad b_i > 0 \quad (36)$$

$$\ddot{\eta} + \beta_a \dot{\eta} + \omega_a^2 (\eta - \xi) = 0 \quad (37)$$

which has the characteristic equation

$$(s^2 + \beta_i s + \omega_i^2) (s^2 + \beta_a s + \omega_a^2) - b_i \omega_i^2 \omega_a^2 = 0 \quad (38)$$

It is trivial to show that a sufficient and necessary condition for stability in this case is

$$b_i < 1 \quad (39)$$

which is also the stability boundary. This obviously is much simpler than the stability boundary of the rate feedback case. Furthermore, it has the nice property that it is independent of all the system and actuator's dynamics! To examine the closed-loop damping characteristic of position feedback, we compute the eigen values of eqn. (38) and plot the real part [represent damping] of the eigen values vs ω_i for fixed b_i , ζ_a , ζ_i , and ω_a . The resulting closed-loop damping characteristic is as shown in Fig. 3. It can be shown [see ref. 7] that the characteristic consists of two parts, the upper and the lower locus which correspond to the actuator and the system, respectively. For sufficiently low gain, the system locus exhibits a resonance peak to the left of ω_a . For higher gain the two locus meet at a cusp which can be shown to be at approximately

$(\omega_a \sqrt{1 - \zeta_a^2}, \frac{\omega_a}{2} [\zeta_a + \zeta_i \sqrt{1 - \zeta_a^2}])$. Thus for modes near the resonance peak, the closed-loop damping can be many times that of the natural damping [the lower asymptotes] while modes away from the peak only have slightly higher than natural damping.

It is such a property that motivates us to the use of "Tuning Filters". Basically these are band-limited electronic devices with dynamics similar to that of the actuator but with a frequency "tuned" to the controlled mode frequency in order to enhance its closed loop damping.

Suppose that there are as many filters as controlled modes, then the damping and frequency of each filter is carefully chosen so that its corresponding controlled frequency lies near the resonance peak [or the cusp].

The overall system is now described by

$$\text{System} \quad M\ddot{x} + D\dot{x} + Kx = S^T z \quad (40)$$

$$\text{Filters} \quad I_{N_A} [\ddot{y}_i + 2\zeta_f \omega_{f_i} \dot{y}_i + \omega_{f_i}^2 y_i] = \omega_{f_i} C_i^{1/2} Sx, \quad i=1, \dots, N_f \quad (41)$$

$$\text{Actuator} \quad \ddot{z} + \beta_a \dot{z} + \omega_a^2 z = \sum_{i=1}^{N_f} \omega_{f_i} C_i^{T/2} [\ddot{y}_i + \beta_a \dot{y}_i + \omega_a^2 y_i] \quad (42)$$

$x \in \mathbb{R}^N; y_i, z \in \mathbb{R}^{N_A}$

$$\text{where} \quad C_i^{T/2} C_i^{1/2} = C_i \quad (43)$$

is the gain matrix for the i^{th} filter which has natural frequency ω_{f_i} and damping ratio ζ_f the same for all filters.

Eqn. (42) implies that:

$$(i) \quad \lim_{t \rightarrow \infty} z = \sum_{i=1}^{N_f} \omega_{f_i} C_i^{T/2} y_i$$

$$(ii) \quad \text{If } z(0) = \dot{z}(0) = y_i(0) = \dot{y}_i(0) = 0 \quad \forall i$$

$$z(t) \equiv \sum_{i=1}^{N_f} \omega_{f_i} C_i^{T/2} y_i \quad (44)$$

so for sufficiently large β_a , z converges to the RHS of (44) rapidly and consequently the actuator dynamics falls out of the picture completely. Equations (40)-(43) just reduce to, after appropriate canonical transformation,

$$\text{System} \quad \ddot{\xi} + D\xi + \Omega\xi = \Phi^T S^T \left[\sum_{i=1}^{N_f} \omega_{f_i} C_i^{T/2} y_i \right] \quad (45)$$

$$\text{Filter} \quad I_{N_A} [\ddot{y}_i + 2\zeta_f \omega_{f_i} \dot{y}_i + \omega_{f_i}^2 y_i] = \omega_{f_i} C_i^{1/2} S\Phi\xi, \quad i=1, \dots, N_f \quad (46)$$

or

$$\begin{aligned}
 & I_{N+N_A} \times N_f \begin{bmatrix} \xi \\ \vdots \\ y_1 \\ \vdots \\ \vdots \\ y_{N_f} \end{bmatrix} + \begin{bmatrix} \mathcal{D} & \dots & 0 \\ 2\zeta_f \omega_{f_1} I_{N_A} & & \vdots \\ \vdots & \ddots & \vdots \\ 0 & & 2\zeta_f \omega_{f_{N_f}} I_{N_A} \end{bmatrix} \begin{bmatrix} \xi \\ \vdots \\ y_1 \\ \vdots \\ \vdots \\ y_{N_f} \end{bmatrix} \\
 & + \begin{bmatrix} \Omega & -E_1^T \omega_{f_1} & \dots & -E_{N_f}^T \omega_{f_{N_f}} \\ -E_1 \omega_{f_1} & \omega_{f_1}^2 I_{N_A} & & 0 \\ \vdots & & \ddots & \vdots \\ -E_{N_f} \omega_{f_{N_f}} & 0 & \dots & \omega_{f_{N_f}}^2 I_{N_A} \end{bmatrix} \begin{bmatrix} \xi \\ y_1 \\ \vdots \\ y_{N_f} \end{bmatrix} = 0 \tag{47}
 \end{aligned}$$

where $E_i = C_i^{1/2} S\Phi$ (48)

The symmetrical structure now enables us to prove for conditional stability as in the following theorem.

Theorem 1: The combined system-filters dynamics are stable if

$$\Omega - \sum_{i=1}^{N_f} (1 + \epsilon_i) B_i \text{ is positive definite} \tag{49}$$

where

$$B_i = \Phi^T S^T C_i S\Phi \tag{50}$$

and ϵ_i are some arbitrarily small positive quantities.

Proof: Define the Liapunov function

$$V = \frac{1}{2} [\dot{\xi}^T \dot{\xi} + \sum_{i=1}^{N_f} \dot{y}_i^T \dot{y}_i] + \frac{1}{2} [\xi^T \Omega \xi + \sum_{i=1}^{N_f} [\omega_{f_i}^2 y_i^T y_i - 2\xi^T E_i^T \omega_{f_i} y_i]] \quad (51)$$

Cauchy Schwartz inequality implies that

$$2\xi^T E_i^T \omega_{f_i} y_i < (1 + \epsilon_i) \xi^T E_i^T E_i \xi + \frac{\omega_{f_i}^2}{(1+\epsilon_i)} y_i^T y_i \quad (52)$$

hence

$$V > \frac{1}{2} [\dot{\xi}^T \dot{\xi} + \sum_{i=1}^{N_f} \dot{y}_i^T \dot{y}_i] + \frac{1}{2} [\xi^T (\Omega - \sum_{i=1}^{N_f} (1 + \epsilon_i) B_i) \xi] + \frac{1}{2} \sum_{i=1}^{N_f} \omega_{f_i}^2 \frac{\epsilon_i}{1+\epsilon_i} y_i^T y_i \quad (53)$$

Differentiating eqn. (51) with respect to time, we obtain

$$\dot{V} = -\dot{\xi}^T D \dot{\xi} - \sum_{i=1}^{N_f} 2\zeta_{f_i} \omega_{f_i} \dot{y}_i^T \dot{y}_i \leq 0 \quad (54)$$

$$\dot{V} \equiv 0 \quad \text{iff} \quad \dot{\xi} = 0, \dot{y}_i = 0 \quad \forall_i$$

Thus if the assumption is true, V is strictly positive with \dot{V} negative semi-definite and hence the combined dynamics is stable by invoking the well-known Liapunov direct method.

It can be shown further [see ref. 7] that a both sufficient and necessary condition for stability is that the matrix P in eqn. (47) be positive definite.

To specify EXACT damping for all the controlled modes will result in solving an unmanageably large set of simultaneous non-linear algebraic equations. For not so large prescribed damping, however, we can ignore the coupling effects from the uncontrolled modes and the first N_A modes can be reduced to N_A decoupled scalar systems with small perturbation error. Suppose that one filter is available for each controlled mode, then the characteristic equation for the i^{th} mode is, approximately

$$(s^2 + \beta_i s + \omega_i^2)(s^2 + \beta_{f_i} s + \omega_{f_i}^2) - b_i \omega_i^2 \omega_{f_i}^2 = 0 \quad (55)$$

Consequently if the closed-loop damping β_{f_i} is specified, the four unknowns $\omega_{q_i}, \omega_{p_i}, \beta_{q_i}, b_i$ can be computed by comparing eqn. (55) with the closed-loop expression

$$(s^2 + \beta_{p_i} s + \omega_{p_i}^2)(s^2 + \beta_{q_i} s + \omega_{q_i}^2) = 0 \quad (56)$$

After some algebra, the solutions are:

$$\beta_{q_i} = \beta_i + \beta_{f_i} - \beta_{p_i} \quad (57)$$

$$G_{1_i} = \omega_i^2 + \omega_{f_i}^2 + \beta_i \beta_{f_i} - \beta_{p_i} \beta_{q_i} \quad (58)$$

$$G_{2_i} = \beta_i \omega_{f_i}^2 + \beta_{f_i} \omega_i^2 \quad (59)$$

$$\omega_{p_i}^2 = (G_{2_i} - \beta_{p_i} G_{1_i}) / (\beta_{q_i} - \beta_{p_i}) \quad (60)$$

$$\omega_{q_i}^2 = (G_{2_i} - \beta_{q_i} G_{1_i}) / (\beta_{p_i} - \beta_{q_i}) \quad (61)$$

$$b_i = 1 - \left[\frac{\omega_{p_i} \omega_{q_i}}{\omega_i \omega_{f_i}} \right]^2 \quad (62)$$

Once the scalar gain b_i for the i^{th} controlled mode is obtained, the corresponding gain matrix C_i can be computed from

$$C_i = (\Phi_1^T S^T)^{-1} B_{11} (S \Phi_1)^{-1} = (\Phi_1^T S^T)^{-1} \begin{bmatrix} 0 & & & 0 \\ & \ddots & & \\ & & 0 & \\ & & & \omega_i^2 b_i \\ 0 & & & & \ddots & \\ & & & & & 0 \end{bmatrix} (S \Phi_1)^{-1} \quad (63)$$

The gains for the uncontrolled modes will subsequently be by-products of these b_i 's.

Hitherto, the choice of ζ_f and ω_{f_i} has remained arbitrary. However, they can be chosen such that the following optimum criteria are achieved.

(i) For a fixed prescribed closed-loop damping, the corresponding scalar gain is to be as small as possible.

(ii) The design should be robust in the sense that slight change in the modal structure will not cause high gain to occur which consequently causes instability.

(iii) If instability ever occurred, we prefer it to occur in the filter [which has inherent saturation characteristics] and not in the system. In other words, crashworthiness is desired.

The first criterion can be easily achieved by designing ω_{f_i} and ζ_f such that the damping for a controlled mode be exactly on the cusp of the damping characteristic. However, this is not a very safe thing to do since slight change in the controlled mode frequency is likely to cause high gain (and consequently instability) to occur. Thus the first and second criteria are unfortunately in conflict. A reasonable compromise is to place the damping of the mode 20% below the cusp to allow for some lateral clearance. The third criterion can be achieved by placing the cusp slightly to the left of the controlled frequencies. This can be explained very simply by means of Root Locus diagram as shown in Fig. 4(i),(ii) and (iii).

With these facts in mind, a reasonably "optimum" choice of the filter's characteristics can be shown to be

$$\zeta_f = \left[\frac{(1.02 \zeta_p)^2}{0.16 + (1.02 \zeta_p)^2} \right]^{1/2} \quad (64)$$

$$\omega_{f_i} = \frac{\omega_i}{1.02 \sqrt{1 - \zeta_f^2}} \quad (65)$$

Note in passing that even though $b_i < 1$ is required for stability, we in general want to keep b_i to be less than about 0.8 to avoid the degeneration into 2 real roots as shown in Fig. 4, because then one root will be less stable than the other.

Lastly, we have so far assumed that a full complement of filters are available; this is in general not necessary. If less than N_A filters are available, we would use one filter each for the lower modes since they are more vulnerable to instability, and several higher controlled modes will share the remaining filters. The damping specification still works out the same except that now we expect slightly poorer performance since we are using less resources to do more work.

IV. NUMERICAL SIMULATION AND RESULTS

For illustration, we shall consider the control of a simply supported discrete shear beam of N elements. The corresponding mass and stiffness matrix take the form

$$M = m_0 I_N \quad (66)$$

$$K = \begin{bmatrix} 2 & -1 & 0 & 0 & \dots & 0 \\ -1 & 2 & -1 & 0 & & \vdots \\ \vdots & -1 & 2 & -1 & & \vdots \\ \vdots & \vdots & & \ddots & & -1 \\ 0 & \dots & -1 & & & 2 \end{bmatrix} \quad (67)$$

We do not know the exact form of the damping matrix D but do know that the canonical damping matrix \mathcal{D} is diagonally dominant, so for simulation purpose we shall assume that

$$(\mathcal{D})_{ij} = 2 \zeta_n \omega_i \delta_{ij} \quad (68)$$

where ω_i is the natural frequencies of the modes, and is easily shown to be

$$\omega_i = \frac{2}{\sqrt{m_0}} \sin \frac{\pi i}{2(N+1)} \quad , \quad i=1, \dots, N \quad (69)$$

with corresponding modal matrix given by

$$(\Phi)_{ij} = \sqrt{\frac{2}{N+1}} \sin \frac{ij\pi}{(N+1)} \quad , \quad i, j = 1, \dots, N, \quad (70)$$

As we would like the first N_A modes to decay at a same rate (as opposed to having the same damping ratio) we shall prescribe an approximate closed-loop damping ratio of ζ_p to the first mode, and then set the damping of all controlled modes to be the same as the first, i.e.,

$$\beta_{p,i} = 2 \zeta_p \omega_i \quad , \quad i=1, \dots, N_A \quad (71)$$

For comparison purposes, we shall carry out simulation for each of the four following cases. In each case, the common parameters are $N=20$, $N_A = 4$, S/A location at $\{3,8,13,19\}$, $\zeta_n = 0.01$, $\zeta_p = 0.3$, $m_0=0.25$.

Case 1: Colocated rate feedback, no actuator dynamics present, feedback gain computed according to eqns. (8) and (9). The closed-loop damping and frequency for each mode are computed from the eigen values of the system in eqn. (4).

Case 2: Colocated rate feedback with actuator dynamics given by $\omega_a = 1.0$, $\zeta_a = 0.7$; No compensation; The feedback gains are the same as in Case 1; the closed-loop damping and frequency are computed from the eigen values of the system in eqns. (15)-(16).

Case 3: Colocated rate feedback with same actuator dynamics as Case 2; compensation with $T_1 = 0.2$, and $T_2 = 1.0$ is included; the feedback gains are the same as in Case 1 and 2; the closed-loop damping and frequency are computed from the eigen values of the system in eqns. (33)-(35).

Case 4. Colocated positive position feedback with actuator dynamics eliminated, 4 tuning filters are used to control first 4 modes; the filter's characteristics are computed from equations (64)-(65); the closed-loop damping and frequency are computed from the eigen values of the system in eqns, (45)-(46).

The outcome of these simulations are tabulated in Tables 1 and 2.

The outcome of the simulations can be summarized by the following points:

(1) In Case 1 where actuator dynamics are absent, colocated rate feedback control works very well and the controlled modes closed-loop damping is fairly close to the prescribed value. Furthermore, all uncontrolled [and expectedly, unmodelled] modes result in higher than natural damping of 1%.

(2) In Case 2 where actuator dynamics are included, we found that the 4th, 5th and 6th modes are unstable. If the scalar gains for these modes are plotted onto Fig. 1, they are found to lie outside the stability region. Hence, this justifies the fact that we can predict stability of a higher order coupled system just by looking at the diagonal elements of β , at least up to first order accuracy anyway. Furthermore, the uncontrolled modes are found to have less than natural closed-loop damping, again consistent with our previous theory.

(3) In Case 3, a lead compensation network is used to raise the phase margins of the unstable modes and it was found that all modes which are previously unstable are now stable. Furthermore, the controlled modes also result in substantially higher damping than the uncompensated case. Unfortunately, this is upset by the decrease in damping of the higher uncontrolled modes,

(4) In Case 4 where positive position feedback with 4 tuning filters is used, the closed-loop performance surpasses the previous case significantly. The closed-loop damping of the first mode is slightly less than specified [within 6% anyway] but all 4 controlled modes have fairly uniform damping. Better still, all uncontrolled [and expectedly, unmodelled] modes result in higher than natural damping.

In addition to what has been observed, position feedback has several advantages over rate feedback as summarized below;

Rate Feedback with Compensation	Position Feedback with Tuning Filters
1. No theorem can be proven to guarantee global stability.	Theorem pertaining to conditional global stability can be proven.
2. Stability is highly dependent on the natural damping of the structure, which remains quite uncertain.	Stability is almost independent of any small natural damping, thus a priori design of the control needs no knowledge of the natural damping.
3. Maximum attainable closed-loop damping is limited depending on the stability boundary.	Maximum attainable damping is, at least in principle, much higher. The resonance peak of the filters damping characteristics is responsible for this.
4. Uncontrolled and unmodelled modes result in lower than natural damping.	Uncontrolled and unmodelled modes result in higher than natural damping.
5. Instability, if ever exists, occurs in the intermediate uncontrolled modes.	Instability can only occur in ill-designed filters.
6. Requires rate sensing.	Requires position (relative) sensing.
7. Requires accurate knowledge of structure than is available in practice.	Only accurate knowledge required is the rigid body mode, which is nevertheless trivial.

V. CONCLUDING REMARKS

In retrospect, the problem of vibration suppression in large space structure has been a complex one, in view of the highly complicated and interactive structure and the vast number of design parameters to be decided upon. In this paper, we specifically address the problem of potential instability caused by actuator dynamics and two ways of overcoming it. Due to restriction in space allocation, we can only present a brief outline of the theory but any missing details can be found in refs. 6 and 7. It is hoped that this paper will stimulate future research to improve existing techniques and dig out finer details which we may have unfortunately neglected.

REFERENCES

1. BALAS, M. J., "Some Trends in Large Space Structure Control Theory: Fondest Hopes; Wildest Dreams," Proc. Joint Automatic Control Conf., Denver, Col., June 17-21, 1979, pp 42-55.
2. BALAS, M. J., "Active Control of Flexible Structures," J. Optimization Theory and Applications, Vol. 25, July 1978, pp 415-436.
3. SCHAECHTER, D. B., "Hardware Demonstration of Flexible Beam Control," J. Guidance and Control, Vol. 5, No. 1, Jan., 1982, pp 48-53.
4. BALAS, M. J., "Direct Velocity Feedback Control of Large Space Structures," J. Guidance and Control, Vol. 2, No. 3, 1979, pp 252-253.
5. CHEN, C. L., "Direct Output Feedback Control of Large Flexible Spacecraft," unpublished Ph.D. thesis, California Institute of Technology, 1982.
6. CAUGHEY, T. K., GOH, C. J., CHEN, C. L., "On Stability Problem Caused by Finite Actuator Dynamics in the Colocated Control of Large Space Structure," in preparation.
7. CAUGHEY, T. K. and GOH, C. J., "Position Feedback Control in the Vibration Suppression of Large Space Structure," in preparation.
8. BALAS, M. J., "Observation Stabilization of Singularly Perturbed Systems," J. Guidance and Control, Vol. 1, No. 1, 1978, pp 93-95.

TABLE I

Mode	Open loop freq.	Scalar gain B_{ii}	Case 1 No Actuator Dynamics			Case 2 Actuator Dynamics $\omega_a=1.0$ $\zeta_a=0.7$		
			C-L	C-L	C-L	C-L	C-L	C-L
			damping	freq.	$\zeta(\%)$	damping	freq.	$\zeta(\%)$
1	0.299	0.1794	-0.0944	0.287	31.28	-0.1105	0.345	30.51
2	0.596	0.1794	-0.0977	0.597	16.16	-0.0468	0.673	6.94
3	0.890	0.1794	-0.1001	0.902	11.03	-0.0127	0.951	1.33
4	1.179	0.1794	-0.1020	1.179	8.62	+0.00158	1.227	-0.13**
5	1.461	0.1816	-0.1085	1.462	7.40	+0.00355	1.494	-0.24**
6	1.736	0.2616	-0.1612	1.732	9.27	+0.00789	1.766	-0.45**
7	2.000	0.2203	-0.1307	1.989	6.56	-0.0003	2.018	0.02
8	2.253	0.0692	-0.0544	2.247	2.42	-0.0169	2.251	0.75
9	2.494	0.2150	-0.1376	2.488	5.52	-0.0107	2.503	0.43
10	2.721	0.1312	-0.0932	2.721	3.42	-0.0196	2.725	0.72
11	2.932	0.1245	-0.0931	2.924	3.18	-0.0229	2.935	0.78
12	3.127	0.1336	-0.0996	3.129	3.18	-0.0252	3.130	0.80
13	3.305	0.0735	-0.0635	3.314	1.92	-0.0301	3.306	0.91
14	3.464	0.0244	-0.2215	3.485	6.35	-0.0254	3.468	0.73
15	3.604	0.0220	-0.1309	3.551	3.68	-0.0281	3.607	0.78
16	3.723	0.1702	-0.1272	3.708	3.43	-0.0315	3.726	0.85
17	3.822	0.3004	-0.1823	3.779	4.82	-0.0285	3.826	0.75
18	3.900	0.1696	-0.0880	3.853	2.28	-0.0336	3.901	0.86
19	3.955	0.1493	-0.1012	3.914	2.59	-0.0350	3.957	0.88
20	3.989	0.1560	-0.0962	3.963	2.43	-0.0352	3.990	0.88
			Actuator 1	-0.6367	0.518	77.55		
			Actuator 2	-0.7310	0.476	83.78		
			Actuator 3	-0.7208	0.534	80.33		
			Actuator 4	-0.7263	0.625	75.78		

** Unstable mode

$\zeta_n=1\%$ in all cases

Table 2

Case 3, Compensated Rate Feedback			Case 4, Positive Position Feedback			
$T_2=1.0$, $T_1=0.2$, Compensator roots are -5.202 , -5.141 , -5.135 , -5.079 .			$\zeta_f=0.6076$			
			$b_1 = 0.3430$			
			$b_2 = 0.2288$			
			$b_3 = 0.1639$			
			$b_4 = 0.1255$			
			$\omega_{f1}=0.369$			
			$\omega_{f2}=0.736$			
			$\omega_{f3}=1.099$			
			$\omega_{f4}=1.455$			
C-L damping	C-L frequency	C-L $\zeta(\%)$	C-L damping	C-L frequency	C-L $\zeta(\%)$	
Actuators			Filters			
-0.5572	0.676	63.58	-0.1396	0.249	48.85	
-0.6530	0.651	70.82	-0.3565	0.508	57.47	
-0.5892	0.585	70.94	-0.5523	0.746	59.50	
-0.5799	0.604	69.25	-0.7972	1.093	58.92	
Mode						
1	-0.1111	0.303	34.45	-0.0875	0.296	28.389
2	-0.0978	0.660	14.65	-0.0931	0.584	15.742
3	-0.0505	0.964	5.23	-0.0964	0.883	10.854
4	-0.0359	1.252	2.86	-0.0918	1.158	7.898
5	-0.0226	1.523	1.49	-0.0365	1.473	2.478
6	-0.0164	1.809	0.91	-0.0220	1.742	1.263
7	-0.0136	2.055	0.66	-0.0218	2.001	1.091
8	-0.0190	2.269	0.84	-0.0242	2.255	1.072
9	-0.0143	2.533	0.57	-0.0260	2.495	1.042
10	-0.0202	2.742	0.74	-0.0279	2.722	1.024
11	-0.0221	2.950	0.75	-0.0302	2.934	1.030
12	-0.0239	3.144	0.76	-0.0336	3.131	1.073
13	-0.0294	3.313	0.89	-0.0334	3.306	1.010
14	-0.0220	3.490	0.63	-0.0350	3.465	1.011
15	-0.0231	3.627	0.64	-0.0364	3.604	1.010
16	-0.0277	3.740	0.74	-0.0377	3.725	1.013
17	-0.0202	3.851	0.53	-0.0387	3.823	1.013
18	-0.0271	3.916	0.69	-0.0394	3.901	1.010
19	-0.0302	3.969	0.76	-0.0398	3.956	1.006
20	-0.0293	4.003	0.73	-0.0403	3.990	1.010

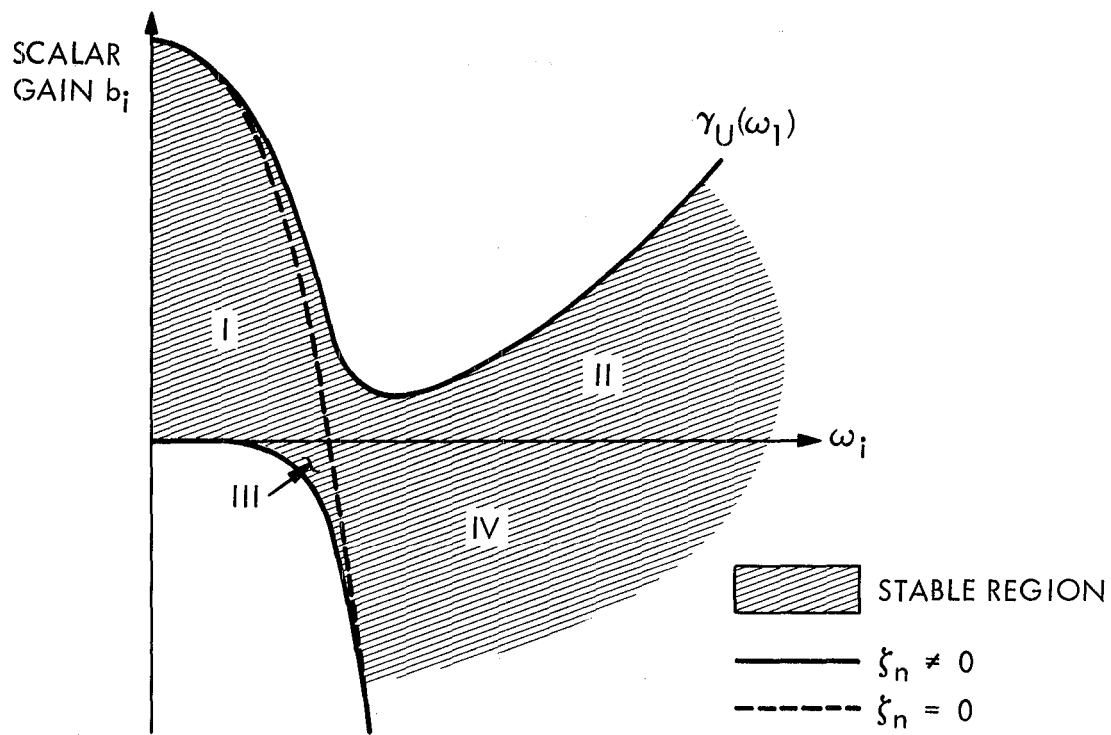


Figure 1. Stability boundary for scalar rate feedback system.
 $\omega_a = 1.0, \zeta_a = 0.7, \zeta_n = 0.01, \beta_p = 2\zeta_p\omega_i$

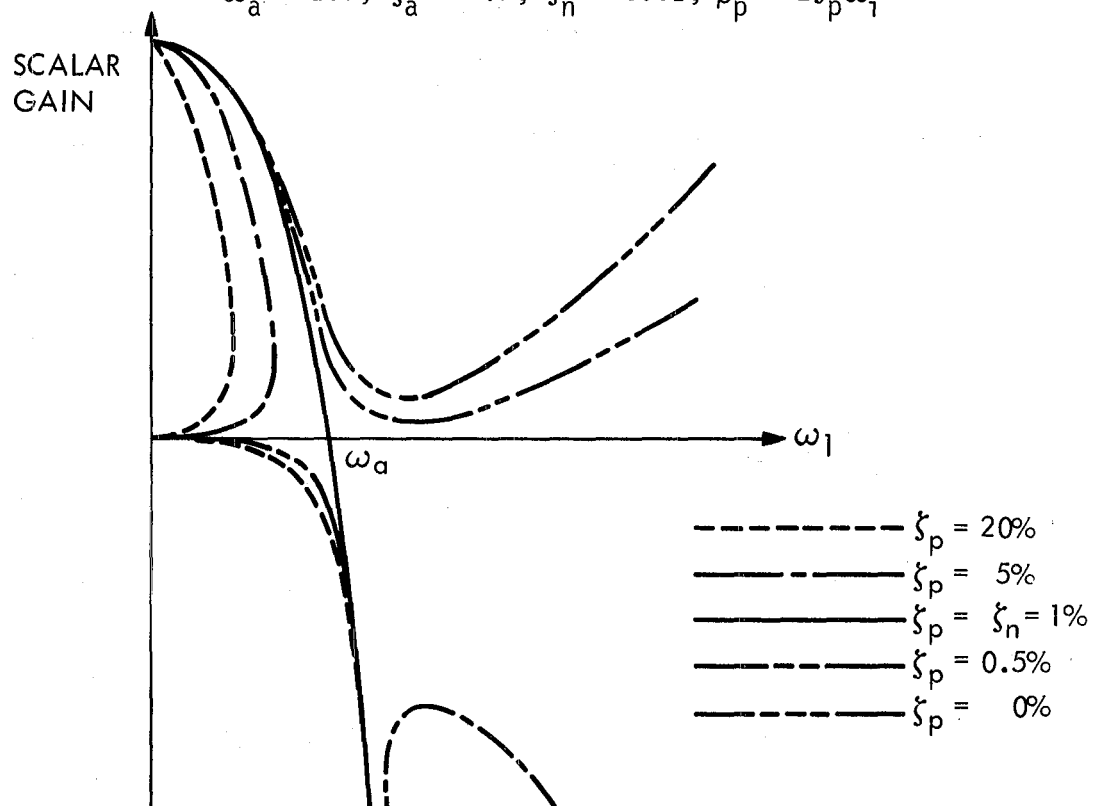


Figure 2. Closed-loop gain characteristic for scalar rate feedback system.

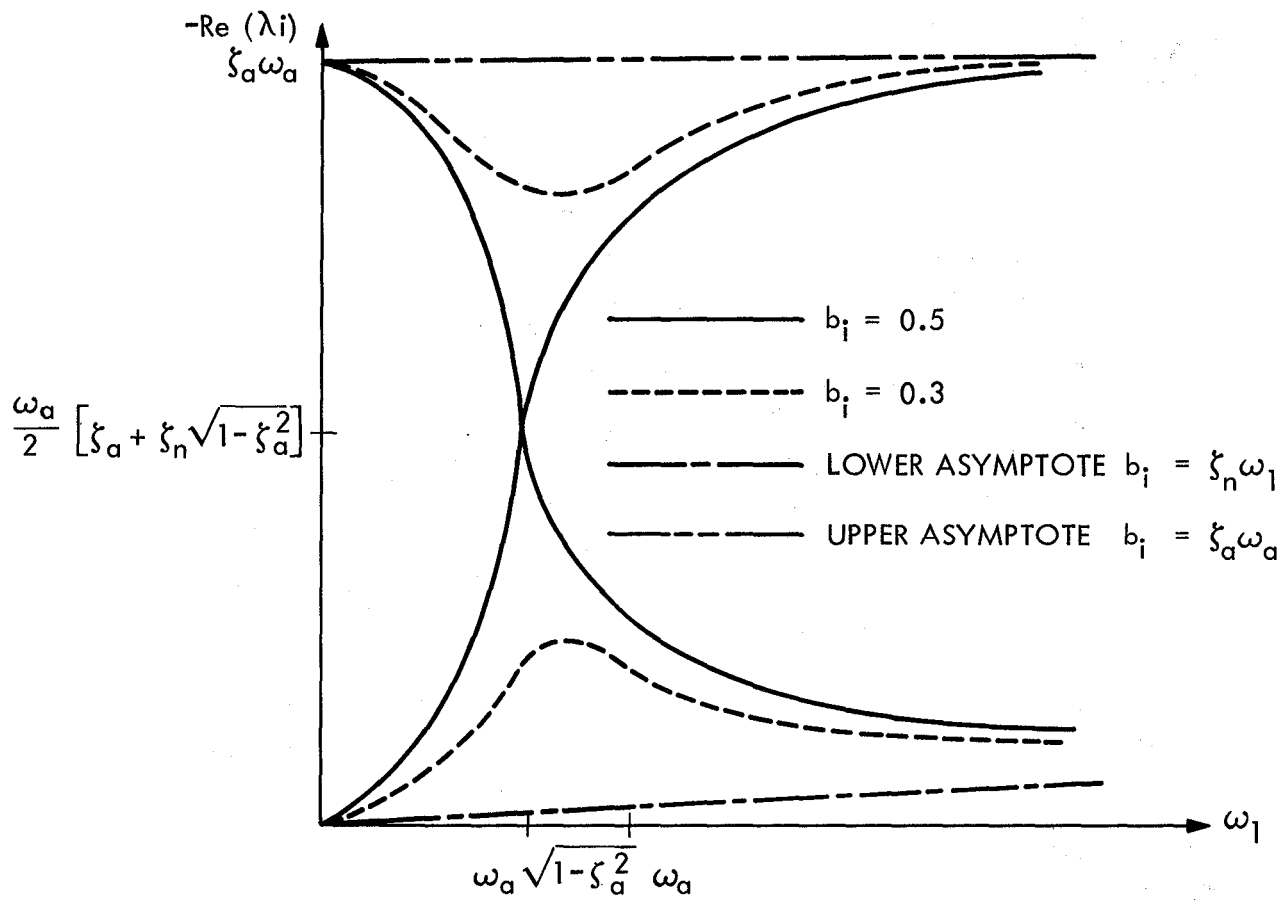


Figure 3. Closed-loop damping characteristics for scalar position feedback $\omega_a = 1.0, \zeta_a = 0.5, \zeta_n = 0.01$.

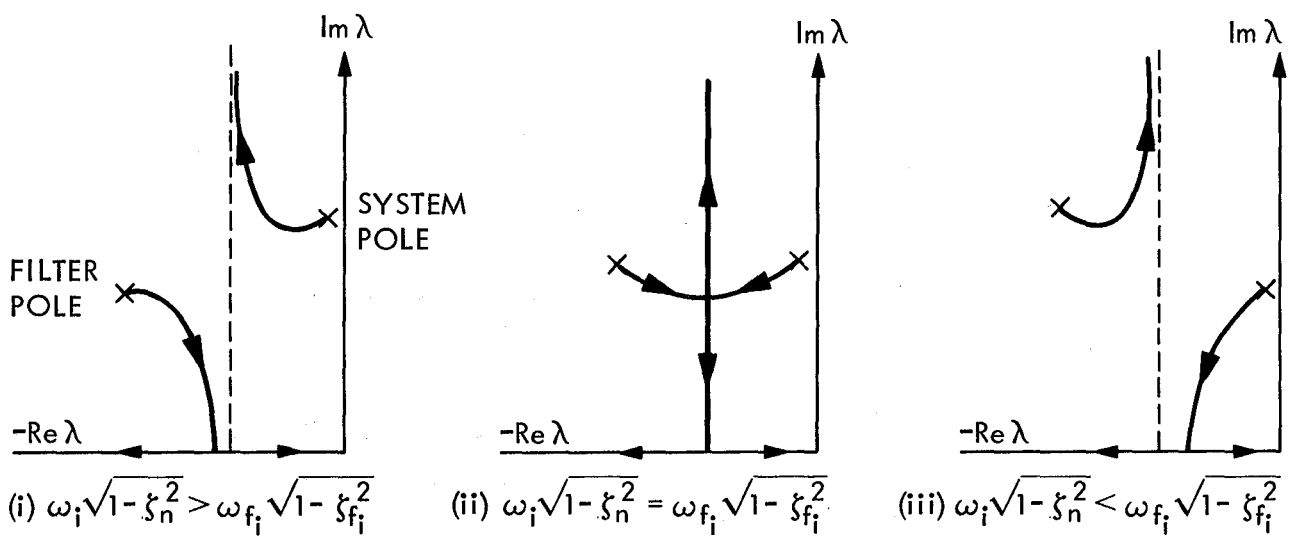


Figure 4. Root locus diagram for 3 situations.

LIST OF SYMBOLS (in Chronological Order)

N	number of modelled system states
N_A	number of sensor/actuator pair = number of controlled modes
$x \in \mathbb{R}^N$	system state vector
$M \in \mathbb{R}^{N \times N}$	system mass matrix
$D \in \mathbb{R}^{N \times N}$	system damping matrix
$K \in \mathbb{R}^{N \times N}$	system stiffness matrix
$S \in \mathbb{R}^{N_A \times N}$	sensor/actuator location matrix
$C \in \mathbb{R}^{N_A \times N_A}$	feedback gain matrix
$\xi \in \mathbb{R}^N$	Canonical (modal) state vector
$\Phi \in \mathbb{R}^{N \times N}$	Canonical (orthogonal) transformation or modal matrix
$D_c \in \mathbb{R}^{N \times N}$	Canonical damping matrix
$K_c \in \mathbb{R}^{N \times N}$	Canonical stiffness matrix
$B_c \in \mathbb{R}^{N \times N}$	modal gain matrix
ϵ, ϵ_i	small scalar parameters
N_K	null space of matrix K
s	Laplace transform domain variable
ω_i	natural frequency of the i^{th} mode
b_i, γ	scalar gain, diagonal elements of B
ζ_n	system natural damping ratio
$\beta_i = 2\zeta_n \omega_i$	twice the open loop damping of the i^{th} mode
ζ_a	actuator damping ratio
$\beta_a = 2\zeta_a \omega_a$	twice the open loop damping of the actuator
ω_a	actuator natural frequency
$z \in \mathbb{R}^{N_A}$	actuator state vector
$n \in \mathbb{R}^N$	Canonical actuator state vector

ζ_p	prescribed (approximate) damping ratio
T_1, T_2	lead compensator time constants
ζ_f	tuning filter damping ratio
ω_{f_i}	natural frequency of the i^{th} tuning filter
λ_i	i^{th} eigen value of relevant systems
V	Liapunov function
$(\dot{\cdot})$	time derivatives of (\cdot)

CONTROL OF ANTENNA-FEED ATTITUDE AND REFLECTOR VIBRATIONS IN LARGE SPACEBORNE ANTENNAS BY MECHANICAL DECOUPLING AND MOVABLE DAMPERS

P.K.C. Wang*, Jet Propulsion Laboratory, California Institute of Technology, Pasadena, CA 91109; E.C. Hong and J.S. Sarina**, Department of System Science, University of California, Los Angeles, Los Angeles, CA 90024

ABSTRACT

Simple, practical methods for damping reflector vibrations and for designing antenna-feed attitude control systems in large deployable spaceborne antennas are proposed. The former involves a movable damper which is positioned so that the rate-of-change of total vibrational energy is minimized. The latter introduces a mechanical decoupler between the flexible boom and the antenna-feed, whereby the feed-attitude control system can be designed independent of boom dynamics. The validity of these approaches are substantiated by analytical studies, computer simulation, and experimental studies.

I. INTRODUCTION

In the design of deployable spaceborne antennas with large flexible dish reflectors and long flexible feed-support booms (see Fig.1), it is of importance to quickly damp out the dish vibrations induced by external disturbances and/or spacecraft motions, and to accurately control the attitude of the antenna-feed with respect to a specified reference frame [1]-[4]. Here, we propose practical design methods which lead to simple implementable feedback systems for controlling the dish vibrations and antenna-feed attitude. For clarity, we shall use simple mathematical models to illustrate the basic ideas and the detailed development and justification of the mathematical results will be omitted.

II. DISH-REFLECTOR VIBRATION CONTROL BY MEANS OF MOVABLE DAMPERS

Consider a circular dish whose vibratory motions about a given static equilibrium configuration (for example, a parabolic cross sectional profile) is describable by the following wave equation in polar coordinates:

*Consultant, Jet Propulsion Laboratory.

**E.C. Hong and J.S. Sarina contributed to Sections III and II respectively.

$$\rho w_{tt} = (Tw_r)_r + Tr^{-1}w_r + r^{-1}(r^{-1}Tw_\theta)_\theta + f \quad (1)$$

defined on the spatial domain $\Omega = \{(r,\theta): 0 \leq \theta \leq 2\pi, 0 < r_{in} < r < r_o\}$ as shown in Fig.2, where w is the displacement about the static equilibrium; $\rho = \rho(r,\theta)$ is the mass density; $T = T(r,\theta)$ is the tension and f corresponds to the control or a damping force. The lettered subscripts denote partial differentiation.

Assuming that the dish is clamped at the inner and outer rims, the boundary conditions are:

$$w(t, r_o, \theta) = w(t, r_{in}, \theta) = 0 \quad \text{for all } t \text{ and } 0 \leq \theta \leq 2\pi. \quad (2)$$

In addition to (2), we have the periodicity requirement:

$$w(t, r, 0) = w(t, r, 2\pi) \quad \text{for } r_{in} < r < r_o. \quad (3)$$

The total energy of the dish at any time t is given by

$$\mathcal{E}(t) = \frac{1}{2} \int_0^{2\pi} \int_{r_{in}}^{r_o} \{\rho |w_t|^2 + T(|w_r|^2 + |r^{-1}w_\theta|^2)\} r dr d\theta. \quad (4)$$

Using (1)-(3) and integration by parts, it can be readily verified that the time rate-of-change of energy is

$$\dot{\mathcal{E}}(t) = \int_0^{2\pi} \int_{r_{in}}^{r_o} f(t, r, \theta) w_t(t, r, \theta) r dr d\theta. \quad (5)$$

A possible approach to vibration damping is to choose the control or damping force f in a given admissible class such that $\dot{\mathcal{E}}(t)$ is minimized [5],[6]. Consequently, the vibrational energy $\mathcal{E}(t)$ is reduced as quickly as possible. A simple choice for f is a spatially distributed feedback control in the form of a linear damping force given by

$$f(t, r, \theta) = -g(t, r, \theta) w_t(t, r, \theta), \quad (6)$$

where g is a positive damping coefficient. Unfortunately, such a distributed control or damper cannot be readily implemented. Therefore, we shall consider a more restricted form of (6) which is amenable to physical implementation.

Let $\Omega_c(t)$ be a proper subset of Ω denoting the effective region for the control at time t . We assume that

$$f(t, r, \theta) = \begin{cases} -g w_t(t, r, \theta) & \text{on } \Omega_c(t), \\ 0 & \text{on } \Omega - \Omega_c(t), \end{cases} \quad (7)$$

where g is a specified positive real number. Let \mathcal{U}_{ad} be the set of all admissible Ω_c 's. We wish to find a $\Omega_c(t) \in \mathcal{U}_{ad}$ such that

$$\dot{\mathcal{E}}(t) = \int_{\Omega} f(t, r, \theta) w_t(t, r, \theta) d\Omega = - \int_{\Omega_c(t)} g |w_t(t, r, \theta)|^2 d\Omega \quad (8)$$

takes on its minimum value. This problem is analogous to that of silencing a large drum as quickly as possible by means of movable damping pads which are effective only over certain portions of the drum surface.

In what follows, we shall consider a special form of movable damper which is suitable for the dish reflector (see Fig.3). Let $\Omega_{co} = \{(r, \theta): 0 < r_{in} < r < r_o; 0 \leq \theta \leq \theta_o \leq 2\pi\}$, where θ_o is a given aperture angle. We define the effective region $\Omega_c(\delta(t))$ for the control (3) as a rotation of Ω_{co} given by

$$\Omega_c(\delta(t)) = \{(r, \theta): 0 < r_{in} < r < r_o; \delta(t) \leq \theta \leq \theta_o + \delta(t)\}. \quad (9)$$

The rotation angle $\delta(t)$ is to be chosen such that $\dot{\mathcal{E}}(t)$ given by (8) is minimized. Let $\delta^*(t)$ denote an optimum angle, then

$$\dot{\mathcal{E}}(t, \delta^*(t)) = - \int_{\delta^*(t)}^{\theta_o + \delta^*(t)} \int_{r_{in}}^{r_o} g |w_t(t, r, \theta)|^2 r dr d\theta. \quad (10)$$

Evidently, $\delta^*(t)$ corresponds to a rotation angle at which the average kinetic energy over the effective control region is maximized. It is of interest to obtain estimates of the total energy decay of the dish with the foregoing optimized movable damper. Unfortunately, useful a priori estimates of the energy decay are not readily obtainable directly from (1)-(3) and the optimized control (7). Therefore, we shall resort to computer simulation at this point.

Consider a dish with constant ρ and T . In this case, we can express the solutions of (1)-(3) with the optimized movable damper in the form:

$$w(t, r, \theta) = \sum_{m, n=1}^{\infty} a_{mn}(t) \phi_{mn}(r, \theta), \quad (11)$$

where ϕ_{mn} is the orthonormalized eigenfunction of the Laplacian operator with boundary conditions (2) and (3) corresponding to the eigenvalue $-\lambda_{mn}^2$ given by the n -th root of the equation:

$$J_m(\lambda r_{in}/\gamma) Y_m(\lambda r_o/\gamma) = J_m(\lambda r_o/\gamma) Y_m(\lambda r_{in}/\gamma), \quad m=1, 2, \dots, \quad (12)$$

where $\gamma^2 = T/\rho > 0$; J_m and Y_m denote the m -th order Bessel functions of the first and second kind respectively.

It can be verified that the modal coefficients $a_{mn}(t)$ satisfy the following countably infinite dimensional system of ordinary differential equations:

$$\begin{aligned} & \ddot{a}_{mn}(t) + g\rho^{-1}\Delta_m(t)\dot{a}_{mn}(t) + \lambda_{mn}^2 a_{mn}(t) \\ & = -g\rho^{-1} \sum_{\substack{k,\ell=1 \\ k \neq m}}^{\infty} \dot{a}_{k\ell}(t) \left\{ \int_{r_{in}}^{r_o} R_{mn}(r)R_{k\ell}(r) r dr \int_0^{\theta_o} \Theta_m(\theta+\delta^*(t))\Theta_k(\theta+\delta^*(t))d\theta \right\} \end{aligned} \quad m,n=1,2,\dots, \quad (13)$$

where

$$\begin{aligned} \phi_{mn}(r,\theta) &= R_{mn}(r)\Theta_m(\theta), \\ R_{mn}(r) &= A_{mn} \{ J_m(\lambda_{mn}r/\gamma) - [J_m(\lambda_{mn}r_{in}/\gamma)/Y_m(\lambda_{mn}r_{in}/\gamma)]Y_m(\lambda_{mn}r/\gamma) \}, \\ \Theta_m(\theta) &= (\pi)^{-\frac{1}{2}} \cos(m\theta + \psi_m), \\ A_{mn} &= \sqrt{2}/[r_o p(r_o) - r_{in} p(r_{in})], \\ p(r) &= J_{m-1}(\lambda_{mn}r/\gamma) - [J_m(\lambda_{mn}r/\gamma)/Y_m(\lambda_{mn}r/\gamma)]Y_{m-1}(\lambda_{mn}r/\gamma), \\ \Delta_m(t) &= \int_{\delta^*(t)}^{\theta_o + \delta^*(t)} |\Theta_m(\theta)|^2 d\theta \\ &= \frac{1}{2\pi} \{ \theta_o - m^{-1} \sin^2 m\theta_o \sin[2(m\delta^*(t) + \psi_m)] \\ &\quad + (2m)^{-1} \sin(2m\theta_o) [1 - 2 \sin^2(m\delta^*(t) + \psi_m)] \}. \end{aligned} \quad (14)$$

It is evident that for large m , the damping coefficient $g\rho^{-1}\Delta_m(t)$ tends to $g\theta_o/(2\pi\rho)$ as $m \rightarrow \infty$.

To gain some idea on the performance of the optimized movable damper, computer simulations are made using truncated versions of (13) with additional small residual damping terms $g_o\rho^{-1}\dot{a}_{mn}(t)$, where $g_o = 0.001$. The numerical values for the dish parameters are:

$$\rho = 0.05 \text{ kg./m}^2, \quad T = 8.9 \text{ kg./sec}^2, \quad r_{in} = 1 \text{ m.}, \quad r_o = 51 \text{ m.}, \quad \text{and } g = 0.1.$$

Fig.4 shows the energy decay for various initial kinetic energy distributions and different forms of movable dampers including a damper sweeping at a constant rate of $20^\circ/\text{sec.}$, a randomly positioned damper and the optimally positioned damper as discussed earlier. In the computer simulations, the dish is partitioned into 36 10° -sectors. The optimal damper position is determined by locating a sector with the highest kinetic energy. In the case of the randomly positioned damper, the damper position at any time is determined by a random number generator. From the numerical results, it is apparent that in all cases,

the total modal energy (first 25 modes) decays monotonically with time. As expected, the fastest energy decay is achieved by the optimally positioned damper. However, it can be seen from Fig.4c that the effectiveness of the optimally positioned damper decreases when all the vibrational energy is concentrated in the high-frequency modes. This is consistent with the fact that the damping coefficient $g\rho^{-1}\Delta_m(t) \rightarrow g\theta_0/(2\pi\rho)$ as $m \rightarrow \infty$ as mentioned earlier.

Although the foregoing results are based on a highly simplified model for the dish, the proposed approach may also be applied to more complex realistic situations where the dish is constructed from elastic ribs covered with thin flexible material. In this case, optimally positioned patch dampers may be more suitable. Finally, the movable dampers proposed here can be implemented either by passive dampers in contact with the dish surface or by active velocity feedback controls. However, passive dampers are preferred from the reliability standpoint, since there is no danger of pumping energy into the dish in case of controller failure.

III. ANTENNA-FEED ATTITUDE CONTROL BY MECHANICAL DECOUPLING

For a typical spaceborne antenna shown in Fig.1, the antenna-feed is rigidly attached to the tip of a flexible boom which could undergo both torsional and bending vibrations. It is required to control the antenna-feed attitude with respect to a given reference frame on the spacecraft. In the usual situation, a control torque and/or force are introduced at the boom-root. Consequently, any control action on the antenna-feed must be transmitted through the flexible boom which is an infinite dimensional system. This greatly complicates the design of the feed-attitude control system. Here, we propose to mechanically decouple the antenna-feed from the boom so that the feed-attitude control system can be designed without taking the boom dynamics into consideration.

To illustrate the basic idea, we consider the special case where the boom vibrations are strictly torsional in nature. The antenna-feed is represented by a rigid disk (with mass polar moment of inertia J_0) attached to the boom-tip as shown in Fig.5. Let P be a point on the disk whose angular position with respect to the fixed y -axis is denoted by θ_0 . First, let the control torque T_C be applied at $x=0$, and it is required to choose T_C such that $\theta_0(t)$ is as close to a specified reference angle θ_R (say $\theta_R=0$) as possible at all times. Here, we observe that any control action $T_C = T_C(t)$ will excite boom vibrations. Hence, T_C must be manipulated in such a way that the desired effective control torque appears at the boom-tip for controlling the feed motion. Moreover, any torsional motion of the boom due to external disturbances will affect θ_0 . These undesirable features greatly complicate the design of the feed-attitude control system. Here, we note that since the relative angle $\theta_R - \theta_0$ is to be controlled, the foregoing undesirable features can be bypassed by introducing a rotary actuator (for example, an electric servomotor with stator moment of inertia J_1) at the boom-tip to decouple J_0 from the boom (see Fig.6). In absence of actuator friction and an actuating signal to the actuator, J_0 rotates freely. Thus, the angular-position control for J_0 can be achieved by applying an appropriate actuating signal depending only on $(\theta_R - \theta_0)$, independent of the boom motion. Note

that a control torque applied to J_o generated by the actuator is always accompanied by a reaction torque on the boom. However, in absence of actuator friction, there is no feedback from the boom motion to J_o . Consequently, the boom motion has no effect on θ_o . In real physical situations, friction coupling between J_o and J_1 always exists. Its effect on the overall system is studied using the following simplified mathematical model:

(a) Torsional vibrations of boom:

$$I_b \theta_{1tt} = (GJ \theta_{1x})_x - \delta \theta_{1t} \quad (15)$$

with boundary conditions:

$$\theta_1(t,0) = 0, \quad (GJ \theta_{1x})|_L = -J_1 \frac{d}{dt}(\theta_{1t}|_L) + c(\dot{\theta}_o - \theta_{1t}|_L) - T_c, \quad (16)$$

where θ_1 is the torsional angle of the boom with respect to the fixed y-axis; I_b and GJ denote the mass moment of inertia and torsional rigidity per unit length of the boom respectively; δ is a positive damping coefficient; c is the actuator stator-rotor friction coupling coefficient, and T_c is the control torque. As in Section II, the lettered subscripts denote partial differentiation and $\dot{\theta}_o = d\theta_o/dt$.

(b) Antenna-feed (J_o) motion:

$$J_o \ddot{\theta}_o = -c(\dot{\theta}_o - \theta_{1t}|_L) + T_c. \quad (17)$$

For simplicity, we assume that the reference angle $\theta_R=0$ and the actuator action is instantaneous. Thus, we can introduce the usual proportional-plus-rate feedback control for positioning J_o :

$$T_c = -(\alpha \theta_o + \beta \dot{\theta}_o), \quad (18)$$

where α and β are given real positive constants. Thus, the complete mathematical model is given by (15)-(18) which can be reformulated as a linear evolution equation defined on a suitable infinite dimensional state space. It is of interest to establish nontrivial sufficient conditions for asymptotic stability of equilibrium in the sense of Lyapunov with respect to the "energy norm" $\|w\|$ defined by

$$\|w\|^2 = \frac{1}{2} \left\{ \int_0^L (I_b |\theta_{1t}|^2 + GJ |\theta_{1x}|^2) dx + J_1 |\theta_{1t}|_L|^2 + J_o \dot{\theta}_o^2 + \alpha \theta_o^2 \right\}. \quad (19)$$

Unfortunately, this task is not straightforward. However, it can be verified [7] that the determination of the eigenvalues or poles of the complete system is reducible to solving the following nonlinear eigenvalue problem: Find all non-trivial pairs $(\theta, \lambda) \in H^2(\Omega) \oplus \mathbb{C}$ satisfying:

$$(GJ\theta_x)_x - \lambda(\delta + \lambda I_b)\theta = 0, \quad (20)$$

$$\theta(0) = 0, \quad (GJ\theta_x)|_L = -\lambda^2 q(\lambda)\theta(L), \quad (21)$$

where $H^2(\Omega)$ denotes the complex Sobolev space of order 2 on $\Omega =]0, L[$; \mathbb{C} denotes the field of complex numbers and

$$q(\lambda) = \frac{J_o J_1 \lambda^2 + [J_1(\beta+c) + cJ_o]\lambda + J_1 \alpha}{J_o \lambda^2 + (\beta+c)\lambda + \alpha}. \quad (22)$$

For this problem, we can deduce the following result [7],[8]: All unstable eigenvalues $\lambda = \lambda_R + j\lambda_I$ are complex and they lie inside the half-disk:

$$\{\lambda \in \mathbb{C}: \lambda_R^2 + \lambda_I^2 < \alpha/J_o, \lambda_R > 0\}.$$

This result gives an upper bound for the growth rates and natural frequencies of the unstable modes. Note that this bound is independent of the boom parameters.

Another aspect having practical importance is the determination of sensitivity of the eigenvalues with respect to the friction coefficients c and δ . This can be studied by a perturbation analysis. Fig.7 shows the loci of eigenvalues with variable parameters δ and c for a 10-meter uniform boom with $I_b = 0.64 \times 10^{-3}$ kg.m., $GJ = 25$ kg.m³/sec², and angular position-control system parameters: $J_1 = 6.4 \times 10^{-4}$ kg.m², $J_o = 1.2 \times 10^{-2}$ kg.m², $\alpha = 0.474$ kg.m²/sec², and $\beta = 0.0754$ kg.m²/sec. It can be seen from Fig.7 that the control system poles for the indicated variations of parameter values for δ and c are clustered around the poles $\lambda = -3.14 + 5.43j$ corresponding to $\delta = 0$ and $c = 0$. This shows that the control system poles are insensitive to variations in the friction coefficients.

The effectiveness of the decoupling is revealed in the computer simulation results given in Figs.8 and 9. Fig.8 shows that for the indicated initial conditions, the ratio of peak magnitudes of the control system positional angle θ_o and the boom-tip deflection is approximately 0.035, which corresponds to a significant reduction in vibration amplitude.

To verify the validity of the proposed decoupling approach, a small scale model of the foregoing system is constructed (see Fig.10). The boom is simulated by a thin steel wire. The effectiveness of the decoupling is clearly shown in Fig.11. Here, the ratio of the peak magnitudes of θ_o and the boom-tip deflection is approximately 0.02. Fig.12 shows the boom vibrations induced by the positional control system motion for different boom stiffnesses. From the experiments, it is found that the friction torques in the servomotor and the sensing potentiometers are predominately static in nature. However, their presence does not alter the effectiveness of decoupling. A more detailed description of the sensitivity analysis and experimental results are given in [9].

The foregoing discussions have been limited to the simplest case with torsional motion only. In an actual antenna system, the flexible boom could undergo both torsional and bending vibrations. It is required to keep a given point on the antenna-feed aligned with a specified point on a reference plane at the boom-root. Here, we may mechanically decouple the boom motion from the feed

positioning control system by introducing a composite rotary and linear actuator as shown in Fig.13. Thus, the antenna-feed may be aligned by a combination of linear and rotary motions of the actuators. Analytical studies and computer simulation for this system are described in reference [8].

From the analytical studies, computer simulation, and experimental studies, the introduction of the proposed mechanical decoupling appears to be a simple and effective approach to the design of implementable antenna-feed attitude control systems for large spaceborne antennas. This approach avoids the consideration of an infinite dimensional model in control system design. To maximize the effectiveness of decoupling, the actuator friction should be as low as possible, and to avoid instability problems, the boom must have sufficient stiffness and structural damping.

ACKNOWLEDGMENTS

The work of the first author was performed at the Jet Propulsion Laboratory, California Institute of Technology, under contract with the National Aeronautics and Space Administration. He also wishes to acknowledge many helpful discussions with Drs. G. Rodriguez and Y.H. Lin of the Jet Propulsion Laboratory.

REFERENCES

- [1] Freeland, R.E. and Campbell, T.G., "Deployable Antenna Technology Development for the Large System Technology Program", Proc. AIAA/NASA Conf. on Advance Technology for Future Space Systems, Hampton, VA., 1979.
- [2] Hamidi, M., Rodriguez, G. and Lin, Y.H., "Results in the Control and Dynamics of LSST Antenna Systems", Jet Propulsion Lab. Engr. Memo. No.347-119, 1981.
- [3] Lin, Y.H., "Control of Large Space Antennas: Wrap-Rib-Hoop/Column", Large Space Systems Technology-1981, NASA Conf. Publication 2215, Part 1, 1982, pp.249-281.
- [4] Tolivar, A.F., "Attitude Control Subsystem Study for the Land Mobile Satellite System Spacecraft", Large Space Systems Technology-1981, NASA Publication 2215, Part 2, 1982, pp.821-839.
- [5] Komkov, V., Optimal Control Theory for the Damping of Vibrations of Simple Elastic Systems, Lecture Notes in Math. No.253, Springer-Verlag, N.Y. 1972.
- [6] Sirazetdinov, T.K., "Analytical Design of Regulators in Processes with Distributed Parameters", Avtomatika i Telemekhanika, Vol.26, No.9, 1965, pp.1449-1457.
- [7] Wang, P.K.C., "A Decoupling Approach to the Control of Large Spaceborne Antenna Systems", Proc. of Third IFAC Symposium on the Control of Distributed-Parameter Systems, Toulouse, France, June, 1982, Paper No.5.1.
- [8] Wang, P.K.C., "Control of Large Spaceborne Antenna Systems with Flexible Booms by Mechanical Decoupling", UCLA Engr. Report ENG-82-33, April, 1982 (to appear in J. Franklin Institute).

- [9] Hong, E.C., "Analytical and Experimental Study of an Angular-position Control System with a Torsional Vibration Decoupler", M.S. Thesis, Department of System Science, Univ. of California, Los Angeles, June, 1982.

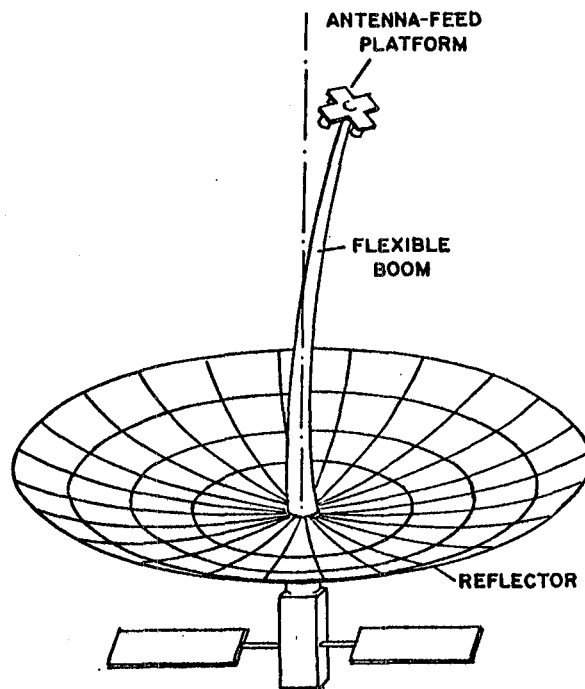


Figure 1. Typical configuration of a spaceborne antenna system with antenna-feed rigidly attached to the tip of a flexible boom.

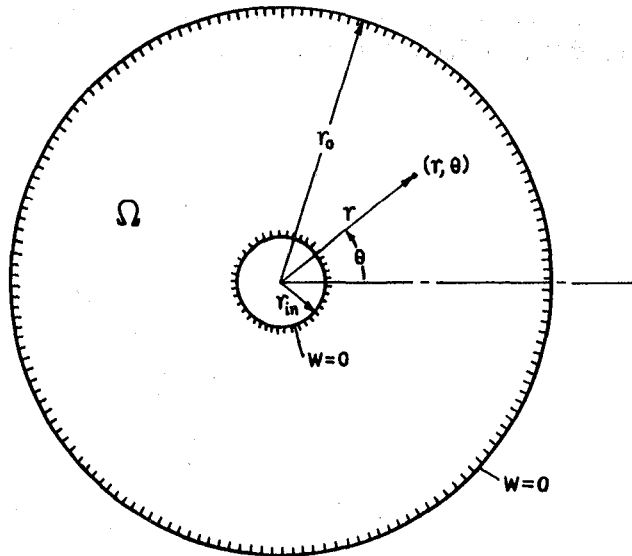


Figure 2. Spatial domain of the dish reflector.

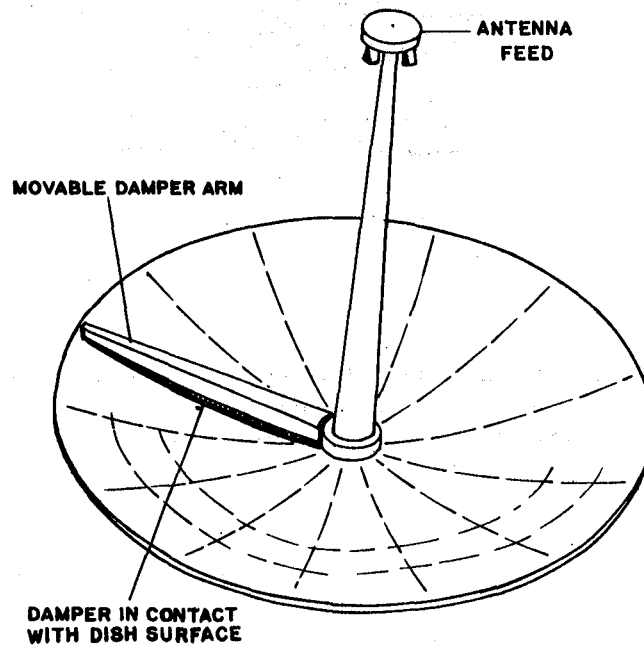


Figure 3. Sketch of dish reflector with a movable damper (The damper may also be placed on the backside of the reflector for reducing its effect on the antenna characteristics).

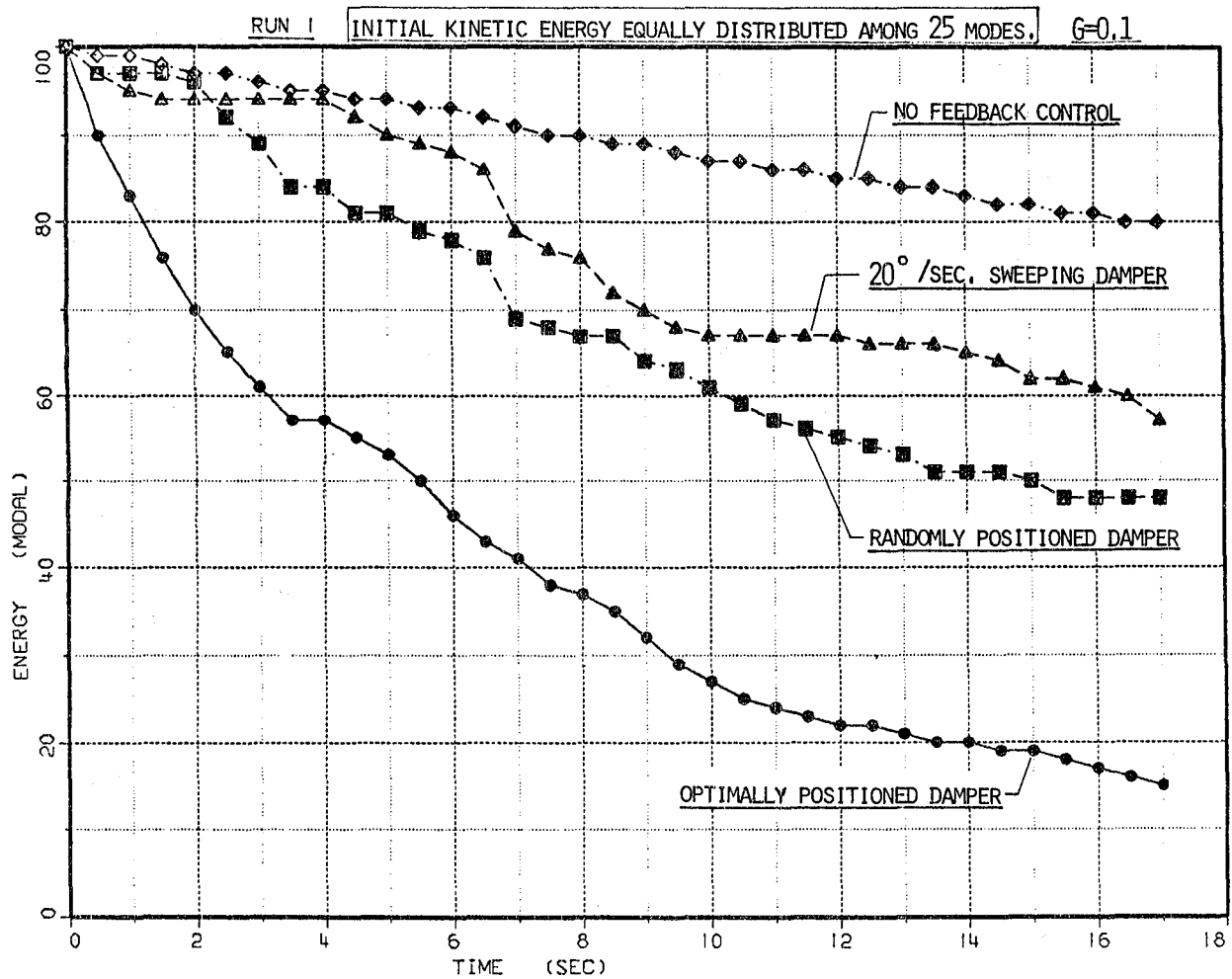


Figure 4a

Figure 4. Energy decay for various initial kinetic energy distributions and different forms of movable dampers.

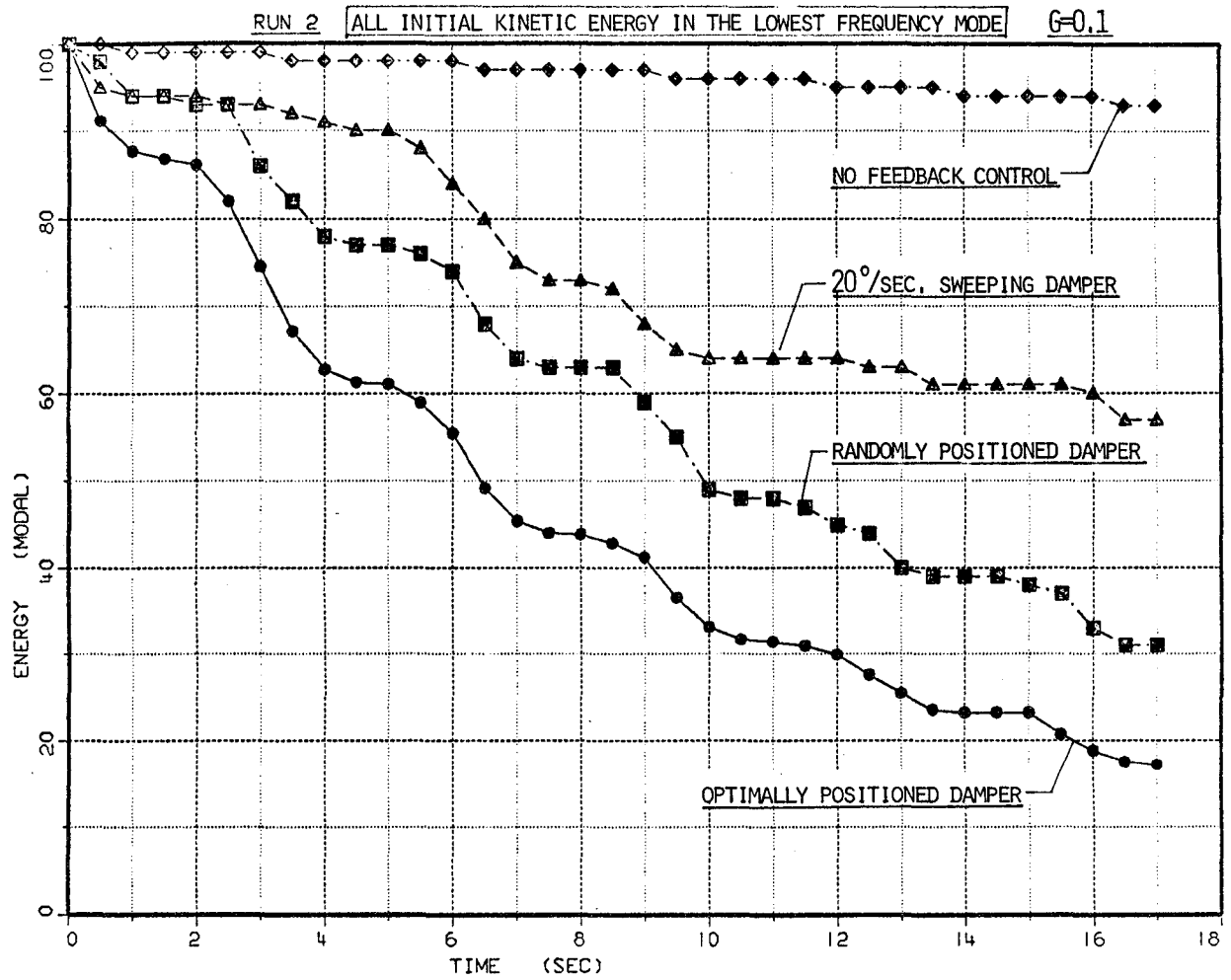


Figure 4b

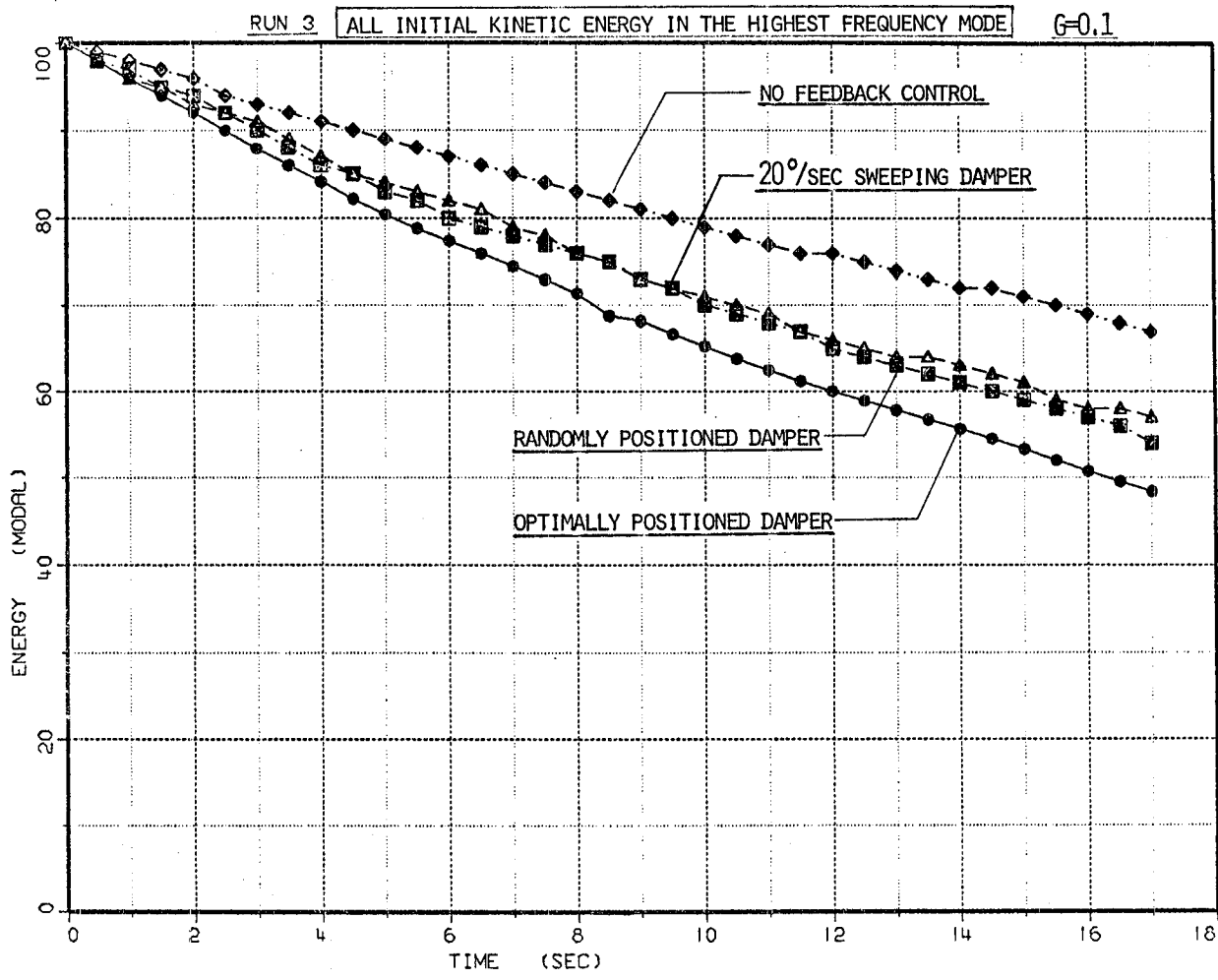


Figure 4c

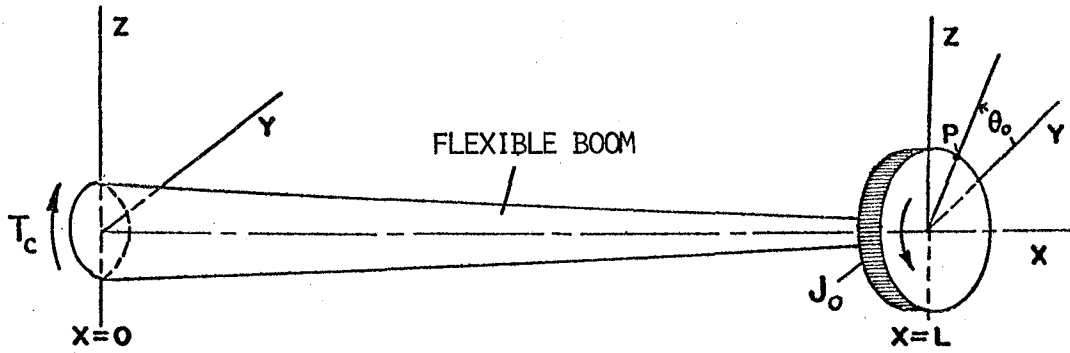


Figure 5. Attitude control of antenna-feed which is rigidly attached to the tip of a flexible boom.

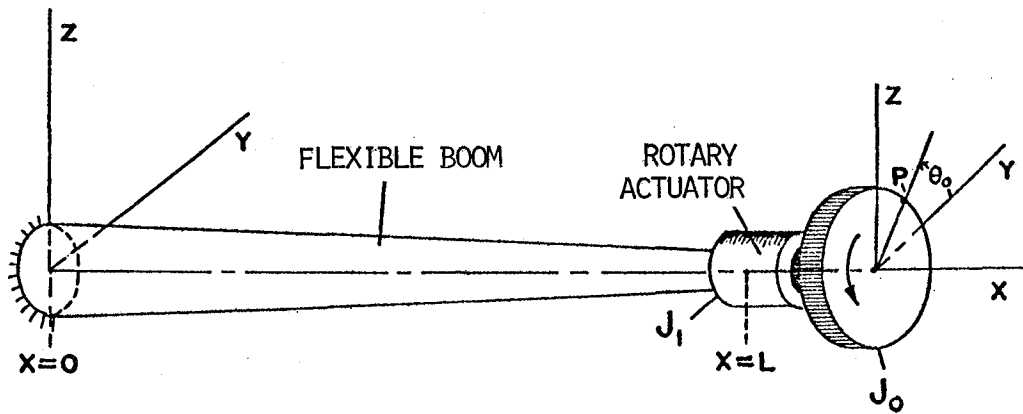


Figure 6. Proposed mechanical decoupling of the antenna-feed from the flexible boom with torsional motion only.

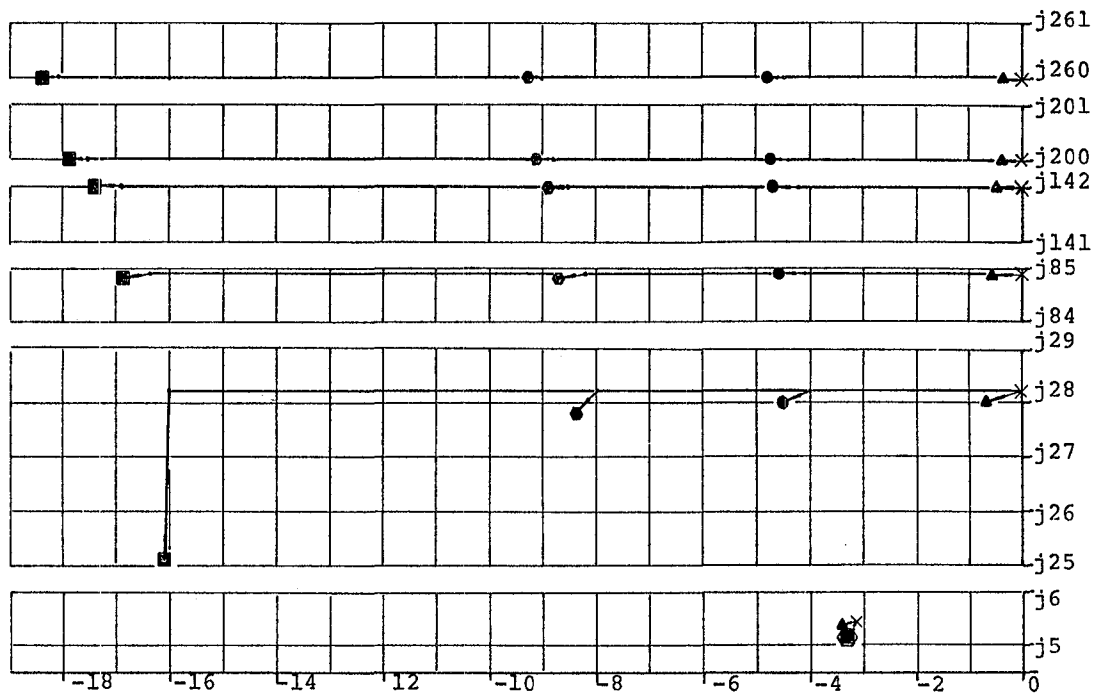


Figure 7. Loci of eigenvalues with variable parameters δ and c for a 10-meter uniform boom.

- × -- $\delta = 0.$, $c = 0.$;
- ▲ -- $\delta = 0.$, $c = 0.005$;
- -- $\delta = 0.00625$, $c = 0.005$;
- ◆ -- $\delta = 0.0125$, $c = 0.005$;
- -- $\delta = 0.025$, $c = 0.005$.

Other parameter values are given in text.

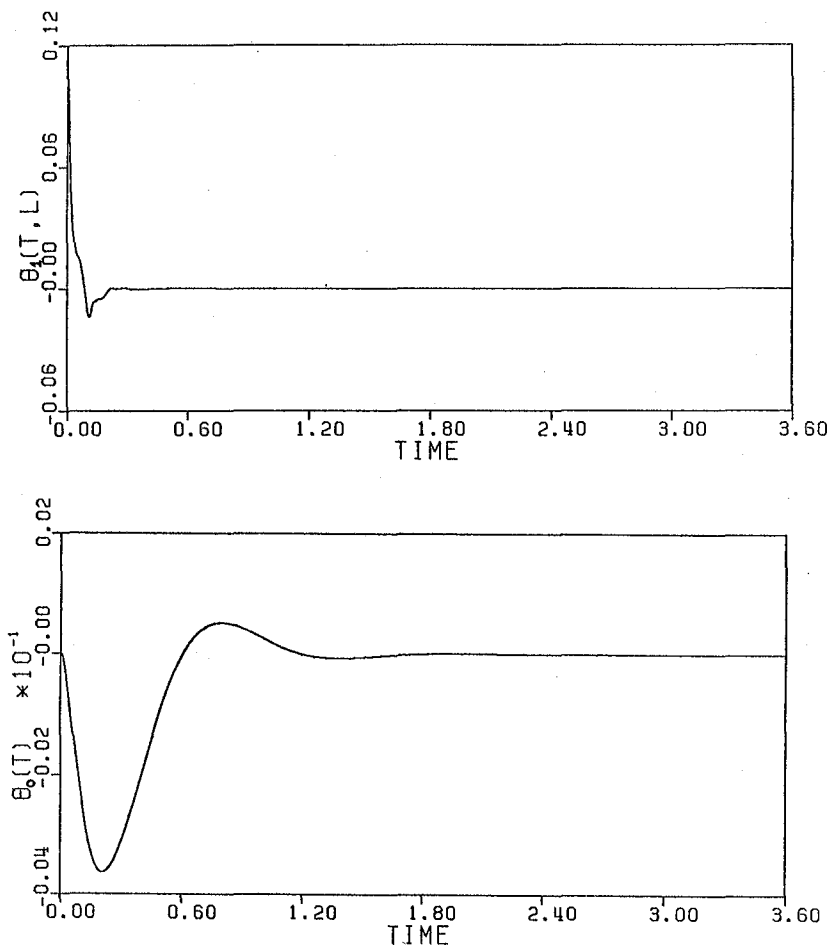


Figure 8. Angular displacements of boom-tip [$\theta_1(t,L)$] and J [$\theta_0(t)$] due to initial torsional deflection of the boom [$\theta_1(0,x) = 0.001x^2$ rad., $\theta_{1t}(0,x) \equiv 0$ rad./sec. $0 \leq x \leq 10$ m.] with J initially at rest. $I_b = 0.64 \times 10^{-3}$ kg.m.; $J_1 = 6.4 \times 10^{-4}$ kg.m.²; $J_0 = 1.2 \times 10^{-2}$ kg.m.²; $GJ = 25$ kg.m.³/sec.²; $\delta = 0.025$ kg.m./sec.; $\alpha = 0.474$, $\beta = 0.0754$ and $c = 0.005$ kg.m.²/sec.

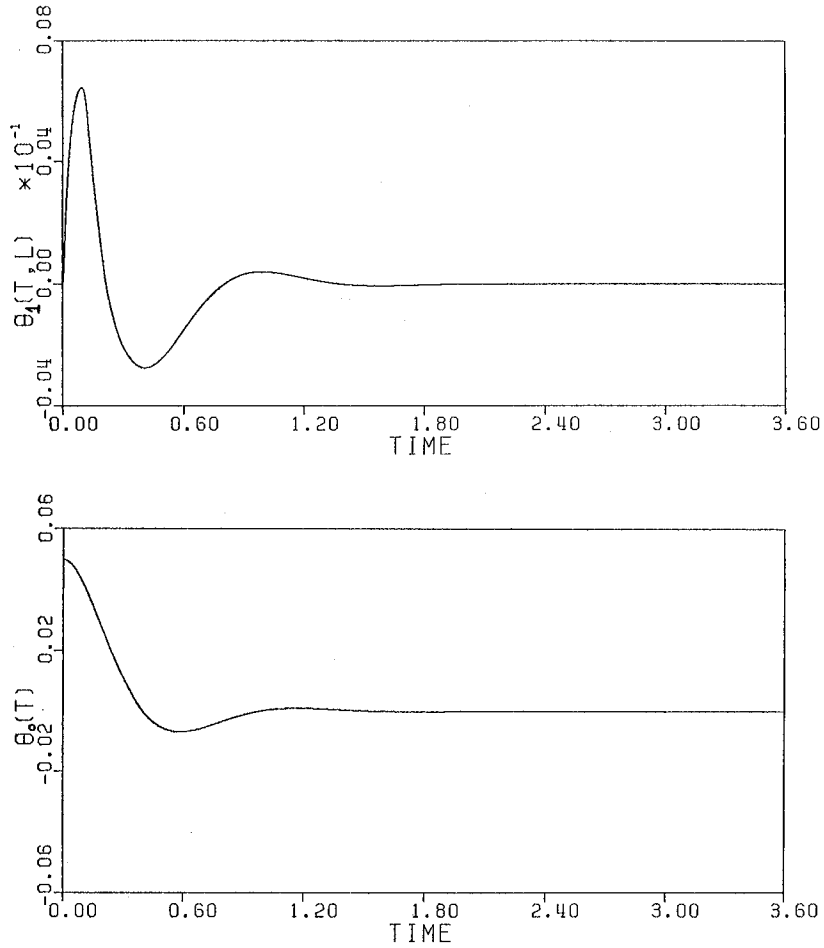


Figure 9. Angular displacements of the boom-tip [$\theta_1(t,L)$] and J_0 [$\theta(t)$] due to initial angular displacement of J_0 [$\theta(0) = 0.05$ rad., $\dot{\theta}(0) = 0$ rad./sec.] with boom initially at rest. The system parameter values are given in Figure 8.

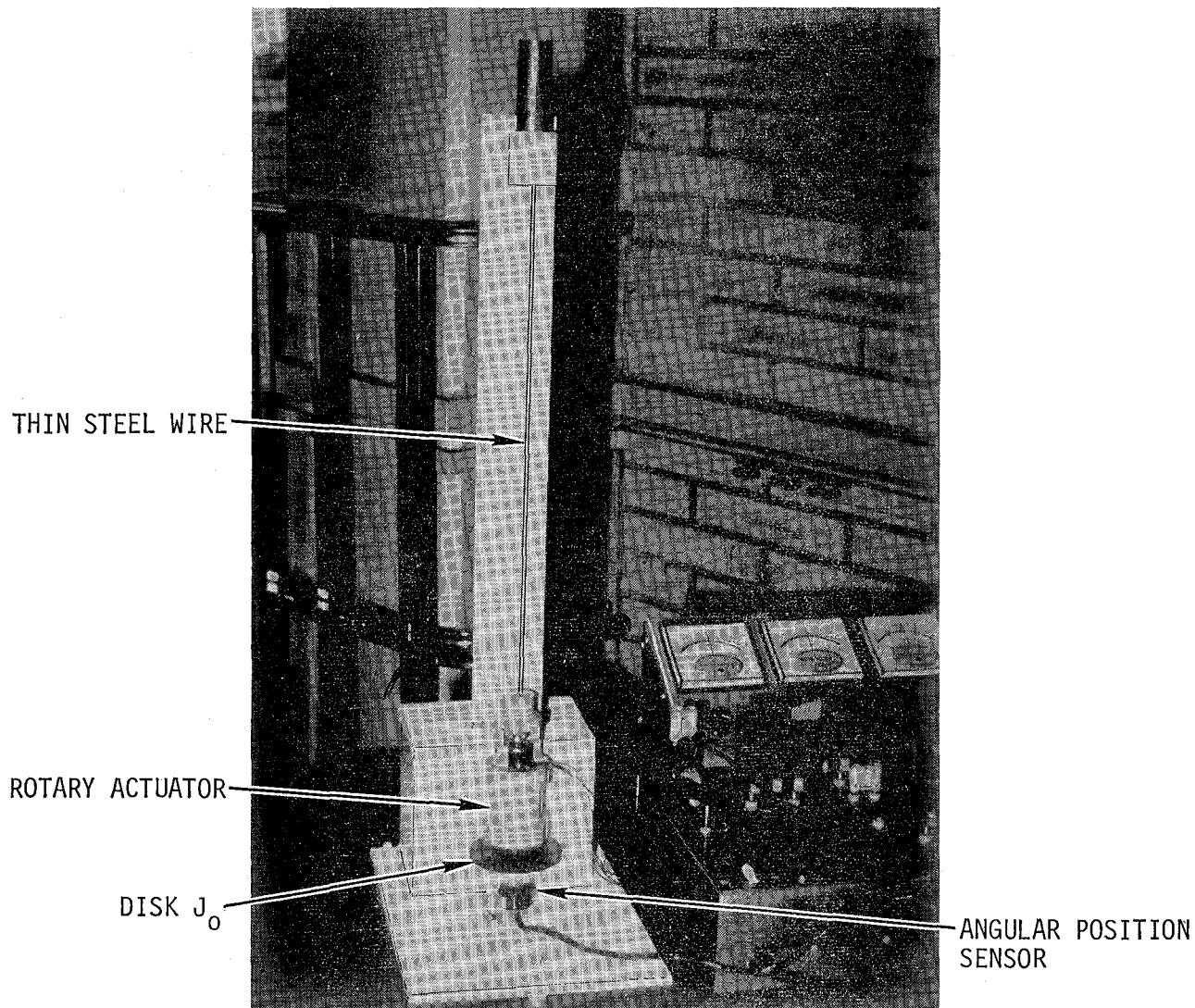


Figure 10. Experimental setup for a small scale model of the proposed antenna-feed angular-position control system with decoupler.

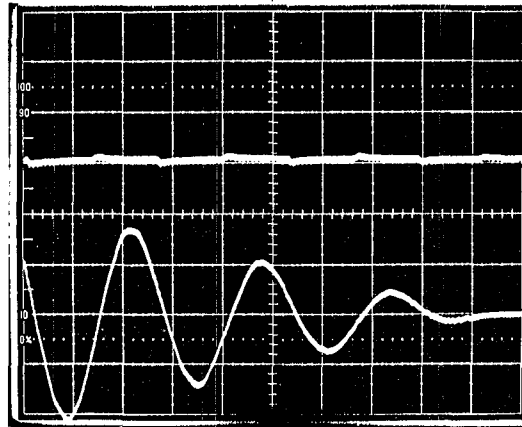
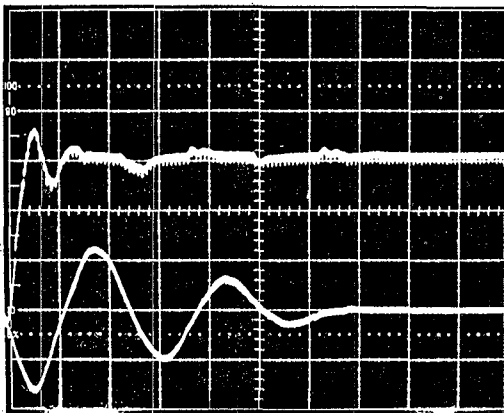
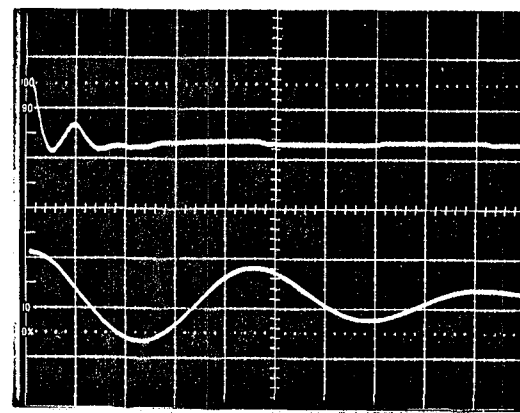


Figure 11. Angular displacements of J_0 (upper trace; scale: $2^\circ/\text{div.}$) and boom-tip (lower trace; scale: $5^\circ/\text{div.}$) due to initial boom displacement, with angular position-control system initially at rest. Time scale: 0.1 sec./div. Equivalent spring constant for boom: $0.1362 \text{ kg.m}^2/\text{sec.}^2$, $J_1 = 2.41 \times 10^{-4} \text{ kg.m}^2$ and $J_0 = 1.32 \times 10^{-4} \text{ kg.m}^2$.



(a)



(b)

Figure 12. Angular displacements of J_0 (upper traces) and boom-tip (lower traces) due to initial displacement of J_0 , with boom initially at rest. (a) Equivalent spring constant for boom: $0.1362 \text{ kg.m}^2/\text{sec.}^2$; scale: upper trace $1^\circ/\text{div.}$, lower trace $5^\circ/\text{div.}$; (b) Equivalent spring constant for boom: $4.52 \times 10^{-2} \text{ kg.m}^2/\text{sec.}^2$; scale: upper trace $5^\circ/\text{div.}$, lower trace $50^\circ/\text{div.}$. The values for J_1 and J_0 are identical to those in Fig.11.

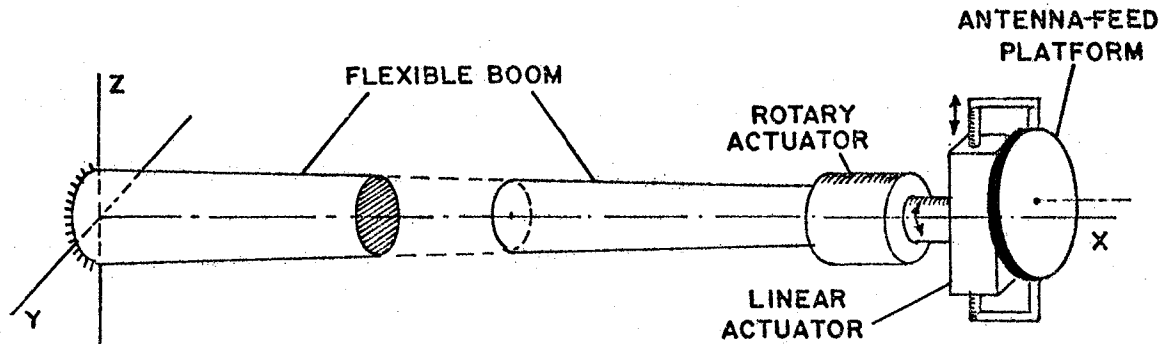


Figure 13. Proposed mechanical decoupling of the antenna-feed from the flexible boom with torsional and bending motions.

A CLOSED-LOOP PRINCIPAL COMPONENT ANALYSIS OF A TETRAHEDRAL TRUSS*

Edmond A. Jonckheere

Department of Electrical Engineering — Systems
University of Southern California
Los Angeles, CA 90007

ABSTRACT

In this paper, a tetrahedral truss, representative of a fairly broad class of large space structures, is considered. A new method, measuring the dynamical importance of each elastic mode when the structure is under feedback control, is presented.

I. INTRODUCTION

The Tetrahedral Truss devised by Charles Stark Draper Labs (Ref. 21) has the simple geometric structure of a tetrahedron, and, despite its simplicity, it models the feeding tower of a large cassegrain antenna (Fig. I.1). It is considered as the simplest nonplanar structure capable of representing a Large Space Structure. The nodes of the tetrahedron are assumed to be torque free, so that the connecting rods are only undergoing traction/compression efforts. The three nodes of the tetrahedral basis are connected to the (inertially stabilized) antenna dish via three bipeds, containing a total of six co-located sensors/actuators. The tetrahedral apex represents the position of the secondary reflector whose motion, because of the nature of the electromagnetic problem, must be controlled extremely accurately. Hence the problem is — control the motion of the tetrahedral apex, by means of actuators located in the bipeds, using sensor information from the bipeds.

The design of the control system for such a distributed parameter, vibrating mechanical structure faces an old, yet not completely resolved, problem — how many vibration modes should the control system take into account to guarantee (robust) stability?

Using Moore's "open-loop principal component analysis" (Ref. 7), the author and Silverman (Refs. 15,16) have shown that the open-loop importance (more precisely, the singular value $\sigma_{2i-1} = \sigma_{2i}$) of each vibrating mode decreases with increasing eigenfrequency, and that the spectrum of the singular values becomes infinitely spread as the relative damping goes to zero.

A delicate issue is whether or not the above conclusion can be extended to

*This research was supported by the USC/TRW University/Industry NSF Grant ECS-8112327.

the closed-loop case. Practical experience ("spillover" problem, Ref. 17) has shown that this is not always the case.

To tackle the closed-loop problem, Skelton (Ref. 9) developed the "cost analysis". More recently, the author and Silverman (Refs. 11,12) have developed a "closed-loop principal component analysis" which is aimed at measuring how much each mode is important when the system is closed-up by a LQG feedback loop. This technique assigns a measure, or "closed-loop singular value", to each mode. The main purpose of this paper is to look at the tetrahedral truss control problem in the light of this "closed-loop principal component analysis." Surprisingly enough, the conclusions of the closed-loop principal component analysis do not quite well corroborate the results of the open-loop analysis. While the spectrum of the open-loop singular values is infinitely spread, the spectrum of the closed-loop singular values is surprisingly concentrated. In more intuitive but less precise terms, this means that, while the modes appear disparately important open-loopwise, they are about equally important closed-loopwise. This discrepancy between the open-loop and the closed-loop analyses can be interpreted as a tentative theoretical explanation of the spillover problem. Also, it turns out that the closed-loop importance of each mode depends on the robustness requirements on the LQG feedback loop. For example, some seemingly unimportant modes can become very important under stringent feedback performance requirements (Refs. 13,14). This paper basically addresses such issues.

II. THE TETRAHEDRAL TRUSS

The motion of the tetrahedral truss is most conveniently represented by its modal state equations:

$$\dot{x}(t) = Ax(t) + Bu(t) \quad (\text{II.1})$$

$$y_r(t) = C_r x(t)$$

In the above, x is the modal state vector; x_{2i-1} is the position of the i th mode, while x_{2i} is the rate of the same mode. A is a block-diagonal matrix with blocks of the form

$$A_i = \begin{bmatrix} 0 & 1 \\ -w_i^2 & 2z_i w_i \end{bmatrix}$$

w_i is the i th modal eigenfrequency; the eigenfrequencies are classified in increasing order. z_i is the relative damping. u is the vector of the six axial forces acting along the legs of the bipeds; the rows of B with odd indices are vanishing, while the rows with even indices contain the coefficients of influence of the actuators on the corresponding mode. y_r is the six-dimensional output vector of the rate sensors located in the bipeds,

and $C_r = B'$.

Some more outputs can be defined: The six-dimensional output y_p of the position sensors located in the bipeds, and the two-dimensional output y_a giving displacement of the tetrahedral apex:

$$y_p(t) = C_p x(t)$$

$$y_a(t) = C_a x(t)$$

Define the transfer functions:

$$G_r(s) := C_r(sI-A)^{-1}B$$

$$G_p(s) := C_p(sI-A)^{-1}B = (1/s)G_r(s)$$

$$G_a(s) := C_a(sI-A)^{-1}B$$

Regardless of mode frequencies and shapes, ISS transfer functions enjoy some remarkable properties (Refs. 18,19). By a fairly general result, the (square) transfer matrix $G_r(s)$ from the (co-located) force actuators to the rate sensors is positive real (or dissipative). Further, the same transfer function is lossless if the relative damping ζ vanishes. Finally, observe that $G_r(s)$ is reciprocal, i.e., $G_r(s) = G_r'(s)$.

The finite element method (NASTRAN) was used by Draper Labs to derive the second order, modal equations of the truss (Refs. 19-21). These equations were further put into the first order, state equation form (II.1) by TRW (Ref. 20). The modal state equations (II.1) contain 12 eigenmodes. Both "nominal" and "perturbed" modal data are available to try out and evaluate control design techniques on the truss. The nominal data is available to the design engineer, while the perturbed data represents a realistic departure from the nominal data. In the nominal and perturbed cases, the eigenfrequencies are, respectively,

ω_1	=	1.3420108,	1.1706554 rad/sec
ω_2	=	1.6647234,	1.4667812
ω_3	=	2.8907117,	2.9646145
ω_4	=	2.9574139,	3.5577479
ω_5	=	3.3981995,	3.8483893
ω_6	=	4.2044821,	5.1494174
ω_7	=	4.6620682,	5.6759052
ω_8	=	4.7552602,	5.7108055
ω_9	=	8.5394174,	8.9396286
ω_{10}	=	9.2505638,	10.303582
ω_{11}	=	10.284775 ,	10.923379
ω_{12}	=	12.905111 ,	13.966664

III. CLOSED-LOOP PRINCIPAL COMPONENT ANALYSIS

Consider a minimal state space representation

$$\dot{x}/dt = Ax + Bu \quad (III.1)$$

$$y = Cx$$

of the plant transfer matrix

$$G(s) := C(sI-A)^{-1}B$$

y is an output available for feedback purposes, while u is the available control action.

The basic philosophy of the "closed-loop principal component analysis" is to measure how much each "mode" (more generally, each state component) participates in the inherent closed-loop behavior of the system. Model reduction and reduced compensation then follow by deleting the unessential modes. There are many ways, depending on the specifications, of closing up a system by a feedback loop, but it is attractive to do this in an optimal way using the Linear-Quadratic-Gaussian approach. This approach is indeed systematic and fairly well understood. It also has the advantage of endowing the design with fairly general robustness properties. More interestingly, the LQG design can be tuned to optimal sensitivity properties by correct adjustment of the the quadratic criterion and the noise covariances. To formulate the problem within the LQG setup, a disturbance Gaussian white noise $d(t)$ is added at the input and a measurement Gaussian white noise $n(t)$ is added at the output, as depicted in Fig. III.1. To tune the LQG design to optimal robustness properties, it is convenient to introduce the quadratic criterion

$$r_0 u'u + q_0 y'y \quad (III.2)$$

together with the noise statistics

$$E(d(t)d'(\tau)) = q_m I \delta(t-\tau) \quad (III.2)$$

$$E(d(t)n'(\tau)) = 0$$

$$E(n(t)n'(\tau)) = r_m I \delta(t-\tau)$$

The q 's and the r 's are (positive) parameters which must be tuned so as to reach satisfactory robustness properties. To understand how this can be done, let $K(s)$ be a causal, stabilizing, strictly proper compensator. A crucial result, apparently due to Youla (Refs. 1,2), connects up the performance $E(q_0 y'y + r_0 u'u)$ of the compensator $K(s)$ with robustness matrices as follows:

$$\begin{aligned}
& E(q_0 y' y + r_0 u' u) = \\
& 1/(2\pi j) \int_{-\infty}^{+\infty} \text{Trace} \{ \\
& q_0 r_m (I - GK)^{-1} G K K_* G_* (I - K_* G_*)^{-1} \\
& + q_0 q_m (I - GK)^{-1} G G_* (I - K_* G_*)^{-1} \\
& + r_0 q_m (I - KG)^{-1} K G G_* K_* (I - G_* K_*)^{-1} \\
& + r_0 r_m (I - KG)^{-1} K K_* (I - G_* K_*)^{-1} \} ds \quad (\text{III.3})
\end{aligned}$$

($K_*(s) := K'(-s)$, that is, the paraconjugate transpose of $K(s)$.) The matrices

$$(I - GK)^{-1} GK, (I - GK)^{-1} G, (I - KG)^{-1} KG, (I - KG)^{-1} K$$

are well known to be related to the robustness properties of the loop; the smaller they are, the better the robustness properties. Intuitively speaking, Equality (III.3) says that minimizing the expected value $E(q_0 y' y + r_0 u' u)$ is equivalent to minimizing the integral over all frequencies of "sizes" of "robustness" matrices. More intuitively, this says that minimizing a quadratic criterion boosts robustness. In the weighted average of the right side of Equation (III.3), the matrices $(I - GK)^{-1} GK$ and $(I - KG)^{-1} KG$ are of particular importance; they are indeed related to the stability margin of the feedback system (Ref. 3); the smaller these matrices, the more the feedback system can accommodate variations of GK and KG , respectively, before the loop becomes unstable. In closed-loop model reduction, the reduction error is considered as plant variation and is expected to be taken care of by the stability margin property of the loop. Hence, for this to be the case, it is imperative that the LQG problem underlying model reduction boosts the stability margin. This can be accomplished by assigning the following values to the parameters:

$$q_0 = 1, r_0 = \epsilon, q_m = \epsilon, r_m = 1$$

and by taking ϵ arbitrarily small. Yet this technique can be further refined by considering colored noises d and n and also by injecting them at other nodes along the loop (Refs. 1,2,3); we postpone these topics to a further paper.

Invoking the Separation Principle, one can split the design into an optimal filtering and an optimal control problem. It is well known (Refs. 4,5) that these optimization problems involve in a crucial way the filtering algebraic Riccati equation

$$A P_m + P_m A' + q_m B B' - P_m C' C P_m / r_m = 0$$

and the control algebraic Riccati equation

$$A' P_0 + P_0 A + q_0 C' C - P_0 B B' P_0 / r_0 = 0$$

The optimal LQG controller consists in the cascade of the optimal filter

$$dw/dt = Aw + Bu + r_m^{-1} P_m C' (z - Cw)$$

and the optimal control gain

$$u = -r_o^{-1} B' P_o w$$

This leads to the following state space representation of the compensator $K(s)$:

$$dw/dt = Fw + Gz$$

$$u = Hw$$

where

$$F := A - B r_o^{-1} B' P_o - P_m C' r_m^{-1} C$$

$$G := P_m C' / r_m$$

$$H := -B' P_o / r_o$$

The following is a fundamental result (Refs. 8, 10-12):

Theorem. Let (A, B, C) be a minimal realization of $G(s)$. Then the eigenvalues of $P_o P_m$ are similarity invariants. Further, these eigenvalues are real and strictly positive. If $\mu_1 > \mu_2 > \dots$ denote the eigenvalues of $P_o P_m$ in decreasing order, then there exists a "balancing" transformation \underline{T} and a "balanced" state space realization $(\underline{A}, \underline{B}, \underline{C}) := (\underline{T} A \underline{T}^{-1}, \underline{T} B, C \underline{T}^{-1})$ in which

$$\underline{P}_o = \underline{P}_m = M$$

where

$$M := \text{diag} \{ \mu_1, \mu_2, \dots \}$$

The physical interpretation of the above-defined quantities (the "closed-loop singular values") should be clear. Assume, for example, that μ_k is "small"; then the balanced state component x_k is "easy" to filter (\underline{P}_m "small" along the k th direction) and "easy" to control (\underline{P}_o "small" along the k th direction); hence, intuitively, x_k is an unessential state component; it is not significantly involved in the closed-loop LQG behavior of the system, and it can be discarded. Technically, this model reduction is done as follows: Assume

$$M = \text{block diag} \{ M_{11}, M_{22} \}$$

with M_{11} "much larger than" M_{22} . Partition both the plant state equations

$$\underline{dx}_1/dt = \underline{A}_{11}\underline{x}_1 + \underline{A}_{12}\underline{x}_2 + \underline{B}_1u$$

$$\underline{dx}_2/dt = \underline{A}_{21}\underline{x}_1 + \underline{A}_{22}\underline{x}_2 + \underline{B}_2u$$

$$y = \underline{C}_1\underline{x}_1 + \underline{C}_2\underline{x}_2$$

and the controller state equations

$$d\underline{w}_1/dt = \underline{F}_{11}\underline{w}_1 + \underline{F}_{12}\underline{w}_2 + \underline{G}_1z$$

$$d\underline{w}_2/dt = \underline{F}_{21}\underline{w}_1 + \underline{F}_{22}\underline{w}_2 + \underline{G}_2z$$

$$u = \underline{H}_1\underline{w}_1 + \underline{H}_2\underline{w}_2$$

conformably with M . The obvious reduced-order model is $(\underline{A}_{11}, \underline{B}_1, \underline{C}_1)$, and it is easily proved that its optimal LQG controller is the obvious reduced-order compensator $(\underline{F}_{11}, \underline{G}_1, \underline{H}_1)$. The problem of the stability of the full plant $G(s)$ closed up by the reduced compensator is tackled in the paper of the author and Silverman (Ref. 12). It is there proved that stability is guaranteed provided M_{22} is "sufficiently small".

Besides this stability result, the closed-loop principal component analysis yields other remarkable results (Ref. 12), relevant to ISS:

Theorem. Let (A, B, C) be a minimal realization of $G(s)$. Take $q_m = r^{-1}$ and $q_0 = r_m^{-1}$. Then $G(s)$ is a reciprocal, lossless transfer matrix if and only if $m_k = 1, k=1, 2, \dots$. Further, in that case, the balanced state space realization is unique within orthogonal similarities and in any such realization $\underline{A} = -\underline{A}'$ and $\underline{C} = \underline{B}'$.

A few words about computations. The main computational burden is the solution to both algebraic Riccati equations. However, there is a fast and reliable procedure for solving the algebraic Riccati equation: the technique of Laub (Ref. 6), which proceeds via the quasi-upper triangular form of the Hamiltonian matrix. Once P_m and P_0 are computed, their simultaneous diagonalization proceeds via the factorization of one of them, say, $P_m = LL'$, followed by the eigenanalysis of $L'P_0L$; see Ref. 8.

IV. RESULTS

In this section, the tetrahedral truss is analysed in the light of the closed-loop principal component analysis. Several plant transfer matrices, corresponding to different combinations of sensors and actuators, are considered. In each case, the modes are classified by order of closed-loop importance. The parameters q and r of the quadratic criterion and the noise statistics are varied so as to determine how the classification is affected by the stability margin requirements. Tentative conclusions for model reduction

are derived.

IV.1. force actuator/rate sensor transfer matrix; nominal data; no damping; $q_o=r_o=q_m=r_m=1$

The 6x6 transfer matrix from the (co-located) force actuators to the rate sensors is lossless and reciprocal; hence all of the μ 's must be equal to 1. Since we know in advance the result, this case is rather a good test of how well the numerical software performs. The software has given the right values, up to a relative error of 10^{-14} ; see Table IV.1. This is quite satisfactory. Regarding the balancing matrix T , which transforms the modal state space representation (A, B, C_r) into the balanced state space representation $(\underline{A}, \underline{B}, \underline{C}_r)$, it is easily found that this transformation can be taken as block diagonal with blocks of the form

$$T = \begin{bmatrix} 0 & (w) & -1/2 \\ & i & \\ -i & (w) & 1/2 \\ & i & 0 \end{bmatrix}$$

However, the balancing transformation is uniquely defined up to orthogonal transformations, and the software does not pick up precisely the above transformation (there are no reasons why it should).

Thus, the closed-loop principal component analysis does not manage to make any discrimination between essential and nonessential modes, when the undamped truss is closed up by a feedback loop from the rate sensors to the force actuators. Intuitively, the reason is that the rate sensors differentiate the modal displacements; this is roughly equivalent to multiplying the modal displacements by their respective eigenfrequencies, thereby boosting the contribution of the high frequency modes and leveling up everything.

IV.2. force actuator/rate sensor transfer matrix; nominal data; nonzero damping; $q_o=r_o=q_m=r_m=1$

Since a ISS exhibits a structural damping, which is poorly known, it is important to determine how the above analysis is affected by the damping and to make sure that the results are consistent over a realistic range of relative damping values.

The results of the closed-loop principal component analysis for $\zeta=0.01$ and 0.001 are given in Table IV.2. The introduction of this damping clearly spreads the spectrum of the μ 's. A distinction between essential and nonessential state components is now possible. Observe that the μ 's appear by pairs of roughly equal values (this was also the case for the open-loop analysis (Ref. 15)); it is therefore tempting to associate each such pair with a particular mode. This intuitive conclusion is validated by the "pattern" of

the balancing transformation shown in Table IV.2. The balancing transformation is very "sparse"; in other words, the balancing transformation merely relabels the modal coordinates. Observe that the pattern of the balancing transformation is not significantly affected by the relative damping. In other words, the closed-loop principal component analysis does not depend too much on the (poorly known) structural damping. Surprisingly enough, observe that the modes are classified by decreasing order of importance as follows:

6,7,8,5,4,3,9,10,2,11,1,12

IV.3. force actuator/rate sensor transfer matrix; nominal data; nonzero damping; $q_o=\epsilon$, $r_o=1$, $q_m=1$, $r_m=\epsilon$

We now examine how the above classification is affected when the quadratic criterion and the noise statistics are chosen so as to boost the inverse return difference $I-(KG_r)^{-1}$, the size of this matrix being somehow proportional to the stability margin. The results are shown in Table IV.3. Somehow they are not quite different from the preceding case. The relative spread of the μ 's is about the same. The balancing transformation is still sparse, thereby relabeling the modal coordinate. The whole analysis is not that much affected by the parameter ϵ . In all of these cases, the closed-loop principal component analysis consistently classifies the modes by order of decreasing importance as follows:

6,7,8,5,4,3,9,10,2,11,1,12

that is, the same as for the preceding case.

IV.4. force actuator/position sensor transfer matrix; nominal data; no damping; $q_o=r_o=q_m=r_m=1$

We now look at the case where the controller utilizes the output y_p of the position sensors located in the bipod legs, that is, in the quadratic criterion (III.2) we take $y=y_p$. We are not yet quite concerned about the stability margin, that is, we normalize the performance criterion and the noise statistics as $q_o=r_o=q_m=r_m=1$. The results of the closed-loop principal component analysis of $G_p(s)$ are given in Table IV.4. All of the μ 's are very close to one, within 10^{-2} . The spectrum of the closed-loop singular values of the transfer function from the force actuators to the displacement sensors is surprisingly concentrated, while the spectrum of the open-loop singular values is much broader (Refs. 15,16). It is thus difficult to classify the modes by order of importance. The balancing transformation is not quite sparse, simply because it is hard to make a distinction between the modes.

IV.5. force actuator/position sensor transfer matrix; nominal data; nonzero damping; $q_o=r_o=q_m=r_m=1$

We now look at how the closed-loop principal component analysis of $G_p(s)$ is

affected by the damping. The results are summarized in Table IV.5. Clearly, the introduction of a relative damping somehow spreads the μ 's, and a classification is now possible. As a result, the balancing transformation is "sparse"; however, the balancing transformation does not exactly relabel the modal coordinates. For example, for $\zeta=0.01$, the balanced coordinates $\underline{x}_5, \underline{x}_6, \underline{x}_7$, and \underline{x}_8 depend on the modal coordinates of both eigenmodes 4 and 7; somehow, the eigenmodes 4 and 7 are intercoupled in the balanced coordinates and can hardly be discriminated importance-wise. Also, the balanced coordinates $\underline{x}_9, \underline{x}_{10}, \underline{x}_{11}$, and \underline{x}_{12} depend on the eigenmodes 3 and 8. Thus the classification of the eigenmodes in decreasing order of importance is as follows:

6,5,(4,7),(3,8),2,1,9,10,11,12

The parentheses indicate that the modes are intercoupled in the balanced coordinates and cannot be discriminated. This classification is not the same as for the case of rate sensor output feedback. Further, this classification is slightly affected by the damping, though an "invariant" feature is that eigenmodes 9, 10, 11, and 12 are always classified as nonimportant.

IV.6. force actuator/position sensor transfer matrix; nominal data; nonzero damping; $q_o=1, r_o=\epsilon, q_m=\epsilon, r_m=1$

The quadratic criterion and the noise statistics are now chosen so as to boost the stability margin, that is, the "size" of $I-(G_p K)^{-1}$, for the position sensor output feedback case. The results are summarized in Table IV.6. The μ 's are about as well spread as for the preceding case. Further, the balancing transformation is about as "sparse" as for the preceding case, which means that the balancing does not exactly reorder the modal coordinates. For $\epsilon=0.1$, the classification is as follows:

(5,6),(4,7),(3,8),2,1,9,10,11,12

For $\epsilon=0.01$, the classification becomes

(3,4,5,6,7,8),2,1,9,10,11,12

Thus, the classification depends on the stability margin requirement. As the stability margin increases, the coupling of some modes, for example, 6, 7, and 8, increases; this is because these modes have very close eigenfrequencies. As the stability margin requirement varies, the only "invariant feature" is that eigenmodes # 9, 10, 11, and 12 are consistently decoupled from the others and classified as nonimportant; this can be justified by the big gap between ω_8 and ω_9 .

IV.7. force actuator/position sensor transfer matrix; nominal data;
nonzero damping; $q_o=\epsilon$, $r_o=1$, $q_m=1$, $r_m=\epsilon$

We still look at the case of a displacement feedback, but we are now concerned about the inverse-return difference matrix $I-(KG_p)^{-1}$. The "size" of this inverse-return difference matrix is boosted if the quadratic criterion and the noise covariances are taken as above. The results are shown in Table IV.7. For $\epsilon=0.1$, the classification, by decreasing order of importance, is the following:

(5,6),(4,7),(3,8),2,1,9,10,11,12

Under the more stringent stability margin requirement $\epsilon=0.01$, this classification becomes

(3,4,5,6,7,8),2,1,9,10,11,12

Thus the classification is the same as for the preceding case. Further, comparing Tables IV.6 and IV.7 shows that this case is very close to the preceding. This observation is reassuring. Indeed, in the multivariable feedback loop, the stability of both transfer matrices $(I-G_p K)^{-1}$ and $(I-KG_p)^{-1}$ is involved, and their stability margins are given by the "sizes" of the inverse-return difference matrices $I-(G_p K)^{-1}$ and $I-(KG_p)^{-1}$, respectively. It is reassuring to observe that the boosting of both stability margins is nonconflicting in this approach.

IV.8. force actuator/position sensor transfer matrix; perturbed data;
nonzero damping; $q_o=\epsilon$, $r_o=1$, $q_m=1$, $r_m=\epsilon$

Needless to say, the modal data of a ISS is highly uncertain. It is therefore useful to determine the extent to which the above analysis, say case # IV.7, is affected by a variation of the mode eigenfrequencies and shapes. The results of the principal component analysis in the perturbed data case are summarized in Table IV.8. Observe that the results are close to those of case study # IV.8. If $\epsilon=0.1$, the classification is as follows:

6,5,(4,7,8),3,2,1,10,11,9,12

Now, if the stability margin requirement is more stringent, i.e., $\epsilon=0.01$, the classification becomes:

(4,5,6,7,8),3,2,1,10,11,9,12

Thus increasing the stability margin requirement produces more intercoupling between some modes, that is, the same tendency as for the nominal data case. It seems, therefore, that the closed-loop principal component analysis picks up the "fine" structure of the system, and does not rely too much on mode eigenfrequencies and shapes. This is reassuring.

IV.9. force actuator/position sensor; nominal data; nonzero damping;
 $E(q_a y_a' y_a + q_o y_p' y_p + r_o u' u)$

In all of the previous cases, we have stabilized the whole system, without particular attention to the deviation of the tetrahedral apex. Here we introduce a quadratic criterion which explicitly penalizes the deviation y_a of the apex. We have taken $q_a=1.0$; the other parameters are taken so as to take care of the stability margin, i.e., $q_o=\epsilon$, $r_o=1$, $q_m=1$, $r_m=g(e)$, with $\epsilon=0.1$. The results are shown in Table IV.9. Observe that the μ 's are fairly well spread, and that the balancing transformation has a much more diagonal structure. This means that, if one is primarily concerned with the deflection of the apex, the modes are somehow classified by decreasing frequencies. Remember, however, that because of the penalty on y_a we lose on the stability margin. There thus appears to be a conflict between precise control of the apex and good stability margin.

V. CONCLUSIONS

We have presented in this paper a procedure for evaluating the "dynamical importance" of each vibration mode in a Large Space Structure operating under feedback control. The main conclusion we have drawn is that the closed-loop importance of each vibration mode depends on the robustness requirements. Also, there appears to be a conflict between precise control of a given node of the structure and stability margin, these two requirements leading to contradictory classifications of the modes by order of importance. A refined version of this analysis, using frequency-dependent weightings (Refs. 1-3) to take care of noise, sensor, and actuator bandwidths, is postponed to a further paper.

ACKNOWLEDGMENT

Some useful discussions on this subject matter with Dr. R.J. Benhabib of the Defense and Space Systems Group of TRW, Redondo Beach, is gratefully acknowledged.

REFERENCES

1. Youla, D.C., Bongiorno, J.J., and Jabr, H.A., "Modern Wiener-Hopf Design of Optimal Controllers--Part I: The Single-Input-Output Case," IEEE Trans. Automat. Contr., Vol. AC-21, 1976, pp. 3-13.
2. Youla, D.C., Jabr, H.A., and Bongiorno, J.J., "Modern Wiener-Hopf Design of Optimal Controllers--Part II: The Multivariable Case," IEEE Trans. Automat. Contr., Vol. AC-21, 1976, pp. 319-338.
3. Safonov, M.G., Laub, A.J., and Hartmann, G.L., "Feedback Properties of Multivariable Systems: The Role and Use of the Return Difference Matrix," IEEE Trans. Automat. Contr., Vol. AC-26, 1981, pp. 47-65.

4. Willems, J.C., "Least Squares Stationary Optimal Control and the Algebraic Riccati Equation," IEEE Trans. Automat. Contr., Vol. AC-16, 1971, pp. 621-634.
5. Rodriguez-Canabal, J.M., "The geometry of the Riccati Equation," Stochastics, Vol. 1, 1973, pp. 129-149.
6. Laub, A.J., "A Schur Method for Solving Algebraic Riccati Equations," IEEE Trans. Automat. Contr., Vol. AC-24, 1979, pp. 913-921.
7. Moore, B.C., "Principal Component Analysis in Linear Systems: Controllability, Observability, and Model Reduction," IEEE Trans. Automat. Contr., Vol. AC-26, 1981, pp. 17-32.
8. Laub, A.J., "Computation of "Balancing" Transformations," Proc. JACC, San Francisco, CA, 1980, FA8-E.
9. Skelton, R.E., and Yousuff, A., "Component cost analysis of large-scale systems," Lecture Notes, School of Aeronautics and Astronautics, Purdue University, West La Fayette, Indiana, 1982.
10. Verriest, E., "Low Sensitivity Design and Optimal Order Reduction for the LQG-Problem," 24th Midwest Symp. on Circuits and Systems, Albuquerque, NM, 1981, pp. 365-369.
11. Jonckheere, E.A., and Silverman, L.M., "A New Set of Invariants for Linear Systems--Application to Approximation," 1981 International Symp. Math. Th. Networks and Syst., Santa Monica, CA, 1981, pp. 129-133.
12. Jonckheere, E.A., and Silverman, L.M., "A New Set of Invariants for Linear Systems--Application to Reduced-Order Compensator Design," IEEE Trans. Automat. Contr., to appear, 1982.
13. Jonckheere, E., "On the Observability of the Deformable Modes in a Class of Nonrigid Satellites," ESA Symp. on Dynamics and Control of Non-Rigid Spacecraft, Frascati, Italy, 1976, pp. 251-262.
14. Jonckheere, E., "Robustness of Observers for Estimating the State of a Deformable Satellite," ESA Conf. on Attitude and Orbit Control Systems, Noordwijk, The Netherlands, 1977, Preprints pp. 191-202.
15. Jonckheere, E.A., and Silverman, L.M., "Singular Value Analysis of Deformable Systems," IEEE CDC, San Diego, CA, 1981, pp. 660-668.
16. Jonckheere, E.A., and Silverman, L.M., "Singular Value Analysis of Deformable Systems," J. Circuits, Systems, and Signal Processing, Special Issue on Rational Approximation for Systems, to appear, 1982.
17. Balas, M.J., "Feedback Control of Flexible Systems," IEEE Trans. Automat. Contr., Vol. AC-23, 1978, pp. 673-679.

18. Benhabib, R.J., Iwens, R.P., and Jackson, R.L., "Stability of Distributed Control for Large Flexible Structures Using Positivity Concepts," AIAA Guidance and Control Conference, Boulder, CO, 1979, pp. 540-548.
19. Benhabib, R.J., "Discrete Large Space Structure Control System Design Using Positivity," IEEE CDC, San Diego, CA, 1981, pp. 715-724.
20. Benhabib, R.J., private communication, 1981.
21. Strunce, R., "Description of Draper Example Structural Model," Charles Stark Draper Labs.

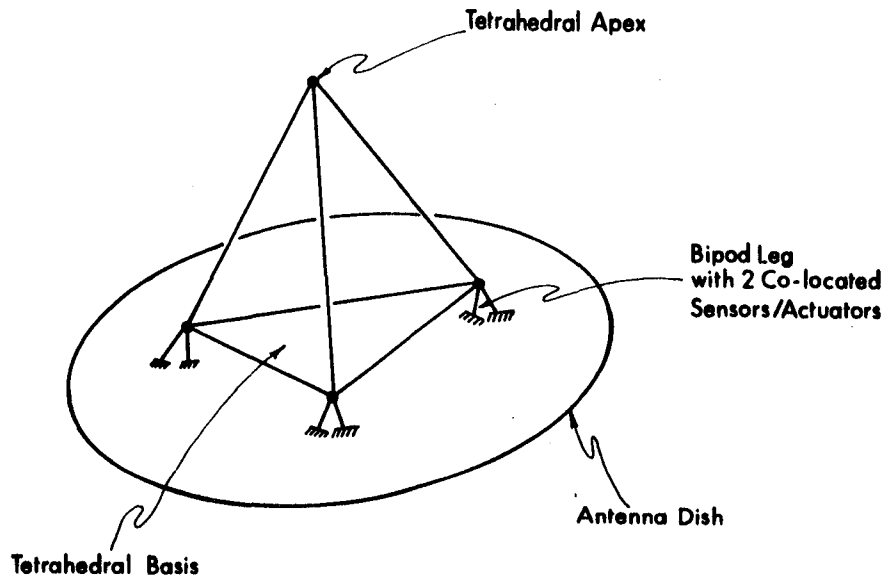


Figure I.1.

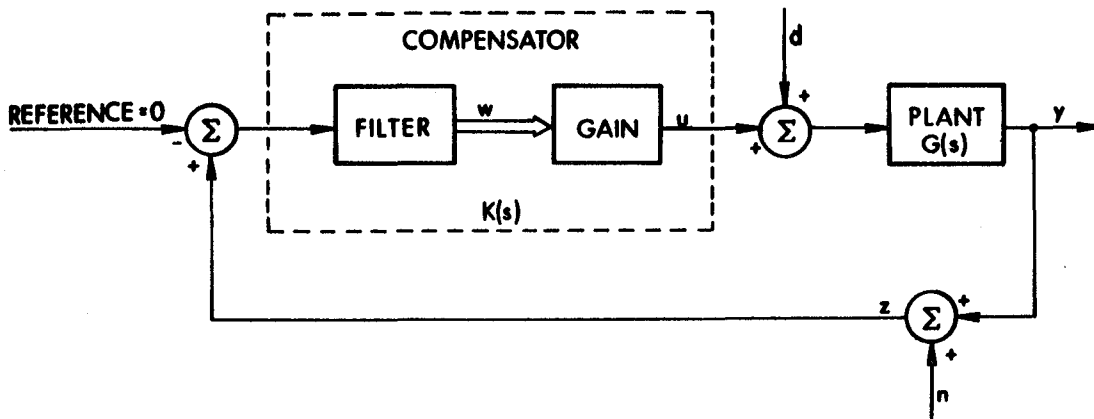
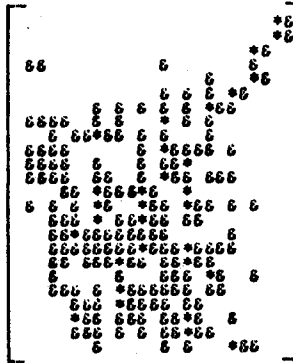


Figure III.1.

TRANSFER FUNCTION FROM FORCE ACTUATORS TO RATE SENSORS
 NOMINAL DATA; RELATIVE DAMPING ZETA = .0000000000000000D+00

MU 1 = .1000000000000000423D+01
 MU 2 = .1000000000000000374D+01
 MU 3 = .1000000000000000031D+01
 MU 4 = .1000000000000000027D+01
 MU 5 = .1000000000000000016D+01
 MU 6 = .1000000000000000009D+01
 MU 7 = .1000000000000000004D+01
 MU 8 = .1000000000000000003D+01
 MU 9 = .1000000000000000003D+01
 MU 10 = .1000000000000000002D+01
 MU 11 = .1000000000000000002D+01
 MU 12 = .1000000000000000001D+01
 MU 13 = .1000000000000000001D+01
 MU 14 = .1000000000000000001D+01
 MU 15 = .1000000000000000000D+01
 MU 16 = .1000000000000000000D+01
 MU 17 = .1000000000000000000D+01
 MU 18 = .999999999999999995D+00
 MU 19 = .999999999999999993D+00
 MU 20 = .999999999999999993D+00
 MU 21 = .999999999999999999D+00
 MU 22 = .999999999999999992D+00
 MU 23 = .9999999999999999978D+00
 MU 24 = .9999999999999999966D+00

X (BALANCED)



X (MODAL)

TABLE IV.1

TRANSFER FUNCTION FROM FORCE ACTUATORS TO RATE SENSORS
 NOMINAL DATA; RELATIVE DAMPING ZETA = .1000000000000000D-02

MU 1 = .983323883786612438D+00
 MU 2 = .983323883784591505D+00
 MU 3 = .980819643938514959D+00
 MU 4 = .980763442337892752D+00
 MU 5 = .979272310893703678D+00
 MU 6 = .979201918591668669D+00
 MU 7 = .977534063997911156D+00
 MU 8 = .977429143876111509D+00
 MU 9 = .9771134919367825376D+00
 MU 10 = .977074542769827732D+00
 MU 11 = .965075548122938087D+00
 MU 12 = .965002572505530646D+00
 MU 13 = .950485531162405975D+00
 MU 14 = .950429884895338641D+00
 MU 15 = .940514519302285285D+00
 MU 16 = .940445267294837664D+00
 MU 17 = .909512697590844786D+00
 MU 18 = .909436605878839803D+00
 MU 19 = .892929319922095508D+00
 MU 20 = .892906020325095011D+00
 MU 21 = .825497002510449850D+00
 MU 22 = .825439295813003594D+00
 MU 23 = .432095616061839846D+00
 MU 24 = .432030408347163280D+00

I =

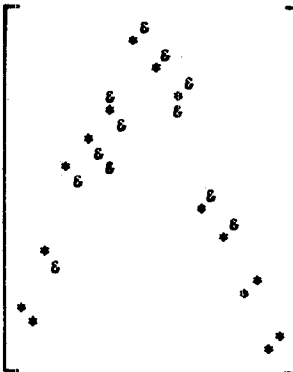


TABLE IV.2

→ Pattern of balancing transformation I
 a blank denotes an entry less than 0.1
 E denotes an entry between 0.1 and 1.0
 B denotes an entry greater than 1.0

TRANSFER FUNCTION FROM FORCE ACTUATORS TO RATE SENSORS
 NOMINAL DATA; RELATIVE DAMPING ZETA = .1000000000000000D-01

MU 1 = .845864248500712689D+00
 MU 2 = .845864248464917286D+00
 MU 3 = .824913388763218445D+00
 MU 4 = .824551441180369514D+00
 MU 5 = .812238846740392822D+00
 MU 6 = .811673644193714442D+00
 MU 7 = .79872430447793288D+00
 MU 8 = .797711638591242474D+00
 MU 9 = .74910068505068248D+00
 MU 10 = .748597316219139735D+00
 MU 11 = .705706226346375584D+00
 MU 12 = .705139674995173724D+00
 MU 13 = .613643709511832253D+00
 MU 14 = .613196037987104590D+00
 MU 15 = .559600061547356764D+00
 MU 16 = .559132087172831184D+00
 MU 17 = .429300531909788405D+00
 MU 18 = .428843536542782594D+00
 MU 19 = .377611090989226210D+00
 MU 20 = .377350619966514385D+00
 MU 21 = .243720340956627955D+00
 MU 22 = .243456190167325270D+00
 MU 23 = .527292682654299050D-01
 MU 24 = .525157243603623179D-01

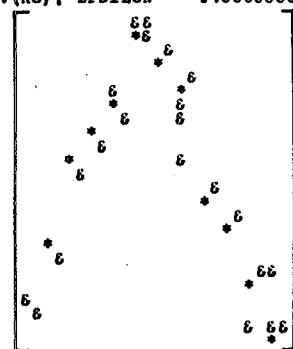
TABLE IV.2



TRANSFER FUNCTION FROM FORCE ACTUATORS TO RATE SENSORS
 NOMINAL DATA; RELATIVE DAMPING ZETA = .1000000000000000D-01
 LQG DESIGN TUNED TO OPTIMAL STABILITY MARGIN 1-INV(KG); EPSILON = .1000000000000000D+00

MU 1 = .238682590369923862D+00
 MU 2 = .238682590362563999D+00
 MU 3 = .229551503854356045D+00
 MU 4 = .229363653422528288D+00
 MU 5 = .224193794989850928D+00
 MU 6 = .223933902014659207D+00
 MU 7 = .218507614629488769D+00
 MU 8 = .218189736890375168D+00
 MU 9 = .199518016624571102D+00
 MU 10 = .199294481609592135D+00
 MU 11 = .184288271324301332D+00
 MU 12 = .184048078722857831D+00
 MU 13 = .155992577047513751D+00
 MU 14 = .155796187859624213D+00
 MU 15 = .141341822268931237D+00
 MU 16 = .141342186957762591D+00
 MU 17 = .109638262674054169D+00
 MU 18 = .109449092941057215D+00
 MU 19 = .977806590633874124D-01
 MU 20 = .976832959936849013D-01
 MU 21 = .674482526367440979D-01
 MU 22 = .673394624204024304D-01
 MU 23 = .162497356124918694D-01
 MU 24 = .161645648258629497D-01

TABLE IV.3



TRANSFER FUNCTION FROM FORCE ACTUATORS TO POSITION SENSORS
 NOMINAL DATA; RELATIVE DAMPING ZETA = .0000000000000000D+00

MU 1 = .101423926472700677D+01
 MU 2 = .101404206879622019D+01
 MU 3 = .101394397358369611D+01
 MU 4 = .101394095085990275D+01
 MU 5 = .101325391592447369D+01
 MU 6 = .101322308021615348D+01
 MU 7 = .100096029059211659D+01
 MU 8 = .100092393735791455D+01
 MU 9 = .100034248685618451D+01
 MU 10 = .100031915399929245D+01
 MU 11 = .100020862324252840D+01
 MU 12 = .100000046204300466D+01
 MU 13 = .999999537959220541D+00
 MU 14 = .99979342027262952D+00
 MU 15 = .999680947827486745D+00
 MU 16 = .999657630400903537D+00
 MU 17 = .999076915514329301D+00
 MU 18 = .999040630681216010D+00
 MU 19 = .986949487754136387D+00
 MU 20 = .986919452551653602D+00
 MU 21 = .986250727076258471D+00
 MU 22 = .986247786912316192D+00
 MU 23 = .986152380428494631D+00
 MU 24 = .985960645360304232D+00

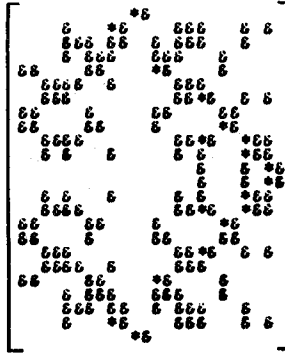


TABLE IV.4

TRANSFER FUNCTION FROM FORCE ACTUATORS TO POSITION SENSORS
 NOMINAL DATA; RELATIVE DAMPING ZETA = .1000000000000000D-01

MU 1 = .526649576012628985D+00
 MU 2 = .508722088066390844D+00
 MU 3 = .500231555295008705D+00
 MU 4 = .484065309965155186D+00
 MU 5 = .464470725932595146D+00
 MU 6 = .451209576729016655D+00
 MU 7 = .450402896576539488D+00
 MU 8 = .438006821993037386D+00
 MU 9 = .422573649241578554D+00
 MU 10 = .412728605442178868D+00
 MU 11 = .410486961420845941D+00
 MU 12 = .401603722416743122D+00
 MU 13 = .293171120375686796D+00
 MU 14 = .286328945045372426D+00
 MU 15 = .188400926772652613D+00
 MU 16 = .184406067425729387D+00
 MU 17 = .15078810665795447D+00
 MU 18 = .112742164852720581D+00
 MU 19 = .883429039589320286D-01
 MU 20 = .865684096999520098D-01
 MU 21 = .432761637985200255D-01
 MU 22 = .424156671872676647D-01
 MU 23 = .414867058042272071D-02
 MU 24 = .406794408008937210D-02

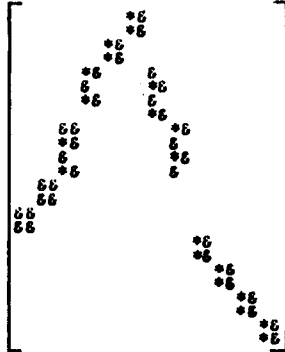


TABLE IV.5

TRANSFER FUNCTION FROM FORCE ACTUATORS TO POSITION SENSORS
 NOMINAL DATA; RELATIVE DAMPING ZETA = .1000000000000000D-01
 LOG DESIGN TUNED TO OPTIMAL STABILITY MARGIN I-INV(GK); EPSILON = .1000000000000000D+00

MU 1 = .134500696377539275D+00
 MU 2 = .127855086172614530D+00
 MU 3 = .127085520058915962D+00
 MU 4 = .121232181320558766D+00
 MU 5 = .119383150560374796D+00
 MU 6 = .115248047125898619D+00
 MU 7 = .113496012191293850D+00
 MU 8 = .110644592148487736D+00
 MU 9 = .109472272110817571D+00
 MU 10 = .106677577956110469D+00
 MU 11 = .104644918919009264D+00
 MU 12 = .102324956644437929D+00
 MU 13 = .793941613916067599D-01
 MU 14 = .768640427959987990D-01
 MU 15 = .74740326020445115D-01
 MU 16 = .528909549704136322D-01
 MU 17 = .348544752948918580D-01
 MU 18 = .340828412125691401D-01
 MU 19 = .271842601313394536D-01
 MU 20 = .266078646131088240D-01
 MU 21 = .135852598312289240D-01
 MU 22 = .13113956411103457D-01
 MU 23 = .131146375390867966D-02
 MU 24 = .128599786708630400D-02

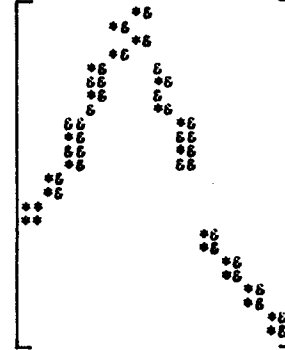


TABLE IV.6

TRANSFER FUNCTION FROM FORCE ACTUATORS TO POSITION SENSORS
 NOMINAL DATA; RELATIVE DAMPING ZETA = .1000000000000000D-01
 LOG DESIGN TUNED TO OPTIMAL STABILITY MARGIN; EPSILON = .1000000000000000D-01

MU 1 = .275889791010572170D-01
 MU 2 = .262213497076064106D-01
 MU 3 = .245606295092365048D-01
 MU 4 = .237682715504828433D-01
 MU 5 = .237471174032811037D-01
 MU 6 = .228789740256103475D-01
 MU 7 = .227902986494801355D-01
 MU 8 = .218264032050708229D-01
 MU 9 = .216587869407960374D-01
 MU 10 = .210987198810891294D-01
 MU 11 = .204130857284760972D-01
 MU 12 = .196406421752567460D-01
 MU 13 = .168796030793629760D-01
 MU 14 = .157123298042878341D-01
 MU 15 = .123937800991666832D-01
 MU 16 = .118089892718795669D-01
 MU 17 = .884204623440648665D-02
 MU 18 = .853731885327878404D-02
 MU 19 = .726248220013023369D-02
 MU 20 = .704686212912609781D-02
 MU 21 = .402667327845060435D-02
 MU 22 = .393475806026910356D-02
 MU 23 = .41357652185338885D-03
 MU 24 = .405625293343716261D-03

$I - (GK)^{-1}$

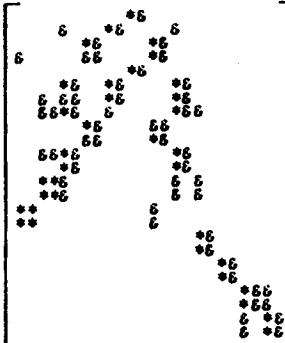


TABLE IV.6

TRANSFER FUNCTION FROM FORCE ACTUATORS TO POSITION SENSORS
 NOMINAL DATA; RELATIVE DAMPING ZETA = .1000000000000000D-01
 LQG DESIGN TUNED TO OPTIMAL STABILITY MARGIN 1-INV(KG); EPSILON = .1000000000000000D+00

MU 1 = .134500696377539370D+00
 MU 2 = .127855086172614498D+00
 MU 3 = .12785520058916040D+00
 MU 4 = .1213218132058795D+00
 MU 5 = .119189150590374658D+00
 MU 6 = .115924804712569223D+00
 MU 7 = .113496012191293767D+00
 MU 8 = .110644592148487405D+00
 MU 9 = .109472272110817620D+00
 MU 10 = .106677577956110426D+00
 MU 11 = .104644938919009229D+00
 MU 12 = .10224956644437943D+00
 MU 13 = .79394161391600529D-01
 MU 14 = .78640427959987789D-01
 MU 15 = .542740326020445139D-01
 MU 16 = .528909549704336127D-01
 MU 17 = .348544752948911637D-01
 MU 18 = .34082841212568053D-01
 MU 19 = .27164260131341757D-01
 MU 20 = .266078646131079940D-01
 MU 21 = .135852599312300037D-01
 MU 22 = .13311395641107759D-01
 MU 23 = .131146375991045269D-02
 MU 24 = .128599786708680984D-02

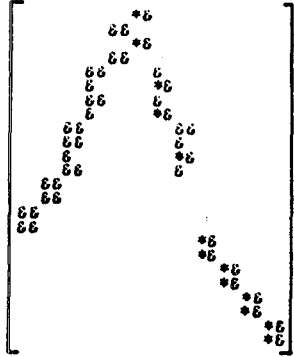


TABLE IV.7

TRANSFER FUNCTION FROM FORCE ACTUATORS TO POSITION SENSORS
 NOMINAL DATA; RELATIVE DAMPING ZETA = .1000000000000000D-01
 LQG DESIGN TUNED TO OPTIMAL STABILITY MARGIN 1-INV(KG); EPSILON = .1000000000000000D-01

MU 1 = .275889791010572974D-01
 MU 2 = .262213497076063345D-01
 MU 3 = .245606295092364501D-01
 MU 4 = .2376277480328083D-01
 MU 5 = .2317927740320037D-01
 MU 6 = .228749740256100791D-01
 MU 7 = .227802986494804812D-01
 MU 8 = .218264032050706403D-01
 MU 9 = .216587869407957664D-01
 MU 10 = .210987198810889048D-01
 MU 11 = .204130857484758624D-01
 MU 12 = .196406307952567339D-01
 MU 13 = .1897964307933493D-01
 MU 14 = .157123299012869639D-01
 MU 15 = .123997800991666841D-01
 MU 16 = .118089892718795438D-01
 MU 17 = .694204623441040925D-02
 MU 18 = .853731885327749655D-02
 MU 19 = .726248220012950422D-02
 MU 20 = .704686212912788575D-02
 MU 21 = .402667327845272071D-02
 MU 22 = .393475608027300050D-02
 MU 23 = .41356765218722513D-03
 MU 24 = .405625293340533149D-03

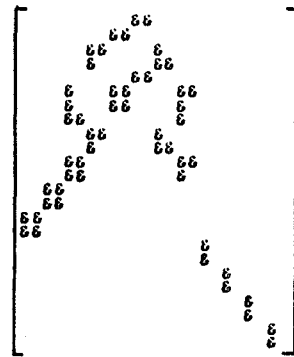


TABLE IV.7

TRANSFER FUNCTION FROM FORCE ACTUATORS TO POSITION SENSORS
 PERTURBED DATA; RELATIVE DAMPING ZETA = .1000000000000000D-01
 LQG DESIGN TUNED TO OPTIMAL STABILITY MARGIN 1-INV(KG); EPSILON = .1000000000000000D+00

MU 1 = .104604445146982473D+00
 MU 2 = .100316193657139951D+00
 MU 3 = .967024488554339602D-01
 MU 4 = .930361233846200964D-01
 MU 5 = .905718691167178525D-01
 MU 6 = .898193899916536494D-01
 MU 7 = .885034095140295110D-01
 MU 8 = .872881788500667901D-01
 MU 9 = .86089212544128630D-01
 MU 10 = .854060589080771586D-01
 MU 11 = .717089129809804272D-01
 MU 12 = .695681549760493563D-01
 MU 13 = .500180940502049705D-01
 MU 14 = .487872915562690576D-01
 MU 15 = .340651083116744841D-01
 MU 16 = .333140223806058059D-01
 MU 17 = .325412325171723332D-01
 MU 18 = .162476865982206172D-01
 MU 19 = .158703977346607295D-01
 MU 20 = .150349545517821074D-01
 MU 21 = .147764721338742269D-01
 MU 22 = .743036868423379882D-03
 MU 23 = .728496889799941810D-03

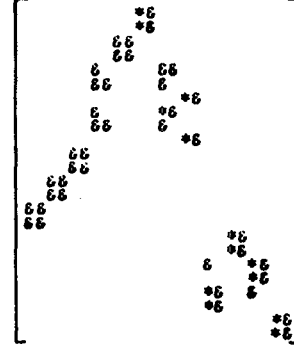


TABLE IV.8

TRANSFER FUNCTION FROM FORCE ACTUATORS TO POSITION SENSORS
 PERTURBED DATA; RELATIVE DAMPING ZETA = .1000000000000000D-01
 LQG DESIGN TUNED TO OPTIMAL STABILITY MARGIN 1-INV(KG); EPSILON = .1000000000000000D-01

MU 1 = .216653638618227531D-01
 MU 2 = .201746606166100215D-01
 MU 3 = .195202985675520740D-01
 MU 4 = .191271448267610856D-01
 MU 5 = .186372021718063833D-01
 MU 6 = .186941817643587852D-01
 MU 7 = .183679750675748411D-01
 MU 8 = .175195127790563220D-01
 MU 9 = .173194912066228307D-01
 MU 10 = .171873170692655855D-01
 MU 11 = .156195591337095647D-01
 MU 12 = .146259891418875765D-01
 MU 13 = .1625473824346389D-01
 MU 14 = .111703596581693107D-01
 MU 15 = .865092222995775079D-02
 MU 16 = .835892982347452205D-02
 MU 17 = .634503303205195538D-02
 MU 18 = .617129459822042235D-02
 MU 19 = .472125535007462991D-02
 MU 20 = .458782771955240079D-02
 MU 21 = .4354243805819679D-02
 MU 22 = .431139055616638373D-02
 MU 23 = .234623206784797151D-03
 MU 24 = .230059680506548157D-03

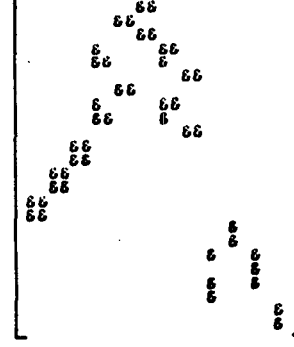


TABLE IV.8

FEEDBACK LOOP FROM POSITION SENSORS TO FORCE ACTUATORS
 NOMINAL DATA; RELATIVE DAMPING ZETA = .1000000000000000D-01
 LOG DESIGN TUNED TO GOOD STABILITY MARGIN I-INV(KG); EPSILON = .1000000000000000D+00
 PENALTY ON THE MISALIGNMENT OF THE TETRAHEDRAL APEX; QA = .1000000000000000D+01

NU 1 = .923241386027993653D+00
 NU 2 = .917532585667735752D+00
 NU 3 = .913531409235174291D+00
 NU 4 = .902003001311227865D+00
 NU 5 = .364732044401400837D+00
 NU 6 = .352242349231984941D+00
 NU 7 = .287613731414219199D+00
 NU 8 = .281470172248874995D+00
 NU 9 = .269929973721119042D+00
 NU 10 = .264429509310469666D+00
 NU 11 = .263332934316548546D+00
 NU 12 = .261840862488049552D+00
 NU 13 = .226924556803458831D+00
 NU 14 = .221005142748028321D+00
 NU 15 = .183596868512355991D+00
 NU 16 = .162424276608593223D+00
 NU 17 = .167689067442477795D+00
 NU 18 = .162499977979763418D+00
 NU 19 = .134501994056115100D+00
 NU 20 = .127086804501346194D+00
 NU 21 = .317992106539145757D-01
 NU 22 = .312940227665405237D-01
 NU 23 = .308946750447977095D-01
 NU 24 = .307323079416590771D-01

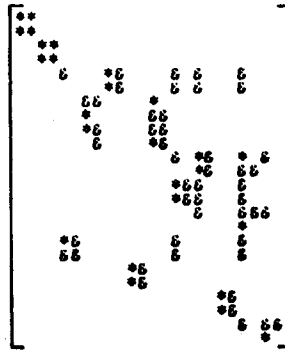


TABLE IV.9

CONTROL OF LARGE SPACE ANTENNAS BASED ON ELECTROMAGNETIC-STRUCTURAL MODELS

Massih Hamidi and Farzin Manshadi, Jet Propulsion Laboratory,
California Institute of Technology
Pasadena, CA 91109

ABSTRACT

A general approach to the optimal control of large space antennas based on their RF/structural characteristics is described. The approach consists of defining a cost functional based on the degradation of the RF performance of the antenna and using the structural model as the dynamic system. The method is applied to the design of an optimal controller for a 55-m, wrap-rib offset-fed antenna. The controller's goal is to minimize the variations of the peak electric field of the antenna due to feed displacements.

INTRODUCTION

The control of the RF properties of antennas is traditionally achieved by implementing and following a set of geometrical considerations such as pointing accuracy, shape distortion, feed position, stability, etc. These geometrical requirements are very stringent because of the way in which they are conceived. The relative importance of different parameters of a geometrical configuration in RF performance degradation usually can not be determined. Each parameter is therefore considered separately and uniform criteria are derived which, in order to meet a worst-case situation, lead to very restrictive conditions. This study aims to use the RF performance degradation directly as the means of defining the controller, and thus to circumvent the stringency of the geometrical methods.

This paper is organized into three sections. The first describes the methods used for the computations of the "far-field" electromagnetic properties of the antenna and for the derivation of the "sensitivity" of these properties to different parameter variations. The second section briefly discusses a general approach to determining quadratic cost functionals based on the RF characteristics of the antenna system. This reduces the RF optimal controller design to a subclass of the linear quadratic optimal controller design problem whose solution is well-known. To illustrate the method, the design of an RF optimal controller for the 55-m, offset-fed, wrap-rib antenna considered in the LMSS [Ref. 1] project is presented in section 3. The goal of the controller is to minimize the variations of the peak electric field of the antenna, caused by feed displacements.

RF MODEL DEVELOPMENT

Consider the reflector antenna shown in Figure 1. The reflector surface Σ is constructed by intersecting a circular cylinder with an arbitrary curved surface. The cylinder axis is taken as the z axis; the x - y plane is perpendicular to the z axis. The projection of Σ on the x - y plane is the circular region σ with radius a . The feed is assumed to be located at some arbitrary point.

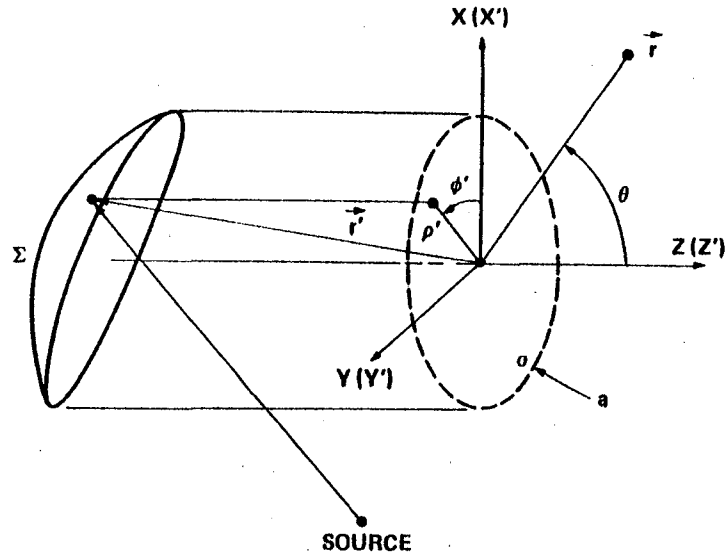


Figure 1. Offset Shaped Reflector Antenna

The far-field approximations for the scattered electric and magnetic fields of the offset-fed antenna are readily evaluated using a technique developed by Y. Rahmat-Samii and V. Galindo-Israel [Ref. 2]. A brief summary of this technique is presented in the following paragraphs.

The electromagnetic fields E and H are given by

$$\begin{cases} H = \nabla \times A \\ E = \frac{1}{j\omega\epsilon} \nabla \times H \end{cases}$$

A is the vector potential expressed as:

$$A = \int_{\Sigma} J \frac{e^{-jk|r-r'|}}{4\pi|r-r'|} ds'$$

where J is the induced current on the reflector surface due to the magnetic field H_s radiated by the source. It is given by [Ref. 3]

$$J = 2\hat{n} \times H_s$$

where \hat{n} is the unit vector normal to the reflector's surface and directed towards the positive direction of the z axis.

Introducing the far-field approximations in the expressions for E and H, one obtains [Ref. 2]

$$\begin{cases} H = jk \frac{e^{-jkr}}{4\pi r} (T_{\phi} \hat{\theta} - T_{\theta} \hat{\phi}) + O(r^{-2}) \\ E = -jk\eta \frac{e^{-jkr}}{4\pi r} (T_{\theta} \hat{\theta} + T_{\phi} \hat{\phi}) + O(r^{-2}) \end{cases}$$

where $\eta = \sqrt{\frac{\mu}{\epsilon}}$, the parameters (r, θ, ϕ) are the coordinates of the observation point, $\hat{\theta}$ and $\hat{\phi}$ the unit vectors corresponding to θ and ϕ , and T the radiation integral given by

$$T = \int_{\Sigma} J(r') e^{jkr' \cdot \hat{r}} ds'$$

It has been found that the radiation integral provides a very accurate solution for predicting the far-field radiations of reflector antennas. The necessity of having an efficient technique for the evaluation of this integral stems from the fact that it has to be computed accurately each time the observation angles change. Moreover, the integrand of the radiation integral oscillates rapidly and thus makes the integration more strenuous for large reflectors.

To circumvent the difficulties in the integration, the radiation integral is first expressed in terms of a summation of Fourier Transforms of an "effective" aperture distribution

$$T = \sum_{p=0}^{P \rightarrow \infty} G_p(\theta) \int_0^{2\pi} \int_0^a Q_p(\rho', \phi') e^{jk\rho' B \cos(\phi - \phi')} \rho' d\rho' d\phi'$$

where B and ϕ are functions of the observation angles θ and ϕ .

The Fourier Transform integrals are then expanded in terms of Jacobi-Bessel series by writing that

$$Q_p(as', \phi') = \sum_{n=0}^{\rightarrow \infty} \sum_{m=0}^{\rightarrow \infty} [pC_{nm} \quad pD_{nm}] \begin{bmatrix} \cos n\phi' \\ \sin n\phi' \end{bmatrix} F_m^n(s')$$

where $F_m^n(\cdot)$ are the modified Jacobi polynomials defined by

$$F_m^n(x) = \sqrt{2(n+2m+1)} P_m^n(1-2x^2) x^n$$

$$P_m^n(x) = \frac{(-1)^{m_2-m}}{m!} (1-x)^{-n} \frac{d^m}{dx^m} [(1-x^2)^m (1-x)^n]$$

and the coefficients pC_{nm} and pD_{nm} are given by

$$\begin{Bmatrix} pC_{nm} \\ pD_{nm} \end{Bmatrix} = \frac{\epsilon_n}{2\pi} \int_0^{2\pi} \int_0^1 Q_p(as', \phi') \begin{Bmatrix} \cos n\phi' \\ \sin n\phi' \end{Bmatrix} F_m^n(s') s' ds' d\phi'$$

$$\epsilon_n = \begin{cases} 1 & n=0 \\ 2 & n \neq 0 \end{cases}$$

Finally, the radiation integral is expressed as

$$T = 2\pi a^2 \sum_{p=0}^{P \rightarrow \infty} G_p(\theta) \sum_{n=0}^{N \rightarrow \infty} \sum_{m=0}^{M \rightarrow \infty} j^n [{}_p C_{nm} \quad {}_p D_{nm}] \begin{bmatrix} \cos n\phi \\ \sin n\phi \end{bmatrix} \sqrt{2(n+2m+1)} \cdot \frac{J_{n+2m+1}(kaB)}{kaB}$$

where $J_n(\cdot)$ indicates the Bessel function of order n .

The method has several important features which may be summarized as follows:

- 1) Higher order coefficients ${}_p C_{nm}$ and ${}_p D_{nm}$ can be calculated from zero order coefficients ${}_0 C_{nm}$ and ${}_0 D_{nm}$ and by use of recursion relations.
- 2) Once ${}_p C_{nm}$ and ${}_p D_{nm}$ are determined they can be used for all observation angles.
- 3) The numerical integrations involved in the computation of ${}_0 C_{nm}$ and ${}_0 D_{nm}$ do not contain the highly oscillatory Fourier Transform kernel of the original expression.

To illustrate the variation of the RF pattern of a reflector antenna as a function of its feed location, the far fields of a 55-m parabolic reflector antenna are plotted for four different feed locations: (1) feed at focal point, (2) feed displaced in the x direction with y and z constant, (3) feed displaced in the y direction with x and z constant, and (4) feed displaced in the z direction with x and y constant. (Figures 2 through 5).

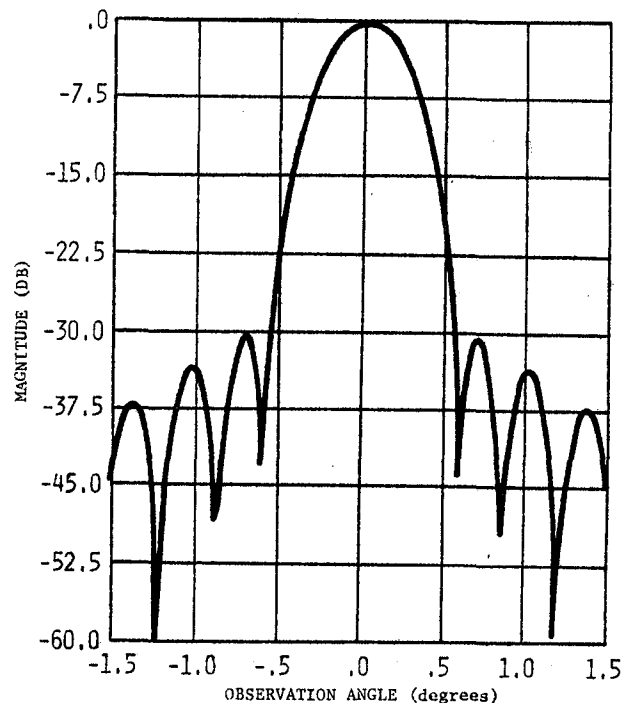


Figure 2. Feed at Focal Point

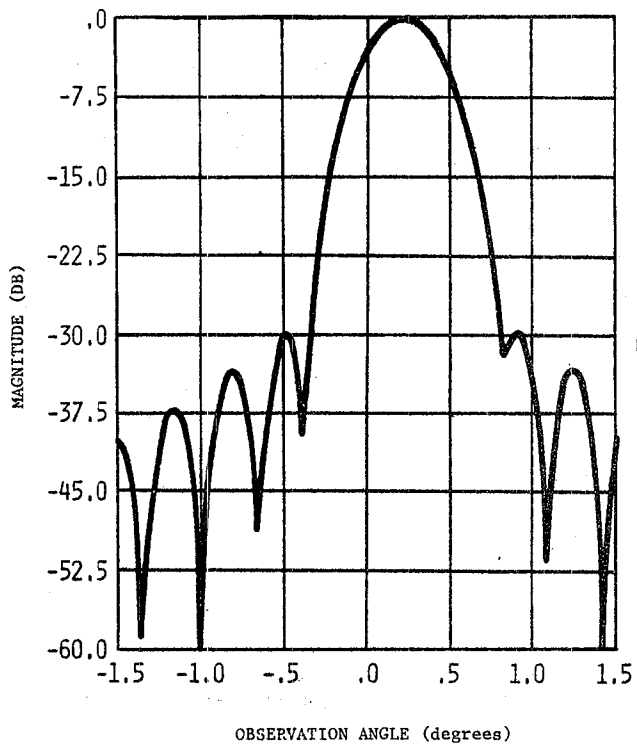


Figure 3. Feed Displaced by 1 Wave-length in x Direction

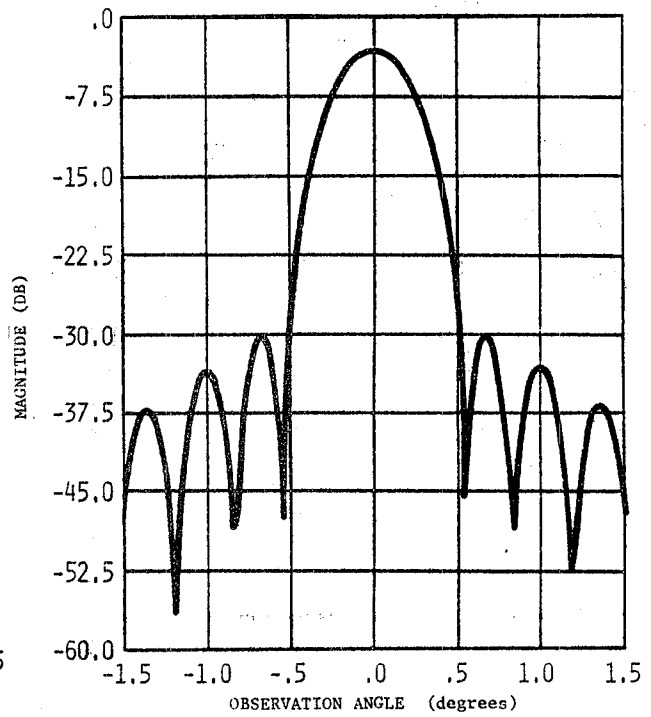


Figure 4. Feed Displaced by 1 Wave-length in y Direction

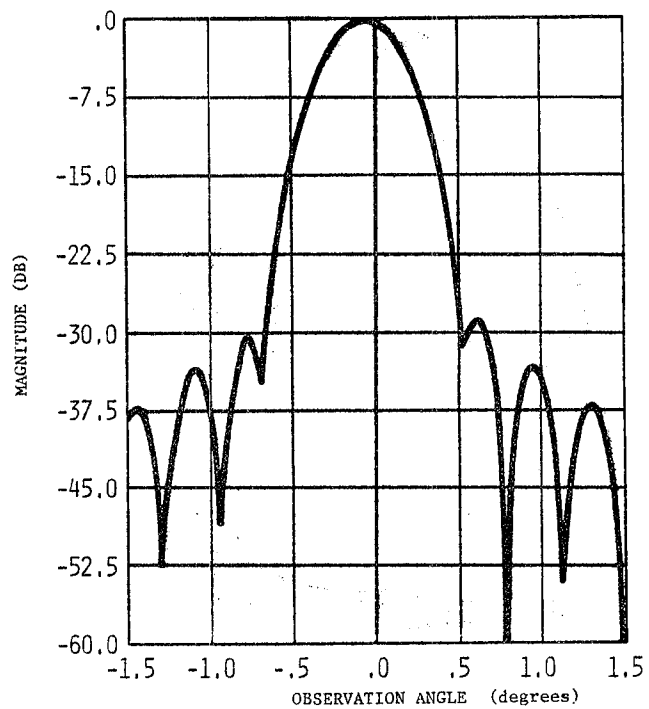


Figure 5. Feed Displaced by 1 Wave-length in z Direction

As can be noticed, displacements along the x and y axes produce significant variations in the gain while displacements along the z axis have almost negligible effects. It can thus be observed that to optimize the gain most of the effort should be concentrated on controlling the feed displacements along the x and y directions and that the control along the z direction can be relatively loose.

COST FUNCTIONAL DERIVATION

Let P be an RF performance parameter to be optimized e.g., gain, bandwidth, magnitude of the electric or magnetic field); Let x_1, x_2, \dots, x_n be the independent variables whose variations affect P: $P = P(x_1, x_2, \dots, x_n)$; and let $x = (x_1 \ x_2 \ \dots \ x_n)^T$. Suppose P assumes its optimal value at $x_0 = (x_{10} \ x_{20} \ \dots \ x_{n0})^T$. Around this point P can be expressed as

$$P(x) = P(x_0) + \nabla P \Big|_{x_0} \cdot \Delta x + \frac{1}{2} \Delta x^T H \Big|_{x_0} \Delta x + \dots$$

where P and H denote the gradient vector and the Hessian matrix of P with respect to x and $\Delta x = x - x_0$.

Since P is optimum at x_0

$$\nabla P \Big|_{x_0} = 0$$

and $H \Big|_{x_0}$ is positive definite or negative definite depending on whether P is minimum or maximum at x_0 .

Hence, around the given point,

$$P(x) = P(x_0) + \frac{1}{2} \Delta x^T H \Delta x + \dots$$

and we can approach the optimum value of P by minimizing $|\frac{1}{2} \Delta x^T H \Delta x|$. Note that if this minimum reduces to zero, we actually attain the optimum value of P. Note also that if $H > 0$,

$$|\frac{1}{2} \Delta x^T H \Delta x| = \frac{1}{2} \Delta x^T H \Delta x$$

and if $H < 0$

$$|\frac{1}{2} \Delta x^T H \Delta x| = \frac{1}{2} \Delta x^T (-H) \Delta x$$

and that in both cases,

$$|\frac{1}{2} \Delta x^T H \Delta x| = \frac{1}{2} \Delta x^T A \Delta x$$

where A is a positive definite matrix.

The antenna is modeled by an equation of the form

$$\ddot{M}y + Ky = Bu \quad y(t_0) = y_0, \quad \dot{y}(t_0) = \dot{y}_0$$

It is always possible to relate Δx to y by an equation of the form $\Delta x = Ty$. Hence, minimizing

$$\frac{1}{2} \Delta x^T A \Delta x$$

and reducing it to zero is equivalent to minimizing

$$\frac{1}{2} \int_0^{\infty} y^T T^T A T y \, dt$$

We can thus formulate a linear quadratic optimal control problem by writing, minimize

$$J = \frac{1}{2} \int_0^{\infty} (y^T T^T A T y + u^T R u) \, dt$$

subject to

$$\ddot{M}y + Ky = Bu \quad y(t_0) = y_0, \quad \dot{y}(t_0) = \dot{y}_0$$

The term

$$\frac{1}{2} \int_0^{\infty} u^T R u \, dt$$

where R is a positive definite matrix, is added to account for the restrictions in energy consumption for the control.

The rest of the procedure is classical. A damping term $\dot{D}y$ is added to the equation, and the system is augmented by considering the state vector $W = (y \ \dot{y})^T$. This leads to the system

$$\dot{W} = \begin{pmatrix} 0 & I \\ -M^{-1}K & -M^{-1}D \end{pmatrix} W + \begin{pmatrix} 0 \\ M^{-1}B \end{pmatrix} u \triangleq FW + Gu$$

associated with the cost functional

$$J = \frac{1}{2} \int_0^{\infty} (W^T Q W + u^T R u) \, dt$$

where

$$Q \triangleq \begin{pmatrix} T^T A T & 0 \\ 0 & 0 \end{pmatrix}$$

The optimal control is given by

$$u(t) = - CW(t)$$

with

$$C = R^{-1}G^TK$$

where K is the positive definite solution of the Riccati equation

$$F^TK + KF + Q - KG^TR^{-1}GK = 0$$

FEED-DISH MOTION COMPENSATION FOR A 55-m, WRAP-RIB, OFFSET-FED ANTENNA

To illustrate the application of the method, in the sequel we describe the design of an RF optimal controller for the 55-m, offset-fed, wrap-rib antenna considered in the LMSS [Ref. 1] project. The controller is designed to minimize the relative feed-dish motion of the antenna.

A schematic diagram of the antenna is given in Figure 6. It is composed of a 55-m diameter reflector dish, a massive feed array, and a long L-shaped boom connecting the dish and the feed. The antenna's operation frequency is 871 MHz which leads to the values of 159.68λ for the dish's diameter and 239.6λ for the focal length (λ is the wavelength at 871 MHz).

Construction of the State Cost Matrix

Let r_0 be the vector from the center of gravity of the spacecraft's bus to the boom's elbow and r_1 the vector from the elbow to the center of gravity of the reflector's dish. The position of the feed is characterized by the vector.

$$S = (x \ y \ z)^T = - (r_0 + r_1)$$

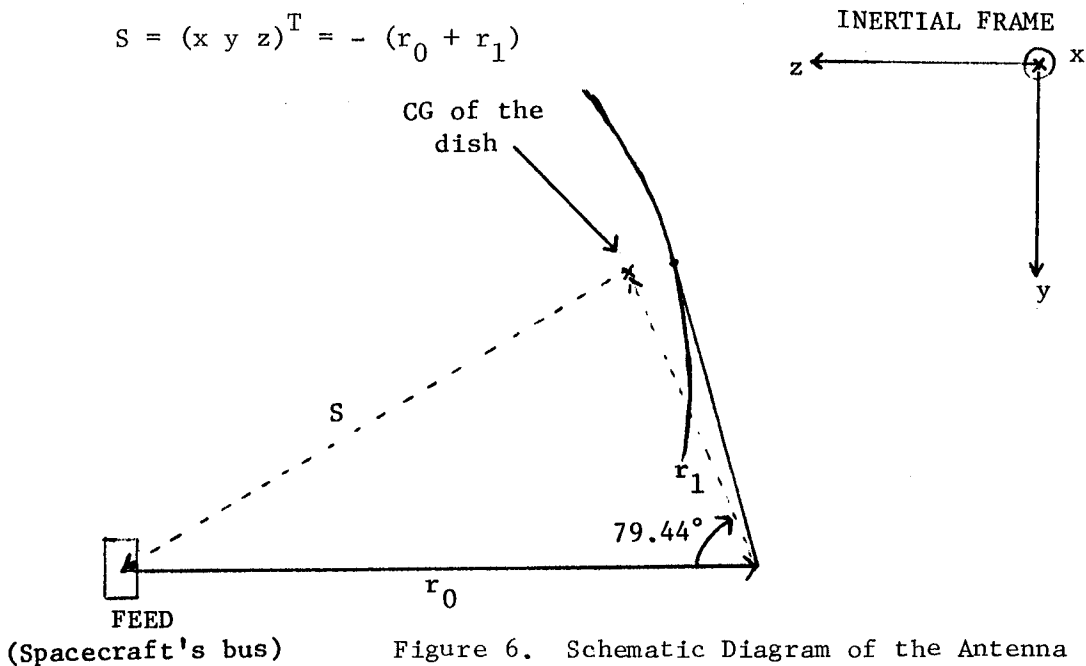


Figure 6. Schematic Diagram of the Antenna

Let $S_0 = (x_0 \ y_0 \ z_0)^T$ be the position for which the electric field is maximized. For the neighborhood of this point

$$E = E(s_0) + \nabla_s E \Big|_{s_0} \cdot \Delta S + \frac{1}{2} \Delta S^T H(s_0) \Delta S + \dots = E(s_0) + \frac{1}{2} \Delta S^T H(s_0) \Delta S + \dots$$

since

$$\nabla_s E \Big|_{s_0} = 0$$

The value of the electric field was evaluated using the algorithm described in the first section of this paper for different feed positions. The following Hessian matrix $H(s_0)$ was obtained through numerical differentiation of the electric field (as a function of feed position):

$$H(s_0) = \begin{pmatrix} -26.0966 & - .00344 & - .0076 \\ - .00344 & -24.231 & 6.396 \\ - .0076 & 6.396 & -1.96 \end{pmatrix}$$

To evaluate ΔS , we interpret the feed-dish motion by considering the feed and the lower boom, r_0 , fixed, and the dish, hence r_1 , rotating about the coordinate axes. Thus,

$$\Delta s = \Delta r_1$$

The antenna's distortions are supposed to be small. This leads to

$$\Delta r_1 = r_1 \times \Gamma$$

where

$$\Gamma = (\gamma_1 \ \gamma_2 \ \gamma_3)^T$$

designates the rotation of r_1 about the x, y and z axes of the inertial frame. Writing Δr_1 in a matrix form, we obtain

$$\Delta s = D \Gamma$$

with

$$D = \begin{pmatrix} 0 & +c & -b \\ -c & 0 & +a \\ b & -a & 0 \end{pmatrix}$$

where a, b, and c are the components of the vector r_1 : $r_1 = (a \ b \ c)^T$.

Thus,

$$\Delta E = E - E(S_0) = \frac{1}{2} \Gamma^T D^T H D \Gamma \triangleq \frac{1}{2} \Gamma^T H' \Gamma$$

$$H' = D^T H D$$

E has a maximum at S_0 . H is therefore negative definite and so is H' . Consequently, the state cost is given by

$$|\Delta E| = \frac{1}{2} \Gamma^T (-H') \Gamma$$

Antenna Model

The antenna is modeled by the linear system

$$M\ddot{y} + Ky = Bu$$

where the state vector y has 12 components as follows: y_1 to y_3 represent the attitude θ_x , θ_y , and θ_z of the spacecraft; y_4 to y_6 the rotations γ_1 , γ_2 , and γ_3 ; and y_7 to y_{12} the six most important modes of the reflector dish.

The values of the matrices M , K , and B are listed in the appendix. The system has a damping of zero on the first three components (rigid body motions) and 0.005 for the rest.

Thus, the state cost weighting matrix takes the form

$$\begin{cases} Q_{ij} = -H'_{(i-3)(j-3)} & 4 \leq i \leq 6, \quad 4 \leq j \leq 6 \\ Q_{ij} = 0 & \text{elsewhere} \end{cases}$$

Optimal Feedback Computation and Simulation

The OPTSYS [Ref. 4] program package was used to determine the optimal gain for the case where a three-dimensional control is applied at the spacecraft's bus. The control cost weighting matrix was taken to be the 3 x 3 identity matrix. The resulting gain matrix is also given at the end of this paper.

The optimal feedback control thus obtained was used to drive the antenna system in simulation studies. The results are given in Figure 7.

CONCLUSION

The RF performance of large flexible antennas is traditionally achieved by imposing stringent geometric restrictions on the structural distortions from a nominal optimum configuration. In this paper, we have presented an approach to alleviate the stringency of the geometrical criteria of satisfactory

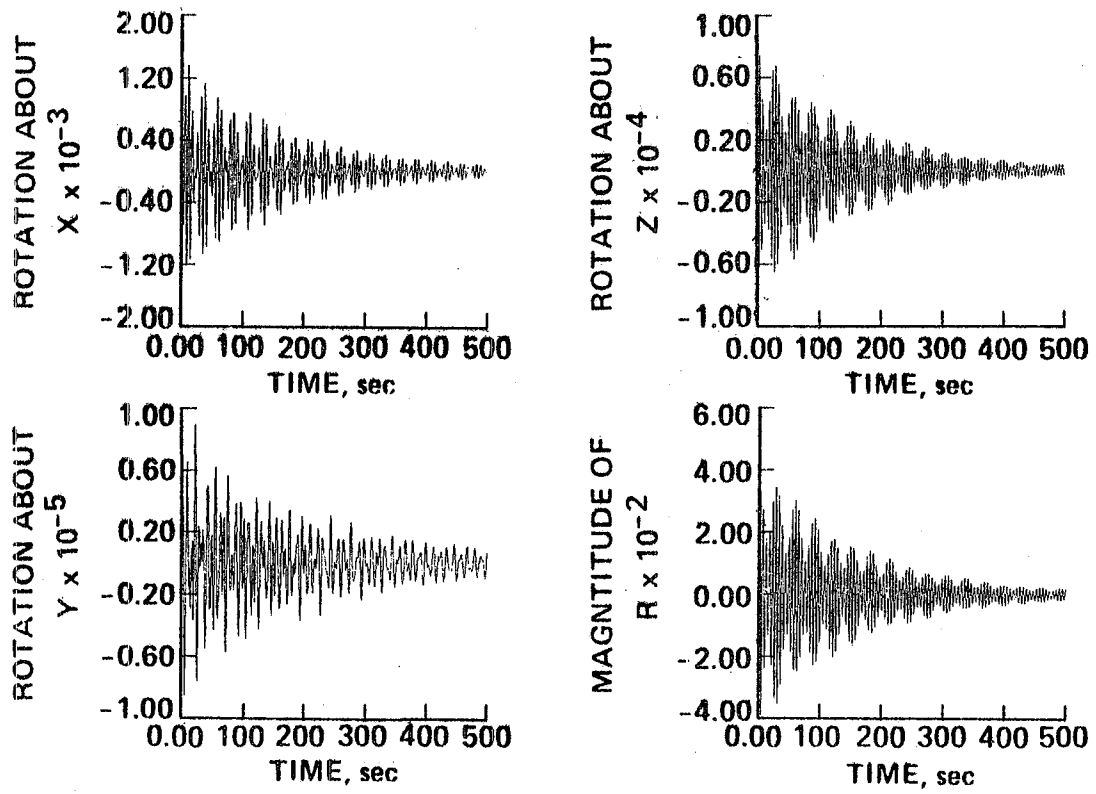


Figure 7. Feed Dish Motion Variation with Time

performance. The approach consists in generating a linear optimal control problem with quadratic cost functional where the cost functional is obtained from the RF characteristics of the antenna and the dynamic system constraint is given by the structural model of the antenna.

The method was applied to the feed-dish motion compensation for a 55-m, wrap-rib, offset-fed antenna and the time simulations presented.

ACKNOWLEDGEMENT

The authors would like to thank Mr. J. Cameron and Dr. D. Schaechter for their invaluable assistance in using the OPTSYS program package.

The research described in this paper was carried out at the Jet Propulsion Laboratory, California Institute of Technology, under contract with the National Aeronautics and Space Administration.

REFERENCES

1. F. Naderi, ed., "Land Mobile Satellite Service, A Conceptual System Design and Identification of the Critical Technology," JPL Publication 82-19, Jet Propulsion Laboratory, February 1982.
2. J. Rahmat-Samii and V. Galindo-Israel, "Shaped Reflector Antenna Analysis Using the Jacobi-Bessel Series," IEEE Trans. Antenna and Propagation, Vol. AP-28, pp. 425-435, July 1980.
3. R.F. Harrington, Time Harmonic Electromagnetic Fields, McGraw-Hill Book Co., 1961.
4. A.E. Bryson, Jr., and W.E. Hall, Jr., "Optimal Control and Filter Synthesis by Eigenvector Decomposition," Stanford University, SUDAR #436, December 1971.

APPENDIX

THE MASS MATRIX IS

	COL 1	COL 2	COL 3	COL 4	COL 5	COL 6	COL 7	COL 8
ROW 1	3.8633086+06	9.9905989+03	2.6100294+03	2.3173954+05	0.0000000	0.0000000	=4.6297059-03	8.9786856+01
ROW 2	9.9905989+03	3.5147213+06	=9.9635939+05	1.9069429+03	1.0663955+05	=1.0865878+06	=5.7304527+01	+7.3592871+02
ROW 3	2.6100294+03	=9.9635939+05	4.6325289+05	=2.6580818+02	=4.4156185+04	4.3388207+05	3.0739090+02	2.2740139+02
ROW 4	2.3173954+05	1.9069429+03	=2.6580818+02	4.1819109+05	0.0000000	0.0000000	=3.0470785-03	=1.1301117+01
ROW 5	0.0000000	1.0663955+05	=4.4156185+04	0.0000000	6.1965110+04	=4.5515826+04	=1.1266795+02	=4.9267653+00
ROW 6	0.0000000	=1.0865878+06	4.3388207+05	0.0000000	=4.5515826+04	4.6328949+05	3.0739090+02	2.4751272+02
ROW 7	=4.6297059-03	=5.7304527+01	3.0739090+02	=3.0470785-03	=1.1266795+02	3.0739090+02	1.0000000+00	1.1119753-16
ROW 8	8.9786856+01	=7.3592871+02	2.2740139+02	=1.1301117+01	=4.9267653+00	2.4751272+02	1.1119753-16	9.6984351-01
ROW 9	6.8179000+02	9.6671560+01	=2.8633031+01	=8.5794042+01	6.4663564-01	=3.2596941+01	0.0000000	5.2833948-11
ROW 10	=4.6663060+02	=1.6841067+00	=3.1364936-01	=3.0711672+02	=1.0826176-04	2.9536953-04	=4.9897100-07	0.0000000
ROW 11	=1.3716475+02	=1.6974841+01	=7.5011154+00	=2.0884245+02	=2.4574875+01	=7.8701537+00	0.0000000	=1.6299311-06
ROW 12	1.8062040+01	=1.2870787+02	=5.8040150+01	2.7459521+01	=1.8688063+02	=5.9918236+01	6.9498455-18	2.8158278-03

	COL 9	COL 10	COL 11	COL 12
ROW 1	6.8179000+02	=4.6663060+02	=1.3716475+02	1.8062040+01
ROW 2	9.6671560+01	=1.6841067+00	=1.6974841+01	=1.2870787+02
ROW 3	=2.8633031+01	=3.1364936-01	=7.5011154+00	=5.8040150+01
ROW 4	=8.5794042+01	=3.0711672+02	=2.0884245+02	2.7459521+01
ROW 5	6.4663564-01	=1.0826176-04	=2.4574875+01	=1.8688063+02
ROW 6	=3.2596941+01	2.9536953-04	=7.8701537+00	=5.9918236+01
ROW 7	0.0000000	=4.9897100-07	0.0000000	6.9498455-18
ROW 8	5.2833948-11	0.0000000	=1.6299311-06	2.8158278-03
ROW 9	9.6984351-01	0.0000000	=2.8158277-03	=1.6299488-06
ROW 10	0.0000000	9.4970845-01	=7.2874412-12	9.1093014-13
ROW 11	=2.8158277-03	=7.2874412-12	9.9973708-01	=9.6786327-13
ROW 12	=1.6299488-06	9.1093014-13	=9.6786327-13	9.9973708-01

THE STIFFNESS MATRIX IS

	COL 1	COL 2	COL 3	COL 4	COL 5	COL 6	COL 7	COL 8
ROW 1	0.0000000	0.0000000	0.0000000	0.0000000	0.0000000	0.0000000	0.0000000	0.0000000
ROW 2	0.0000000	0.0000000	0.0000000	0.0000000	0.0000000	0.0000000	0.0000000	0.0000000
ROW 3	0.0000000	0.0000000	0.0000000	0.0000000	0.0000000	0.0000000	0.0000000	0.0000000
ROW 4	0.0000000	0.0000000	0.0000000	6.3766433+05	0.0000000	0.0000000	0.0000000	0.0000000
ROW 5	0.0000000	0.0000000	0.0000000	0.0000000	1.8365554+04	0.0000000	0.0000000	0.0000000
ROW 6	0.0000000	0.0000000	0.0000000	0.0000000	0.0000000	9.9449838+04	0.0000000	0.0000000
ROW 7	0.0000000	0.0000000	0.0000000	0.0000000	0.0000000	0.0000000	1.3057600+00	0.0000000
ROW 8	0.0000000	0.0000000	0.0000000	0.0000000	0.0000000	0.0000000	0.0000000	1.4208640+00
ROW 9	0.0000000	0.0000000	0.0000000	0.0000000	0.0000000	0.0000000	0.0000000	0.0000000
ROW 10	0.0000000	0.0000000	0.0000000	0.0000000	0.0000000	0.0000000	0.0000000	0.0000000
ROW 11	0.0000000	0.0000000	0.0000000	0.0000000	0.0000000	0.0000000	0.0000000	0.0000000
ROW 12	0.0000000	0.0000000	0.0000000	0.0000000	0.0000000	0.0000000	0.0000000	0.0000000

	COL 9	COL 10	COL 11	COL 12
ROW 1	0.0000000	0.0000000	0.0000000	0.0000000
ROW 2	0.0000000	0.0000000	0.0000000	0.0000000
ROW 3	0.0000000	0.0000000	0.0000000	0.0000000
ROW 4	0.0000000	0.0000000	0.0000000	0.0000000
ROW 5	0.0000000	0.0000000	0.0000000	0.0000000
ROW 6	0.0000000	0.0000000	0.0000000	0.0000000
ROW 7	0.0000000	0.0000000	0.0000000	0.0000000
ROW 8	0.0000000	0.0000000	0.0000000	0.0000000
ROW 9	1.4208640+00	0.0000000	0.0000000	0.0000000
ROW 10	0.0000000	2.2162439+01	0.0000000	0.0000000
ROW 11	0.0000000	0.0000000	2.2179390+01	0.0000000
ROW 12	0.0000000	0.0000000	0.0000000	2.2179390+01

THE MATRIX B IS

	COL 1	COL 2	COL 3
ROW 1	1.0000000+00	0.0000000	0.0000000
ROW 2	0.0000000	1.0000000+00	0.0000000
ROW 3	0.0000000	0.0000000	1.0000000+00
ROW 4	0.0000000	0.0000000	0.0000000
ROW 5	0.0000000	0.0000000	0.0000000
ROW 6	0.0000000	0.0000000	0.0000000
ROW 7	0.0000000	0.0000000	0.0000000
ROW 8	0.0000000	0.0000000	0.0000000
ROW 9	0.0000000	0.0000000	0.0000000
ROW 10	0.0000000	0.0000000	0.0000000
ROW 11	0.0000000	0.0000000	0.0000000
ROW 12	0.0000000	0.0000000	0.0000000

THE MATRIX C IS

	COL 1	COL 2	COL 3	COL 4	COL 5	COL 6	COL 7	COL 8
ROW 1	3.1622700-01	4.1714300-09	-4.5876100-09	1.8341600-02	3.1813400-04	1.2572100-04	-1.7964400-06	8.0114399-06
ROW 2	4.5156800-11	3.1622700-01	2.4704700-06	7.9090100-03	1.3217300-01	1.8114600-01	4.5278200-05	1.6210600-05
ROW 3	3.3257200-09	-2.4707100-06	3.1622700-01	-1.0675900-01	-9.3888400-01	-1.4103000+00	4.4507000-04	-4.7270900-04
	COL 9	COL 10	COL 11	COL 12	COL 13	COL 14	COL 15	COL 16
ROW 1	5.6080000-05	-3.7757000-05	-1.0939500-05	1.3021500-06	1.5631200+03	2.2295400+00	1.2069300+00	9.3762700+01
ROW 2	-1.2061500-05	-4.6951200-06	-7.8795800-05	-5.7721500-04	2.2295200+00	1.4526600+03	-3.3567000+02	7.8414700-01
ROW 3	2.7802800-04	6.8976900-05	4.8196600-04	3.3056700-03	1.2069400+00	-3.3568500+02	4.2463300+02	-1.5358700+00
	COL 17	COL 18	COL 19	COL 20	COL 21	COL 22	COL 23	COL 24
ROW 1	-3.0828100-02	3.3378400-01	-4.8242000-04	3.6675300-02	2.7579900-01	-1.8880100-01	-5.5466600-02	7.5448500-03
ROW 2	3.8571100+01	-3.9126200+02	1.0731300-01	-2.9501100-01	3.8310100-02	-5.8629000-04	-1.2842000-02	-9.8965800-02
ROW 3	-3.1577400+01	2.4733600+02	4.2061500-01	9.3221200-02	-9.1390799-03	3.6252000-04	-1.4768200-02	-1.2054800-01

ACTIVE CONTROL OF SPACE STRUCTURES (ACOSS) MODEL 2

Timothy C. Henderson
Charles Stark Draper Laboratory, Inc.
Cambridge, MA 02139

1.0 Introduction

In order to assess the performance, sensitivity, and hardware requirements of the various active structural control methods which are being developed, a universal system model is required. This report contains a complete description of ACOSS Model #2 which is a simple but realistic evaluation model. The design of this system was driven by the desire to incorporate certain attributes into the overall system characteristics. The desired features were

- structural design based on realistic sizes and weights
- a simple unclassified optical system with associated performance measures and tolerances
- a set of disturbances typical of equipment vibration and attitude control (slew).

The resulting model is described in detail in section 2.0 along with the resulting mode shapes and natural frequencies of the system. Section 4.1 contains a description of the line-of-sight (LOS) performance measure including theory and implementation.

2.0 Structural Design

ACOSS Model #2 is shown in Figure 1. It consists of two subsystems. The optical support structure and the equipment section, which are connected by springs at three points to allow either passive or active vibration isolation. The optical support structure contains the four optical surfaces which are assumed to be a rigid central section with two flexible solar panels cantilevered from it.

2.1 Optical Support Structure

The optical support structure consists of the upper mirror support truss, the lower mirror support truss and the metering truss which maintains mirror separation. The finite element model of this subsystem is shown in Figure 2. The model contains 35 node points and 117 beam elements. The structure is designed

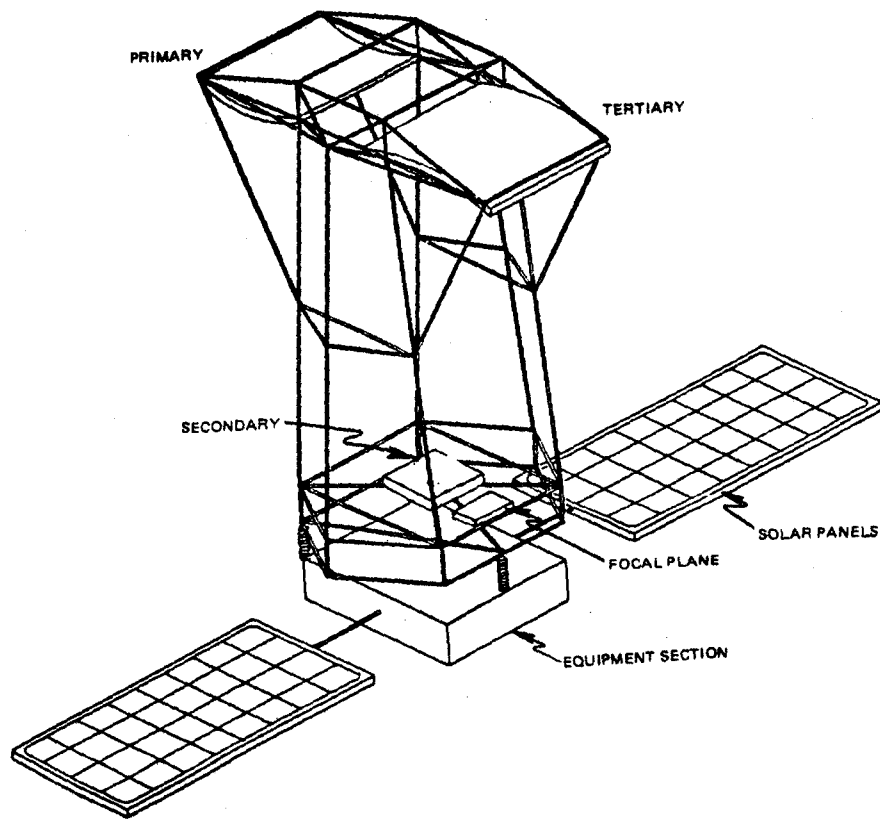


Figure 1. ACOSS Model No. 2

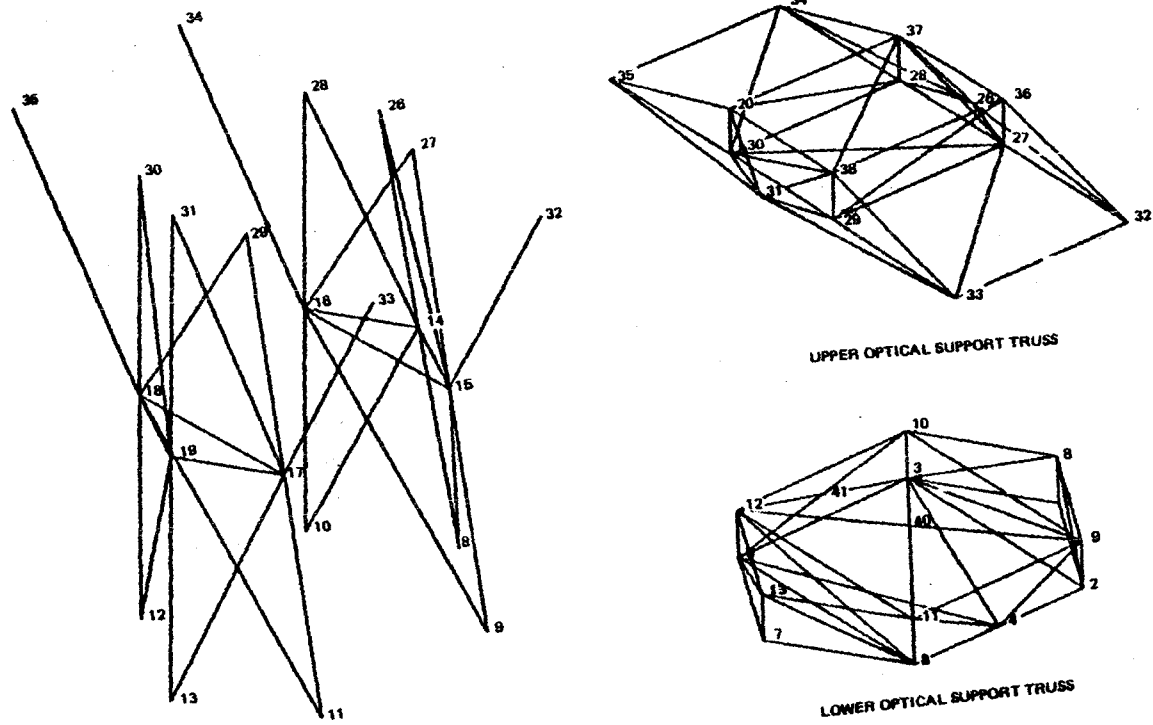


Figure 2. ACROSS Model No. 2 - Finite Element Model

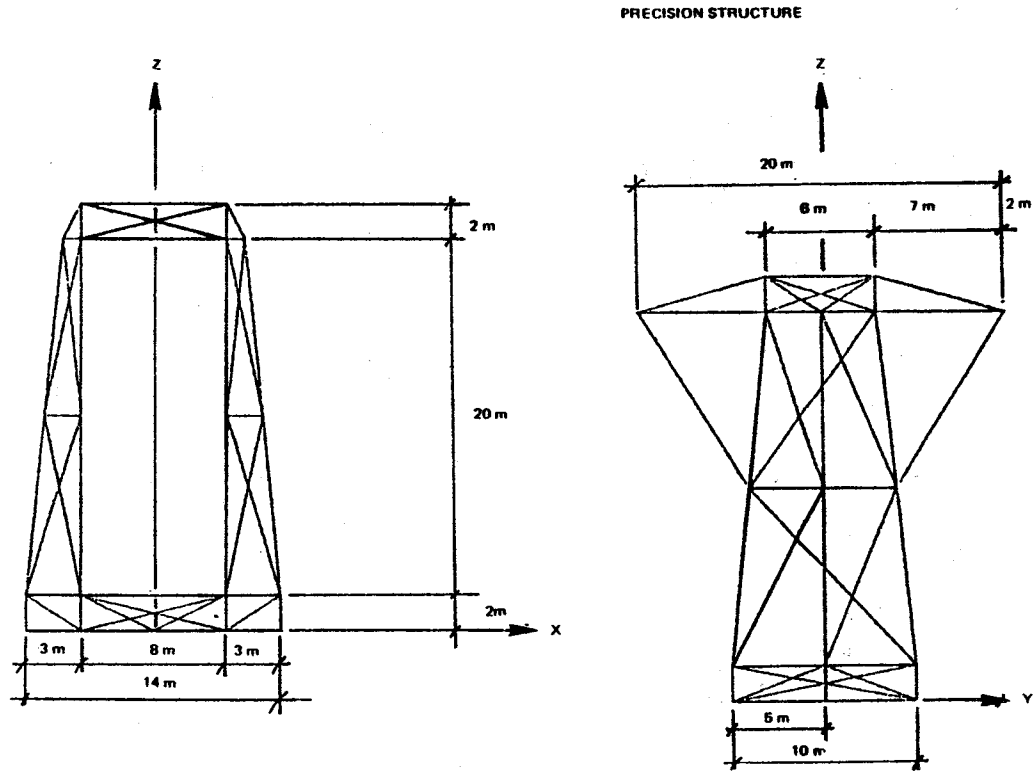


Figure 2. ACOSS Model No. 2 - Finite Element Model (Continued)

to act as a truss but it is assumed that all joints allow a full moment connection. Thus, both bending and axial stiffness are included for all members. All structural elements are assumed to be hollow graphite epoxy tubes. Four different sizes of tubes are used in this model and their dimensions and section properties are listed in Table 1. The optical surfaces are assumed to be rigid and kinematically mounted on the structure so that they will have no effect on the overall stiffness. The mass of the mirrors will increase the inertia of the system and has been included in the model. The total mass of this subsystem, 5084 kg which includes the structure, optical surfaces, and equipment, has been lumped at 18 node points as shown in Figure 3.

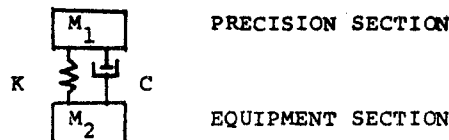
2.2.2 Equipment Section

The equipment section is modelled as a central rigid body with two flexible solar panels cantilevered from it. The finite element model is given in Figure 4. It has been assumed that the rigid body portion contains all of the equipment, guidance and navigation, control systems, power supplies, that are necessary for operation of the system. Therefore, a relatively large portion of the total mass, 3500 kg, is concentrated in the rigid section at node 44. Also included at node 44 are the rotational inertias due to distribution of the mass over the triangular area. These inertia terms are listed in Figure 7.

The solar panels are assumed to have an area of 120 m² each and are supported by graphite epoxy support booms. The mass and rotational inertia of the solar panels are lumped at three nodes on each boom. The lumped masses are listed in Figure 4.

2.2.3 Isolation System

The optical support structure and the equipment section are connected by a passive isolator at three points by springs acting in all three translational directions. The isolator is designed to reduce the amount of force transmitted from the equipment section to the optics. This is accomplished by designing an isolator with the natural frequency much lower than expected disturbance frequencies. In addition, the isolator frequency should be lower than the optical structure bending frequency. A passive isolator consists of a spring and a viscous dashpot in parallel as shown in Figure 5.



$$F_{isol} = \frac{1}{2\pi} \sqrt{\frac{K(M_1 + M_2)}{M_1 M_2}}$$

Figure 5. Passive isolator.

Table 1: Member properties

TYPE 200

20 cm dia. x .1 cm Round Tube

$$A = 6.250 \times 10^{-4} \text{ m}^2$$

$$I = 3.075 \times 10^{-6} \text{ m}^4$$

$$J = 6.189 \times 10^{-6} \text{ m}^4$$

TYPE 300

20 cm dia x .05 cm Round Tube

$$A = 3.133 \times 10^{-4} \text{ m}^2$$

$$I = 1.559 \times 10^{-6} \text{ m}^4$$

$$J = 3.118 \times 10^{-6} \text{ m}^4$$

TYPE 400

25 cm dia x .05 cm Round Tube

$$A = 3.919 \times 10^{-4} \text{ m}^2$$

$$I = 3.0496 \times 10^{-6} \text{ m}^4$$

$$J = 6.099 \times 10^{-6} \text{ m}^4$$

TYPE 500

40 cm dia x .075 cm Round Tube

$$A = 9.407 \times 10^{-4} \text{ m}^2$$

$$I = 1.874 \times 10^{-5} \text{ m}^4$$

$$J = 3.749 \times 10^{-5} \text{ m}^4$$

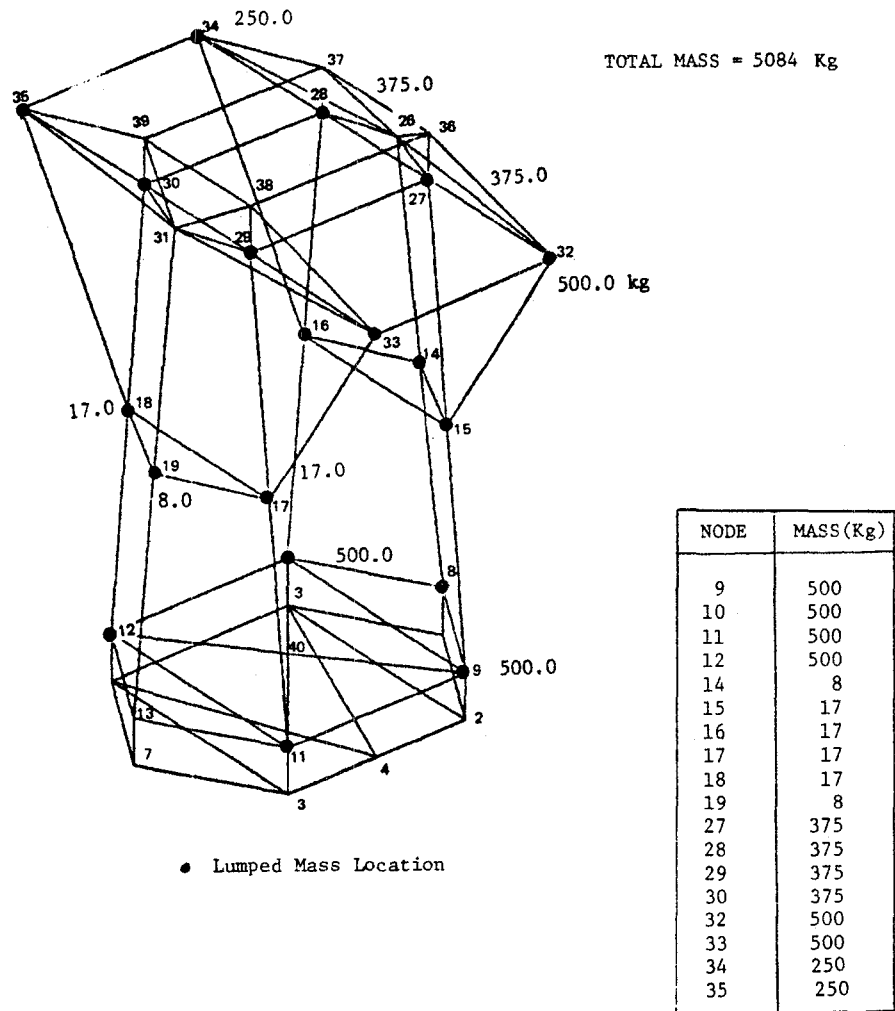
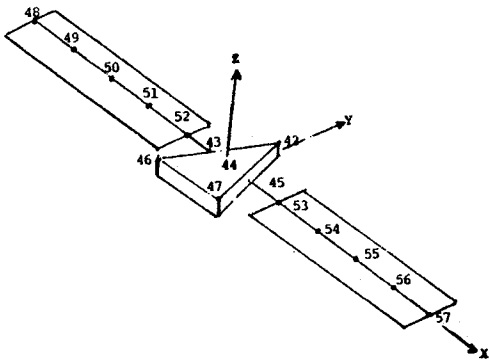


Figure 3. Optical support structure mass distribution

EQUIPMENT SECTION & SOLAR PANELS



NODE LOCATIONS (m)			
NODE	X	Y	Z
42	0.0	5.0	0.0
43	-2.0	0.0	0.0
44	0.0	0.0	0.0
45	2.0	0.0	0.0
46	-4.0	-5.0	0.0
47	4.0	-5.0	0.0
48	-26.0	0.0	0.0
49	-21.0	0.0	0.0
50	-16.0	0.0	0.0
51	-11.0	0.0	0.0
52	-6.0	0.0	0.0
53	6.0	0.0	0.0
54	11.0	0.0	0.0
55	16.0	0.0	0.0
56	21.0	0.0	0.0
57	26.0	0.0	0.0

EQUIPMENT SECTION - ELEMENT CONNECTIONS

- NODES 42-47 RIGID PLATE
- SOLAR PANEL BOOMS

ELEMENT #	NODE A	NODE B	PROPERTY #
131	48	49	500 ↑ ↓
132	49	50	
133	50	51	
134	51	52	
135	52	43	
136	45	53	
137	53	54	
138	54	55	
139	55	56	
140	56	57	

LUMPED MASSES

NODE	M(Kg)	Ixx	Iyy	Izz
44	3500	2100	2100	4200
48	90	270	0	0
50	180	540	0	0
52	90	270	0	0
53	90	270	0	0
55	180	540	0	0
57	90	270	0	0

Figure 4. Equipment section and solar panels

If the isolator frequency is lower than the lowest natural frequencies of the two sections, they can be modelled by their inertia properties only. For this system, the isolator was sized to have a frequency of 0.5 Hz. The dashpot size has not been specified as it is assumed to be part of the overall control design. The spring constants are given in Table 2.

3.0 Structural Analysis

A model analysis was performed using the NASTRAN finite element program. This model contains 84 dynamic degrees of freedom, thus 84 frequencies and mode shapes were extracted. Table 3 gives a list of frequencies and descriptions of the first fifty mode shapes.

4.0 System Performance Evaluation

The performance of this system is measured by the ability to maintain line-of-sight (LOS) rotation and defocus within specified tolerances. By making some simplifying assumptions a set of linear equations relating the LOS rotations and defocus to the displacements of node points in the finite element model have been developed. This results in a performance evaluation model which has the same level of accuracy as the finite element model.

4.1 LOS Error Algorithm

The optical system used in ACROSS model #2 is shown in Figure 6. The primary and tertiary mirrors are off axis sections of rotationally symmetric coaxial surfaces. The secondary mirror and the focal surface are flat. We assume that the mirrors maintain their nominal shape and that their motion is a linear function of the displacements of the nodes at the support points. Using these assumptions and first order optics equations, expressions relating mirror translations and rotations to the translation and rotation of the image are given. Translations and rotations of the mirrors are assumed to be the displacements of the vertices of the surfaces, located on the optical axis (Figure 7). The displacements of the vertices can be extrapolated from the displacements of the node points at the mirror supports.

The general form of the expressions for LOS rotation and defocus is

$$\text{LOSX} = Y/F \quad \text{LOS Y} = X/F \quad \text{DEFOCUS} = Z \quad (4-1)$$

Where

$$X = [-X_p + X_t - R_p \theta Y_p + 2\theta Y_s \left(\frac{R_p}{2} + t_1 - 2 Y_t T \right) \frac{R_t}{2T - R_t}] \quad (4-2)$$

$$+ X_t - X_f + \theta_f Y_I$$

$$Y = [-Y_p + Y_t + R_p \theta X_p - 2\theta X_s \left(\frac{R_p}{2} + t_1 + 2\theta X_t T \right) \frac{R_t}{2T - R_t}] \quad (4-3)$$

$$+ Y_t - Y_f - \theta_f X_I$$

Table 2. Isolator spring connectivities

SPRING A	NODE A	DOF	NODE B	DOF
1	4	1	42	1
2	4	2	42	2
3	4	3	42	3
4	3	1	46	1
5	3	2	46	2
6	3	3	46	3
7	6	1	47	1
8	6	2	47	2
9	6	3	47	3

$K = 5790 \text{ N/m}$

Table 3. Frequencies and mode shapes

	Freq. (Hz)	Description		Freq. (Hz)	Description
1-6	0.0	rigid body	17	1.72	torsion
7	.145	Isolator Y-rotation	18	1.82	2 nd S.P. X-Z plane
8	.263	Isolator Z-rotation	19	1.82	2 nd S.P. X-Y plane
9	.317	1 st S.P. X-Z plane	20	1.89	1 st S.P. torsion asym
10	.333	1 st S.P. X-Y plane	21	2.36	1 st bending
11	.443	Isolator Z-trans	22	2.99	1 st S.P. torsion sym
12	.577	Isolator Y-trans	23	3.18	3 rd S.P. X-Y plane
13	.581	Isolator X-trans	24	3.39	3 rd S.P. X-Z plane
14	1.22	2 nd S.P. X-Z plane	25	5.16	2 nd S.P. torsion
15	1.30	2 nd S.P. X-Y plane	26	5.26	2 nd S.P. torsion
16	1.35	Isolator X-rotation	27	7.87	3 rd S.P. torsion

	FREQ(HZ)	DESCRIPTION		FREQ(HZ)	DESCRIPTION
28	8.11	LEG TORSION	39	15.65	LEG & LOWER TRUSS BENDING
29	8.36	3 rd S.P. TORSION	40	16.07	LEG BENDING
30	8.57	LEG TORSION	41	16.52	UPPER TRUSS BENDING
31	8.81	3 rd S.P. X-Y PLANE	42	16.75	UPPER TRUSS BENDING
32	8.81	3 rd S.P. X-Z PLANE	43	17.16	UPPER AND LOWER BENDING
33	11.35	4 th S.P. X-Y PLANE	44	17.83	STRUCTURAL BENDING X-Y
34	11.50	LEG BENDING	45	19.07	LOWER TRUSS BENDING
35	12.73	LEG BENDING	46	23.77	UPPER TRUSS BENDING
36	13.58	4 th S.P. X-Z PLANE	47	24.41	UPPER & LOWER BENDING
37	13.71	LEG BENDING	48	25.91	UPPER TRUSS AXIAL
38	14.16	LEG & LOWER TRUSS BENDING	49	26.36	UPPER TRUSS BENDING
			50	26.43	S.P. AXIAL

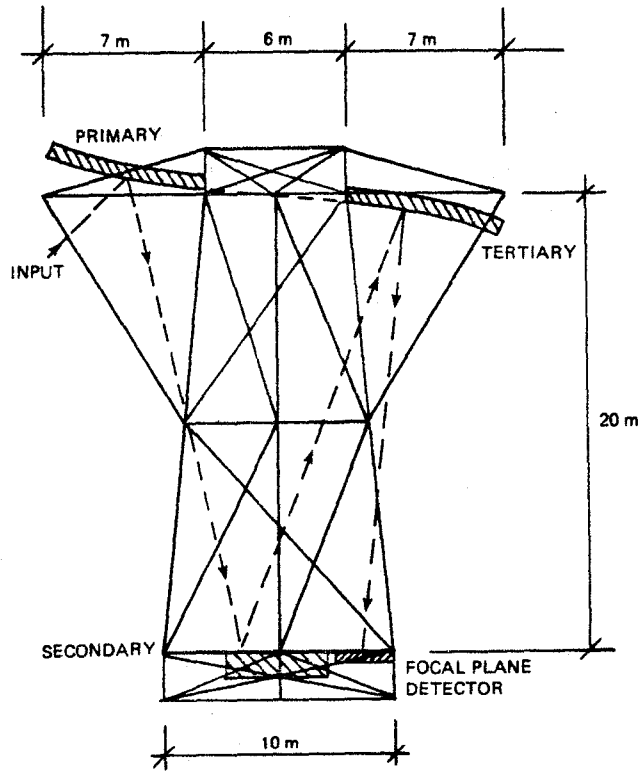


Figure 6. Optical system

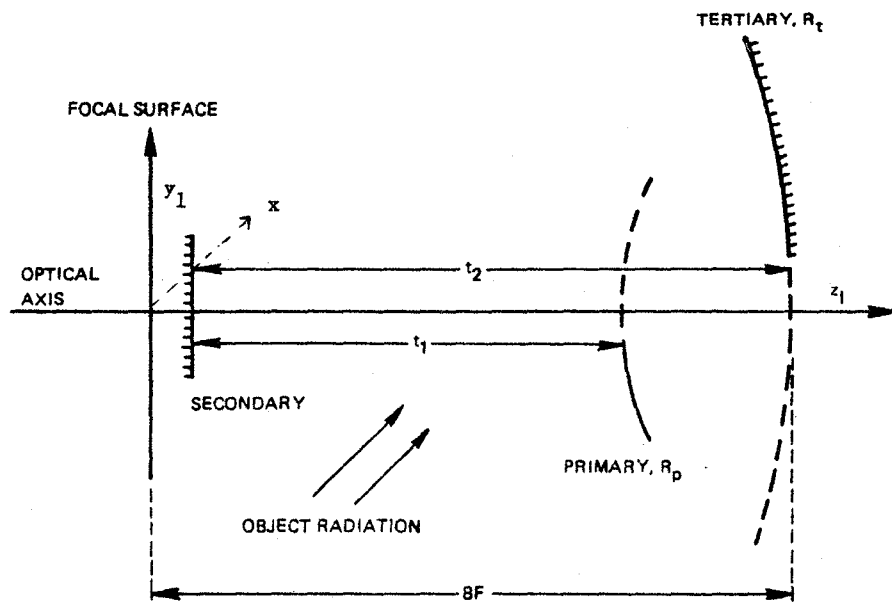


Figure 7. Three-mirror system

$$Z = (Z_p - 2Z_s + Z_t) \frac{R_t^2}{[R_p - R_t + 2(t_1 - t_2)]^2} + Z_t - Z_f \quad (4-4)$$

$$+ \Theta Y_f \cdot X_I - \Theta X_f \cdot Y_I$$

the terms X_i , Y_i , Z_i , ΘX_i , ΘZ_i refer to the translations and rotations in the global X, Y, and Z directions of the primary (p) and secondary (s), tertiary (t), and focal plane (f). The variables in the equations which relate to the size of the optical system are

- R_p = radius of curvature of the primary
- R_t = radius of curvature of the tertiary
- t_1 = axial distance between the primary and the secondary
- t_2 = axial distance between the secondary and the tertiary
- X_I, Y_I = location of a point on the focal plane
- F = focal length
- $= \frac{R_t R_p}{2(2T - R_t)}$
- T + $\frac{R_p}{2} + t_1 + t_2$

the location of the image plane is a function of the parameters of the three-mirror optical system. The distance BF between the tertiary mirror and the image plane (see Figure 7) is given by

$$BF = \frac{R_t T}{2T - R_t} \quad (4-5)$$

and for all cases the focal surface must be placed at this location, or, alternately the radius of curvature of the tertiary should be calculated using

$$R_t = \frac{2T \cdot BF}{T + BF} \quad (4-6)$$

so that the final image coincides with the focal plane.

To simplify implementation we can rewrite the previous equations in matrix form. Equation 4-1, relating the line-of-sight errors to the translational defocus terms becomes

$$\begin{Bmatrix} \text{LOSX} \\ \text{LOS Y} \\ Z \end{Bmatrix} = [A] \begin{Bmatrix} X \\ Y \\ Z \end{Bmatrix} \quad (4-7)$$

where: X, Y, Z - translational defocus terms defined in Eqs. (4-2) to (4-4)

$$[A] = \begin{bmatrix} 0 & 1/F & 0 \\ 1/F & 0 & 0 \\ 0 & 0 & 1 \end{bmatrix}$$

Equations (4-2), (4-3), and (4-4) can be rewritten in matrix form as

$$\begin{Bmatrix} X \\ Y \\ Z \end{Bmatrix} = [B] \{U_m\} \quad (4-8)$$

where: U_m = vector of mirror vertex motions

B = matrix relating U_m to translational defocus terms (X, Y, Z)

The optical system used in ACROSS model #2 has the following parameters:

$$R_p = 53.9 \text{ m}$$

$$R_t = 30.8 \text{ m}$$

$$t_1 = t_2 = 20.0 \text{ m}$$

$$X_I = Y_I = 0.0 \text{ m}$$

$$F = 8.051 \text{ m}$$

$$T = 66.95 \text{ m}$$

The radius of curvature of the tertiary, R_t , was found using Eq. (4-6) and the requirements that $BF = 20.0 \text{ m}$.

These parameters are then used to form the terms in matrices A and B.

4.2 LOS Error Algorithm Implementation

The motion of the vertex of each mirror can be extrapolated from the displacements of the support points since all mirrors are assumed to be rigid. The mirrors are supported by kinematic mounts so that there is no elastic deformation in the mirrors. A displacement transformation matrix which relates the motion of each mirror to the displacements of the support points in the global coordinate system can be constructed. The relationship is of the form

$$U_m = C U_n \quad (4-9)$$

where: U_m = vector of mirror displacements and rotations

U_n = vector of displacements at support node points

C = displacement transformation matrix

The final form of the equations relating LOS errors to displacements at the support node points is

$$\begin{Bmatrix} \text{LOSX} \\ \text{LOS Y} \\ Z \end{Bmatrix} = [A] [B] [C] \{U_n\} \quad (4-10)$$

using terms that have been previously defined. If modal superposition is used in the analysis, Eq. (4-10) can be rewritten as

$$\begin{Bmatrix} \text{LOSX} \\ \text{LOS Y} \\ Z \end{Bmatrix} = [\phi_{\text{LOS}}] \{\eta\} \quad (4-11)$$

where: $\{\eta\}$ = modal displacements

$$[\phi_{\text{LOS}}] = [A] [B] [C] [\phi]$$

This matrix, $[\phi_{\text{LOS}}]$ is a simple way to relate LOS errors to the modal displacements which will be the result of the analysis if a modal model is used.

5.0 Conclusion

Further information on this model is contained in CSDL Report C-5437.

This Page Intentionally Left Blank

TRAVELLING WAVE EFFECTS IN LARGE SPACE STRUCTURES

Andy von Flotow
Stanford University
Stanford, CA 94305

Abstract:

This paper investigates several aspects of travelling waves in Large Space Structures (LSS). The dynamic similarity among LSS's, electric power systems, microwave circuits and communications networks is noted. The existence of time lags between actuation and response is illuminated with the aid of simple examples, and their prediction is demonstrated. To prevent echoes, communications lines have matched terminations; this idea is applied to the design of dampers of one dimensional structures. Periodic structures act as mechanical band pass filters. Implications of this behaviour are examined on a simple example. It is noted that the implication is twofold; continuum models of periodic lattice structures may err considerably; on the other hand, it is possible to design favourable transmission (and resonance) characteristics into the structure.

Introduction:

Large space structures have been proposed with dimensions of many kilometers (1), (2). More realistically, for the near future, reflectors and antennas with dimensions as large as 100 metres are planned (3). Some of these structures will be composed entirely of networks of long, slender, essentially one dimensional structural members. Others will have their flexibility concentrated predominantly in one dimensional appendages and components. These components will be flexible to the point where several of the member's frequencies of free vibration will be within the frequency range of interest. For such structures, it becomes reasonable to visualize the response to a disturbance as consisting of elastic waves, slowly travelling along structural members, reflecting and transmitting at nodes and discontinuities. This view becomes ever more valid as the disturbance is concentrated in space and time.

The limit of several free vibration frequencies of individual elements being within the frequency range of interest has been reached in several relevant fields within electrical engineering. Microwave circuits (4) typically operate at wavelengths of a few millimetres with circuit elements as large as a few centimetres. Power distribution networks (5), have electrical wavelengths of 3000 miles (at 60 Hz), while circuit dimensions of the same scale are being used. Communications lines, with wavelengths as small as a few miles (corresponding to a 10 KHz voice transmission) and line lengths of many hundreds of miles are an extreme example (6). In these fields, a balanced approach to dynamic analysis is used. System behaviour is investigated with both travelling wave and modal methods. The importance of travelling wave concepts is greatest in communication line analysis, where the wavelength to circuit dimension ratio is smallest.

There is a relatively clear conceptual relationship between travelling wave and modal analysis. Modes of free vibration are derivable from a travelling wave analysis by invoking the phase closure principle (7). A travelling wave, in one complete circumnavigation of the structure, must close on itself with a total phase change (due to travelled distance and reflections) of $2n\pi$. For one-dimensional problems the phase closure principle can yield the modes and frequencies of free vibration with minimum effort. This paper concerns itself with insights gained into the dynamic behaviour of one-dimensional structural elements when considered from a travelling wave perspective.

Travelling Wave Concepts

An ideal one-dimensional structural member is described by a system of partial differential equations together with appropriate boundary conditions. The system of PDE's may have arbitrarily high order in space and time. The simplest well known equation

$$\frac{\partial^2 U}{\partial t^2} - \frac{\partial^2 U}{\partial x^2} = f(x, t) \quad (1)$$

modelling torsion and longitudinal compression of solid sections and transverse motion of cables, is second order in space and time. The well known Bernoulli-Euler beam model is fourth order in space, second order in time, while the Timoshenko beam model is fourth order in both space and time (8). Continuum models for lattice beams have been proposed (9, 10) which are large as eighth order in space and eighth order in time.

Assumption of a travelling wave solution of the form

$$U(x, t) = U_o e^{i(Kx - \omega t)}$$

(where U is a vector of deflection variables, K is the wave number, ω the circular frequency) and substitution into the homogenous system of partial differential equations yields a polynomial matrix equation

$$[P_{ij}(\omega, K)]U_o = 0$$

The condition $\det [P_{ij}] = 0$ yields a polynomial frequency equation in ω and K , and the associated eigenvectors U_o give participation of the various deformation variables in the travelling

wave. The identity $\omega = Kc_p$ (where c_p is phase speed) can be used in the frequency equation above to arrive at the equivalent dispersion equation, a polynomial in c_p and K .

To clarify the above discussion, and to introduce the phenomenon of dispersion, the following two examples are given.

Cable on Elastic Foundation (8):

$$\text{Governing PDE:} \quad \frac{\partial^2 u}{\partial x^2} - \Delta U = \frac{\partial^2 u}{\partial t^2} \quad (2)$$

$$\text{Frequency equation:} \quad K^2 + \Delta - \omega^2 = 0 \quad (\text{figure 1})$$

$$\text{Dispersion equation:} \quad K^2(1 - c_p^2) + \Delta = 0$$

Also indicated in figure 1 is the use of the phase-closure principle to determine modal frequencies of a finite structure, directly from the frequency vs wave number curve.

Timoshenko Beam (8):

Governing PDE's :

$$\frac{\partial^2 \psi}{\partial x^2} + \frac{1}{\gamma} \left(\frac{\partial y}{\partial x} - \psi \right) - \frac{\partial^2 \psi}{\partial t^2} = 0 \quad (3a)$$

$$\frac{\partial^2 y}{\partial t^2} - \frac{1}{\gamma} \left(\frac{\partial^2 y}{\partial x^2} - \frac{\partial \psi}{\partial x} \right) = 0 \quad (3b)$$

where γ is relative shear flexibility, y is lateral deflection, $\psi - \frac{\partial y}{\partial x}$ is shear deformation.

Shear deformation effects may be neglected by setting $\gamma = 0$. The resulting system is that studied by Rayleigh, the rotary inertia term being instrumental in producing a more realistic dispersion curve than the Bernoulli-Euler equation (figure 3b).

Assumption of

$$\begin{pmatrix} \psi \\ y \end{pmatrix} = \begin{pmatrix} \psi_0 \\ y_0 \end{pmatrix} e^{i(kx - \omega t)}$$

leads to the matrix equation:

$$\begin{bmatrix} -K^2 + \omega^2 - 1/\gamma & iK/\gamma \\ iK/\gamma & -\omega^2 + K^2/\gamma \end{bmatrix} \begin{pmatrix} \psi_0 \\ y_0 \end{pmatrix} = 0 \quad (4)$$

Thus the frequency equation is (figure 2);

$$K^4 - K^2\omega^2(1 + \gamma) + \omega^2(\omega^2\gamma - 1) = 0$$

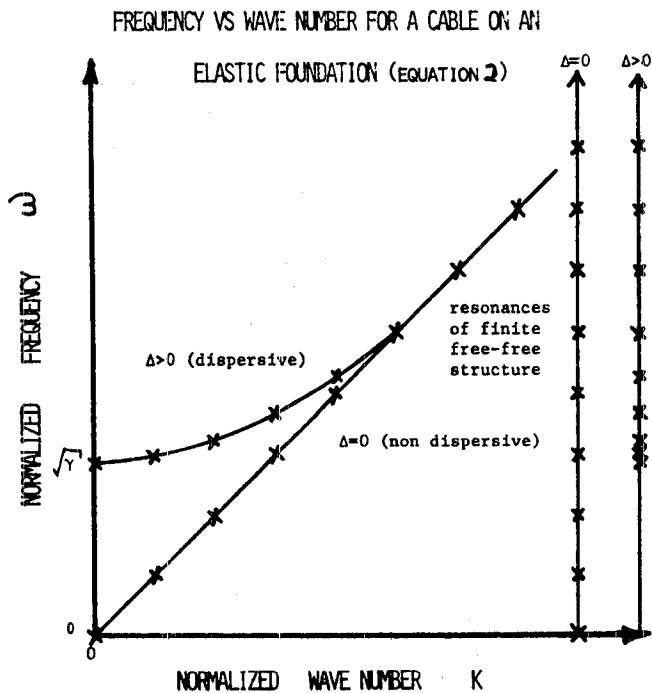


FIGURE 1

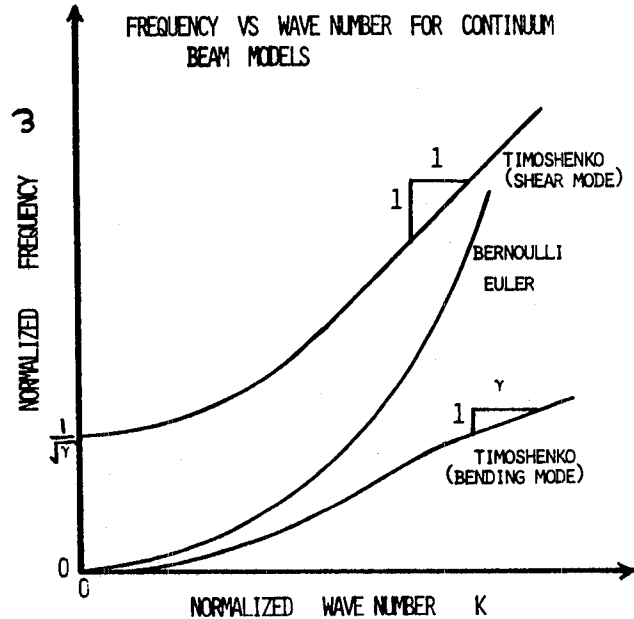
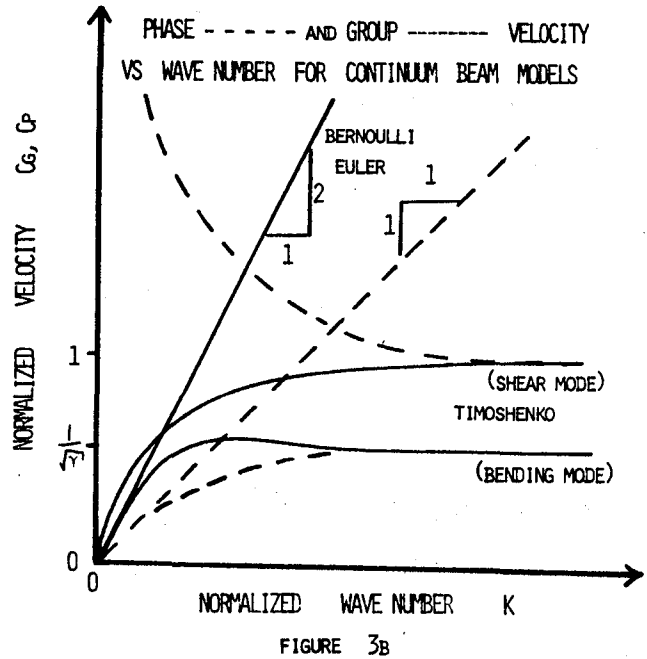
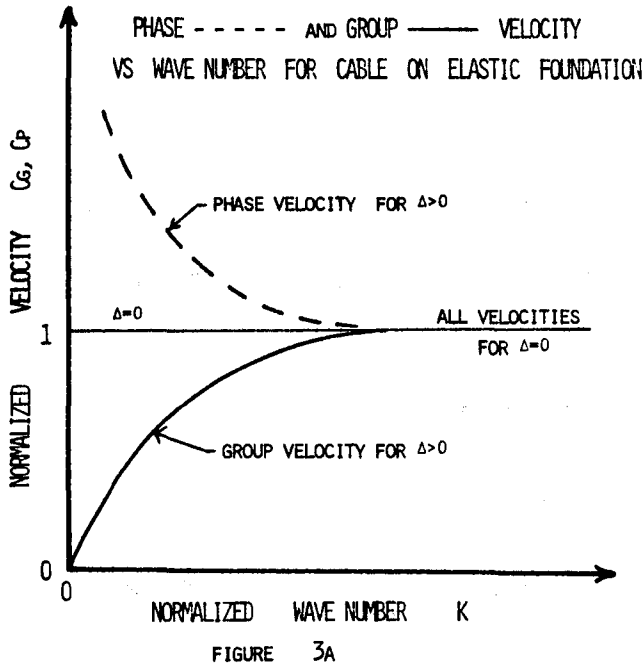


FIGURE 2

and the dispersion equation is (figure 3b);

$$K^2(1 - c_p^2(1 + \gamma) + c_p^4\gamma) - K^2 c_p^2 = 0$$

The comparison in figures 2 and 3b with the Bernoulli-Euler beam model should be noted. The Bernoulli-Euler beam model predicts infinite phase speeds for infinitesimal wave numbers. Since the phase speeds determine the model frequencies (from the phase-closure principle), the higher frequencies tend to be over-predicted. Timoshenko models of typical built-up beams (11) have shown them to have non-dimensional shear stiffness $\frac{1}{\gamma}$ much less than unity. Thus, for these structures, the shear deformation included in the Timoshenko beam model becomes important surprisingly early.



Dispersion, Velocity Definitions

A medium for which the phase speed $c_p = \omega/K$ is dependent on frequency (or wavelength) is called dispersive. For such a medium the concept of signal propagation may become poorly defined. The signal distorts as it propagates, and may become unidentifiable. For these media, other velocities may be meaningfully defined. Group, signal, and energy transmission velocities have all been studied in the literature (12). Group velocity, also a function of frequency, is the velocity with which a group of harmonic disturbances of almost identical frequency will propagate. Signal velocity is loosely defined as the speed at which the first detectable portion of a disturbance propagates. Energy transmission velocity, also loosely defined, is the average speed at which the bulk of the energy in a disturbance is propagated. For a non-dispersive medium, all velocities are equal to the phase velocity, and independent of frequency.

It has been shown (12) that the signal and energy transmission velocities are equal to the group velocity when the frequency equation is linear in ω and K . Moreover, when this restriction is almost satisfied, or when the disturbance has a frequency decomposition primarily restricted to the linear portions of the frequency equation, the group velocity determines speed of propagation of disturbances. Only in case of anomalous dispersion characteristics must other speeds be considered.

As has been stated, the group velocity is the speed of propagation of a group of harmonic waves of only slightly varying frequencies. It is defined as $c_G = \frac{\partial \omega}{\partial k}$ and can be calculated from the frequency equation. The group velocity of the two examples introduced above is graphed in figures 3a and 3b.

Exact solutions exist for some loading conditions in both these examples. The impulse response of the cable on an elastic foundation is a travelling, distorting Bessel function, whose discontinuous front travels with the maximum group velocity (8), $c = 1$ (refer to fig. 3a). The transient response of the Timoshenko beam model admits some closed-form solutions (13). Two limiting velocities are identified; discontinuities in shear force and lateral velocity propagate with nondimensional velocity $c = 1$, while discontinuities in bending moment and angular velocity travel with non-dimensional velocity $c = 1/\sqrt{\gamma}$ (refer to fig 3b). Although no proof is known, it is proposed to generalize these results, and to make the following claim for media with smooth, quasi-linear frequency-wave number relationships: disturbances travel with a velocity no greater than the maximum group velocity.

Time Lags:

An effect clearly illuminated by a travelling wave approach is the existence of finite time lags between actuation and response when actuator and sensor are not co-located. Actually, due to multiple wave paths and reflection, many time lags will be present, however, experience indicates that in most real, dissipative and dispersive structures, only the first lag will be clearly observable. Since the response time lags depend on the structure's dimension and on group velocity, while modal periods depend on dimension, boundary condition, and phase velocity, one can expect lags independent of modal periods, possibly much larger than the period of the lowest mode.

Recent experiments with flexible structures have demonstrated significant lags, on the order of modal periods of the second and third modes (2, 14). A flexible built-up beam at Stanford University (1.1 metre long) exhibited lags in tip deflection response to root torques of approximately 100 milliseconds (14). This compares with the period of the third flexible mode, measured as 110 milliseconds. Figure 4a gives a rough description of the beam and relevant experimental results.

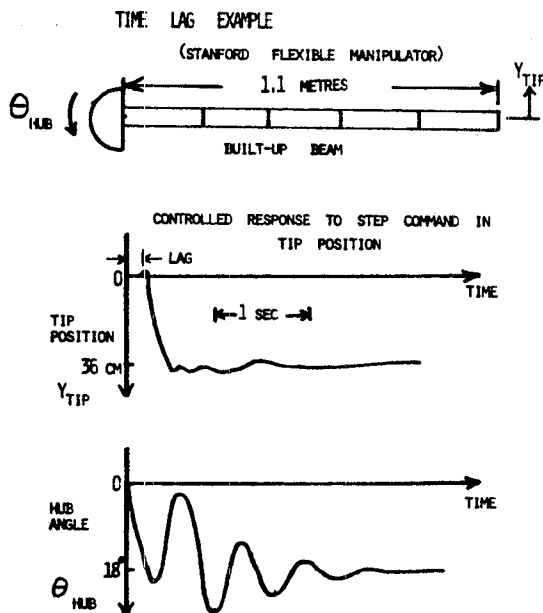


FIGURE 4a

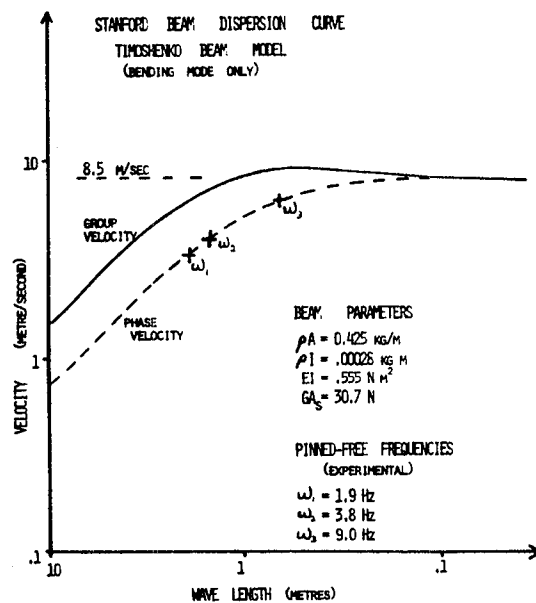


FIGURE 4b

Figure 4b shows the dispersion curve of a Timoshenko model of the Stanford beam. The four beam parameters were estimated by smearing stiffness, mass and rotary inertia, then adjusted to predict the first two experimentally measured clamped-free modes of vibration.

The applied root torque enters the beam as a bending moment, and the disturbance can be expected to travel (13) with non-dimensional limit velocity $c = 1/\sqrt{\gamma}$, or from figure 4, $c = 8.5$ metre/sec. Thus, the calculated lag is 129 milliseconds.

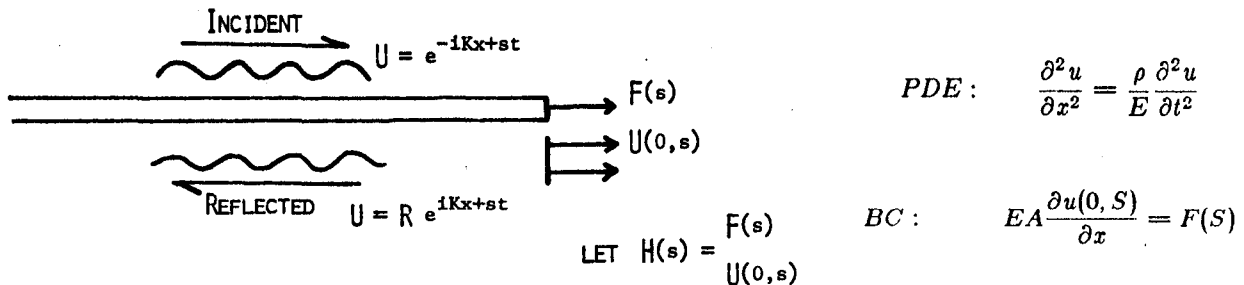
Matched Terminations:

An idea which originates in the field of communications is that of a matched termination for a transmission line (6). Such a termination prevents reflection (echoes) by imitating the behaviour of a semi-infinite continuation of the transmission line. The resulting response lacks modes of vibration entirely, and the line's transfer function may be simplified to that of a single integrator.

The idea of matched terminations can be extended to the design of active or passive dampers at the boundaries of structural elements. For the one-dimensional structures considered in this paper, the matched termination is expressed as a set of transfer functions relating tip displacements and applied forces. The practical implementation of the required transfer functions may be difficult; however the idea provides a basis for passive damper design. Two examples involving simple structural models follows.

Matched Termination Example 1:

Simple wave equation; model of torsion and longitudinal compression of solid section, transverse motion of tensioned cable;



where ρ is the material mass density, E is the modulus of material, and A is the cross-sectional area.

Application of boundary condition yields for the reflection coefficient

$$R = \frac{H(S) + iKEA}{iKEA - H(S)}$$

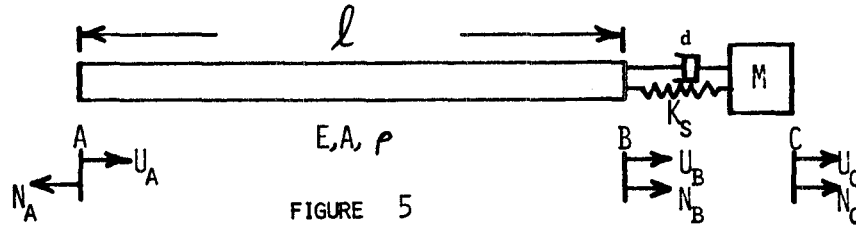
but the PDE imposes the frequency equation;

$$iK = \sqrt{\rho/E} S$$

so

$$R = \frac{H(S) + A\sqrt{\rho E}S}{A\sqrt{\rho E}S - H(S)}$$

for $H(S) = -A\sqrt{E\rho}S$ (a daspot) $R = 0$ (no reflection occurs).



Thus, a properly sized dashpot yields a matched termination for this class of problems. To study the effect of mismatched terminations on the transfer function of a finite structure, the state-vector transition matrix method of Pestel (15) is employed. This method proves valuable in the analysis of periodic structures and is introduced in this example. With reference to figure 5, the deformation of a rod (of length ℓ , area A , modulus E) in longitudinal compression is described by state vector $(\bar{U}, \bar{N})^T$ where \bar{U} is non-dimensional displacement U/ℓ , \bar{N} is non-dimensional internal force N/EA .

The state vectors at two points in a structure are related by the transition matrix

$$\begin{pmatrix} \bar{U} \\ \bar{N} \end{pmatrix}_B = [T_{AB}] \begin{pmatrix} \bar{U} \\ \bar{N} \end{pmatrix}_A$$

For the rod, the transition matrix is given by

$$[T_{AB}] = \begin{bmatrix} \cosh \bar{s} & \frac{\sinh \bar{s}}{\bar{s}} \\ \bar{s} \sinh \bar{s} & \cosh \bar{s} \end{bmatrix} \quad \text{where } \bar{s} = s \sqrt{\frac{\rho}{E}}$$

Note that the state vector at points B and C may be related by another transition matrix (15):

$$\begin{pmatrix} U_C \\ N_C \end{pmatrix} = \begin{bmatrix} 1 & \frac{1}{K_S + s d} \\ s^2 M & 1 + \frac{s^2 M}{K_S + s d} \end{bmatrix} \begin{pmatrix} U_B \\ N_B \end{pmatrix}$$

So, multiplication of matrices yields the global transition matrix:

$$\begin{pmatrix} \bar{U}_C \\ \bar{N}_C \end{pmatrix} = \begin{bmatrix} \cosh \bar{s} + \frac{\bar{s} \sinh \bar{s}}{\gamma + \bar{s} \Delta} & \frac{\sinh \bar{s}}{\bar{s}} + \frac{\cosh \bar{s}}{\gamma + \bar{s} \Delta} \\ \bar{s}^2 \mu \left(\cosh \bar{s} + \frac{\bar{s} \sinh \bar{s}}{\gamma + \bar{s} \Delta} \right) + \bar{s} \sinh \bar{s} & \bar{s}^2 \mu \left(\frac{\sinh \bar{s}}{\bar{s}} + \frac{\cosh \bar{s}}{\gamma + \bar{s} \Delta} \right) + \cosh \bar{s} \end{bmatrix} \begin{pmatrix} \bar{U}_A \\ \bar{N}_A \end{pmatrix}$$

where $\mu = m/\rho A \ell$ (mass fraction)
 $\gamma = K_S \ell / EA$ (stiffness ratio)
 $\Delta = d / A \sqrt{E \rho}$ (non-dimensional damping constant)

Various transfer functions can be extracted from the above matrix equation. In the present case, $\bar{N}_C = 0$, so the second row gives the transfer function

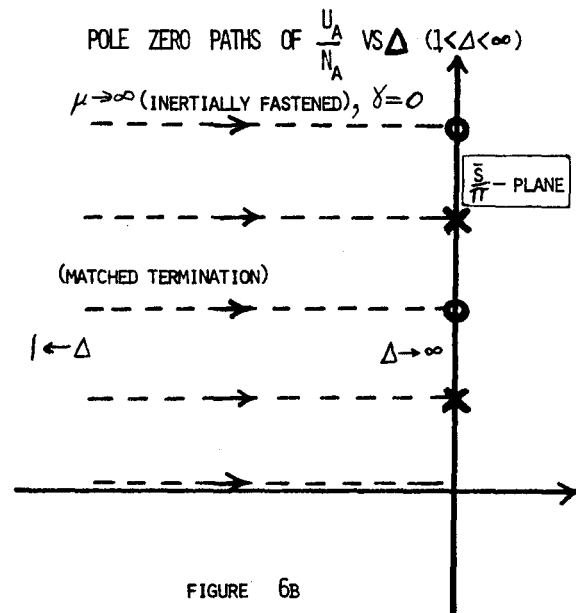
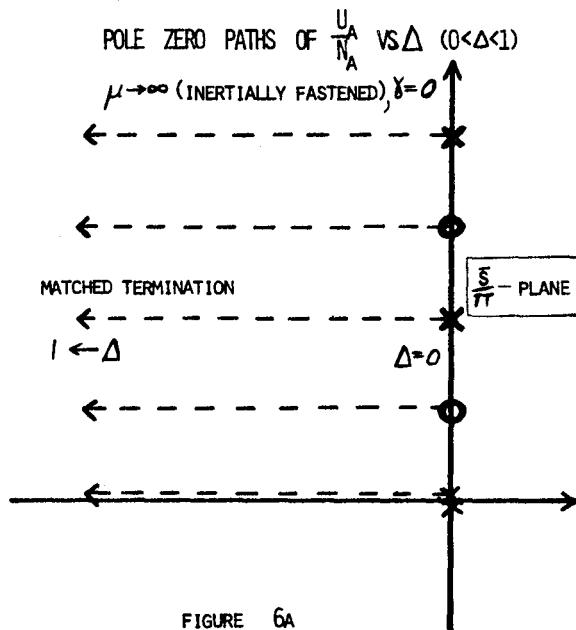
$$\frac{U_A(\bar{s})}{N_A(\bar{s})} = -\frac{\frac{1}{\bar{s}} \mu(\gamma + \bar{s}) \bar{s} \sinh \bar{s} + (\mu \bar{s}^2 + \Delta \bar{s} + \gamma) \cosh \bar{s}}{\mu(\gamma + \bar{s}) \bar{s} \cosh \bar{s} + (\frac{1}{\mu} \bar{s}^2 + \Delta \bar{s} + \gamma) \sinh \bar{s}}$$

For the matched termination calculated above, ($\gamma = 0, \Delta = 1, \mu \rightarrow \infty$), this becomes

$$\frac{U_A(\bar{s})}{N_A(\bar{s})} = -\frac{1}{\bar{s}}$$

a single integrator, also (with a redefinition of the length non-dimensionalisation) the transfer function of a semi-infinite rod.

The poles and zeroes of the transfer function (1) are shown in figures 6. Figures 6a, b show the effect of damper mismatch, with an inertial reference point available (infinite mass ratio). Figure 6c uses more realistic mass ratios of 1% and 5% and shows the root locus versus damper strength. The optimum damper strength is seen to be a function of mass ratio and mode to be damped. Modal damping ratios as large as 1% can be obtained with a 1% mass penalty. The picture could be complicated by inclusion of a spring $\gamma \neq 0$, however, such a search for an optimum tuned damper has been described elsewhere (16,17).

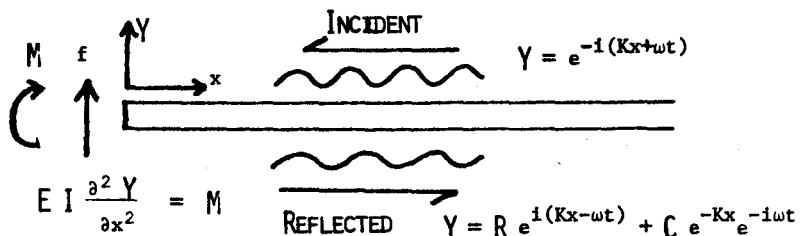


Matched Termination Example 2:

Bernoulli-Euler beam model:

PDE; $E I \frac{\partial^4 Y}{\partial x^4} + \frac{\partial^2 Y}{\partial t^2} = 0$

BC's; (at $x=0$) $E I \frac{\partial^3 Y}{\partial x^3} = f$



Note that the PDE admits two types of time-harmonic solutions, one a travelling unattenuated wave, the other a near field effect, attenuated with distance. Assume that an external moment M and force f can be applied in response to end deflection and slope

$$M(\omega) = M_0(\omega)y(0, \omega) + M_1(\omega)\frac{\partial y}{\partial x}(0, \omega)$$

$$f(\omega) = f_0(\omega)y(0, \omega) + f_1(\omega)\frac{\partial y}{\partial x}(0, \omega)$$

This assumption is in the interest of practicality. If moments proportional to curvature and forces proportional to $\frac{\partial^3 y}{\partial x^3}$ could be applied, it would become easy to imitate the behaviour of a semi-infinite continuation. Using the assumed solution

$$y(x, t) = e^{-i(Kx + \omega t)} + B e^{i(Kx - \omega t)} + C e^{-Kx} e^{-i\omega t}$$

and application of the above boundary line yields

$$\begin{bmatrix} M_0 + iK M_1 + E I K^2 & M_0 - M_1 K - E I K^3 \\ f_0 + iK f_1 + iE I K^3 & f_0 - f_1 K + E I K^3 \end{bmatrix} \begin{pmatrix} B \\ C \end{pmatrix} = \begin{bmatrix} -M_0 + iK M_1 - E I K^2 \\ -f_0 + i f_1 + E I K^3 \end{bmatrix}$$

Combinations of boundary transfer functions M_0, M_1, f_0, f_1 , which yield $B = C = 0$ are perfectly matched boundary conditions. If $C = 0$, reflection occurs, however the reflected signal does not propagate. Figure 7 presents some candidate combinations. All choices involve springs or dashpots which are dependent on disturbance frequency. A square root frequency dependence is approximated by many types of rubber (17), however, an $\omega^{3/2}$ dependence is likely to present difficulties. A practical implementation of these ideas would likely use the above matched terminations only as guidelines in a more comprehensive damper design.

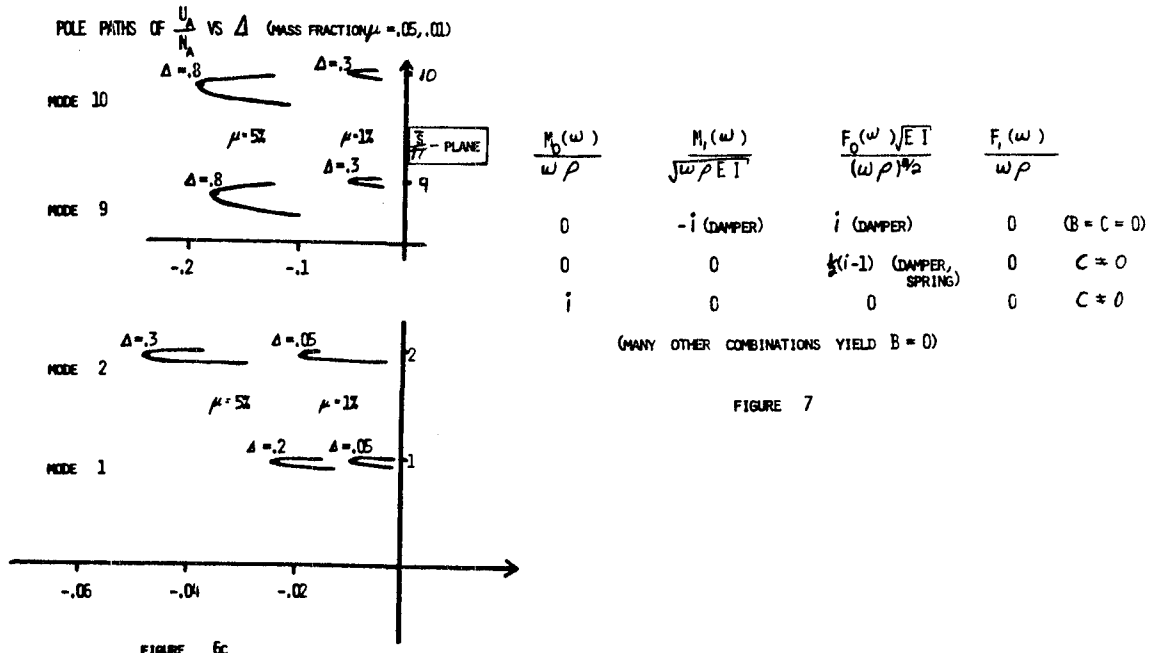


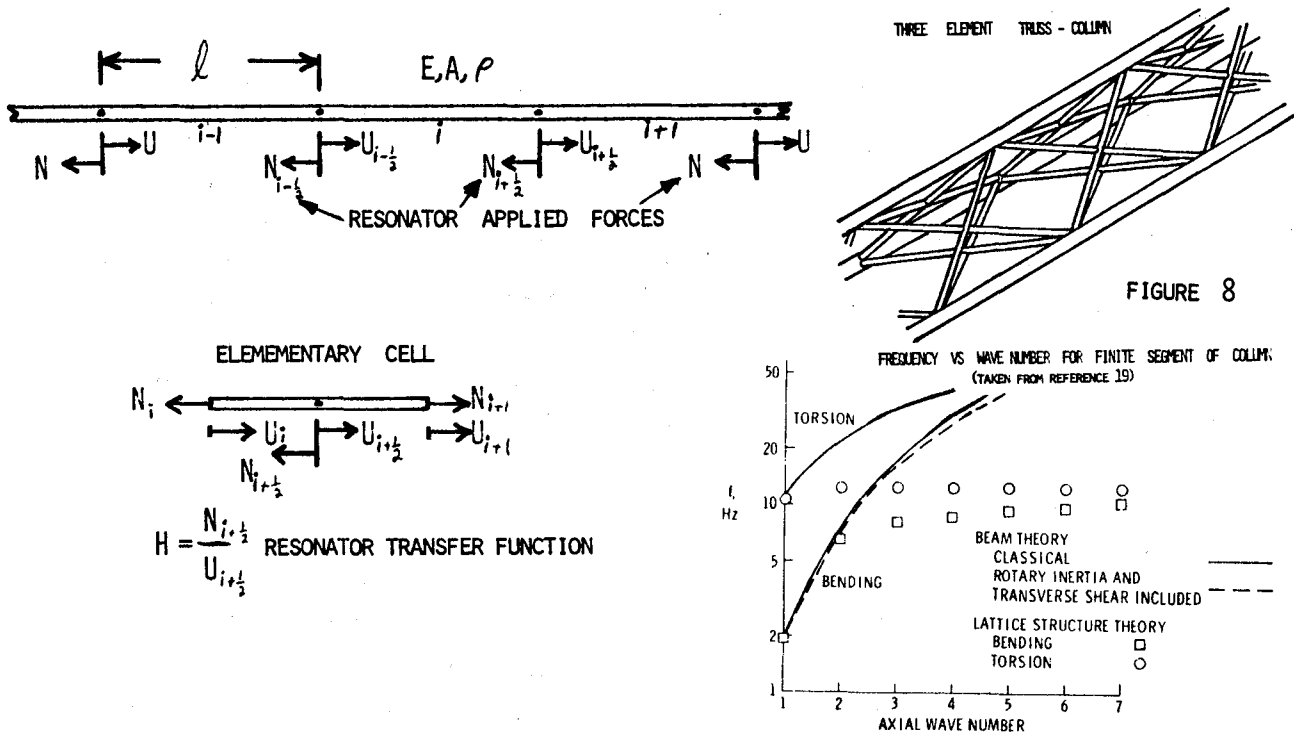
FIGURE 6c

Periodic Structures

A periodic one-dimensional wave guide exhibits anomalous dispersion characteristics (18). The frequency-wave number relationship has a banded structure, with passing and stopping bands. There will be as many passing bands as there are degrees of freedom in the elementary cell, disturbances at frequencies outside these passing bands are spacially attenuated. A continuous wave guide with periodically attached resonators will exhibit two types of structure; there will be stopping bands due to the periodicity, and stopping bands due to the poles and zeroes of the attached resonant systems.

These effects can make continuum modelling of periodic lattice beams difficult. Figure 8, taken from a paper by Anderson, (19) compares modal frequencies for a pinned-pinned lattice beam calculated in two ways. The equivalent continuum beam model, adequate for description of static deformation, errs seriously (by 300% in mode 4), in predicting modal frequencies. Anderson discovered that "the reason for this result is that the clamped end frequency of the diagonal members is 12.3 Hz which becomes an upper limit for the lowest frequency for each n number."

The essential features of wave propagation and resonances in a continuous-periodic structure are demonstrated by the following example. The system to be studied consists of a uniform rod in longitudinal compression.



It is loaded by identical resonant systems periodically attached. Using the state vector representation and symbols of a previous example, the transition matrix corresponding to an elementary cell is

$$\begin{pmatrix} \bar{U} \\ \bar{N} \end{pmatrix}_{i+1} = \begin{bmatrix} \cosh \bar{s} + \bar{H}(\bar{s}) \frac{\sinh \bar{s}}{2\bar{s}} & \frac{\sinh \bar{s}}{\bar{s}} - \bar{H}(\bar{s}) \frac{(1 - \cosh \bar{s})}{2\bar{s}^2} \\ \bar{s} \sinh \bar{s} + \frac{\bar{H}(\bar{s})}{2} (1 + \cosh \bar{s}) & \cosh \bar{s} + \bar{H}(\bar{s}) \frac{\bar{s} \sinh \bar{s}}{2\bar{s}} \end{bmatrix} \begin{pmatrix} \bar{U} \\ \bar{N} \end{pmatrix}_i$$

where $\bar{s} = s l \sqrt{\frac{\rho}{E}}$

$\bar{U} = U/l$

$\bar{N} = N/EA$

$\bar{H} = H/lEA$

Symbolically, the approach to obtaining the poles and zeroes of a finite periodic structure would consist of the same steps used in the previous example. The global transition matrix is obtained by multiplication of local matrices. The boundary conditions are used to extract the frequency determinant or transfer function from the global matrix. The transfer function is searched for its poles and zeroes. This approach leads to numerical difficulties, and a more intuitive method using the phase-closure principle is described.

Wave Propagation along Second Order Periodic-Continuous Structures:

A second order continuous structure with periodically attached resonant systems will have a 2x2 elementary transition matrix

$$[T] = \begin{bmatrix} T_{11} & T_{12} \\ T_{21} & T_{22} \end{bmatrix}$$

A single wave that propagates along this infinite structure is characterized by the fact that the state vector is multiplied by a complex factor ξ as the wave passes through the cell

$$\begin{pmatrix} \bar{U} \\ \bar{N} \end{pmatrix}_{i+1} = \xi \begin{pmatrix} \bar{U} \\ \bar{N} \end{pmatrix}_i$$

Thus, the transmission coefficient ξ may be determined as the eigenvalues of the local transition matrix

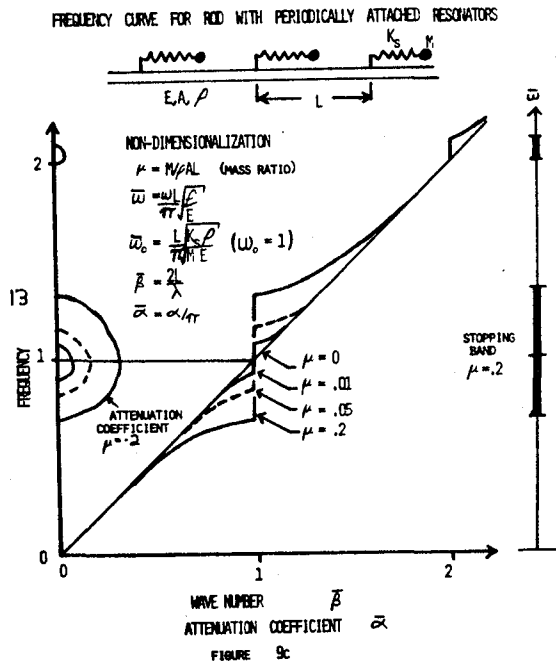
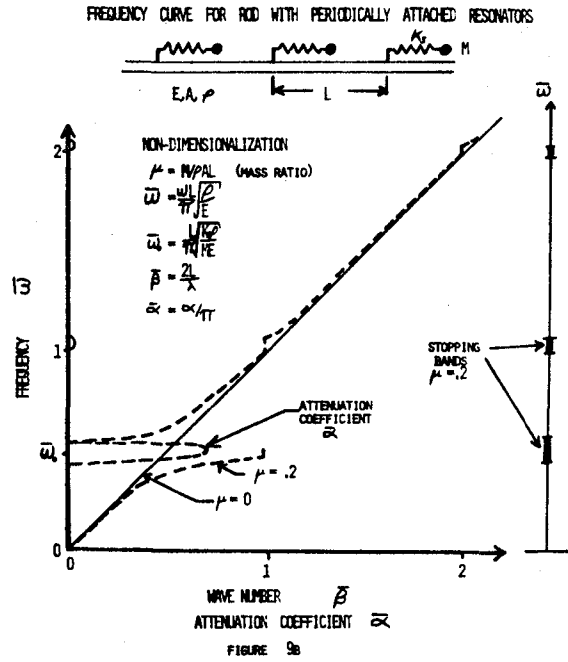
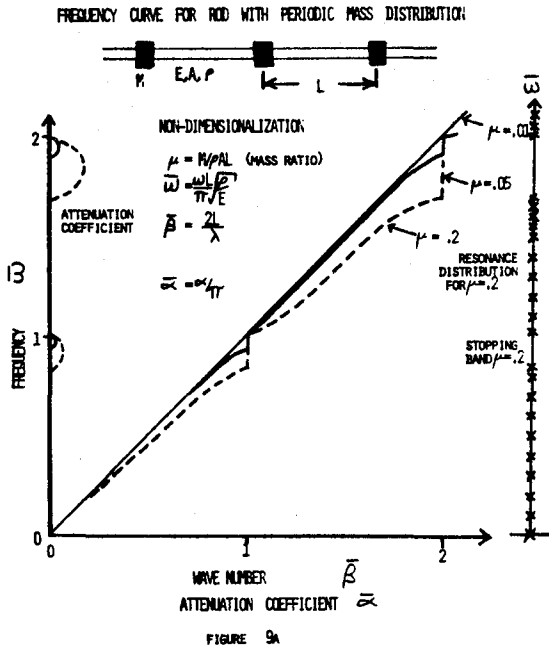
$$\xi^2 - (T_{11} + T_{22})\xi + 1 = 0$$

(where the energy conservation property, $\det [T] = 1$, valid for conservative systems, has been used). This quadratic has the property that its two roots satisfy $\xi_1 \xi_2 = 1$. Thus, if $\xi_1 = e^{-\gamma} = e^{-\alpha - i\beta}$ then $\xi_2 = e^{\alpha + i\beta}$. Here α is the attenuation coefficient per cell, β the phase change. Unattenuated propagation occurs if $\alpha = 0$ i.e. $|T_{11} + T_{22}| < 2$. When spacial attenuation occurs, resonances in finite structures are prevented.

In the second order case described above, it is interesting to note the exact analogy with Floquet theory and Hill's equation (20).

The procedure outlined above was used to calculate the frequency-wave number relationship for the example structure. Point transfer functions $\bar{H}(\bar{S})$ representing rigidly attached masses and elastically attached masses were considered. Results are graphed in figures 9. These figures display the banded frequency distribution. The first branch of the curve in figure 9b should be compared with Anderson's results in figure 8. Anderson also mentions the existence of the higher branches, but does not show them. The existence of this banded resonant structure is a hindrance to continuum modelling of lattice beams. However, it also provides opportunities to the designer. With prescribed tuning, the stopping bands may be placed where desired. Resonance-free frequency ranges may be designed into structural members and used for vibration isolation or control spillover amelioration. In this model the width of the first stopping band depends on the mass ratio and on the tuning.

Since the elastically attached mass is a simplified representation of internal lattice members, it is difficult to speak of a weight penalty. However, in this model, a mass penalty of 5% (figure 9c) yielded a resonant-free frequency range of relative bandwidth 15%. Inclusion of light damping in the spring-mass system would potentially double the effective resonant-free range.



Summary:

This paper has examined various aspects of travelling wave effects in one-dimensional structures. The existence of time lags was indicated, and a simple method of their prediction was demonstrated. The possibility of passive damper design based on the matched terminations of communications engineering was explored with the help of two examples. Insight was gained into the continuum modelling of periodic lattice beams and the possibility of custom-designing desirable transmission-resonance characteristics was pointed out.

Acknowledgments:

This research was supported in part by Air Force Office of Scientific Research under contract AFOSR 0062 and in part by National Aeronautics and Space Administration under Grant NAG-1-97 from Langley Research Centre. I would like to express my appreciation to my advisor, Prof. Holt Ashley, for providing an excellent environment in which to work.

References

1. Ivan Bekey, John E. Naugle, "Just Over the Horizon in Space," *Astronautics and Aeronautics*, May 1980.
2. Richard H. MacNeal, "Structural Dynamics of the Heliogyro," NASA CR-1745, May 1971.
3. A. F. Tolivar, "NASA LSS Missions and Control Requirements," presented at NASA Workshop on Applications of Distributed System Theory to the Control of LSS, July 14-16, 1982, JPL, Pasadena.
4. B. Lax, K. J. Button, Microwave Ferrites and Ferrimagnetics, McGraw-Hill, 1962.
5. P. M. Anderson, A. A. Fouad, Power System Control and Stability, Iowa State University Press, Iowa, 1977.
6. P. Grivet, P. W. Hawkes, The Physics of Transmission Lines at High and Very High Frequencies, Academic Press, 1970.
7. L. Cremer, M. Heckl, E. E. Ungar, Structure Borne Sound, Springer Verlag, 1973.
8. K. F. Graff, Wave Motion in Elastic Solids, Ohio State University Press, 1975.
9. A. K. Noor, M. P. Nemeth, "Micropolar Beam Models for Lattice Grids with Rigid Joints," *Comp Mthd Appl Mech Engng.*, 21 (1980) 249-263.
10. A. K. Noor, C. M. Andersen, "Analysis of Beam-Like Lattice Trusses," *Comp Mthd Appl Mech Engng.*, 20 (1979) 53-70.
11. C. T. Sun, B. J. Kim, J. L. Bogdanoff, "On the Derivation of Equivalent Simple Models for Beam and Plate-Like Structures in Dynamics Analysis," AIAA paper 81-0624.
12. Leon Brillouin, Wave Propagation and Group Velocity, Academic Press, 1960.
13. B. A. Boley, C C Chao, "Some Solutions of the Timoshenko Beam Equations," *J Appl Mech*, 22 (1955) 579-86.
14. R. H. Cannon, E Schmitz, "Initial Experiments on Control of a Very Flexible Robot Link Using End Point Sensing," (to be published).
15. E. C. Pestel, F A Leckie, Matrix Methods in Elastomechanics, McGraw-Hill, 1963.
16. J. B. Hunt, Dynamic Vibration Absorbers, Mechanical Engineering Publications, London, 1979.
17. J. C. Snowdon, Vibration and Shock in Damped Mechanical Systems, Wiley and Sons, 1968.
18. Leon Brillouin, Wave Propagation in Periodic Structures, Dover, 1946.
19. M. S. Anderson, "Vibration of Prestressed Periodic Lattice Structures," *AIAA J*, 19 (1981) 782-8.
20. J. J. Stoker, Nonlinear Vibrations in Mechanical and Electrical Systems, Interscience, 1950.

This Page Intentionally Left Blank

DISTRIBUTED CONTROL OF LARGE SPACE ANTENNAS

J.M. Cameron, M. Hamidi, Y.H. Lin, and S.J. Wang
Jet Propulsion Laboratory, California Institute of Technology
Pasadena, CA 91109

ABSTRACT

In this paper, a systematic way to choose control design parameters and to evaluate performance for large space antennas is presented. The structural dynamics and control properties for a Hoop and Column Antenna and a Wrap-Rib Antenna are characterized. Some results of the effects of model parameter uncertainties to the stability, surface accuracy, and pointing errors are presented. Critical dynamics and control problems for these antenna configurations are identified and potential solutions are discussed.

I. INTRODUCTION

Large space antennas and other large space structures will play an important role in the coming decades as commercial applications of space become feasible - especially in the area of communications. Structures from 10 m to 120 m and larger have been considered by NASA and other government agencies for future missions (Reference 1). As the structural size and mass distribution change drastically from that of conventional spacecraft, many difficult control problems arise. The basic problem, however, comes in modeling highly flexible structures. Structures of this type are known to have a large number of packed modes at very low frequencies; mode shapes and frequencies can not be accurately predicted or measured even for a small number of modes at preflight time. This means that there are always model uncertainties. Model uncertainties in the control loop can cause serious consequences including the possibility of making the system unstable. Model order is another problem with great impact in control design. Using today's inflight computer capability, one can only expect to have a modest low order controller - which often means model truncation and will cause further performance deterioration. Dynamics and control problems for specific configurations must be characterized and evaluated in terms of incomplete knowledge of the system dynamics so that the required performance can be ensured and risk reduced.

In this paper, the structural dynamics and the control properties for a 64-meter diameter center fed antenna and a 55-meter offset fed antenna are investigated. Some interesting results are presented on the effects of model parameter uncertainties to the system stability, surface accuracy, and pointing accuracy. Critical control problems are identified and potential solutions are recommended. In Section II the antenna configurations and the structural dynamic properties are briefly described. The control design, disturbance assessment, and construction of weighting matrices are summarized in Section III. Finally, numerical results and conclusions are given in Sections IV and V, respectively.

II. ANTENNA CONFIGURATIONS AND STRUCTURAL DYNAMIC PROPERTIES

A. Antenna Configurations

Several antenna concepts are under development (References 1,2,3). However, there are two concepts that have drawn particular attention in recent years; they are the structurally balanced center fed quad aperture hoop and column antenna and the offset fed wrap-rib antenna. The hoop and column antenna chosen for analysis is a pretensioned mesh deployable structure. Figure 1 shows the deployed 100 mD antenna and the major components are depicted in Figure 2. The basic structural components are the feed assemblies, the mast, the hoop, and the reflector mesh surface. The mast and the support cables suspend the hoop and together the assembly provides the stiffness of the structure. The mesh is suspended by the hoop and the mast and the surface shape is controlled by the shape cables through a secondary draw surface and tie cords. The cables are stranded quartz cords. The hoop consists of 48 hollow sections made of graphite fiber. The adjacent sections are joined together through hinges. The reflector is made of gold plated poly-wire mesh. The four circular surface areas are separately illuminated by the feed elements that form the offset feed quad-aperture arrangement.

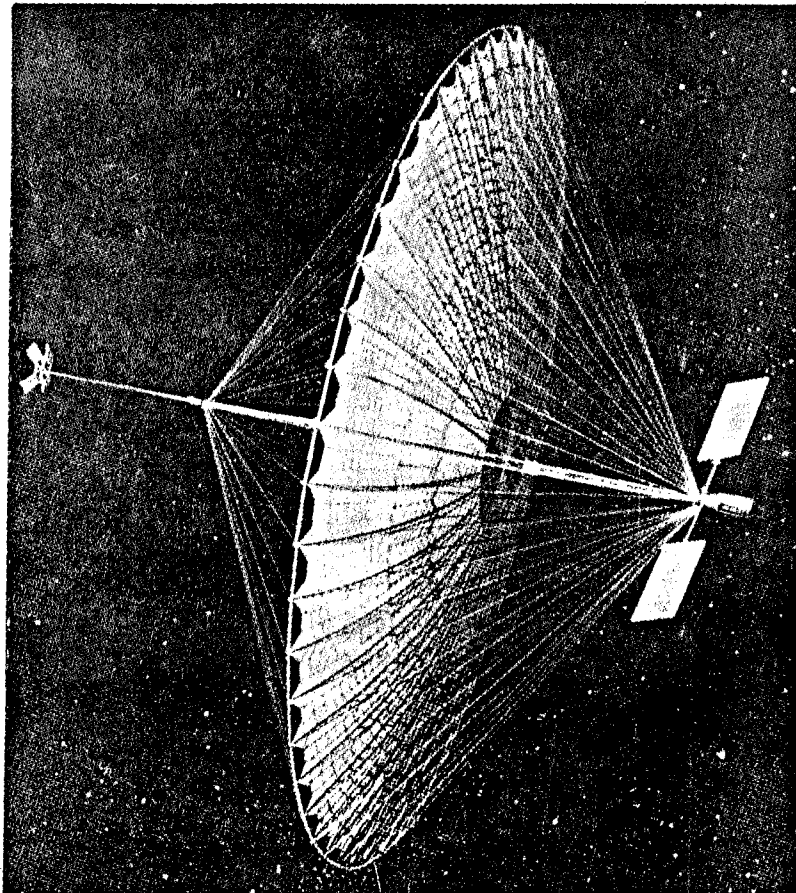


Figure 1. Deployed 100 mD Hoop and Column Antenna.

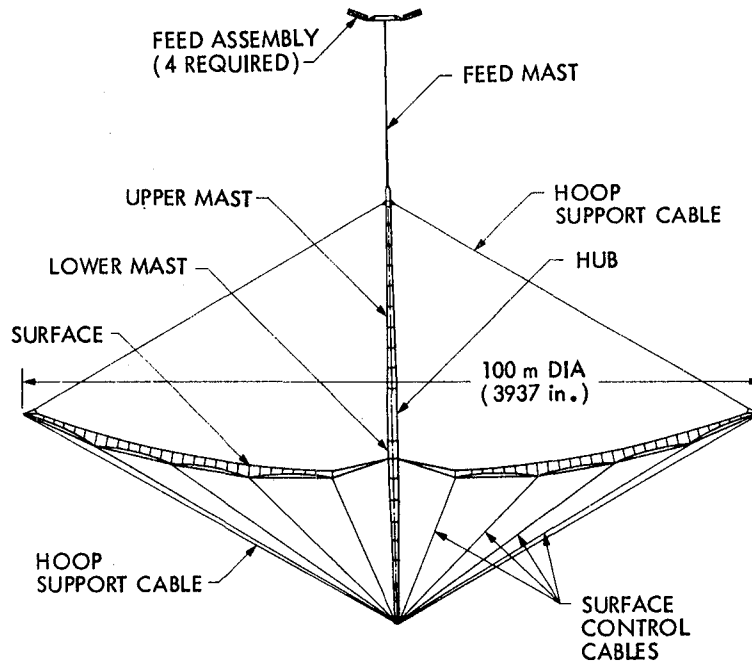


Figure 2. Side View of 100 mD Hoop and Column Antenna.

The wrap-rib antenna consists of a 55-meter diameter mesh reflector, a feed array mounted on a spacecraft bus, and a long L-shaped boom connecting the reflector and the bus. A typical configuration is shown in Figure 3.

The reflector consists of a number of radial ribs which are cantilevered from a central hub structure. For parabolic or other curved shape reflectors, the ribs are formed in accordance with the required surface shape, and the mesh gores are attached between the ribs.

B. Structural Dynamic Properties

The total weight of the hoop and column antenna system is 2790 kg of which the feed assembly weighs approximately 30%, the hoop and the mast, 20%, and the solar panels and the spacecraft weigh 50%. Since mass distribution affects modal frequencies, it is appropriate to point out that based on a subsequent study of a 122 mD LMSS (Land Mobile Satellite Service) antenna a much heavier (approximately 50%) mass concentration at the feed area is more realistic.

To assess performance, a finite element model of a 64 mD hoop and column antenna (Reference 4) has been adopted. The reflector and the hoop were modeled by a two-for-one model with 24 gore and hoop sections and 120 grid points. The feeds, the solar panels, the mast, etc., were represented by 86 grid points. Bar elements were used to model the mast and the feed and solar panels; and rod elements for the hoop joints, hoop support and surface shaping cables.

The finite element analysis revealed that the lowest mode is the first torsional mode which has a frequency of 0.10 Hz; the next higher modes are the

TOTAL MASS 9695 LBS

$$\text{MOMENTS OF INERTIA} \begin{cases} I_x = 2.91 \times 10^6 \text{ SLUG-FT}^2 \\ I_y = 2.64 \times 10^6 \\ I_z = 0.37 \times 10^6 \end{cases}$$

$$\text{PRODUCTS OF INERTIA} \begin{cases} I_{xy} = -3.56 \times 10^3 \\ I_{xz} = -4.22 \times 10^3 \\ I_{yz} = 0.72 \times 10^6 \end{cases}$$

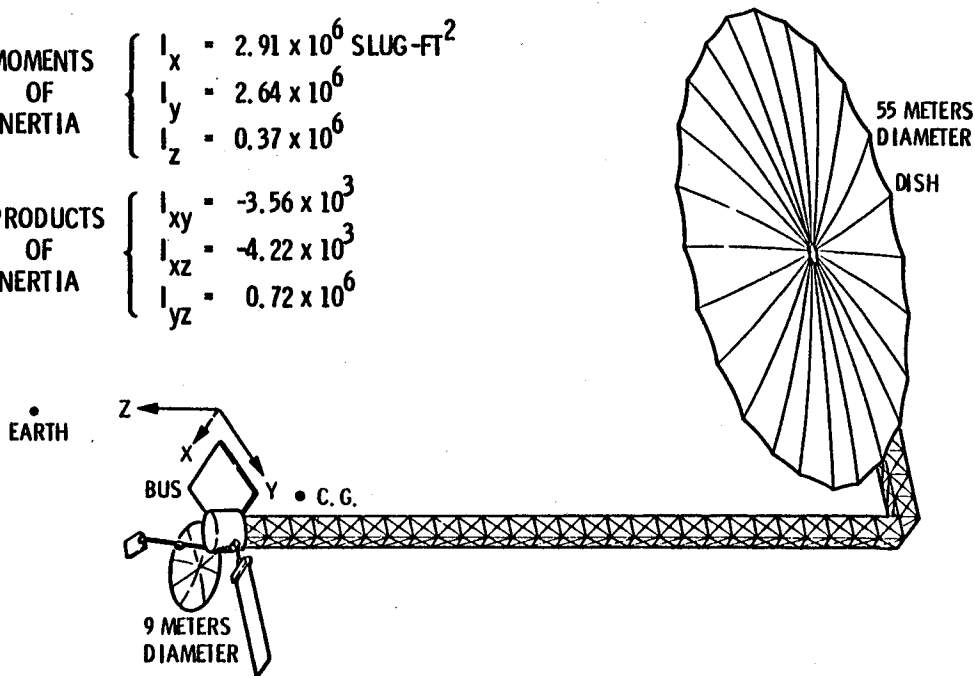


Figure 3. The Wrap-Rib Offset Fed Antenna Configuration

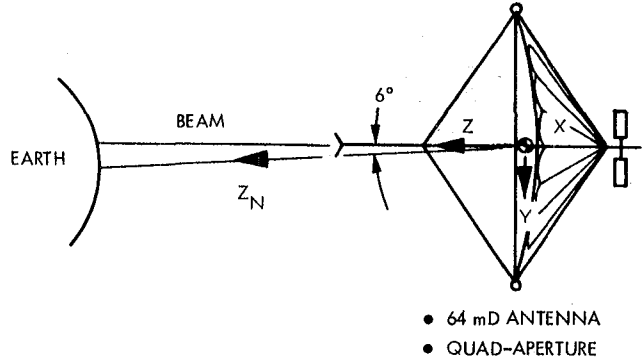
two orthogonal mast bending modes with frequencies 0.43 Hz; the next two modes are the second and third mast torsion modes which are followed by two orthogonal second mast and dish bending modes. Figure 4 shows the modal and mass properties. It is interesting to note that the antenna has relatively high bending stiffness and weak torsional stiffness. The high radial separation of the hoop and the mast, the large hoop moment of inertia, and the small moment arm of the hoop cables at the mast make the mast very loosely coupled to the hoop so that the mast alone dominates the torsional modes.

The total weight of the wrap-rib antenna system is 4,407 kg (9695 lb), 80% of which is concentrated at the feed/bus area. The remaining 20% is attributed to the reflector and the hub. Moments of inertia are 3.95×10^6 , 3.58×10^6 , $.502 \times 10^6$ kg-m². The largest cross product of inertia is $.976 \times 10^6$ kg-m², which is due to the inherent imbalance of the offset feed configuration. The axis of least moment-of-inertia is approximately along an imaginary line connecting the bus and the reflector hub. This results in a 16° offset between the least moment-of-inertia axis and the local vertical.

Mode shapes and mode frequencies of the wrap-rib antenna system were obtained in two steps. First, reflector modes and offset boom modes were obtained from finite element methods. Second, the modes of these two substructures were then combined through the process of modal synthesis on the assumption that the interface at the hub structure is rigid. Figure 5 provides the first seven flexible mode frequencies and mode shape description of the wrap-rib antenna system.

• MODAL FREQUENCIES

NO.	FREQ, HZ	DESCRIPTIONS
7	0.10	1ST MAST TORSION
8	0.43	1ST MAST ROLL BENDING
9	0.43	1ST MAST PITCH BENDING
10	0.58	2ND MAST TORSION
11	1.07	3RD MAST TORSION
12	1.83	2ND MAST/DISH ROLL BDG
13	1.90	2ND MAST/ DISH PITCH BDG
14	3.20	DISH WARPING
15	3.28	DISH WARPING
16	3.36	DISH WARP MAST BENDING
17	3.37	DISH WARP MAST BENDING
18	4.43	DISH WARP MAST BENDING



• MASS PROPERTY

- MASS: 2790 Kg
- MOMENT OF INERTIA
 - $1.42 \times 10^6 \text{ Kg-m}^2$
 - 1.42×10^6
 - 2.73×10^5

• MAX DISTURBANCE TORQUES

- GRAVITY GRADIENT $1.89 \times 10^{-3} \text{ Nm}$
- GYROSCOPE 6.30×10^{-4}
- SOLAR PRESSURE 6.23×10^{-3}

• BALANCED CONFIGURATION

Figure 4. Structural Properties for the 64 mD Hoop and Column Antenna

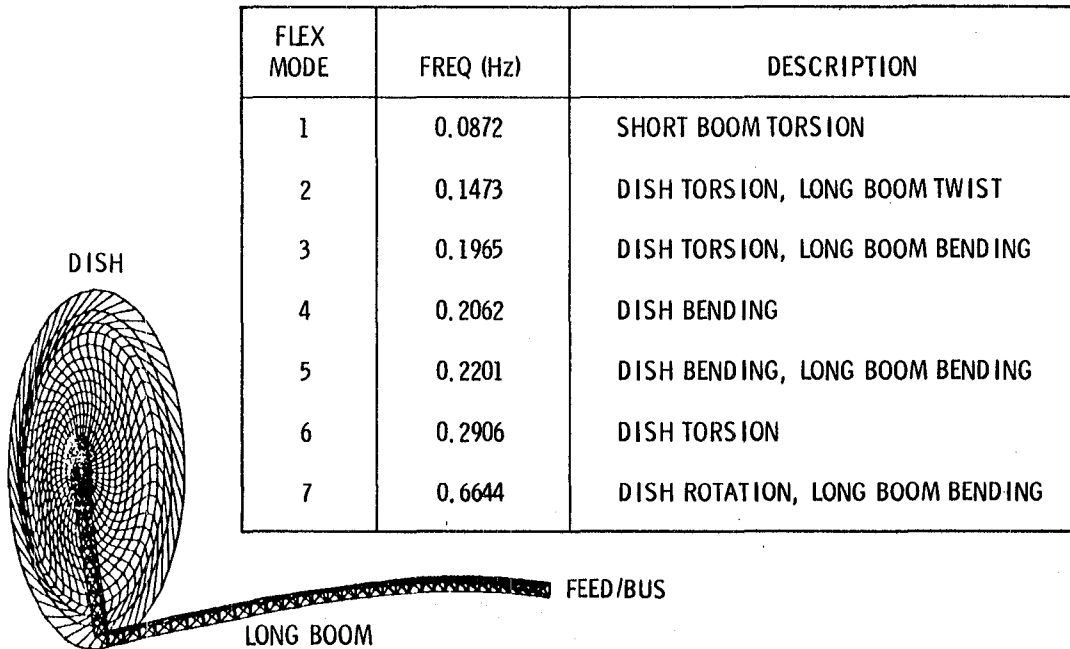


Figure 5. Wrap-Rib Antenna Mode Frequencies/Shapes

III. ATTITUDE AND STRUCTURAL CONTROL SYSTEMS

A. Equations of Motion

For small perturbations about the equilibrium, the dynamics of this system may be described by the finite element method. For the hoop and column system, let q be the 18-modal amplitude vector, Φ the 1236x18-eigenvector matrix, and f the vector of the applied forces. The dynamic equations are, in component form

$$\ddot{q}_k = \phi_k^T f \quad k = 1, \dots, 6 \quad (1a)$$

$$\ddot{q}_k + 2\zeta_k \omega_k \dot{q}_k + \omega_k^2 q_k = \phi_k^T f, \quad k = 7, \dots, 18 \quad (1b)$$

where the modal frequencies, ω_k , may be obtained from Figure 4 and the estimated values for the damping ratios, ζ_k , are .01 for $k = 7, \dots, 10$ and .02 for $k = 11, \dots, 18$.

Due to the existence of numerical sensitivity problems the rigid modes were not used and instead Euler's equations were used to describe the rigid body motion. Referring to Figure 4, let X, Y, Z be the body-fixed coordinates. Consider a nadir pointing configuration with the satellite moving in a circular synchronous orbit. The Euler's equations for the rigid body rotation are

$$I_x \ddot{\phi} + 4\omega_o^2 (I_y - I_z) \phi + \omega_o (I_y - I_x - I_z) \dot{\psi} = T_{dx} + T_{cx} \quad (2a)$$

$$I_y \ddot{\theta} + 3\omega_o^2 (I_x - I_z) \theta = T_{dy} + T_{cy} \quad (2b)$$

$$I_z \ddot{\psi} + \omega_o^2 (I_y - I_x) \psi + \omega_o (I_x - I_y + I_z) \dot{\phi} = T_{dz} + T_{cz} \quad (2c)$$

where $I_x, I_y, I_z, \omega_o, \phi, \theta,$ and ψ are the principal moments of inertia, the orbital rate, and the roll, pitch, and yaw angles, respectively. $T_{dx}, T_{dy}, T_{dz}, T_{cx}, T_{cy},$ and T_{cz} are the disturbance and control torques, respectively. Note that since the gravity gradient torques and the gyroscopic torques are already included in the left-hand side of Eq. (2), they are excluded from T_d . The angles ϕ, θ, ψ and their derivatives in Eq. (2) are assumed small and they are related to inertial angular rates by the following approximate relations.

$$\omega_x = \dot{\phi} - \psi \omega_o \quad (3a)$$

$$\omega_y = \dot{\theta} - \omega_o \quad (3b)$$

$$\omega_z = \dot{\psi} + \phi \omega_o \quad (3c)$$

The equations of motion of the wrap-rib antenna system were developed in Reference 5. The approach there was based on LaGrange's formulation. The set of equations developed reproduces mode shapes and frequencies very close to those generated using finite element methods (Figure 5). However, the approach in

Reference 5 permits convenient and inexpensive model parameter changes.

The equations of motion have the following general form:

$$\ddot{Mx} + Kx = F \quad (4)$$

where x consists of 3 rigid-body rotations, and boom and reflector flexible modes. M and K are the mass and the stiffness matrices, respectively. And F represents all non-conservative forces on the antenna system. In this study, 3 boom modes and 6 reflector modes were selected for analysis, and therefore Eq. (4) is a 12 x 12 second order system.

To consider natural damping of the system, the following equation was adopted:

$$\ddot{Mx} + D\dot{x} + Kx = F \quad (5)$$

where $D = \Phi^T [2Z\Omega]\Phi$; Φ and Ω are the eigenfunctions and eigenvalues of Eq. (4). And Z represents the diagonal matrix of damping ratios:

$$Z = \text{diag} (\zeta_i) , \quad (6)$$

where, in this study, $\zeta_i = 0$ for $i = 1,2,3$, and $\zeta_i = .005$ for all other i .

B. Control Hardware Placement

The beam pointing accuracy is determined by the orientations of the feed and the dish and their relative motions. Sensor and actuator placement is dictated by the observability and controllability properties and the structural constraints. By examining the eigenvectors of the elastic modes at various potential locations, it can be seen that sensors and actuators placed at the feed assembly and the spacecraft bus can most effectively control the attitude and the important elastic modes. Figure 6 shows the two-site 3-axis attitude and structural control system for the hoop and column configuration considered in this paper. Basic control devices are the inertial sensors and momentum wheels. Reflector shape control can be achieved with the addition of optical sensors such as SHAPES (Reference 6) and shape-cable actuators. Hoop motion can be controlled with a SHAPES sensor and thrusters on the hoop sections.

Three options in control hardware placement have been considered for the wrap-rib antenna. Option 1 has all attitude sensors and actuators lumped together and mounted on the bus. This concept represents current attitude controllers for 3-axis spacecraft stabilization.

Option 2 represents a departure from option 1 in that it calls for an additional optical sensor mounted on the bus to perform multi-point distributed sensing of the reflector as shown in Figure 7. The purpose of having this optical sensor is to obtain distortion and vibration information of the reflector and boom directly by measurements.

Option 3 is option 2 plus additional control devices at the reflector hub. It represents a spatially distributed control scheme for the antenna such that the distortions of the short boom can also be controlled effectively with actuators located at the reflector hub.

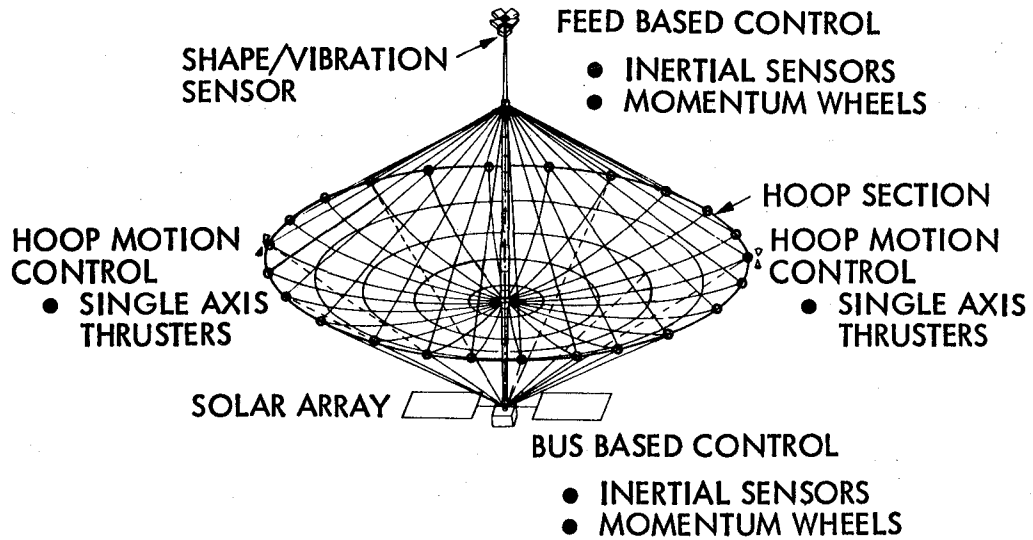


Figure 6. Two-Site Control System for Hoop and Column Antenna

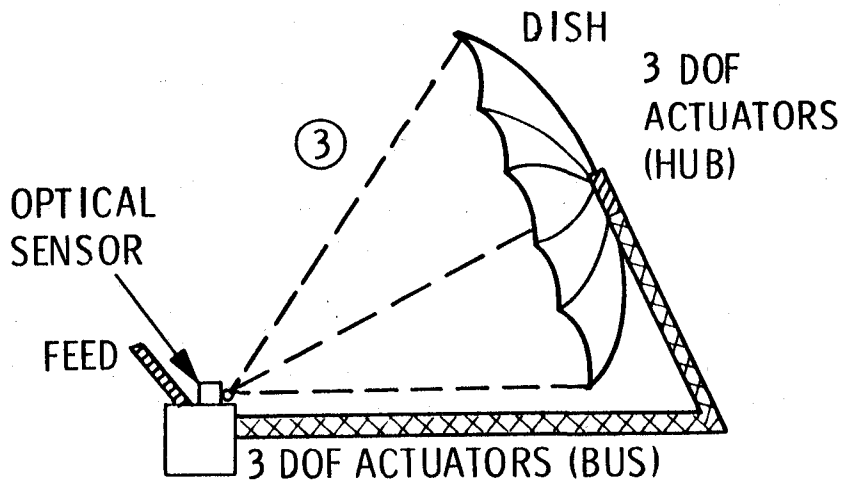


Figure 7. Wrap-Rib Control for Option 3.

C. Characterization of Disturbances

The disturbances discussed here are limited to the gravity gradient and gyroscopic torques due to nonprincipal axis pointing, solar pressure torques, and torques caused by thruster firings for wheel dumping and station keeping.

Consider the LMSS antenna applications. With the current hoop and column antenna design, the body z-axis must tilt 6° from nadir in order to provide the necessary communication coverage. The orbital configuration is shown in Figure 8a. A gravity gradient torque and gyroscopic torque of -2.52×10^{-3} N-m is created about the x-axis. Since this torque is noncyclic, a periodic wheel dumping at the rate of 217.73 N-m-s for every 24 hours is required. The solar pressure torques, on the contrary, are cyclic. With the availability of a detailed configuration for a 122 mD antenna, the solar pressure torques for the latter have been computed for arbitrary sun inclination and orbital position. The solar pressure torques for the 64 mD antenna are obtained by scaling and considering the shift of the center of mass. The projected solar pressure torques are shown in Figure 8b.

For the wrap-rib antenna, due to the structurally imbalanced configuration a -16° tilt of the principal axis results. This pronounced non-principal axis pointing has created a non-cyclic x-axis gravity gradient and gyroscopic torque of 2.06×10^{-2} N-m. The solar pressure torques are cyclic. Figure 9 shows these torques over a 24-hour period.

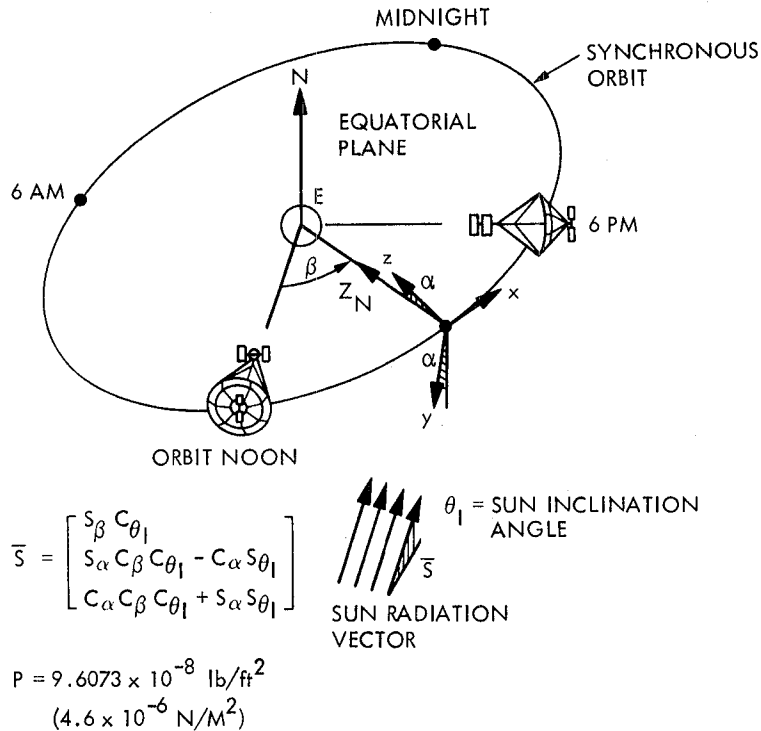


Figure 8a. Orbital Configuration (α = tilt angle, β = orbit angle)

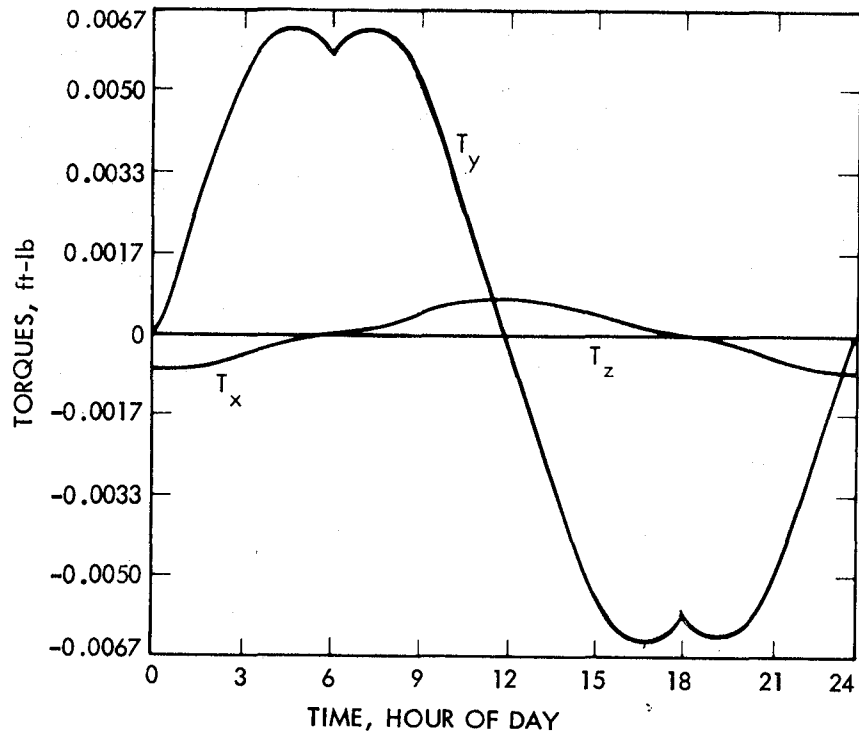


Figure 8b. Solar Pressure Disturbance Torques for Hoop and Column Antenna ($\alpha = 6^\circ$ and $\theta_I = 0^\circ$).

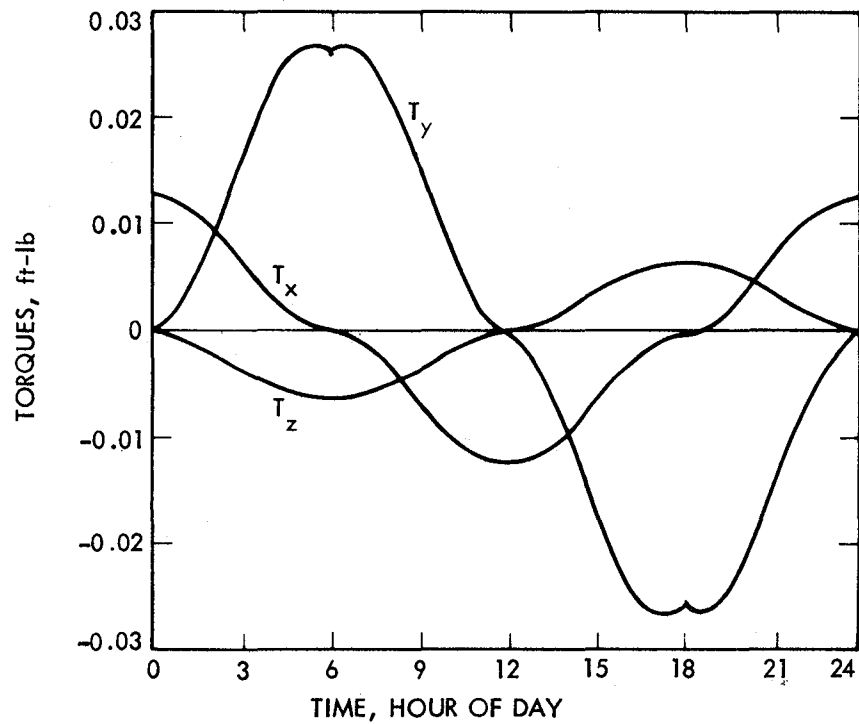


Figure 9. Solar Pressure Disturbance Torques for Wrap-Rib Antenna ($\alpha = 16^\circ$, $\theta_I = 0^\circ$).

D. Control Design

Consider the steady state stochastic linear optimal output feedback regulator problem. The following formulation applies to both the hoop and column and the wrap-rib configurations; the only differences are in the assignment of variables and coefficient matrices. Let x and \hat{x} be the state vector and the state estimate and let z be the measurement vector. Let F , G , Γ , and H be the assumed state matrix, control influence matrix, disturbance distribution matrix, and the measurement distribution matrix, respectively. The state and the state estimator equations are:

$$\dot{\hat{x}} = Fx + Gu + \Gamma w \quad (7a)$$

$$z = Hx + v \quad (7b)$$

$$u = -K_c \hat{x} \quad (7c)$$

$$\dot{\hat{x}} = F\hat{x} + Gu + K_e(z - H\hat{x}) \quad (7d)$$

The cost index to be minimized is

$$J = \frac{1}{2} E \left\{ \int_0^{\infty} (x^T A x + u^T B u) dt \right\} \quad (8)$$

The optimal control gains K_c and the filter gains K_e are, respectively

$$K_c = B^{-1} G^T S \quad (9a)$$

$$K_e = P H^T R^{-1} \quad (9b)$$

where S and P satisfy the following algebraic equations, respectively

$$SF + F^T S - SGB^{-1}G^T S + A = 0 \quad (10a)$$

$$FP + PF^T - PH^T R^{-1} HP + \Gamma Q \Gamma^T = 0 \quad (10b)$$

where A and B are the state and the control weighting matrices and u is the control vector; and w and v are the plant disturbances and the measurement noise vector, respectively. Q and R are the power spectral density matrices for the plant disturbances and the measurement noises, respectively. The F matrix is block diagonal and can be constructed from the equations of motion; the G , H , and Γ matrices can be obtained from the eigenvector data.

For the hoop and column antenna, consider the three rigid body modes and the first seven elastic modes. Examination of the eigenvectors of the elastic modes reveals that for small deformations and attitude excursion, the interactions between the pitch axis and the roll and yaw axes are negligible. Therefore, the pitch controller can be treated separately from the roll and yaw controller. Let p be the subscript for the pitch controller, and γ for the roll and yaw controller, then the state vectors, the measurement vectors, etc., for the hoop and column controllers are assigned as follows:

$$\mathbf{x}_p = (\theta, \dot{\theta}; q_9, \dot{q}_9; q_{13}, \dot{q}_{13})^T \quad (11a)$$

$$\mathbf{z}_p = (\theta_{pb}, \dot{\theta}_{pb}; \theta_{pf}, \dot{\theta}_{pf})^T \quad (11b)$$

$$\mathbf{w}_p = (T_{dyb}, T_{dyf}; F_{dxb}, F_{dxf})^T \quad (11c)$$

$$\mathbf{v}_p = (v_{yab}, v_{yrb}; v_{yaf}, v_{yrf})^T \quad (11d)$$

$$\mathbf{u}_p = (T_{yb}, T_{yf})^T \quad (11e)$$

and

$$\mathbf{x}_\gamma = (\phi, \dot{\phi}; \psi, \dot{\psi}; q_7, \dot{q}_7; q_8, \dot{q}_8; q_{10}, \dot{q}_{10}; q_{11}, \dot{q}_{11}; q_{12}, \dot{q}_{12})^T \quad (12a)$$

$$\mathbf{z}_\gamma = (\phi_{\gamma b}, \dot{\phi}_{\gamma b}; \psi_{\gamma b}, \dot{\psi}_{\gamma b}; \phi_{\gamma f}, \dot{\phi}_{\gamma f}; \psi_{\gamma f}, \dot{\psi}_{\gamma f})^T \quad (12b)$$

$$\mathbf{w}_\gamma = (T_{dxb}, T_{dxf}; T_{dzb}, T_{dzf}; F_{yb}, F_{yf})^T \quad (12c)$$

$$\mathbf{v}_\gamma = (v_{xab}, v_{xrb}; v_{zab}, v_{zrb}; v_{xaf}, v_{xrf}; v_{zaf}, v_{zrf})^T \quad (12d)$$

$$\mathbf{u}_\gamma = (T_{xb}, T_{xf}; T_{zb}, T_{zf})^T \quad (12e)$$

where in Eqs. (11) and (12), f refers to feed base, b refers to spacecraft bus, a and r refer to attitude and rate, respectively.

Hardware sizing allows for assessment of onboard disturbances. Using the subscripts SK for station keeping and WD for wheel dumping, the estimated power spectral density (PSD) matrices for the random disturbances are

$$Q_{pSK} = \text{Diag} (.02, .02; 4.82 \times 10^{-3}, 9.68 \times 10^{-4}) \quad (13a)$$

$$Q_{pWD} = \text{Diag} (.02, .02) \quad (13b)$$

$$Q_{\gamma SK} = \text{Diag} (.02, .02; .02, .02; 4.82 \times 10^{-3}, 9.68 \times 10^{-4}) \quad (14a)$$

$$Q_{\gamma WD} = \text{Diag} (.02, .02; .02, .02; 9.68 \times 10^{-4}, 9.68 \times 10^{-4}) \quad (14b)$$

The PSD for the measurement noises are assumed as follows:

$$R_p = \text{Diag} (3.2 \times 10^{-10}, 3.06 \times 10^{-9}; 3.2 \times 10^{-10}, 3.06 \times 10^{-9}) \quad (15)$$

and

$$R_\gamma = \text{Diag} (3.2 \times 10^{-10}, 3.06 \times 10^{-9}; \dots; 3.2 \times 10^{-10}, 3.06 \times 10^{-9}) \quad (16)$$

The selection of the state and control weighting matrices determines the control design. The state weighting matrix must reflect the control objectives such as requirements on stability, surface and pointing errors, etc. Consider the pitch control. Let $A_p = \text{Diag}(a_1, a_2; a_3, a_4; a_5, a_6)$. The odd elements, in general, contribute to the stiffness of the closed-loop state and the even terms affect the damping.

The a_{2n+1} terms are determined by the weighted normalized mean square structural attitude angles, feed displacements, and dish deformations; or more specifically, they may be expressed as follows:

$$a_1 = \frac{g_\theta}{(S_\theta)^2} \quad (17a)$$

$$a_3 = \frac{g_F}{n_F (S_F)^2} \sum_{i_F} (\phi_{9xi}^2 + \phi_{9yi}^2 + \phi_{9zi}^2) + \frac{g_D}{n_D (S_D)^2} \sum_{i_D} (\phi_{9xi}^2 + \phi_{9yi}^2 + \phi_{9zi}^2) \quad (17b)$$

$$a_5 = \frac{g_F}{n_F (S_F)^2} \sum_{i_F} (\phi_{13xi}^2 + \phi_{13yi}^2 + \phi_{13zi}^2) + \frac{g_D}{n_D (S_D)^2} \sum_{i_D} (\phi_{13xi}^2 + \phi_{13yi}^2 + \phi_{13zi}^2) \quad (17c)$$

where the subscripts F and D refer to feed and dish, respectively; n_D is the number of grid points on the dish, i_D means grid point i on the dish, ϕ_{9xi} is the translational mode shape for mode 9 at grid i ; S_D is the specified rms surface displacement. Other parameters are similarly defined. The weighting factors g_θ , g_F , and g_D reflect the relative importance of the individual requirements. The values for the weighting factors were chosen to be 10, 20, 5, respectively. This selection was guided by the feed and reflector optical properties. The construction of the roll and yaw state weighting matrix is similar.

For the wrap-rib antenna control design, the state vector contains 24 elements representing the 12 modal amplitudes and the 12 modal rates. In the first half of the state vector, the first three states are the antenna attitude (roll, pitch, yaw), the next three are associated with boom distortions, and the last six are dish vibration modes.

Similar to the hoop-column antenna control designs, the development of control and estimator gains requires good engineering judgment in selecting weighting matrices A, B, Q, and R. Here A is a 24 x 24 matrix of the form

$$A = \text{Block diag } (A_{\theta}, A_B, A_D, A_{\dot{\theta}}, A_{\dot{B}}, A_{\dot{D}}) \quad (18)$$

where

A_{θ} is 3 x 3 weighting for attitude

A_B is 3 x 3 weighting for boom distortion

A_D is 6 x 6 weighting for dish distortion

$A_{\dot{\theta}}, A_{\dot{B}},$ and $A_{\dot{D}}$ are corresponding rate weightings.

For all wrap-rib antenna control designs, matrix A stays fixed throughout, elements of which are chosen as discussed in the following paragraphs.

A_{θ} is chosen with weighting matrix B such that the closed-loop rigid body modes have equivalent frequencies of about 1/5 of the lowest open-loop vibration frequency of the system (which is 0.55 rad/sec). To achieve this, the following relation has been used to define A_{θ}

$$A_{\theta}^T = I^T B I U b_w^4 \quad (19)$$

where

I represents the 3 x 3 inertia tensor of system

B is the 3 x 3 control weighting matrix

U is the 3 x 3 identity matrix

b_w is the desired bandwidth

A_B is chosen as a 3 x 3 diagonal matrix, with each element equal to the inverse of the required boom distortion error squared. For this study, boom distortion is given in terms of angles at the boom joint and the requirement is set at 0.01° for each axis. Therefore,

$$A_B = \text{Diag } (3.27 \times 10^7, 3.27 \times 10^7, 3.27 \times 10^7) \quad (20)$$

A_D is the weighting for dish modes and is chosen to minimize dish RMS surface errors. The following relation is used to determine A_D :

$$\begin{bmatrix} x_7 \\ x_8 \\ \vdots \\ x_{12} \end{bmatrix}^T A_D \begin{bmatrix} x_7 \\ x_8 \\ \vdots \\ x_{12} \end{bmatrix} = \frac{[\text{dish RMS surface error in meters}]^2}{[\text{dish RMS surface required accuracy in meters}]^2} \quad (21)$$

the denominator is set at $(12 \times 10^{-3})^2$ for the 12 mm dish RMS surface accuracy requirement. The dish RMS surface error is given by

$$\left\{ \frac{1}{6624} \begin{bmatrix} x_7 \\ x_8 \\ \vdots \\ x_{12} \end{bmatrix}^T \Phi_D^T \Phi_D \begin{bmatrix} x_7 \\ x_8 \\ \vdots \\ x_{12} \end{bmatrix} \right\}^{1/2} \quad (22)$$

where Φ_D is the 6 selected mode shapes of the dish and thus its dimension is 6624×6 , with 6624 being the number of nodes of the dish.

From Eq. (21) and Eq. (22), A_D is given by

$$A_D = \frac{1}{6624} \cdot \frac{1}{(12 \times 10^{-3})^2} \cdot \Phi_D^T \Phi_D \quad (23)$$

The values for $A_{\dot{D}}$, $A_{\ddot{D}}$, and $A_{\dot{D}}$ have been set to zero. Matrix B is diagonal and each element is the inverse of the square of the maximum control torque specified for each axis.

After choosing A and B, weighting matrices Q and R were selected to obtain desired closed-loop estimator poles for the rigid body modes. The relation used was

$$Q^T = I^T R I U b_w^4 \quad (24)$$

Due to the use of the above relation in designing the estimator, the power spectral density matrix Q assumes different values in the design than in the performance evaluation. For system performance evaluation, the actual process disturbance PSD was used. However, sensor measurement noise PSD is identical for design and evaluation processes. In particular, the Q matrix for performance evaluation of systems 1 and 2 is given by

$$Q = \text{Diag} (9.8 \times 10^{-5}, 7.688 \times 10^{-5}, 3.528 \times 10^{-5}) \quad (25)$$

and for System 3 by

$$Q = \text{Diag} (9.8 \times 10^{-5}, 7.688 \times 10^{-5}, 3.528 \times 10^{-5}, 9.8 \times 10^{-9}, 7.68 \times 10^{-9}, 3.52 \times 10^{-9}) \quad (26)$$

The R matrix for design and evaluation is given by

$$R = \text{Diag} (3 \times 1.52 \times 10^{-13}, 3 \times 1.88 \times 10^{-13}) \quad (27)$$

for 3 angular and 3 rate measurement noises. If an optical sensor is used for dish measurement of 15 points, R has 15 additional terms, i.e.,

$$R = \text{Diag} (3 \times 1.52 \times 10^{-13}, 3 \times 1.88 \times 10^{-13}, 15 \times 8.0 \times 10^{-9}) \quad (28)$$

E. Model Parameter Error Problem and Performance Evaluation Model

In Section IIID the control system has been defined with the assumption that the structural parameters were known. However, in reality large space system parameters can not be accurately predicted on the ground. The result of this model error could seriously destabilize the system. Let F' be the actual state matrix and F be the modeled state matrix. Let e be the estimator error, $\hat{x}-x$. The closed-loop system may be represented as

$$\underbrace{\begin{bmatrix} \dot{\hat{x}} \\ \dot{e} \end{bmatrix}}_{x_C} = \underbrace{\begin{bmatrix} F' - GK_c & -GK_c \\ F - F' & F - K_e H \end{bmatrix}}_{F_C} \underbrace{\begin{bmatrix} x \\ e \end{bmatrix}}_{x_C} + \underbrace{\begin{bmatrix} \Gamma & 0 \\ -\Gamma & K_e \end{bmatrix}}_{\Gamma_C} \underbrace{\begin{bmatrix} w \\ v \end{bmatrix}}_{w_C} \quad (29)$$

In the absence of model errors, i.e., $F'=F$, the eigenvalues of the closed-loop system are those determined by $\det(F-GK_c)$ and $\det(F-K_e H)$. For this type of controller, the system is asymptotically stable. However, when $F' \neq F$, stability can not be guaranteed and destabilization can occur if F' is sufficiently different from F as demonstrated in the next section. Note in Eq. (29) the gain matrices are designed based on the modeled system parameters.

The control system performances that are of particular interest are (1) the attitude and surface accuracy achievable in the projected disturbance environment, (2) the relative stability, and (3) the robustness of the controller in the presence of model parameter errors. These performance measures may be evaluated through computer simulations of the transient responses or the steady state analysis of the statistical averages. The relative stability can be obtained from the closed-loop eigenvalues. The parameter error sensitivity problem can be evaluated using Eq. (29) and the following formulation. In the remainder of this subsection we shall concentrate on the development of the evaluation models for the attitude errors, surface deformations, etc. using the state covariance matrix, X_C .

Let X_{CP} and X_{CY} be the augmented state covariance matrices for pitch and roll and yaw control and estimation, respectively. The values for X_{CP} and X_{CY} may be obtained by solving the following matrix algebraic equations:

$$F_{CP} X_{CP} + X_{CP} F_{CP}^T + \Gamma_{CP} Q_{CP} \Gamma_{CP}^T = 0 \quad (30)$$

$$F_{CY} X_{CY} + X_{CY} F_{CY}^T + \Gamma_{CY} Q_{CY} \Gamma_{CY}^T = 0 \quad (31)$$

where F_{CP} , F_{CY} , Γ_{CP} , and Γ_{CY} are defined in Eq. (29) and Q_{CP} and Q_{CY} are the power spectral densities of w_{CP} and w_{CY} , respectively, also defined in Eq. (29). The rms attitude error σ_A for the structure, the rms dish deformation σ_D , and the rms feed displacement σ_F may be defined in terms of the covariance matrices as follows:

$$\sigma_A = (X_\phi + X_\theta + X_\psi)^{1/2} \quad (32)$$

$$\sigma_D = \left[\frac{1}{n_D} \text{tr} (\phi_{Dp}^T \phi_{Dp} X_{qp}) + \frac{1}{n_D} \text{tr} (\phi_{D\gamma}^T \phi_{D\gamma} X_{q\gamma}) \right]^{1/2} \quad (33)$$

$$\sigma_F = \left[\frac{1}{n_F} \text{tr} (\phi_{Fp}^T \phi_{Fp} X_{qp}) + \frac{1}{n_F} \text{tr} (\phi_{F\gamma}^T \phi_{F\gamma} X_{q\gamma}) \right]^{1/2} \quad (34)$$

where X_ϕ , X_θ , X_ψ , X_{qp} , and $X_{q\gamma}$ are submatrices of X_p and X_γ ; and ϕ_{Dp} , $\phi_{D\gamma}$, ϕ_{Fp} , and $\phi_{F\gamma}$ are submatrices of the eigenvector matrix ϕ . For instance, X_{qp} and ϕ_{Dp} are

$$X_{qp} = \begin{bmatrix} E(q_9^2) & E(q_9 q_{13}) \\ E(q_9 q_{13}) & E(q_{13}^2) \end{bmatrix} \quad (35)$$

and

$$\phi_{Dp} = \begin{bmatrix} \phi_{9x15} \cdots \phi_{9x134} & \phi_{9y15} \cdots \phi_{9y134} & \phi_{9z15} \cdots \phi_{9z134} \\ \phi_{13x15} \cdots \phi_{13x134} & \phi_{13y15} \cdots \phi_{13y134} & \phi_{13z15} \cdots \phi_{13z134} \end{bmatrix}^T \quad (36)$$

360x2

and in Eqs. (33) and (34) tr is the trace of the matrix in the argument.

The rms control effort is also of interest and can be obtained from the control covariance matrices as follows:

$$U_p = K_{pc} X_p K_{pc}^T \quad (37a)$$

$$U_\gamma = K_{\gamma c} X_\gamma K_{\gamma c}^T$$

$$U_{\text{rms}} = [\text{tr}(U_p + U_\gamma)]^{1/2} \quad (37c)$$

The rms attitude error in Eq. (32) is the attitude of the entire structure or the rigid body attitude. It is, therefore, not the beam pointing attitude. The actual beam pointing error is a function of the relative motions of the feed, the dish, and the dish surface deformation in addition to the structural attitude defined in Eq. (32).

The attitude errors at the feed and at the bus can be easily defined, however, in terms of the variables discussed in this section.

IV. DISCUSSION OF RESULTS

A. Hoop and Column Control Performance

Designs discussed in the preceding subsections have yielded reasonable performance. Figure 10 shows the feed and the bus pointing errors with parameter

error varying from 70% to 130%. The controller becomes unstable if parameter errors exceed these boundaries. Figure 11 shows a similar result for the feed displacement. In all cases when the actual frequencies increased, the performance has improved somewhat. This is because when frequency increases, the structure becomes stiffer.

One important question that needs to be addressed here is how much a two-site control is better than a one-site control system. Figure 12 demonstrates that the two-site control system is more robust than either of the two one-site control systems.

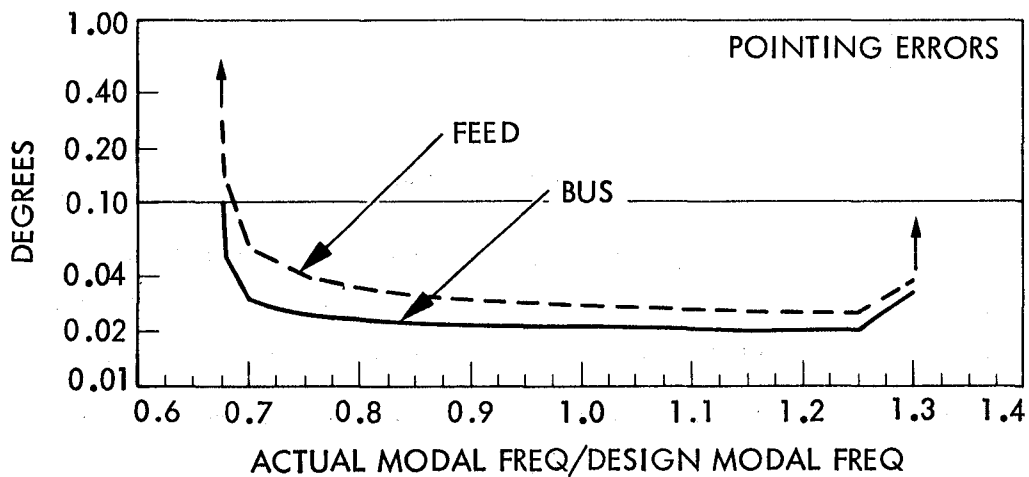


Figure 10. RMS Pointing Accuracy for Hoop and Column Antenna.

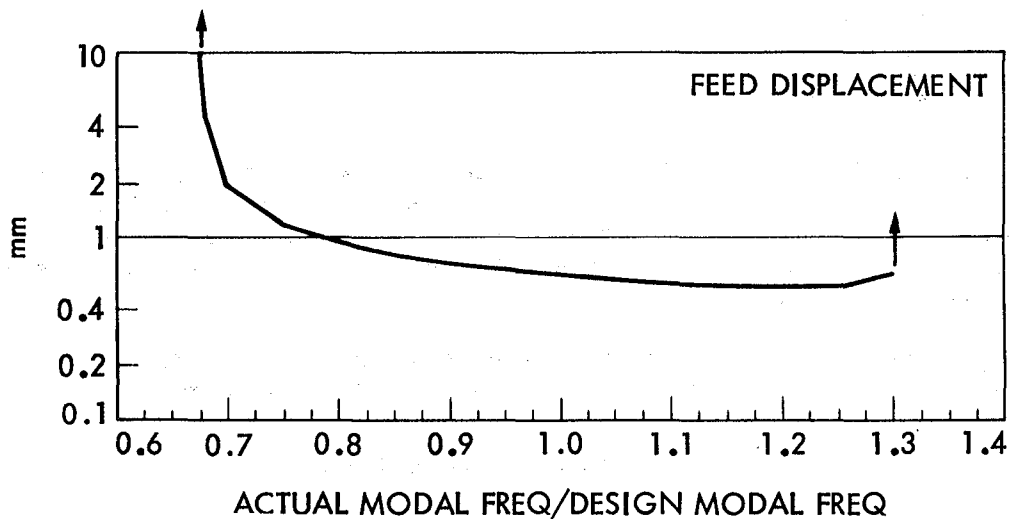


Figure 11. RMS Feed Displacement for Hoop and Column Antenna.

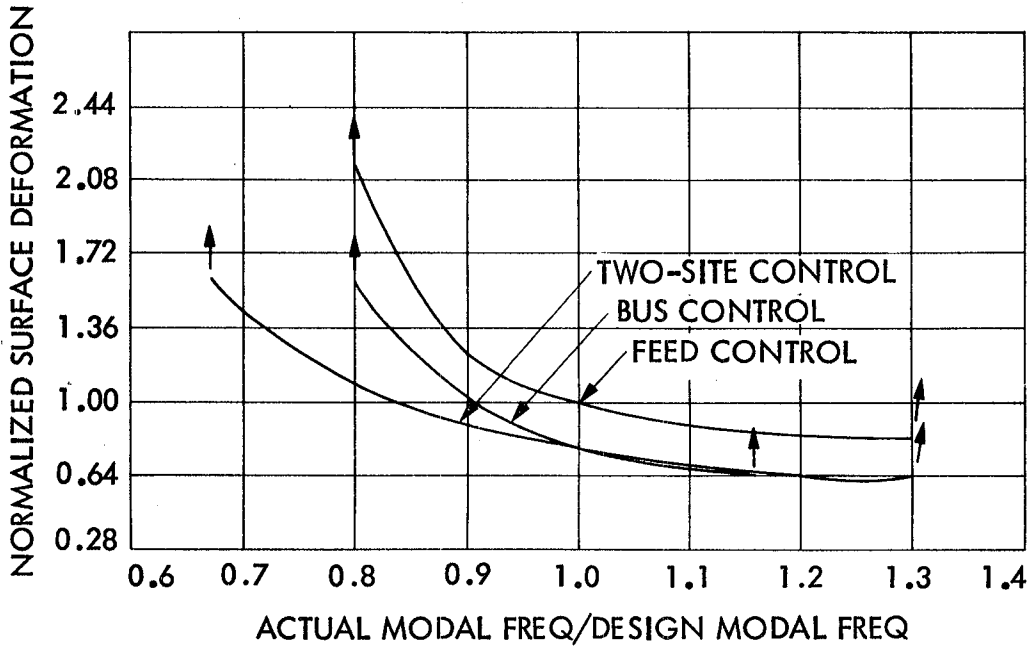


Figure 12. Stability Regions for Three Control Systems for Hoop and Column Antenna

Further comparisons for the three control concepts are in Figure 13 where the identifications of critical modal parameters are made. The bending modes are less critical to all but the single-site feed control system. The torsional modes are critical to all the systems and they set the stability limits for both the single-site bus control and the two-site control systems.

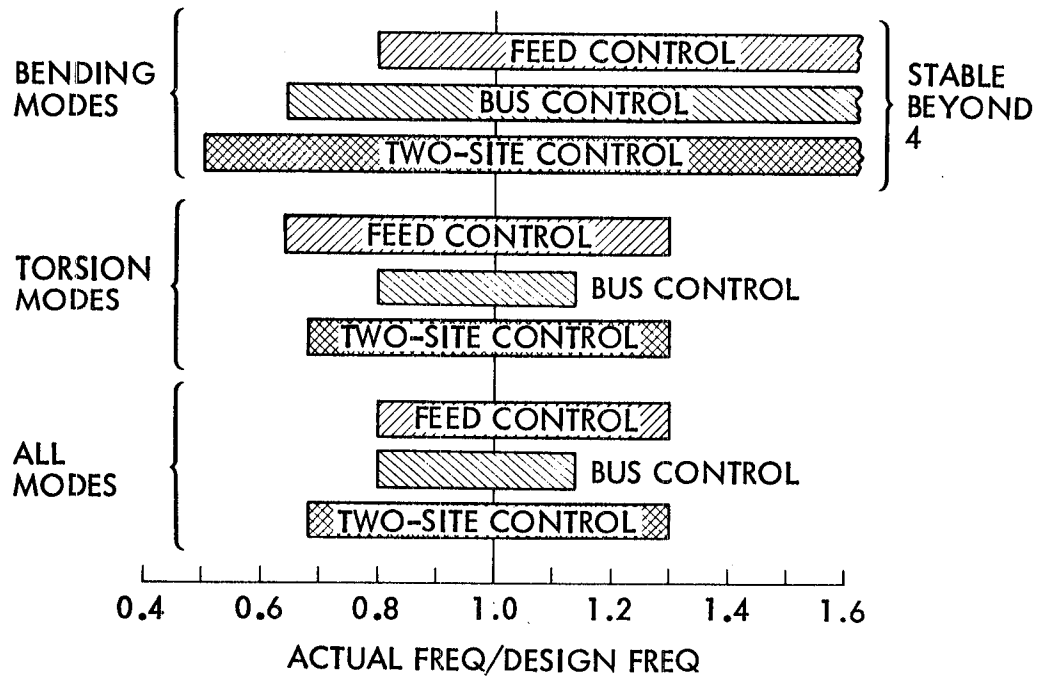


Figure 13. Stability Regions Subject to Parameter Errors for Hoop and Column Antenna

B. Wrap-Rib Control Performance

Consider the first case where actual boom frequencies are the same as the boom frequencies used in the control designs. Figure 14 shows the dish LOS (Line-of-Sight) stability error as a result of having 1 newton-meter sinusoidal disturbance torque applied to the antenna. For example, in cases where the disturbing sinusoidal torque has the same frequency as the first vibration frequency of the antenna at 0.55 rad/sec, the dish LOS error will be 0.03° for control system 1, 0.015° for control system 2, and 0.002° for control system 3. This means that having capabilities of optical sensing and extra control at dish hub, system 3 is able to bring peak errors down by an order of magnitude and distribute the errors more uniformly.

In addition, system 3 provides more stable and robust performance than the other two systems as actual boom frequencies decrease. This is illustrated in Figures 15 and 16. As actual boom frequencies decrease to 62.5% of the design frequencies, the peak LOS errors for system 3 is about 2.5 times better than that of system 2, whereas system 1 is already unstable. Similarly, in the last case where actual boom frequencies are 60% of the design boom frequencies, the peak LOS error for system 3 is at about 0.02° , and both system 1 and system 2 are unstable.

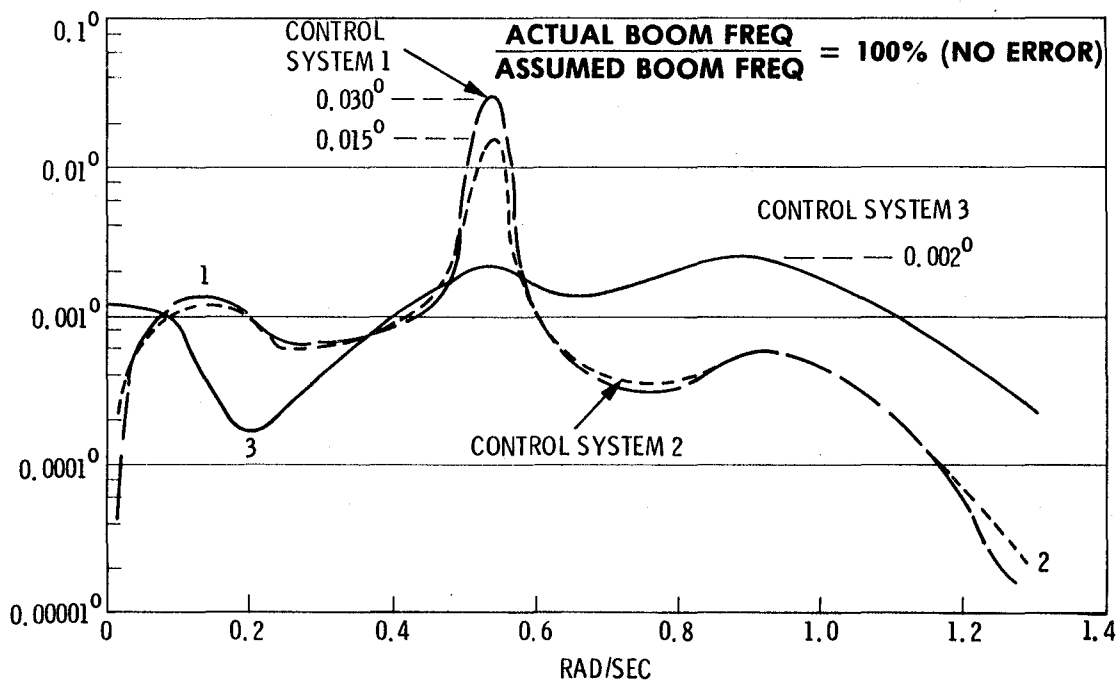


Figure 14. Wrap-Rib Dish Line-of-Sight Error with Exact Boom Frequency in Model.

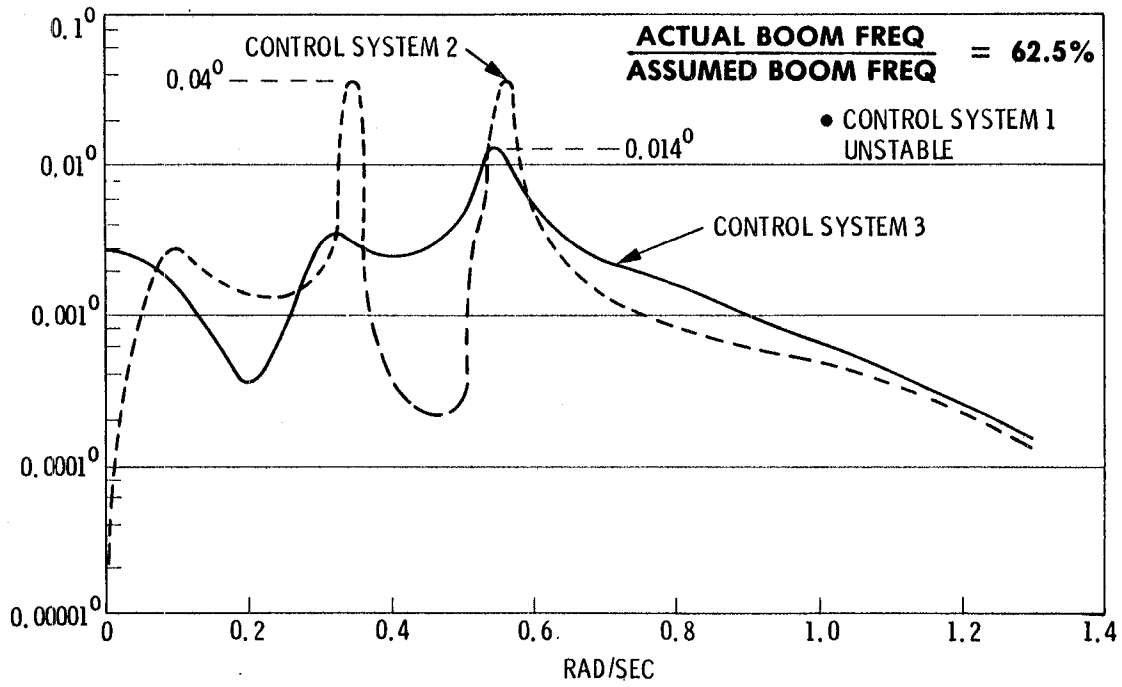


Figure 15. Wrap-Rib Dish Line-of-Sight Error

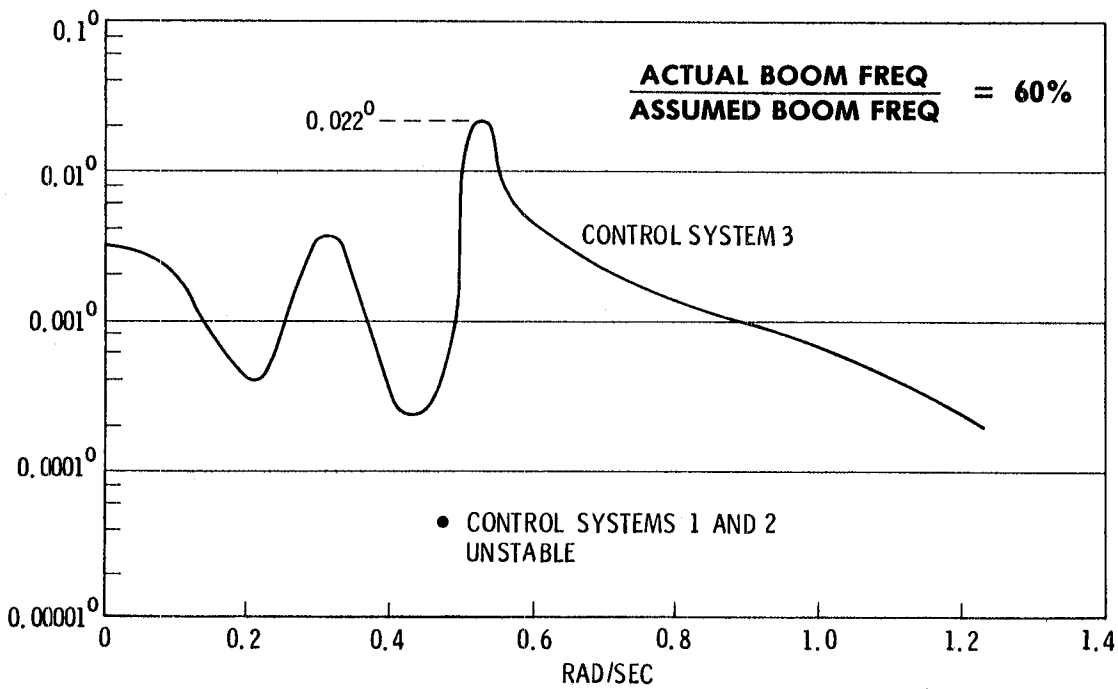


Figure 16. Wrap-Rib Dish Line-of-Sight Error

Figure 17 shows the peak dish LOS error for the three systems as functions of boom frequency errors which has further illustrated the superior performance of System 3 than those of Systems 1 and 2.

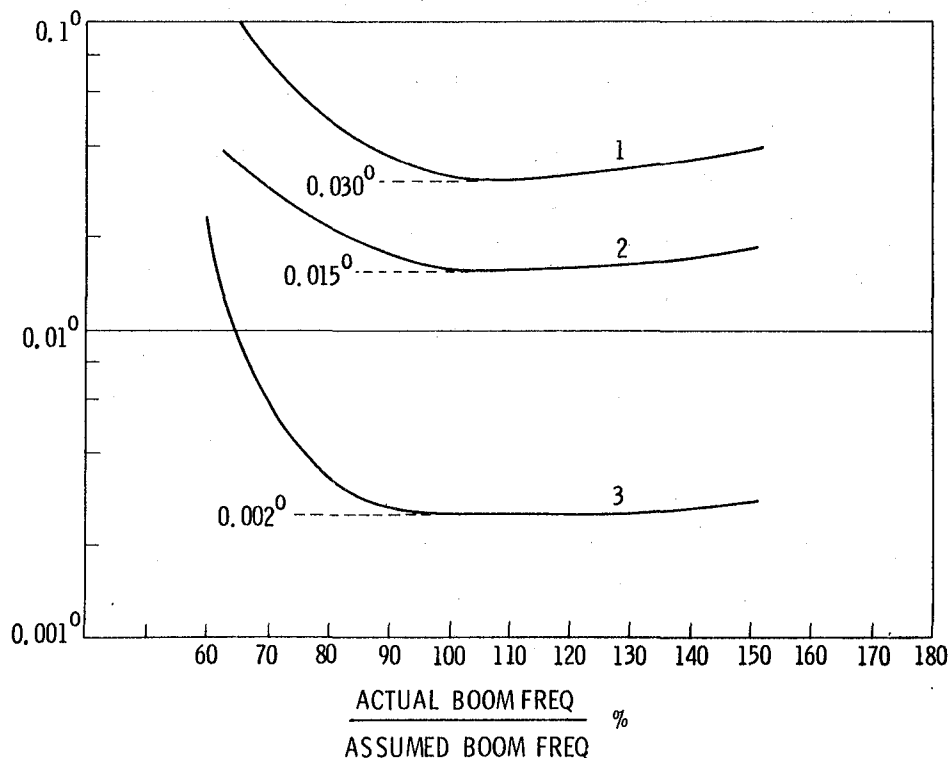


Figure 17. Wrap-Rib Peak Dish Line-of-Sight Error vs. Boom Frequency Error.

V. CONCLUSIONS

1. Structural uncertainties and model error can cause serious performance deterioration and can even destabilize the controllers.
2. For the hoop and column antenna, large hoop and long mast and the lack of stiffness between the two substructures result in low structural frequencies. Performance can be improved if this design can be strengthened.
3. The two-site control system is more robust than either single-site control systems for the hoop and column antenna. The two-site control concept has resulted in reasonable hardware requirements when applied to LMSS communication missions.
4. For the wrap-rib antenna, the uncertainties in boom dynamics and its stiffness are critical to the control design.
5. By adding hub sensor and hub actuators, System 3 has out performed Systems 1 and 2 by a great margin in the wrap-rib configuration.
6. Flight tests and in-orbit system identification of critical structural modes will insure performance and reduce risk for large space antenna missions.

VI. REFERENCES

1. Russell, R.A., T.G. Campbell, and R.E. Freeland, "A Technology Development Program for Large Space Antennas," Paper No. IAF-80 A33, 31st International Astro. Congress of the International Astro. Fed., Sept. 21-28, 1980, Tokyo, Japan.
2. Tankerslay, B.D., "Maypole (Hoop/Column) Deployable Reflector Concept Development for 30 to 100 Meter Antenna," Conference on Advanced Technology for Future Space Systems, Hampton, VA, May 8-10, 1979.
3. "LSST Hoop/Column Antenna Development Program, Phase I Final Program Review," NAS1-15763, Volume 1 of 2, October, 1980, Harris Corp., Melbourne, Florida.
4. Private Communication.
5. Hamidi, M., G. Rodriguez, and D. Schaechter, "Distributed System Modeling of a Large Space Antenna," Proceedings of Workshop on Applications of Distributed System Theory to the Control of Large Space Structures, July 14-16, 1982, Jet Propulsion Laboratory, Pasadena, California.
6. McLauchlan, J.M., W.C. Goss, and E.F. Tubbs, "SHAPES: A Spatial High-Accuracy, Position-Encoding Sensor for Space Systems Control Applications," Paper No. AAS 32-032, Presented at the AAS Annual Rocky Mountain Guidance and Control Conference, Keystone, Colorado, Jan. 30-Feb. 3, 1980.

This Page Intentionally Left Blank

SESSION III: DISCUSSION - LSS CONTROL PROBLEMS

Moderator: **R.R. Strunce**, Charles Stark Draper Laboratory, Inc.

Panel Members: **N.K. Gupta**, Integrated Systems, Inc., **J. Sesak**, General Dynamics,
and **A.F. Tolivar**, Jet Propulsion Laboratory

SYNOPSIS*

Each panel member gave an opening statement, then a general discussion with the audience followed.

N. K. GUPTA: The problem may be divided into three areas for discussion: analytical developments, real-time processing, and actuators and sensors.

In analytical developments, insufficient emphasis has been placed on numerical techniques. Adequate numerical processing techniques do not exist to deal with the high-order models used in control of large space structures.

Real-time processing will be needed at very high computation rates, perhaps 10 million to 100 million operations per second. The DoD Very High Speed Integrated Circuits (VHSIC) program may provide a partial solution. It may be necessary to look into other techniques involving both analytical and real-time processor developments.

Reliability will be extremely important in these very complex systems. The problem of developing high-order languages, etc., that will allow convenient and reliable real-time processing and verification of control laws must be looked into.

Actuators and sensors that have to operate in the space environment for several years are very important. Basic actuator and sensor limitations should be taken into account in analytical developments. For example, some robustness proofs are not valid when actuator and sensor dynamics are considered.

It is a very big jump going from analytical studies to full space flight experiments. It seems that intermediate steps of simulation and laboratory experiments would be very useful and cost-effective before going into flight experiments.

J. SESAK: My discussion focuses on experiments for large space structures technology. Most laboratory experiments conducted to date have been with very simple examples, such as beams and flat plates. Nothing tested resembles, even

*This synopsis attempts to capture the main points discussed but has not been reviewed or endorsed by the speakers.

remotely, an actual space structure. More complex structures and tests that closely represent actual space structures should be used in experiments. Flight experiments will be necessary to achieve realistic data, particularly with respect to damping, in the space environment.

There is the need for actuator technology for operation at very low frequencies (fractions of Hz). Flight tests are needed not only for verifying theories but also for actuator and sensor hardware.

A. F. TOLIVAR: The problem with large space structures is not just one of high frequencies, but of extending the actuator and sensor hardware capability down into the very low frequency ranges, essentially to quasi-static conditions.

In several technical areas, the theory that has been developed to date needs to be made ready for flight. The theory should be developed to the point where efficient packages exist that can operate on-board the spacecraft with confidence. For example, if one were asked for an autonomous system identification program for a complex 100-meter space system, it would not be possible to accomplish that in a cost-effective manner with today's level of technology.

How do we convince a project manager that the technology is indeed ready for mission applications? It is through demonstrating the technology both with laboratory and flight experiments on realistic articles.

R. R. STRUNCE: The fundamental issue is how to design a finite compensator to control infinite-dimensional structures. There are four major technology areas to pursue: simultaneous achievement of performance and robustness; system identification; reduced-order compensators; and sensor/actuator technology. An important question for this workshop is: do we have a solution looking for a problem or do we have a real problem that needs solution? Maybe it is time to move into a technology demonstration activity.

Comments and Questions from the Audience

A. N. MADIWALE, MIT Lincoln Lab: Major problems in control of large structures are the parameter uncertainties or inaccuracies in the large scale models. The uncertainties could be from 20% to 100%. A workshop paper by Hyland and Madiwale presents a technique that directly incorporates the parameter uncertainties into the modeling process and designs an optimum controller around these uncertainties. Certain robustness properties are obtained by this process.

V. KOMKOV, West Virginia University: There certainly are problems with modeling large structures with very slender members. Modeling that represents the physical reality has not been developed very well. The assumptions used in modeling, for example in the Euler-Bernoulli theory, are not looked at very carefully and often do not apply. One might throw in all kinds of uncertainties but it really does not solve the problem of having a reasonable theory.

L. WEISSTEIN, Lockheed Missiles and Space Co. (LMSC): There are available analytical models that have parameters of real space structures far beyond the simple problems characterized by the experiments discussed here. Some continuum models have been developed for such structures as two-layer tetrahedral

trusses, hexagonal trusses, periodic trusses, and framework structures. These would certainly aid in applying control theories to more real-life structures. The manuscript listed below presents an extensive bibliography.*

A. M. MEYSTEEL, University of Florida: There are two different areas which apply to large space structures: control in the small and control in the large. The only topics covered here have been linked with small motions. Large, quick motions should also be considered for which neither linear quadratic gaussian (LQG) nor other approaches discussed here apply. Research should concentrate on other approaches than LQG that can treat "control in the large."

We should separate in our discussions "theory for design" from "theory for control." They are two different topics and should be treated differently. The model used for preliminary system design may be very different from the one used in real-time, on-line control.

There are many methods for decoupling control, but special techniques must be developed for on-line decoupling for large scale systems.

The issues of actuator resolution and dynamics in the zero-g environment should be given more attention.

Probably the most important step that should be taken is for NASA to define future applications and specifications for control of large space structures so that the control community can focus on the same problems.

A. F. TOLIVAR: In response to Professor Leonard Meirovitch's question about the state of the art of distributed actuation and sensing, I have the following comments.

The problem of including actuator dynamics in the model of a large space structure has not been addressed to any great extent. Instrumentation hardware and associated measurement algorithms that satisfy the performance requirements that are space-qualified are not available. Similarly, for the actuation area, there does not exist a technology for a space-qualified actuator that operates at very low frequencies, perhaps 1/100th of 1 Hz. Hundreds of sensors and actuators may be needed for a single space system and there is basically no space-qualified hardware available in this area.

R. R. STRUNCE: Fault tolerance becomes a major issue when considering systems with hundreds of sensors and actuators. How will the wires (or fiber optics) be run? How will failures be accommodated? How will the control laws perform with internal failures? It seems that this major area is being overlooked.

B. R. HANKS, Langley: It is surprising to find that in this workshop, as in most others on control of large flexible structures, there are so few structural dynamicists. Keep in mind that stiffening up the structure may be the best

*L. S. Weisstein, Continuum Models for Repetitive Beamlike Structures, unpublished master's thesis, George Washington University, 1982.

solution in many cases. If actuators required for rigid-body control are not adequate for flexible-mode control, then maybe they are being designed the wrong way. Maybe passive stiffening and damping are better.

R. S. GRAN, Grumman Aerospace: The structural dynamics people first of all find our problem boring because we all talk about linear systems and they stopped talking about them 20 years ago. The structural dynamics research problems now are very complicated and involve nonlinear partial differential equations and so on. Control engineers like linear models and those are boring. The issue of doing control has to be divided into two parts: Open-loop control of the nonlinear system to give a nominal trajectory; then, closed-loop linear control of perturbations about the nominal trajectory. If the control law does a good job, then the motion will always consist of small perturbations, and the linear model will be valid.

B. R. Hanks has a very good point. A piece of wire is a lot cheaper than a control system.

H. A. REDISS, Milco: There is a clear need to perform large-scale flight experiments in space, but has everything been done in laboratory experiments that is possible to develop and verify techniques?

B. R. HANKS, Langley: You can not practically do laboratory experiments of large flexible structures that have modes on the order at 0.1 Hz or less because the suspension systems become an inherent part of the structure. Also, damping in a structure is very dependent on the frequency, so scaling of stiffer structural models down to the very low frequencies will not work. Laboratory experiments cannot solve the total problem.

NUMBER AND PLACEMENT OF CONTROL SYSTEM SENSORS CONSIDERING POSSIBLE FAILURES

Wallace E. Vander Velde* and Craig R. Carignan**

Department of Aeronautics and Astronautics

Massachusetts Institute of Technology

Cambridge, MA 02139

ABSTRACT

In the future design of active control systems for large, flexible space structures there is likely to be some freedom as to the placement of the control system sensors and actuators. Certainly the designer will have some choice over the number of these components which he specifies. The answer to the question of how many control system components should be used and where they should be placed on the structure is not likely to be obvious. The matter becomes even more obscure when one considers the likelihood that some of these components will fail during the operating lifetime of the system.

This paper presents a methodology which is intended to assist the designer in this process with respect to sensors. The suggested approach begins with definition of a Degree of Observability of the system for a given set (number and location) of sensors. This measure of observability is a quantitative indicator of how well the system can be observed with a given set of sensors. The issue of component unreliability is then introduced by computing an average Degree of Observability over the operating lifetime of the system accounting for the likelihood of various combinations of component failures. This measure reflects the basic capability of the sensor set to observe the system state in the context of the failures which will probably occur. Having defined this average measure of the performance capability of the set of sensors, one can optimize the locations of a given number of components by maximizing the measure, and one can see how this optimized measure varies with the number of components. This provides the designer with a meaningful basis for choice of number and location of control system sensors.

INTRODUCTION

The dimensions of space structures being considered for future applications are on the order of several hundred meters to several kilometers and will require a large number of actuators and sensors for attitude and shape control. A solar power satellite, for instance, may require hundreds of control moment gyros and thrusters to damp out surface vibrations caused by periodic disturb-

*Professor **Graduate Student

ances such as solar and gravity gradient torques. One of the first decisions a designer of the control system for such an assembly must make is how many sensors and actuators to use and where to place them on the structure. Placement represents a substantial degree of freedom available to the designer and is usually not a very straightforward question. It is even less apparent when one considers redundancy in the system to allow for failures; even if the "optimal" position of a sensor is known, it may not be so clear where a backup sensor should be placed. The number of components to be used must reflect the trade-off of cost, weight, power, etc. vs. system performance—and the evaluation of performance should recognize the likelihood of some component failures during the lifetime of the system.

The effect of component failures is emphasized here because even an elementary analysis demonstrates that component unreliability will have a dominating influence on the behavior of these systems. The control system must be configured with the capability to accommodate component failures, and the likely effect of these failures on the performance of the system must be anticipated from the beginning of the design process. As one example of this, suppose a system is to operate for three years between visits for maintenance and re-supply. If the control system utilizes a total of 400 sensors and actuators—each with an exponential distribution of time to failure with a mean time to failure of 100,000 hours (optimistic by today's standards)—the probability that none of these components will fail in this interval is about $2 \cdot 10^{-46}$, which indicates virtual certainty that one or more failures will occur. In fact, many failures are likely to occur—about one every 10 days on average!

In this work we develop a methodology for measuring the performance of a system which reflects the type, number and placement of the sensors on the structure. The measure also reflects the expected loss of performance due to component failures. This performance measure is intended to be especially useful as a guide to the choice of sensor number and placement in the earliest phase of system design.

Problem Definition

It would be most helpful to the control engineer to have some criterion at his disposal for placing sensors. Unfortunately, modern control theory does not provide any such measure of "observability." Observability is simply a binary concept—either a system is observable or it is not. It does not say how observable a system is with a given set of sensors.

Some work has appeared in recent literature which addresses this question. Juang and Rodriguez (Ref. 1) formulate the linear quadratic regulator problem with an infinite time horizon. The solution defines the optimal cost as an explicit function of the initial state, and indirectly as a function of the number and location of the actuators and sensors. The expectation is taken over a defined distribution of initial conditions—producing the expected cost as a function of the actuator and sensor set only. While this approach has some appeal, we found several objections to the method: (1) The weighting of control effort versus state excursions in the cost function is rather arbitrary; (2) If there is a particular direction in the state space in which the state is not

very observable, this fact is largely lost when the cost is averaged over the distribution of initial states; (3) The expected cost is an inverse measure in which larger cost means poorer observability and becomes infinite when the system is unobservable; and (4) The expected cost depends on both the actuator set and the sensor set whereas it may be more useful to have separate measures of observability and controllability.

Skelton and Hughes (Ref. 2) define measures in terms of controllability and observability "norms" which apply to the individual modes of a system rather than to the system as a whole. Their approach is also tailored to "linear mechanical systems" which have a special form of representation as a second order matrix differential equation. Although that form applies to space structure dynamics, we prefer to define measures which have a physical interpretation in terms of control or estimation error characteristics for general linear systems.

What we seek, then, is a quantitative measure of how well the system state can be observed with a given set—number and location—of sensors. This measure should have as clear an interpretation as possible, be easy to compute, and should not depend on the design of the control system. Moreover, it should properly reflect the loss of capability due to the sensor failures which are likely to occur over the mission period.

Dynamic Measure of Observability

Any measure of the observability of a dynamic system should reflect as directly as possible the amount of information which can be derived about the system states from the sensor outputs in a given amount of time. The means of obtaining this information is by attaching to the system an observer whose states, \hat{x} , are estimates of the true states of the system. The more information that is obtained about the system, the smaller the estimation error becomes.

In the parallel problem of indicating the controllability of a system with a given set of actuators it is not obvious how the control should be used so as to realize the best possible control of the system. What is "best" might be defined in a number of reasonable ways. But in this case, if we use a linearized description of the system dynamics from the outset, then the best way to process the sensor data so as to minimize estimation error is obvious. The linear estimator which minimizes the state estimation error vector, $e = \hat{x} - x$, in a mean square sense, i.e., minimizes

$$S = e^T M e \quad (1)$$

where M is some weighting matrix, is the Kalman Filter.

With the state dynamics and measurement relation given as

$$\dot{x} = Ax + Bu + w \quad (2)$$

$$y = Cx + v \quad (3)$$

the estimation error covariance matrix with Kalman filtering obeys the equation

$$\dot{P} = AP + PA^T - PC^T N^{-1} CP + Q \quad (4)$$

where P is the estimation error covariance matrix, and N and Q are the measurement and driving noise intensity matrices, respectively. But the estimation error, or its covariance matrix, is an inverse indication of the amount of information one has about the state. We wish the measure of observability to be a direct indicator of information, so to that end we introduce the information matrix—the inverse of the error covariance matrix.

$$J = P^{-1} \quad (5)$$

One other consideration is that the observability measure should be a property of the system and a set of sensors—nothing else. Since the measurement noise is a property of the set of sensors being evaluated, we retain its inclusion in (4) in the form of N but do not include the effect of state driving noise, because that is an external influence not related to the sensor set. Thus, if we set $Q = 0$, then (4) in terms of J becomes

$$\dot{J} = -JA - A^T J + C^T N^{-1} C \quad (6)$$

Take as the standard situation the case in which there is no information about the state initially and data is collected up to a specified time T . Then $J(0) = 0$ and one is interested in $J(T)$.

Having the information matrix at time T , we need some scalar measure of how large the matrix is as an indication of how much information has been generated by optimal processing of the sensor data. One way of measuring the size of $J(T)$ is by reference to the quadratic surface

$$v^T J^{-1} v = 1 \quad (7)$$

Equation (7) defines an ellipsoidal surface in v -space. If J is a diagonal matrix (one can always transform to principal coordinates), one observes that increasing an element J_{ii} will expand the ellipsoid in the direction v_i . Thus the larger J becomes, the larger the volume encompassed by the surface in (7) so that the more information obtained about the system, the larger the volume becomes.

Typically, however, some components of x will be of greater concern than others—especially considering that different units will apply to different components. Regardless of how one were to approach the definition of a measure of observability, it is clear that a scaling of the state variables to reflect their relative importance to the success of the mission would be required. To that end, define the transformation

$$z = Fv$$

$$F = \begin{bmatrix} |e_{1\max}| & \text{○} \\ \vdots & \vdots \\ \text{○} & |e_{n\max}| \end{bmatrix} \quad (8)$$

where $e_{i\max}$ is the maximum error one is willing to tolerate in the direction x_i . The more error one is willing to tolerate in that direction, the greater the transformed state so the larger the volume becomes. Thus the scaling is consistent with the requirement that the more important a variable is (smaller $|e_{i\max}|$) the smaller it will appear in the transformed space and the less observable it appears unless the sensor set is adjusted to favor that variable. Also note that v has units of reciprocal error, so z is dimensionless.

Now that the axes have been scaled so that it is equally important to obtain information in each direction, one can interpret the size of the surface generated by the information matrix in terms of the volume enclosed by that surface. But the volume alone does not reflect the shape of the surface. An ideal allocation of sensors would produce a sphere in the space of equally important variables. Thus if two sensor sets produce surfaces enclosing equal volume, we would favor the set which produced the more nearly spherical surface.

After considering a number of alternatives, the degree of observability was chosen to be the following:

$$DO = \left[V_S + \frac{V_S}{V_E} (V_E - V_S) \right]^{1/n} \quad (9)$$

where V_E is the n -dimensional volume of the ellipsoid in the transformed space and V_S is the volume of the largest inscribed sphere; n is the dimension of the state space. The first term on the right side of (9) is the predominant term in the observability measure; it reflects the smallest magnitude of reciprocal error relative to the maximum tolerable error (largest value of error relative to $e_{i\max}$) which remains after optimal processing of the sensor data for time T starting with no initial information. If the sensors were ideally allocated, the surface would be a sphere and V_S would be the observability measure. The second term in (9) adds a smaller amount to DO to recognize the additional information derived about the other variables if the surface is not spherical. The additional volume, $V_E - V_S$, is scaled by V_S/V_E so that the most this term can add, as $V_E \rightarrow \infty$, is V_S and so that DO is zero if there is any direction in which the system does not derive information at all. This is the case of traditional unobservability, and $V_S = 0$. The n th root of the weighted volume

is taken as the observability measure to make it proportional to the linear dimensions of the region in which information is produced. The volume weighting scheme for a two-dimensional case (volumes are areas) is depicted in Figures 1(a-c).

Once one accepts (9) as a reasonable assessment of the observability of the system, what remains to be shown are the mechanics of computing the n-dimensional volumes V_S and V_E . The volume enclosed in any quadratic surface is proportional to the product of the reciprocals of the square roots of the eigenvalues of the matrix which generates the quadratic surface. Since volume has little intuitive significance in spaces of dimension greater than 3, we omit the constant of proportionality and the volume is taken to be simply

$$V = \left(\prod_{i=1}^n \frac{1}{\sqrt{\lambda_i}} \right)^{-1} \quad (10)$$

To apply this result to the case at hand, first substitute (8) into (7) to obtain the equation of the ellipsoidal surface in the space of z :

$$1 = z^T (FJ(T)F^T)^{-1} z \quad (11)$$

V_E is then given by (10) where λ_i are the eigenvalues of $(FJ(T)F^T)^{-1}$. More simply, if v_i denotes the eigenvalues of $FJ(T)F^T$, the ellipsoidal volume is also given by

$$V_E = \pi \prod_{i=1}^n \sqrt{v_i} \quad (12)$$

and the spherical volume is the shortest distance to the surface, $1/\sqrt{\lambda_{\max}}$, to the nth power, or alternatively,

$$V_S = \left(\sqrt{v_{\min}} \right)^n \quad (13)$$

The remaining issue is computation of $J(T)$. It is always possible to integrate (6) for an interval T starting from a zero initial condition. But in Ref. 3 an analytic solution is given for the case of flexible space structure dynamics expressed in decoupled modal form. Since it is always possible to express the dynamics in this form it is always possible to compute the Degree of Observability, DO , by evaluating closed-form expressions and solving for the eigenvalues of a real, symmetric matrix.

RECOGNITION OF COMPONENT FAILURES

Because of the realistic possibility of components failing during the operating lifetime of the system, one would like the Degree of Observability to

be averaged in some way over the set of component failure combinations which the system may experience. To this end, let f be an indicator of the state of failures of the components, and let the vector \underline{l} represent their locations. Then for a given set of operating sensors, one can compute the Degree of Observability, $DO(\underline{l}, f)$, using the method previously described.

The component locations indicated by \underline{l} are deterministic; they will subsequently be adjusted to optimize the Degree of Observability. But f is a random variable with a time-dependent probability distribution. Thus $DO(\underline{l}, f)$ is also a random variable with a time-dependent probability distribution defined by the distribution of f . To define a meaningful deterministic performance measure, one would logically use the expected value of $DO(\underline{l}, f)$ with the expectation taken over the distribution of f , the failure state for the system components. This yields a performance measure which depends on time, t . It represents a measure of the expected performance of the system at time t in view of the probabilities of the various failure states at that time.

But this control system is required to operate over a certain period T_m which might represent the time between maintenance visits. Rather than optimize the Degree of Observability at any one time, such as the end of that period, it would seem more meaningful to optimize the average Degree of Observability over the whole period. In this average, the performance resulting from failure states which are likely over longer periods would be weighted more heavily than those likely to exist over shorter periods. And a probability-weighted measure of performance over the whole operating period is obtained rather than just a measure of performance at one time.

The average of the expected Degree of Observability over the mission period T_m is taken as the final measure:

$$DO_{AVE}(\underline{l}) = \frac{1}{T_m} \int_0^{T_m} \overline{DO(\underline{l}, f)} dt \quad (14)$$

But the expected DO is simply a weighted sum over the different failure states,

$$\overline{DO(\underline{l}, f)} = \sum_i DO(\underline{l}, f_i) P_i(t) \quad (15)$$

where $P_i(t)$ is the probability of failure state f_i at time t . The final measure can be expressed as

$$DO_{AVE}(\underline{l}) = \sum_i DO(\underline{l}, f_i) \frac{1}{T_m} \int_0^{T_m} P_i(t) dt \quad (16)$$

and depends on T_m and the component failure statistics as well as the locations.

To illustrate the calculation of the average probabilities for the failure states, take the usual assumptions of independence of component failures and the exponential distribution of time to failure for each component. Then for the j th component, the probability that it is working at time t is

$$P(\text{jth component working at } t) = e^{-\lambda_j t} \quad (17)$$

where λ_j is the failure rate for this component, the reciprocal of its mean time to failure. Let the i th failure state be characterized by two sets of indices, J_W and J_F , with all components having indices j in the set J_W working and all components having indices j in the set J_F failed. Note that the index of each component in the system must be contained in one or the other of J_W or J_F , but not both. Then the probability of this failure state at t is

$$P_i(t) = \left[\prod_{j \in J_W} e^{-\lambda_j t} \right] \left[\prod_{j \in J_F} (1 - e^{-\lambda_j t}) \right] \quad (18)$$

With the definition

$$\lambda_W = \sum_{j \in J_W} \lambda_j \quad (19)$$

this can be written as

$$P_i(t) = e^{-\lambda_W t} \prod_{j \in J_F} (1 - e^{-\lambda_j t}) \quad (20)$$

The average, over the mission period T_M , of this probability—as is required for the calculation of the Degree of Observability given in Eq. (16)—can be expressed as

$$\frac{1}{T_M} \int_0^{T_M} P_i(t) dt = \sum_{k=0}^{N_F} (-1)^k \text{Sum}(k) \quad (21)$$

where

$$\text{Sum}(k) = \sum_{\ell=1}^{(NF)} \frac{1}{(\lambda_W + \sum_k^{\ell} \lambda_j)^{T_M}} \left[1 - e^{-(\lambda_W + \sum_k^{\ell} \lambda_j)^{T_M}} \right] \quad (22)$$

$$\binom{NF}{k} = \frac{N_F!}{k! (N_F - k)!}$$

N_F = the number of elements in J_F (the number of failed components)

$\sum_k^{\ell} \lambda_j$ = for each ℓ , the sum of a different combination of $k \lambda_j$ with $j \in J_F$

The first term in the sum of Eq. (21) requires interpretation in the case of no working components. In the usual case with some components working, λ_W given by Eq. (19) is greater than zero and

$$\text{Sum}(0) = \frac{1}{\lambda_W^{T_M}} (1 - e^{-\lambda_W^{T_M}}) \quad \lambda_W > 0 \quad (23)$$

If there are no working components, define $\lambda_W = 0$, and $\text{Sum}(0) = 1$.

These expressions can be simplified in the special case of all component failure rates equal. Call the number of working components N_W and the number of failed components N_F as before. Then if all $\lambda_j = \lambda$,

$$\frac{1}{T_M} \int_0^{T_M} P_i(t) dt = \sum_{k=0}^{N_F} \frac{(-1)^k \binom{N_F}{k}}{(N_W + k)^{\lambda T_M}} \left[1 - e^{-(N_W + k)\lambda T_M} \right] \quad (24)$$

As before, if $N_W = 0$, the term corresponding to $k = 0$ is 1.

OPTIMUM SENSOR PLACEMENT

Having a computable measure of how well the structure can be observed with any given set of sensors, with the expected effect of component failures throughout the mission reflected in the measure, one can then seek to optimize the choice of component locations, for a given number, so as to maximize the performance measure. This task may be computationally burdensome when dealing

with a large number of components but it is conceptually straightforward.

A constraint which will likely apply in most applications is that sensor placement will be restricted to a discrete set of permissible locations. Structural considerations, for example, may require that instrument packages be mounted only at the joints of a truss structure. If this is true of all the components, then the placement optimization problem is in the nature of an integer programming problem. Many algorithms have been described in the literature for solving integer programming problems; nothing has been added to that art in this work. The examples which follow are intended only to illustrate the nature of this step. They were restricted to a small number of components and optimization was accomplished by global search—by testing all admissible combinations of component locations.

CHOICE OF COMPONENT NUMBER

Having the optimum set of sensor locations and the corresponding maximum Degree of Observability for a given number of components, one can compute this maximum performance measure for several choices of component number. The choice of how many sensors to use in the system cannot be resolved as an optimization problem unless additional factors are incorporated in the criterion. The Degree of Observability will always improve with additional sensors if the best locations are used in each case.

However, it should be informative to observe the trend of the performance measure with number of components. Some locations are more advantageous than others—such as the placement of rate gyros near the nodes of important modes. With the realistic restriction that only one component can be placed at any one of the allowable locations, one should expect to see diminishing returns in performance with increasing number as the more favorable locations are occupied. This information should be helpful to the designer in making the trade-off between improved performance and increased cost, power required, etc.

APPLICATION TO BEAM

To illustrate the methodology defined above, sensor placement and number were considered for the case of a free-free beam. The beam was modeled as in Reference 3 with the states representing the modal amplitudes and rates of the first three flex modes; translation rate sensors were used for observation. In all trials the amplitude rate states were scaled by the factor ω_i relative to the amplitude states where ω_i is the corresponding modal frequency. The sensors were assumed equally noisy ($N = 1$). As an aid to interpretation of the results that follow, the mode shapes for the three modeled modes are shown in Figure 2.

The Degree of Observability as a function of the position of a single translation rate sensor along the length of the beam is shown in Figure 3 with the beam modeled by the dynamics of the first mode only. This case is shown to demonstrate that the computed DO gives the result that is intuitively obvious in this instance—the DO reflects the shape of the first mode and is zero

when the sensor is located at either node because the mode is unobservable by this type of sensor placed at a node. The use of the observability measure will be more important when dealing with more complex systems where the results will not be so predictable. A suggestion of this is given in Figure 4 which shows the DO as a function of the location of a single sensor with the beam modeled by the dynamics of the first three flex modes. In this case the pattern is more complex with the measure going to zero at each node of any mode—because unobservability of any decoupled mode constitutes unobservability of the system. No sensor failures have been considered in these results.

The Degree of Observability achieved with two sensors is shown in Figure 5 with the beam represented by the dynamics of the first two flex modes. In this case one sensor is fixed at the end of the beam and DO is shown as a function of the location of the other sensor. At no point does DO become zero because both modes are observable by the sensor at the end. The observability measure is dominated by the observability of the first mode as is indicated by the similarity of this curve to that of Figure 3 for first mode dynamics only.

The effect of possible sensor failures on the observability measure is indicated in Figure 6 which shows the Degree of Observability for a two-mode representation of the dynamics of the beam as a function of the location of one sensor with another fixed at the end of the beam. The upper curve is the same as Figure 5 in which no failures are accounted for. The lower curve in Figure 6 is the average expected DO with the mean time to failure for each sensor equal to the mission period. This gives a probability of 0.63 that each sensor will fail before the end of the mission. This system is unobservable if both sensors fail or if one sensor is located at a node of either mode and the other sensor fails. These possibilities are accounted for with the proper probabilities in the measure of observability.

As in Figure 5, the DO in Figure 6 is dominated by the observability of the first mode. In this case the maximum tolerable error in the estimate of both modal amplitudes was taken equal ($e_{1_{\max}} = e_{3_{\max}}$). This characteristic is changed if the relative importance of the two modes is different. This is illustrated in Figure 7 which is the same case as in Figure 6 except that the second mode has been declared 5 times more sensitive than the first mode ($e_{3_{\max}} = 1/5 e_{1_{\max}}$). The relative weighting of each rate state to the corresponding amplitude state has been retained as ω_i , the modal frequency, as before. In this figure, the DO as a function of the location of the variable sensor has essentially the character of the magnitude of the second mode shape. This is because of the greater importance that has been assigned to that mode.

Figure 7 also illustrates a very important point related to the importance of accounting for the possibility of component failures early in the design process. That point is the fact that recognition of the likely effects of component failures can alter the optimal locations for those components. The quantitative significance of this point is small in this example but the qualitative truth of the proposition is established. Looking at the upper curve in Figure 7 one can see that if the possibility of sensor failures is ignored, the Degree of Observability is nearly the same with one sensor at the end of the beam and a second sensor located either at test position 2 or 7—actually, the observability is slightly better at position 7. So without considering failures one would say that the optimum locations for two sensors on the beam are at

test positions 1 and 7. But from the lower curve which accounts for the likely failures it is clear that locations 1 and 2 are optimal in that case. In drawing these conclusions we hold the constraint that only one sensor can be allowed at one location and only the test positions shown in Figure 2 are permitted. In particular, we search only half the length of the beam; sensors located on the other half of the beam would give symmetric results.

The interpretation of the results on optimum sensor placement is that position 7 is near the antinode of mode 2 and so is a good location for observing that mode which has been given great importance in this example. But position 7 is near the node of mode 1 and so is not a good choice of location for observing that mode. If no failures are admitted, the optimal sensor locations represent the risky choice of placing one sensor at location 7 to gain good observability of mode 2 because mode 1 is well observed by the sensor at position 1, the end of the beam. But if failures are anticipated, the failure of the sensor at position 1 leaves mode 1 so poorly observed by a sensor at position 7 that the more conservative choice of placing the second sensor at position 2 is preferable. At position 2, the sensor does not observe the second mode quite as well, but has better observability of mode 1 compared with a sensor at position 7.

Finally, the variation of Degree of Observability with optimized sensor locations as the number of sensors is increased is shown in Figure 8. In general one would expect to see diminishing returns of observability with more sensors as the more favorable locations are occupied. The designer must then base his choice of number of sensors to use on the trade-off of increased performance against increased cost, weight, power, etc. In this case diminishing returns are not evident in Figure 8 because there are several locations which are nearly equally effective after the position at the end of the beam has been occupied. If the curve were extended to a larger number of sensors it would surely begin to flatten out.

CONCLUSIONS

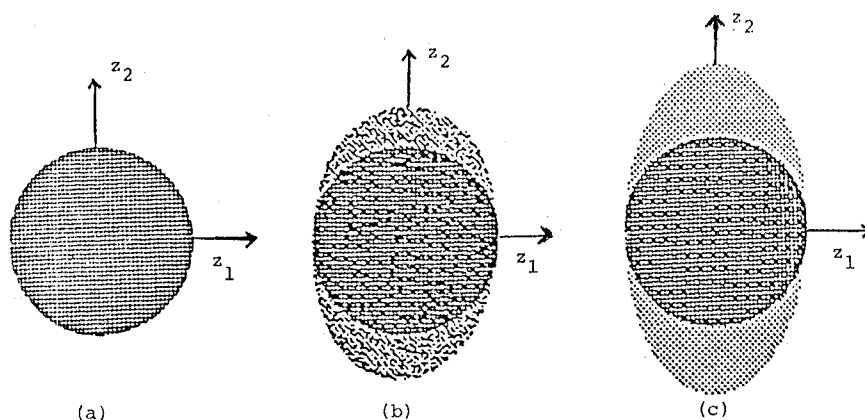
A methodology has been presented which is intended to assist the designer of a control system for a large space structure to decide how many sensors should be incorporated in the system and where they should be placed on the structure. This approach is intended to be especially useful in the early stages of the evolution of the system, before a complete control system concept has been defined. This methodology is based on a quantitative measure of the observability of the system for a given set of sensors. The effect of possible component failures during the mission period was incorporated in the measure. The question of sensor placement is then resolved by finding the locations which maximize the performance measure. The number of components to use cannot be determined by optimizing the measure because the observability always improves with increased number of sensors if they are optimally located. However, the improvement in the measure with component number can be determined, and this information can be used along with data on cost, power required, etc. to decide how many sensors to use.

REFERENCES

1. Juang, J.N. and Rodriguez, G., Formulations and Applications of Large Structure Actuator and Sensor Placement, Proc. of 2nd VPI & SU/AIAA Symposium (Dynamics and Control of Flexible Spacecraft), Blacksburg VA, June 1979.

2. Hughes, P.C. and Skelton, R.E., "Controllability and Observability for Flexible Spacecraft," J. Guidance and Control, Vol. 3 No. 5, Sept-Oct 1980.
3. Vander Velde, W.E. and Carignan, C.R., "A Dynamic Measure of Controllability and Observability for the Placement of Actuators and Sensors on Large Space Structures," MIT Space Systems Laboratory Report No. 2-82, Massachusetts Institute of Technology, Cambridge, Mass., January 1982.
4. Carignan, C.R. and Vander Velde, W.E., "Number and Placement of Control System Components Considering Possible Failures," MIT Space Systems Laboratory Report No. 5-82, Massachusetts Institute of Technology, Cambridge, Mass., March 1982.

FIGURES



Figures 1a-c: Volume weighting scheme for computing degree of observability - (a) ideal distribution, (b) slightly distorted distribution, (c) very distorted distribution. Shading indicates relative weighting.

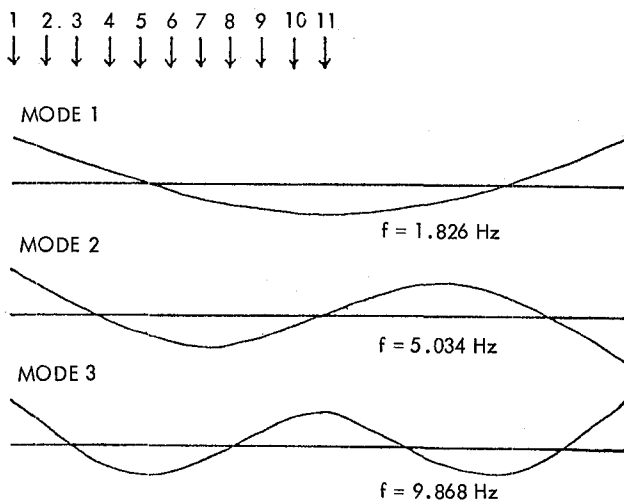


Figure 2. Modeled Mode Shapes and Sensor Test Positions.

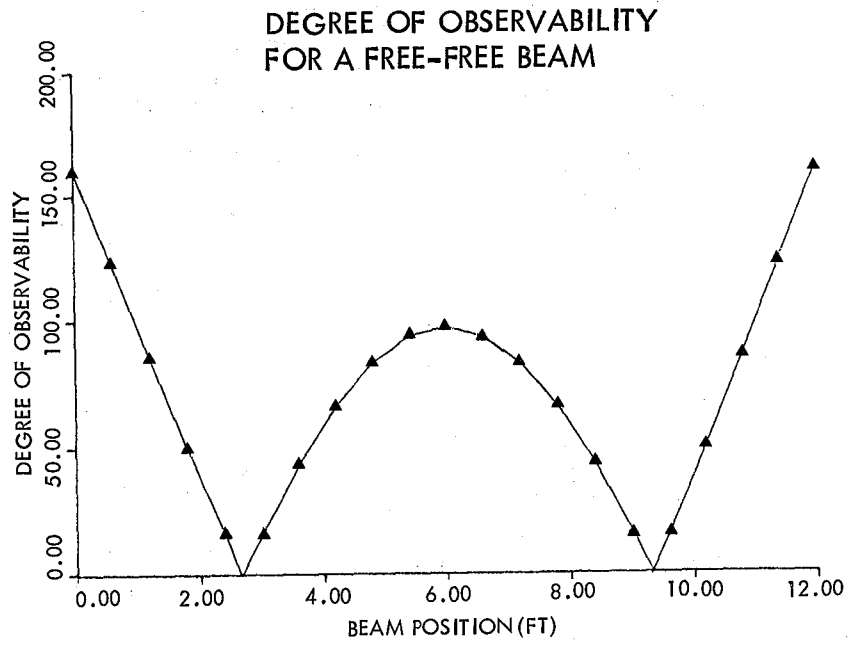


Figure 3. DO vs. Sensor Position for First Mode Representation of the Beam.

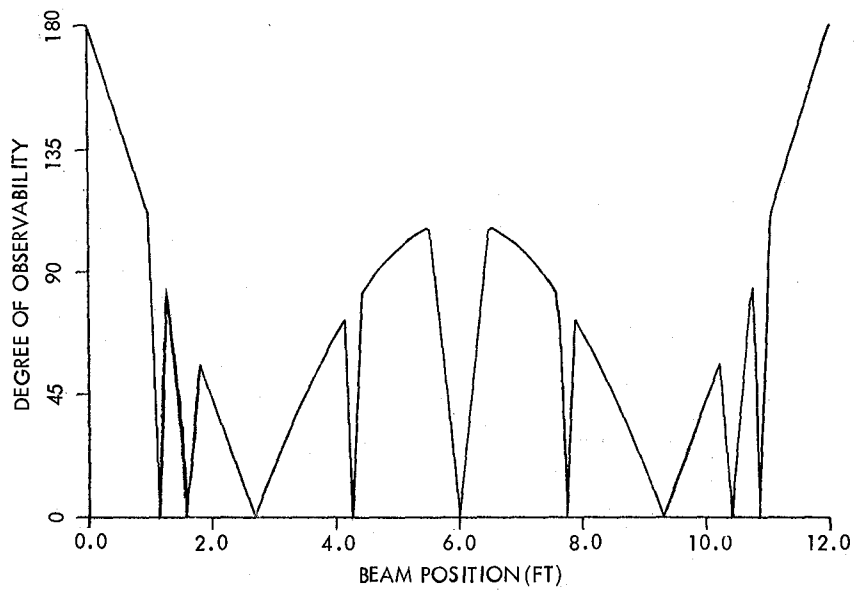


Figure 4. DO vs. Sensor Position for a Three-Mode Representation of the Beam.

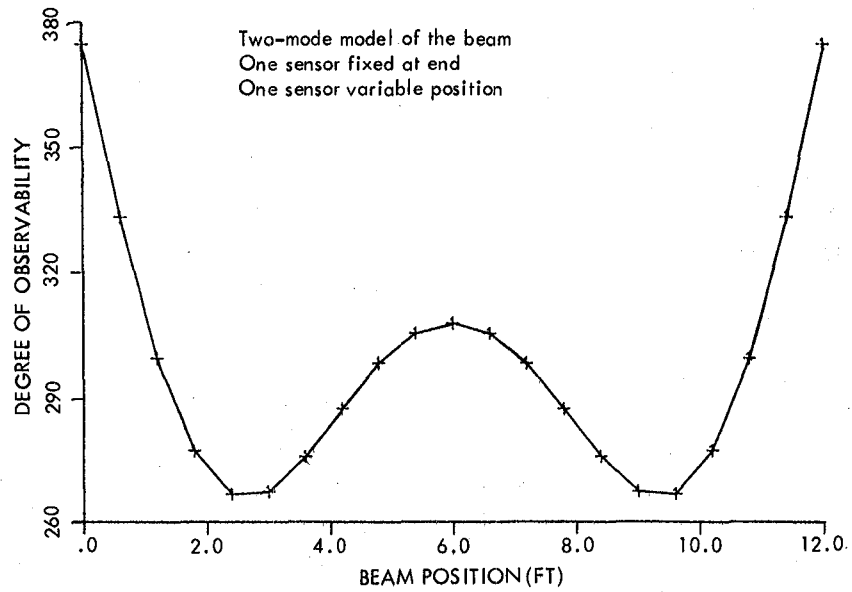


Figure 5. Degree of Observability with Two Sensors.

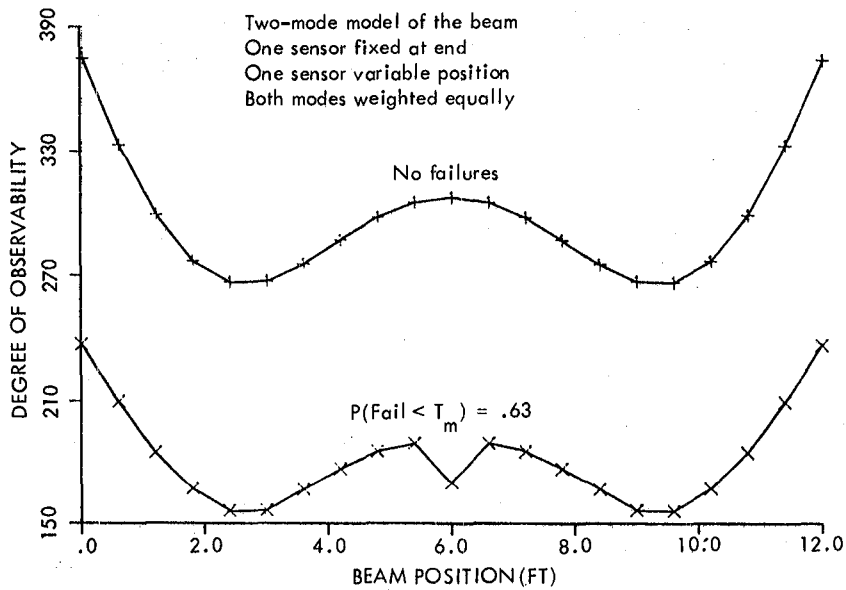


Figure 6. Degree of Observability with Two Sensors.

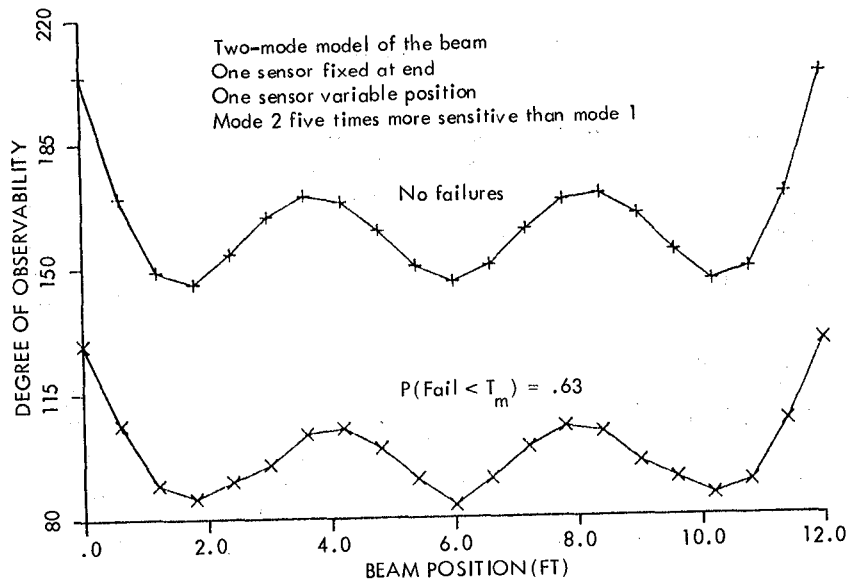


Figure 7. Degree of Observability with Two Sensors.

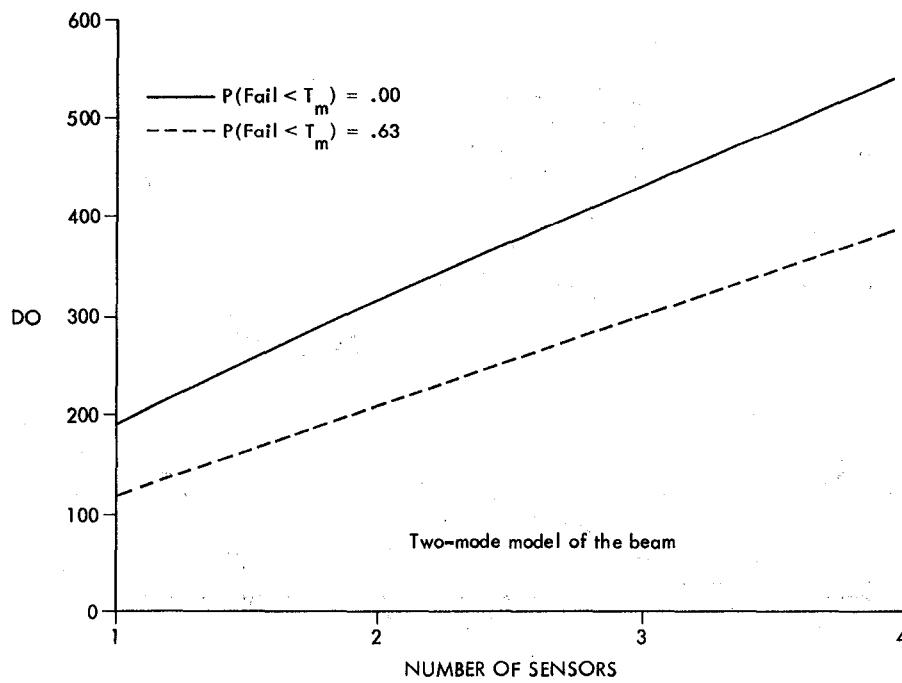


Figure 8. Maximum DO vs. Number of Sensors.

THE TOYSAT STRUCTURAL CONTROL EXPERIMENT

J.A. Breakwell and G.J. Chambers
Lockheed Missiles and Space Company
Sunnyvale, CA 94304

ABSTRACT/FOREWORD

This paper describes in detail the Lockheed TOYSAT experiment. The experiment was designed to test hypothesis concerning the application of optimal control theory to flexible spacecraft. The theory is presented, and results described.

Hardware Setup. A drawing of the TOYSAT experimental setup is shown in Fig. 1. The test setup consists of a 12-ft. flexible beam fastened to the side of a 1.3-ft. square block of aluminum. To accentuate bending, a 2-lb. weight is attached to each end of the beam. The beam is suspended from the ceiling in such a way as to allow free motion in the horizontal plane.

Control of the motion of the specimen is provided by two linear actuators. When the actuators act together, translational motion results, and when equal but opposite commands are given, pure rotational motion results. Sensing is provided by accelerometers mounted at the ends of the flexible beam and by linear position sensors mounted in tandem with the linear actuators. The average of the two accelerometer measurements indicates the translational motion, and their difference measures the rotational motion. The same holds true for the position sensors. The separation of rotation and translation in both controller and sensor, as well as in the physical behavior of the TOYSAT, allows independent and separate design of translational and rotational control laws.

Figure 2 shows how the TOYSAT is connected by way of A/D and D/A converters to a computer where the digital control law is implemented. The large number of computations necessary to carry out the control law is handled by an array processor which allows a sampling rate of 80 Hz.

The frequencies, dampings, and mode shapes for the assembled system are shown in Table 1. These data result from a judicious combination of analysis and testing. The rigid body modes and the first two bending modes in both translation and rotation are used in controls synthesis and implementation. The remaining modes are used to evaluate the effect of spillover. The frequencies and dampings (ω_j , ξ_j) are assembled in the usual block diagonal form to give the F matrix, the η_j give the G matrix, and the $\phi_j(0)$ and $\phi_j(\ell)$ give the H_1 and H_2 matrix components corresponding to the linear sensors and accelerometers respectively. (These matrices are defined by their use in Eq. 2).

Controls Synthesis. The controller implemented in the hardware has the form:

$$\begin{aligned}\hat{x}_{n+1} &= \Phi' \hat{x}_n + \Gamma' u_n + K z_n \\ u_n &= C x_n,\end{aligned}\tag{1}$$

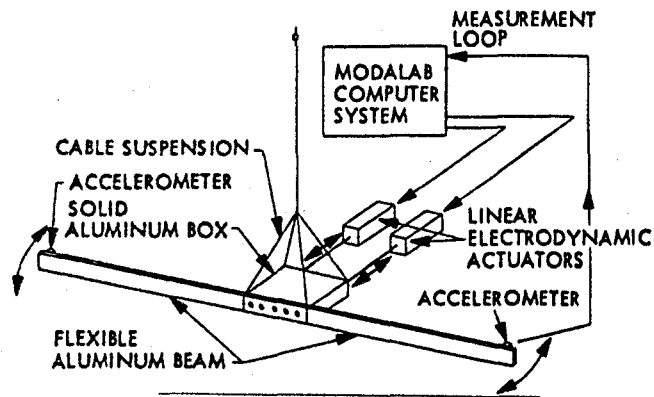


Fig. 1 TOYSAT Test Setup

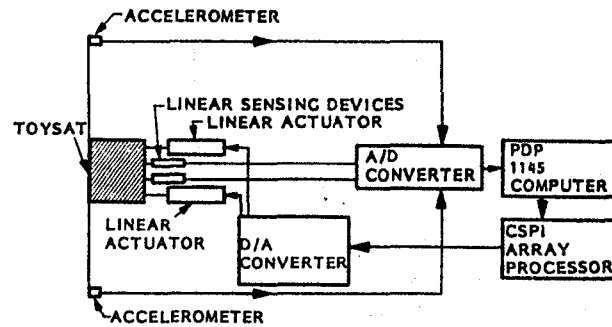


Fig. 2 Measurement and Control Flow Diagram

Table 1 TOYSAT MODAL FREQUENCIES, DAMPINGS, MODE SHAPES, AND INFLUENCE COEFFICIENTS

	ω_i (Hz)	ζ_i (%)	ϕ_i (o)	ϕ_i (l)	η_i
<u>Trans</u>					
R.B.	0.19	70.0*	1.0	1.0	3.24
1	0.98	0.58	0.0842	-0.952	4.21
2	9.06	0.29	0.0365	0.365	1.83
3	28.02	0.54	0.0210	-0.229	1.05
4	57.69	0.74	0.0147	0.0164	0.735
5	98.15	0.1	0.0113	-0.128	0.565
6	149.38	0.1	0.0092	0.105	0.460
<u>RT</u>					
R.B.	0.0	0.0	1.0	72.0	0.00712
1	2.64	0.33	0.252	-0.471	1.54
2	9.87	0.30	0.127	0.335	0.774
3	28.4	0.54	0.055	-0.226	0.335
4	57.94	0.88	0.033	0.163	0.201
5	98.33	0.1	0.022	-0.127	0.134
6	149.53	0.1	0.017	0.104	0.104
Total Mass = 2.708 slugs Total Inertia = 140.37 in.-lb-s ²					
*An approximation for a phenomenon that cannot be accounted for by modal damping.					

where Φ' denotes the transition matrix, and Γ' , K , C are constant matrices to be determined. This deceptively simple form conceals a multitude of complexities involved in choosing the gains K and C . The controller separates naturally into a part which estimates the modal amplitudes and another part which outputs these estimates, multiplied by some gain, to the control actuators. In accordance with this separation we will present first the estimator synthesis and then the control gains synthesis.

Filter Synthesis. The problem is defined in the continuous domain by Eq. 2 below. (The state covariance is specified in the continuous domain).

$$\begin{aligned} \dot{x} &= Fx + Gu + w_c \\ z &= H_1x + H_2\dot{x} + v_c \end{aligned} \quad (2)$$

w_c is white noise, zero mean, covariance Q_c ;
 v_c is white noise, zero mean, covariance R_c .

The extra term H_2 is necessary because the standard form does not allow for acceleration measurements. The specific entries in the matrices for the separate translation and rotation plants are given in Table 1.

The first step in the synthesis process is to convert the continuous system given in Eq. 2 to a discrete system,

$$\begin{aligned} x_{n+1} &= \Phi x_n + \Gamma u_n + w_d \\ z_n &= H_1 x_n + H_2 \dot{x}_n + v \end{aligned} \quad (3)$$

w_d is zero mean white noise, covariance Q_d ;
 v is zero mean white noise, covariance R .

$$Q_d = E \{w_d w_d^T\} = \int_0^T \Phi(t) Q_c \Phi^T(t) dt \quad (4)$$

ϕ and A are derived from F and $1G$ using standard numerical matrix exponential procedures. T is the step length. The covariance of the discrete noise R is taken as an input and is not derived from the continuous measurement noise R_c . Eq. 3 is put into standard Kalman filter form in two steps. First x_n equation by means of Eq. 2, leaving

$$z_n = H_1 x_n + H_2 F x_n + H_2 G u_n + H_2 w_c + v \quad (5)$$

Then to the first of Eq. 3 we add the identically zero quantity

$$\begin{aligned} L \{ & z_n - H_1 x_n - H_2 F x_n \\ & - H_2 G u_n - H_2 w_c - v \} \end{aligned} \quad (6)$$

where L is to be determined later. The result is

$$\begin{aligned} x_{n+1} &= \left[\Phi - LH_1 - LH_2 F \right] x_n \\ &+ \left[\Gamma - LH_2 G \right] u_n + L z_n \\ &+ w_d - LH_2 w_c - Lv. \end{aligned} \quad (7)$$

Equations 5 and 7 together constitute the usual Kalman filter problem if L is chosen so that the measurement noise ($H_2 w_c + v$) and the state noise ($w_d - L H_2 w_c - L v$) are uncorrelated. Equation 8 shows the choice of L that accomplishes this.

$$L = \Phi(T) Q_c H_2^T [H_2 Q_c H_2^T + R]^{-1} \quad (8)$$

Standard optimal techniques may now be used to obtain the filter gains K . The resulting filter has the form

$$\begin{aligned} x_{n+1} = & \left[\Phi - (L + K)(H_1 + H_2 F) \right] x_n \cdot \\ & + \left[\Gamma - (L + K) H_2 G \right] u_n + (L + K) z_n \end{aligned} \quad (9)$$

Φ' and Γ' shown in Eq. 1 are just the appropriate coefficients of x_n and u_n from Eq. 9.

Control Gains. The control segment of the problem is specified by

$$\dot{x} = Fx + Gu \quad (10)$$

with the cost functional

$$J = \int_0^{\infty} (x^T A x + u^T B u) dt .$$

Again, as with the filter, this problem is converted to a discrete problem

$$x_{n+1} = \Phi x_n + \Gamma u_n , \quad (11)$$

but now the cost function is specified by

$$J = \sum_{n=1}^{\infty} (x_n^T \tilde{Q} x_n + u_n^T \tilde{S} u_n + 2 u_n^T \tilde{R} x_n), \quad (12)$$

where the weights Q , S , R , of the discrete problem are given by

$$\tilde{Q} = \int_0^{-T} \Phi^T(t) A \Phi(t) dt$$

$$\tilde{S} = \int_0^T \Gamma^T(t) A \Phi(t) dt$$

$$\tilde{R} = \int_0^T \{B + \Gamma^T(t) A \Gamma(t)\} dt \quad (13)$$

Equations 11 and 12 specify a standard discrete optimal control problem that is easily solved by standard methods. The resulting gains C are those implemented in the controller specified by Eq. 1.

Evaluation of Controller. When the six-state controller for either translation or rotation is completed, it is tested on an augmented fourteen-state evaluation model. The eigenvalues of the six-state controller operating on the fourteen-state plant are investigated for signs of spillover. These eigenvalues are those of the matrix shown in Fig. 3. The superscripts 14 in this figure refer to the fourteen-state evaluation model.

Specific Controls Design. The actual gain selection procedure, like the theory, divides into separate estimator and control gains selections. First a filter was designed and tested on the open-loop system. When that seemed to be working, the loop was closed with an appropriate set of control gains.

To obtain filter gains, the parameters to be selected were the continuous state noise covariance matrix Q_C (defined in Eq. 2) a six-by-six matrix for either translation or rotation, and the state noise covariance matrix R (defined in Eq. 3), a two-by-two matrix assumed to be diagonal.

The approach to choosing Q_C and R was to pick Q_C so as to maximize the separation of the estimator poles. When done correctly, this assures that the separate states in the Kalman filter contain just the intended modal amplitude and very little of the others. That is, Q_C is picked to minimize crosstalk between modes in the Kalman filter.

$$\left[\begin{array}{c|c} \Phi^{14} & \Gamma^{14} C \\ \hline (K + L) \left[H_1^{14} + H_2^{14} F^{14} \right] & \Phi - (K + L) \left[H_1 + H_2 F + (K + L) H_2 G \right] C \\ & + (K + L) H_2^{14} G^{14} C \end{array} \right]$$

Fig. 3 Matrix For Eigenvalues of Six-State Controller

Figure 4 shows the time history of the estimates of the state vector for a good choice of Q_c . The specimen had been excited by a four-second chirp (a fast sine sweep varying linearly in frequency), and the outputs of the estimator were recorded. The rigid body channels contain all the low frequency movement, while the modal channels separate the remaining frequencies nicely.

The measurement covariance matrix R was chosen to force good convergence of modal reconstruction of the measurements with the actual measurements. That is, individual components of R are increased until corresponding components of Hx converge with the actual measurements fairly quickly. Figures 5 and 6 show that the modal reconstruction of the rotational displacement and tip acceleration converge quite quickly with the actual measurements. Again, in this case the specimen had been perturbed by a four-second chirp and then allowed to settle.

Once a filter design has been established, the selection of control gains is straightforward. Since there was no obvious physical quantity such as a line of sight on the TOYSAT, the control weights were picked to give fast and roughly equal settling times for all modes. The values for the covariance matrices and control weighting matrices which generated the nominal controller are shown in Table 2 for the translation controller and in Table 10 for the rotation controller. Also shown are the resulting filter and control pole locations.

TOYSAT Experimental Results. The hardware tests of the control system described in the previous section are slight variations of a standard modal identification tests. A four-second chirp containing frequencies from 0 to 40 Hz is applied simultaneously in rotation and translation through the Electroseis shakers. This open-loop command is superimposed upon any feedback commands which may be generated by the control law given in Eq. 1. The open-loop chirp command is also communicated to the estimator. Data are taken for twelve seconds. Since the chirp begins sometime in the first second, this allows for roughly eight seconds of data after the chirp has expired. Data saved during the test run include the open- and closed-loop control commands, all four measurements, and the twelve Kalman filter states during the run. Post-experiment processing allows analysis of the data in the frequency domain as well as in the time domain.

Figures 7 through 12 illustrate various forms of results from the control system test described in Tables 2 and 3. Figures 7 and 8 show comparisons of the four measurements taken during two separate test runs; one without controls, and one with the control system loop control. The closed-loop data show much faster settling time than do the data from the open-loop test. Also, peak excursions during the chirp excitation are considerably smaller. Figure 9 shows the Kalman filter states during the closed-loop test. This may be compared with Fig. 4 which describes the same states during the open-loop test.

Figures 10 and 11 present frequency domain comparisons of open- and closed-loop transfer functions for tip accelerations to inputs through the central shakers. Figure 10 shows that the translation controller reduces the response of the first two bending modes (at 1 and 9 Hz) to below the level of the third unmodeled bending mode (28 Hz). The first mode amplitude is reduced by a factor of eight, a number which is proportional to the increase in damping.

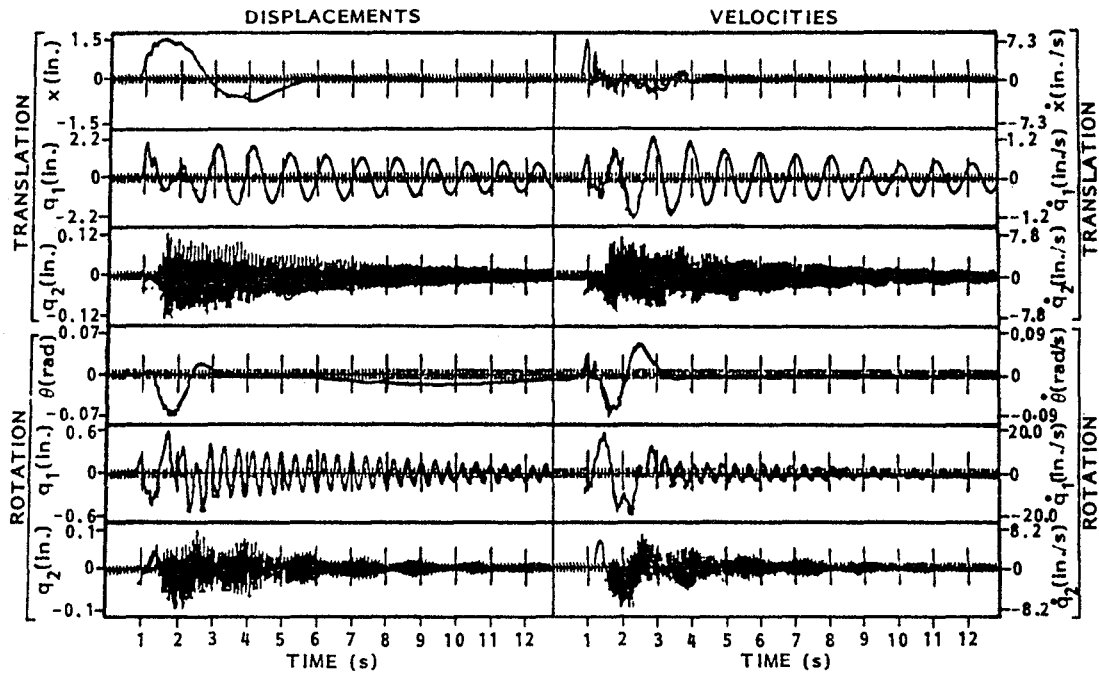


Fig. 4 Open-Loop Kalman Filter Output (Response to 4-s Chirp)

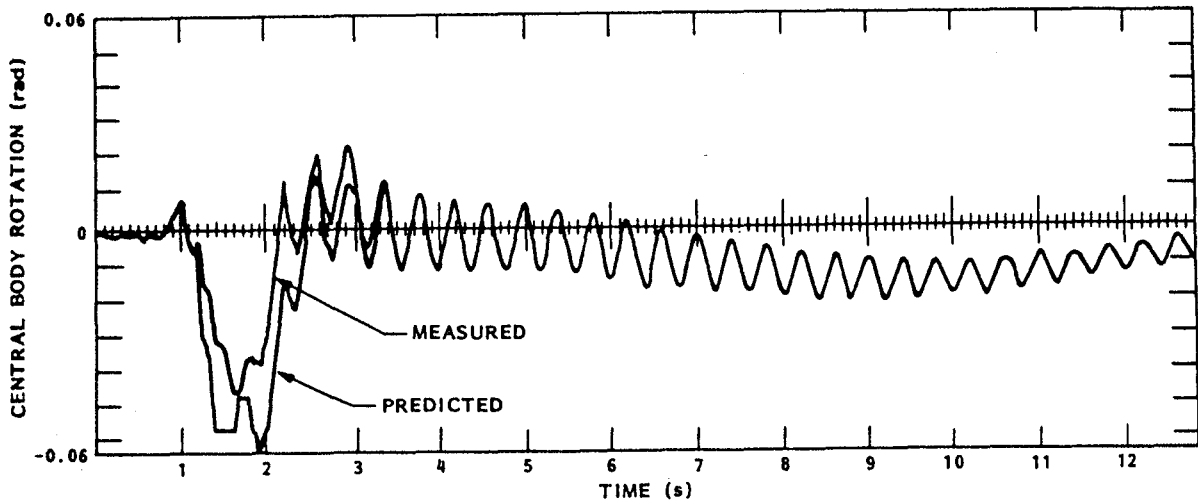


Fig. 5 Measured and Predicted Open-Loop Central Body Rotation (Response to 4-s Chirp)

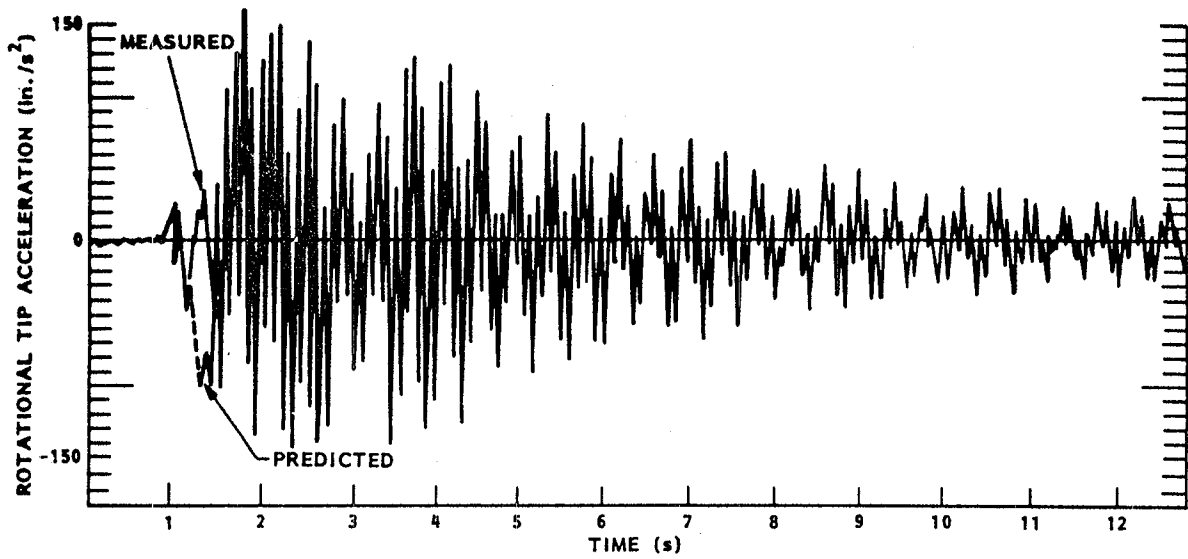


Fig. 6 Measured and Predicted Open-Loop Rotational Tip Acceleration (Response to 4-s Chirp)

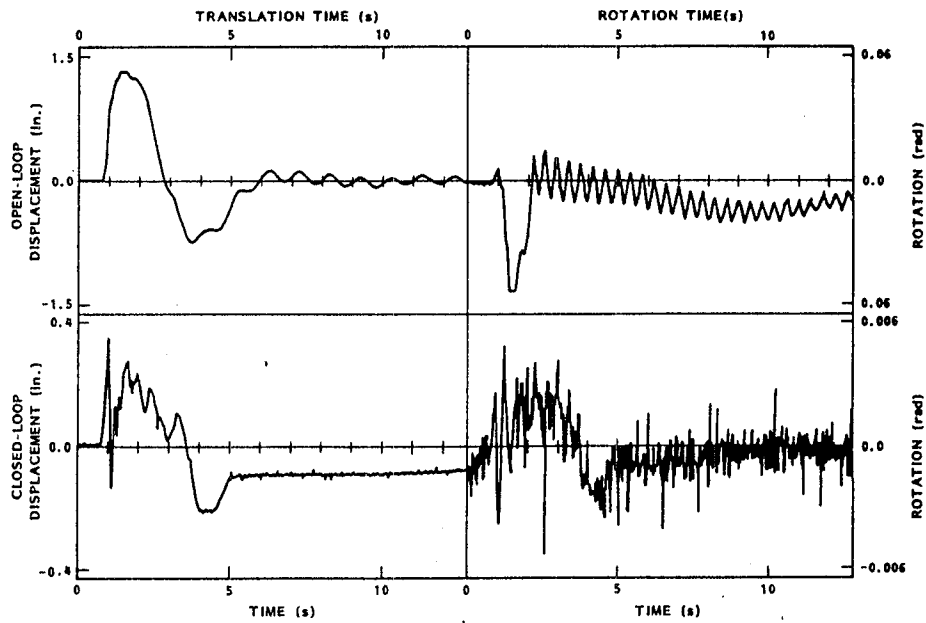


Fig. 7 Open- and Closed-Loop Central Body Measurements

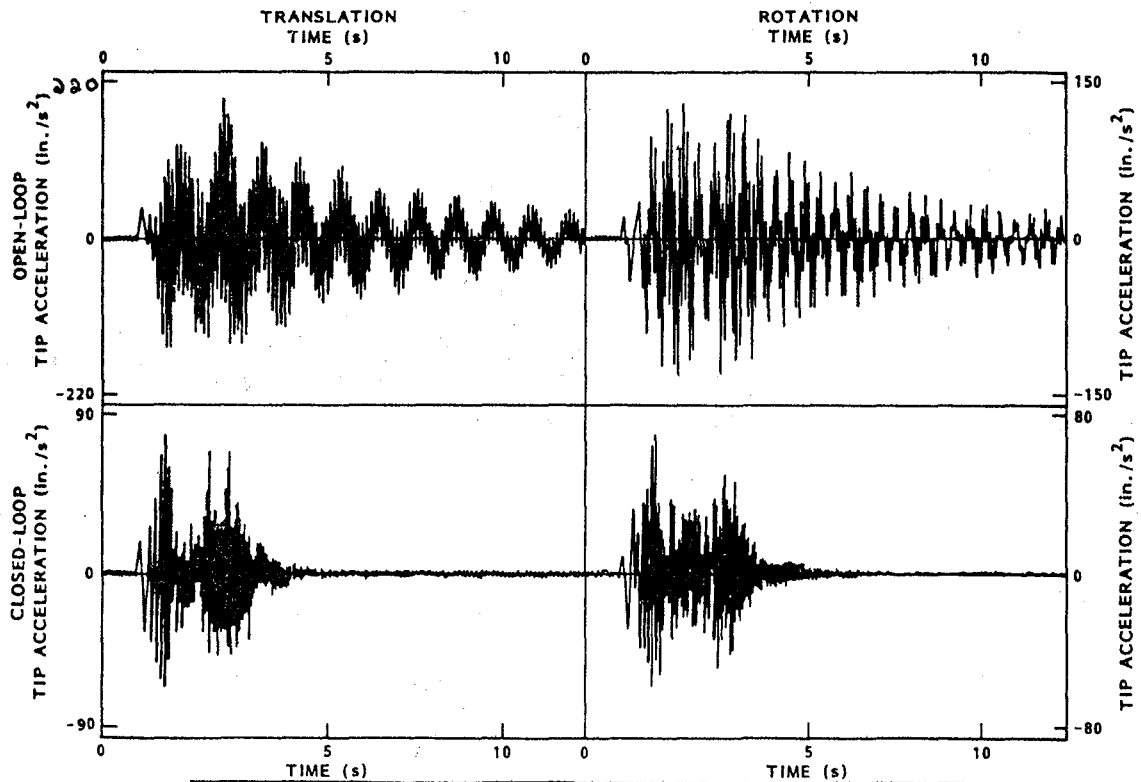


Fig. 8 Open- and Closed-Loop Tip Acceleration Measurements

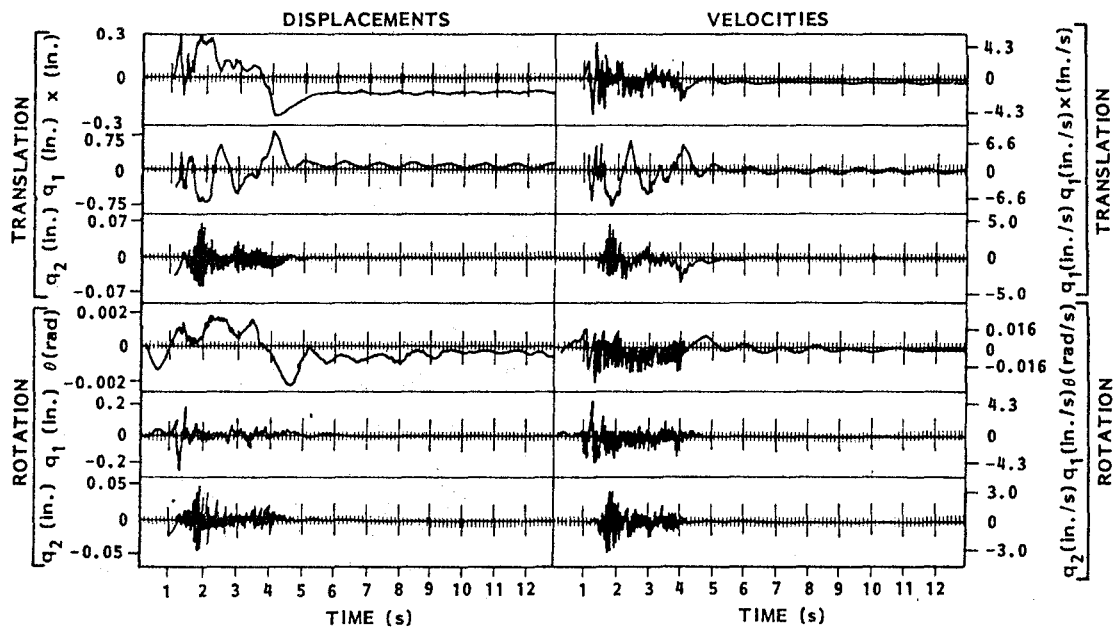


Fig. 9 Closed-Loop Kalman Filter Output (Response to 4-s Chirp)

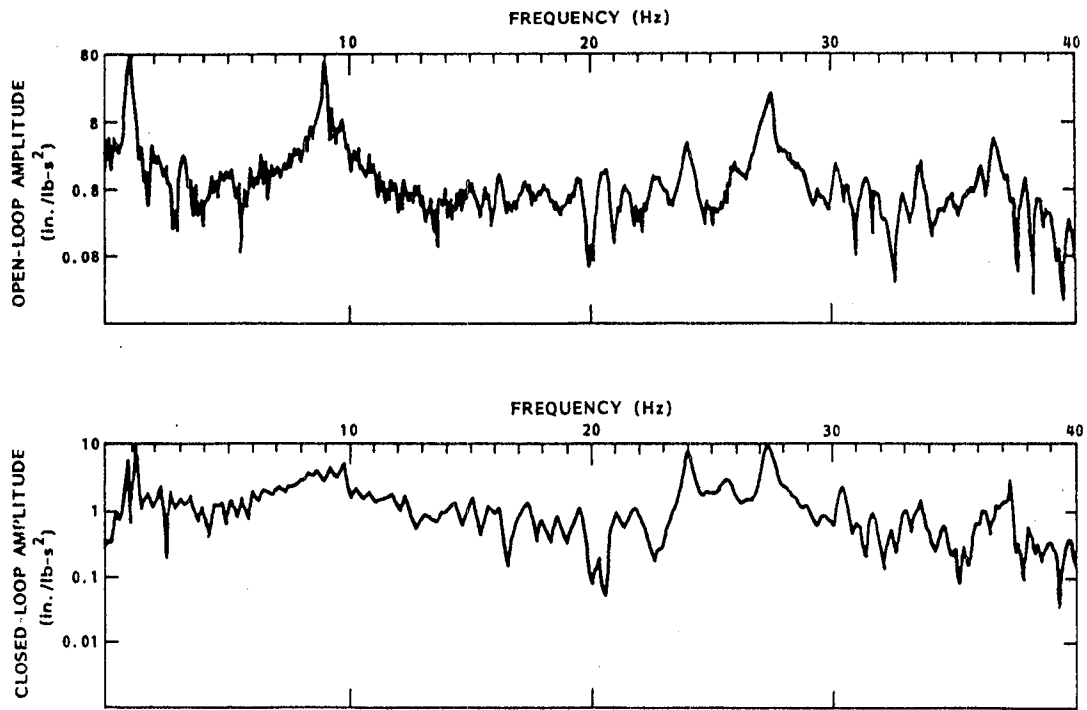


Fig. 10 Open- and Closed-Loop Transfer Functions; Translational Tip Acceleration/Input Chirp

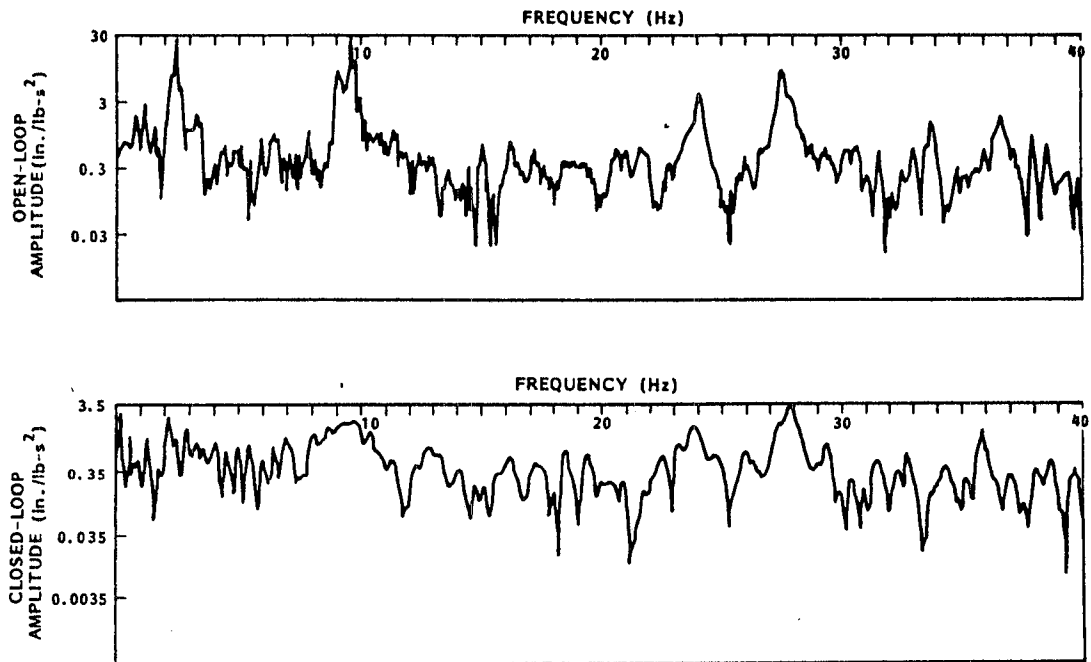


Fig. 11 Open- and Closed-Loop Transfer Functions; Rotational Tip Acceleration/Input Chirp

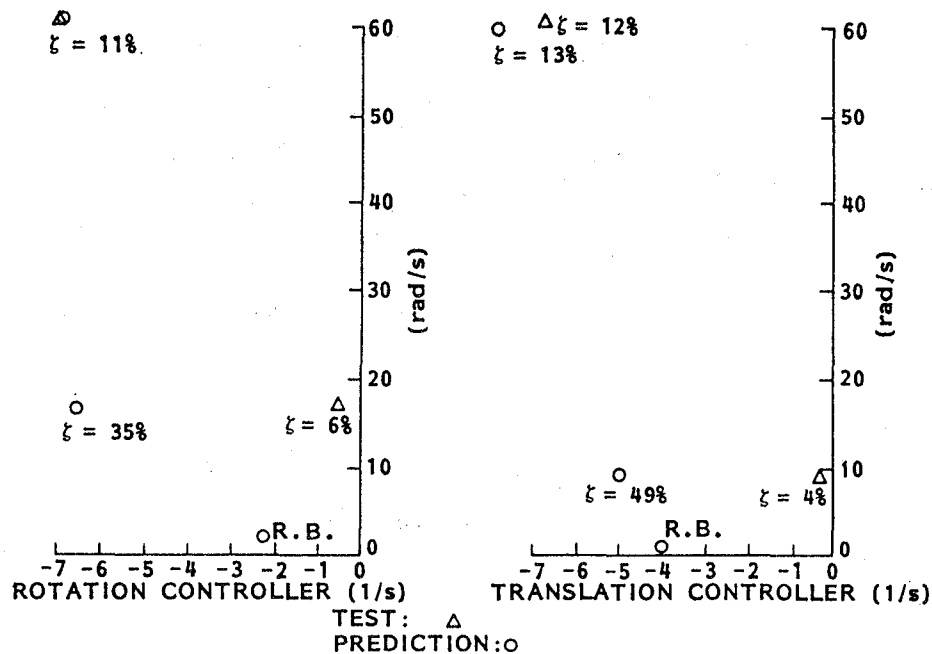


Fig. 12 Closed-Loop Pole Location; Predicted Versus Test

The damping was measured by fitting second order models to the transfer function. The closed-loop was roughly 4 percent for the first mode (versus 0.29 percent open-loop) and 11 percent for the second mode (versus 0.54 percent open-loop). For the rotation controller, the first and second modes (2.6 and 9.8 Hz) were also reduced below the level of the third mode (28 Hz). Again, the ratio of the reduced amplitude was proportional to the increase in damping. The first mode closed-loop damping was roughly 6 percent (versus 0.33 percent open-loop), and the second mode was 12 percent (versus 0.3 percent open-loop).

The damping measured from test data does not agree with the analytically predicted pole locations shown in Tables 2 and 3. The predictions for the second mode behaviour were reasonably close, but the first mode predictions were quite inaccurate. These differences are dramatically illustrated by the charts in Fig. 12.

Figure 13 shows the result of a deliberate attempt to provoke the phenomena commonly known as spillover. A new control system was generated by reducing the weight on the translation control by a factor of one hundred from that given in Table 2. The analysis predicted that this controller would cause the first unmodeled mode (at 29 Hz) to go unstable. Test results given in Fig. 13 demonstrate that indeed something did go unstable. The frequency domain transfer function in Fig. 14 confirms that it was the 29 Hz mode which dominated the instability.

Finally, two quick test runs were made, more as demonstrations to suggest further work than to prove any point in themselves. The first was a demonstration of a low sample rate Kalman filter; it ran at 20 Hz while

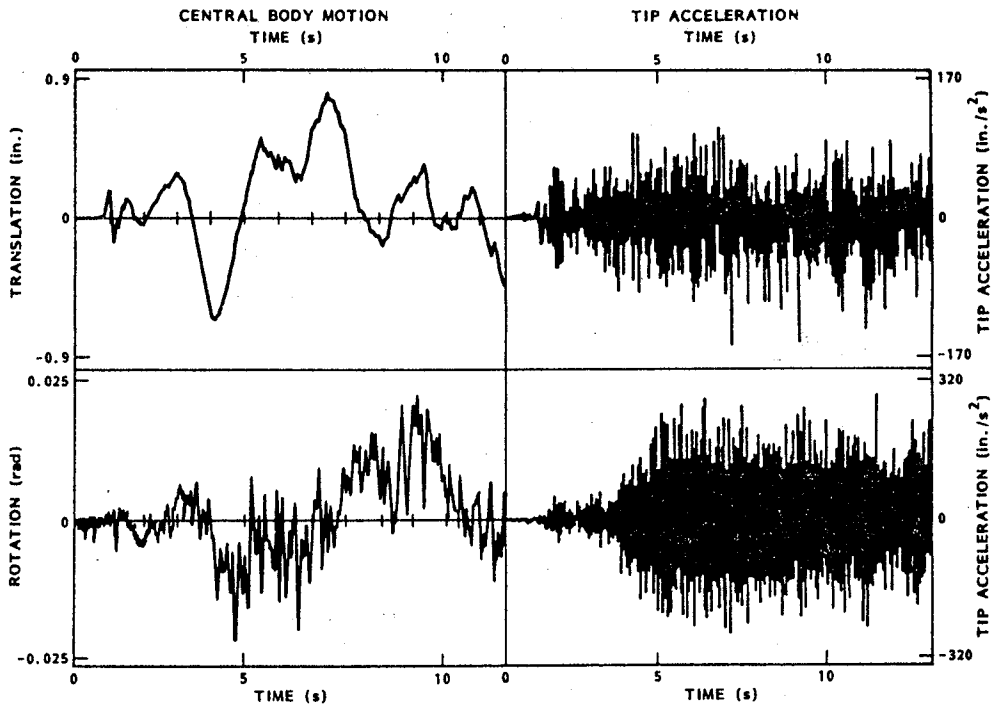


Fig. 13 Measurements for Case With Provoked Spillover

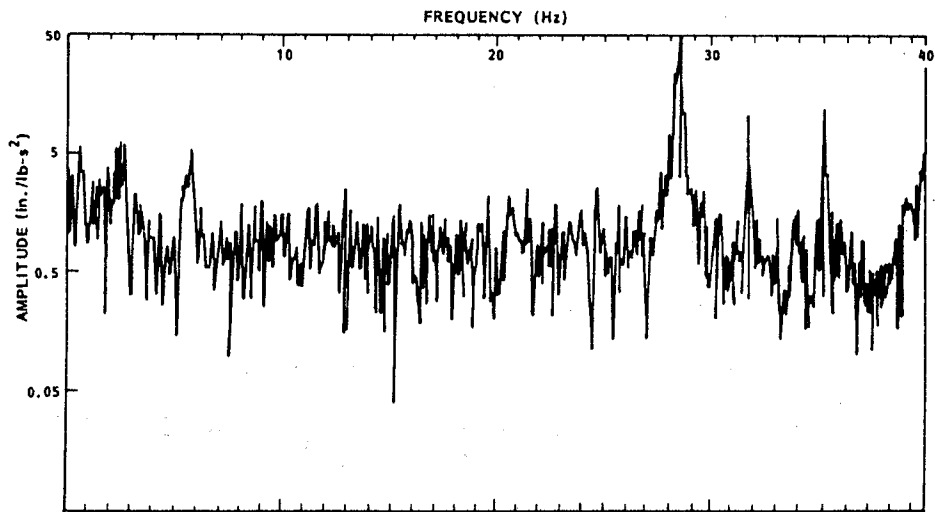


Fig. 14 Transfer Function; Spillover Case Rotational Tip Acceleration/ Input Chirp

estimating behavior up to 10 Hz. The results were not spectacular, but they are shown in Fig. 15. It shows a comparison of the filter prediction (z) with the actual measurement of the central body rotation. Theory suggests that the filters should work at even lower frequencies, but we were unable to make this happen in the test.

The last figure, Fig. 16 shows a test devised in response to criticisms claiming that the optimal control theory is too sensitive to knowledge of the system parameters. A two pound weight was removed from one of the tips of the flexible beam. This destroyed the symmetry of the TOYSAT, and changed its rotational inertia by 70 percent. Yet the control system designed to work on the original system did not do badly, as the figure shows. Admittedly, this is not a rigorous test of robustness, and there are some parameters that the control system must know very accurately in order to function properly. However, it is a dramatic exhibition of the control system working despite a massive perturbation.

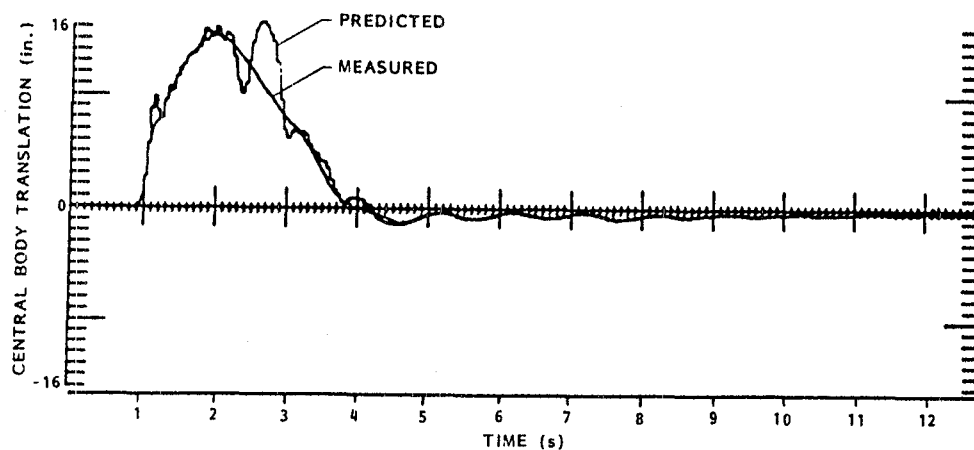


Fig. 15 Measured and Predicted Open-Loop Central Body Rotation for a 20 Hz Sample Rate Kalman Filter

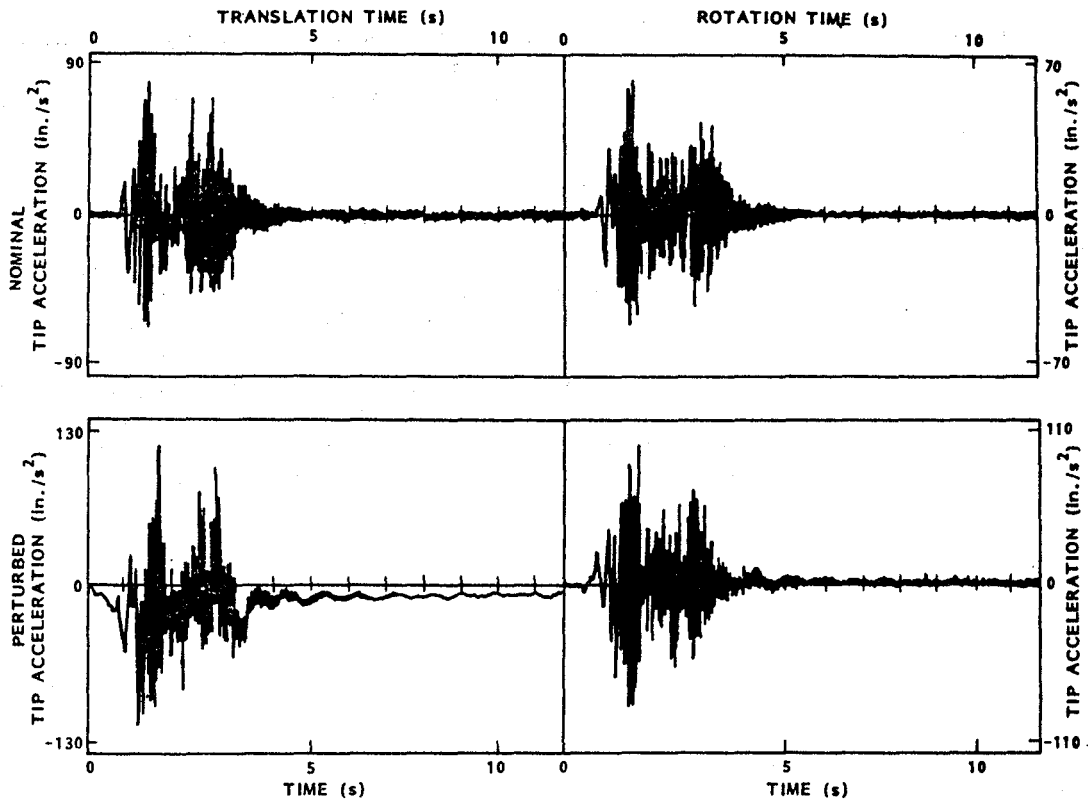


Fig. 16 Measured Tip Acceleration for Two Closed-Loop Tests, One With Nominal Configuration, One With One 2-lb Tip Mass Removed

Conclusion. Long after concluding the testing, we found an analytical "oversight" which could very well have caused the discrepancy between test and prediction of the lowest bending mode (Fig. 12). Not mentioned in the filter synthesis was what we used as noise statistics to get the gains for the filter is Eq. 7. It's rather straight forward to obtain the state covariance as

$$Q_d - \phi(t) Q_c H_2^T L^T - L H_2 Q_c \phi^T(T) + L H_2 Q_c H_2^T L^T + L R L^T$$

However the measurement covariance should be taken as

$$\frac{1}{\Delta t} (H_2 Q H_2^T + R_c)$$

where Δt is the sample time.

We had carelessly taken it as

$$\frac{1}{\Delta t} H_2 Q H_2^T + R$$

until Herb Rauch corrected our error.

The result of choosing the latter value is that the lower frequency modes will rely excessively on the accelerometer measurement to the exclusion of the position measurements. Thus, two integration constants are lost (or two poles are trapped at the origin). This is particularly disastrous for the lower frequency modes, and could easily have caused the discrepancy between the predicted lapping result and that obtained by test. A further correction is that the right hand side of Eq. 8 should be preceded by a $1/2$. But this has little effect on the outcome.

This Page Intentionally Left Blank

LARGE SPACE STRUCTURE MODEL REDUCTION AND CONTROL SYSTEM DESIGN BASED UPON ACTUATOR AND SENSOR INFLUENCE FUNCTIONS

Y. Yam, J.H. Lang, T.L. Johnson, S. Shih, and D.H. Staelin, Research Laboratory of Electronics, Massachusetts Institute of Technology
Cambridge, MA 02139

ABSTRACT

A model reduction procedure based on aggregation with respect to sensor and actuator influences rather than modes is presented for large systems of coupled second-order differential equations. Perturbation expressions which can predict the effects of spillover on both the aggregated and residual states are derived. These expressions lead to the development of control system design constraints which are sufficient to guarantee, to within the validity of the perturbations, that the residual states are not destabilized by control systems designed from the reduced model. A numerical example is provided to illustrate the application of the aggregation and control system design method.

INTRODUCTION

The model reduction issue for large space structures is particularly acute because model reduction is essential for easy finite-dimensional control system design, yet its use introduces the possibility of inadvertent system destabilization. Ordinary methods of model truncation result in control energy being coupled to the neglected system through spillover. This makes a priori performance estimation difficult. Furthermore, the control gains enter the coupling coefficients so that the control system design and evaluation processes must be iterated. By contrast, the model reduction method presented here, based on aggregation with respect to sensor and actuator influence functions rather than the system dynamic matrix, results in spillover coupling that is independent of the control system. As a consequence, the effect of spillover can be more readily predicted and is done here using perturbation theory.

Aggregation with respect to sensor and actuator influence functions was developed for first-order systems by Johnson and Lin [1]. In this paper, the method is applied to systems in second-order form which are representative of large space structures. The use of perturbation theory to estimate pole shifts due to spillover has been developed by Balas [2] and Lang [3]. However, their expressions involve the controller gains in a way which is more difficult to use for design purposes than the expressions presented here. Aubrun [4] applied perturbation theory to evaluate the effects of small control gains on stability. In the limit of small control gains and small spillover, his approximation agrees with the one given in this paper.

The present model reduction procedure has numerical advantages. Further, it allows the perturbation results to be extended in special cases to yield control system design constraints sufficient to guarantee, to within the validity of the perturbations, the non-destabilization of the residual system.

Accordingly, a control system should be designed to produce acceptable aggregated system behavior, and to satisfy the residual-system stability conditions. The design of such control systems is more complex. The compensating advantage is that more reliable performance estimates can be obtained.

AGGREGATION OF LSS MODELS

In modal analysis, the dynamic model for many large space structures (LSSs) can be written as

$$\ddot{\eta} + \beta \dot{\eta} + \Omega^2 \eta - D_e \eta = Bu \quad (1)$$

$$y = C\eta + D\dot{\eta} \quad (2)$$

where η is an n_η -vector of modal deflections, u is an n_u -vector of control forces and y is an n_y -vector of modal deflections and velocities. The matrices β and Ω^2 are assumed to satisfy

$$\beta = \text{diag}[\beta, \dots, \beta]; \quad \Omega^2 = \text{diag}[\omega_1^2, \dots, \omega_{n_\eta}^2] \quad (3)$$

where β is a uniform modal damping coefficient, and $\omega_i^2 > 0$, $i = 1, \dots, n_\eta$ are the squared modal frequencies. The matrix D_e represents the destabilizing forces in the system, and is assumed here to be of the form $D_e = \text{diag}[d, \dots, d]$. A general D_e can actually be put in a form readily treated with the present analysis. The ability to handle open-loop unstable systems is important to certain LSSs [5]. The open loop poles of the system (1) are

$$\rho_i^\pm = -\frac{\beta}{2} \pm \sqrt{\left(\frac{\beta}{2}\right)^2 + d - \omega_i^2} \quad i = 1, \dots, n_\eta \quad (4)$$

Let

$$C = \Pi_{CB} B^T + \tilde{C} \quad \tilde{C} \cdot B = 0 \quad (5)$$

$$D = \Pi_{DB} B^T + \Pi_{DC} \tilde{C} + \tilde{D} \quad \tilde{D} \cdot B = 0, \quad \tilde{D} \cdot \tilde{C}^T = 0 \quad (6)$$

be projection decompositions of C along B^T , and D along B^T and \tilde{C} , where a superscript T denotes algebraic transposition. Assuming \tilde{C} and \tilde{D} are of full rank, the partitioned matrix

$$[B \quad \tilde{C}^T \quad \tilde{D}^T] = \begin{bmatrix} B_a & \tilde{C}_a^T & \tilde{D}_a^T \\ B_r & \tilde{C}_r^T & \tilde{D}_r^T \end{bmatrix} = \begin{bmatrix} E_a \\ E_r \end{bmatrix} \quad (7)$$

can be formed where E_a is $n_a \times n_a$ and E_r is $n_r \times n_r$, $n_a = n_u + 2n_y$, and $n_r = n_\eta - n_a$. If \tilde{C} and \tilde{D} are not of full rank, only their significant and independent rows are retained and n_a can be reduced. \tilde{C} represents the component of displacement measurement which is not collocated with the actuators, and \tilde{D} represents the component of velocity measurement which is not collocated with either the actuators or displacement sensors. Next, let the ordering of the modes in (1) be such that E_a is invertible. In this case, it is possible to define the similarity transformation U such that

$$U = \begin{bmatrix} E_a^T & E_a^T S^T \\ -S & I \end{bmatrix} \quad (8)$$

with

$$U^{-1} = U^T (UU^T)^{-1} = \begin{bmatrix} E_a & -S^T \\ S E_a & I \end{bmatrix} \begin{bmatrix} M_a^{-1} & 0 \\ 0 & M_r^{-1} \end{bmatrix}$$

where

$$M_a = E_a^T (I + S^T S) E_a = \begin{bmatrix} B^T B & 0 & 0 \\ 0 & \tilde{C} \tilde{C}^T & 0 \\ 0 & 0 & \tilde{D} \tilde{D}^T \end{bmatrix}$$

$$M_r = (I + S S^T)$$

$$S \equiv E_r E_a^{-1}$$

Here, S is termed the spillover matrix.

Defining $\bar{\eta} = U\eta$, the original system of (1) and (2) can be transformed into a particularly favorable form.

$$\ddot{\bar{\eta}} + \beta I \dot{\bar{\eta}} + \bar{\Omega}^2 \bar{\eta} - d I \dot{\bar{\eta}} = \bar{B} u \quad (9)$$

$$y = \bar{C} \bar{\eta} + \bar{D} \dot{\bar{\eta}} \quad (10)$$

where

$$\bar{\Omega}^2 = \begin{bmatrix} \bar{\Omega}_{aa}^2 & \bar{\Omega}_{ar}^2 \\ \bar{\Omega}_{ra}^2 & \bar{\Omega}_{rr}^2 \end{bmatrix} = \begin{bmatrix} E_a^T (\Omega_1^2 + S^T \Omega_2^2 S) E_a M_a^{-1} & E_a^T (-\Omega_1^2 S^T + S^T \Omega_2^2) M_r^{-1} \\ (-S \Omega_1^2 + \Omega_2^2 S) E_a M_a^{-1} & (\Omega_2^2 + S \Omega_1^2 S^T) M_r^{-1} \end{bmatrix} \quad (11)$$

$$\bar{B} = \begin{bmatrix} \bar{B}_a \\ 0 \end{bmatrix} \quad \bar{B}_a = \begin{bmatrix} B^T B \\ 0 \\ 0 \end{bmatrix}$$

$$\bar{C} = [\bar{C}_a \quad 0] \quad \bar{C}_a = [\Pi_{CB} \quad I \quad 0]$$

$$\bar{D} = [\bar{D}_a \quad 0] \quad \bar{D}_a = [\Pi_{DB} \quad \Pi_{D\tilde{C}} \quad I]$$

with Ω_1^2 and Ω_2^2 given by

$$\Omega_1^2 = \text{diag}[\omega_1^2 \cdots \omega_{n_a}^2]; \quad \Omega_2^2 = \text{diag}[\omega_{n_a+1}^2, \cdots, \omega_{n_\eta}^2].$$

If $\bar{\eta}$ is partitioned such that $\bar{\eta} = \begin{bmatrix} \bar{\eta}_a \\ \bar{\eta}_r \end{bmatrix}$, where $\bar{\eta}_a : n_a \times 1$ and $\bar{\eta}_r : n_r \times 1$, then the aggregated and residual models associated with the transformation U are

$$\ddot{\bar{\eta}}_a + \beta I \dot{\bar{\eta}}_a + \bar{\Omega}_{aa}^2 \bar{\eta}_a - d I \bar{\eta}_a = \bar{B}_a u \quad (12)$$

$$y = \bar{C}_a \bar{\eta}_a + \bar{D}_a \dot{\bar{\eta}}_a \quad (13)$$

and

$$\ddot{\bar{\eta}}_r + \beta I \dot{\bar{\eta}}_r + \bar{\Omega}_{rr}^2 \bar{\eta}_r - d I \bar{\eta}_r = 0. \quad (14)$$

Note that spillover has been transformed from control and observation spillover, as in modal truncation, into the present form of dynamic coupling matrices, $\bar{\Omega}_{ra}^2$ and $\bar{\Omega}_{ar}^2$, between the aggregated and residual models. Any other aggregation procedures will generally result in spillover appearing in both forms. The set of states included in the aggregated model is solely a reflection of the sensor and actuator influences. A reasonable design of sensors and actuators, for instance, should effectively sense and excite only certain critical modes. As a result, the aggregated states would be primarily composed of the critical modes and the spillover matrix S would be numerically small.

Denote the eigenvalues and left and right eigenvectors of $\bar{\Omega}_{aa}^2$ and $\bar{\Omega}_{rr}^2$ as

$\lambda_{a_i}^2, \ell_{a_i}, \gamma_{a_i}, i = 1, \dots, n_a$ and $\lambda_{r_i}^2, \ell_{r_i}, \gamma_{r_i}, i = n_a + 1, \dots, n_\eta$, respectively. Then, the open loop poles of the aggregated and residual model are

$$\rho_{a_i}^\pm = -\frac{\beta}{2} \pm \sqrt{\left(\frac{\beta}{2}\right)^2 + d - \lambda_{a_i}^2} \quad i = 1, \dots, n_a \quad (15)$$

$$\rho_{r_i}^\pm = -\frac{\beta}{2} \pm \sqrt{\left(\frac{\beta}{2}\right)^2 + d - \lambda_{r_i}^2} \quad i = n_a + 1, \dots, n_\eta \quad (16)$$

The sensors and actuators should be so designed that the $\rho_{r_i}^\pm$ are stable. Note that in this case the margin of stability for the residual states is $\frac{\beta}{2}$, the same as that for stable $\rho_{a_i}^\pm$.

Consider a compensator for (1) and (2) having the form

$$\begin{aligned} \dot{z} &= Fz + Gy \\ u &= Hz + Ky \end{aligned} \quad (17)$$

so that

$$\frac{d}{dt} \begin{bmatrix} z \\ \eta_a \\ \dot{\eta}_a \\ \eta_r \\ \dot{\eta}_r \end{bmatrix} = \begin{bmatrix} \hat{A}_{aa} & \hat{A}_{ar} \\ \hat{A}_{ra} & \hat{A}_{rr} \end{bmatrix} \begin{bmatrix} z \\ \eta_a \\ \dot{\eta}_a \\ \eta_r \\ \dot{\eta}_r \end{bmatrix} \quad (18)$$

where

$$\hat{A}_{aa} = \begin{bmatrix} F & \overline{GC}_a & \overline{GD}_a \\ 0 & 0 & I \\ \overline{B}_a H & dI - \overline{\Omega}_{aa}^2 + \overline{B}_a \overline{KC}_a & -\beta I + \overline{B}_a \overline{KD}_a \end{bmatrix} \quad (19a)$$

$$\hat{A}_{ar} = \begin{bmatrix} 0 & 0 \\ 0 & 0 \\ -\overline{\Omega}_{ar}^2 & 0 \end{bmatrix} \quad (19b)$$

$$\hat{A}_{ra} = \begin{bmatrix} 0 & 0 & 0 \\ 0 & -\bar{\Omega}_{ra}^2 & 0 \end{bmatrix} \quad (19c)$$

$$\hat{A}_{rr} = \begin{bmatrix} 0 & I \\ dI - \bar{\Omega}_{rr}^2 & -\beta I \end{bmatrix} \quad (19d)$$

Denote the i th eigenvalues and left and right eigenvectors of \hat{A}_{aa} as ζ_{a_i} , \mathcal{L}_{a_i} , \mathcal{R}_{a_i} . Note that \hat{A}_{aa} is the closed loop dynamic matrix of compensator (17) applied directly to aggregated model (12)-(13) and \hat{A}_{rr} is the untouched residual model dynamic matrix. The compensator thus has a direct effect on the aggregated model and an indirect effect on \hat{A}_{rr} through the coupling matrices \hat{A}_{ar} and \hat{A}_{ra} . The effect of this coupling on the original eigenvalues of \hat{A}_{aa} and \hat{A}_{rr} can be approximated by perturbation techniques, see Appendix A. The original eigenvalues of \hat{A}_{aa} and \hat{A}_{rr} , which are ζ_{a_i} and $\rho_{r_i}^{\pm}$, are shifted by $\Delta\zeta_{a_i}^{(2)}$ and $\Delta\rho_{r_i}^{\pm(2)}$, respectively, where the superscript 2 denotes that the shifts are second order in the elements of the coupling matrices. The terms $\Delta\zeta_{a_i}^{(2)}$ and $\Delta\rho_{r_i}^{\pm(2)}$ are given by

$$\Delta\zeta_{a_i}^{(2)} = -\mathcal{L}_{a_i} \begin{bmatrix} 0 \\ 0 \\ -\bar{\Omega}_{ar}^2 \end{bmatrix} [dI - \bar{\Omega}_{rr}^2 - \zeta_{a_i}^2 I]^{-1} [0 \quad -\bar{\Omega}_{ra}^2 \quad 0] \mathcal{R}_{a_i} \quad (20)$$

$$\Delta\rho_{r_i}^{\pm(2)} = -\frac{1}{(\beta + 2\rho_{r_i}^{\pm})} \mathcal{L}_{r_i} \bar{\Omega}_{ra}^2 [\lambda_{r_i}^2 I - \bar{\Omega}_{aa}^2 + \bar{B}_a \tilde{K}(\rho_{r_i}^{\pm}) \tilde{Q}(\rho_{r_i}^{\pm})]^{-1} \bar{\Omega}_{ar}^2 \gamma_{r_i} \quad (21)$$

where
$$\tilde{K}(\rho_{r_i}^{\pm}) = K - H(F - \rho_{r_i}^{\pm} I)^{-1} G \quad (22)$$

$$\tilde{Q}(\rho_{r_i}^{\pm}) = \bar{C}_a + \rho_{r_i}^{\pm} \bar{D}_a. \quad (23)$$

The terms $\zeta_{a_i}^c \equiv \zeta_{a_i} + \Delta\zeta_{a_i}^{(2)}$, $\rho_{r_i}^{\pm c} \equiv \rho_{r_i}^{\pm} + \Delta\rho_{r_i}^{\pm(2)}$ are then the approximated closed loop poles of the overall system. They would be an adequate approximation of the actual values if the coupling between \hat{A}_{aa} and \hat{A}_{rr} were weak. Such a weak coupling condition can be achieved by designing a reasonably small S and by shifting the poles of \hat{A}_{aa} away from those of \hat{A}_{rr} by means of feedback.

Equations (20) and (21) do not conveniently allow a quick estimation of the effect of spillover because they contain quantities as Ω_{ar}^2 , ℓ_{r_i} , λ_{r_i} , etc. which require appreciable computation. For simplified expressions, one can retain in (20) and (21) only terms quadratic in S; see Appendix B. In this case aggregated and residual pole placement is given by

$$\zeta_{a_i}^{S^2} = \zeta_{a_i} - \mathcal{L}_{a_i} \begin{bmatrix} 0 \\ 0 \\ E_a (-\Omega_1^2 S^T + S^T \Omega_2^2) \end{bmatrix} [dI - \Omega_2^2 - \zeta_{a_i}^2 I]^{-1} [0 \quad (-S\Omega_1^2 + \Omega_2^2 S)(E_a^T)^{-1} \quad 0] \mathcal{R}_{a_i} \quad (24)$$

$$\rho_{r_i}^{\pm} = \rho_i^{\pm} + \frac{1}{(\beta + 2\rho_i^{\pm})} S_{r_i} E_a \begin{bmatrix} I \\ 0 \\ 0 \end{bmatrix} \tilde{K}(\rho_i^{\pm}) \tilde{Q}(\rho_i^{\pm}) E_a^T \left[I + (\omega_i^2 I - \Omega_1^2)^{-1} E_a \begin{bmatrix} I \\ 0 \\ 0 \end{bmatrix} \tilde{K}(\rho_i^{\pm}) \tilde{Q}(\rho_i^{\pm}) E_a^T \right]^{-1} S_{r_i}^T \quad (25)$$

where S_{r_i} denotes the i th row of S and the superscript S^2 indicates that (24) and (25) retain only terms quadratic in S. Equations (24) and (25) contain only readily available quantities such as Ω_1^2 , ρ_i^{\pm} , etc. and yield quick estimates of the effect of spillover. Furthermore, since the next higher order are terms proportional to S^4 , they can come quite close to equations (22) and (23) in value for spillover that is not too strong.

COLLOCATED SENSORS AND ACTUATORS

In the case of collocated sensors and actuators, $C = \Pi_{CB} B^T$ and $D = \Pi_{DB} B^T$, so that $B = \begin{bmatrix} E_a \\ E_r \end{bmatrix}$. Only n_u independent columns are used in forming U. Since

$$M_r \bar{\Omega}_{rr}^2 = \bar{\Omega}_{rr}^2 M_r$$

it follows from the symmetry of Ω_1^2 and Ω_2^2 that

$$\gamma_{r_i} = M_r \ell_{r_i}^T \quad (26)$$

In this case, (21) can be solved for the real part of $\Delta\rho_{r_i}^{\pm(2)}$, giving

$$\text{Real}(\Delta\rho_{r_i}^{\pm(2)}) = \text{Real} \frac{1}{(\beta + 2\rho_i^{\pm})} \Gamma_i^{\pm*} \tilde{K}(\rho_i^{\pm}) \tilde{Q}(\rho_i^{\pm}) \Gamma_i^{\pm} \quad (27)$$

where

$$\Gamma_i^{\pm} \equiv B^T B [\lambda_{r_i}^2 M_a - E_a^T (\Omega_1^2 + S^T \Omega_2^2 S) E_a + B^T B \tilde{K}(\rho_i^{\pm}) \tilde{Q}(\rho_i^{\pm}) M_a]^{-1} E_a (-\Omega_1^2 S^T + S^T \Omega_2^2) \ell_{r_i}^T \quad (28)$$

and a superscript * denotes complex conjugation.

It is a concern in designing F, G, H, K that $\rho_{r_i}^{\pm}$ not be destabilized. Suppose that F has distinct roots and that T is its transformation to Jordan form.

$$F = T \Xi T^{-1} \quad (29)$$

where $\Xi = \text{diag}[\xi_1, \dots, \xi_{n_z}]$. Then sufficient conditions for the shift (27) to be non-positive can be derived for several feedback forms.

For displacement measurement,

$$\begin{aligned} (1) \quad & K\Pi_{CB} \text{ be symmetric} \\ (2) \quad & (HT)^* = (T^{-1}G\Pi_{CB}) \quad (30) \\ (3) \quad & -\left|\frac{1}{2}(\beta + 2\rho_{r_i}^{\pm})\right| \leq \text{Im}(\xi_k) \leq \left|\frac{1}{2}(\beta + 2\rho_{r_i}^{\pm})\right| \quad \begin{array}{l} i = n_u + 1, \dots, n_\eta \\ k = 1, \dots, n_z \end{array} \end{aligned}$$

For velocity measurement,

$$\begin{aligned} (1) \quad & K\Pi_{DB} \text{ be symmetric and negative semi-definite, and either} \\ (2a) \quad & F, G, H = 0 \quad (31) \\ & \text{or} \\ (2b) \quad & (HT)^* = -(T^{-1}G\Pi_{DB}) \\ & \text{Re}(\xi_k) \leq -\frac{1}{2}\beta \quad k = 1, \dots, n_z \\ & -\left|\frac{1}{2}(\beta + 2\rho_{r_i}^{\pm})\right| \leq \text{Im}(\xi_k) \leq \left|\frac{1}{2}(\beta + 2\rho_{r_i}^{\pm})\right| \quad \begin{array}{l} i = n_u + 1, \dots, n_\eta \\ k = 1, \dots, n_z \end{array} \end{aligned}$$

For displacement and velocity measurement,

$$\begin{aligned} (1) \quad & \Pi_{CB} = a\Pi_{DB} \quad \text{where } a \text{ is a scalar} \\ (2) \quad & K\Pi_{DB} \text{ be symmetric and negative semi-definite, and either} \\ (3a) \quad & F, G, H = 0 \quad (32) \\ & \text{or, if } a - \frac{\beta}{2} < 0, \\ (3b) \quad & (HT)^* = -(T^{-1}G\Pi_{DB}) \\ & \text{Re}(\xi_k) \leq -\frac{1}{2}\beta \quad k = 1, \dots, n_z \\ & -\left|\frac{1}{2}(\beta + 2\rho_{r_i}^{\pm})\right| \leq \text{Im}(\xi_k) \leq \left|\frac{1}{2}(\beta + 2\rho_{r_i}^{\pm})\right| \quad \begin{array}{l} i = n_u + 1, \dots, n_\eta \\ k = 1, \dots, n_z \end{array} \end{aligned}$$

It is interesting to observe that for displacement measurement, nonzero F, G, H, e.g. a velocity observer, are needed to introduce additional damping into the residual states. With velocity measurement, no additional dynamics are required. Because of (16), the condition

$$-\left|\frac{1}{2}(\beta + 2\rho_{r_i}^{\pm})\right| < \text{Im}(\xi_k) < \left|\frac{1}{2}(\beta + 2\rho_{r_i}^{\pm})\right| \quad \begin{array}{l} i = n_u + 1, \dots, n_\eta \\ k = 1, \dots, n_z \end{array} \quad (33)$$

requires only the knowledge of the smallest eigenvalues of $\bar{\Omega}_{rr}^2$. The shift $\Delta\zeta_{a_i}^{(2)}$ usually generates less concern since the designed ζ_{a_i} should have a large margin of stability.

EXAMPLE

For the case of collocated sensors and actuators with the displacement measurement $y = B^T \Pi_{CB} = I$, choose F, G, H, K of the following form:

$$\begin{aligned} n_z &= n_u = n_a \\ F &= - \begin{bmatrix} \xi_1 & & & \\ & \ddots & & \\ & & \ddots & \\ & & & \xi_{n_z} \end{bmatrix} & \xi_i > 0 \text{ for } i=1, \dots, n_z \\ G &= \begin{bmatrix} g_1 & & & \\ & \ddots & & \\ & & \ddots & \\ & & & g_{n_z} \end{bmatrix} R_a^{-1} \\ H &= (R_a^T)^{-1} \begin{bmatrix} g_1 & & & \\ & \ddots & & \\ & & \ddots & \\ & & & g_{n_z} \end{bmatrix} \\ K &= -(R_a^T)^{-1} \begin{bmatrix} k_1 & & & \\ & \ddots & & \\ & & \ddots & \\ & & & k_{n_z} \end{bmatrix} R_a^{-1} \end{aligned} \quad (34)$$

where $R_a \equiv \text{columns}[\gamma_{a_1} \dots \gamma_{a_{n_u}}]$. Equation (34) satisfies the sufficient conditions (30) for displacement measurements. Substituting (34) into (19a), the eigenvalues of the resulting \hat{A}_{aa} can be seen to be the union of the eigenvalues of the matrices \hat{a}_{aa_i} $i = 1, \dots, n_u$, where

$$\hat{a}_{aa_i} = \begin{bmatrix} -\xi_i & g_i & 0 \\ 0 & 0 & 1 \\ g_i & d - \lambda_{a_i}^2 - k_i & -\beta \end{bmatrix}; \quad (35)$$

see Appendix C.

The compensator of the form (34) affects different eigenmodes of the aggregated model independently so that ξ_i , g_i , and k_i can be separately designed for each i . Denote the three poles of \hat{a}_{aa_i} by $\rho_{a_i}^t$, $t = 0, +, -$, where 0 represents the real eigenvalue and + and - represent the complex conjugate pair. The necessary and sufficient conditions for $\rho_{a_i}^t$ to be stable are

$$g_i^2 + \xi_i(d - \lambda_{a_i}^2 - k_i) < 0 \quad (36)$$

which necessarily requires $(d - \lambda_{a_i}^2 - k_i) < 0$. With k_i so chosen, the following scaled quantities can be defined.

$$\tilde{\rho}_{a_i}^t = \frac{\rho_{a_i}^t}{|d - \lambda_{a_i}^2 - k_i|^{1/2}} \quad \tilde{\xi}_i = \frac{\xi_i}{|d - \lambda_{a_i}^2 - k_i|^{1/2}} \quad \tilde{g}_i = \frac{g_i}{|d - \lambda_{a_i}^2 - k_i|^{3/4}} \quad (37)$$

Figure 1 shows the eigenvalues $\tilde{\rho}_{a_i}^0$ and $\tilde{\rho}_{a_i}^+$ for different values of $\tilde{\xi}_i$ and \tilde{g}_i .

Only the case for $\beta = 0$ is shown since weak inherent damping typical of LSS systems would be swamped by the feedback.

The important result from the figure is that the eigenvalues of \hat{a}_{aa_i} , given by $\rho_{a_i}^t = |d - \lambda_{a_i}^2 - k_i|^{1/2} \tilde{\rho}_{a_i}^t$, hence those of \hat{A}_{aa} , are indeed on the left half plane and can in principle be pushed arbitrarily to the left by choosing an arbitrary large k_i . Such a compensator given by (34) would therefore stabilize the aggregated model, preserve the validity of the perturbation technique and guarantee the non-destabilization of the residual states.

As a numerical example, consider a vibrating string with fixed ends in the region $0 \leq r \leq 1$, with two collocated sensor and actuator pairs. For simplicity, the system model consists of 3 modes, includes only displacement measurement ($\Pi_{CB} = I$, $\Pi_{DB} = 0$), and exhibits a destabilizing mechanism. Thus,

$$\ddot{\eta} = - \begin{bmatrix} \pi^2 & 0 & 0 \\ 0 & 4\pi^2 & 0 \\ 0 & 0 & 9\pi^2 \end{bmatrix} \eta + d\dot{\eta} + \begin{bmatrix} b_{11} & b_{12} \\ b_{21} & b_{22} \\ b_{31} & b_{32} \end{bmatrix} u_o$$

$$y_o = \begin{bmatrix} b_{11} & b_{21} & b_{31} \\ b_{12} & b_{22} & b_{32} \end{bmatrix} \eta \quad (38)$$

where $b_{ij} = \sqrt{2} \int_0^1 f_j(r) \sin i\pi r dr$, $f_j(r)$ is the influence function of the j th sensor actuator pair, and $\sqrt{2} \sin i\pi r$ is the eigenfunction of the i th mode.

Defining the new control $u = \begin{bmatrix} b_{11} & b_{12} \\ b_{21} & b_{22} \end{bmatrix} u_o$ and the new measurement $y = \begin{bmatrix} b_{11} & b_{21} \\ b_{12} & b_{22} \end{bmatrix}^{-1} y_o$, (38) becomes

$$\ddot{\eta} = - \begin{bmatrix} \pi^2 & 0 & 0 \\ 0 & 4\pi^2 & 0 \\ 0 & 0 & 9\pi^2 \end{bmatrix} \eta + d\dot{\eta} + \begin{bmatrix} 1 & 0 \\ 0 & 1 \\ s_1 & s_2 \end{bmatrix} u \quad (39)$$

$$y = \begin{bmatrix} 1 & 0 & s_1 \\ 0 & 1 & s_2 \end{bmatrix} \eta$$

where $(s_1 s_2) = [b_{31} \quad b_{32}] \begin{bmatrix} b_{11} & b_{12} \\ b_{21} & b_{22} \end{bmatrix}^{-1}$. The aggregation transformation U is

$$U = \begin{bmatrix} 1 & 0 & s_1 \\ 0 & 1 & s_2 \\ -s_1 & -s_2 & 1 \end{bmatrix} \quad (40)$$

and the transformed system is given by

$$\ddot{\bar{\eta}} = - \bar{\Omega}^2 \bar{\eta} + d\dot{\bar{\eta}} + \bar{B}u \quad (41)$$

$$y = \bar{C} \bar{\eta}$$

where

$$\bar{\Omega}^2 = \frac{\pi^2}{(1 + s_1^2 + s_2^2)} \begin{bmatrix} 1 + 9s_1^2 + s_2^2 & 8s_1 s_2 & 8s_1 \\ 5s_1 s_2 & 4 + 4s_1^2 + 9s_2^2 & 5s_2 \\ 8s_1 + 3s_1 s_2^2 & 5s_2 - 3s_1^2 s_2 & 9 + s_1^2 + 4s_2^2 \end{bmatrix}$$

$$\bar{B} = \begin{bmatrix} 1 + s_1^2 & s_1 s_2 \\ s_1 s_2 & 1 + s_2^2 \\ 0 & 0 \end{bmatrix}$$

$$\bar{C} = \begin{bmatrix} 1 & 0 & 0 \\ 0 & 1 & 0 \end{bmatrix}$$

For this example, $d = 2\pi^2$ so that the lowest mode in the system is destabilized. Choose the compensator F, G, H, and K as in (34). Let $k_1 = k_2 = k\pi^2$ be the only undetermined compensator parameter and

$$\tilde{\xi}_1 = \tilde{\xi}_2 = 1.4, \quad \tilde{g}_1 = \tilde{g}_2 = 1.0412.$$

Then from Fig. 1, with $\dot{i} = \sqrt{-1}$,

$$\tilde{\rho}_{a_1}^0 = \tilde{\rho}_{a_2}^0 = -0.60954 \quad \tilde{\rho}_{a_1}^\pm = \tilde{\rho}_{a_2}^\pm = -0.39523 \pm 0.60164 \dot{i}.$$

The eigenvalues of the closed loop aggregated matrix \hat{A}_{aa} are thus, $t=0,+,-$

$$\rho_{a_1}^t = \tilde{\rho}_{a_1}^t |2\pi^2 - \lambda_{a_1}^2 - k\pi^2|^{1/2} \quad \text{and} \quad \rho_{a_2}^t = \tilde{\rho}_{a_2}^t |2\pi^2 - \lambda_{a_2}^2 - k\pi^2|^{1/2}$$

and the eigenvalues of the residual model

$$\rho_r^\pm = \pm \dot{i} \pi \sqrt{\frac{9 + S_1^2 + S_2^2}{1 + S_1^2 + S_2^2}}$$

Due to the nonzero coupling matrices \hat{A}_{ar} and \hat{A}_{ra} , these eigenvalues will be shifted. Figures 2 through 5 show the designed poles $\rho_{a_1}^t$, $\rho_{r_3}^+$, the perturbation corrected poles $\rho_{a_1}^{tc}$, $\rho_{r_3}^{+c}$ and $\rho_{a_1}^{tS^2}$, $\rho_{r_3}^{+S^2}$ for different values of k for the cases of weak spillover, $S_1 = S_2 = 0.2$, and strong spillover, $S_1 = S_2 = 0.8$. For comparison, the exact value of the corresponding poles are also included. On comparison, several points are noted. First, as k is increased, the validity of the perturbation result is enhanced due to the growing distance between the poles of \hat{A}_{aa} and \hat{A}_{rr} , this is most apparent in Figs. 4 and 5. Second, as expected, the validity of the perturbation technique increases with decreasing spillover. However, the damping introduced to the residual states increases as S_1^2 and S_2^2 . Third, for very large k , the beneficial spillover damping in the residual states is reduced. This is again a result of the increasing distance between the poles of \hat{A}_{aa} and \hat{A}_{rr} . Fourth, given their ease of evaluation, the $\rho_{a_1}^{tS^2}$ and $\rho_{r_3}^{+S^2}$ expressions yield quite reasonable estimates of the exact values, especially for the weak spillover case. Finally, and most importantly, it is indeed possible, as illustrated by this example, to have a reduced order compensator designed based on the aggregated model and still guarantee the stability of the overall system.

CONCLUSIONS

Spillover cannot be eliminated by aggregation procedures. The present method merely transforms control and observation spillover into the form of dynamic coupling matrices. The effect of spillover in this form can then be more readily approximated using perturbation techniques. Two sets of perturbation-corrected pole shifts were derived. The first set gives very close approximation to reality if the validity of the perturbation technique is preserved. Further, it yields sufficient conditions that guarantee the non-destabilization of the residual states. The second set of pole shifts, obtained by truncating the first set to retain only quadratic terms in the spillover matrix S , enables quick estimations of the pole shifts.

As illustrated by a numerical example for the collocated sensor and actuator case with displacement measurement, a reduced order compensator which yields

stability for the overall system can be obtained adopting the present approach. Damping is indeed introduced to the residual states through spillover. The amount of damping introduced is proportional to spillover squared. Thus proper actuator and sensor design should result in spillover values such that relatively large damping can be introduced while the validity of the perturbation technique at the designed control gains is still maintained. Spillover need not always be minimized.

The present method yields an aggregated model order related to the number of sensors and actuators. Further control of aggregation model order can be obtained using combined (synthetic) sensors and actuators in the design procedure. This topic is presently under study.

The authors wish to thank the Lockheed Missiles and Space Company and the U.S. Joint Services Electronics Program (Contract DAAG-29-78-C-0020) for their support during the course of this research.

REFERENCES

1. Johnson, T. L., and Lin, J. G., "An Aggregation Method for Active Control of Large Space Structures," Proceedings of the 18th IEEE Conference on Decision and Control, December 1979, pp. 1-3.
2. Balas, M. J., "Feedback Control of Flexible Systems," IEEE Trans. Automat. Control, Vol. 23, 1978, pp. 673-679.
3. Lang, J. H., "A Perturbation Analysis of Spillover in Closed-Loop Distributed-Parameter Systems," Proceedings of the IEEE Conference on Decision and Control, December 1980, pp. 991-993.
4. Aubrun, J. N., "Theory of the Control of Structures by Low-Authority Controllers," J. Guidance and Control, Vol. 3, No. 5, September 1980, pp. 444-451.
5. J. H. Lang and D. H. Staelin, "Electrostatically Figured Reflecting Membrane Antennas for Satellites," IEEE Trans. Automat. Control, Vol. 27, No. 3, June 1982, pp. 666-670.

APPENDIX A: EIGENVALUE PERTURBATION DUE TO COUPLING MATRICES

Consider the matrix $\hat{A} = \begin{bmatrix} \hat{A}_{aa} & \hat{A}_{ar} \\ \hat{A}_{ra} & \hat{A}_{rr} \end{bmatrix}$. Denote the i th eigenvalue, left and right eigenvector of \hat{A}_{aa} and \hat{A}_{rr} by ζ_{a_i} , \mathcal{L}_{a_i} , \mathcal{R}_{a_i} and $\rho_{r_i}^{\pm}$, $\hat{\ell}_{r_i}^{\pm}$, $\hat{\gamma}_{r_i}^{\pm}$, respectively. If \hat{A}_{ar} and \hat{A}_{ra} were zero, the ζ_{a_i} and $\rho_{r_i}^{\pm}$ would be the eigenvalues of \hat{A} . However, due to the coupling between \hat{A}_{aa} and \hat{A}_{rr} through the partitions \hat{A}_{ar} and \hat{A}_{ra} , ζ_{a_i} and $\rho_{r_i}^{\pm}$ will be shifted. According to perturbation theory, the shifts, denoted by $\Delta\zeta_{a_i}^{(2)}$ and $\Delta\rho_{r_i}^{\pm(2)}$, are given to second order in the elements of the coupling matrices by

$$\Delta\zeta_{a_i}^{(2)} = - \mathcal{L}_{a_i} \hat{A}_{ar} [\hat{A}_{rr} - \zeta_{a_i} I]^{-1} \hat{A}_{ra} \mathcal{R}_{a_i} \quad (42)$$

$$\Delta\rho_{r_i}^{\pm(2)} = -\hat{\ell}_{r_i}^{\pm}\hat{A}_{ra}[\hat{A}_{aa} - \rho_{r_i}^{\pm}I]^{-1}\hat{A}_{ar}\hat{\gamma}_{r_i}^{\pm} \quad (43)$$

With \hat{A}_{rr} as given in (19), $\hat{\ell}_{r_i}^{\pm}$, $\hat{\gamma}_{r_i}^{\pm}$ are related to ℓ_{r_i} , γ_{r_i} as follows:

$$\hat{\ell}_{r_i}^{\pm} = \begin{bmatrix} \frac{(\beta + \rho_{r_i}^{\pm})}{(\beta + 2\rho_{r_i}^{\pm})} \ell_{r_i} & \frac{1}{(\beta + 2\rho_{r_i}^{\pm})} \ell_{r_i} \end{bmatrix} \quad \hat{\gamma}_{r_i}^{\pm} = \begin{bmatrix} \gamma_{r_i} \\ \rho_{r_i}^{\pm} \gamma_{r_i} \end{bmatrix}. \quad (44)$$

Equations (20) and (21) are then obtained by substituting (19) into (42) and (19) and (44) into (43), respectively, and applying the matrix identity

$$\begin{bmatrix} M_{11} & M_{12} \\ M_{21} & M_{22} \end{bmatrix}^{-1} = \begin{bmatrix} M_{11}^{-1} + M_{11}^{-1}M_{12}(M_{22} - M_{21}M_{11}^{-1}M_{12})^{-1}M_{21}M_{11}^{-1} & -M_{11}^{-1}M_{12}(M_{22} - M_{21}M_{11}^{-1}M_{12})^{-1} \\ -(M_{22} - M_{21}M_{11}^{-1}M_{12})^{-1}M_{21}M_{11}^{-1} & (M_{22} - M_{21}M_{11}^{-1}M_{12})^{-1} \end{bmatrix}$$

APPENDIX B: EXPRESSIONS OF SECOND ORDER ACCURACY IN S

To reduce equations (20) and (21) to second order accuracy in S, notice from (11) that $\bar{\Omega}_{ar}^2$ and $\bar{\Omega}_{ra}^2$ each have lowest order terms first order in S. Their products are second order in S, thus the quantities ℓ_{r_i} , γ_{r_i} , $\lambda_{r_i}^2$, etc. in (20) and (21) can be replaced by their zero order values in S. As a result, substitutions in (20) and (21) can be made as follows:

$$M_a \rightarrow E_a^T E_a; \quad M_r \rightarrow I; \quad \bar{\Omega}_{aa}^2 \rightarrow E_a^T \bar{\Omega}_a^2 (E_a^T)^{-1}; \quad \bar{\Omega}_{rr}^2 \rightarrow \Omega_2^2; \quad \bar{\Omega}_{ar}^2 \rightarrow E_a^T (-\Omega_1^2 S^T + S^T \Omega_2^2); \quad \bar{\Omega}_{ra}^2 \rightarrow (-S \Omega_1^2 + \Omega_2^2 S) (E_a^T)^{-1}; \quad \ell_{r_i} \rightarrow [0, \dots, 0, 1, 0, \dots, 0]; \quad \gamma_{r_i} \rightarrow [0, \dots, 0, 1, 0, \dots, 0]^T; \quad \rho_{r_i}^{\pm} \rightarrow \rho_i^{\pm}.$$

The new equations yield $\Delta\zeta_{a_i}^{(2)S^2}$ and $\Delta\rho_{r_i}^{\pm(2)S^2}$, which denote equations (20) and (21) reduced to quadratic terms in S, respectively. The relation $\zeta_{a_i}^{S^2} = \zeta_{a_i} + \Delta\zeta_{a_i}^{(2)S^2}$ is then (24) while the relation

$$\begin{aligned} \rho_{r_i}^{\pm S^2} &= \rho_{r_i}^{\pm} + \Delta\rho_{r_i}^{\pm(2)S^2} \\ &= \rho_{r_i}^{\pm} - \frac{1}{(\beta + 2\rho_{r_i}^{\pm})} S_{r_i} (\Omega_1^2 - \omega_i^2 I) \left[\omega_i^2 I - \Omega_1^2 + E_a \begin{bmatrix} I \\ 0 \\ 0 \end{bmatrix} \tilde{K}(\rho_{r_i}^{\pm}) \tilde{Q}(\rho_{r_i}^{\pm}) E_a^T \right]^{-1} (\Omega_1^2 - \omega_i^2 I) S_{r_i}^T, \end{aligned} \quad (45)$$

with S_{r_i} denoting the i th row of S, can be further manipulated to become (25).

For F, G, H, K = 0,

$$\rho_{r_i}^{\pm S^2} = \rho_{r_i}^{\pm} + \frac{1}{(\beta + 2\rho_{r_i}^{\pm})} S_{r_i} (\Omega_1^2 - \omega_i^2 I) S_{r_i}^T \quad (46)$$

It is known that the exact eigenvalues of the system without feedback are ρ_i^{\pm} .

Thus (46) is ρ_i^{\pm} expressed to second order in S, and the approximation

$$\rho_{r_i}^{\pm} + \frac{1}{(\beta + 2\rho_i^{\pm})} S_{r_i} (\Omega_1^2 - \omega_i^2 I) S_{r_i}^T \approx \rho_i^{\pm} \quad (47)$$

introduces an error by terms which are fourth order in S . Since the expressions of concern are to second order in S , this error can be neglected. Putting (47) into (45) and making use of the matrix identity

$$(M_1 + M_2)^{-1} = M_1^{-1} - M_1^{-1} M_2 (I + M_1^{-1} M_2)^{-1} M_1^{-1}.$$

results in (25). In this manner, (47) acts as an "initial condition" in that it provides equality between $\rho_{r_i}^{\pm S^2}$ and the exact values in the absence of feedback.

APPENDIX C: EIGENVALUES OF \hat{A}_{aa} WITH F, G, H, K AS GIVEN IN (34).

Two relations between γ_{a_i} and ℓ_{a_i} should be noted. First, as in (26), $\gamma_{a_i} = M_a^T \ell_{a_i}$. Second, the orthonormalization condition $\ell_{a_i}^T \gamma_{a_j} = \delta_{ij}$ is adopted. With $M_a = B^T B$ for the collocated sensor and actuator case, $R_a = \text{column}[\gamma_{a_1}^T \dots \gamma_{a_{n_u}}^T]$ and $L_a^T = \text{column}[\ell_{a_1}^T \dots \ell_{a_{n_u}}^T]$, it can be shown that

$$\begin{aligned} R_a &= B^T B L_a^T \\ R_a &= L_a^{-1} \end{aligned} \quad (48)$$

Substitute (34) into (19), apply a similarity transform to the resultant \hat{A}_{aa} with

$$V = \begin{bmatrix} I & 0 & 0 \\ 0 & L_a & 0 \\ 0 & 0 & L_a \end{bmatrix} \quad \text{and} \quad V^{-1} = \begin{bmatrix} I & 0 & 0 \\ 0 & R_a & 0 \\ 0 & 0 & R_a \end{bmatrix}$$

and make use of (48). The result is that

$$V \hat{A}_{aa} V^{-1} = \begin{bmatrix} \begin{bmatrix} \xi_1 & & \\ & \ddots & \\ & & \xi_{n_u} \end{bmatrix} & \begin{bmatrix} g_1 & & \\ & \ddots & \\ & & g_{n_u} \end{bmatrix} & 0 \\ 0 & 0 & I \\ \begin{bmatrix} g_1 & & \\ & \ddots & \\ & & g_{n_u} \end{bmatrix} & \begin{bmatrix} d - \lambda_{a_1}^2 & -k_1 & & \\ & \ddots & \ddots & \\ & & d - \lambda_{a_{n_u}}^2 & -k_{n_u} \end{bmatrix} & -\beta I \end{bmatrix} \quad (49)$$

By rearranging the columns and rows of (48), it can be seen that the eigenvalues of $V \hat{A}_{aa} V^{-1}$, hence those of \hat{A}_{aa} , are given by the union of the eigenvalues of \hat{a}_{aa_i} , $i = 1, \dots, n_u$, with \hat{a}_{aa_i} as given by (35).

FIGURES

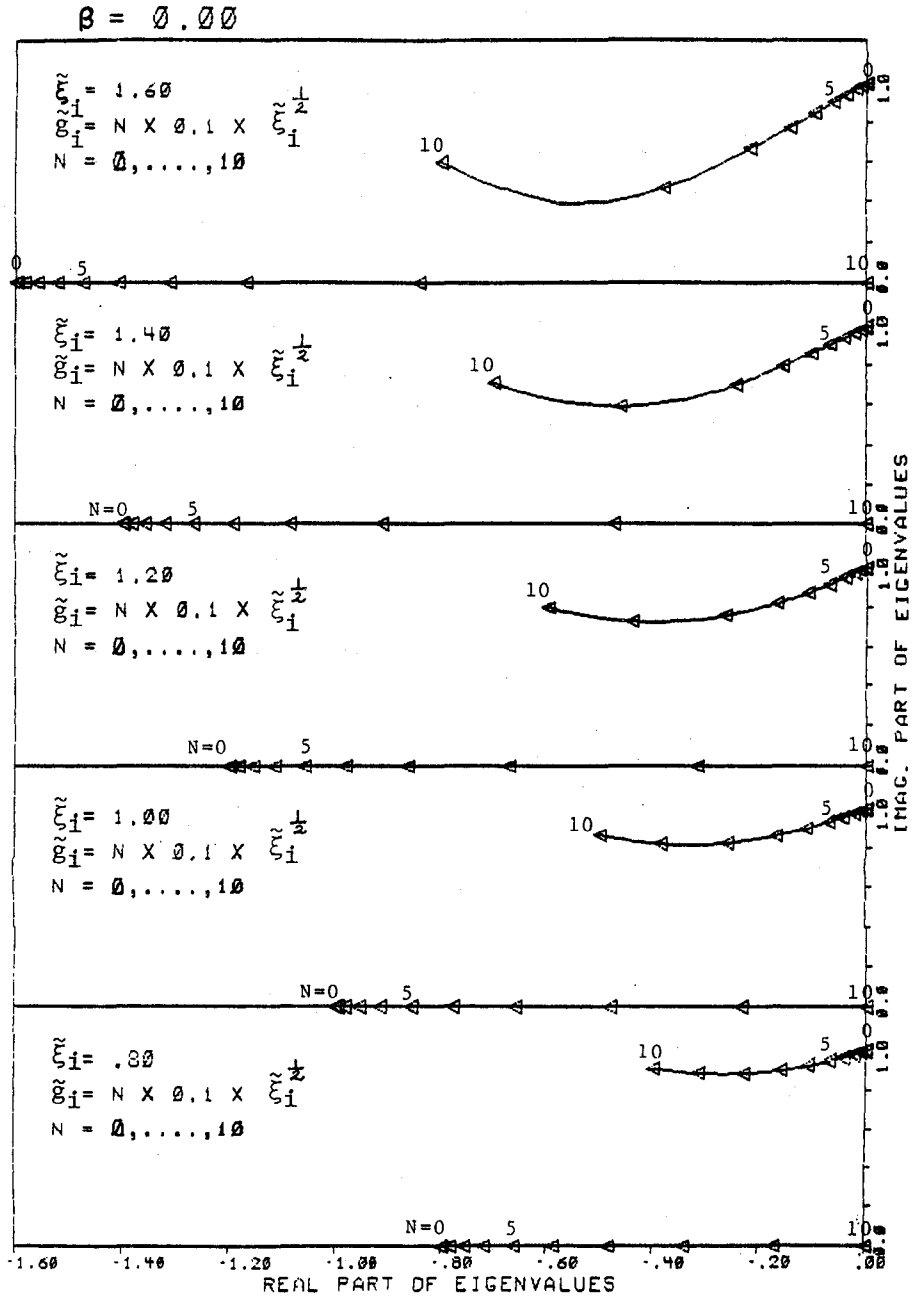


Fig. 1. $\tilde{\rho}_{a_i}^0$ locus (real) and $\tilde{\rho}_{a_i}^+$ locus (complex) at different values of $\tilde{\zeta}_i$ and \tilde{g}_i for the case $\beta = 0.0$.

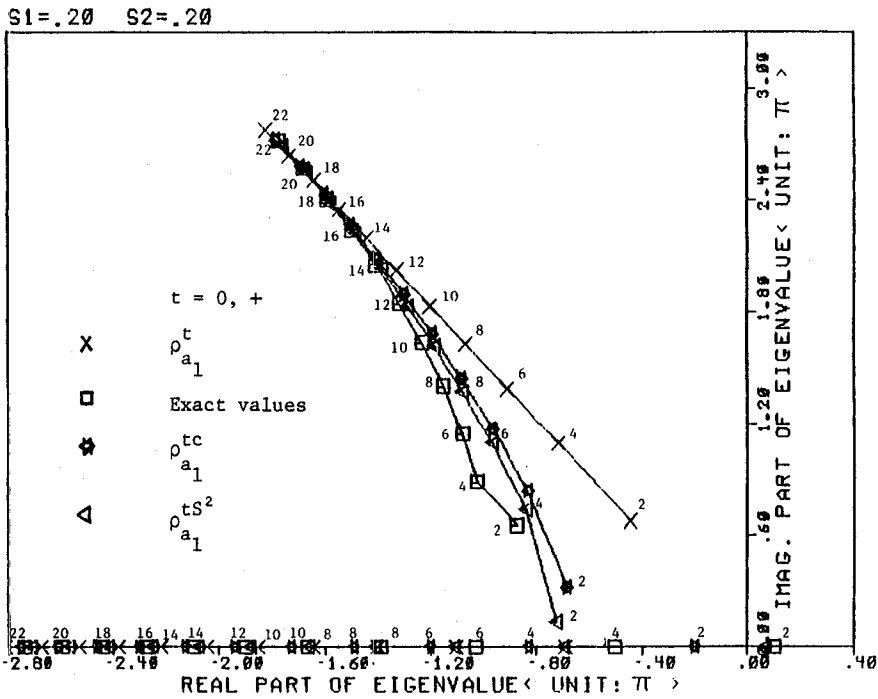


Fig. 2. Comparison between the designed, exact and approximated closed-loop eigenvalues of the first aggregated state in the examined numerical example, with $S_1 = S_2 = 0.2$ and k , the sole undetermined compensator parameter, takes on different values.

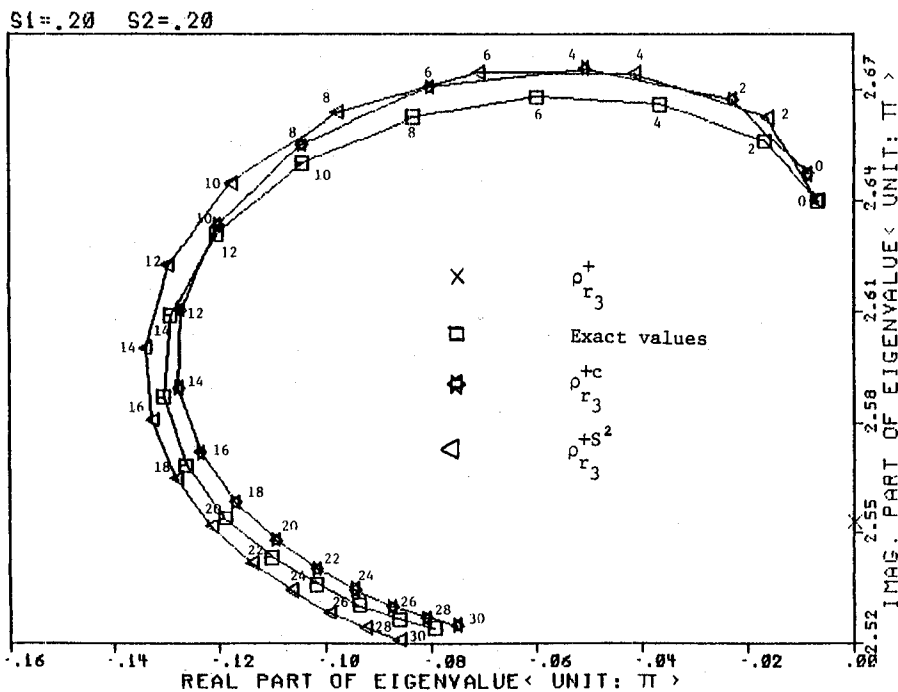


Fig. 3. Comparison between the designed, exact and approximated closed-loop eigenvalues of the residual state in the examined numerical example, with $S_1 = S_2 = 0.2$ and k , the sole undetermined compensator parameter, takes on different values.

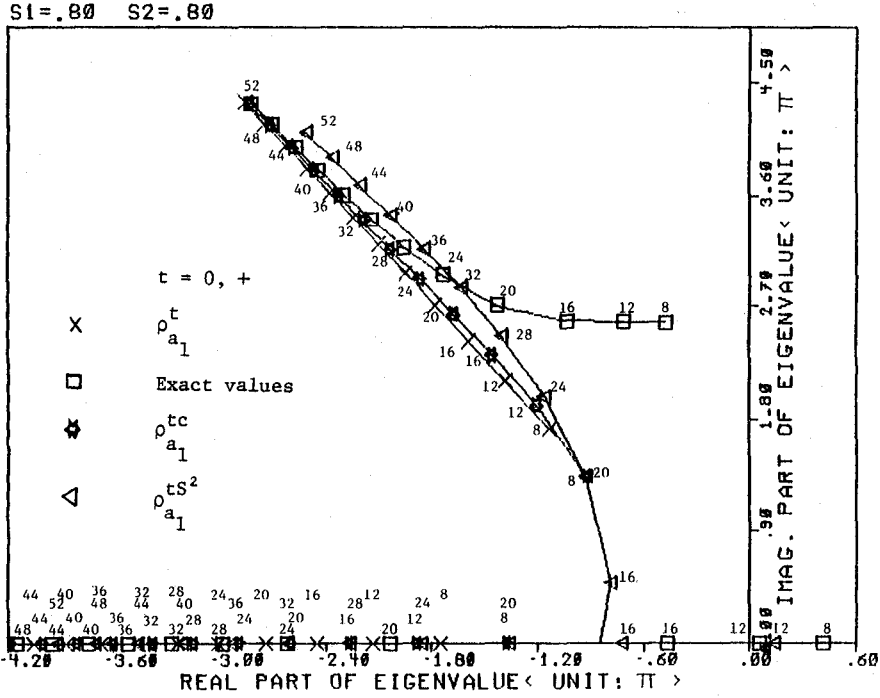


Fig. 4. Comparison between the designed, exact and approximated closed-loop eigenvalues of the first aggregated state in the examined numerical example, with $S_1 = S_2 = 0.8$ and k , the sole undetermined compensator parameter, takes on different values.

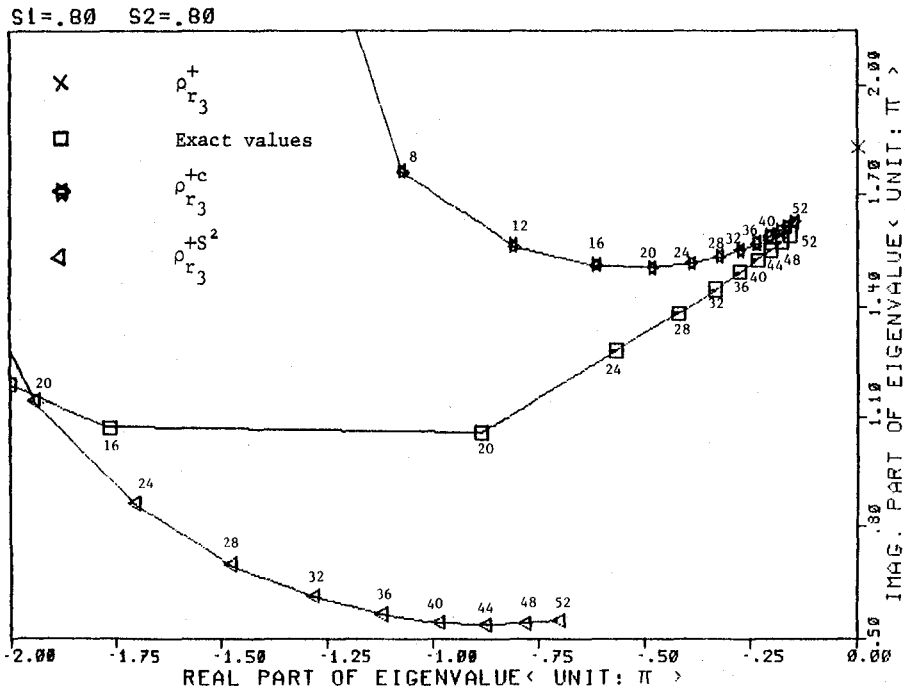


Fig. 5. Comparison between the designed, exact and approximated closed-loop eigenvalues of the residual state in the examined numerical example, with $S_1 = S_2 = 0.8$ and k , the sole undetermined compensator parameter, takes on different values.

A DESIGN PROCEDURE FOR ACTIVE CONTROL OF BEAM VIBRATIONS

Stephen L. Dickerson and George Jarocki
Mechanical Engineering, Georgia Institute of Technology
Atlanta, GA 30332

ABSTRACT

This work analyzes the transverse vibrations of beams and presents a methodology for the design of an active damping device.

The Bernoulli-Euler equation is used to derive a transcendental transfer function, which relates a torque applied at one end of the beam to the rotational position and velocity at that point. The active damping device consists of a wire, a linear actuator and a short torque arm attached to one end of the beam. The action of the actuator varies a tension in the wire and creates a torque which opposes the rotation of the beam and thus damps vibration.

A contribution of the paper is a design procedure for such an active damper. This procedure shows the relationships and trade-offs between the actuator stroke, power required, stress levels in the wire and beam and the geometry of the beam and wire.

It is shown that by consideration of the frequency response at the beam natural frequencies, the aforementioned relationships can be greatly simplified. Similarly, a simple way of estimating the effective damping ratios and eigenvalue locations of actively controlled beams is presented.

SYMBOLS

- A cross sectional area of a beam (or wire if sub w)
- b feedback gain
- d length of moment arm
- E modulus of elasticity
- f tension in wire
- G open loop transfer function
- H closed loop transfer function
- J moment of cross section of beam

L	length of beam (or wire if sub w)
p	open loop poles
P	power
s	d/dt operator
x	beam length coordinate
y	beam displacement
z	extension of wire
z_n	open loop zeros
δ	normalizing factor for time
η	normalized length coordinate
θ	rotational angle
ξ_{cn}	closed loop damping ratio of n^{th} pole pair
σ	negative of real part of eigenvalue
τ	normalized time
ω	frequency of oscillation

MODEL OF BEAM WITH RATE FEEDBACK

A beam of constant cross-section and material properties with no internal damping and shear deformation may be described by the Bernoulli-Euler equation.

$$EJ \frac{\partial^4 y}{\partial x^4} + A\rho \frac{\partial^2 y}{\partial t^2} = 0 \quad (1.1)$$

If the beam is of length L it is convenient to normalize this equation using

$$\eta \equiv \frac{1}{L} x \quad \text{and} \quad \tau \equiv \delta t \quad (1.2)$$

where $\delta \equiv \sqrt[4]{EJ/\rho AL}$ to obtain the partial differential equation

$$\frac{\partial^4 y}{\partial \eta^4} + \frac{\delta^2 y}{\delta \tau^2} = 0 \quad (1.3)$$

For the case of a beam pinned at both ends the boundary conditions $y=0$ and $\delta^2 y / \delta \tau^2 = 0$ at $\eta=0$ and $\eta=1$ yields the modal solutions

$$y(\eta, \tau) = C_n \sin(\omega_n \tau + \phi) \sin \sqrt{\omega_n} \eta \quad (1.4)$$

where $\omega_n = \pi^2 n^2$, $n=1,2,3,\dots$

Such a beam if excited oscillates with frequency components ω_n . These oscillations can be damped by applying a moment at either or both ends that opposes the rotational rate. That is, the boundary condition at $\eta=0$ becomes

$$M(0, t) = -b \frac{d}{dt} \theta(0, t) \quad (1.5)$$

where $\theta \equiv \delta y / \delta \eta$ and $M \equiv -\delta^2 y / \delta \eta^2$. The sign convention on M is necessary to make a positive moment result in a positive θ and y .

A moment opposed to rotational velocity will damp oscillations because it removes energy. Points other than $\eta=0$ are acceptable but examination of Eq. 1.4 shows that there are values of η on the modal solution where $\delta^2 y / \delta x \delta t$ (i.e., $d\theta/dt$) is zero. Such modes will not be damped if the moment is applied at these points.

To examine the effect of variation of the damping constant b in Eq. 1.5 it is possible to consider b as a gain in a feedback control system as shown in Fig. 1. The transfer function $G(s)$ is derived relating the input moment M to the rotational velocity at $\eta=0$. The result is

$$G(s) = \frac{\sqrt{2s}(\sin\sqrt{2s} - \sinh\sqrt{2s})}{2(\cos\sqrt{2s} - \cosh\sqrt{2s})} \quad (1.6)$$

where s can be interpreted as the derivative operator, d/dt . The "poles" of the transfer function are the zeros of the denominator or

$$p_n = j\pi^2 n^2, \quad n=1,2,3,\dots \quad (1.7)$$

There is also a pole at infinity since the numerator is of order greater than the denominator. The "zeros" are given by the zeros of the numerator or

$$\begin{aligned} z_0 &= 0 \\ z_n &= j\pi^2 (n+0.25)^2, \quad n=1,2,3,\dots \end{aligned} \quad (1.8)$$

Actually the z_n expressions ($n>0$) are slight approximations. $z_1=15.418$ instead of 15.421 as given by Eq. 1.8. The approximation for $n>1$ is much better. From the zero and pole locations one can write

$$G(s) = \frac{s \prod_{n=0}^{\infty} \left(1 + \frac{s^2}{\pi^4 (n+0.25)^4}\right)}{3 \prod_{n=1}^{\infty} \left(1 + \frac{s^2}{n^4 \pi^4}\right)} \quad (1.9)$$

where the $1/3$ comes from Eq. 1.6 using the limit as s approaches zero of $G(s)/s = 1/3$. With feedback as shown in Fig. 1 or as suggested by Eq. 1.5 the overall transfer function is

$$H(s) = \frac{G(s)}{1+bG(s)} \quad (1.10)$$

or

$$H(s) = \frac{\frac{s}{3} \prod_{n=1}^{\infty} \left(1 + \frac{s^2}{\pi^4 (n+0.25)^4}\right)}{\prod_{n=1}^{\infty} \left(1 + \frac{s^2}{n^4 \pi^4}\right) + \frac{s}{3} b \prod_{n=1}^{\infty} \left(1 + \frac{s^2}{n^2 (n+0.25)^4}\right)} \quad (1.11)$$

which can be written as

$$H(s) = \frac{s \prod_{n=1}^{\infty} \left(1 + \frac{s^2}{\pi^4 (n+0.25)^4}\right)}{3(1+Ts) \prod_{i=1}^{\infty} \left(1 + \frac{2\xi_n}{\omega_{cn}} s + \left(\frac{s}{\omega_{cn}}\right)^2\right)} \quad (1.12)$$

where the closed loop natural frequencies ω_{cn} and damping ratios are evident. The form of the denominator is arrived at by consideration of the root locus discussed in subsequent sections.

VARIATION OF SYSTEM EIGENVALUES WITH FEEDBACK GAIN

The characteristic equation of $H(s)$ is $1+bG(s)=0$. A numerical solution for the root locus for the first few branches is presented in Fig. 2. This numerical solution uses the transcendental form of $G(s)$, Eq. 1.6, and finds

values of s for which the imaginary part of $G(s)$ is zero and then calculates b from "minus inverse b = real part of $G(s)$."

For light damping (small b) a good approximation for the closed loop damping ratios, ξ_n , can be found by (1) assuming $\omega_{cn} = \omega_n$, (2) realizing that $H(j\omega_n) = 1/b$ and (3) neglecting the complex portion of most of the denominator terms as follows.

$$H(m\pi^2 j) = \frac{1}{b} = \frac{m^2 \pi^2}{3|1 + Tm^2 \pi^2 j|} \cdot \frac{\prod_{n=1}^{\infty} \left| 1 - \left(\frac{m}{n+0.25} \right)^4 \right|}{\prod_{n=1}^{\infty} \left| 1 - \left(\frac{m}{n} \right)^4 + 2\xi_n \left(\frac{m}{n} \right)^2 j \right|} \quad (2.1)$$

Now if the imaginary terms in the denominator above are neglected except for $n = m$ then

$$\frac{1}{b} \approx \frac{m^2 \pi^2}{6\xi_n} a_m \quad \text{where} \quad a_m \equiv \frac{\prod_{n=1}^{\infty} \left| 1 - \left(\frac{m}{n+0.25} \right)^4 \right|}{\prod_{\substack{n=1 \\ n \neq m}}^{\infty} \left| 1 - \left(\frac{m}{n} \right)^4 \right|} \quad (2.2)$$

$$\text{Thus } \xi_m \approx \frac{m^2 \pi^2 b a_m}{6}$$

From numerical calculation this reduces to

$$\xi_m \approx b, \quad m = 1, 2, 3, \dots \quad (2.3)$$

From Fig. 2 it is apparent that this approximation is good for small b .

"Small" b appears to depend on the m value. From numerical results the maximum possible damping ratio for the m^{th} eigenvalue is apparently given approximately by

$$\xi_{m \text{ MAX}} \approx \frac{0.28}{n} \quad (2.4)$$

From Fig. 2 and Table 1 it is apparent that "low" values of b damp higher frequency oscillations better while "high" values of b (but not greater than 0.3) damp the low frequency oscillations which are more important to damp actively.

An approach similar to the above can be used to estimate the closed loop eigenvalues for "large" b . From Eq. 1.11 the characteristic equation is

$$3 \prod_{n=1}^{\infty} \left(1 + \frac{s^2}{n^4 \pi^4}\right) + b s \prod_{n=1}^{\infty} \left(1 + \frac{s^2}{\pi^4 (n+0.25)^4}\right) = 0 \quad (2.5)$$

Let a solution be $s = j\pi^2(m+0.25)^2 - \sigma_m$ where σ_m is "small" and positive. Then substituting into Eq. 2.5 the magnitude part becomes

$$3 \prod_{n=1}^{\infty} \left| 1 - \left(\frac{m+0.25}{n}\right)^4 + \frac{\sigma_m^2}{n^4 \pi^4} - j \frac{2\sigma_m}{n^4 \pi^4} (m+0.25)^2 \right|$$

$$+ b \left| j\pi^2(m+0.25)^2 - \sigma_m \prod_{n=1}^{\infty} \left| 1 - \left(\frac{m+0.25}{n+0.25}\right)^4 + \frac{\sigma_m^2}{\pi^4 (n+0.25)^4} \right. \right. \quad (2.6)$$

$$\left. \left. - j2\sigma_m \frac{(m+0.25)^2}{\pi^2 (n+0.25)^4} \right| = 0$$

If the imaginary parts (except for $m=n$ in the second product) and the σ_m^2 terms are neglected, then

$$\sigma_m \approx \frac{1}{b} \left(\frac{3}{2} \frac{\prod_{n=1}^{\infty} \left| 1 - \left(\frac{m+0.25}{n}\right)^4 \right|}{\prod_{\substack{n=1 \\ n \neq m}}^{\infty} \left| 1 - \left(\frac{m+0.25}{n+0.25}\right)^4 \right|} \right) \quad (2.7)$$

which by numerical calculation reduces to

$$\sigma_m \approx \frac{2}{b} \quad (2.8)$$

From Fig. 2 and Table 2 it is apparent that this approximation is good for "large" b and is better for large m for a given value of b .

Incidentally, the time constant associated with the real closed loop eigenvalue is approximated by $T = b/3$ for "large" b . For "small" b the time constant approaches zero and in most cases is thus unimportant.

To summarize, the eigenvalues associated with mode m ($m = 1, 2, 3, \dots$) have damping ratios approximated by Eq. 2.3 for "small" b . Eq. 2.4 and Table 1 provide a dividing line between "large" and "small" b which depends on m .

Eq. 2.8 gives the approximate real part of the eigenvalue (negative) for "large" b. A graphical interpretation of eigenvalue placement is given by Figure 3.

ACTIVE DAMPER CHARACTERISTICS

An active damper construction is illustrated by Fig. 4. A linear actuator varies the tension in a wire stretched between the beam ends. The tension force $f(t)$ developed by the linear actuator acting on the torque arm of length d creates a moment which opposes the angular velocity at the beam end and thus damps vibrations by removing energy from the beam. The resulting control loop at the beam support where the torque is applied is depicted in Fig. 1.

The moment equation, no longer normalized, is

$$M = -b\dot{\theta} = -fd \quad (3.1)$$

Note that b (normalized) must be multiplied by $EJ/L\delta$ to get the actual feedback gain b . If z is defined as the extension of the actuator then z has two components--that due to rotation of the moment arm and that due to elongation of the wire. Thus

$$z = d\theta - \frac{fL_{\omega}}{A_{\omega}E_{\omega}} \quad (3.2)$$

Using Eq. 3.1 we have

$$z = (d - Bbs)\theta \quad \text{where} \quad B \equiv \frac{L_{\omega}}{dA_{\omega}E_{\omega}} \quad (3.3)$$

and as before s stands for d/dt .

For simplicity any initial tension in the wire has been excluded from this analysis but is necessary in a practical application. The reader should imagine a constant tension device in parallel with the dynamic actuator to provide this tension. Naturally, this affects the force variations allowed in the wire to prevent breakage or slackness.

The instantaneous power is given by $-(sz)(f)$ or

$$P = -[s(d-Bbs)\theta] \left[\frac{bs}{d}\theta \right] \quad (3.4)$$

Suppose for now that the moment provided by the actuator is a known amount at a frequency ω .

$$M = M_0 \sin \omega t \quad (3.5)$$

Then

$$\dot{\theta} = s\theta = -\frac{M_0}{b} \sin \omega t, \quad \theta = \frac{M_0}{b\omega} \cos \omega t, \quad \text{and } s^2\theta = \frac{-M_0\omega}{b} \cos \omega t$$

Substitution into Eqs. 3.1, 3.3 and 3.4 gives

$$\begin{aligned} f_{\text{MAX}} &= \frac{M_0}{d} = -f_{\text{MIN}} \\ z_{\text{MAX}} &= M_0 \sqrt{B^2 + \left(\frac{d}{b\omega}\right)^2} = -z_{\text{MIN}} \\ P_{\text{MAX}} &= \frac{M_0^2}{2b} \left[\sqrt{1 + \left(\frac{Bb}{d}\right)^2} - 1 \right] \\ P_{\text{MIN}} &= \frac{-M_0^2}{2b} \left[\sqrt{1 + \left(\frac{Bb}{d}\right)^2} + 1 \right] \\ P_{\text{AVE}} &= -\frac{M_0^2}{2b} \end{aligned} \quad (3.6)$$

Each of f , z and P are sinusoidal at frequency ω except P is at frequency 2ω .

To apply the above relationships one needs to interpret the significance of f_{MAX} , z_{MAX} , P_{MAX} , etc.

f_{MAX} is the greatest force which the actuator must deliver. It plus any initial tension in the wire is the greatest tension in the wire. An initial tension would usually exceed f_{MAX} in order that the wire never go slack.

Two times z_{MAX} is the stroke required of the actuator.

P_{MAX} is the greatest instantaneous power required from the actuator. It is zero if the wire is inelastic or $B=0$. The average work done by the actuator over a cycle is always negative since the actuator is being used to remove energy from the beam. P_{MIN} is always negative and represents the maximum energy absorption rate of the actuator.

$M_0 \sin(\omega t)$ could be interpreted as a moment applied at $x=0$ if $\omega = \omega_n$. Under these conditions the actuator must, in the steady state, absorb exactly the moment applied by an external excitation.

Alternatively for a lightly damped case where the motion associated with any mode is approximately sinusoidal M_0 can be related to an initial displacement or velocity of the beam. For instance, referring to Eq. 1.4 if the

maximum midpoint displacement of a mode is 1, then

$$\theta = \frac{\partial y}{\partial \eta} = \sqrt{\omega_n} \sin \omega_n \tau$$

$$s\theta|_{MAX} = \frac{\partial^2 y}{\partial \eta \partial \tau} = [\omega_n]^{3/2} = n^3 \pi^3$$

from which $M = bn^3 \pi^3$, b normalized.

NUMERICAL EXAMPLE

Consider the American Standard S6x17.25 I-beam for which

$$E = 29 \times 10^6 \text{ psi} \qquad J = 26.3 \text{ in}^4$$

$$\rho = 7.36 \times 10^{-4} \text{ lb sec}^2/\text{in}^4 \qquad A = 5.07 \text{ in}$$

Suppose the active damper applies a maximum moment of 20,000 in.lb. and that the length of the torque arm is 6 in., in this case equal to the depth of the beam, and that the wire is 0.375 inches in diameter of carbon steel with $E = 29 \times 10^6$ psi. This gives a maximum stress of 30,193 psi which must be approximately doubled to prevent slack.

If the initial displacement in the beam, which needs to be damped, is taken as that which results from a 50,000 psi max stress in the beam from the first mode shape, then the mode shape is given by

$$y(x,0) = C \sin\left(\frac{\pi x}{600}\right)$$

where $C = 20.96$ inches.

Since $\theta_{MAX} = 0.1098$ rad and $\delta = 1.256/\text{sec}$, $\omega_1 = \pi^2 \delta = 12.39$ rad/sec, from which $\dot{\theta}_{MAX} = 1.361$ rad/sec. The maximum b allowed is 1.47×10^4 in.lb.sec. from the relationship $1.361 b = 20,000$. In normalized terms

$$b = b \frac{L\delta}{EJ} = 0.0145$$

This can be interpreted as adding a damping ratio of 1.45% to the low frequency modes and moving the "high" frequency modes to

$$-\sigma = \frac{-2}{b} = -138 \text{ (normalized)} = -173/\text{sec.}$$

The "high" frequency modes in this case begin at about the 20th mode and are probably unimportant. However, the same wire and actuator could be used to provide much greater low frequency damping ratios if the amplitude of oscillation were greatly less than 21 inches.

SOME PRACTICAL CONSIDERATIONS

Unfortunately, no real control system--measurement, computation, actuation--can realize a simple gain b at all frequencies. Fortunately, no real beam can realize zero damping at any frequency and as a rule that damping expressed as a damping ratio increases for higher modes. From root-locus arguments it is possible to conclude that as b realizes a phase lag at higher frequencies some of the loci will tend toward the imaginary axis--a generally undesirable situation. The amount of motion toward the imaginary axis is reduced by the magnitude attenuation of b at higher frequencies. If the beam has no inherent or passively supplied damping the system would be unstable. Thus as a practical matter the actuator must have a "flat" frequency response up to a frequency at which the beam has a high inherent damping or the magnitude of b must be restricted by considerations of effects on high mode eigenvalues.

BIBLIOGRAPHY

1. Meirovitch, L., Elements of Vibration Analysis. McGraw-Hill, Inc., 1975.
2. Pestel, E., and Leckie, A., Matrix Methods in Elastomechanics. McGraw-Hill, Inc., 1971.
3. Takahashi, Y., Rabins, J., and Auslander, M., Control and Dynamics Systems, Addison-Wesley, Inc., 1970.
4. Brown, F. T., "A Unified Approach to the Analysis of Uniform One-Dimensional Distributed Systems," A.S.M.E. Journal of Basic Eng., June 1967.
5. Vaughan, D. R., "Application of Distributed Parameter Concepts to Dynamic Analysis and Control of Bending Vibrations," A.S.M.E. Paper of unknown source.
6. Rockwell, T. H., and Lawther, J. M., "Theoretical and Experimental Results on Active Vibration Dampers," Journal of the Acoustical Society of America, August 1964.

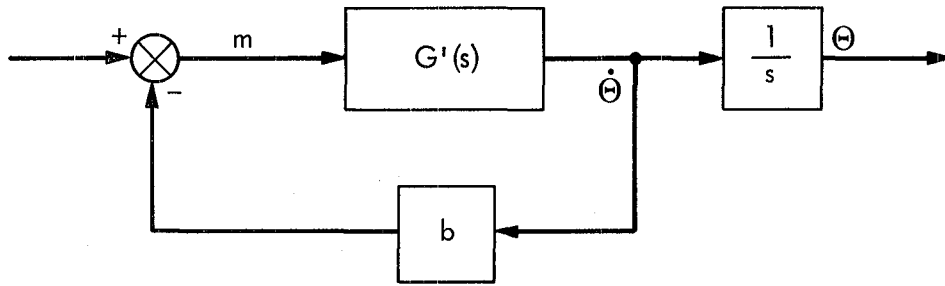


Figure 1. Block Diagram of Feedback Control System.

Table 1. Maximum Damping Ratio and Corresponding Value of b (Numerically Determined)

Mode, m	$\xi_{m,MAX}$	b
1	0.289	0.378
2	0.143	0.201
3	0.0946	0.139
4	0.0707	0.107
5	0.0565	0.0866
6	0.0471	0.0784
10	0.0282	0.0441

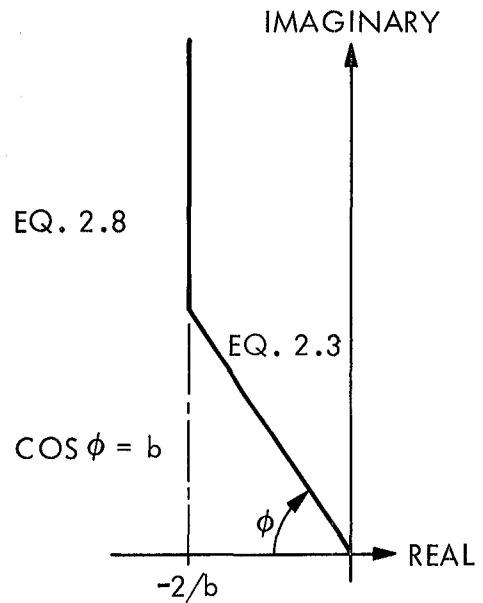


Figure 3. Eigenvalue Placement Asymptotic Values

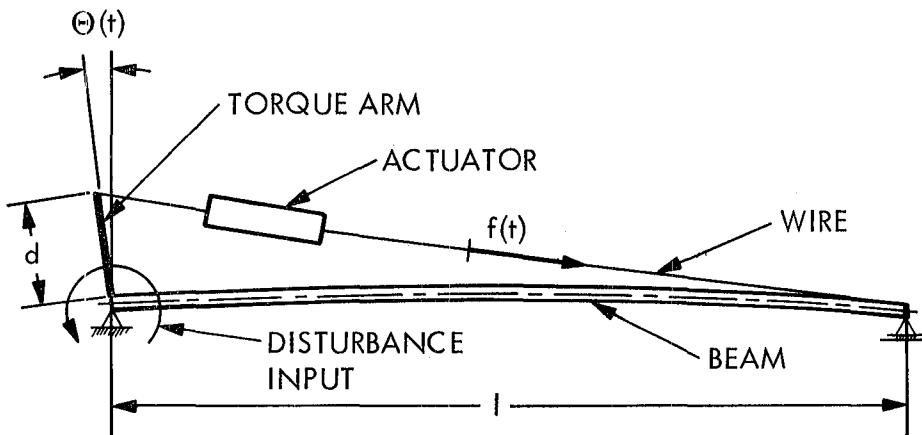


Figure 4. Construction of Active Beam Damper

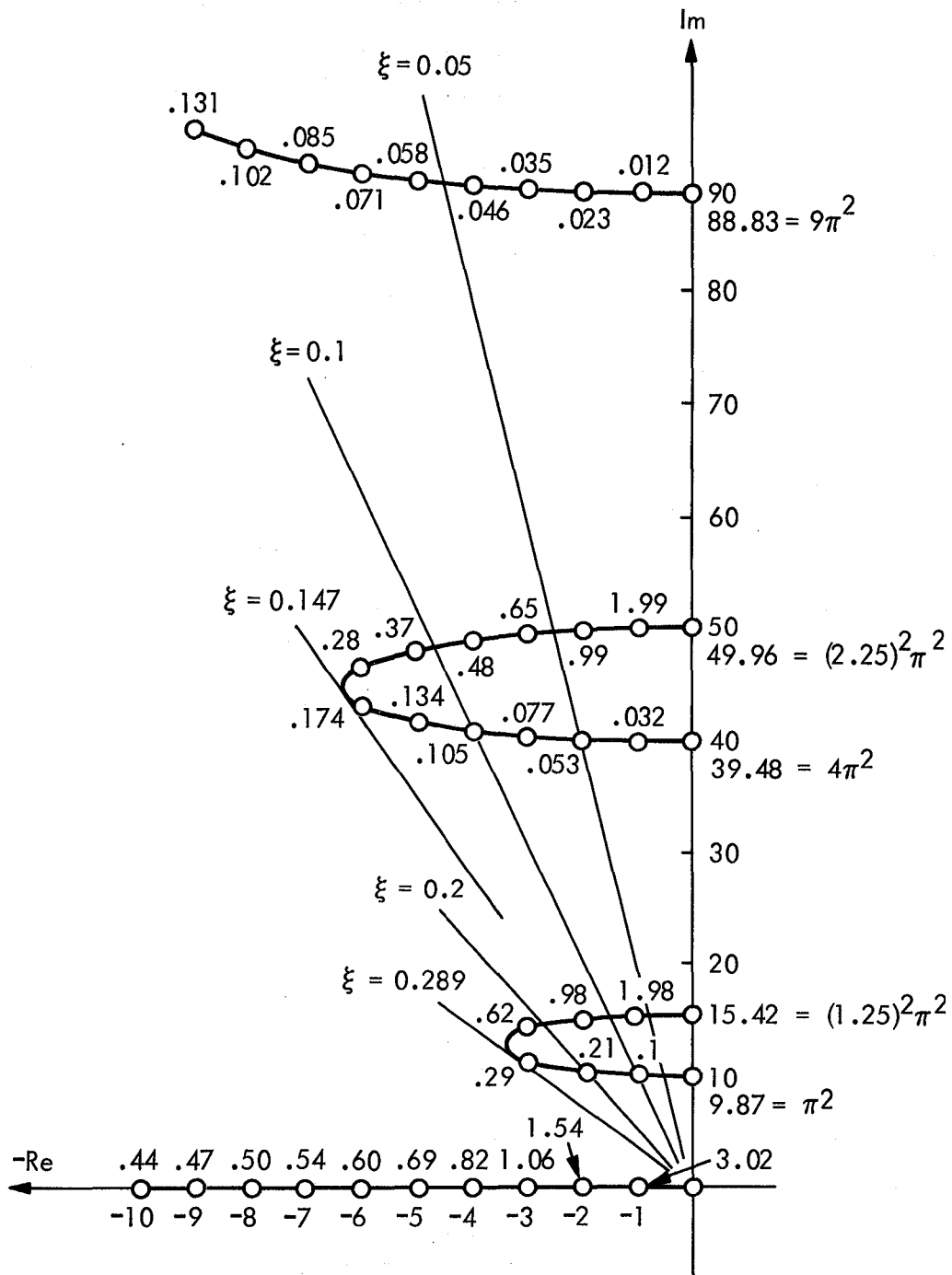


Figure 2. Root Locus for Lower Frequency Modes (circles on loci are labelled with the values of b .)

ON VIBRATION CONTROL OF TETHERED SATELLITE SYSTEMS

D.M. Xu and A.K. Misra

Department of Mechanical Engineering
McGill University
Montreal, Quebec, Canada H3A 2K6

V.J. Modi

Department of Mechanical Engineering
University of British Columbia
Vancouver, B.C., Canada V6T 1W5

ABSTRACT

The general dynamics of a shuttle supported tethered subsatellite system taking into account the longitudinal and three dimensional transverse vibrations is considered. It is noted that control of inherently unstable dynamics during retrieval of the subsatellite can be carried out by letting the rate of change of length depend on the state variables in an appropriate manner. Control laws using linear feedback of inplane state variables and nonlinear feedback of out-of-plane state variables are proposed.

INTRODUCTION

Tether connected multibody systems have various potential applications. A description of these applications is given in a report¹ by the Preliminary design Office of the Marshall Space Flight Center. A shuttle supported tethered subsatellite system similar to the Skyhook² proposed by the Smithsonian Institution for low altitude scientific experiments is being considered by NASA. To ensure successful operation, analysis and control of the dynamics of the system during deployment, stationkeeping and retrieval stages must be carried out. The general dynamics of tethered satellites is rather complex. The degrees of freedom involved are:

- a) three dimensional rotational motions of the endbodies;
- b) three dimensional rotations of the tether;
- c) longitudinal oscillations of the tether; and
- d) three dimensional transverse vibrations.

The major environmental effect in the case of shuttle supported systems is that due to the aerodynamic drag. A comparison of the models used in various investigations of the shuttle supported tethered subsatellite systems has been carried out by Misra and Modi³.

Control of the dynamics of the tethered subsatellite systems is likely to be carried out by using either a tension control law or a length rate law i.e., by letting either the tension in the tether or rate of change of its length to depend on the state variables in specific ways. Rupp⁴ formulated a control procedure in which the tension was proportional to the actual and commanded lengths and the length rate. However, only the rotation of the tether in the orbital plane was considered. Baker et al⁵ and Bainum and Kumar⁶ improved the control performance by choosing a superior set of gains. A simulation using a Rupp type control during deployment and retrieval was carried out by Kulla⁷. Although the transverse vibrations of the tether were included, the longitudinal oscillations and the out-of-plane motion of the system were ignored. Kalaghan et al⁸ analyzed the Skyhook system in detail, taking various environmental effects into account. The tether was not treated as a continuum, but longitudinal oscillations were considered. Although References 7 and 8 incorporated certain vibrations in the dynamical models, the control laws had no vibrational feedback. During retrieval and under certain circumstances during deployment the vibrations of the tether increase gradually indicating that appropriate vibrational feedback must be used. The objective of this paper is to do just that.

DESCRIPTION OF THE SYSTEM

The Shuttle/Tethered Subsattellite System is shown in Figure 1. The subsatellite having a mass m_s is supported by the shuttle through a tether having a mass per unit length ρ_t and instantaneous nominal length L . The instantaneous centre of mass S of the system may be assumed to coincide with the centre of mass of the shuttle, since the mass of the subsatellite or the tether is very small compared to that of the shuttle. S can be located with respect to the centre of the Earth E by the radial distance R_0 , inclination i of the orbit to the equatorial plane, argument of the perigee θ_p and true anomaly θ . The tether is nominally along the local vertical. The instantaneous orientation of the line joining the two ends of the tether is defined by two rotations, roll γ and pitch α , in that order. The tether is stretched longitudinally due to the gravity gradient and aerodynamic drag. This longitudinal strain varies along the tether, but for short tethers, this variation is small. Since most of the problems in controlling the system are associated with short tether lengths during retrieval, it is assumed that the longitudinal strain is uniform and the instantaneous stretched length L_s given by

$$L_s = L (1 + \epsilon) \quad (1)$$

The transverse vibrations u and v perpendicular to and in the plane of the orbit, respectively, are superposed on the stretched tetherline. These transverse vibrations may be expanded in series form in terms of a set of admissible functions:

$$u = \sum_{k=1}^{\infty} \phi_k(L, y) A_k(t) , \quad (2a)$$

$$v = \sum_{k=1}^{\infty} \phi_k(L, y) B_k(t) , \quad (2b)$$

where

$$\phi_k(L, y) = \sqrt{2} \sin(k\pi y/L) . \quad (2c)$$

It may be noted that ϕ_k is not invariant with time.

The equations of motion corresponding to the generalized co-ordinates $\alpha, \gamma, \epsilon, A_k, B_k, k = 1, 2, \dots, \infty$, are obtained using a Lagrangian formulation. Linearizing the vibratory terms, but retaining the nonlinearities in rotations which may be large, one gets a set of nonlinear equations with time dependent coefficients. For example, the equation for B_k degree of freedom is

$$\begin{aligned} \ddot{B}_k + (\dot{L}/L) \dot{B}_k + [\omega_k^2 - \omega_{xc}^2 - \omega_{yc}^2 + (\mu/R_0^3)(1 - 3\ell_{zc}^2)] B_k \\ + \sum_{n=1}^{\infty} [(\dot{B}_n - \omega_{yc} A_n)(\dot{L}/L)(C_{nk} - C_{kn}) - (\dot{L}/L)^2 D_{nk} B_n + (\dot{L}/L) C_{nk} B_n] \\ - 2\omega_{yc} \dot{A}_k - \{\omega_{yc} - \omega_{zc} \omega_{xc} + (3\mu/R_0^3)\ell_{zc} \ell_{xc} + (\dot{L}/L)\omega_{yc}\} A_k \\ - [\sigma_k L \{(\omega_{xc} + \omega_{yc} \omega_{zc} - (3\mu/R_0^3)\ell_{yc} \ell_{zc})(1 + \epsilon) + 2\omega_{xc} \dot{\epsilon}\} + 2\delta_k \dot{L}(1 + \epsilon)\omega_{xc}] = Q_{bk}/\rho_t L, \quad (3) \end{aligned}$$

where $\mu, \delta_k, \sigma_k, C_{nk}, D_{nk}, \omega_k, \omega_{xc}, \omega_{yc}, \omega_{zc}, \ell_{xc}, \ell_{yc}, \ell_{zc}$, are as defined in Appendix A. Other equations are also given in Appendix A. The generalized forces are due to the atmospheric drag. The equations are nondimensionalized by changing the independent variable from time \tilde{t} to true anomaly θ , using a new set of vibrational variables

$$\tilde{A}_k = A_k/L \quad (4a)$$

$$\tilde{B}_k = B_k/L \quad (4b)$$

and defining a nondimensional length

$$\eta = \ln(L/L_{ref}) , \quad (4c)$$

where L_{ref} is an arbitrary reference length. Note that α, γ , and ϵ are nondimensional to start with. It was found convenient to use the final unstretched tether length as L_{ref} . Eq. 3 can now be rewritten as

$$\begin{aligned}
\ddot{\tilde{B}}_k'' + (3\eta' - F) \tilde{B}_k' + [\tilde{\omega}_k^2 + \eta'' + 2\eta'^2 - F\eta' - (\alpha' + c\gamma)^2 - (\gamma' s\alpha - s\gamma c\alpha)^2 + G(1 - 3s^2\alpha c^2\gamma)] \tilde{B}_k \\
+ \sum_{j=1}^{\infty} [(B_j' + \eta' \tilde{B}_j - (\gamma' s\alpha - s\gamma c\alpha) \tilde{A}_j) (C_{jk} - C_{kj}) \eta' - \eta'^2 D_{jk} \tilde{B}_j + (\eta'' + \eta'^2 - F\eta') C_{jk} \tilde{B}_j] \\
- 2(\gamma' s\alpha - s\gamma c\alpha) \tilde{A}_k' - [\gamma'' s\alpha - 2\gamma' c\alpha c\gamma - (3G+1)s\alpha s\gamma c\gamma + (3\eta' - F)(\gamma' s\alpha - s\gamma c\alpha)] \tilde{A}_k \\
- \sigma_k [(1+\epsilon)\{\alpha'' - 2\gamma' s\gamma c^2\alpha - F(\alpha' + c\gamma) + \gamma'^2 s\alpha c\alpha + (3Gc^2\gamma - s^2\gamma)s\alpha c\alpha\} + 2(\alpha' + c\gamma)\epsilon'] \\
+ 2\delta_k \eta'(1+\epsilon)(\alpha' + c\gamma) = \tilde{Q}_{bk}
\end{aligned} \tag{5}$$

where

$$F = 2 e s \theta G$$

$$G = (1 + e c \theta)^{-1}$$

$$\tilde{\omega}_k^2 = (\omega_k^2 / \Omega^2) \{ (1 - e^2)^3 / (1 + e c \theta)^4 \}$$

Ω = mean orbital rate

e = eccentricity of the orbit.

Nondimensional equations corresponding to the other degrees of freedom are omitted here for brevity. Defining x as the state vector comprising of the generalized co-ordinates and their derivatives, the equations of motion can be abbreviated as

$$\underline{A} \dot{x} = f \tag{6}$$

If N_i and N_o are the number of admissible functions retained in the modelling of inplane and out-of-plane transverse vibrations, respectively, then there would be $2(3+N_i+N_o)$ elements in x . Note that \underline{A} is a square matrix dependent on x as well as dimensionless time $\tilde{\theta}$ and f is a vector of rather lengthy nonlinear functions of x and $\tilde{\theta}$.

DYNAMICS AND CONTROL DURING RETRIEVAL OF THE SUBSATELLITE

Deployment of the tethered subsatellite to the required altitude and its subsequent retrieval can be carried out by either providing appropriate tension in the tether or controlling the rotation of the tether feedout spool, thereby controlling the rate of change of the undeformed length of the tether. The second approach is followed here, i.e., η' is specified.

Deployment is basically a stable operation³. Hence, attention is focused on the dynamics and control during retrieval. Figure 2 shows the out-of-plane portion of the uncontrolled retrieval dynamics using

$$\dot{L} = CL \tag{7}$$

where $c = -2 \times 10^{-4} \text{ sec}^{-1}$ ($\bar{c} = c \times 10^4 = -2$). The shuttle is in a polar orbit with its major axis 220 km larger than the earth's radius and having an eccentricity 0.001. The mass of the subsatellite is 150 kg and that of the tether per unit length is 1.5 kg/km. One may note the growth of roll and transverse vibrations. Numerical integration was terminated when the displacements became too large.

Clearly, some sort of control is required to eliminate the dynamical instability associated with retrieval of the subsatellite. It must be pointed out that it is not necessary to have stringent shape and attitude control during retrieval. The objective of a control procedure is to arrest the unlimited growth of the displacements and bound them to reasonable limits. For nonlinear systems having time varying coefficients, it is difficult to devise such a control procedure. Hence, to gain some insight linearized system equations valid for zero eccentricity are examined, although subsequent numerical simulation is carried out without any approximation. Considering A_k and B_k degrees of freedom one has

$$\begin{aligned} \ddot{A}_k'' + 3\eta' \dot{A}_k' + (\eta'' + 2\eta'^2 + 1 + \omega_k^2) \ddot{A}_k + \sum_{j=1}^{\infty} [\eta' (C_{jk} - C_{kj}) \dot{A}_j' + \{\eta'' C_{jk} + \eta'^2 (2C_{jk} - C_{kj} - D_{kj})\} \ddot{A}_j] \\ - \sigma_k (\gamma'' + 4\gamma') - 2\delta_k \eta' \gamma' = \ddot{Q}_{ak} \end{aligned} \quad (8a)$$

$$\begin{aligned} \ddot{B}_k'' + 3\eta' \dot{B}_k' + (\eta'' + 2\eta'^2 + \omega_k^2) \ddot{B}_k + \sum_{j=1}^{\infty} [\eta' (C_{jk} - C_{kj}) \dot{B}_j' + \{\eta'' C_{jk} + \eta'^2 (2C_{jk} - C_{kj} - D_{kj})\} \ddot{B}_j] \\ - \sigma_k (\alpha'' + 2\epsilon' + 3\alpha) + 2\delta_k \eta' (\alpha' + \epsilon) = \ddot{Q}_{bk} - 2\delta_k \eta' \end{aligned} \quad (8b)$$

and

$$\epsilon'' + 2\mu_1 \eta' \epsilon' + [\tilde{\omega}_\epsilon^2 + \mu_1 (\eta'' + \eta'^2)] \epsilon - 2\mu_2 \sum_{j=1}^{\infty} \sigma_j (\tilde{B}_j' + 3\eta' \tilde{B}_j) - 2\alpha' = \ddot{Q}_\epsilon + 3 + \mu_1 (\eta'' + \eta'^2), \quad (8c)$$

where $\mu_1 = (m_s + \frac{1}{2} \rho_t L) / (m_s + \frac{1}{3} \rho_t L)$

and $\mu_2 = \rho_t L / (m_s + \frac{1}{3} \rho_t L)$

Similar equations for α and γ are omitted here for brevity. The presence of the terms $2\delta_k \eta'$ and η'' in the right hand side of Eqs. (8b) and (8c), respectively suggests that inplane transverse vibrations and oscillations may be reduced by letting the length rate η' depend linearly on transverse vibrational rate and longitudinal strain. However, no such term is present for out-of-plane vibrations and a nonlinear control law in conjunction with nonlinear equations must be considered for that case. This conclusion of linear state feedback of out-of-plane vibrations is parallel to the case of rotational control for which it has been shown⁹ that nonlinear equations of motion must be considered and an appropriate control law is

$$\eta' = K_\theta [1 + K_\alpha \alpha' + K_\gamma \gamma'^2], \quad (9)$$

where K_α and K_γ are negative constants and K_θ is, in general, a negative function of θ defining the commanded or nominal retrieval rate.

It may be noted that 'modal decoupling' is possible only for a constant length tether (i.e., $\eta' = 0$), but not during retrieval. This is due to the

fact that there are no conventional normal modes for a tether having a time varying length and the modal co-ordinates (loosely termed) are coefficients of admissible functions which are time dependent. This coupling turns out to be useful due to the following: δ_k and hence $2\delta_k\eta'$ is zero for an even k and without coupling vibrational feedback to η' would have no effect (except of second order) on even modes.

The length rate chosen to control the general dynamics is of similar form as Eq.(9) and is given by

$$\eta' = K_0 [1 + K_i^T x_i + K_0^T g(x_0)] \quad (10)$$

where x_i and x_0 are the inplane and out-of-plane portion of the state vector, K_i and K_0 are a set of gain vectors and g is a nonlinear vector function of x_0 . There are no standard procedures to determine K_i and K_0 . Here, they are chosen so that in approximated forms of Eq(8), the negative damping due to negative η' is eliminated.

The pitch and roll behaviour of the system during retrieval of the subsatellite using

$$\eta' = \frac{c}{\Lambda} (1 - \alpha' - 9\gamma'^2) \quad , \quad c = -2 \times 10^{-4} \text{sec}^{-1} \quad (11)$$

is shown to be stable limit cycles in Reference 9. The vibrational behaviour using the same length rate is shown in Figure 3. The longitudinal oscillation grows rather fast and the transverse vibrations are building up slowly. Numerical integration was stopped when the longitudinal oscillation became too large.

Figure 4 shows the response of the system when the length rate is:

$$\eta' = \frac{c}{\Lambda} (1 - \gamma' - 9\gamma'^2 - K_\epsilon \epsilon) \quad , \quad K_\epsilon = 30, \quad c = -2 \times 10^{-4} \text{sec}^{-1}, \quad (12)$$

Axial vibrations are more or less eliminated. The transverse displacements represented by A_1 , A_2 , B_1 , and B_2 and the resultant transverse deflection of the midpoint of the tether denoted by R also are small towards the end of retrieval. The dimensionless modal co-ordinates \tilde{A}_1 , \tilde{A}_2 , \tilde{B}_1 , and \tilde{B}_2 are bounded within reasonable limits, although they have grown during retrieval. Using a length rate

$$\eta' = \frac{c}{\Lambda} (1 - \alpha' - 9\gamma'^2 - K_{b1} B_1^1) \quad , \quad (13)$$

with $K_{b1} = 10$ and employing a viscous damper to provide a force proportional to the longitudinal strain rate, one obtains the system response shown in Figure 5. This response is very similar to that in Figure 4, except that the transverse vibrations are slightly smaller. The retrieval dynamics up to a tether length of 250 m using Eq.(12) is described in Figure 6. K_ϵ is 30 for $L > 1.2\text{km}$, but is 300 for $L < 1.2\text{km}$. It may be noted that the vibrations remain small up to the end of retrieval.

CONCLUDING REMARKS

The salient features of the analysis may be summarized as follows:

- (i) Control of longitudinal and transverse vibrations of a shuttle supported tethered system during its retrieval can be carried out by letting the length rate depend on the vibrational state variables.
- (ii) Linear feedback of inplane state variables and nonlinear feedback of out-of-plane state variables are used.
- (iii) Several control procedures with reasonable success are proposed.

(iv) It is suggested that some effort should be directed towards developing suitable procedures for control of flexible systems where nonlinearities and time dependence of system parameters cannot be ignored.

REFERENCES

1. Preliminary Design Office, "Shuttle/Tethered Satellite System Conceptual Design Study", NASA TM x-73365, Marshall Space Flight center, December 1976.
2. Colombo, G. et al., "Shuttle-Borne Skyhook", Smithsonian Astrophysical Observatory Report in Geoastronomy No.1, September 1974.
3. Misra, A.K. and Modi, V.J., "Deployment and Retrieval of Shuttle Supported Tethered Satellites", Journal of Guidance, Control and Dynamics, Vol.5, No.3, May-June 1982, pp.278-285.
4. Rupp, C.C., "A Tether Tension Control Law for Tethered Subsatellites Deployed Along Local Vertical", NASA TM x-64963, Marshall Space Flight Center, September 1975.
5. Baker, W.P. et al., "Tethered Subsatellite Study". NASA TM x-73314, Marshall Space Flight Center, March 1976.
6. Bainum, P.M. and Kumar, V.K., "Optimal Control of the Shuttle-Tethered-Subsatellite Study", Acta Astronautica, Vol. 7, No.12, 1980, pp.1333-1348.
7. Kulla, P., "Dynamics of Tethered Subsatellites", Proceedings of the Symposium on Dynamics and Control of Non-Rigid Spacecraft, Frascati, Italy, May 1976, pp.349-354.
8. Kalaghan, P.M., et al., "Study of the Dynamics of a Tethered Satellite System (Skyhook)", Final Report, Contract NAS8-32199, Smithsonian Institution, Astrophysical Observatory, Cambridge, Mass., March 1978.
9. Xu, D.M., Misra, A.K., and Modi, V.J., "Three Dimensional Control of the Shuttle Supported Tethered Satellite Systems during Retrieval", 3rd VPISU / AIAA Symposium on Dynamics and Control of Large Flexible Spacecraft, Blacksburg, Va., June 1981.

APPENDIX A

Equations for A_k and ϵ degrees of freedom are as follows:

$$\begin{aligned} \ddot{A}_k + (\dot{L}/L)\dot{A}_k + [\omega_k^2 - \omega_{yc}^2 - \omega_{zc}^2 + (\mu/R_0^3)(1 - 3\ell_{xc}^2)]A_k + \sum_{j=1}^{\infty} [(\dot{A}_j + \omega_{yc}B_j)(C_{jk} - C_{kj})(\dot{L}/L) \\ - (\dot{L}/L)^2 D_{jk}A_j + (\dot{L}/L)C_{jk}A_j] + 2\omega_{yc}\dot{B}_k + \{\dot{\omega}_{yc} + \omega_{xc}\omega_{zc} - (3\mu/R_0^3)\ell_{xc}\ell_{zc} + (\dot{L}/L)\omega_{yc}\}B_k \\ - [\sigma_k L \{\dot{\omega}_{zc} - \omega_{xc}\omega_{yc} + (3\mu/R_0^3)\ell_{xc}\ell_{yc}\}(1 + \epsilon) + 2\delta_k \dot{L}(1 + \epsilon)\omega_{zc}] = Q_{bk}/\rho_t L \end{aligned} \quad (A-1)$$

$$\begin{aligned}
& \ddot{\epsilon} + 2\mu_1(\dot{L}/L)\dot{\epsilon} + [\omega_\epsilon^2 + \mu_1(\dot{L}/L)]\epsilon - [\omega_{XC}^2 + \omega_{ZC}^2 - (\mu/R_0^3)(1-3\ell_{YC}^2) - \mu(\dot{L}/L)] \\
& - 2(\mu_2/L) \sum_{k=1}^{\infty} \sigma_k [\omega_{XC} \{ \dot{B}_k + 2(\dot{L}/L)B_k \} - \omega_{ZC} \{ \dot{A}_k + 2(\dot{L}/L)A_k \}] \\
& - (\mu_2/L) [\dot{\omega}_{XC} - \omega_{YC}\omega_{ZC} - (3\mu/R_0^3)\ell_{YC}\ell_{ZC}] \sum_{k=1}^{\infty} \sigma_k A_k = Q_\epsilon / \ell^2 (m_S + 1/3 \rho_t L)
\end{aligned} \tag{A-2}$$

where μ = gravitational constant of the earth

$$\mu_1 = (m_S + 1/2 \rho_t L) / (m_S + 1/3 \rho_t L)$$

$$\mu_2 = \rho_t L / (m_S + 1/3 \rho_t L)$$

$$\sigma_k = \sqrt{2} (-1)^{k-1} / k\pi$$

$$\delta_k = 2\sqrt{2} / k\pi \text{ for odd } k, 0 \text{ for even } k$$

$$C_{jk} = \begin{cases} 2jk / (k^2 - j^2), & j \neq k \\ 1/2, & j = k \end{cases}$$

$$D_{jk} = \begin{cases} 4jk(j^2 + k^2) / (j^2 - k^2)^2, & j \neq k \\ 1/2 + k^2\pi^2/3, & j = k \end{cases}$$

$$\omega_k^2 = (k\pi/L)^2 (EAE/\rho_t)$$

$$\omega_\epsilon^2 = EA / (m_S + 1/3 \rho_t L) L$$

$$\omega_{XC} = \dot{\alpha} + \dot{\theta}c\gamma$$

$$\omega_{YC} = \dot{\gamma}s\alpha - \dot{\theta}s\gamma c\alpha$$

$$\omega_{ZC} = \dot{\gamma}c\alpha + \dot{\theta}s\gamma s\alpha$$

$$\ell_{XC} = sr$$

$$\ell_{YC} = c\alpha c\gamma$$

$$\ell_{ZC} = -s\alpha c\gamma$$

Equations for α and γ are given in Reference 9.

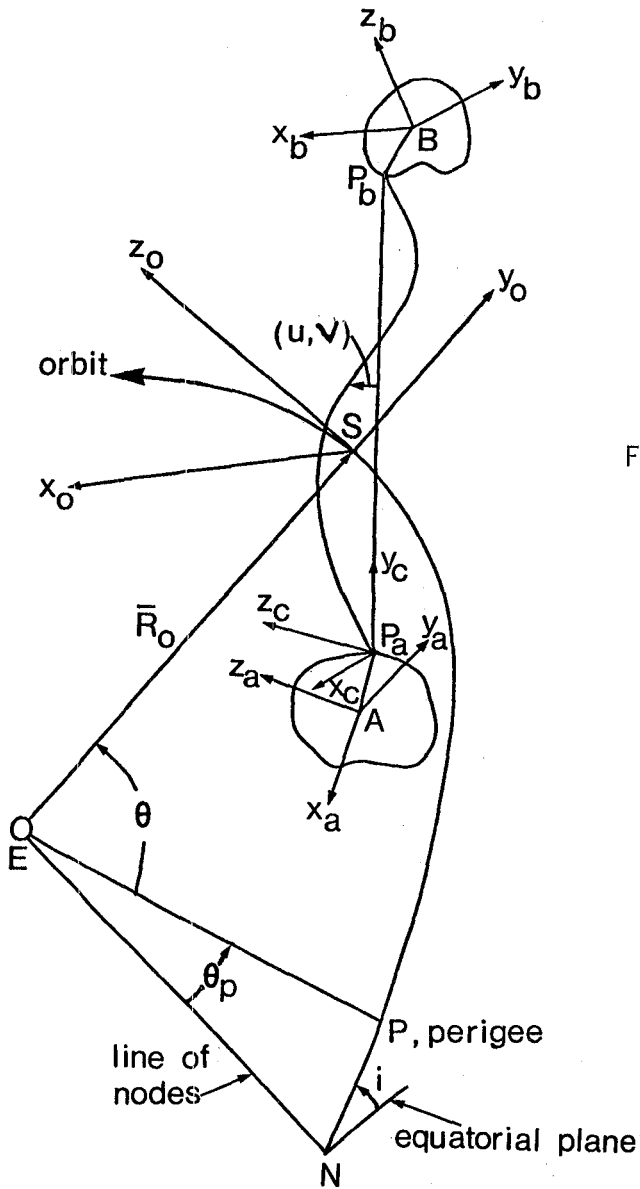


Figure.1. Geometry of motion.

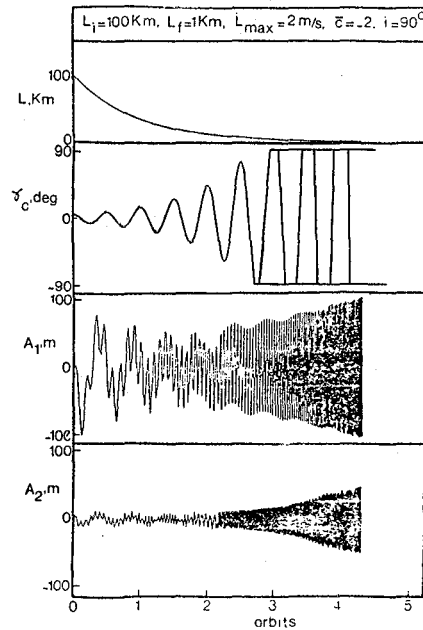


Figure 2. Typical out-of-plane response during uncontrolled retrieval.

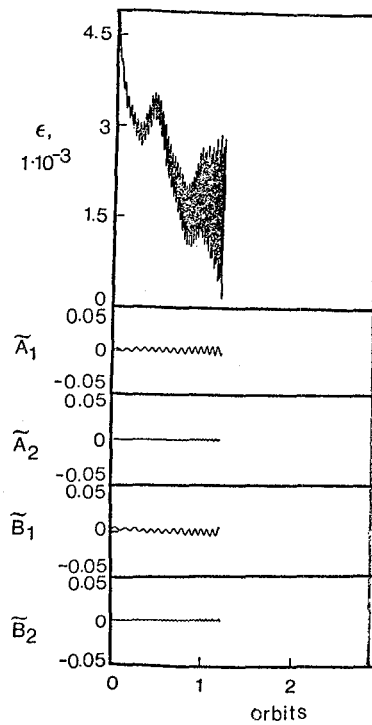


Figure 3. Vibrational response in the presence of rotational control.

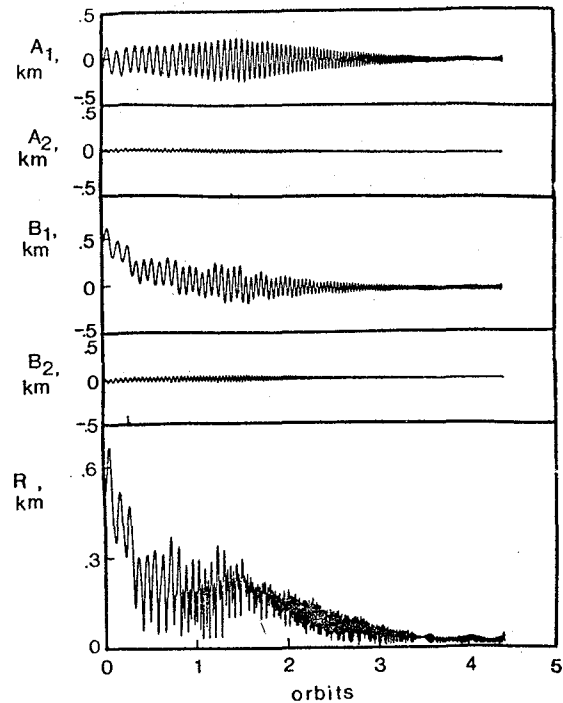
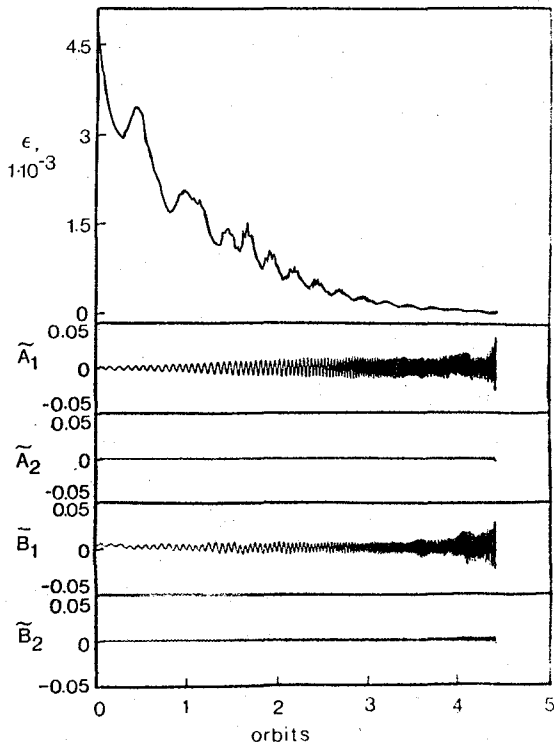
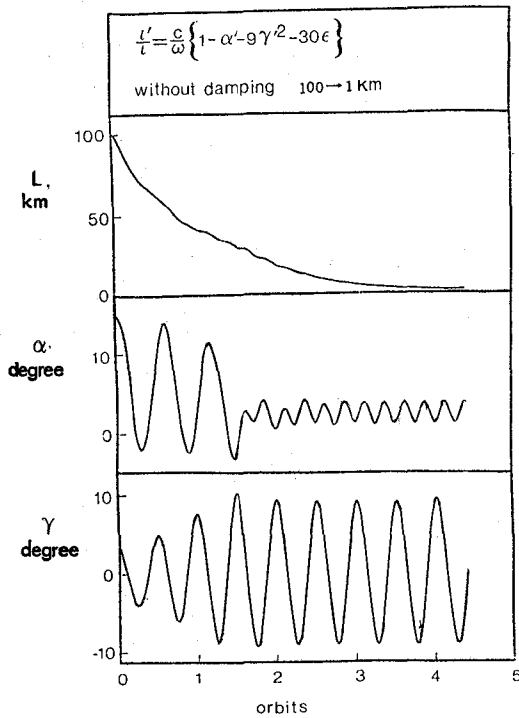


Figure 4. Response of the system using a length rate $\eta' = \frac{c}{\omega} (1 - \alpha' - 9\gamma'^2 - K_{\epsilon}\epsilon)$, $K_{\epsilon} = 30$

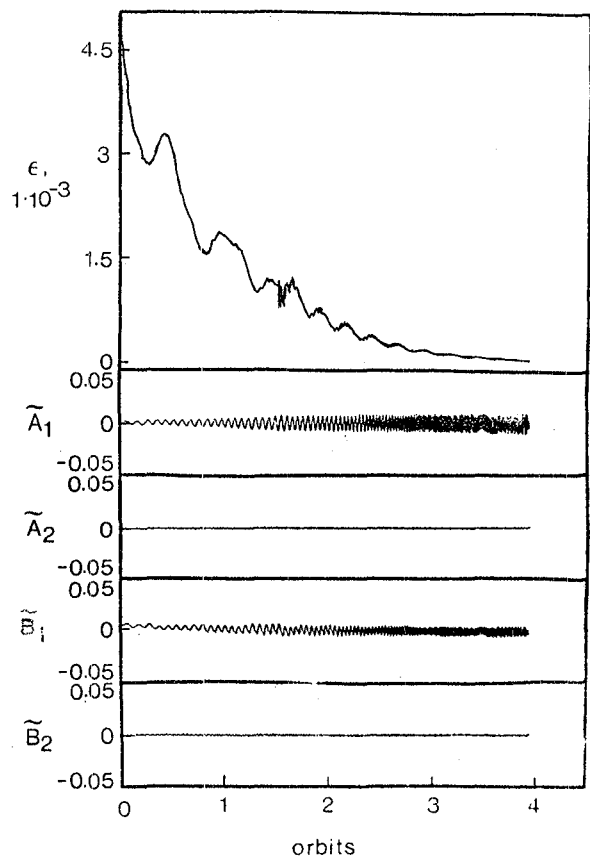


Figure 5. Vibrational response using $\eta' = \frac{c}{\Lambda}(1 - \alpha' - 9\gamma'^2 - 10\tilde{B}_1')$

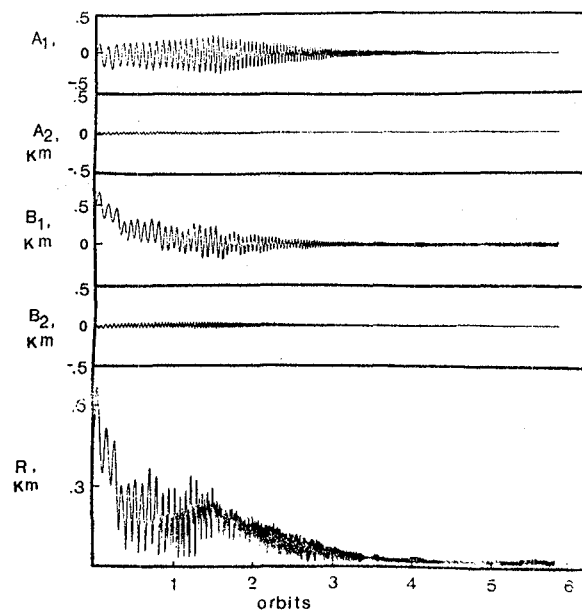


Figure 6. Vibrational response using $\eta' = \frac{c}{\Lambda}(1 - \alpha' - 9\gamma'^2 - K_\epsilon \epsilon)$; $K_\epsilon = 30, L > 1.2$; $K_\epsilon = 100, L < 1.2 \text{ km}$.

This Page Intentionally Left Blank

ORBITING CHAINS AND RINGS

John V. Breakwell

Department of Aeronautics/Astronautics
Stanford University
Stanford, CA 94305

ABSTRACT

This paper summarizes some recently published analyses of the hanging chain and the orbiting ring.

1. INTRODUCTION

This paper describes two very different, highly flexible, space structures which have been proposed during the last decade and which involve analytical solution of certain partial differential equations.

The first structure is an array, or "hanging chain" of aluminum beads [1] which would serve as a convenient communicator (see Fig. 1) if, under the influence of the earth's gravity gradient, it assumes a local vertical orientation as it circles the earth. The analysis for small deviations from vertical uses a continuous-chain model, and pitch and roll frequencies and mode shapes are readily obtained. Except for the lower, rigid, modes, damping is provided by fluid in the joints (see Fig. 2) between the aluminum beads. Two passive schemes have been proposed for damping the rigid modes: (i) twist the wire at the ends to provide non-zero moment of inertia about the vertical [1], thereby inducing relative motion of the two tips during rigid pitch or roll, and thus exercising a damper; (ii) introduce weak lossy springs [2] between the end sections and the main section; thereby providing linear coupling between the springs and all the in-plane (pitch) modes. Damping of the rigid roll is achieved by tuning the spring constant so that one of the in-plane combination modes has frequency 4 times orbital frequency. Nonlinear coupling then provides slow energy transfer back and forth between rigid roll and the particular in-plane combination mode, and hence, eventually, damping of the rigid roll.

The second structure, for some future generation(!), is a complete ring of satellites cabled together at synchronous altitude [3]. By a slight increase in altitude, the cable is in tension. This configuration is, however, unstable, and an active feedback control scheme is required to stabilize it. A possible scheme [3] involves local cable length adjustment based on measurement of local altitude and shape variations and their rates.

2. THE HANGING CHAIN

For launch, the array is coiled in a container. Deployment consists in driving the array out of the container, one end first. If the scattering elements were supported by a wire, the array would retain an unacceptable residual curvature. A freely jointed, bead-chain construction, on the other hand, would rely on the rather weak gravity gradient at synchronous altitude for straightening. Some inaccuracy, however, in deployment could result in an initially tumbling motion, and as this tumbling motion is slowed by damping (see later), there will be periods of compression rather than tension in the chain (see Fig. 3), which could result in the chain tying itself into knots. A happy compromise consists in a support structure of about 100 sections of relatively stiff wire connected by joints that are free up to about 3° of motion (see Fig. 2). Residual curvature of the sections is now tolerable, and knotting is impossible. Gravity gradient and damping can be relied upon to align and straighten the array.

Modeling the chain as a perfectly flexible cable of length L and linear density σ , the tension in a vertical equilibrium position is:

$$T_e = \frac{3}{2} \sigma n^2 \left\{ \left(\frac{L}{2} \right)^2 - x^2 \right\} \quad (1)$$

where n is the (constant) orbital angular rate.

Adopting the coordinate system of Fig. 4 and a dimensionless independent variable, $\xi = 2x/L$, the partial differential equations of motion become:

$$(1-\xi^2) \frac{\partial^2 y}{\partial \xi^2} - 2\xi \frac{\partial y}{\partial \xi} = \frac{2}{3n^2} \frac{\partial^2 y}{\partial t^2} \quad (2)$$

$$(1-\xi^2) \frac{\partial^2 z}{\partial \xi^2} - 2\xi \frac{\partial z}{\partial \xi} - \frac{2}{3} z = \frac{2}{3n^2} \frac{\partial^2 z}{\partial t^2}$$

The mode-shapes are Legendre polynomials:

$$y_l(\xi) = z_l(\xi) = AP_l(\xi)$$

and the frequencies are given by:

$$(\omega_y/n)^2 = (\omega_z/n)^2 - 1 = \frac{3}{2} l(l+1) \quad (3)$$

Damping in the joints may be represented by small additions to the equations of motion. In-plane, for example:

$$(1-\xi^2)y_{\xi\xi} - 2\xi y_{\xi} + \frac{2}{3} \left(\frac{\omega_y}{n} \right)^2 y = j\eta y_{\xi\xi\xi\xi} \quad (4)$$

where η is a small dimensionless damping parameter, and the rate of energy loss in the l^{th} mode is approximately

$$\frac{3}{8} \eta \omega_y \sigma L n^2 A^2 \int_{-1}^1 P_l''^2(\xi) d\xi \quad ,$$

providing damping of all but the rigid mode: $l = 1$.

The first passive scheme proposed [1] for damping the rigid pitch and roll modes is illustrated in Figs. 5, 6 and 7. For a chain of length 150 m and "tip inertias" of radius 5 m, it was estimated that in-plane libration could be decreased by a factor 2 in $5 \frac{1}{2}$ days, and out-of-plane libration a little faster.

The second passive scheme requires the tuning of springs inserted between the end portions of the chain and the main portion. The spring constants must be adjusted so that one of the odd in-plane combination modes has frequency at or close to twice that of rigid roll, i.e., 4 times orbital frequency n . This provides for a slow interchange of energy between the rigid roll and the particular in-plane mode. The necessity for choosing an odd rather than an even in-plane mode. The necessity for choosing an odd rather than an even in-plane mode arises from the requirement that the two springs act together rather than in opposition. It was estimated that, if the time-constant of the in-plane mode was 10 days, due to energy loss either in the spring or in the cable joints, a 2 1/2% mismatch to the frequency $4n$ could still reduce a rigid roll amplitude from 30° (unacceptable) to 4° (acceptable?) in about 60 days.

3. THE ORBITING RING

Treating the ring [3] as a continuous, perfectly flexible, chain with longitudinal elasticity in circular orbit at radius R about a spherical planet, the equilibrium tension is:

$$T_e = \sigma R (n^2 R - \mu / R^2) \quad , \quad (5)$$

proportional to the difference between centrifugal and gravitational acceleration. The tension in a displaced position is:

$$T = T_e + k \frac{\partial(\Delta s)}{\partial \alpha} = T_e + k(x + y_\alpha) \quad (6)$$

where α is the angular position of an element of the ring. Introducing two non-dimensional parameters:

$$\omega^2 = T_e / (n^2 \sigma R^2) = 1 - \mu / (n^2 R^3) \quad (7)$$

typically much less than unity, and

$$\omega_1^2 = k / (n^2 \sigma R) \quad (8)$$

typically much greater than unity, and the non-dimensional time:

$$\tau = nt \quad (9)$$

the equations of motion are:

$$y_{\tau\tau} - 2y_\tau - (3 - 2\omega^2)x - \omega^2(x_{\alpha\alpha} - y_\alpha) + \omega_1^2(x + y_\alpha) = 0$$

$$y_{\tau\tau} + 2x_\tau - \omega^2 x_\alpha - \omega_1^2(x_\alpha + y_{\alpha\alpha}) = 0$$

$$z_{\tau\tau} + (1 - \omega^2)z - \omega^2 z_{\alpha\alpha} = 0$$

Modal solutions have x, y, z proportional to $e^{j(m\alpha + \Omega_m \tau)}$, m being an integer, yielding the following characteristic equations:

$$\begin{aligned} \Omega_m^4 - [1 + (m^2 + 2)\omega^2 + (m^2 + 1)\omega_1^2]\Omega_m^2 + 4m(\omega^2 + \omega_1^2)\Omega_m \\ + m^2(m^2\omega^2\omega_1^2 - \omega^4 - 3\omega_1^2) = 0 \quad (10) \end{aligned}$$

arising from the in-plane coupled x, y equations, and

$$\Omega_m^2 - m^2\omega^2 - (1-\omega^2) = 0 \quad , \quad (11)$$

arising from the out-of-plane z equation.

The ring is unstable unless both characteristic equations lead to real, distinct, values of Ω_m , for each $m \geq 0$. The out-of-plane motion is thus clearly linearly stable.

In the limiting case ($\omega_1^2 = \infty$) of the inextensible ring, the in-plane characteristic equation for $m = 1$ yields $\Omega_1 = 1 \pm j\sqrt{\frac{1-\omega^2}{2}}$, leading to instability, corresponding in fact [3] to a growing rigid translation out of position. Numerical investigation of the extensible case, $\omega_1^2 < \infty$, revealed that, although the mode $m = 1$ could become stable in the unlikely case that ω_1^2 were sufficiently small in comparison to ω^2 , some other mode would always go unstable.

Stability for $m = 1$ is, moreover, impossible when elastic damping is taken into account. To see this, we replace k by $k(1+\beta j\Omega_1)$, where β is real and positive, and hence ω_1^2 by $j\beta K(\Omega_1 - j/\beta)$, where K is the undamped value of ω_1^2 . A typical root-locus vs K , for fixed β greater than zero, is sketched in Fig. 8. Since one branch immediately enters the lower half Ω_1 -plane, instability occurs for all $K > 0$.

It has been shown [3] that, at least for $\omega_1^2 \gg 1$ and $\omega^2 \ll 1$, the following control law stabilizes all modes:

$$T = T_0 + k(x + y_\alpha - u) \quad , \quad (12)$$

u being a local cable length change, given by:

$$u = \left[1 - \frac{3-2\omega^2}{K(1+\beta s)} \right] x + 3x_{\alpha\alpha} - \frac{As}{K(1+\beta s)} \left[x - \frac{1}{4}\omega^2 x_{\alpha\alpha} \right] + \frac{A}{K(1+\beta s)} \left[\frac{1}{4}y + \frac{1}{12}\omega^2 y_{\alpha\alpha} \right] \quad , \quad (13)$$

where the Laplace variable s indicates differentiation w.r.t. time. Indeed, the resulting characteristic equation takes the form:

$$\Delta_4(\Omega_m) - j\Delta_3^*(\Omega_m) = 0 \quad , \quad (14)$$

where

$$\Delta_3^*(\Omega_m) \equiv A\Delta_3(\Omega_m) + K\beta\Delta_2(\Omega_m) \quad , \quad (15)$$

and where the polynomials $\Delta_i(\Omega_m)$ have zeros as indicated in Fig. 9. Since the zeros of $\Delta_3^*(\Omega_m)$, like those of $\Delta_3(\Omega_m)$, always separate those of $\Delta_4(\Omega_m)$, the root-locus vs A has all branches entering the upper half Ω_m -plane as soon as $A > 0$, and some damping of all modes is assured.

It is interesting to note that the system is not completely controllable: an initial error in total ring angular momentum cannot be removed. Nevertheless, the control law (13), applied to the "uniform" mode $m = 0$, removes the angular error y of all points of the ring by adjusting the cable length and hence the radial increment x .

REFERENCES

- [1] Breakwell, J.V. and G.B. Andeen, "Dynamics of a Flexible Passive Space Array," *J. of Spacecraft & Rockets*, vol. 14, no. 9, Sept. 1977, pp. 556-561.
- [2] Breakwell, J.V. and G.B. Andeen, "A Flexible Passive Space Array with Springs (II)," *Proceedings of Dynamics of Multibody Systems*, IUTAM Symposium, Aug. 29-Sept. 3, 1977, Munich, Germany.
- [3] Breakwell, J.V., "Stability of an Orbiting Ring," *J. Guid. & Contr.*, vol. 4, no. 2, March-April 1981, pp. 197-200.

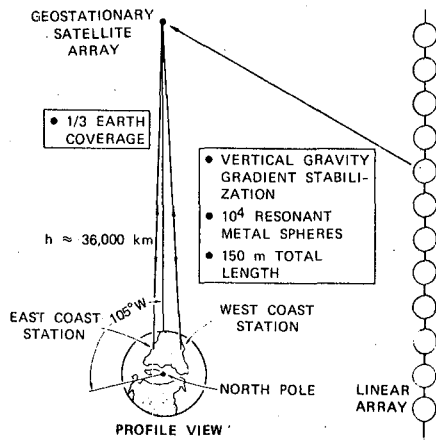


Fig. 1 Configuration of feasibility demonstration.

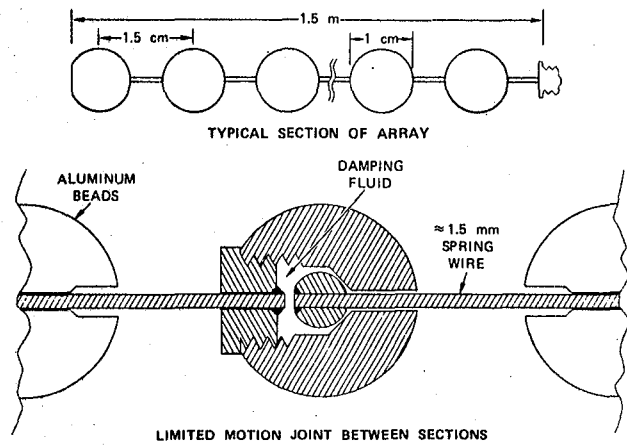


Fig. 2 Array construction

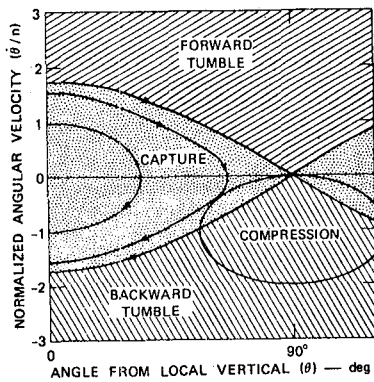


Fig. 3 Phase-plane plot for the in-plane motion of a rigid rod.

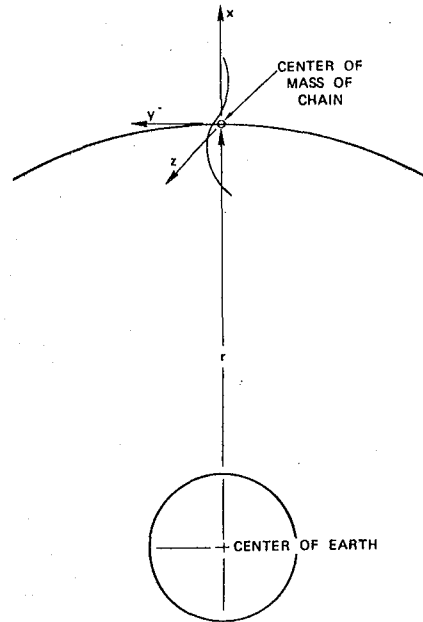


Fig. 4 Coordinate system.

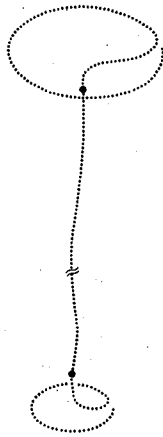


Fig. 5 Array of inertial tips.

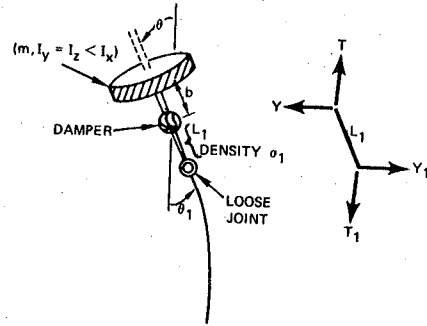


Fig. 6 Dynamic model of tip inertia.

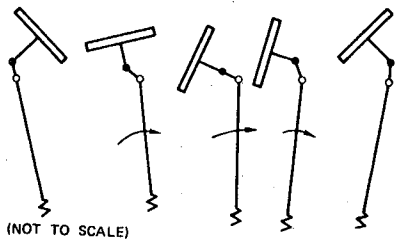


Fig. 7 Libration of tip inertia (1/2 cycle).

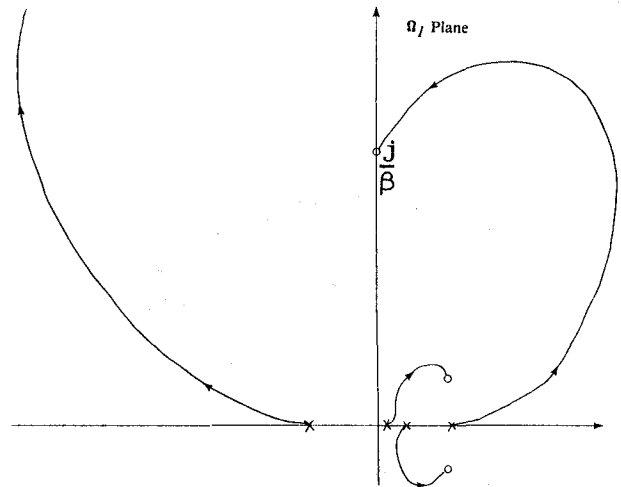
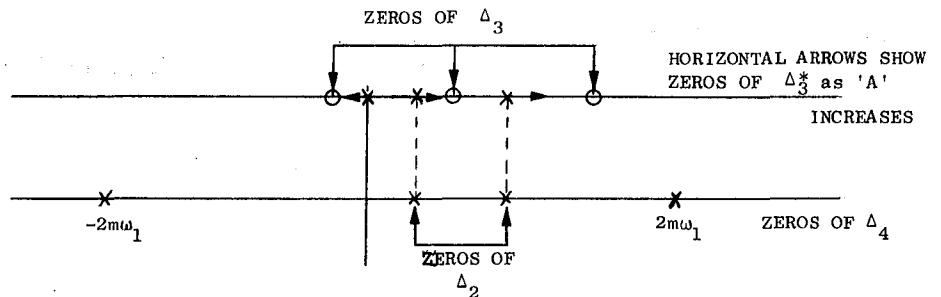


Fig. 8 Root locus for Ω_1 vs $K = \text{Re}(\omega_I^2)$, fixed β .

Fig. 9 Zeros of Δ_3^* and Δ_4 .



HARDWARE VERIFICATION OF DISTRIBUTED/ADAPTIVE CONTROL

Daniel B. Eldred and David B. Schaechter

Jet Propulsion Laboratory
California Institute of Technology
Pasadena, CA 91109

ABSTRACT

Adaptive control techniques are being studied for their future application to the control of large space structures, where uncertain or changing parameters may destabilize standard control system designs. The approach used in this paper is to examine an extended Kalman filter estimator, in which the state vector is augmented with the unknown parameters. The associated Riccati equation is linearized about the case of exact knowledge of the parameters. By assuming that parameter variations occur slowly, the filter complexity is reduced further yet. Simulations on a two degree-of-freedom oscillator demonstrate the parameter-tracking capability of the filter, and an implementation on the JPL Flexible Beam Facility using an incorrect model shows the adaptive filter/optimal control to be stable where a standard Kalman filter/optimal control design is unstable.

INTRODUCTION

This paper contains the derivation of a simplified, state space adaptive filter/controller, which can be used in real time to adapt to changing or uncertain dynamic models. The application of the simplified extended Kalman filter approach to a two degree-of-freedom oscillator is compared to the more complex complete extended Kalman filter. It will be seen that the simplified filter compares quite well with the full order filter. In addition, the simplified filter has been implemented on an experimental facility consisting of a large, flexible hanging beam. Experiments on the facility show that the adaptive filter/optimal control can stabilize a system whereas the Kalman filter/optimal control destabilizes it, if the system model is incorrect.

As usual, the problem formulation begins with a dynamic system in state variable format

$$\begin{aligned}\dot{\mathbf{x}} &= \mathbf{F}\mathbf{x} + \mathbf{G}\mathbf{u} + \mathbf{\Gamma}\mathbf{w} \\ \mathbf{z} &= \mathbf{H}\mathbf{x} + \mathbf{v}\end{aligned}\tag{1}$$

In the case that the dynamic system in (1) is precisely known, a state estimator of the following form may be constructed,

$$\dot{\hat{\mathbf{x}}} = \hat{\mathbf{F}}\hat{\mathbf{x}} + \mathbf{G}\mathbf{u} + \mathbf{K}(\mathbf{z} - \hat{\mathbf{H}}\hat{\mathbf{x}})\tag{2}$$

Optimal estimator gains K may be selected by minimizing the trace of the estimate error covariance, $P = E(\tilde{x}\tilde{x}^T)$. Letting $\tilde{x} = x - \hat{x}$, differencing (1) and (2) gives

$$\dot{\tilde{x}} = (F - KH)\tilde{x} + \Gamma w - K v \quad (3)$$

then

$$\dot{P} = E(\dot{\tilde{x}}\dot{\tilde{x}}^T) + E(\tilde{x}\dot{\tilde{x}}^T) = (F-KH)P + P(F-KH)^T + \Gamma Q \Gamma^T + K R K^T \quad (4)$$

Picking K to minimize the trace of the estimate error covariance gives the usual result

$$K = P H^T R^{-1} \quad \text{and} \quad \dot{P} = F P + P F^T + \Gamma Q \Gamma^T - P H^T R^{-1} H P \quad (5)$$

Notice that for the case of a precisely known dynamic system, the estimator gain may be precomputed, even in the event of a time varying system. The analysis used in the case of unknown system parameters closely parallels the preceding development.

Adaptive Control Formulation

Adaptive control may be required in the case that the model in (1) is unknown, uncertain, or dependent upon the system configuration. The modifications that need to be made in (1) in order to include the effects of an uncertain parameter are given below

$$\begin{aligned} \dot{\tilde{x}} &= F(a)\tilde{x} + G(a)u + \Gamma w \\ \dot{a} &= w_a \\ z &= Hx + v \end{aligned} \quad (6)$$

As can be seen from (6), the system dynamics are now a function of the vector of parameters, a . Furthermore, these parameters are assumed to be randomly varying constants, so that they may be adjoined to the state vector. An adaptive state estimator may now be written as

$$\begin{aligned} \dot{\hat{x}} &= F(\hat{a})\hat{x} + G(\hat{a})u + K_x(z - H\hat{x}) \\ \dot{\hat{a}} &= K_a(z - H\hat{x}) \end{aligned} \quad (7)$$

Now, both the state vector and the vector of parameters is updated using the measurements. Determination of the adaptive gains K_x and K_a still remains.

Proceeding as before, and assuming $\tilde{a} = a - \hat{a}$ is small

$$\begin{aligned} \dot{\tilde{x}} &= (F(\hat{a}) - K_x H)\tilde{x} + \left(\frac{\partial F}{\partial \hat{a}} \hat{x} + \frac{\partial G}{\partial \hat{a}} u\right) \tilde{a} + \Gamma w - K_x v \\ \dot{\tilde{a}} &= -K_a H \tilde{x} + w_z - K_a v \end{aligned} \quad (8)$$

An optimal choice of gains may be selected by minimizing the trace of the estimate error covariance,

$$\begin{aligned} K_x &= P_x H^T R^{-1} \\ K_a &= P_{ax} H^T R^{-1} \end{aligned}$$

and

$$\begin{aligned} \begin{bmatrix} \dot{P}_x & \dot{P}_{ax}^T \\ \dot{P}_{ax} & \dot{P}_a \end{bmatrix} &= \begin{bmatrix} F & \left(\frac{\partial F}{\partial \hat{a}} \hat{x} + \frac{\partial G}{\partial \hat{a}} u\right) \\ 0 & 0 \end{bmatrix} \begin{bmatrix} P_x & P_{ax}^T \\ P_{ax} & P_a \end{bmatrix} \\ &+ \begin{bmatrix} P_x & P_{ax}^T \\ P_{ax} & P_a \end{bmatrix} \begin{bmatrix} F^T & 0 \\ \left(\frac{\partial F}{\partial \hat{a}} \hat{x} + \frac{\partial G}{\partial \hat{a}} u\right)^T & 0 \end{bmatrix} \\ &+ \begin{bmatrix} \Gamma & 0 \\ 0 & I \end{bmatrix} \begin{bmatrix} Q & 0 \\ 0 & Q_a \end{bmatrix} \begin{bmatrix} \Gamma^T & 0 \\ 0 & I \end{bmatrix} \\ &- \begin{bmatrix} P_x & P_{ax}^T \\ P_{ax} & P_a \end{bmatrix} \begin{bmatrix} H & 0 \end{bmatrix}^T R^{-1} \begin{bmatrix} H & 0 \end{bmatrix} \begin{bmatrix} P_x & P_{ax}^T \\ P_{ax} & P_a \end{bmatrix} \end{aligned} \quad (9)$$

In addition to the increased dimension of (9) over (5), the feature that distinguishes these two cases is the appearance of \hat{x} term in (9). \hat{x} is the estimate of the state, and therefore cannot be known a priori. Therefore, both the state estimator and the augmented order matrix Riccati equation must be solved in real time in order to implement the extended Kalman filter. On

line solution of the matrix differential equation tremendously increases the required computation. Several approximations will be made in an attempt to reduce this computational complexity.

Extended Kalman Filter Approximation (EKF)

In the case when there are no uncertain parameters (and, of course, under suitable observability conditions), the estimator gains tend to a steady state value. A reasonable choice for simplifying the EKF is to linearize the solution about the case of perfectly known parameters. Toward this end, it will be assumed that $P = P_0 + \epsilon P_1 + \epsilon^2 P_2 \dots$, where P_0 is a constant matrix and ϵ is a small parameter, and that the process noise driving the parameters has a spectral density Q_a of order ϵ^2 . In the limiting case, for $\epsilon = 0$, the solution reduces to the familiar steady state gains for a perfectly known system. Letting

$$F_a \hat{x} = \frac{\partial F}{\partial \hat{x}} \hat{x} + \frac{\partial G}{\partial \hat{a}} u,$$

expanding (9) and collecting like powers of ϵ gives the following intermediate results:

zeroth order

$$0 = F P_{x_0} + P_{x_0} F^T + F_a \hat{x} P_{ax_0} + P_{ax_0}^T (F_a \hat{x})^T + \Gamma Q \Gamma^T - P_{x_0} H^T R^{-1} H P_{x_0} \quad (10a)$$

$$0 = P_{ax_0} F^T + P_{a_0} (F_a \hat{x})^T - P_{ax_0} H^T R^{-1} H P_{x_0} \quad (10b)$$

$$0 = P_{ax_0} H^T R^{-1} H P_{ax_0}^T \quad (10c)$$

first order

$$\dot{P}_{x_1} = F P_{x_1} + P_{x_1} F^T + F_a \hat{x} P_{ax_1} + P_{ax_1}^T (F_a \hat{x})^T - P_{x_0} H^T R^{-1} H P_{x_1} - P_{x_1} H^T R^{-1} H P_{x_0} \quad (11a)$$

$$\dot{P}_{ax_1} = P_{ax_1} F^T + P_{a_1} (F_a \hat{x})^T - P_{ax_0} H^T R^{-1} H P_{x_1} - P_{ax_1} H^T R^{-1} H P_{x_0} \quad (11b)$$

$$\dot{P}_{a_1} = -P_{ax_0} H^T R^{-1} H P_{ax_1}^T - P_{ax_1} H^T R^{-1} H P_{ax_0}^T \quad (11c)$$

From (10c), $P_{ax_0} = 0$. Using this result in (10b) gives $P_{a_0} = 0$. Using both these results in (10a) gives the familiar steady state results for a plant with known parameters, as was expected. The results obtained from (10) can now be used to simplify (11). A summary of the simplified results is given below:

zeroth order

$$0 = FP_{x_0} + P_{x_0}F^T + \Gamma Q \Gamma^T - P_{x_0}H^T R^{-1} H P_{x_0} \quad (12a)$$

$$0 = P_{ax_0} \quad (12b)$$

$$0 = P_{a_0} \quad (12c)$$

first order

$$\dot{P}_{x_1} = (F - K_{x_0} H) P_{x_1} + P_{x_1} (F - K_{x_0} H)^T + (F_a \hat{x}) P_{ax_1} + P_{ax_1}^T (F_a \hat{x})^T \quad (13a)$$

$$\dot{P}_{ax_1} = P_{ax_1} (F - K_{x_0} H)^T + P_{a_1} (F_a \hat{x})^T \quad (13b)$$

$$\dot{P}_{a_1} = 0 \quad (13c)$$

where

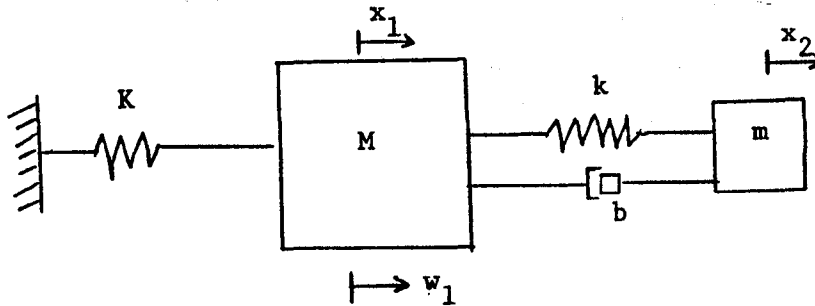
$$K_{x_0} = P_{x_0} H^T R^{-1}$$

Even after simplification, (12) and (13) require an on line integration of a matrix equation in order to generate the adaptive gains. A further simplification that can be made (and later be verified with simulation) is to assume the derivatives on the left hand side of (13) are identically zero. This allows for computation of the adaptive gains in terms of the current value of the state using a simple matrix multiplication, rather than a matrix integration. The final results of this simplification are shown in (14)

$$\begin{aligned}
0 &= P_{x_0} F + P_{x_0} F^T + \Gamma Q \Gamma^T - P_{x_0} H^T R^{-1} H P_{x_0} \\
\dot{P} &= P_{ax_1} (F - K_{x_0} H)^T + P_{a_1} (F_{ax_1})^T \\
P_{a_1} &= \text{constant} \\
K &= \begin{bmatrix} K_x \\ K_a \end{bmatrix} = \begin{bmatrix} P_{x_0} H^T R^{-1} \\ P_{ax_1} H^T R^{-1} \end{bmatrix}
\end{aligned}
\tag{14}$$

Adaptive Control Simulation

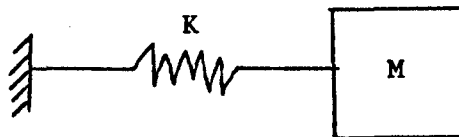
The extended Kalman Filter (EKF) and the approximation to the EKF derived in the previous simulation are compared using a simplified model for the computer simulation. The model used is shown below.



The equations of motion are:

$$\begin{aligned}
M\ddot{x}_1 &= -Kx_1 + k(x_2 - x_1) + b(\dot{x}_2 - \dot{x}_1) + w_1 \\
m\ddot{x}_2 &= -k(x_2 - x_1) - b(\dot{x}_2 - \dot{x}_1)
\end{aligned}
\tag{15}$$

The simulation consists of modeling the system shown in the previous schematic by simply:



At $t = 2$ on the computer generated charts shown in Figures 1-6, a step change in the natural frequency from 1.0 to 1.25; i.e. at 25% error in natural frequency is made. The adaptive filters are supposed to detect this error in the presence of process noise w_1 , a truncated mode, and measurement noise in the position of M. Virtually indistinguishable results are obtained for the estimator using the full EKF, vs. the estimator using the simplified EKF. On the computer charts, true values are shown by solid lines, and dashed lines show the corresponding estimated value.

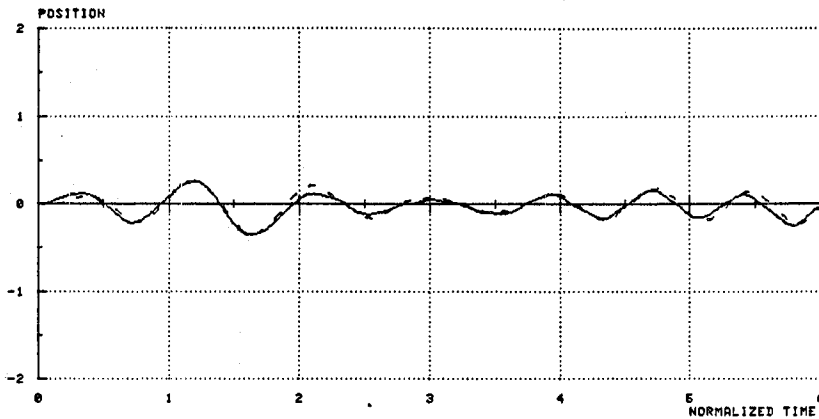


Figure 1. Extended Kalman Filter

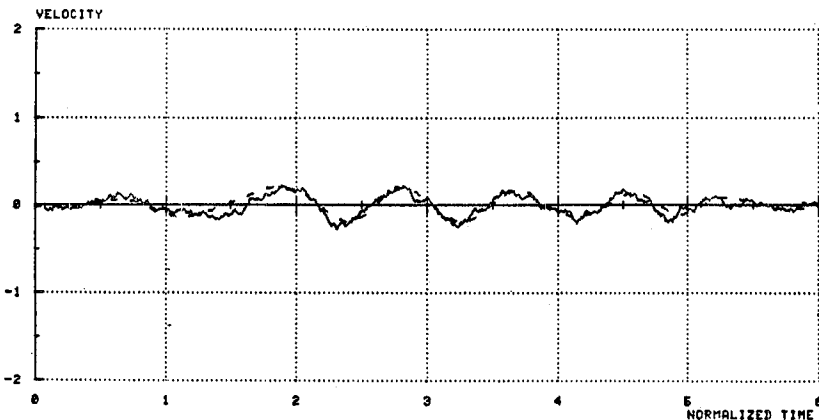


Figure 2. Extended Kalman Filter

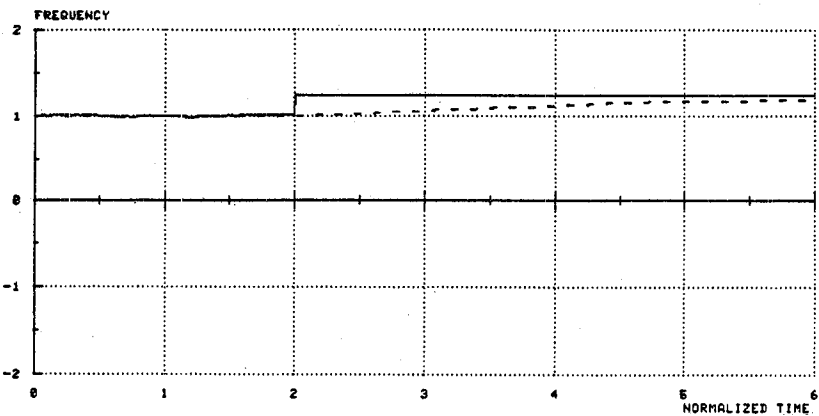


Figure 3. Extended Kalman Filter

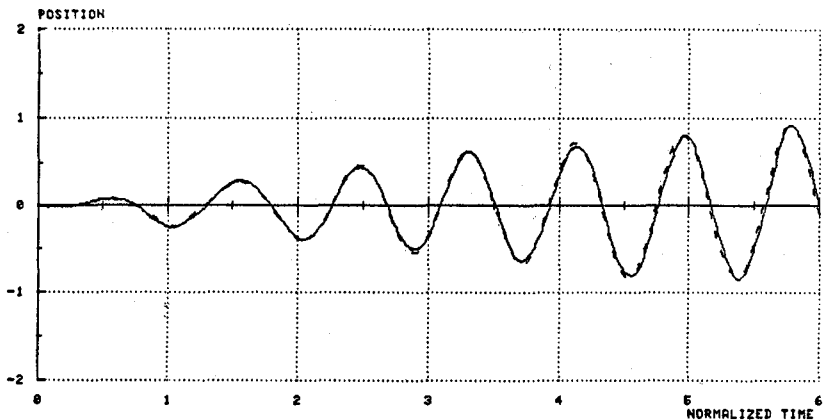


Figure 4. Adaptive Filter

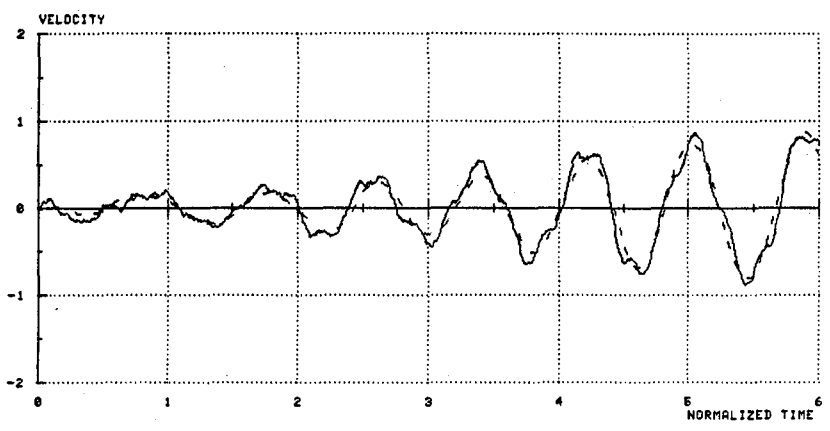


Figure 5. Adaptive Filter

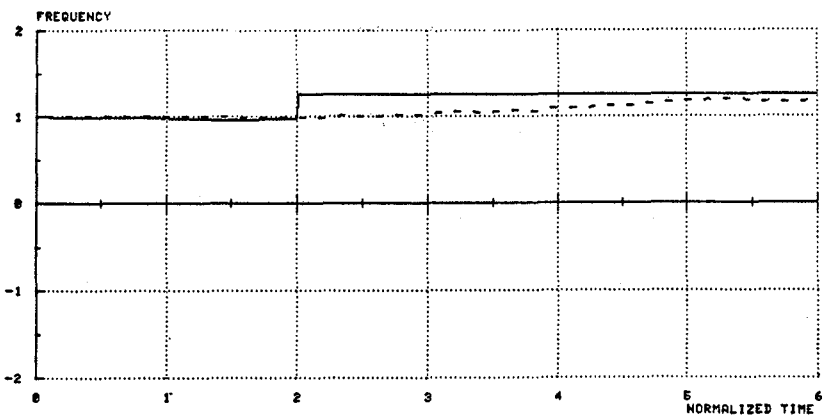


Figure 6. Adaptive Filter

The JPL Flexible Beam Facility

A facility has been constructed to experimentally validate a variety of control technologies associated with large, flexible space structures and to gain insight into their implementation. To date, Kalman filter/optimal control, distributed control, and static figure control have been demonstrated using the Flexible Beam.

The facility consists of a 12-1/2 foot long, by 6 inch wide, by 1/32 inch thick, hanging stainless steel beam. A large tower was constructed for the sole purpose of supporting the beam and isolating it from vibrations in the ground. Sensing with a range of ± 1 inch is performed by up to four eddy current sensors, and actuation is by three D.C. brushless motors capable of outputting 5 ounces to the beam.

All control functions are handled by a SYM microcomputer, which uses a 6502 microprocessor operating at 1 megahertz. Four 12-bit digital-to-analog converters on two circuit boards allow interfacing between the microcomputer and the sensors and actuators. In addition, a 9511 floating-point arithmetic processor performs the mathematical computations associated with digital filtering. Previously, computations were performed in software using two-byte fixed point precision; the 9511 executes four-byte floating point precision calculations in approximately 1/5 the time, allowing the implementation of more complex control laws.

Additional features of the facility include an ASCII keyboard, a video monitor, and a small printer. The microcomputer features an advanced monitor, for machine language debugging; an editor-assembler, for program development; and BASIC, which provides the interface between the user and machine language programs. Commonly used routines are stored on either erasable, programmable read-only memories (EPROMS), or digitally on inexpensive audio cassettes.

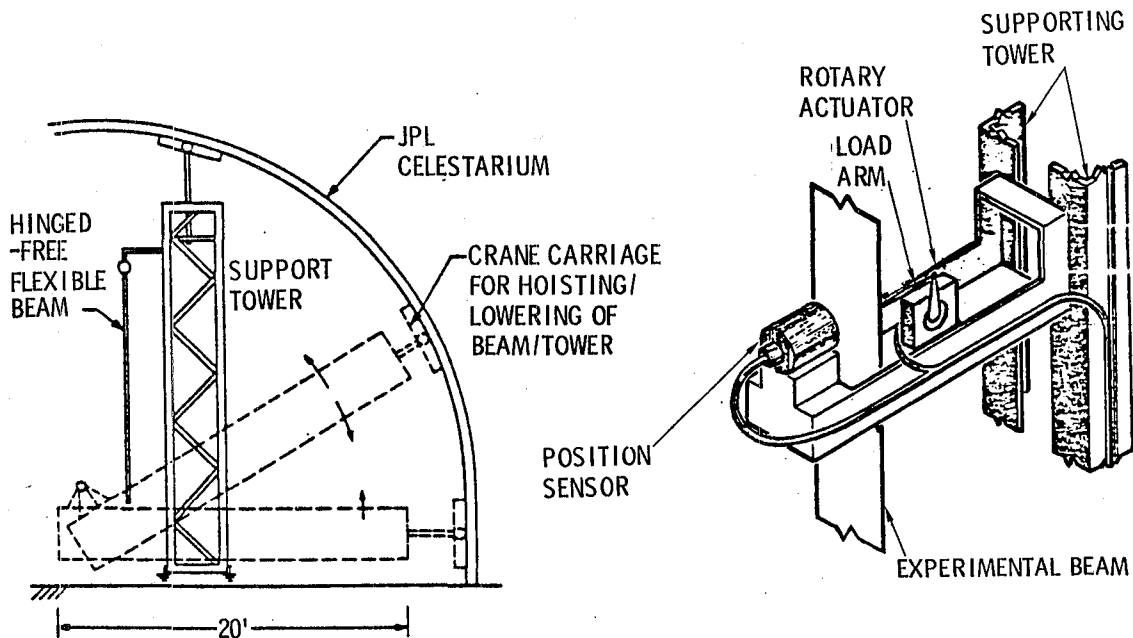


Figure 7. The JPL Flexible Beam Facility

A general purpose machine - language program has been written for the purpose of implementing control algorithms. Due to the predominance of matrices in digital control design, the program treats matrices as the primary data type. Single instructions allow matrices to be multiplied, added, stored, or recalled from memory. Additional instructions sample sensors, output controls, or set a timer (to maintain a constant control loop time). Every effort has been made to make the program fast and easy to use.

Additional documentation of the facility can be found in the references.

Beam Analysis

An exact solution to the partial differential equation for the beam

$$\frac{\partial^2}{\partial t^2} y(x,t) + \frac{\partial^2}{\partial x^2} (EI \frac{\partial^2 y}{\partial x^2}) - \frac{\partial}{\partial x} (pg(l-x) \frac{\partial y}{\partial x}) = f(x) \quad (16)$$

was unobtainable due to the presence of gravity. An approximation scheme, whereby the mode shapes were assumed to be a superposition of beam modes and hanging-chain modes, yielded the correct eigenvalues only approximately. A finite element model was therefore developed to obtain normal mode frequencies and mode shapes. From Table 2, it is clear that the predicted eigenvalues are very close to their experimental values.

Variable	Value	Description
l	149.875 in.	Beam Length
ρ	.6444 lb/ft	Linear Density
EI	424,352 lb-in ²	Beam Stiffness

Table 1. Beam Parameters

n	Finite Element Model	Experimental
0	.308 Hz	.34
1	.755	.75
2	1.38	1.37
3	2.21	2.15
4	3.24	3.16
5	4.47	4.38

Table 2. Normal Mode Frequencies

Implementation of Adaptive Estimation/Control

A three mode (six state), plus the highest frequency, adaptive filter/controller using one sensor and one actuator (at the lower end of the beam) was developed for experimental testing. A digital implementation of (7) should take into account the time delays associated with discrete-time sampling and actuation, (in this case, .030 sec). An attempt to derive a digital analog of (7) proved fruitless; instead, the filter gain K_x was obtained from a discrete Kalman filter analysis and the simple approximation

$$\hat{a}_{i+1} = \hat{a}_i + K_a (Z_i - H\hat{X}_i) \delta T \quad (17)$$

was made for the parameter updating. Since parameter variations are very slow compared to system response (by assumption), this approximation should not present any problems. In addition, the control gains were obtained from a discrete optimal control analysis.

The following plots show the beam response to an impulse at its lower end, and the control effort exerted, for the adaptive estimator/optimal control and the Kalman filter/optimal control. In one case, the assumed model is the correct model, and the other case, the third eigenvalue was intentionally made 20% too large to reflect an uncertain model. A discussion of each plot is included.

SUMMARY AND CONCLUSIONS

Although in theory, the extended Kalman filter is quite complex to implement in real time, this paper has shown that suitable approximations can make implementation quite tractable, while at the same time yielding excellent results. Of course, the virtues of adaptive estimators/control must be weighed against the extra computation time required; however, if the system is evolving in time or the model is inaccurate, then an adaptive estimator/controller is ideal.

REFERENCES

1. Bryson, A.E., and Y.C. Ho, Applied Optimal Control, John Wiley & Sons, New York, 1975.
2. Schaechter, David B., "Hardware Demonstration of Flexible Beam Control," 1980 AIAA Guidance and Control Conference, Danvers, Mass.
3. Eldred, Daniel B., "Finite Element Model for the LSST Beam," JPL Internal Document EM 347-101, 1981.
4. Eldred, Daniel B., and D.B. Schaechter, "Experimental Demonstration of Static Shape Control," 1981 AIAA Guidance and Control Conference, Albuquerque, N.M.

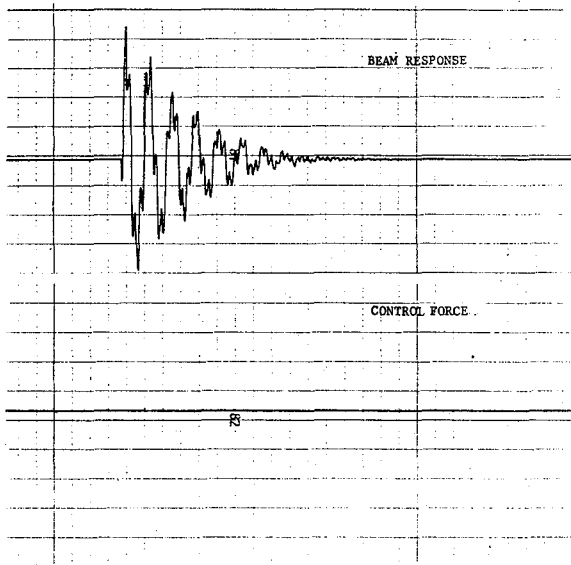


Figure 8. Natural Structural Damping

An impulse was applied to the beam and the resulting open-loop response recorded. Note the light structural damping which is characteristic of large, flexible space structures. The slight displacement offset of the beam is caused by a slight curvature (due to hard use).

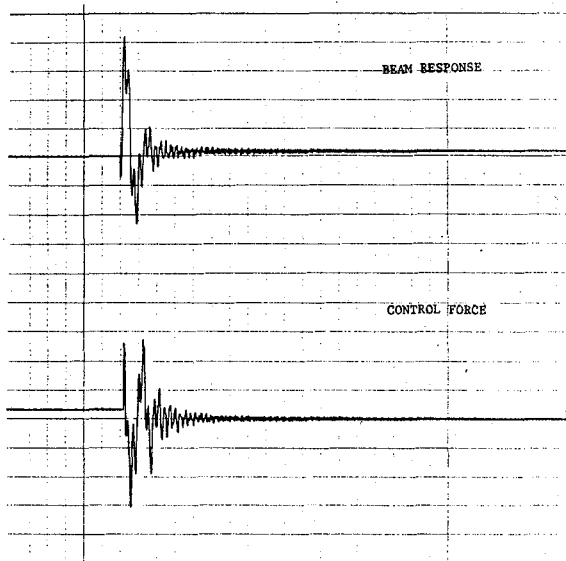


Figure 9. Kalman Filter/Optimal Control

In this case, a six-state Kalman filter/optimal control was switched on immediately following the impulse. The resulting closed-loop response damps out much more rapidly than the open loop system. Residual oscillations are due to the unmodeled 2.2 Hz mode. The particular Kalman filter/optimal control design has the best performance of any tried to date.

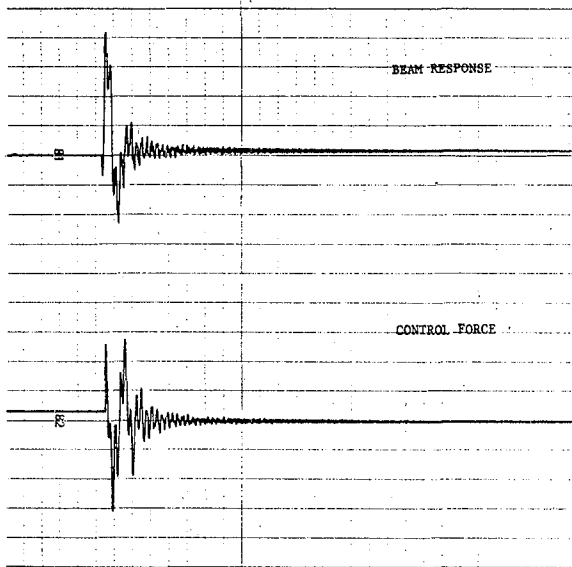


Figure 10. Adaptive Filter/Optimal Control

The Kalman filter was replaced by an adaptive filter which estimates the third modal frequency in addition to the state. Since the initial model was exact, the beam response is virtually identical to the Kalman filter/optimal control response.

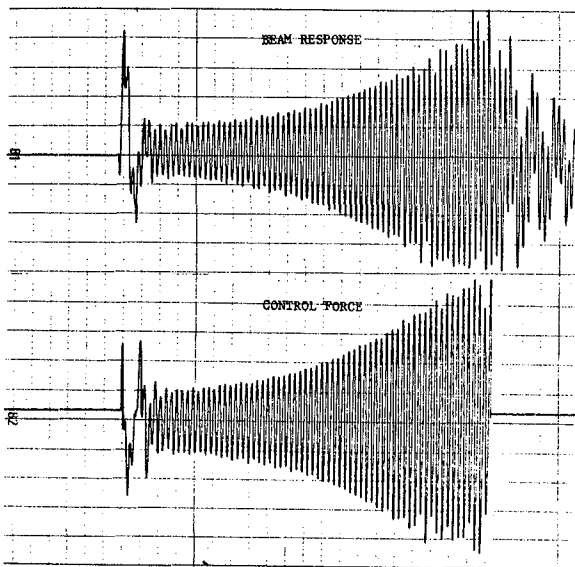


Figure 11. Kalman Filter/Optimal Control with Model Error

The initial value for the third eigenvalue was set 20% too large. The Kalman filter/optimal control design cannot cope with the erroneous model and the system goes unstable.

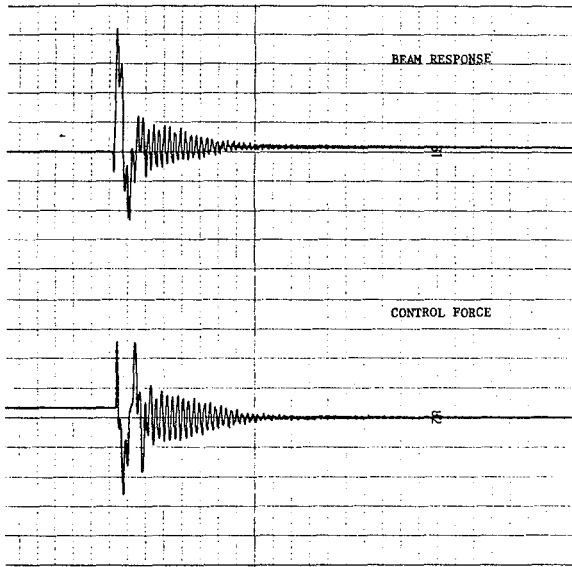


Figure 12. Adaptive Filter/Optimal Control with Model Error

Again, the initial value of the third eigenvalue was 20% too large. Unlike the Kalman filter/optimal control, which was unstable, the adaptive filter effectively damps the system after an initial identification period.

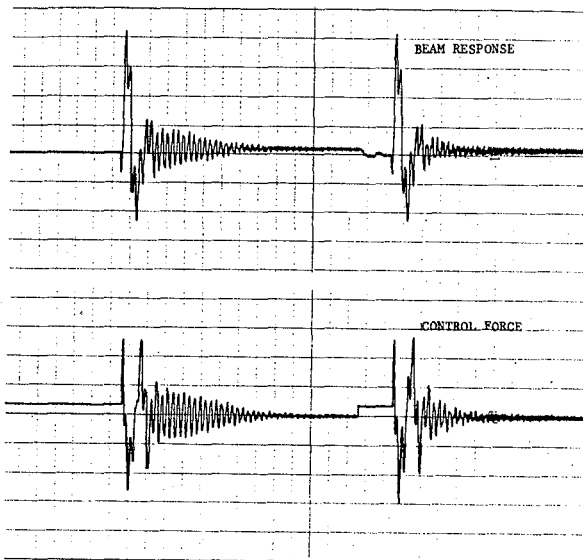


Figure 13. Memory Effect of the Adaptive Filter

Once the model has been correctly identified, the closed loop response is virtually identical to that using the correct model initially.

SOME REMARKS ON THE CURRENT STATUS OF THE CONTROL THEORY OF SINGLE SPACE DIMENSION HYPERBOLIC SYSTEMS*

D.L. Russell**

Department of Mathematics, University of Wisconsin
Madison, WI 53706

ABSTRACT

We review various aspects of the control theory of hyperbolic systems, including controllability, stabilization, control canonical form theory, etc. To allow a unified and not excessively technical treatment, we restrict attention to the case of a single space variable; the multi-dimensional case is treated in our more extensive review [36]. The paper concludes with a short discussion of the newly developed procedure of canonical augmentation.

SOME ASPECTS OF THE CONTROL THEORY OF THE WAVE EQUATION AND RELATED SYSTEMS

The systematic study of control systems governed by partial differential equations, a special, but exceptionally important, subcategory of distributed parameter systems began in the early 1960's with the work of the Soviet scientists A. G. Butkovskii [3], [4], Yu. V. Egorov [11] and others. These works were primarily concerned with the extension of Pontryagin's Maximum Principle [26] to certain classes of processes which could not be satisfactorily modelled by finite dimensional mathematical systems. Controllability questions were raised but were usually subsidiary to questions of optimality. One of the first systematic controllability studies, in connection with the heat equation, was presented by Gal'chuk in [14]. One of the most important of the early American contributions to the subject was the 1963 thesis of Fattorini [13], which also treated parabolic systems and was one of the first works to recognize the strong relationship between distributed parameter control studies

* Supported in part by the Air Force Office of Scientific Research under Grant AFOSR 79-0018.

** Also associated with Mathematics Research Center, University of Wisconsin, Madison.

and classical results in analytic function theory.

The author's own interest in distributed parameter control theory arose out of consulting experience with Honeywell, Inc., and NASA, starting around 1965 or 1966. In developing the Saturn launch vehicle for the Apollo program, NASA has encountered the problem of transverse vibrations of the booster structure and interaction of those vibrations with liquid sloshing modes in the immense Saturn fuel tanks. While the eventual treatment of that problem was based on finite modal approximations, the problem stimulated a great deal of research aimed at an understanding of the control of vibrations in various distributed parameter settings.

First looking at this problem, under Honeywell-NASA auspices, we thought of modelling the booster structure as an "Euler" beam, the displacement $w(x, t)$, which we may take to be scalar here, satisfying

$$\rho(x) \frac{\partial^2 w}{\partial t^2} + \frac{\partial^2}{\partial x^2} (EI(x) \frac{\partial^2 w}{\partial x^2}) = 0 \quad (1.1)$$

along with appropriate boundary conditions including the control inputs, at the longitudinal extremities $x = 0$, $x = L$. We got nowhere with our study of this problem initially because the equation (1.1) is not particularly well understood from the mathematical standpoint. There seemed to be no "handles" to grasp. It would not be until the 1969 thesis of Quinn [27] that we would understand how this system works and that it is, in fact, controllable in a rather strong sense.

We knew about the control theory of ordinary differential equations from various papers and from notes and lectures which would later be incorporated into the 1967 treatise on control theory by Lee and Markus [20]. We also knew that hyperbolic partial differential equations in two independent variables reduce to ordinary differential equations satisfied along the characteristics. It was natural, therefore, to look for hyperbolic models which might fit our purpose. Such was provided by the Timoshenko beam equations

$$I \rho(x) \frac{\partial^2 \psi}{\partial t^2} - k(x) \left(\frac{\partial y}{\partial x} - \psi \right) - \frac{\partial}{\partial x} (EI(x) \frac{\partial \psi}{\partial x}) = 0 \quad (1.2)$$

$$\rho(x) \frac{\partial^2 y}{\partial t^2} - \frac{\partial}{\partial x} (k(x) \left(\frac{\partial y}{\partial x} - \psi \right)) = 0, \quad (1.3)$$

which may be viewed as two coupled wave equations. By "wave equations" here, we mean the equation

$$r(x) \frac{\partial^2 z}{\partial t^2} - \frac{\partial}{\partial x} \left(s(x) \frac{\partial z}{\partial x} \right) = 0. \quad (1.4)$$

All coefficient functions shown in (1.2), (1.3), (1.4) are positive on $0 \leq x \leq L$. It may be verified that (1.2), (1.3) and (1.4) are hyperbolic in the sense described in [8], [25], e.g.. Since (1.4) is conceptually simpler, it was studied first, with accompanying boundary conditions

$$z(0, t) = 0 \quad (1.5)$$

$$\frac{\partial z}{\partial x}(L, t) = u(t), \quad (1.6)$$

the latter incorporating the control force $u(t)$.

While the practical goal in mind was appropriate form of stabilization, we knew that in the case of finite dimensional systems

$$\dot{x} = Ax + Bu$$

an affirmative resolution of the controllability problem, steering from a given $x(0) = x_0$ to a given $x(T) = x_1$, implied the property of stabilization; hence we felt justified in first looking at the state to state controllability problem for (1.4), (1.5), (1.6). The "energy" form for (1.4) is

$$\mathcal{E}(z, \frac{\partial z}{\partial t}) = \frac{1}{2} \int_0^L r(x) \left(\frac{\partial z}{\partial t}(x, t) \right)^2 + s(x) \left(\frac{\partial z}{\partial x}(x, t) \right)^2 dx. \quad (1.7)$$

Given initial and terminal states

$$z(x, 0) = z_0(x), \quad \frac{\partial z}{\partial t}(x, 0) = y_0(x) \quad (1.8)$$

$$z(x, T) = z_1(x), \quad \frac{\partial z}{\partial t}(x, T) = y_1(x) \quad (1.9)$$

of finite energy, i.e. $\mathcal{E}(z_0, v_0) < \infty$, $\mathcal{E}(z_1, v_1) < \infty$, we asked if there exists $u \in L^2[0, T]$ for which the solution of (1.4), (1.5), (1.6) corresponding to the initial state (1.8) assumes the desired terminal state (1.9) at time $t = T$. The answer, a qualified "yes", came from two different approaches to the problem. The relationship between these two approaches has, over the years, grown ever more fundamental and has led to a great many very interesting developments. See [34] and [45] in particular.

The first method explored was, as we have already indicated, the method of characteristics. If we let

$$c(x) = \sqrt{\frac{s(x)}{r(x)}} \quad (1.10)$$

and consider families X^+ , X^- of "characteristic" curves satisfying

$$\frac{dx^+}{dt} + c(x) = 0, \quad \frac{dx^-}{dt} - c(x) = 0, \quad (1.11)$$

respectively, and then set

$$v^+(x, t) = \frac{\partial z}{\partial t}(x, t) + c(x) \frac{\partial z}{\partial x}(x, t),$$

$$v^-(x, t) = \frac{\partial z}{\partial t}(x, t) - c(x) \frac{\partial z}{\partial x}(x, t),$$

we see readily that on $X^+ = \{(x^+(t), t)\}$, $X^- = \{(x^-(t), t)\}$, respectively, we have

$$\frac{d}{dt} v^+(x^+(t), t) = c'(x^+(t)) \frac{v^+(x^+(t), t) - v^-(x^+(t), t)}{2} \quad (1.12)$$

$$\frac{d}{dt} v^-(x^-(t), t) = c'(x^-(t)) \frac{v^+(x^-(t), t) - v^-(x^-(t), t)}{2} \quad (1.13)$$

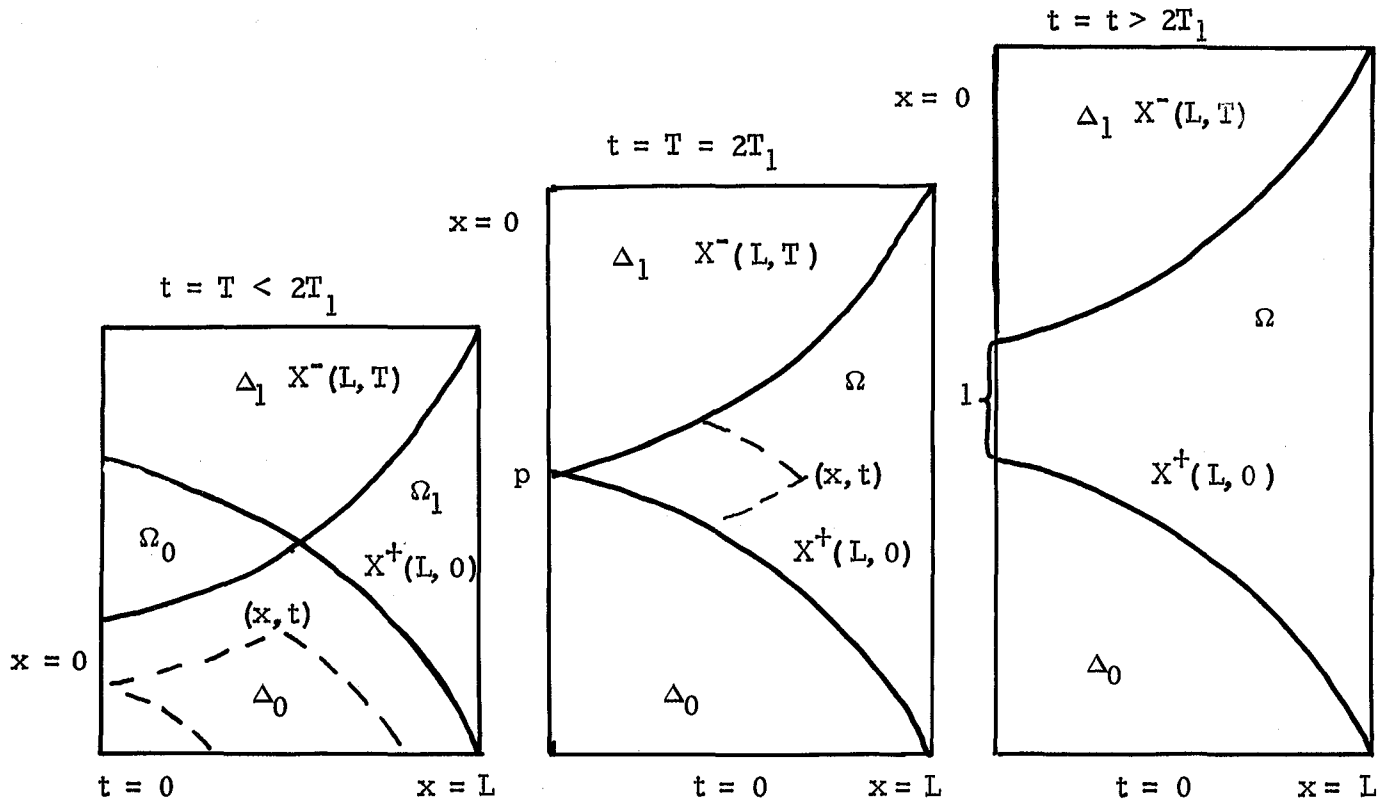


Fig. 1.1: The Method of Characteristics

Because these differential equations are satisfied on different families of characteristics, the coupling between them is more complicated than for the usual system of ordinary differential equations. Nevertheless there is a method of successive approximations, described in [30], [36], which enables solution of these equations in certain regions provided with appropriate boundary data. Such a region is the roughly triangular domain Δ_0 shown in Fig. 1.1, bounded by $t = 0$, $x = 0$ and the characteristic $X^+(L, 0)$, of the first family described by (1.11), passing through the point $(L, 0)$. Together with the boundary data provided by (1.5) and (1.8), it may be seen that the differential equations (1.12), (1.13) determine v^+ and v^- , and hence $z(x, t)$, throughout the domain Δ_0 . Similarly, these equations together with the data provided by (1.5) and (1.9) determine $z(x, t)$ in the domain Δ_1 bounded by $x = 0$, $t = T$ and the characteristic curve $X^-(L, T)$, described by the second equation in (1.11) and passing through the point (L, T) . Thus the initial and terminal states, described by (1.8), (1.9), together with the boundary condition (1.5) determine $z(x, t)$ in both Δ_0 and Δ_1 .

Whether Δ_0 and Δ_1 are disjoint, or have a region, Ω_0 , of overlap, depends on the time T allotted for control. The time required for the curve $X^+(0, L)$ to pass from $X = L$ to $x = 0$ is

$$T_1 = \int_0^L \frac{dx}{c(x)} \quad (1.14)$$

and this is also the time required for $X^-(L, T)$ to pass from $x = 0$ to $x = L$. We summarize the control situation, depending on the relationship between T and T_1 .

Case $T < 2T_1$. Here Δ_0 and Δ_1 overlap and the determinations of $z(x, t)$ in the overlap region $\Omega_0 = \Delta_0 \cup \Delta_1$ provided by (1.8) and (1.9) need not and, in general, will not agree. There can, in such cases of disagreement, be no solution of (1.4), equivalently (1.12), (1.13), in the region $R_T = \{(x, t) | 0 \leq x \leq L, 0 \leq t \leq T\}$. The control function $u(t)$, shown in (1.6), never enters the picture because it cannot affect the solution of (1.4) in Δ_0 or Δ_1 if (1.8), (1.9) are satisfied at $t = 0$, $t = T$, respectively.

Case $T = 2T_1$. Here the two "domains of determinacy", Δ_0 and Δ_1 , just fail to overlap; their boundaries have exactly one point in common, $t = T_1$, $x = 0$. The initial and terminal conditions (1.8) and (1.9) determine $z(x, t)$ in Δ_0 and Δ_1 , respectively. Another process of integration of the coupled

differential equations (1.12) and (1.13) permits unique extension of $z(x, t)$, equivalently $v^+(x, t)$, $v^-(x, t)$, into the domain Ω . The control steering (1.8) to (1.9) is then uniquely determined from this extension and (1.6).

The determinations of $z(x, t)$ in Δ_0 and Δ_1 may fail to match smoothly at the point $p: x = 0, t = T_1$. This results in discontinuities of v^+ along $X^+(L, 0)$ and of v^- along $X^-(L, T)$ in general.

Case $T > 2T_1$. The only difference between this case and the case $T = 2T_1$ lies in the line segment $l: x = 0, T_1 < t < T - T_1$, which replaces the point p of the case $T = 2T_1$. Extension of $z(x, t)$ from $\Delta_0 \cup \Delta_1$ into Ω cannot be carried out until the boundary condition (1.5), which yields $\partial z / \partial t(0, t) = 0$, is augmented by arbitrary data

$$\frac{\partial z}{\partial x}(0, t) = \zeta(t), \quad (0, t) \in l. \quad (1.15)$$

Once this is done, extension of $z(x, t)$ into Ω proceeds much as before. (See [30], [36] for details of the extension process.) The arbitrary function $\zeta(t)$ can be designed so as to eliminate discontinuities of the solution along $X^+(L, 0)$ and $X^-(L, T)$, to satisfy some criterion of optimality (see [30] e. g.) or to fulfill any other appropriate design objective.

If the partial differential equation (1.4) is combined with boundary conditions different from (1.5), (1.6), but still admissible for (1.4), the cases $T < 2T_1$, $T > 2T_1$ remain as above. The rather delicate situation at $T = 2T_1$ depends on the specific form of the boundary conditions. For example, the boundary conditions

$$z(0, t) = 0, \quad z(L, t) = u(t)$$

lead, in case $T = 2T_1$, to a situation where the desired control is not unique; it has the form

$$u(t) = \hat{u}(t) + \gamma \tilde{u}(t)$$

where $\tilde{u}(t)$ is a non-zero control steering the zero initial state into the zero final state and γ is an arbitrary constant. By contrast, the boundary conditions

$$\frac{\partial z}{\partial x}(0, t) = 0, \quad \frac{\partial z}{\partial x}(l, t) = u(t) \quad (1.16)$$

lead, in case $T = 2T_1$, to a situation where the desired control $u(t)$ does not, in general, exist. (See [31], [37] for more details.)

The analysis of more complicated systems of hyperbolic equations, such

as the Timoshenko system (1.2), (1.3), is in general rather complicated but there are some special cases, including appropriate boundary conditions, for which the analysis is fairly simple. In [M] a discussion is given permitting analysis of the free boundary case

$$\frac{\partial \psi}{\partial x}(0, t) = 0, \quad \psi(0, t) - \frac{\partial y}{\partial x}(0, t) = 0, \quad (1.17)$$

$$\frac{\partial \psi}{\partial x}(L, t) = u_1(t), \quad \psi(L, t) - \frac{\partial y}{\partial x}(L, t) = u_2(t). \quad (1.18)$$

It may be shown that all cross-coupling is of low order and the problem is essentially equivalent to two problems (1.4) with boundary conditions (1.16). Two critical times are involved. With (cf. (1.14))

$$c_1(x) = \left(\frac{EI(x)}{I\rho(x)} \right)^{\frac{1}{2}}, \quad T_1 = \int_0^L \frac{dx}{c_1(x)}, \quad (1.19)$$

$$c_2(x) = \left(\frac{k(x)}{\rho(x)} \right)^{\frac{1}{2}}, \quad T_2 = \int_0^L \frac{dx}{c_2(x)}, \quad (1.20)$$

it may be shown that finite energy states are controllable if and only if

$$T \geq 2 \max\{T_1, T_2\}.$$

The essential details of the analysis are given in [30] and are quite similar to what we have briefly outlined here for (1.4), (1.5), (1.6).

It is immediately clear that the method of characteristics is specially adapted to controls $u(t)$ acting at a point, as in (1.6). This is true because the control determination occurs at the very last stage of the analysis, after the controlled solution has been computed. If the control $u(t)$, itself scalar, acts on the system through a "control distribution function" $g(x)$, as in (cf. (1.4))

$$r(x) \frac{\partial^2 z}{\partial t^2} - \frac{\partial}{\partial x} \left(s(x) \frac{\partial z}{\partial x} \right) = g(x) u(t), \quad (1.21)$$

homogeneous boundary conditions (cf. (1.5), (1.6))

$$z(0, t) = 0, \quad \frac{\partial z}{\partial x}(L, t) = 0 \quad (1.22)$$

applying at the boundaries, we face what appears at first glance to be a rather different situation than what obtains in (1.4), (1.5), (1.6), for even the equations corresponding to (1.12), (1.13) will involve the unknown control $u(t)$ in this situation; one cannot proceed by filling out $z(x, t)$ in successive domains as before; a completely different approach is required. Such an approach can be found in the study of moment problems - a technique developed

by several authors (see [3], [12], [15], [14], [23]). The technique has the advantage, from the point of view of approximation of being intimately connected with the modal representation of the system based on the natural modes of vibration, or eigenfunctions of the operator $-r(x)^{-1}(\partial/\partial x)(s(x)(\partial z/\partial x))$.

It is known (see [1], [7]) that the operator

$$Lz = -r(x)^{-1} \frac{\partial}{\partial x} (s(x) \frac{\partial z}{\partial x}) \quad (1.23)$$

with boundary conditions conformable with (1.22) has eigenvalues

$$\lambda_k = \left(\frac{2k-1}{2}\right)^2 \frac{\pi^2}{T_1^2} + \varepsilon_k, \quad k = 1, 2, 3, \dots \quad (1.24)$$

where the ε_k are uniformly bounded and T_1 is related to $c(x)$ by (1.14). The corresponding eigenfunctions, $\varphi_k(x)$, $k = 1, 2, 3, \dots$, form an orthonormal basis for $L_r^2[0, L]$ (which consists of the same functions as $L^2[0, L]$ but has the inner product

$$(\varphi, \psi)_r = \int_0^L r(x) \varphi(x) \psi(x) dx. \quad (1.25)$$

Every finite energy solution $z(x, t)$ of (1.21), (1.22), i. e. every solution for which the integral (1.7) is bounded for all t , can be expanded in the form

$$\ddot{z}(x, t) = \sum_{k=1}^{\infty} z_k(t) \varphi_k(x)$$

where, if we assume the control distribution function $f(x)$ has the expression

$$g(x) = \sum_{k=1}^{\infty} g_k \varphi_k(x)$$

convergent in $L_r^2[0, L]$, the $z_k(t)$ satisfy

$$z_k + \lambda_k z_k = g_k u(t), \quad k = 1, 2, \dots \quad (1.26)$$

Letting

$$\omega_k = \lambda_k^{\frac{1}{2}}, \quad k = 1, 2, 3, \dots$$

and using the transformation

$$\begin{pmatrix} z_k \\ \dot{z}_k \end{pmatrix} = \begin{pmatrix} 1/i\omega_k & -1/i\omega_k \\ 1 & 1 \end{pmatrix} \begin{pmatrix} \eta_k \\ \zeta_k \end{pmatrix} \quad (1.27)$$

one arrives at the system

$$\begin{pmatrix} \dot{\eta}_k \\ \dot{\zeta}_k \end{pmatrix} = \begin{pmatrix} i\omega_k & 0 \\ 0 & -i\omega_k \end{pmatrix} \begin{pmatrix} \eta_k \\ \zeta_k \end{pmatrix} + \begin{pmatrix} g_k/2 \\ g_k/2 \end{pmatrix} u(t). \quad (1.28)$$

It may be seen that finite energy states are those for which

$$\sum_{k=1}^{\infty} [(\dot{z}_k)^2 + \lambda_k (z_k)^2] < \infty$$

and this becomes, in terms of η_k, ζ_k ,

$$\sum_{k=1}^{\infty} (|\eta_k|^2 + |\zeta_k|^2) < \infty. \quad (1.29)$$

Integrating (1.28), we have, for $T > 0$,

$$\eta_k(T) - e^{i\omega_k T} \eta_k(0) = \frac{g_k}{2} \int_0^T e^{i\omega_k(T-t)} u(t) dt$$

$$\zeta_k(T) - e^{i\omega_k T} \zeta_k(0) = \frac{g_k}{2} \int_0^T e^{-i\omega_k(T-t)} u(t) dt.$$

Assuming the controllability condition

$$g_k \neq 0, \quad k = 1, 2, 3, \dots$$

we see that the problem of steering between the given states at times 0 and T reduces to the moment problem

$$\int_0^T e^{i\omega_k s} f(s) ds = \frac{\alpha_k}{g_k}, \quad k = 1, 2, 3, \dots, \quad (1.30)$$

$$\int_0^T e^{-i\omega_k s} f(s) ds = \frac{\beta_k}{g_k}, \quad k = 1, 2, 3, \dots, \quad (1.31)$$

where $s = T-t$, $f(s) = u(T-s)$, and

$$\alpha_k = 2(\eta_k(T) - e^{i\omega_k T} \eta_k(0)), \quad \beta_k = 2(\zeta_k(T) - e^{-i\omega_k T} \zeta_k(0)) \quad (1.32)$$

are square summable.

To solve the moment problem we resort to the theory of nonharmonic Fourier series as developed by Paley and Wiener [24], Levinson [21], Schwartz [42] and many others. (An excellent expository treatment [49] by R. Young has recently appeared.) The following is known; the three cases being divided in a manner conformable with the three cases discussed earlier.

Case $T < 2T_1$. The functions $e^{i\omega_k t}, e^{-i\omega_k t}$, $k = 1, 2, 3, \dots$, are linearly dependent in $L^2[0, T]$ in a rather strong sense. Any one of these functions, indeed, any finite number of them, lie in the closed span of the remaining functions (which, in fact, is equal to the whole space $L^2[0, T]$). As a result the moment problem (1.30), (1.31) cannot, in general, be solved.

Suppose, e. g., all but finitely many of the α_k, β_k , say $k = K+1, K+2, \dots$, were equal to zero, while some of the α_k, β_k , $k = 1, 2, \dots, K$, are non-zero. The linear dependence just referred to shows that such a problem can have no solution; the equations

$$\int_0^T e^{i\omega_k s} f(s) ds = \int_0^T e^{i\omega_k s} f(s) ds = 0, \quad k > K$$

imply that the same equations must hold for $k \leq K$.

Case $T = T_1$. Here the functions $e^{i\omega_k s}, e^{-i\omega_k s}$, $k = 1, 2, 3, \dots$ form a Riesz basis for $L^2[0, 2T_1]$. Every function $h \in [0, 2T_1]$ has the unique convergent expansion

$$h(s) = \sum_{k=1}^{\infty} [h_k e^{i\omega_k s} + h_{-k} e^{-i\omega_k s}] \quad (1.33)$$

and there are positive numbers c, C , such that

$$c^{-2} \|h\|_{L^2[0, 2T]}^2 \leq \sum_{k=1}^{\infty} (|h_k|^2 + |h_{-k}|^2) \leq C^2 \|h\|_{L^2[0, 2T]}^2 \quad (1.34)$$

Further, there is a unique dual basis of biorthogonal elements $p_k, p_{-k} \in L^2[0, 2T_1]$ such that

$$\int_0^{2T_1} e^{i\omega_k s} p_l(s) ds = \delta_{k,l}, \quad \begin{matrix} k = \pm 1, \pm 2, \dots \\ l = \pm 1, \pm 2, \dots \end{matrix} \quad (1.35)$$

$$\delta_{kl} = \begin{cases} 1, & k = l \\ 0, & k \neq l \end{cases}$$

which engenders expansions similar to (1.33), the roles of c, C in the inequalities paralleling (1.34) being reversed. The formal solution of (1.30), (1.31) is then uniquely given by

$$f(s) = \sum_{k=1}^{\infty} \frac{1}{g_k} [\alpha_k p_k(s) + \beta_k p_{-k}(s)]. \quad (1.36)$$

If we have

$$\lim_{k \rightarrow \infty} |g_k| = 0, \quad (1.37)$$

as would be the case, e. g., if $g \in L^2[0, L]$, then the conditions for convergence of (1.36) are more stringent than just the square summability of the α_k, β_k given by (1.32). We need

$$\sum_{k=1}^{\infty} \left(\left| \frac{\alpha_k}{g_k} \right|^2 + \left| \frac{\beta_k}{g_k} \right|^2 \right) < \infty.$$

As a consequence we can steer (1.21) from any finite energy initial state to a dense (in the energy norm) subspace of final states, or vice versa, but we cannot steer between arbitrary finite energy states during $[0, 2T_1]$ if (1.37) is true. The case of boundary control (1.6), already treated by the method of characteristics, will be discussed more extensively below. In that case the coefficients g_k in (1.26) are bounded and bounded below. The result is, in that situation, that we obtain the same result this way as by the method of characteristics - given finite energy initial and terminal states, there is a unique control $u \in L^2[0, 2T_1]$ steering the one to the other.

Case $T > 2T_1$. The main difference between this case and the preceding is that here the functions $e^{i\omega_k s}$, $e^{-i\omega_k s}$, $k = 1, 2, 3, \dots$, form a Riesz basis for a proper subspace, E , of $L^2[0, T]$. The biorthogonal functions p_k , p_{-k} exist, but are unique only if we require that they lie in E — or we impose some comparable condition. If we agree that \tilde{p}_k , \tilde{p}_{-k} belong to E , then any elements

$$p_k = \tilde{p}_k + q_k, \quad p_{-k} = \tilde{p}_{-k} + q_{-k}$$

with $q_k, q_{-k} \in E^\perp \subset L^2[0, T]$ still form a biorthogonal set relative to the $e^{i\omega_k s}$, $e^{-i\omega_k s}$. The convergence properties of series involving the \tilde{p}_k , \tilde{p}_{-k} are much the same as in the preceding case. As a result we have the same control capability as in the case $T = 2T_1$ but controls are not unique. Indeed, if \tilde{u} is a control steering between two given states, the family of controls $\tilde{u} + \hat{u}$, $\hat{u} \in E^\perp$, all realize the same control objective. Again, this non-uniqueness should be compared with the similar property observed for $T > 2T_1$ in applying the method of characteristics.

Using the theory of distributions and related material, boundary value control situations such as (1.6) can be included in the same framework as (1.26) but with g in a larger space than $L^2[0, L]$; g should be a linear functional (in general unbounded on $L^2[0, L]$) whose domain includes the domain, $\mathfrak{D}(L)$, of the self adjoint operator L , given by (1.23), with the given homogeneous boundary conditions. The g_k are the values which g assumes at the eigenfunctions $\varphi_k \in \mathfrak{D}(L)$. A detailed study of these "admissible input elements" is provided in [17]. In this way a unification of the boundary and distributed control cases may be achieved. One consequence of this is that the biorthogonal functions p_k , p_{-k} which play such an

important role in the method based on the moment problem (1.30), (1.31) can actually be obtained through the more constructive method of characteristics as controls steering from a zero initial state (say) to final states constructed using a single eigenfunction φ_k of L .

We began our discussion here with the Euler beam equation (1.1). For definiteness, let us add a distributed control term (scalar input) and specific boundary conditions so that we have

$$\rho(x) \frac{\partial^2 w}{\partial t^2} + \frac{\partial^2}{\partial x^2} (EI(x) \frac{\partial^2 w}{\partial x^2}) = g(x) u(t) \quad (1.38)$$

$$\frac{\partial^2 w}{\partial x^2} (0, t) = \frac{\partial^3 w}{\partial x^3} (0, t) = 0, \quad (1.39)$$

$$\frac{\partial^2 w}{\partial x^2} (L, t) = \frac{\partial^3 w}{\partial x^3} (L, t) = 0. \quad (1.40)$$

In 1969 J.P. Quinn, in his doctoral thesis [27], studied the controllability properties of a class of systems including this one. Here the operator

$$Aw = \frac{1}{\rho(x)} \frac{\partial^2}{\partial x^2} (EI(x) \frac{\partial^2 w}{\partial x^2})$$

on the domain in $H^4[0, L]$ consisting of functions obeying boundary conditions conformable with (1.39), (1.40) has eigenfunctions $\varphi_k(x)$ forming an orthonormal basis for $L^2[0, L]$ and the corresponding eigenvalues λ_k grow like k^4 as $k \rightarrow \infty$. With $\omega_k = \lambda_k^{\frac{1}{2}}$ we obtain a system similar to (1.28), using a transformation like (1.27) applied to the second order differential equations resulting from the eigenfunction decomposition:

$$\ddot{w}_k + \lambda_k w_k = g_k u(t), \quad k = 0, 1, 2, 3, \dots$$

(a slight modification of (1.27), (1.28) is necessary for $\lambda_0 = 0$; see [34]).

Again there results

$$\begin{pmatrix} \dot{\eta}_k \\ \dot{\zeta}_k \end{pmatrix} = \begin{pmatrix} i\omega_k & 0 \\ 0 & -i\omega_k \end{pmatrix} \begin{pmatrix} \eta_k \\ \zeta_k \end{pmatrix} + \begin{pmatrix} \frac{g_k}{2} \\ \frac{g_k}{2} \end{pmatrix} u(t) \quad (1.41)$$

and the energy expression for (1.38) is, equivalently,

$$\frac{1}{2} \int_0^L \left[\rho(x) \left(\frac{\partial w}{\partial t} \right)^2 + EI(x) \left(\frac{\partial^2 w}{\partial x^2} \right)^2 \right] dx$$

or

$$\frac{1}{2} \sum_{k=0}^{\infty} [(\dot{w}_k)^2 + \lambda_k (w_k)^2]$$

or

$$\frac{1}{2} \sum_{k=0}^{\infty} |\eta_k|^2 + |\zeta_k|^2,$$

all $< \infty$ for "finite energy" states.

Quinn was able to show in this case that the functions $e^{i\omega_k s}, e^{-i\omega_k s}$, $k = 0, 1, 2, 3, \dots$ (for $k = 0$ replace $e^{i\omega_k s}, e^{-i\omega_k s}$ by $1, s$) are linearly independent in $L^2[0, T]$ for every $T > 0$ (this result by itself had already been obtained much earlier by Ingham [18] who shows, in effect, that these functions form a Riesz basis for a closed subspace of $L^2[0, T]$ for every $T > 0$) and, additionally, that there is a positive number, $M(T)$, such that if the (non-unique) biorthogonal functions $p_k(s), p_{-k}(s)$ are appropriately selected in $L^2[0, T]$, these functions are continuous and satisfy the pointwise bounds

$$|p_k(s)| \leq M(T), \quad |p_{-k}(s)| \leq M(T), \quad s \in [0, T]. \quad (1.42)$$

The fact that the $e^{i\omega_k s}, e^{-i\omega_k s}$ form a Riesz basis for a closed subspace of $L^2[0, T]$, $T > 0$, implies that initial states and terminal states with (in terms of (1.41)) expansion coefficients $\eta_{k,0}, \zeta_{k,0}$ and $\eta_{k,1}, \zeta_{k,1}$ can be steered, one to the other, during $[0, T]$ with $u \in L^2[0, T]$, provided that

$$\sum_{k=0}^{\infty} (|\frac{\eta_{k,0}}{g_k}|^2 + |\frac{\zeta_{k,0}}{g_k}|^2) < \infty, \quad \sum_{k=0}^{\infty} (|\frac{\eta_{k,1}}{g_k}|^2 + |\frac{\zeta_{k,1}}{g_k}|^2) < \infty.$$

The boundedness property (1.42) shows we can also control states for which

$$\sum_{k=0}^{\infty} (|\frac{\eta_{k,0}}{g_k}| + |\frac{\zeta_{k,0}}{g_k}|) < \infty,$$

$$\sum_{k=0}^{\infty} (|\frac{\eta_{k,1}}{g_k}| + |\frac{\zeta_{k,1}}{g_k}|) < \infty,$$

this being possible with a control function $u(t)$ uniformly bounded and continuous on $[0, T]$.

We have noted in connection with the Timoshenko beam system (1.2), (1.13)

(1.17), (1.18), that an adequate control theory, based on the method of characteristics, exists when we have two separate control functions, $u_1(t)$ and $u_2(t)$, with which to control the lateral deflection and shear deformation separately. An open question is the adequacy of control using a single control input, so that (1.17), (1.18) becomes, e.g.,

$$\frac{\partial \psi}{\partial x}(L, t) = \alpha u(t), \quad \psi(L, t) - \frac{\partial y}{\partial x}(L, t) = \beta u(t)$$

with $\alpha^2 + \beta^2 \neq 0$. This problem is a special case of the more general question of the controllability of linear hyperbolic systems of dimension $n = 2m$, involving m pairs of characteristics, each pair describing a given wave mode propagating in two opposite directions, by means of fewer than m control inputs. Some work has been done in this direction by R. G. Teglus in his thesis [45] and by N. Wick [47], but it is safe to say that no very general criteria for this problem have yet appeared. Particularly valuable, it seems to this author, would be a study of the Timoshenko beam system from the singular perturbation standpoint, elucidating the behavior of solutions and controllability properties as the modulus of elasticity in shear, $k(x)$ in (1.2), (1.3), tends to infinity.

STABILIZATION, CANONICAL FORMS, EIGENVALUE PLACEMENT, etc.

As all practicing engineers will know, controllability in itself is rarely the prime goal of control system design. Stability, and related criteria such as robustness, insensitivity to particular input frequency bands, etc., are more commonly uppermost in mind. Additionally, there is the question of state estimation from lower dimensional, noisy observations in order to implement linear feedback control policies. These subjects have been pursued almost ad nauseum for linear, finite dimensional systems. In the case of distributed parameter systems, and hyperbolic systems in particular, the literature on this subject remains rather sparse and spotty in its coverage.

As in the case of linear finite dimensional systems, stability and stabilization studies for linear partial differential equations have tended to cluster around two dominant approaches: the Liapounov approach, primarily carried out in connection with systems involving some form of "conservation of energy" law, and the spectral approach, determining if, or making certain that, the

eigenvalues of the system lie in an appropriate subset of the left half plane. The spectral approach suffers from the disadvantages of greater intricacy of computation and the need to show that the spectrum location does, in fact, determine the asymptotic behavior of the system. The latter brings in questions of completeness and linear independence of the eigenvectors of the system.

We will begin with a short discussion of what has been done with Liapounov methods. On the theoretical side one can start with a system

$$\dot{x} = Cx, \quad (2.1)$$

C generating a strongly continuous semigroup $S(t)$ in the Hilbert space X (we may have started with a control system $\dot{x} = Ax + Bu$, set $u = Kx$, then $C = A + BK$). We set up a quadratic functional

$$V(x) = (x, Qx),$$

where Q is a bounded, positive, self adjoint operator on X with $Q \geq qI$ for some $q > 0$, to serve as a Liapounov function. One may then show that for $t_2 > t_1$ and $x(t) = S(t)x_0$ a "solution" of (2.1), that

$$\begin{aligned} & (x(t_2), Qx(t_2)) - (x(t_1), Qx(t_1)) \\ & = - \int_{t_1}^{t_2} (x(s), Wx(s)) ds \end{aligned}$$

for some positive self adjoint operator W so that, in some sense which one needs to make precise in individual cases,

$$C^*Q + QC + W = 0, \quad (2.2)$$

the Liapounov operator equation, is satisfied. An important result, due to Datko [10], states that if

$$\int_0^{\infty} (x(t), Qx(t)) dt < \infty \quad (2.3)$$

for every initial state $x_0 \in X$, then the semigroup $S(t)$ is exponentially damped, i.e.

$$\|S(t)\| \leq Me^{-\gamma t}, \quad t \geq 0,$$

for positive numbers M, γ . The condition (2.3) is satisfied if $W \geq wI$ for some $w > 0$, as may easily be verified.

Consider the linear symmetric hyperbolic system in $L_n^2[0, L] = (L^2[0, L])^n$

$$E(x) \frac{\partial w}{\partial t} = A(x) \frac{\partial w}{\partial x} + B(x)w + f(x, t) \quad (2.4)$$

where $E(x), A(x), B(x)$ are continuously differentiable $m \times m$ matrices defined for $x \in [0, L]$, $E(x)$ symmetric and positive definite, $A(x)$

symmetric. The wave and Timoshenko equations can be written in this form. The "energy" usually is expressed as

$$e(t) = \frac{1}{2} \int_0^L (w(x, t), E(x) w(x, t)) dx .$$

With appropriately "conservative" or "dissipative" boundary conditions at $x = 0, x = L$, one finds that for $t_2 > t_1$

$$e(t_2) - e(t_1) = \int_{t_1}^{t_2} \left\{ \frac{1}{2} \int_0^L (w(x, t), [B(x) + B(x)^* - \dot{A}(x)] w(x, t)) dx + \int_0^L (w(x, t), f(x, t)) dx \right\} dt .$$

If $B(x) + B(x)^* - \dot{A}(x)$ is uniformly negative definite or if the n dimensional control function $f(x, t)$ may be arbitrarily specified as a function of x and t , one may use feedback

$$f(x, t) = K(x) w(x, t) \tag{2.5}$$

in such a way that

$$e(t_2) - e(t_1) = - \int_{t_1}^{t_2} \int_0^L (w(x, t), W(x) w(x, t)) dx dt \tag{2.6}$$

with $W(x)$ uniformly positive definite and symmetric on $[0, L]$. Then one can apply Datko's result, or more simple arguments, to show that solutions of (2.3), (2.4) are uniformly exponentially damped in $L_n^2[0, L]$ norm.

Note, however, that if $B(x) + B(x)^* - \dot{A}(x) = 0$ or for some other reason fails to be positive definite, and if

$$f(x, t) = D(x) u(x, t) \quad \text{or} \quad f(x, t) = D(x) u(t)$$

with $\dim u(x, t) = r < R$ in the first instance, u a function of t only in the second instance, then we cannot, in general, achieve (2.5) with $W(x)$ uniformly positive definite. Comparable difficulties arise when boundary control is employed. In such cases it is a form of the La Salle "invariance principle" (see, e. g. [19]) which must be appealed to, rather than the basic Liapounov theory, for an analysis of presumed asymptotic stability properties of the system. This has been discussed in some detail in [36] and [33] and we give only the briefest outline here.

The "invariance principle", as it applies to finite dimensional systems, relies heavily on the compactness of the " ω -limit set" of the system in order to reach the final conclusion of asymptotic stability. Comparable compactness properties associated with the solutions of an infinite dimensional system are

generally difficult to realize but the initial attempts to extend the theory nonetheless relied on establishing some sort of compactness property. One of the first contributions in this direction was due to Dafermos [9] who studied weak damping of the wave equation, relying on the almost periodic nature of the system solutions to provide the required compactness. Slemrod [43] studied the boundary damped wave equation by introducing suitably weakened topologies — as compared with the usual topology associated with the energy norm — and was able to conclude a correspondingly weakened form of asymptotic stability.

Knowing that controllability implies stabilizability in the case of autonomous finite dimensional linear systems, we are not surprised to find controllability playing a role in the study of asymptotic stability and stabilization properties of autonomous infinite dimensional linear systems. This is discussed in some detail in the paper [28] by J. P. Quinn and the author and also in [33]. Systems of the form (2.3), but with the control appearing in the boundary conditions, are studied in [28] prior to the main discussion on the boundary damped, higher dimensional wave equation. We can give an idea of the flavor of the arguments employed using a simple example based on the wave equation (1.4) with control appearing in the boundary conditions (1.5), (1.6). If in this system one employs the feedback law

$$u(t) = -\gamma \frac{\partial w}{\partial t}(L, t), \quad (2.7)$$

the closed loop system is (1.4), (1.5) together with the "closed-loop" Robin type boundary condition

$$\frac{\partial w}{\partial x}(L, t) + \gamma \frac{\partial w}{\partial t}(L, t) = 0. \quad (2.8)$$

Here a short computation shows that with the energy $\mathcal{E}(t)$ defined by the expression (1.7) we have, for $t_2 > t_1$,

$$\mathcal{E}(t_2) - \mathcal{E}(t_1) = -\gamma p(L) \int_{t_1}^{t_2} \left(\frac{\partial w}{\partial t}(L, t) \right)^2 dt. \quad (2.9)$$

It is not feasible to fit this situation into the general pattern based on the Liapounov operator equation (2.2) but, since we expect (correctly) that, along with (1.4), (1.5), (2.8)

$$\frac{\partial w}{\partial t}(L, t) \equiv 0 \implies w(x, t) \equiv 0,$$

an "invariance principle" type of argument appears to be in order. But we will use a variation on this procedure which makes use of the controllability already established in Section 1. Let $v(x, t)$ be a controlled solution of

(1.4), (1.5), (1.6), $u(t)$ being selected so as to steer the initial state

$$v(x, 0) = w(x, 0), \quad \frac{\partial v}{\partial t}(x, 0) = \frac{\partial w}{\partial t}(x, 0), \quad (2.10)$$

agreeing with the initial state of the solution $w(x, t)$ of (1.4), (1.5), (2.8), to the zero final state

$$v(x, T_1) = 0, \quad \frac{\partial v}{\partial t}(x, T_1) = 0, \quad (2.11)$$

T_1 as described earlier. Defining the "energy inner product"

$$\langle w(\cdot, t), v(\cdot, t) \rangle = \int_0^L [\rho(x) \frac{\partial w}{\partial t}(x, t) \frac{\partial v}{\partial t}(x, t) + p(x) \frac{\partial w}{\partial x}(x, t) \frac{\partial v}{\partial x}(x, t)] dx$$

it is found, using (1.5), (2.8), (2.10), (2.11), that

$$\begin{aligned} \langle w(\cdot, 0), v(\cdot, 0) \rangle - \langle w(\cdot, 2T_1), v(\cdot, 2T_1) \rangle &= \|w(\cdot, 0)\|_{\mathcal{E}}^2 = \\ &= -p(L) \int_0^{2T_1} \left[\frac{\partial w}{\partial x}(L, t) \frac{\partial v}{\partial t}(L, t) + \frac{\partial v}{\partial x}(L, t) \frac{\partial w}{\partial t}(L, t) \right] dt \\ &= p(L) \int_0^{2T_1} \frac{\partial w}{\partial t} \left[\gamma \frac{\partial v}{\partial t}(L, t) + \frac{\partial v}{\partial x}(L, t) \right] dt \\ &= p(L) \int_0^{2T_1} \frac{\partial w}{\partial t}(L, t) \left[\gamma \frac{\partial v}{\partial t}(L, t) + u(t) \right] dt. \end{aligned}$$

Here $\|w(\cdot, 0)\|_{\mathcal{E}}^2$, the energy norm at $t = 0$, is $2\mathcal{E}(0)$. Applying the Schwartz inequality

$$\begin{aligned} 4\mathcal{E}(0)^2 &\leq p(L) \int_0^{2T_1} \frac{\partial w}{\partial t}(L, t)^2 dt \\ &\quad \cdot \int_0^{2T_1} \left(\gamma \frac{\partial v}{\partial t}(L, t) + u(t) \right)^2 dt. \end{aligned} \quad (2.12)$$

A slightly more detailed study of the control problem for (1.4), (1.5), (1.6) in the case $T = 2T_1$ (or $T > 2T_1$) shows that control from an initial state $w(x, 0)$, $\frac{\partial w}{\partial t}(x, 0)$ to $0, 0$ at time $2T_1$ is realized with a control $u(t)$ which satisfies

$$\int_0^{2T_1} u(t)^2 dt \leq K_0 \mathcal{E}(0)$$

and, for the resulting controlled solution we have

$$\int_0^{2T_1} \frac{\partial v}{\partial t}(L, t)^2 dt \leq K_1 \mathcal{E}(0)$$

for certain positive constants K_0 and K_1 . Then (2.12) easily yields

$$\gamma p(L) \int_0^{2T_1} \frac{\partial w}{\partial t}(L, t)^2 dt \geq \frac{\mathcal{E}(0)^2}{2(K_0 + \gamma^2 K_1) \mathcal{E}(0)} \equiv K \mathcal{E}(0)$$

and, setting $t_1 = 0$, $t_2 = 2T_1$ in (2.9), we have

$$\varepsilon(2T_1) \leq \varepsilon(0) - K\varepsilon(0) = (1-K)\varepsilon(0). \quad (2.13)$$

Since $\varepsilon(2T_1)$ is, from (2.9), (2.13), positive and less than or equal to $\varepsilon(0)$ we conclude $0 < 1-K < 1$.

Repeating the above argument on successive intervals $[0, 2T_1]$, $[2T_1, 4T_1]$, \dots , $[2kT_1, 2(k+1)T_1]$, \dots and using the monotonicity of $\varepsilon(t)$, as implied by (2.9), we conclude that $\varepsilon(t)$ decays exponentially to 0 as $t \rightarrow \infty$. The same general argument can be used with a fairly wide class of boundary damped linear symmetric hyperbolic systems (2.4) and with many other systems which are energy conserving in the uncontrolled situation and suitably strong controllability properties. The Timoshenko system (1.2), (1.3), with appropriate boundary conditions, is in this class. As far as the author is aware, the Euler beam model (1.1) has not yet been studied from this point of view.

The spectral approach, as we have already indicated, involves a direct analysis of the eigenvalues and eigenfunctions or, more generally, the spectrum and invariant subspaces, of the generating operator C for a given system $\dot{x} = Cx$, possibly derived from a control system $\dot{x} = Ax + Bu$ by the use of linear feedback $u = Kx$ so that $C = A + BK$. A fairly common case, which can be treated with minimal difficulty, arises when all but finitely many of the eigenvalues of C have negative real parts. Under generically valid controllability-type conditions it is then possible to move the unstable eigenvalues into the left half plane while either keeping the stable eigenvalues fixed or else maintaining a certain margin of stability. Work of this sort has been carried out by Triggiani [46], Sakawa [40], [41] and others.

A somewhat more challenging task arises when one starts with a system having infinitely many eigenvalues in the closed right half plane (usually one considers a conservative system wherein all of the eigenvalues of C are purely imaginary) and one attempts to devise a feedback law to move all of these eigenvalues over into the open left half plane. A number of procedures have been examined in this connection.

In [32] a second order system with scalar control

$$\ddot{x} + Ax = bu, \quad x, b \in X, \quad (2.14)$$

is studied, X being a real Hilbert space and A an unbounded positive self adjoint operator on X . Assuming that A has a Riesz basis of eigenvectors ϕ_k , $k = 1, 2, 3, \dots$, in X , and corresponding positive eigenvalues λ_k ,

increasing with k , $k = 1, 2, 3, \dots$, x and b may be expanded as

$$x = \sum_{k=1}^{\infty} x_k \phi_k, \quad b = \sum_{k=1}^{\infty} b_k \phi_k, \quad (2.15)$$

convergent in X , with square summable coefficients. We assume the minimal condition for approximate controllability

$$b_k \neq 0, \quad k = 1, 2, 3, \dots$$

The energy form is $\frac{1}{2} [(\dot{x}, \dot{x}) + (x, Ax)] = \mathcal{E}$ and elementary computations show that for (2.14) and for any $T > 0$

$$\mathcal{E}(T) - \mathcal{E}(0) = \int_0^T (\dot{x}(t), b) u(t) dt. \quad (2.16)$$

It follows that with

$$u(t) = -\gamma (\dot{x}(t), b) \quad (2.17)$$

the energy $\mathcal{E}(t)$ is non-increasing with increasing t . So far this is basically a Liapounov approach employing what is known in the engineering literature as an ILAF (Identical Location of Accelerometer and Forces) approach. The resulting closed loop system is, still in second order form,

$$\ddot{x} + B\dot{x} + Ax = 0 \quad (2.18)$$

with B defined by

$$B\dot{x} = \gamma (\dot{x}, b) b. \quad (2.19)$$

With $y = \dot{x}$, one may consider the equivalent first order system in $X \times X$,

$$\begin{pmatrix} \dot{x} \\ \dot{y} \end{pmatrix} = C \begin{pmatrix} x \\ y \end{pmatrix}, \quad C = \begin{pmatrix} 0 & I \\ -A & -B \end{pmatrix}, \quad (2.20)$$

and ask: what are the eigenvalues and eigenvectors of C ? It is here that one leaves the second method of Liapounov and returns to his first. In [32] a perturbation analysis is carried out, valid for small values of γ in (2.17), (2.19). It is shown that, under the separation assumption

$$w_{k+1} - w_k \geq d > 0, \quad w_k = \sqrt{\lambda_k}, \quad (2.21)$$

the eigenvalues of C , which for $\gamma = 0$ are $\pm iw_k$, $k = 1, 2, 3, \dots$, all have negative real parts for $\gamma > 0$ and, moreover, designating the perturbed eigenvalues by $\zeta_k(\gamma)$, $k = \pm 1, \pm 2, \pm 3, \dots$, $\zeta_k(0) = iw_k$, $\zeta_{-k}(0) = -iw_k$, we have (cf. (2.21))

$$\zeta_k(\gamma) = iw_k - \frac{\gamma}{2} |b_k|^2 + o(\gamma^2 \frac{1}{|w_k|^2}), \quad k \rightarrow \infty \quad (2.22)$$

$$\zeta_{-k}(\gamma) = -i\omega_k - \frac{\gamma}{2} |b_k|^2 + \mathcal{O}\left(\gamma^2 \frac{1}{|w_k|^2}\right), \quad k \rightarrow \infty. \quad (2.22)$$

It is also possible to show that the perturbed eigenvectors continue to form a Riesz basis for the space $X \times X$. From this it follows that all solutions of (2.18) tend strongly to zero in the energy norm, though not at a uniform exponential rate.

Following Wonham's initial results [48] on the finite dimensional case, there has been considerable interest displayed in the question of spectral determination via linear feedback for distributed parameter systems. In terms of the system (2.14), equivalently,

$$\begin{pmatrix} \dot{x} \\ \dot{y} \end{pmatrix} = \begin{pmatrix} 0 & I \\ -A & 0 \end{pmatrix} \begin{pmatrix} x \\ y \end{pmatrix} + \begin{pmatrix} 0 \\ b \end{pmatrix} u, \quad (2.23)$$

with initial ($u=0$) eigenvalues $\pm i\omega_k$, $k = 1, 2, 3, \dots$, the question may be phrased as follows: we suppose use of a linear feedback functional

$$u = (A^{\frac{1}{2}}x, k_1) + (y, k_2), \quad k_1, k_2 \in X, \quad (2.24)$$

bounded relative to the energy norm $(x, Ax) + (y, y) = (A^{\frac{1}{2}}x, A^{\frac{1}{2}}x) + (y, y)$ in $X \times X$. With

$$K_1 x = (A^{\frac{1}{2}}x, k_1)b, \quad K_2 y = (y, k_2)b \quad (2.25)$$

the closed loop system is

$$\begin{pmatrix} \dot{x} \\ \dot{y} \end{pmatrix} = \begin{pmatrix} 0 & I \\ -A + K_1 & K_2 \end{pmatrix} \begin{pmatrix} x \\ y \end{pmatrix}. \quad (2.26)$$

One can now ask: What eigenvalues can be achieved for the closed loop system (2.24) by appropriate selection of k_1, k_2 in (2.25)? For some time the author was under the impression that his approach via canonical forms [35] (more on this below) was the first treatment of this question but, in fact, it appears that this credit must go to Prof. Sun S.-H. of Szechuan University who treated this problem by a more sophisticated application of the perturbation technique used by the author in [32] to obtain the result. Sun was able to show, with an assumption similar to (2.21) and the Riesz basis assumption on the open loop eigenvectors, that the totality of spectra, \sum , achievable by use of (2.25) coincides with sequences ζ_k, ζ_{-k} , $k = 1, 2, 3, \dots$ for which, assuming the $b_k \neq 0$ as before,

$$\sum_{k=1}^{\infty} \left(\left| \frac{\zeta_2 - iw_k}{b_k} \right|^2 + \left| \frac{\zeta_{-k} + iw_k}{b_k} \right|^2 \right) < \infty .$$

His very important paper has been translated by Ho L.-F. in [44]. Some comparable, but necessarily weaker, results have been obtained by Reid in his thesis [29] for the equation of linear surface waves where (2.21) is not satisfied and, in fact, $\lim_{k \rightarrow \infty} (w_{k+1} - w_k) = 0$. Other results in this direction, for hyperbolic systems of various types, have been obtained by Clark [5], [6] and by Ho in his thesis [16].

Much of the initial impetus for the study of control canonical forms, both for finite and infinite dimensional systems, came from the spectral determination question discussed above, but the subject is interesting in its own right and shows some promise of being adaptable for "real world" control implementation. The reader will recall that a finite dimensional controllable system

$$\dot{x} = Ax + bu, \quad x \in \mathbb{R}^n,$$

with scalar control u is equivalent, via a state space similarity transformation (see [20], [35]) to a system in rational canonical form corresponding to the n -th order scalar equation

$$y^{(n)} + a_1 y^{(n-1)} + \dots + a_{n-1} y' + a_n y = u, \quad (2.27)$$

where

$$p(\lambda) = \det(\lambda I - A) = \lambda^n + a_1 \lambda^{n-1} + \dots + a_{n-1} \lambda + a_n$$

is the characteristic polynomial of the matrix A . Comparable, but somewhat more intricate, results are available for systems with higher control dimension [20], [2]. In [38] we note that if one employs a scalar linear observation

$$y = h^* x = (x, h), \quad (2.28)$$

there is exactly one observation vector $h \in \mathbb{R}^n$ for which (2.28) satisfies (2.27); for general h the right hand side will involve the derivatives of u of order $\leq u - 1$. Systems (2.27) are particularly easy to deal with. Closed loop eigenvalues $\zeta_1, \zeta_2, \dots, \zeta_n$ may be realized simply by forming the polynomial

$$q(\lambda) = \prod_{k=1}^n (\lambda - \zeta_k) = \lambda^n + c_1 \lambda^{n-1} + \dots + c_{n-1} \lambda + c_n$$

and determining u by linear feedback on the observation y and its

derivatives ,

$$u = \sum_{k=1}^n (a_k - c_k) y^{(n-k)} .$$

Apparently less well known, but quite obvious, is that the control problem for (2.27) is, in a sense, trivial. Let us suppose the initial instant is taken to be $t = 0$ and control is to be effected during $0 \leq t \leq T$. Let the initial state be specified by

$$y^{(n-k)}(0) = Y_{n-k+1}, \quad k = 1, 2, \dots, n \quad (2.29)$$

and the terminal state by

$$y^{(n-k)}(T) = Y_{n-k+1}, \quad k = 1, 2, \dots, n . \quad (2.30)$$

If $y(t)$ satisfies (2.29) and

$$y^{(n)}(t) = v(t), \quad 0 \leq t \leq T \quad (2.31)$$

then we see readily that for $k = 1, 2, \dots, n$

$$y^{(n-k)}(t) = \sum_{\ell=1}^k Y_{n-\ell+1} \frac{t^{k-\ell}}{(k-\ell)!} + \int_0^t (t-s)^{k-1} v(s) ds$$

and (2.30) is achieved just in case

$$\int_0^T (t-s)^{k-\ell} v(s) ds = Y_{n-k-1} - \sum_{\ell=1}^k Y_{n-\ell-1} \frac{T^{k-\ell}}{(k-\ell)!} ,$$

$$k = 1, 2, \dots, n .$$

This is easily solved for v in various function classes, e.g. polynomials of degree $\leq n - 1$, etc. and, it should be noted, the solution has nothing to do with the coefficients in (2.27) so the calculation can be carried out once for any given T and recorded for use ever after. Then in a given canonical system (2.27) we need only set

$$u(t) = v(t) - \sum_{k=1}^n a_k y^{(n-k)}(t) \quad (2.32)$$

to realize the desired control objective.

Since, in a given control context, it is not likely that the available observation (2.28) will be the particular one for which (2.27) obtains, the above result might seem to be a generally useless curiosity. It turns out, however, that in canonical form theory there is a counterpart to the more widely known observer theory. If C is any $n \times n$ matrix whose minimal and

characteristic polynomials coincide, it is possible to select (non-uniquely) r , d and j such that the augmented system

$$\dot{x} = Ax + bu \quad (2.33)$$

$$\dot{z} = ry + Cz + du \quad (= rh^*x + Cz + du \quad \text{since } y = h^*x) \quad (2.34)$$

with augmented observation

$$w = y + j^*z = h^*x + j^*z \quad (2.35)$$

is in canonical form, so that for some coefficients $\alpha_1, \alpha_2, \dots, \alpha_{2m}$

$$w^{(2n)} + \alpha_1 w^{(2n-1)} + \dots + \alpha_{2m-1} w' + \alpha_{2m} w = u.$$

The adjoined system (2.34) can be realized electronically, just as an observer system is, and the considerable freedom in choice of C , r , d and j provides much design flexibility. In some cases the dimension of (2.34) can be reduced. The proof that (2.33), (2.34), (2.35) can be made a canonical system appears in [38].

A parallel control canonical form theory has been developed for certain hyperbolic distributed parameter systems, involving neutral functional equations in place of the n -th order scalar equation (2.27). The theory is quite complex, especially as it applies to partial differential equations with variable coefficients (see [35], [16], [38], [39] e.g.). To give an idea how the theory is developed we will consider the constant coefficient case of (1.4) which, without loss of generality, we can take to be

$$\frac{\partial^2 w}{\partial t^2} - \frac{\partial^2 w}{\partial x^2} = 0, \quad t \geq 0, \quad 0 \leq x \leq 1, \quad (2.36)$$

$$w(0, t) = 0, \quad \frac{\partial w}{\partial x}(1, t) = u(t). \quad (2.37)$$

The normalized eigenfunctions of the corresponding homogeneous system are

$$\phi_k(x) = \sqrt{2} \sin \frac{2k-1}{2} \pi x, \quad k = 1, 2, 3, \dots \quad (2.38)$$

Setting $w_k = \frac{2k-1}{2} \pi$ and forming the expansions

$$w(x, t) = \sum_{k=1}^{\infty} w_k(t) \phi_k(x), \quad (2.39)$$

$$\frac{\partial w}{\partial t}(x, t) = \sum_{k=1}^{\infty} v_k(t) \phi_k(x), \quad (2.40)$$

followed by the transformation

$$\begin{pmatrix} w_k \\ v_k \end{pmatrix} = \begin{pmatrix} \frac{1}{iw_k} & -\frac{1}{iw_k} \\ 1 & 1 \end{pmatrix} \begin{pmatrix} \eta_k \\ \zeta_k \end{pmatrix} \quad (2.41)$$

we have, for $k = 1, 2, 3, \dots$

$$\dot{\eta}_k = iw_k \eta_k + \frac{(-1)^{k-1}}{\sqrt{2}} u(t), \quad \dot{\zeta}_k = -iw_k \zeta_k + \frac{(-1)^{k-1}}{\sqrt{2}} u(t). \quad (2.42)$$

Consider now the neutral delay equation

$$y(t+2) + y(t) = u(t+2). \quad (2.43)$$

The characteristic function of the homogeneous equation is

$$p(\lambda) = e^{2\lambda} + 1 = 2e^\lambda \cosh \lambda$$

and the zeros of $p(\lambda)$ are precisely the eigenvalues $\pm iw_k$ appearing in (2.42). The transfer function for (2.43) is

$$T_0(\lambda) = \frac{e^{2\lambda}}{e^{2\lambda} + 1} = \frac{1}{2} \frac{\sinh \lambda}{\cosh \lambda} + \frac{1}{2} \quad (2.44)$$

which can be rewritten as

$$T_0(\lambda) = \sum_{k=1}^{\infty} \frac{\lambda}{\lambda^2 + \omega_k^2} + \frac{1}{2}, \quad \omega_k = \frac{2k-1}{2} \pi. \quad (2.44)$$

If we define an observation $y(t)$ on (2.42) by

$$y(t) = \sum_{k=1}^{\infty} [h_k \eta_k(t) + g_k \zeta_k(t)] + \frac{1}{2} u(t)$$

the transfer function for y is, formally,

$$\sum_{k=1}^{\infty} \left[\frac{h_k (-1)^{k-1} \frac{1}{\sqrt{2}}}{\lambda - i\omega_k} + \frac{g_k (-1)^{k-1} \frac{1}{\sqrt{2}}}{\lambda + i\omega_k} \right] + \frac{1}{2}$$

which may be seen to agree with (2.44) just in case

$$h_k = g_k = \frac{(-1)^k}{\sqrt{2}}.$$

Using (2.38), (2.39), (2.41), (2.42) it may be seen that this choice of h_k, g_k corresponds to

$$y(t) = \frac{1}{2} \frac{\partial w}{\partial t}(1, t) + \frac{1}{2} u(t) = \frac{1}{2} \left(\frac{\partial w}{\partial t}(1, t) + \frac{\partial w}{\partial x}(1, t) \right). \quad (2.45)$$

This observation on (2.42), and no other, satisfies the scalar equation (2.43) which serves as the control canonical form for (2.42). The details of the above

calculations and some idea of the form of a general theory appear in [38] and [39].

If the canonical observation (2.45) were actually available, so that we have (2.43), its usefulness is quite clear. For, with the causal feedback law

$$u(t+2) = (1-\gamma)y(t) - \int_0^2 c(s)y(t+s)ds \quad (2.46)$$

(2.43) transforms to

$$y(t+2) + \gamma y(t) + \int_0^2 c(s)y(t+s)ds = 0 \quad (2.47)$$

and it is known from [35], [44] that the exponential solution $e^{\zeta_k t}$, $e^{\zeta_{-k} t}$ of (2.47) can be made such that

$$\zeta_k = i\omega_k + \alpha + \varepsilon_k, \quad \zeta_{-k} = i\omega_k + \alpha + \varepsilon_{-k},$$

where α is a complex number (ordinarily negative) determined by γ and ε_k , ε_{-k} are arbitrary complex numbers, determined by $c \in L^2[0,2]$, such that

$$\sum_{k=1}^{\infty} (|\varepsilon_k|^2 + |\varepsilon_{-k}|^2) < \infty.$$

It may be shown that these are the eigenvalues of the closed loop system (2.36), (2.37), (2.45), (2.46).

In a given application, however, it is entirely likely that the particular "canonical" observation (2.46) will not be available. Indeed, in the example indicated, since this observation is taken at the same point where control is applied and might, therefore, be subject to a certain amount of noise disturbance, it might not be desirable to use this observation in practice. To illustrate the use of the technique of canonical augmentation (or "canonical compensation", perhaps) let us consider the same system (2.36), (2.37), but suppose the available observation is

$$y(t) = \frac{\partial w}{\partial x}(0, t). \quad (2.48)$$

It is not hard to show in this case that $y(t)$ satisfies

$$y(t+2) + y(t) = u(t+1) \quad (2.49)$$

rather than (2.43). This "central" control canonical form is not as usable as the "backward" form (2.43) because, unlike (2.46),

$$u(t+1) = (1-\gamma)y(t) - \int_0^2 c(s)y(t+s)ds$$

is not a causal feedback law and cannot be implemented. But now couple (2.49) with

$$z(t+2) + \rho z(t) = au(t+2) + bu(t+1) + cy(t+1) + dy(t) \quad (2.50)$$

and let

$$w(t) = y(t) + z(t).$$

One ordinarily will take $|\rho| < 1$ so that the homogeneous part of (2.50) is asymptotically stable, thus avoiding the growth of parasitic solutions in the compensator. Since

$$[y(t+4) + y(t+2) - u(t+3)] + \rho [y(t+2) + y(t) - u(t+1)] = 0$$

while

$$[z(t+4) + \rho z(t+2) - au(t+4) - bu(t+3) - cu(t+1) - cy(t+3) - dy(t+2)] + [z(t+2) + \rho z(t) - au(t+2) - bu(t+1) - cy(t+1) - dy(t)] = 0$$

we find that

$$\begin{aligned} w(t+4) + (1+\rho)w(t+2) + \rho w(t) &= au(t+4) + [1+b]u(t+3) \\ &+ au(t+2) + [\rho+b]u(t+1) + c[y(t+3) + y(t+1)] \\ &+ d[y(t+2) + y(t)] = (\text{using (2.49)}) \\ &au(t+4) + [1+b]u(t+3) + [a+c]u(t+2) + [\rho+b+d]u(t+1). \end{aligned}$$

Then it is easy to see that with

$$a = 1, \quad 1+b = a+c = \rho+b+d = 0,$$

i.e. with

$$a = 1, \quad b = -1, \quad c = -1, \quad d = 1 - \rho,$$

we arrive at the "backward" canonical form satisfied by $w(t)$:

$$w(t+4) + (1+\rho)w(t+2) + \rho w(t) = u(t+4)$$

for which causal feedback laws

$$\begin{aligned} u(t+4) &= -\gamma_1 w(t+3) + [1+\rho - \gamma_2] w(t+2) - \gamma_3 w(t+1) \\ &+ [\rho - \gamma_4] w(t) - \int_0^4 c(s) w(t+s) ds \end{aligned} \quad (2.51)$$

may be implemented, yielding overall closed loop systems

$$w(t+4) + \gamma_1 w(t+3) + \gamma_2 w(t+2) + \gamma_3 w(t+1) + \gamma_4 w(t) + \int_0^4 c(s) w(t+s) ds = 0. \quad (2.52)$$

It is necessary to check separately that the system (2.49), (2.50), (2.51) is observable in any given case.

The exponential solutions of (2.52), and hence the eigenvalues of (2.36), (2.37), (2.48), (2.50), (2.51) may be determined with the same flexibility as already noted for (2.47). This is discussed in some detail in the thesis of R. G. Teglus [45]. A complete theory of canonical compensation for hyperbolic systems remains to be developed but, we hope, the example given here gives reason to believe that the method is a promising one. It is clear that there are some connections with observer theory as developed in [22] and elsewhere; these connections remain to be worked out.

REFERENCES

1. Birkhoff, G. D., and G. -C. Rota Ordinary Differential Equations. Ginn and Co., New York, 1959.
2. Brunovsky, P., "A Classification of Linear Controllable Systems," *Kybernetika*, Vol. 6, 1970, pp. 173-188.
3. Butkovskiy, A. G., "The Method of Moments in the Theory of Optimal Control of Systems with Distributed Parameters," *Automat. Rem. Contr.*, Vol. 24, 1963, pp. 1106-1113.
4. _____, *Theory of Optimal Control of Distributed Parameter Systems*. American Elsevier Pub. Co., New York, 1969.
5. Clarke, B. M. N., "Control Canonical Forms and Eigenvalue Assignment by Feedback for a Class of Linear Hyperbolic Systems," *SIAM J. Cont. and Opt.*, Vol. 19, 1981, pp. 711-729.
6. _____, "Eigenvalue Assignment of an Augmented Hyperbolic System by Linear Feedback," *Macquarie Mathematics Reports*, No. 80-0017, School of Mathematics and Physics, Macquarie University, North Ryde, Australia, 1980.
7. Coddington, E. H., and N. Levinson, *Theory of Ordinary Differential Equations*. McGraw Hill Book Co., New York, 1955.
8. Courant, R., and D. Hilbert, *Methods of Mathematical Physics, Vol II: Partial Differential Equations*. Interscience Pub. Co., New York, 1962.
9. Dafermos, C. M., "Wave Equations with Weak Damping," *SIAM J. Appl. Math.*, Vol. 18, 1970, pp. 759-767.

10. Datko, R., "A Linear Control Problem in an Abstract Hilbert Space," *J. Diff. Eq'ns*, Vol. 9, 1971, pp. 346-359.
11. Egorov, Yu. V., "Some Problems in the Theory of Optimal Control," *Soviet Mathematics*, Vol. 3, 1962, pp. 1080-1084.
12. _____, "Optimal Control on Banach Space," *Ibid.*, Vol. 4, 1963.
13. Fattorini, H. O., "Control in Finite Time of Differential Equations in Banach Space," *Comm. Pure Appl. Math.*, Vol. 19, 1966, pp. 17-34.
14. Gal'chuk, L. I., "Optimal Control of Systems Described by Parabolic Equations," *SIAM J. Control*, Vol. 7, 1969, pp. 546-558.
15. Herget, C. J., "On the Controllability of Distributed Parameter Systems," *Inter. J. Control*, Vol. 11, 1970, pp. 827-833.
16. Ho, L. F., "Controllability and Spectral Assignability of a Class of Hyperbolic Control Systems with Retarded Control Canonical Forms," Thesis, University of Wisconsin, Madison. August 1981.
17. Ho, L.F., and D. L. Russell, "Admissible Input Elements for Linear Systems in Hilbert Space and a Carleson Measure Criterion. To appear.
18. Ingham, A. E., "Some Trigonometrical Inequalities in the Theory of Series," *Math. Zeitschr.*, Vol. 41, 1936, pp. 367-379.
19. LaSalle, J. P., and S. Lefschetz, *Stability by Liapounov's Direct Method with Applications*. Academic Press, New York, 1961.
20. Lee, E. B., and L. W. Markus, *Foundations of Optimal Control Theory*. Wiley, New York, 1967.
21. Levinson, N., "Gap and Density Theorems," *Amer. Math. Soc. Colloquium Pub.*, Vol. 26, 1940.
22. Luenberger, D. G., "An Introduction to Observers," *IEEE Trans. Auto. Control*, Vol. AC-16, 1971, pp. 596-602.
23. Mizel, V. J., and T. I. Seidman, "Observation and Prediction for the Heat Equation," *J. Math. Anal. Appl.*, Vol. 28, 1969, pp. 303-312. Part II: *Ibid.*, Vol. 38, 1972, pp. 149-166.
24. Paley, R. E. A. C., and N. Wiener, "Fourier Transforms in the Complex Domain," *Amer. Math. Soc. Coll. Pub.*, Vol. 19, Providence, 1934.
25. Petrovski, I. G., *Partial Differential Equations*. Iliffe Books, London, 1967.
26. Pontryagin, L. S., V. G. Boltyanskii, R.V. Gamkrelidze, E.F. Mishchenko, *The Mathematical Theory of Optimal Processes*. Interscience Pub., New York, 1962.

27. Quinn, J. P., Time Optimal Control of Linear Distributed Parameter Systems, Thesis, University of Wisconsin, Madison, August 1969.
28. Quinn, J. P., and D. L. Russell, "Asymptotic Stability and Energy Decay Rates for Solutions of Hyperbolic Equations with Boundary Damping," Proc. Royal Soc. Edinburgh, Vol. 77A, 1977, pp. 7-12.
29. Reid, R. M., Some Controllability and Stabilizability Properties of Linear Water Waves, Thesis, University of Wisconsin, Madison, August 1979.
30. Russell, D. L., On Boundary Value Controllability of Linear Symmetric Hyperbolic Systems, in Mathematical Theory of Control, Academic Press, New York, 1967, pp. 312-321.
31. _____, "Nonharmonic Fourier Series in the Control Theory of Distributed Parameter Systems," J. Math. Anal. Appl., Vol. 18, 1967, pp. 542-559.
32. _____, "Linear Stabilization of the Linear Oscillator in Hilbert Space," J. Math. Anal. Appl., Vol. 25, 1969, pp. 663-675.
33. _____, "Decay Rates for Weakly Damped Systems in Hilbert Space Obtained With Control-Theoretic Methods," J. Diff. Eqns., Vol. 19, 1975, pp. 344-370.
34. _____, "Control Theory of Hyperbolic Equations Related to Certain Questions in Harmonic Analysis and Spectral Theory," J. Math. Anal. Appl., Vol. 40, 1972, pp. 336-368.
35. _____, "Canonical Forms and Spectral Determination for a Class of Hyperbolic Distributed Parameter Control Systems," Ibid., Vol. 62, 1978, pp. 186-225.
36. _____, "Controllability and Stabilization Theory for Linear Partial Differential Equations: Recent Progress and Open Questions," SIAM Review, Vol. 20, 1978, pp. 639-739.
37. _____, Closed Loop Eigenvalue Specification for Augmented and Deficient Hyperbolic Systems, Technical Summary Report 2021. Mathematics Research Center, University of Wisconsin, Madison, 1979.
38. _____, Control Canonical Structure for a Class of Distributed Parameter Systems, Proceedings of Third IMA Conf. on Control Theory, Sheffield, 1980.
39. _____, Functional Equations as Control Canonical Forms for Distributed Parameter Systems and a State Space Theory for Certain Differential Equations of Infinite Order, Proceedings Conf. on Functional Eq'ns. and Control Theory, Blacksburg, Va., 1981, to appear.
40. Sakawa, Y., "Observability and Related Problems for Partial Differential Equations of Parabolic Type," SIAM J. Control, Vol. 13, 1975, pp.14-27.

41. _____, Feedback Control of Second Order Evolution Equations with Damping, to appear.
42. Schwartz, L., Etude des sommes d'exponentielles. deuxième édition, Hermann, Paris, 1959.
43. Slemrod, M., "Asymptotic Behavior of a Class of Abstract Dynamical Systems," J. Diff. Eq'ns., Vol. 7, 1970, pp. 584-600.
44. Sun, S. -H., "On Spectrum Distribution of Completely Controllable Linear Systems," SIAM J. Cont. and Opt., Vol. 19, 1981, pp. 730-743.
45. Teglas, R. G., A Control Canonical Form for a Class of Linear Hyperbolic Systems. Thesis, University of Wisconsin, Madison, June 1981.
46. Triggiani, R., "On the Stabilizability Problem in Banach Space," J. Math. Anal. Appl., Vol. 52, 1975, pp. 383-403.
47. Weck, N., "A Remark on Controllability for Symmetric Hyperbolic Systems in one Space Dimension," SIAM J. Contr. and Opt., Vol. 20, 1982, pp. 1-8.
48. Wonham, W. M., "On Pole Assignment in Multi-input Controllable Linear Systems," IEEE Trans. Auto. Contr., Vol. AC-12, 1967, pp. 660-665.
49. Young, R. M., An Introduction to Non-harmonic Fourier Series. Academic Press, New York, 1980.

This Page Intentionally Left Blank

APPROXIMATION IN CONTROL OF FLEXIBLE STRUCTURES, THEORY AND APPLICATION

J.S. Gibson

University of California, Los Angeles
Los Angeles, CA 90024

1. Introduction

Several recent papers by the present author have applied the modern theory of the infinite dimensional regulator problem to problems in active control of flexible structures ([2], [3], [4], [5], [6]).

We study the sense in which the feedback control law based on an approximate finite dimensional model of a continuous structure approximates a control law which is optimal for the distributed, or infinite dimensional, model of the structure. From the analysis of the various control and stability issues associated with this basis question, we can gain useful information for designing finite dimensional compensators which produce near-optimal performance in infinite dimensional systems.

Our most important analytical tools are the properties of the infinite dimensional Riccati equation and approximation theory for its approximate solution by means of finite dimensional Riccati matrix equations. In this paper, we hope to indicate some of the important predictions that can be made about large-order finite dimensional control laws, using the theory of infinite dimensional Riccati equations.

2. The Infinite Dimensional Problem

We consider an abstract second order (in time) linear system

$$(1) \quad \ddot{x} + C_0 \dot{x} + A_0 x = B_0 u,$$

where the state vector $x(t)$ is in a real

Hilbert space H and the control vector $u(t)$ is a real m -vector for some finite m . The linear operator A_0 is a self-adjoint operator in H with compact resolvent, $C_0 = C_0^* \geq 0$ and C_0 is A_0 -bounded, and B_0 is bounded. With $y = (x, \dot{x})$, (1) takes the first order form

$$(2) \quad \dot{y} = Ay + Bu.$$

See [2] for details. The state vector $y(t)$ is cast in a Hilbert space E such that $\frac{1}{2} \|y(t)\|_E^2$ is essentially the total energy in the system.

In the infinite dimensional optimal control problem, we choose u to minimize

$$(3) \quad J = \int_0^{\infty} (\langle Dy, y \rangle_E + \|u\|^2) dt,$$

where $D = D^* \geq 0$ and D is bounded.

If J can be made finite for each $y(0)$, then an optimal control exists for each $y(0)$ and has the feedback form

$$(4) \quad u(t) = -B^* P y(t),$$

where $P = P^*$ is nonnegative and bounded and satisfies the infinite dimensional Riccati equation

$$(5) \quad A^* P + PA - PBB^* P + D = 0.$$

See [1], [2].

When P exists for D positive definite, then the closed-loop semigroup generated

by $A - BB^*P$ is uniformly exponentially stable.

3. Approximation

To approximate (4) and (5), we define E_n to be the subspace of E spanned by the first n eigenvectors of A_0 , and project the infinite dimensional problem onto E_n to obtain the n th finite dimensional problem. Again, see [2] for details.

The eigenvectors of A_0 are the natural mode shapes of free vibration, so that we are using modal approximation.

Projecting the operators A , B , and D onto E_n yield the corresponding operators A_n , B_n , and D_n . For the n th problem, we then obtain the Riccati equation

$$(6) \quad A_n^* P_n + P_n A_n - P_n B_n B_n^* P_n + D_n = 0.$$

This equation amounts to an $2n \times 2n$ Riccati matrix equation because the operators involved are all finite dimensional. Our analysis hinges on when and in what sense P_n approximate P if P exists.

From here on, we will assume that A_0 is positive definite and that $\frac{1}{2} \|y(t)\|_E^2$ is equal to the total energy in the structure. According to [2], if D is positive definite (coercive) and $C_0 = 0$ (no damping in the free structure), then P does not exist and $\|P_n\|$ increases without bound as n increases. On the other hand, if C_0 is positive definite, then P exists and $P_n \Lambda_n$ converges strongly to P , where Λ_n is the projection operator mapping E onto E_n . Also when C_0 is positive definite, the closed-loop semigroup generated by

$A - BB^* P \Lambda_n$ approximates the semigroup generated by $A - BB^* P$ in norm, and hence is uniformly exponentially stable for n sufficiently large.

4. Example

We take a simply-supported beam whose first natural frequency is 10 hz.; i.e., the lowest eigenvalue of the operator A_0 in (1) is 100. The control force is distributed over a pad whose length is five per cent of the beam's length. For damping, we assume $C_0 = c_0 A_0^{1/2}$, which yield the same damping ratio for each mode. We denote by $x(t, \eta)$ the displacement of a point a distance η from the left end at time t .

In the optimal control problem, we take

$$(7) \quad J = \int_0^\infty (2E(t) + u^2(t)) dt,$$

where $E(t)$ is the total energy in the beam. When a solution to (3) exists, (4) becomes

$$(8) \quad u(t) = - \int_0^L f''(\eta) x''(t, \eta) d\eta - \int_0^L g(\eta) \dot{x}(t, \eta) d\eta,$$

where $(\cdot)'' = \frac{\partial^2}{\partial \eta^2}$. (Details are in [7].)

From the n th approximate problem we obtain approximations f_n and g_n to f and g by using the solution to the Riccati equation (6). We should note that f_n and g_n give graphical representations of the modal control law

$$(9) \quad u_n = -B_n^* P_n y_n(t)$$

that would be used in a finite dimen-

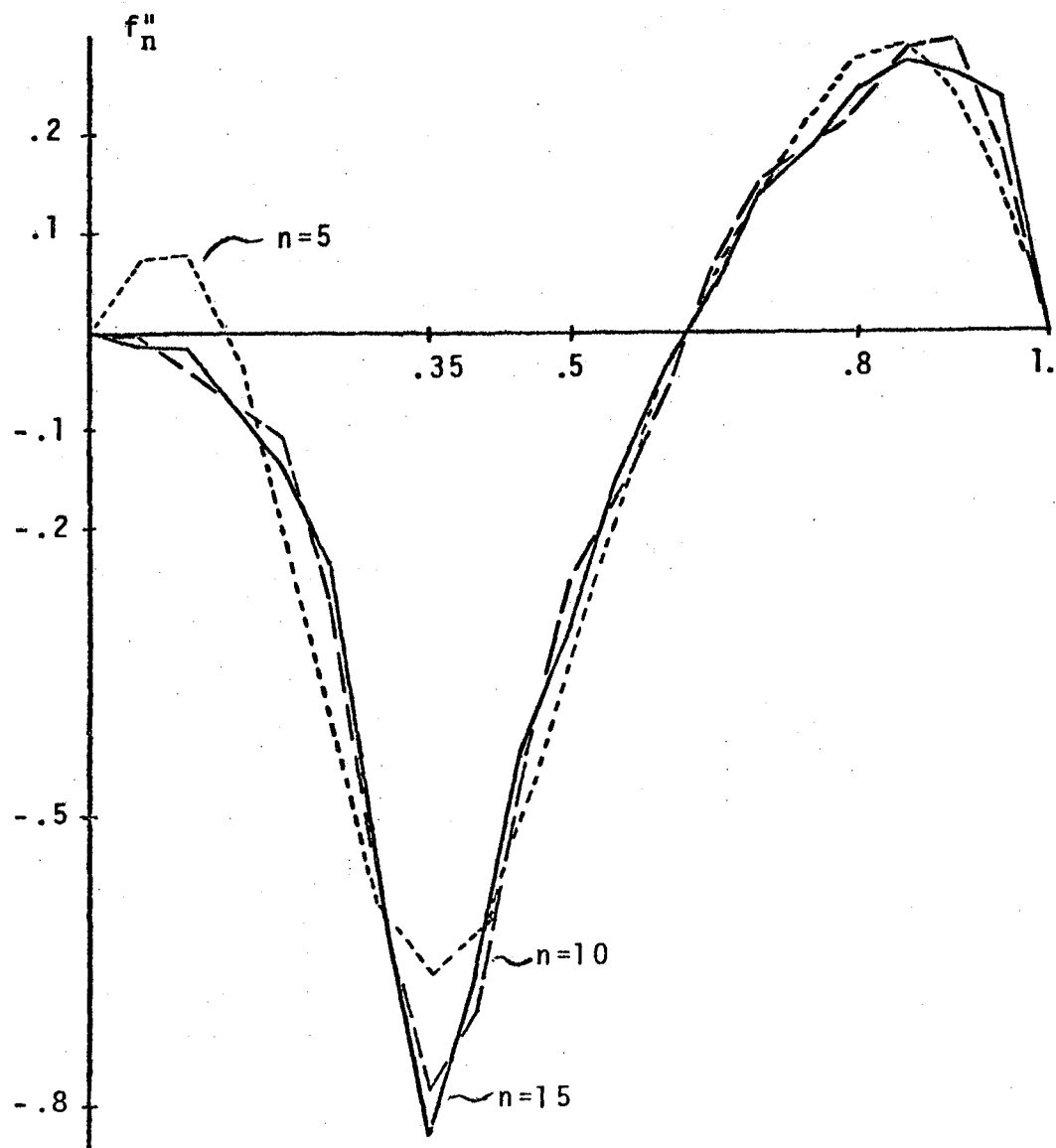
sional compensator based on an n-mode model of the beam (see [2], [7]).

Figures 1, 2, and 3 show our numerical results for f_n and g_n with increasing n. Note the important role of inherent system damping when large numbers of modes are modeled. Perhaps our most significant results pertain to the importance of modeling damping in large numbers of modes.

7. J. S. Gibson, "Approximation Theory for Linear-quadratic Optimal Control and Estimation of Hyperbolic Systems," to appear.

REFERENCES

1. J. S. Gibson, "The Riccati Integral Equations for Optimal Control Problems on Hilbert Spaces", SIAM J. Control Opt., July 1979.
2. J. S. Gibson, "An Analysis of Optimal Modal Regulation: Convergence and Stability," SIAM J. Contr. Opt., September 1981.
3. J. S. Gibson, "A Note on Stabilization of Infinite Dimensional Linear Oscillators by Compact Linear Feedback, SIAM J. Contr. Opt., May 1980.
4. J. S. Gibson, "Convergence and Stability in Linear Modal Regulation of Flexible Structures," Second VIP & SU Symposium on Spacecraft Control, June 1979.
5. J. S. Gibson and M. Navid, "Approximate Solution of Riccati Algebraic Equations," International Symposium on Math. Thy. of Networks, Santa Monica, CA, August 1981.
6. J. S. Gibson and M. Navid, "Optimal Control of Flexible Structures," CDC, December 1981.



$c_0 = 0$

Figure 1a

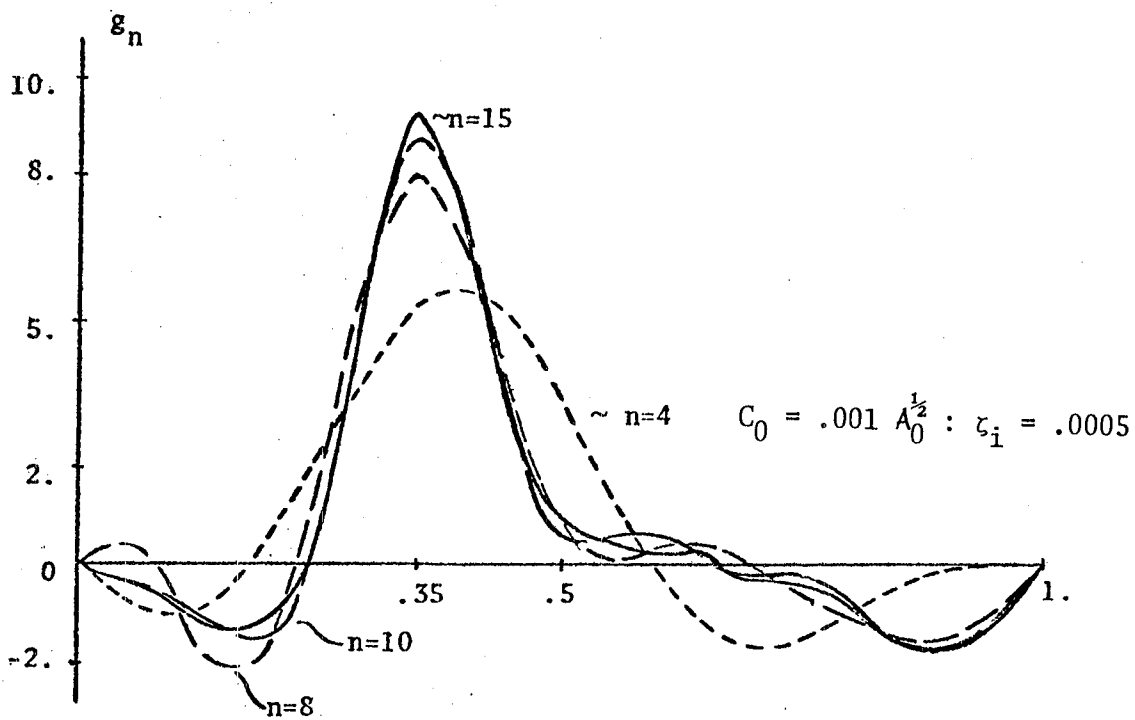
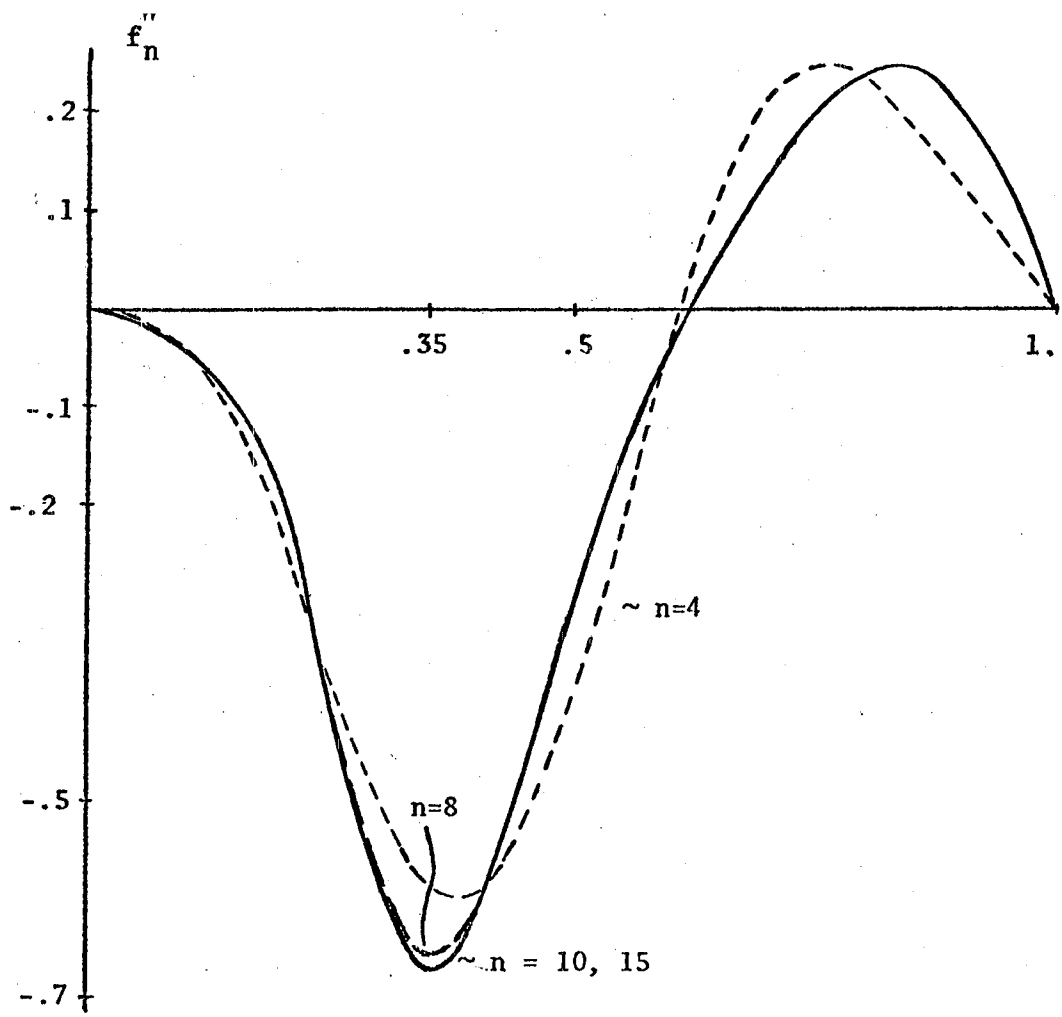
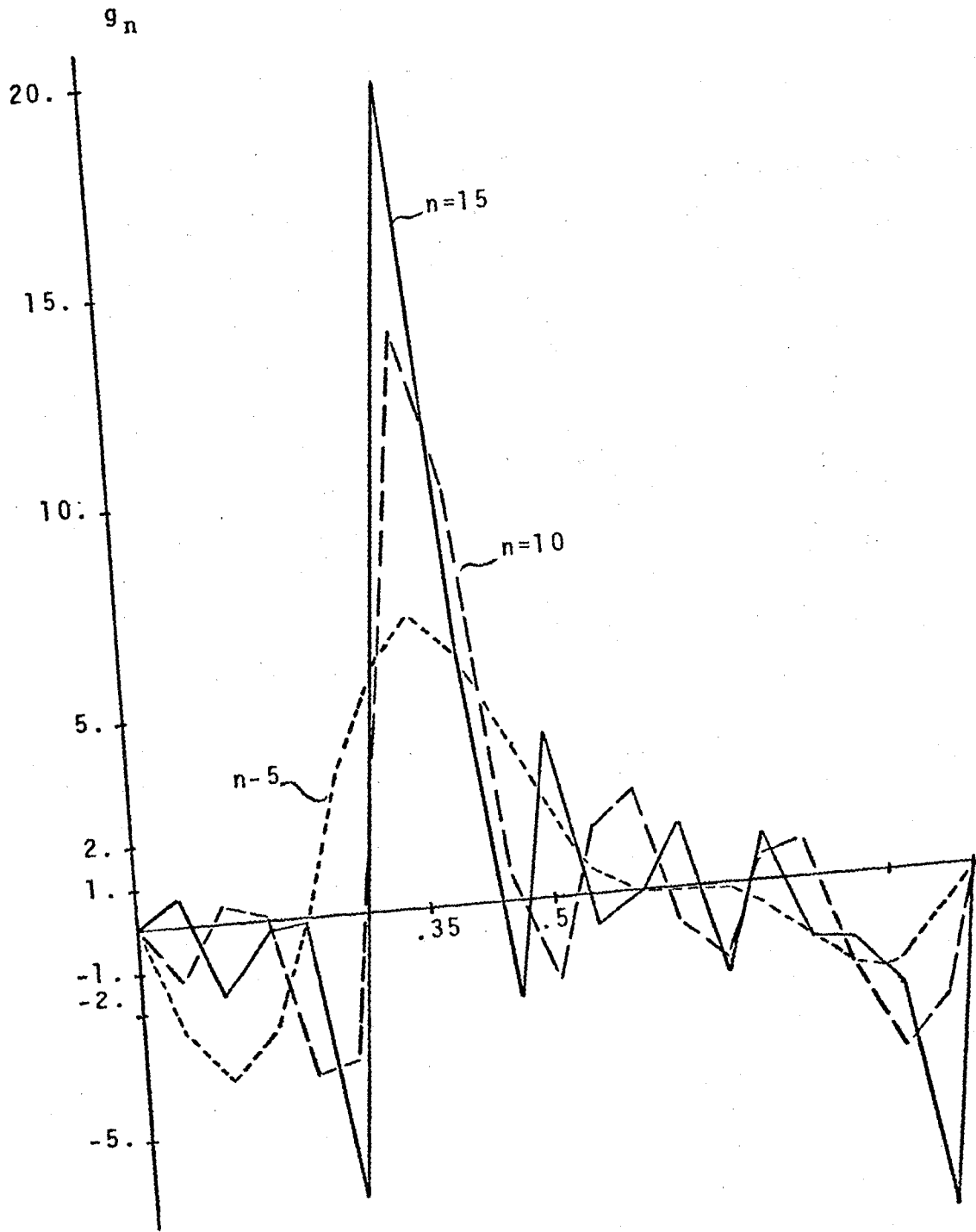
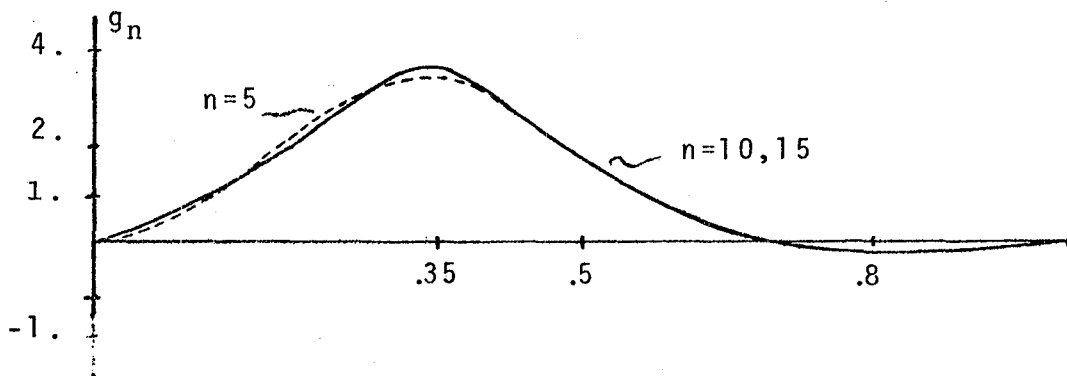
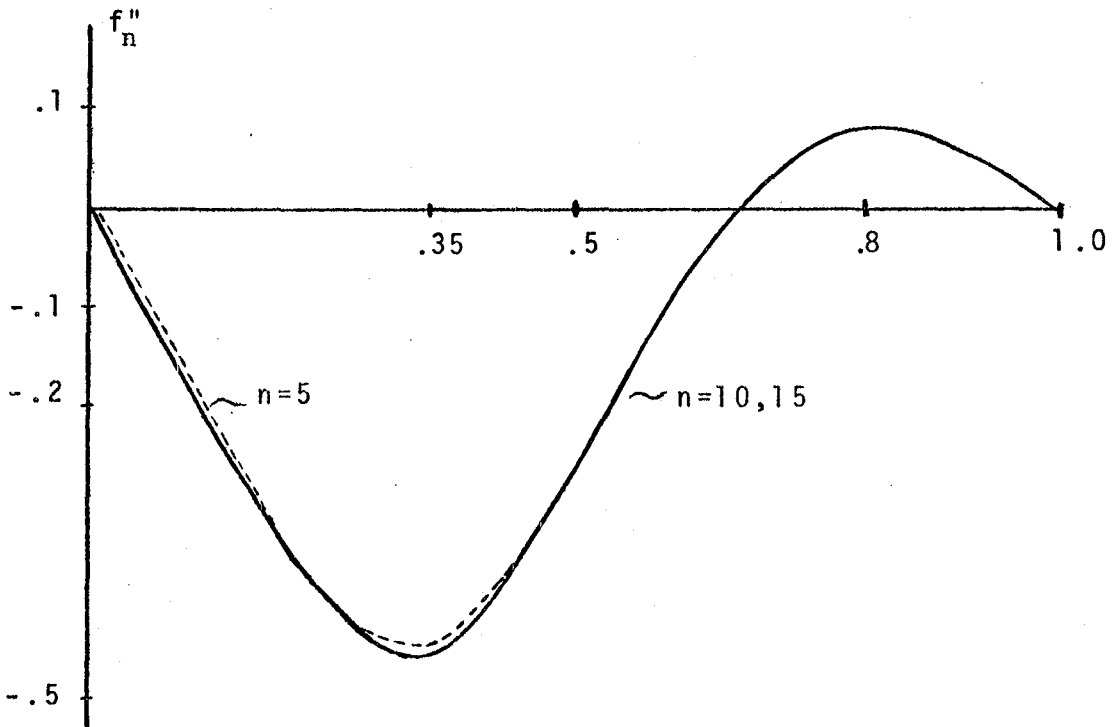


Figure 2



$$C_0 = 0$$

Figure 1b



$$C_0 = .02A_0^{1/2} : \zeta_i = .01$$

Figure 3

This Page Intentionally Left Blank

SIMULTANEOUS CONTROL AND OPTIMIZATION FOR ELASTIC SYSTEMS*

Vadim Komkov

Department of Mathematics, West Virginia University
Morgantown, WV 26505

ABSTRACT

We consider the dynamic response of beams and plates to loads which are extreme within a certain class of admissible loads. Two approaches to this problem are suggested. In approach one, Pontrjagin's maximality principle is regarded as an additional constraint. The optimality of design is then determined by standard numerical techniques.

Secondly, we proceed with the "adjoint variable approach" to sensitivity of structural design for a given inhomogeneous term. The inhomogeneous term is an extremal element of admissible load vectors, which constitute a closed subspace of a Sobolëv space. Again, we invoke the maximality principle. While only beam and plate theory problems are used as examples, generalizations are easy to perceive.

0. NOTATION AND SOME BASIC ASSUMPTIONS

Symbols used in the discussion of beam theory have the following meaning:

ρ denotes the material density per unit length.

E denotes Young's modulus, which is assumed to be constant ($E > 0$) in our discussion.

A is the cross-sectional area ($A(x) > 0, \forall x \in [-\ell, +\ell]$).

I is the moment of inertia of the cross-sectional area about the neutral axis of bending, i.e., a line whose length remains unchanged locally as the beam undergoes deformation. I is not assumed to be constant, but is a positive function.

t denotes time.

The Cartesian coordinate system is used. The x -axis coincides with the undeformed axis of the beam, which occupies the interval $\Omega = [-\ell, +\ell]$. $W(x,t)$

*This research was supported by NSF Grant CMS 80-05677.

denotes the displacement function which is an element of Sobol'ev space H determined by the existence of the following integrals:

$$\int_{-\ell}^{+\ell} \left\{ E I(x) \left(\frac{\partial^2 w(x,t)}{\partial x^2} \right)^2 \right\} dx$$

$$\int_{-\ell}^{+\ell} \left[\rho A(x) \frac{\partial w(x,t)}{\partial t} \right] dx,$$

for all values of t in a given time interval $[0, T]$. The inner product in H is given by

$$(0.1) \quad \langle w_1, w_2 \rangle_{\Omega} = \int_{-\ell}^{+\ell} \left[E I(x) \left(\frac{\partial^2 w_1(x,t)}{\partial x^2} \cdot \frac{\partial^2 w_2(x,t)}{\partial x^2} \right) \right] dx \\ + \int_{-\ell}^{+\ell} \left[\rho A(x) \left(\frac{\partial w_1(x,t)}{\partial t} \cdot \frac{\partial w_2(x,t)}{\partial t} \right) \right] dx.$$

This is distinguished from the usual L_2 (inner) product

$$(f, g) = \int_{\Omega} [f(x,t) g(x,t)] dx.$$

The total energy of the beam is identified with the energy norm

$$(0.2) \quad \frac{1}{2} \| \| w(x,t) \| \| = \frac{1}{2} \langle w, w \rangle_{\Omega} = \epsilon(t),$$

which differs from $L_2(\Omega)$ norm $\|W\|_{L_2} = (W, W)_\Omega^{1/2}$. We assume that $A(x)$ and $l(x)$ depend uniquely on the choice of m -tuple of design parameters

$$\{s_1(x), s_2(x), \dots, s_m(x)\} = \underline{s};$$

that is,

$$A = A(\underline{s}(x); x)$$

and

$$l = l(\underline{s}(x); x).$$

The vector $\underline{s}(x)$ consists of m -design functions, such as thickness of the web, width of the flanges, etc., which are to be determined an optimal, or near-optimal design. The functions $s_i(x)$, $i = 1, 2, \dots, m$, $-l \leq x \leq +l$, obey certain constraints, such that $0 < G_i \leq s_i(x) \leq \Sigma_i$, where G_i , Σ_i are some constants determined by manufacturing limitations. The set \mathcal{S} of designs obeying these constraints is called admissible. The set of admissible loads includes all bounded (Lebesgue) measurable functions in Ω , and linear combinations of the spatial Dirac delta function and its first derivative concentrated at finite number of points in Ω multiplied by an $L_2(0, T)$ function of time; that is, an admissible load $q(x, t)$ is of the form:

$$(0.3) \quad q(x, t) = g(x, t) + \sum_{j=1}^{n_1} a_j \delta(x - \xi_j) \phi_j(t) + \sum_{j=1}^{n_2} b_j \delta'(x - \xi_j) \psi_j(t),$$

where $g(x, t)$ is a bounded measurable function on $\Omega \times [0, T]$; a_i , $i = 1, 2, \dots, n_1$, and b_i , $i = 1, 2, \dots, n_2$, are constants while the $\phi_i(t)$, $\psi_j(t)$ are bounded $L_2[0, T]$ functions.

$\|q(x,t)\|_Q$ is the $H^{-1}\{\Omega\} \times L_2[0,T]$ norm given by

$$\|q(x,t)\|_Q = \sup |(q,w)|$$

$$\|w\|_{L_2} \leq 1$$

The admissible loads $q(x,t) \in Q$ obey the constraint $\|q(x,t)\|_Q \leq M$ for some fixed constant $M > 0$.

The deflection function $W(x,t)$ obeys the state equation

$$(0.4) \quad L \left(W(\underline{s}(x); x, t) \right) = \rho A(\underline{s}(x), x) \frac{\partial^2 W(\underline{s}(x); x, t)}{\partial t^2} + \frac{\partial^2}{\partial x^2} \left(E I(\underline{s}(x), x) \right) \frac{\partial^2 W(\underline{s}(x); x, t)}{\partial x^2} = q(x, t),$$

where $q(x,t)$ is an admissible load, and $\underline{s}(x)$ an admissible design. Equation 0.4 can be rewritten as a system

$$(0.5) \quad \begin{cases} M(x,t) = - E I(\underline{s}(x), x) \cdot \frac{\partial^2 W(\underline{s}(x); x, t)}{\partial x^2} \\ \frac{\partial^2 M(x,t)}{\partial x^2} + \rho A(\underline{s}(x), x) \cdot \frac{\partial^2 W(\underline{s}(x); x, t)}{\partial t^2} = q(x, t) \end{cases}$$

The boundary conditions are

$$(0.6) \quad \left. \begin{array}{l} W(\underline{s}(\bar{x}); \bar{x}, t) \equiv 0 \\ M(\bar{x}, t) \equiv 0 \end{array} \right\} \quad \begin{array}{l} \text{for all } t \in [0, T], \\ \bar{x} = -l, \text{ or } \bar{x} = +l. \end{array}$$

The initial conditions in most realistic problems are not known. Here, we assume for the sake of simplicity that

$$(0.7) \quad \begin{aligned} W(\underline{S}(x), x, 0) &\equiv 0. \\ M(x, 0) &\equiv 0. \end{aligned}$$

1. STATEMENT OF THE PROBLEM

We consider a cost functional $J(\underline{S}(x); W(\underline{S}(x)); q(x, t); t)$ and we wish to find a design $\hat{\underline{S}}(x) \in \mathcal{P}$, such that

$$\hat{\underline{S}}(x) \rightarrow \min_{\underline{S} \in \mathcal{P}} \left[\max_{t \in [0, T]} \left\{ \sup_{q \in Q} \left(J(\underline{S}(x); W(\underline{S}(x)); q(x, t); t) \right) \right\} \right].$$

For example, we may wish to minimize the total energy

$$J(\underline{S}(x); W(\underline{S}(x)); q(x, t), t) = \varepsilon(\underline{S}, q, t)$$

Our problem consists in finding $\hat{\underline{S}}(x) \in \mathcal{P}$ such that

$$(1.1) \quad \hat{\varepsilon}(\hat{\underline{S}}, \tilde{q}, \tilde{t}) = \min_{\underline{S} \in \mathcal{P}} \left\{ \max_{t \in [0, t]} \left(\sup_{q \in Q} \varepsilon(\underline{S}; q, t) \right) \right\}.$$

In what follows we shall always assume that the set Q of admissible loads is bounded in the Q -norm and convex. For the sake of convenience let subscripts, from now on, denote partial differentials, i.e.,

$$W_x \equiv \frac{\partial W}{\partial x}, \quad W_t = \frac{\partial W}{\partial t}, \quad \text{etc.}$$

To prove some preliminary lemmas we need the following known identity (for stated boundary conditions)

$$(1.2) \quad \frac{d}{dt} \langle W_1, W_2 \rangle_{\Omega} = \left(L W_1, W_2 \right)_t_{\Omega} + \left(L W_2, W_1 \right)_t_{\Omega}$$

Hence,

$$(1.3) \quad \frac{d}{dt} \left\| \left\| W(q(x,t)) \right\| \right\|_{\Omega} = (q, W_t)_{\Omega}.$$

Clearly, if $\text{sign } q(x,t) = \text{sign } W_t(x,t)$ for some $x \in \Omega$ on a set of positive measure in Ω , and $q(x,t) = 0$ elsewhere in Ω , we must have

$$(1.4) \quad \frac{d}{dt} \left\| \left\| W(q(x,t)) \right\| \right\|_{\Omega} > 0.$$

Of course, we do not know whether such design exists. However, the following lemma is easy to prove.

Lemma 1

For any fixed $t \in [0, T]$ and fixed $\tilde{S} \in \mathcal{P}$ $\sup_{q \in Q} \varepsilon(\tilde{S}; q, t)$ exists and for a fixed \tilde{S}

$$\max_{t \in [0, T]} \left(\sup_{q \in Q} \varepsilon(\tilde{S}, q, t) \right) = \sup_{q \in Q} \varepsilon(\tilde{S}, q, T).$$

Proof

The first statement follows trivially from boundedness of the set of all numbers $\varepsilon(\tilde{S}, q, t)$, $\tilde{S} \in \mathcal{P}$, $q \in Q$, $t \in [0, T]$.

The second statement can be proven as follows. Suppose that for some choice of $q \in Q$, $\tilde{S} \in \mathcal{P}$ $\varepsilon_0 = \max_{t \in [0, t]} \varepsilon(\tilde{S}, q, t) > 0$ occurs at some time $t = \tau < T$.

Let us suppose that force $q \equiv 0$ is applied to the beam on a time interval (t, t_1) , $t < t_1 < T$. Clearly, t_1 can be chosen so that $W_t(x, t_1) \neq 0$ on some subset of Ω containing an interval $[x_1, x_2] \in \Omega$. Applying an admissible load $\tilde{q}(x, t)$ such that either $\text{sign } \tilde{q}(x, t) = \text{sign } W_t(x, t)$ on $[x_1, x_2]$ and $q(x, t) \equiv 0$ otherwise, or $\tilde{q}(x, t) = 0$ on some subset of $[x_1, x_2]$ for $t \in [t_1, t_2] \subset [t_1, T]$ with $[t_1, t_2]$ chosen sufficiently small, we obtain $\varepsilon(\tilde{S}, q, t_2) > \varepsilon_0$ which is a contradiction, proving our contention that $\tau = T$. Hence, the problem is reduced to finding a design $\hat{S} \in \mathcal{P}$ such that

$$\hat{\varepsilon}(\hat{S}, \hat{q}, T) = \min_{\tilde{S} \in \mathcal{P}} \left(\sup_{q \in Q} \varepsilon(\tilde{S}, q, T) \right).$$

2. PONTRJAGIN'S PRINCIPLE

For a fixed design $\tilde{\xi} \in \mathcal{P}$ the extremal control $\hat{q} \in Q$ satisfies Pontrjagin's maximality principle in the form given in References 1 and 2. Specifically, let $\hat{W}_H(\tilde{\xi}, x, t)$ be a solution of the homogeneous equation

$$(2.1) \quad \left(E I (\tilde{\xi}(x); x) \left(\hat{W}_H(\tilde{\xi}(x); x, t) \right)_{xx} \right)_{xx} + \rho A (\tilde{\xi}(x); x) \left(\hat{W}_H(\tilde{\xi}(x); x, t) \right)_{tt} = 0,$$

where \hat{W}_H obeys the boundary conditions of Equation 0.6 at $x = \pm \ell$, and satisfies an energy condition

$$(2.2) \quad \varepsilon \left(\left(\hat{W}_H(\tilde{\xi}(x); x, T) \right)_t \right) \geq \varepsilon \left(\left(\hat{W}_H(\tilde{\xi}(x); x, T) \right)_t \right)$$

for any other solution $\tilde{W}_H(\tilde{\xi}(x); x, t)$ satisfying the same boundary conditions. (Note that the design $\tilde{\xi}(x)$ is fixed!)

Then the following inequality must be true for all values of time on the interval $[0, T]$

$$(2.3) \quad \int_{-\ell}^{+\ell} -\hat{q}(x, t) \hat{W}_{H_t}(\tilde{\xi}(x); x, t) dx = \max_{q \in Q} \int_{-\ell}^{+\ell} \left[-q(x, t) \hat{W}_{H_t}(\tilde{\xi}(x); x, t) \right] dx$$

for an extremal control $\hat{q}(x, t)$. Let us make the following comments. For a fixed $\tilde{\xi} \in \mathcal{P}$ the final state $W(\tilde{\xi}(x), x, T)$, which maximizes the total energy at $t = T$, is not unique.

3. DUHAMEL'S PRINCIPLE

This differs sharply from the theorem established in Reference 2 for optimal controls minimizing the final energy. The reason for this difficulty is the nonconvexity of final states. To prove some properties of extremal energy states we proceed to postulate a strong form of Duhamel's principle. There exists a kernel function $G(x, \xi, t, \tau)$, which depends only on the coefficients ρ , E , I , and A of the Equation 0.4 and on the assigned boundary conditions, but

is independent of the initial data and of the inhomogeneous term $q(d,t)$, and such that the solution of Equation 0.4 can be written as

$$(3.1) \quad W(x,t) = \int_{\xi=-\ell}^{\xi=+\ell} \int_{t=0}^{t=T} \left[G(x,\xi,t,\tau) q(\xi,\tau) \right] d\xi d\tau + W_H(x,t)$$

For example, in the static deflection case for a freely supported beam, this kernel is of the form

$$(3.2) \quad \zeta(\xi,x) = \left(1 - \frac{x}{\ell}\right) \left(1 - \frac{\xi}{\ell}\right) \int_0^{\xi} \frac{\eta^2}{EI(\eta)} d\eta$$

$$+ \xi \left(1 - \frac{x}{\ell}\right) \int_{\xi}^x \frac{(1 - \eta/\ell)}{EI(\eta)} d\eta$$

$$+ \xi x \int_x^{\ell} \frac{(1 - \eta/\ell)^2}{EI(\eta)} d\eta ,$$

with the kernel $G(\xi,x)$ defined on $[0,\ell] \times [0,\ell]$ by the relation:

$$(3.3) \quad \left. \begin{aligned} G(\xi,x) &= \zeta(\xi,x) && \text{if } 0 \leq \xi \leq x \leq \ell \\ G(\xi,x) &= \zeta(x,\xi) && \text{if } 0 \leq x \leq \xi \leq \ell \end{aligned} \right\}$$

and

The solution of the homogeneous equation $W_H(x,t)$ satisfies the stated boundary conditions.

Lemma 3.1

We assume a fixed design $\tilde{\xi} \in \mathcal{P}$. Suppose that $\hat{q}_1(x,t), \hat{q}_2(x,t)$ are extremal admissible loads maximizing the energy ε at the time $t = T$, with zero initial conditions. Then the corresponding extremal displacements $\hat{W}_1(x,t), \hat{W}_2(x,t)$ obey the condition $\langle \hat{W}_1, \hat{W}_2 \rangle_{\Omega} |_{t=T} \leq 0$.

Proof

We use the convexity of the set of admissible loads. Hence, if \tilde{q}_1, \tilde{q}_2 are admissible $1/2(\tilde{q}_1 + \tilde{q}_2)$ is admissible. Using Formula 3.1, we conclude that the corresponding displacement is $1/2(\tilde{W}_1 + \tilde{W}_2)$, where \tilde{W}_1, \tilde{W}_2 correspond to the loads \tilde{q}_1, \tilde{q}_2 , respectively. (We recall that $W_H(x,t) \equiv 0$ in the Formula 3.1 because of our assumption concerning initial conditions.) Suppose that $\hat{q}_1(\tilde{\xi}), \hat{q}_2(\tilde{\xi})$ are two external loads such that $\varepsilon(\hat{q}_1(\tilde{\xi}), T) = \hat{\varepsilon}(\hat{q}_2(\tilde{\xi}), T) \geq \varepsilon(q(\tilde{\xi}), T)$ for any admissible load $q(x,t) \in Q$. Let $\hat{W}_1(\tilde{\xi}(x), x, t)$ be the displacement corresponding to \hat{q}_1 and $\hat{W}_2(\tilde{\xi}(x), x, t)$ displacement corresponding to \hat{q}_2 . We compute

$$\begin{aligned} \varepsilon\left(\frac{1}{2}(\hat{W}_1 + \hat{W}_2)\right)_{t=T} &= \frac{1}{2} (\langle \hat{W}_1, \hat{W}_2 \rangle + 2\langle \hat{W}_1, \hat{W}_2 \rangle + \langle \hat{W}_2, \hat{W}_2 \rangle)_{t=T} = \frac{1}{2} (\hat{\varepsilon} + 2 \langle \hat{W}_1, \hat{W}_2 \rangle + \hat{\varepsilon})_{t=T} \\ &= \hat{\varepsilon}(T) + 2 \langle \hat{W}_1, \hat{W}_2 \rangle_{t=T}. \end{aligned}$$

Since $\hat{\varepsilon}(T)$ is the maximal attainable energy level at $t = T$, we have

$$\langle \hat{W}_1, \hat{W}_2 \rangle_{\Omega} |_{t=T} \leq 0.$$

Lemma 3.2

The final state at $t = T$ corresponding to a maximal optimal control with zero initial condition results in a first eigenmode vibration if the beam vibrates freely on any interval $[T, T_1]$ (with $q \equiv 0$).

Outline of Proof

We shall assume that $q \in Q$ implies $\|q\|_Q \leq 1$. Let us suppose that the final state $\{\hat{W}(x,T), \hat{W}_t(x,T)\}$ cannot be attained as a state corresponding to the first eigenfunction of the system $\phi_1(x,t)$.

The homogeneous solution $W_H(x,t)$ such that $W_H(x,T) = \hat{W}(x,T)$ and $W_{H_t}(x,T) = \hat{W}_t(x,T)$ can be expanded in terms of eigenfunctions of the operator given by Equation 0.4 on the ray

$$(T, \infty) \cdot W_H(x,t) = \sum_{i=1}^{\infty} c_i \phi_i(d,t),$$

where $\{\phi_i(x,t)\}$ form an orthonormal system.

We only need to show that some extremal admissible load (i.e., $\|q\| = 1$) brings the system to rest at $t = 2T$ starting at energy level $\epsilon = \hat{\epsilon}$ at $t = T$, but that system with identical initial energy is controllable on $[T, 2T]$ if the initial state corresponded to the second (or higher) eigenfunction.

This is a technical computation comparing the work done by opposing maximal velocity point with a Dirac delta force over the interval $[T, 2T]$ as the beam vibrates in a second fundamental mode. The key to this argument is the fact that the mean velocity over one cycle of vibration is lower at the point of maximum velocity than the one measured in the fundamental mode of vibration. The proof of this technical lemma follows some arguments of D. L. Russell and will be published elsewhere.

Theorem 3.1

Let us assume a design \mathcal{S} which does not correspond to the coalescing point of first two fundamental frequencies. Then the (maximal) optimal control $q(x,t)$, $x \in \Omega$, $t \in [0, T]$, maximizing the total energy of a beam at $t = T$, with the state function $W(x,t)$ satisfying zero initial conditions, results in a unique finite condition $\{W(x,T), W_t(x,T)\}$ at $t = T$ within a plus or minus sign.

Proof

This theorem can be regarded as a corollary to Lemmas 3.1 and 3.2. Clearly, if $\hat{q}(x,t)$ is optimal, then so is $-\hat{q}(x,t)$. Consequently, it is easy to show that any optimal displacements \hat{W}_1, \hat{W}_2 corresponding to linearly independent controls \hat{q}_1 and \hat{q}_2 satisfy orthogonality condition

$$\langle W_1, W_2 \rangle_{\Omega} |_{t=T} = 0.$$

Choosing $-\hat{q}_2$ as an admissible control, the displacement $-\hat{w}_2$ corresponding to $-\hat{q}_2$ satisfies the inequality

$$-\langle w_1, w_2 \rangle_{\Omega} \Big|_{t=T} = 0.$$

Hence,

$$(\hat{w}_2, \hat{w}_2)_{\Omega} \Big|_{t=T} = 0.$$

Lemma 3.2 indicates that either \hat{w}_1 or \hat{w}_2 is the state corresponding to a fundamental frequency Ω_1 . Hence, without any loss of generality suppose that $w_1(x, T) = \phi_1(x, t) \Big|_{t=T}$, $\phi_1(x, t)$ corresponding to fundamental frequency Ω_1 . Then $w_2(x, t)$ cannot be optimal unless it corresponds to the same eigenvalue, i.e., the same frequency Ω_1 . Since this case is precluded, the proof is complete.

4. SIMULTANEOUS OPTIMIZATION AND CONTROL

The Direct Approach

As before we seek a minimum over the set of optimal designs ξ of the maximal total energy $\hat{\varepsilon}(T)$ attained by an admissible control $\hat{q} \in Q$. We assume $\|\hat{q}\|_Q \leq 1$. The theorem on uniqueness of the finite state is crucial in establishing a direct computational technique and in estimating errors. For a given design $\xi \in \mathcal{P}$ let $C(t, \xi(x))$ denote the

$$\max_{\|\hat{q}\|_Q \leq 1} \left\{ \int_{\Omega} [q(x, t) w_{H_t}(x, t)] dx \right\},$$

where $w_H(x, t)$ obeys the unique finite conditions at $t = T$. We make use of weak compactness of the set of admissible finite states for each design $\xi \in \mathcal{P}$ to assert the existence of $C(t, \xi(x))$ for almost all $t \in [0, T]$. If constraints are of the form

$$(4.1) \quad \int_{\Omega} \phi_i(\xi(x) w(\xi(x, t))) dx \leq 0 \quad i = 1, 2, \dots, r,$$

then at each S_0 and $t \in [0, T]$, which is a regular point of

$$\int_{\Omega} \left[\hat{q}(x, t) W_{H_t}(x, t) \right] dx,$$

use of Lagrangian multipliers can be justified and we could consider minimization over \mathcal{P} of the functional

$$(4.2) \quad J(\underline{S}) = \hat{\varepsilon}(\underline{S}(x), \hat{q}(x, t), T) + \sum_{i=1}^r \mu_i \phi(\underline{S}(x), t) + \mu_0(t) C(t; \underline{S}(x))$$

with $\mu_i \leq 0$ $i = 1, 2, \dots, r$, and $\mu_0 \geq 0$, at each regular point $t \in [0, T]$.

Note

A number of known "tricks of the trade" can be employed to change local constraints to a global form Equation 4.1. (See References 3 or 4.) If one assumes the existence of a simple fundamental frequency $\omega_1(\underline{S})$, then using recent results of Haug and Rousselet (Reference 5) one can prove Fréchet differentiability of the differential operator L with respect to the design vector. (Actually, one can prove more than that, but detailed results are not needed here.) Therefore, it is legal to proceed with formal differentiation with respect to the design vector function $\underline{S} = \{S_1(x) \dots S_n(x)\}$. Regarding $\delta \underline{S} = \{\delta S_1, \dots, \delta S_n\}$ as an arbitrary increment, such that $S_0 + \delta \underline{S}$ is admissible, we could copy the approach given by Kómkov and Coleman in Reference 6.

The formal differentiation procedure produces incorrect designs if the two lowest eigenvalues coalesce, thus leading to erroneous conclusions. This is a crucial point in the computational techniques based on heuristic arguments. Optimization results in numerical minimization of weight at constant eigenfrequency led in the past to many difficulties including appearance of singularities, discontinuities in design, and questionable local optima.

Bearing this in mind, we now proceed to optimize the design in the simplest possible case, when the structural system (in our case a single beam) is statically determinate. The bending moment $M(x, t)$ does not depend on the design \underline{S} ; it depends only on the load $\hat{q}(x, t)$, which maximizes $\varepsilon(T)$.

Identifying the potential energy with strain energy, we use the Hooke's law formula to evaluate $\varepsilon(t)$.

$$(4.3) \quad \varepsilon(t) = \frac{1}{2E} \int_0^{\ell} \left[\frac{M^2(x,t)}{I(\underline{S}(x);x)} \right] dx + \frac{1}{2} \int_0^{\ell} \rho \left[A(x) W_t \right]^2 dx.$$

Since M is independent of $\underline{S}(x)$ we can evaluate the sensitivity vector $dJ/d\underline{S} \in B^*$ (the dual of the normed space B of which \mathcal{P} is a bounded, closed convex subset).

We compute formally

$$\begin{aligned} \left\langle \frac{dJ}{d\underline{S}}, \delta\underline{S} \right\rangle &= \frac{1}{2E} \int_0^{\ell} \left[\left(\hat{M}^2(\hat{q}(x,T), x, T) \right) I^{-2} \left(\underline{S}(x); x \right) \frac{dI(\underline{S}(x))}{d\underline{S}} \right] \delta\underline{S} \\ &+ \frac{\rho}{2} \left[\frac{dA(\underline{S}(x); x)}{d\underline{S}} W_t(\underline{S}(x); x, T) + A(\underline{S}(x); x) \frac{dW_t}{d\underline{S}}(\underline{S}(x); x, T) \right] \delta\underline{S} dx \\ &+ \mu_0 \left[\frac{d}{d\underline{S}} (q(x,t) \hat{W}_{H_t}(x,t)) - \left\langle \frac{dC(t, \underline{S}(x))}{d\underline{S}}, \delta\underline{S} \right\rangle \right] \\ &+ \sum_{i=1}^r \mu_i \left\langle \frac{\partial \phi_i(\underline{S}(x), x)}{\partial \underline{S}}, \delta\underline{S} \right\rangle, \end{aligned}$$

where

$$\frac{d}{d\underline{S}} = \begin{bmatrix} \frac{d}{dS_1} \\ \vdots \\ \frac{d}{dS_n} \end{bmatrix}$$

Since the last term contains only design constraints which are time-independent and the first term is specifically evaluated at $t = T$, we conclude that the term

$$H_0 \left[\frac{d}{dS} \left((q \hat{W}_H) - c(t; S(x)) \right) \cdot \delta S \right]$$

is also time independent and can be evaluated at $t = T$. Hence, for statically determinate cases we can design a fairly simple computational algorithm similar to the one offered in Reference 6 allowing us to compute iteratively the optimal control and the improvements in design. A simple example of such computation was carried out in Reference 6 for the case of energy minimizing control.

Our results of Sections 2 and 3 indicate that this technique is appropriate to optimal excitation, that is, to energy maximizing controls. The lack of convexity apparently does not destroy the effectiveness of the basic theory based on Pontrjagin's principle. Basically, these results duplicate the conclusions made in Reference 6, but in a theoretically more difficult case. However, a check must be maintained on absence of multiple eigenvalues when a change in design causes a corresponding change in $\hat{W}_{H_t}(x, t)$.

5. THE ADJOINT VARIABLE TECHNIQUES

We consider a weak form of the state Equation 0.4, i.e.,

$$(5.1) \quad \langle \Lambda, (L(S)W(\underline{S}(x), x, t) - q(x, t)) \rangle_{\Omega} = 0,$$

subject to boundary conditions and spatial constrains

$$\phi_i(x, \underline{S}(x), W(x, t)) = \tilde{\phi}_i(x) = 0, \quad i = 1, 2, \dots, r.$$

It is known that solutions exist to Equation 0.4 in the Sobolëv space H whose structure is determined by energy inequalities of Equations 0.2 and 0.3, if one prescribes Cauchy data, such as $W(x, 0) = \phi(x) \in C^1(\Omega)$, $W_t(x, 0) = \psi(x) \in C^1(\Omega)$, and suitable boundary conditions, such as, for example, free support at $x = \pm \ell$. Hence, Equation 5.1 is satisfied for any choice of sufficiently smooth $\Lambda(x, t)$. Let J denote the functional given by Equation 4.2.

Λ satisfies the equation

$$(5.2) \quad L^* \Lambda = \sum_{i=1}^r \mu_i \frac{\partial \phi_i}{\partial W} + \frac{\partial J}{\partial W} = \frac{\partial a(\mu_i, \phi_i, J, \underline{S})}{\partial W},$$

in $\Omega \times [0, T]$ and satisfies terminal condition $\Lambda(x, T) = 0$.

The invariance of state equation when the design is perturbed is expressed by the condition

$$(5.3) \quad \frac{d}{d\underline{S}} \{ \langle \Lambda, L W \rangle_{\Omega} - \langle \Lambda, \hat{q} \rangle_{\Omega} \} = 0.$$

Since Λ does not depend on \underline{S} , Equation 5.3 can be rewritten as a system of r -equations

$$(5.4) \quad \langle \Lambda, L_{\underline{S}} W \rangle + \langle L^* \Lambda, W_{\underline{S}} \rangle - \langle \Lambda, \hat{q}_{\underline{S}} \rangle = 0,$$

where

$$L_{\underline{S}} \cdot = \frac{\partial^2}{\partial x^2} \left(\left(E \frac{\partial I(\underline{S})}{\partial \underline{S}} \right) \frac{\partial^2}{\partial x^2} \cdot \right) + \rho \frac{\partial A(\underline{S})}{\partial \underline{S}} \left(\frac{\partial^2}{\partial t^2} \cdot \right).$$

Recalling Equation 5.2, we note that

$$\frac{da(\mu_i, \phi_i, J, \underline{S})}{d\underline{S}} = \frac{\partial a}{\partial W} W_{\underline{S}} + \frac{\partial a}{\partial \underline{S}}.$$

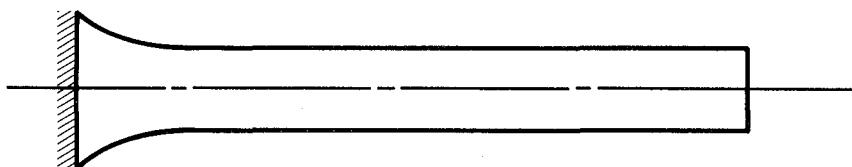
Hence,

$$\langle L^* \Lambda, W_{\underline{S}} \rangle = \langle \frac{\partial a}{\partial W}, W_{\underline{S}} \rangle = \frac{da}{d\underline{S}} - \frac{\partial a}{\partial \underline{S}}.$$

The very important term da/dS is essential in deciding sensitivity of the cost functional, in this case of the total energy at final time. We observe da/dS can be computed if one knows the state function $W(x,t)$, the solution Λ of the adjoint Equation 5.2 and the multipliers μ .

The most troublesome term W_{ξ} has been removed. One could immediately apply gradient projection technique perfected for this problem by Haug, Arrora, and Feng (Reference 7), if we apply a fixed control $q(x,t)$. For example, choosing a specific design, computing the natural frequency, fixing a maximum weight of the beam, the maximum permissible displacement, and the minimum sizes of the beam, we adopt a load which is a Dirac delta function applied to the free end of a cantilevered beam, with frequency input $\cos(80\pi t)$, for $t > 0$. The constants were taken to be $E = 30 \cdot 10^6$ psi, $\alpha A^2 = 1$, $\alpha = .3$, $l = 40''$.

This problem was analyzed at the University of Iowa on an IBM 360/65 computer. The beam was divided into ten finite element sections.



The optimal shape of the beam is illustrated above. Changes due to the term $C(\xi,t)$, which is absent in the Iowa analysis, do not appear to affect seriously the optimal shape. We recall that the term

$$\hat{C}(s,t) - \hat{W}_{H_t}(x,t) \cdot \hat{q}(x,t)$$

is independent of time and only depends on frequency and, therefore, on ξ . Small changes in design and small changes in optimal control, particularly if the first two eigenvalues of the operator L are not close to each other, do not affect seriously the sensitivity, or the iterative techniques incorporating changes in control.

Numerical studies indicate that assignment of constraints on minimum sizes of admissible designs prevents this difficulty. However, any numerical studies must incorporate the study of changes in spectrum of the operator L .

6. A BRIEF DISCUSSION OF APPLICATIONS

A question which engineers find hard to answer concerns the design of a system. Is the design "good"? Generally, a check is made to determine whether the design is safe and reasonably economical. Traditionally, little effort was made to improve a "satisfactory" design. However, in the last ten years a concentrated effort was made to develop a theory and algorithms for iterative improvements of even very complex mechanical and structural systems, particularly of systems modelled by equations with distributed parameters. Some of the most difficult theoretical problems arise almost casually in any consideration of what is a "good" design. Questions of identification (i.e., how good is the mathematical model), of reliability of data, of our knowledge of physics of the basic processes, and specifically of the loads applied to the system can never be answered completely or satisfactorily. In most structural systems, at least in some part, the loads are unknown or random. When designing structures to withstand random wind gusts, earthquake loads, or unpredictable dynamic loading from other causes, one must design the structure for the worst set of conditions encountered in past years or expected in the foreseeable future.

Clearly one cannot design for some average loads or average winds. A reasonable assumption is to study the "worst" data available. The techniques outlined in this paper apply to basic concepts of engineering design if it is assumed that Mother Nature conspires to present the worst possible set of controls over a reasonable time period $[0, T]$ corresponding to a duration of extreme wind gusts, of an earthquake, or of some other extreme dynamic loads. Even then our assumptions are open to many criticisms; but so are other assumptions when one tries to model and predict physical phenomena.

REFERENCES

1. Komkov, V., "Optimal Control theory for the damping of vibrations of simple elastic systems," Lecture Notes in Mathematics, No. 253, Springer Verlag, Berlin, 1972.
2. Komkov, V., "Classification of boundary conditions in optimal control theory of beams and plates," in Proceedings International Conference on Control Theory, IFAC, Banff, Canada, 1971, No. 5.5, pp. 1-11.
3. Haug, E. J., and J. S. Arrora, Applied Optimal Design, John Wiley - Interscience, New York, 1979.
4. Haug, E. J., and T. T. Feng, "Optimization of distributed parameter structures under dynamic loads," in Control and Dynamic Systems, C. T. Leondes, editor, Vol. 12, 1978, pp. 299-307.
5. Haug, E. J., and B. Rousselet, "Design Sensitivity analysis in structural mechanics I," Structural Mech. Vol. 8, No. 1, 1980, pp. 17-41.

6. Komkov, V., and N. Coleman, "Optimality of design and sensitivity analysis of beam theory," *Int. J. Control*, Vol. 18, No. 4, 1973, pp. 731-740.
7. Haug, E. J., J. S. Arrora, and T. T. Feng, "Optimal Structural design and optimization of structures under dynamic loads," *Int. J. for Num. Methods in Engineering*, Vol. 11, No. 1, 1977, pp. 39-52.

FIXED-ORDER DYNAMIC COMPENSATION THROUGH OPTIMAL PROJECTION*

David C. Hyland and Appasaheb N. Madiwale
Massachusetts Institute of Technology Lincoln Laboratory
Lexington, MA 02173

ABSTRACT

This paper reviews a formulation for the design of fixed-order dynamic compensation for flexible mechanical systems which is based upon explicit optimality conditions derived under the minimum data/maximum entropy stochastic modelling approach. The optimality conditions give rise to the novel concept of "optimal projection" which provides significant insight with regard to the compensator structure and permits earlier, more restricted and/or ad hoc design schemes to be seen as special cases of the present formulation.

1. INTRODUCTION

A satisfactory theory of structural control design for large, flexible space systems must secure desirable system properties in the face of inevitable errors arising in the construction of large order structural models and should successfully address the optimization of implementable dynamic compensation. Ref. [1] reviewed recent developments leading to the minimum data/maximum entropy approach to modelling and mean-square optimization. Accepting system parameter uncertainties at their *a priori* levels, this formulation incorporates such uncertainties directly within the design process by the use of an explicitly stochastic design model of the plant. By virtue of the underlying maximum entropy principle, the resulting stochastic design approach acknowledges the minimum possible prior information on parameter statistics and is capable of directly securing robust stability and mean-square optimality.

The design ramifications of this modelling approach in the case of full-state feedback regulation are summarized in the companion paper¹. This paper addresses further optimization issues. In particular, we review the development, under the minimum data/maximum entropy model, of optimality conditions for fixed-order dynamic compensation. It will be seen that, quite apart from the inclusion of parameter uncertainties, the present formulation of mean-square optimal, fixed-order compensation is novel. In particular, explicit optimality conditions are made available, and a rigorous and tractable design scheme for implementable compensation is obtained. The compensator form which naturally emerges from this formulation is fully defined by the gains and by a projection (an idempotent matrix) whose row and column spaces are the observation and control subspaces of the compensator. The optimality conditions given herein are of such a form that they determine this "optimal projection" together with the optimal gains. Since

* This work is sponsored by the Department of the Air Force. The U.S. Government assumes no responsibility for the information presented.

the compensator control and observation subspaces are not restricted at the outset to consist only of selected modal coordinates, the present formulation achieves greater design flexibility than the more conventional approaches.

After setting forth the basic maximum entropy design model in the following section, we present the main optimality and stability results in Section 3. Section 4 describes the relations between the formulation considered here and earlier treatments of more idealized controller forms. The remaining sections offer various geometric interpretations and elucidate the approximate character of the "modern modal control" approach (modal truncation followed by LQG design) in the light of the present, more general developments.

2. MAXIMUM ENTROPY MODELLING AND MEAN-SQUARE OPTIMIZATION

Consider control design for a structural system modelled by n of its elastic modes. Extensions needed to include rigid body modes are straightforward and will not be explicitly considered here. The system equation assumes the form:

$$\begin{aligned} \dot{\xi} &= \mu\xi + \beta u + w_1 & \text{a.} \\ \eta &= \gamma\xi + w_2 & \text{b.} \\ \xi \in \mathcal{C}^{2n}, u \in \mathbb{R}^\ell, \eta \in \mathcal{C}^p & & \text{c.} \end{aligned} \quad (1)$$

where ξ is the plant state, μ is the plant dynamics map and β and γ are the control input and sensor output maps, respectively. Also, w_1 is a white disturbance noise with intensity matrix $v_1 \geq 0$ and w_2 is observation noise with intensity $v_2 > 0$.

Due to various sources of error arising in the process of structural modelling, there may exist *a priori* uncertainties in μ , β and γ . It is supposed here that (1) is written in the eigenbasis of the structural system with the nominal or expected values of the parameters. In this case as Refs. [2,3] show, a wide class of parameter uncertainties (embracing errors in the structural stiffness matrix and in actuator and sensor placement) may be represented by skew-hermitian perturbations in μ alone. Thus, arranging the state vector appropriately, μ assumes the form:

$$\mu = \bar{\mu} + v(t), \quad v = -v^H \quad (2)$$

where v is a zero-mean random matrix and $\bar{\mu}$ is the expected value:

$$\bar{\mu} = \text{diag}\{\bar{\omega}_1(i-\eta_1), \bar{\omega}_1(-i-\eta_1), \dots, \bar{\omega}_n(i-\eta_n), \bar{\omega}_n(-i-\eta_n)\} \quad (3)$$

with $\bar{\omega}_k$ and η_k the nominal modal frequencies and damping ratios, respectively.

While explicitly recognizing the stochastic character of the plant dynamics map, it is desired to secure a controller which is optimal in an averaged sense by selecting the input, $u(t)$, to minimize the mean-square (steady-state) performance:

$$J_s = \lim_{t_1 - t_0 \uparrow \infty} \frac{1}{t_1 - t_0} \int_{t_0}^{t_1} dt E[\xi^H r_1 \xi + u^T r_2 u] \quad \left. \vphantom{J_s} \right\} \quad (4)$$

$$r_1 \geq 0, r_2 > 0$$

where the ensemble average, $E[.]$, embraces the v -ensemble.

In addressing this stochastic design problem, it must be recognized that a complete probabilistic description of $v(t)$ is never accessible to the design analyst from the necessarily incomplete empirical statistical data. To resolve this difficulty, Refs. [4,5] introduced the use of a maximum entropy principle for the construction of a full probability model which is consistent with available data while being maximally unconstrained otherwise. Moreover, the work reviewed in Ref. [1] identified a minimum set of parameter statistical data which must be acknowledged as empirically available in order that a well-defined probability model may be induced via the maximum entropy principle. The minimum data/maximum entropy model is thus literally the maximum entropy model induced by this minimum data set.

Since the maximum entropy modelling approach entails a measure of design conservatism and implicitly imposes robustness constraints without recourse to ad hoc procedures, we adopt its use here for the modelling of $v(t)$ in (2). Although all of the following results can be obtained or trivially extended to the general formulation outlined in Ref. [1], we limit consideration, for simplicity in the exposition, to uncertainties in the open loop frequencies of system (1):

$$v(t) = \text{diag} [i \text{Im}(\bar{v}_{kk}) \delta_k(t)] \quad (5)$$

where $\text{Im}(\cdot)$ denotes the imaginary part.

Within the maximum entropy model, and by virtue of (5), system (1) has the Itô differential representation:

$$\left. \begin{aligned} d\xi(t) &= \bar{\mu}_m \xi(t) dt + \beta u dt + dv(t)\xi(t) + dW_1(t) \\ d\eta(t) &= \gamma d\xi(t) + dW_2(t) \end{aligned} \right\} \quad (6)$$

where:

$$\bar{\mu}_m \triangleq \bar{\mu} - \frac{1}{2}I, \quad I \triangleq \text{diag} \left[\frac{1}{T_k} \right] \quad (7)$$

where T_k is the so-called "relaxation time" associated with the $\delta_k(t)$ in (5). Assigned numerical values for the T_k constitute the minimum data set in this case and, referring to the expressions given in Ref. [1], it is seen that the T_k are real, non-negative and inversely proportional to the overall magnitudes of the frequency deviations.

Within the above conditions, the stochastic design approach consists in accepting (6) as the plant model and then determining $u(t)$ to minimize J_s of (4). This plan has been elaborated for a variety of specific controller forms. In

particular, for full-state feedback regulation as well as full-order dynamic compensation, Refs. [6,7] succeeded in showing various desirable properties of the stochastic design approach - notably, guaranteed closed-loop stochastic stability under the stochastic design model and the automatic emergence of an inherently robust control law for high levels of modelled uncertainty. These and additional results described in Ref. [1] strongly motivate extension of the approach to consideration of fixed-order compensation.

3. FIXED-ORDER COMPENSATION: BASIC FORMULATION AND OPTIMALITY CONDITIONS

Quite apart from the issues connected with parameter uncertainty, there is a need for re-examination of previous methods for fixed-order compensator design. Perhaps the earliest approach to the design of fixed-order compensation for flexible mechanical systems involves the retention, in the design model, of relatively few modal coordinates and the use of familiar LQG techniques for the reduced-order model. As is presently well known, this scheme spawns a host of spillover instability problems. Furthermore, various techniques advanced over the past few years which retain the use of modal-coordinate space decompositions (i.e., reduced-order modal coordinate models) for the purpose of spillover suppression^{8,9} or model reduction^{10,11} are themselves subject to unwanted spillover effects and cannot guarantee stability or robustness for the full order system.

From the above considerations, increasing attention has been directed to the general approach (originated by Newton, Gould and Kaiser¹²) which accepts a high order model of the system while limiting the compensator order to some fixed number. Using the technique recommended by Kwakernaak and Sivan for gradient computations together with a parameter optimization algorithm, Martin and Bryson¹³ have recently applied this approach to flexible spacecraft control. The formulation of Martin and Bryson assumes a positive definite weight (in the usual quadratic performance index) on the control input and permits feedthrough only for the non-noisy portion of the sensor output. In marked contrast, Johnson¹⁴ allows unrestricted sensor output feedthrough and places no weight on the control input. Actually, these two formulations are extreme cases of a more general scheme which allows limited feedthrough combined with limited control input weighting in a manner which avoids singularity in the performance index. This general situation is certainly of interest, but, to fix ideas, we consider the problem formulation of Martin and Bryson under non-singular observation noise.

Thus, consider the closed-loop system equations comprising (6) for the plant together with:

$$\begin{array}{rcl}
 u & = & -\kappa q & \text{a.} \\
 \dot{q} & = & \alpha q + f_n & \text{b.} \\
 q \in \mathcal{C}^N q ; N_q \leq 2n & & & \text{c.}
 \end{array} \quad \left. \vphantom{\begin{array}{rcl} u \\ \dot{q} \\ q \end{array}} \right\} (8)$$

where κ and f are the (time-invariant) compensator gains, q is the compensator state (of dimension $N_q \leq 2n$) and α the corresponding dynamics map. With these restrictions, we should like to determine κ , f and α to minimize J_s .

Although the parameter optimization approach to this problem is reasonably well developed (at least for the case of a deterministically parametered plant) and its computational burden does not seem prohibitive, it yields little theoretical insight and no guarantee of global optimality. Thus there is a need for explicit optimality conditions of a form analogous to the results of Levine, Athans and Johnson¹⁵ for the optimal output feedback problem.

Such conditions were derived, for the first time, in Ref. [16]. Of course, the stationary conditions initially obtained comprised a system of non-linear matrix equations of formidable complexity. However, the condition that the gradient of the performance index with respect to elements of the compensator dynamics matrix vanish results in an identity. In fact, the stationary conditions furnish no determination of the compensator dynamics matrix and there is thus considerable latitude of choice. It was shown that by judicious choice of the compensator dynamics, the originally very complex stationary conditions may be reduced to relatively simple forms. Defining:

$$\{M\} \triangleq \text{diag} [M_{11}, M_{22}, \dots, M_{2n,2n}] \quad (9.a)$$

for any $M \in \mathcal{C}^{2n \times 2n}$ and introducing the notation:

$$\sigma \triangleq \beta r_2^{-1} \beta^H, \quad \bar{\sigma} \triangleq \gamma^H v_2^{-1} \gamma \quad (9.b)$$

the final results of Ref. [16] which are the object of the present discussion may be summarized as follows:

Theorem 1 - Consider:

$$\left. \begin{aligned} 0 &= (\bar{\mu}_m - \sigma P \tau)^H P + P (\bar{\mu}_m - \sigma P \tau) + I \{P + \tau \hat{P} \tau\} + r_1 + \tau^H P \sigma P \tau & a. \\ 0 &= (\bar{\mu}_m - \tau Q \bar{\sigma}) Q + Q (\bar{\mu}_m - \tau Q \bar{\sigma})^H + I \{Q + \tau \hat{Q} \tau^H\} + v_1 + \tau Q \bar{\sigma} Q \tau^H & b. \end{aligned} \right\} (10)$$

$$\left. \begin{aligned} 0 &= \tau^H [(\bar{\mu}_m - Q \bar{\sigma})^H \tau^H \hat{P} \tau + \tau^H \hat{P} \tau (\bar{\mu}_m - Q \bar{\sigma}) + P \sigma P] & a. \\ 0 &= \tau [(\bar{\mu}_m - \sigma P) \tau \hat{Q} \tau^H + \tau \hat{Q} \tau^H (\bar{\mu}_m - \sigma P)^H + Q \bar{\sigma} Q] & b. \end{aligned} \right\} (11)$$

where:

$$\tau \triangleq g^H \Gamma; \quad g, \Gamma \in \mathcal{C}^{N \times 2n} \quad (12.a)$$

such that Γ and g satisfy:

$$\Gamma g^H = I_{N_q} \quad (12.b)$$

If Γ , g and positive semi-definite P , \hat{P} , Q and \hat{Q} exist satisfying (10)-(12), then with the choice:

$$\alpha = \Gamma (\bar{\mu}_m - f \gamma - \beta \kappa) g^H \quad (13)$$

for α in (8.b), the gains:

$$\kappa = \hat{\kappa} g^H, \quad f = \Gamma \hat{f} \quad (14)$$

where:

$$\hat{\kappa} = r_2^{-1} \beta^H P, \quad \hat{f} = Q \gamma^H v_2^{-1} \quad (15)$$

determine an extremum of the performance index (4) under the constraints imposed by (6) and (8). The extremum value, J_s^* of J_s is given by:

$$J_s^* = \text{tr}[P v_1 + \tau^H P \tau (v_1 + Q \bar{\sigma} Q)] \quad (16)$$

Proof: See Theorem 2 and Corollary 1 of Ref. [16].

As is evident from (13) the present approach does not fix the structure of the compensator dynamics in advance but, rather, determines it together with the gains. The consequent form of the closed-loop system under the maximum entropy model of the plant is seen to be:

$$\begin{aligned} \dot{\xi} &= \mu \xi - \beta \hat{\kappa} g^H q + w_1 \\ \dot{q} &= \Gamma (\bar{\mu}_m - \hat{f} \gamma - \beta \hat{\kappa}) g^H q + \Gamma \hat{f} (\gamma \xi + w_2) \end{aligned} \quad (17)$$

where μ is to be interpreted in accordance with (2), (5) and (6).

Equations (10)-(12) clearly form the core of the design formulation and these relations indicate that the projection τ (note: $\tau = \tau^2$ and $\text{rank} \tau = N_q$ are implied by (12)) plays a central role. With the exception of the results of Theorem 4 below, necessary and sufficient conditions for the existence of solutions to (10)-(12) remain the object of research. It is possible, however, to illustrate the consequences of existence, particularly with regard to stochastic stability and the minimum property.

To facilitate the statement of the following result, denote by $\langle \tau M \tau \rangle \in \mathcal{C}^{N_q \times N_q}$ the matrix of the map, M , restricted to the subspace upon which τ is the projection with restricted codomain. Then we have:

Theorem 2 - Given N_q , suppose that full rank g and Γ and positive semi-definite P , Q , $\tau^H P \tau$ and $\tau Q \tau^H$ exist satisfying (10)-(12) with $(\langle \tau^H P \sigma P \tau \rangle^{\frac{1}{2}}, \langle \tau (\bar{\mu}_m - Q \bar{\sigma}) \tau \rangle)$ detectable. Then:

- A. System (17) under the minimum data/maximum entropy model for μ is second mean and almost surely exponentially stable. Also, (17) with $\mu = \bar{\mu}$ (that is, the system with nominal values of parameters) is exponentially stable.
- B. The gains, (14), determine a minimum of the performance index (4) under the constraints imposed by (6) and (8).

Proof: See Theorem 2 of Ref. [17].

Thus, under mild restrictions the formulation of Theorem 1 not only secures stability for the nominal system but also guarantees a considerable degree of stochastic stability. The above results, particularly part B, now justify use of the term "optimality conditions" in connection with (10)-(12). Accordingly, we now devote the remainder of the paper to discussion of various properties of relations (10)-(12).

4. QUALITATIVE FEATURES - RELATIONS TO PREVIOUS RESULTS

The principal requirements of Theorem 1 are seen to consist of two modified Riccati equations, (10), and two modified Lyapunov equations, (11). The Riccati-like equations, (10), are each similar in structure to the stochastic Riccati equation arising in the case of full-state feedback regulation. To recapitulate, earlier work, Refs. [4,6], the time invariant gain, κ , where

$$u = -\kappa \xi$$

which extremalizes J_s is given by

$$\kappa = r_2^{-1} \beta^H P \quad (18)$$

where P is the positive semi-definite solution to the stochastic Riccati equation:

$$0 = (\bar{\mu}_m - \sigma P)^H P + P(\bar{\mu}_m - \sigma P) + I\{P\} + r_1 + P\sigma P \quad (19)$$

Now examine the qualitative features of this equation. The modifications which distinguish (19) from the standard Riccati equation are the term $-\frac{1}{2}I$ in $\bar{\mu}_m$ as defined in (7) and the term $I\{P\}$. Both of these obviously arise from the influence of frequency uncertainty and are responsible for important effects.

To better understand the properties of (19) described in Ref. [1], let us re-write (19) in the form:

$$0 = \bar{\mu}^H P + P\bar{\mu} + \sum_{k=1}^{2n} \frac{1}{T_k} [B_k, [P, B_k]] - P\sigma P + r_1 \quad (20)$$

where $[A, B]$ denotes the commutator $(AB - BA)$ and the matrices B_k :

$$(B_k)_{\ell m} = \begin{cases} 1 & ; \ell = m = k \\ 0 & ; \text{otherwise} \end{cases} \quad (21)$$

are the "direction matrices" for uncertainties of the form (5). The structure of the modification term in (20) suggests that for large uncertainty in the k^{th} open-loop frequency (T_k small), the commutator $[P, B_k]$ will be suppressed - and this is indeed the case. As noted in Refs. [4,5], if all uncertainty levels are made to increase without bound (all the T_k approach zero), then P approaches an asymptotic solution which commutes with all the B_k - i.e., it is diagonal (and is given in closed analytical form). Precisely because all the $[P, B_k]$ vanish, a simple Lyapunov argument shows that the resulting rate-feedback control is stable regardless of the values of modal frequencies. In the more general case in which lower order modes are well known while frequency uncertainty increases with modal order, analogous results are obtained and the third term in (20) leads to robustness levels comparable to modelled uncertainty levels and reduced computational burden for the high order, poorly-known modes. With regard to the explicit appearance of terms connected with uncertainty, Eqs. (10) have the same structure as (20) and similar effects are to be expected.

Now, previous developments proceeded in generalizing results obtained under the regulator problem by first removing the assumption of full-state feedback. Supposing state information to be available only through a finite number of sensors (with non-singular observation noise), Ref. [7] derived optimality conditions for full-order dynamic compensation under the maximum entropy model. Let us first note that both the conditions of Ref. [7] and standard LQG theory can be obtained as special cases of the conditions given in Theorem 1:

Lemma 1

A. Under the problem formulation of Section 3, suppose that $N_q = 2n$. Then (10)-(12) are satisfied by $\tau = I_{2n} = \Gamma = g$ and by P, Q, \hat{P} and \hat{Q} satisfying:

$$\left. \begin{aligned} 0 &= \bar{\mu}_m^{-H} P + P \bar{\mu}_m + I\{P + \hat{P}\} - P\sigma P + r_1 & \text{a.} \\ 0 &= \bar{\mu}_m Q + Q \bar{\mu}_m^{-H} + I\{Q + \hat{Q}\} - Q\sigma Q + v_1 & \text{b.} \end{aligned} \right\} (22)$$

$$\left. \begin{aligned} 0 &= (\bar{\mu}_m - Q\sigma)^H \hat{P} + \hat{P} (\bar{\mu}_m - Q\sigma) + P\sigma P & \text{a.} \\ 0 &= (\bar{\mu}_m - \sigma P) \hat{Q} + \hat{Q} (\bar{\mu}_m - \sigma P)^H + Q\sigma Q & \text{b.} \end{aligned} \right\} (23)$$

and the extremalizing gains are given by:

$$\kappa = \hat{\kappa} = r_2^{-1} \beta^H P, \quad f = \hat{f} = Q \gamma^H v_2^{-1} \quad (24)$$

B. If, in addition to $N_q = 2n$, there is no parameter uncertainty, i.e., $I = 0$, then the extremal gains are (24) but with P and Q satisfying

$$\left. \begin{aligned} 0 &= \bar{\mu}_m^{-H} P + P \bar{\mu}_m - P\sigma P + r_1 \\ 0 &= \bar{\mu}_m Q + Q \bar{\mu}_m^{-H} - Q\sigma Q + v_1 \end{aligned} \right\} (25)$$

(Thus, LQG theory is seen to be a very special case in the formulation of Theorem 1).

Proof: Immediate from Theorem 1.

Of course, (22) and (23) are precisely the conditions first obtained in Ref. [7]. Observe that in the absence of the terms $I\{\hat{P}\}$ and $I\{\hat{Q}\}$, (22) are of the form of the stochastic Riccati equation, (19). In general, however, (22.a) and (22.b) are coupled through $I\{\hat{P}\}$ and $I\{\hat{Q}\}$ so that the effects of modal frequency uncertainty preclude the separation principle. Also, the coupling terms effectively augment the diagonal elements of r_1 and v_1 , thereby demanding greater control authority and stabilization. Moreover, from (23), \hat{P} and \hat{Q} tend to increase with controller input, $\kappa^H R_2 \kappa$ and its dual $f^H v_2 f$. We may say that \hat{P} and \hat{Q} represent the effect of error "leaking through" the regulator to the observer and vice versa by virtue of parameter uncertainty.

Additional properties of the full-order compensation formulation together with illustrative numerical results are presented in Ref. [7]. In particular, the behavior of solutions to (22,23) for large uncertainties is analogous to the

regulator case and a closed-form asymptotic solution (which is inherently robust) can again be obtained.

Finally, Ref. [16] removed the restriction $N_q = 2n$ to obtain the results stated in Theorem 1. Clearly (10) and (11) are very similar in structure to (22) and (23) and exhibit all the features noted above. A fundamentally new element, however, is introduced by the appearance of the projection τ . Note particularly, that in the present formulation, the compensator dynamics matrix as well as the gains are determined by the optimality conditions (10)-(12). Furthermore, these conditions also determine the N_q -dimensional row spaces of Γ and g which serve to complete the definition of the compensator. Thus, we shall attempt to clarify the central role played by τ in the following section.

5. GEOMETRIC INTERPRETATIONS: THE OPTIMAL PROJECTION

The geometric structure of the compensator of Theorem 1 is best illustrated by the quasi-full-order compensator interpretation given in Ref. [16]. Specifically, if we introduce the quasi-full-state estimate, $\hat{\xi}$:

$$\hat{\xi} \stackrel{\Delta}{=} g^H q \in \mathcal{C}^{2n} \quad (26.a)$$

so that $\tau \hat{\xi} = \hat{\xi}$ and:

$$q = \Gamma \hat{\xi} \in \mathcal{C}^{N_q} \quad (26.b)$$

then, the closed-loop system, (17), may be written:

$$\left. \begin{aligned} \dot{\hat{\xi}} &= \mu \hat{\xi} - \beta \hat{\kappa} \tau \hat{\xi} + w_1 \\ \dot{\hat{\xi}} &= \tau (\bar{\mu} - \hat{f} \gamma - \beta \hat{\kappa}) \tau \hat{\xi} + \tau \hat{f} (\gamma \hat{\xi} + w_2) \end{aligned} \right\} (27)$$

Thus, although the implemented compensator has the state $q = \Gamma \hat{\xi} \in \mathcal{C}^{N_q}$, it may be viewed as a quasi-full-order compensator whose structure is defined by the projection τ . Clearly, sensor inputs, $\hat{f} \eta$, are annihilated unless they are contained in $\text{Im}(\tau^H)$ (the row space of Γ), while the quasi-full-order state estimate, $\tau \hat{\xi}$, employed in control input is contained in $\text{Im}(\tau)$ (the row space of g). In consequence, we may call $\text{Im}(\tau)$ and $\text{Im}(\tau^H)$ the control and observation (respectively) subspaces of the compensator. Complements of these spaces are, of course, $\text{Im}(\tau_{\perp}^H)$ and $\text{Im}(\tau_{\perp})$, where

$$\tau_{\perp} \stackrel{\Delta}{=} I_{2n} - \tau \quad (28)$$

To distinguish these subspaces, we shall term $\text{Im}(\tau_{\perp}^H)$ and $\text{Im}(\tau_{\perp})$ the "secondary" control and observation (respectively) subspaces.

As can be seen from the above discussion, the optimality conditions of Theorem 1 determine a projection which, in turn, induces all of the important subspaces of the problem. For this reason, we may call the approach of Theorem 1 that of "optimal projection".

Now consider in what manner the optimality conditions (10)-(12) specifically determine τ . First note that (10) are analogous to the corresponding relations,

(22), determining P and Q for full-order compensation and do not constrain τ directly. Next examine (11). For convenience, denote the quantities within brackets on the right of (11.a) and (11.b) by Λ_P and Λ_Q respectively. Then (11) require that $\text{Ker}[\tau^H \Lambda_P] = \text{Ker}[\tau \Lambda_Q] = \mathcal{C}^{2n}$. But since $\mathcal{C}^{2n} = \text{Im}(\tau) \oplus \text{Im}(\tau_{\perp}) = \text{Im}(\tau^H) \oplus \text{Im}(\tau_{\perp}^H)$, (11) gives rise to the four conditions:

$$0 = \tau^H \Lambda_P \tau, \quad 0 = \tau \Lambda_Q \tau^H \quad (29.a,b)$$

$$0 = \tau^H \Lambda_P \tau_{\perp}, \quad 0 = \tau \Lambda_Q \tau_{\perp}^H \quad (30.a,b)$$

Expanded out, (29) assume the form of Lyapunov equations (very similar to (23)) which serve to determine $(\tau^H \hat{P} \tau)$ and $(\tau \hat{Q} \tau^H)$ but not τ . On the other hand, with Λ_P and Λ_Q dictated primarily by (10) and (29), conditions (30) require that 1) the secondary control subspace, $\text{Im}(\tau_{\perp})$, be Λ_P -invariant and 2) the secondary observation subspace, $\text{Im}(\tau_{\perp}^H)$, be Λ_Q -invariant. Thus, (30) do constrain τ .

Actually, (30) are the only direct requirements on τ since (12) merely demand that there exist a basis in \mathcal{C}^{2n} (the "canonical basis") for which the matrix of τ assumes the projection canonical form:

$$\tau^* \triangleq \begin{bmatrix} I_{N_q} & 0 \\ 0 & 0 \end{bmatrix} \quad (31)$$

In other words (see Lemma 1 of Ref. [17]), there exists a non-singular $\varphi \in \mathcal{C}^{2n \times 2n}$ such that:

$$\tau = \varphi^{-1} \tau^* \varphi \quad (32)$$

Thus, solution of (10)-(12) is tantamount to determination of non-singular φ and positive semi-definite P, Q, \hat{P} and \hat{Q} with τ defined by (31) and (32). Further consideration reveals that the total number of unknown parameters to be determined exceeds the number of independent conditions implicit in (10)-(12) with (31) and (32) by N_q^2 . This merely reflects the fact that (10)-(12) can determine τ only to within an arbitrary transformation of the compensator state. In particular, we may re-state Lemma 2 of Ref. [17]:

Lemma 2 - Let $u \in \mathcal{C}^{N_q \times N_q}$ be non-singular. Under the transformation:

$$\Gamma = u \tilde{\Gamma}, \quad g = u^{H-1} \tilde{g}; \quad \tilde{\Gamma} \tilde{g}^H = I_{N_q} \quad (33)$$

relations (10)-(12) retain their form except for the substitutions:

$$g \rightarrow \tilde{g}, \quad \Gamma \rightarrow \tilde{\Gamma} \quad (34)$$

Moreover with (34) and:

$$\tilde{u} \triangleq u^{-1} \quad (35)$$

the closed-loop system equations for $\begin{pmatrix} \xi \\ \tilde{q} \end{pmatrix}$ retain the form of (17).

Thus, there is still some latitude with regard to the choice of τ and we may impose N_q^2 additional conditions upon g and Γ so as to simplify their form. One representation of τ which is particularly useful in applications is given as follows. Assuming that there exist τ , \hat{P} and \hat{Q} satisfying (10)-(12), they may be written in the forms:

$$\tau = \begin{bmatrix} I & -LG^H \\ & G^H \end{bmatrix} [I, L] \quad (36)$$

$$\begin{aligned} \hat{P} &= \begin{bmatrix} I \\ L^H \end{bmatrix} \hat{P} [I, L] & \text{a.} \\ \hat{Q} &= \begin{bmatrix} I & -LG^H \\ & G^H \end{bmatrix} \hat{Q} [I \ -GL^H, G] & \text{b.} \end{aligned} \quad (37)$$

where

$$\begin{aligned} G, L &\in \mathcal{C}^{N_q \times (2n - N_q)} \\ \hat{P}, \hat{Q} &\in \mathcal{C}^{N_q \times N_q} \geq 0 \end{aligned} \quad (38)$$

Moreover, the transformation φ of (32) is:

$$\varphi = \begin{bmatrix} I & L \\ -G^H & I - G^H L \end{bmatrix}; \quad \varphi^{-1} = \begin{bmatrix} I & -LG^H & -L \\ & G^H & I \end{bmatrix} \quad (39)$$

where I denotes either I_{N_q} or I_{2n-N_q} , according to context.

With (36), (12) are seen to be satisfied identically. Furthermore, the explicit equations obtained upon substitution of (36) and (37) into (10) and (11) are given in Lemma 3 of Ref. [17]. Here we note that the relations corresponding to (29) consist of two $N_q \times N_q$ Lyapunov equations determining \hat{P} and \hat{Q} . Equations (30) give rise to two asymmetric Riccati equations for L and G . As will be illustrated in the next section, when $\|L\|$ and $\|G\|$ are small, these equations may be approximated by two Lyapunov equations which, in essence, determine first order corrections to φ such that (32) is more nearly satisfied.

6. ALMOST IGNORABLE STATES - RELATIONSHIPS TO MODERN MODAL CONTROL

To further illustrate the relations of the present approach with earlier, more conventional formulations, we now consider a situation in which control and observation subspaces are well approximated (in some sense) by N_q -dimensional, μ -invariant subspaces. Specifically, let all system matrices be expressed in the eigenbasis of the nominal system dynamics, as in Section 2 and suppose that:

$$\begin{aligned}
r_1 &= \begin{bmatrix} R_1 & \epsilon R_{12} \\ \epsilon R_{12}^H & \epsilon^2 R_2 \end{bmatrix}, & v_1 &= \begin{bmatrix} V_1 & \epsilon V_{12} \\ \epsilon V_{12}^H & \epsilon^2 V_2 \end{bmatrix} & & \left. \begin{array}{l} \text{a,b} \\ \text{c,d} \end{array} \right\} \\
\sigma &= \begin{bmatrix} \sigma_1 & \epsilon \sigma_{12} \\ \epsilon \sigma_{12}^H & \epsilon^2 \sigma_2 \end{bmatrix}, & \bar{\sigma} &= \begin{bmatrix} \bar{\sigma}_1 & \epsilon \bar{\sigma}_{12} \\ \epsilon \bar{\sigma}_{12}^H & \epsilon^2 \bar{\sigma}_2 \end{bmatrix} & & (40) \\
R_1, V_1, \sigma_1, \bar{\sigma}_1 &\in \mathcal{C}^{N_q \times N_q} \quad (N_q \text{ even}) & & & & \left. \begin{array}{l} \\ \\ \text{e} \end{array} \right\}
\end{aligned}$$

where $\epsilon \geq 0$ and all sub-blocks R_1, R_{12}, \dots etc. are bounded and independent of ϵ . Clearly, for ϵ sufficiently small, (40) implies that the last $2n - N_q$ states are only slightly weighted in the performance index, weakly disturbed and nearly unobservable and uncontrollable - whence the term "almost ignorable" may be applied to these states for $0 < \epsilon \ll 1$.

First, we consider the case $\epsilon = 0$ and determine a solution to (10)-(12) which corresponds to the familiar "modern modal control" approach wherein the last $2n - N_q$ states are dropped and a full-order compensator is designed for the reduced-order model. For $\epsilon = 0$, the main result is:

Theorem 3 - Assume conditions (40) with $\epsilon = 0$. Partitioning all matrices in accordance with (40), suppose that μ_2 is asymptotically stable (in accordance with the assumptions of Section 2) and:

$$\left. \begin{aligned}
(\bar{\mu}_1, \sigma_1^{1/2}), & \quad (\bar{\mu}_1, V_1^{1/2}) \quad \text{controllable} \\
(R_1^{1/2}, \bar{\mu}_1), & \quad (\sigma_1^{1/2}, \bar{\mu}_1) \quad \text{reconstructible}
\end{aligned} \right\} (41)$$

Then the fixed-order compensator optimality conditions (10)-(12) are satisfied by

$$\begin{aligned}
\tau &= \begin{bmatrix} I_{N_q} & 0 \\ 0 & 0 \end{bmatrix} & & (42) \\
P &= \begin{bmatrix} P_1^O & 0 \\ 0 & 0 \end{bmatrix}, & Q &= \begin{bmatrix} Q_1^O & 0 \\ 0 & 0 \end{bmatrix} & & \left. \begin{array}{l} \text{a,b} \\ \text{c,d} \end{array} \right\} \\
\hat{P} &= \begin{bmatrix} \hat{P}^O & 0 \\ 0 & 0 \end{bmatrix}, & \hat{Q} &= \begin{bmatrix} \hat{Q}^O & 0 \\ 0 & 0 \end{bmatrix} & & (43)
\end{aligned}$$

where P_1^O, Q_1^O, \hat{P}^O and \hat{Q}^O are the unique positive definite solutions to:

$$\left. \begin{aligned}
0 &= \bar{\mu}_{m1}^H P_1^O + P_1^O \bar{\mu}_{m1} + I_1 \{P_1^O + \hat{P}^O\} + R_1 - P_1^O \sigma_1 P_1^O \\
0 &= \bar{\mu}_{m1} Q_1^O + Q_1^O \bar{\mu}_{m1}^H + I_1 \{Q_1^O + \hat{Q}^O\} + V_1 - Q_1^O \sigma_1 Q_1^O
\end{aligned} \right\} (44)$$

$$\left. \begin{aligned} 0 &= (\bar{\mu}_{m1} - Q_1^o \sigma_1^o)^H \hat{\hat{P}}^o + \hat{\hat{P}}^o (\bar{\mu}_{m1} - Q_1^o \sigma_1^o) + P_1^o \sigma_1^o P_1^o \\ 0 &= (\bar{\mu}_{m1} - \sigma_1^o P_1^o) \hat{\hat{Q}}^o + \hat{\hat{Q}}^o (\bar{\mu}_{m1} - \sigma_1^o P_1^o)^H + Q_1^o \sigma_1^o Q_1^o \end{aligned} \right\} (45)$$

Proof: See Theorem 3 of Ref. [17].

Conditions (44) and (45) are simply the full-order compensation optimality conditions (22)-(23) for the reduced order model comprising the first N_q states. Since N_q is even, τ also assumes the canonical form (31) in the usual modal coordinate basis. Thus the modern modal control approach (which proceeds by modal truncation) amounts to the assumption that (42) is a decent approximation for τ .

For $\epsilon > 0$, this simple state of affairs no longer prevails. However, it should be expected that solutions of (10)-(12) "in the vicinity" of (42) and (43) do exist provided ϵ is sufficiently small. Under modest restrictions, this is the case - as the following emphasizes:

Theorem 4 - Suppose that $\epsilon > 0$, but otherwise retain the conditions of Theorem 3. Expressing τ , \hat{P} and \hat{Q} according to (36) and (37), consider the formal series expansions:

$$L = \sum_{k=1}^{\infty} \epsilon^k L^k, \quad G = \sum_{k=1}^{\infty} \epsilon^k G^k \quad (46)$$

and

$$\hat{\hat{P}} = \sum_{k=0}^{\infty} \epsilon^k \hat{\hat{P}}^k \quad (47)$$

with similar expressions for $\hat{\hat{Q}}$, P and Q . Here, the leading terms for P , Q , $\hat{\hat{P}}$ and $\hat{\hat{Q}}$ are given by (43)-(45), and all remaining terms are obtained by regular perturbation expansion applied to (10) and (11).

Under these conditions, there exists an $\bar{\epsilon} > 0$ such that for all $\epsilon \leq \bar{\epsilon}$, the series (46)-(47) are absolutely convergent to solutions of (10)-(12).

Proof: See Lemmas 4 and 5 and Theorem 4 of Ref. [17].

This result confirms the expectation that the problem is well posed in some neighborhood of $\epsilon = 0$. Of course, the radius of convergence of (46)-(47) remains to be determined. However, this question will be deferred to a subsequent report since our main interest here is the qualitative behavior of solutions for ϵ sufficiently small but non-zero.

7. SMALL ϵ -SOLUTIONS - SPILLOVER ACCOMMODATION THROUGH OPTIMAL PROJECTION

Supposing that ϵ is sufficiently small in the case of almost ignorable states, the last theorem above guarantees existence of solutions to the optimality conditions of Theorem 1 and provides a perturbation expansion which has the modern modal control approximation of Theorem 3 as its point of departure. Although more general existence results and more satisfactory computational methods will be presented subsequently, let us pursue the developments of the last section in order to illustrate the manner in which the present formulation modifies the usual modern modal control approach.

To simplify the algebra somewhat in developing explicit expressions, consider only the case of a deterministic plant:

$$I = 0, \quad \bar{\mu}_m = \bar{\mu} \quad (48)$$

and suppose the primary and secondary modes to be independently weighted and disturbed:

$$V_{12} = R_{12} = 0 \quad (49)$$

With these restrictions, the results of Theorem 3 would apply were it not for the non-zero values of σ_{12} and $\bar{\sigma}_{12}$ in (40.c,d). These terms arise from the controllability and observability of the almost ignorable states.

To illustrate the effects of non-zero σ_{12} and $\bar{\sigma}_{12}$, let us develop the series solutions of Theorem 4 up to and including terms of order ϵ^2 . The results (see Corollary 1 of Ref. [17]) may be summarized as follows: $P \geq 0$, $Q \geq 0$ and τ satisfying (10)-(12) may be approximated by:

$$\begin{aligned} P &= \tilde{P} + O(\epsilon^3), \quad Q = \tilde{Q} + O(\epsilon^3) & \text{a,b} \\ \tau &= \begin{bmatrix} I & -LG^H \\ & G^H \end{bmatrix} [I, L] + O(\epsilon^3) & \text{c.} \end{aligned} \quad (50)$$

where \tilde{P} , \tilde{Q} , L and G are determined by:

$$0 = \bar{\mu}^{-H} \tilde{P} + \tilde{P} \bar{\mu} - \tilde{P} \bar{\sigma} \bar{\sigma}^H \tilde{P} + \tilde{R}, \quad 0 = \bar{\mu} \tilde{Q} + \tilde{Q} \bar{\mu}^H - \tilde{Q} \bar{\sigma} \bar{\sigma}^H \tilde{Q} + \tilde{V} \quad \text{a,b} \quad (51)$$

$$\begin{aligned} 0 &= L \bar{\mu}_{m2} + \hat{P}^{o-1} (\bar{\mu}_{m1} - Q_1^o \bar{\sigma}_1^o)^H \hat{P}^o L - \epsilon Q_1^o \bar{\sigma}_{12} & \text{a.} \\ 0 &= G \bar{\mu}_{m2} + \hat{Q}^{o-1} (\bar{\mu}_{m1} - \sigma_1 P_1^o) \hat{Q}^o G - \epsilon P_1^o \sigma_{12} & \text{b.} \end{aligned} \quad (52)$$

where:

$$\tilde{R} \triangleq r_1 + \begin{bmatrix} 0 & 0 \\ 0 & L^H P_1^o \sigma_1 P_1^o L \end{bmatrix}, \quad \tilde{V} \triangleq v_1 + \begin{bmatrix} 0 & 0 \\ 0 & G^H Q_1^o \bar{\sigma}_1 Q_1^o G \end{bmatrix} \quad \text{a,b} \quad (53)$$

and where σ^o and $\bar{\sigma}^o$ denote σ and $\bar{\sigma}$, respectively, with $\epsilon = 0$ in (40.c,d) while P_1^o , Q_1^o , \hat{P}^o and \hat{Q}^o are determined according to (44) and (45) with $I_1 = 0$.

(50)-(53) now give an explicit, approximate solution of (10)-(12) for sufficiently small ϵ which incurs errors of order ϵ^3 . For $\epsilon > 0$ and, in contrast to the modern modal control approximation of Theorem 3, (50.c) and (52) show that the optimal projection is not in the canonical form in the modal coordinate basis. Rather, the vectors spanning the compensator observation and control subspaces (the row vectors of $[I, L]$ and $[I - GL^H, G]$, respectively) have small ($O(\epsilon)$) components along the almost ignorable states, represented by L and G . As (52) shows, the magnitudes of these are dictated by the control and observation spillover terms, σ_{12} and $\bar{\sigma}_{12}$, respectively. Thus, some accommodation is made for spillover effects by "rotating" the compensator subspaces in the direction of the almost ignorable states. The manner in which this directly enhances stabilization for the last $2n - N_q$ states is described more fully elsewhere.

A second major qualitative feature can be seen from (51) and (53). It is evident that the present optimality conditions effectively augment the state weighting and disturbance noise intensity for the almost ignorable states. This augmentation occurs through the terms $L^H P_1^0 \sigma_1 P_1^0 L$ and $G^H Q_1^0 \bar{\sigma}_1 Q_1^0 G$ appearing in (53). In consequence, conditions (10)-(12) automatically impose additional control authority on the almost ignorable states in direct proportion to the magnitudes of observation and control spillover effects.

Thus, in summary, rather than demanding the suppression of spillover, the optimality conditions (10)-(12) automatically accommodate for spillover effects so as to achieve overall closed-loop stability.

8. CONCLUDING REMARKS

The approach, presented here, for design of mean-square optimal, fixed-order dynamic compensation is seen to possess the following salient aspects:

(1) The formulation is predicated upon a maximum entropy stochastic model of the plant which not only recognizes the design impact of structural parameter uncertainties but also incorporates a minimum of *a priori* statistical information. Such a maximally unpresumptive stochastic modelling approach provides an implicit mechanism for the attainment of robust stability.

(2) The approach eschews both ad hoc model reduction schemes and the purely computational parameter optimization technique and is based upon explicit optimality conditions presented in Theorem 1. Such conditions reveal that the "optimal projection" defining the compensator structure plays a crucial role and provides significant theoretical insight. Moreover, under mild restrictions, existence of solutions to the optimality conditions guarantees closed-loop stochastic stability under the maximum entropy design model.

Furthermore, we attempted in Sections 4 and 5 to provide insight into the significance of the fixed-order compensation optimality conditions and their relation to earlier, more restricted formulations. In particular, the last two sections above presented explicit results revealing the familiar modern modal control approach as a special approximation under the present formulation. Most importantly, it was seen that the optimality conditions of Theorem 1 can secure global stability without necessitating suppression of observation and control spillover.

Clearly, the above features tend to remedy many of the deficiencies of current design methods. Computational techniques and illustrative numerical results will be given in a subsequent publication. Finally, just as in the case of full-order compensation considered previously, we may anticipate that the optimality conditions (10)-(12) possess simple asymptotic solutions associated with the high-order, poorly-known modes. This feature tends to reduce the burden of design computation and permits the use of very high order design models.

REFERENCES

1. D.C. Hyland, "Minimum Information Modelling of Structural Systems with Uncertain Parameters", JPL Workshop on Applications of Distributed System Theory to the Control of Large Space Structures, Pasadena, CA, 14-16 July 1982.
2. D.C. Hyland, "Maximum Entropy Stochastic Approach to Control Design for Uncertain Structural Systems", No. 9475, American Control Conf., June 1982.
3. D.C. Hyland, "Robust Spacecraft Control Design in the Presence of Sensor/Actuator Placement Errors", No. 82-1405, AIAA Astrodynamics Conf., August 1982.
4. D.C. Hyland, "Active Control of Large Flexible Spacecraft: A New Design Approach Based on Minimum Information Modelling of Parameter Uncertainties", VPI&SU/AIAA Symposium on Dynamics and Control of Large Flexible Spacecraft, Blacksburg, VA, June 1981.
5. D.C. Hyland, "Optimal Regulation of Structural Systems with Uncertain Parameters", Technical Report 551, MIT, Lincoln Laboratory, 2 February 1981, DDC AD-A099111/7.
6. D.C. Hyland, "Optimal Regulator Design Using Minimum Information Modelling of Parameter Uncertainties: Ramifications of the New Design Approach", Proc. VPI&SU/AIAA Symposium, June 1981.
7. D.C. Hyland and A.N. Madiwale, "A Stochastic Design Approach for Full-Order Compensation of Structural Systems with Uncertain Parameters", AIAA Guidance and Control Conf., No. 81-1830, Albuquerque, NM, August 1981.
8. J.R. Sesak, "Control of Large Space Structures Via Singular Perturbation Optimal Control", AIAA Conf. on Large Space Platforms, Los Angeles, CA, No. 78-1690, 17-19 September 1978.
9. T. Coradetti, "Orthogonal Subspace Reduction of Optimal Regulator Order", AIAA Guidance & Control Conf., Boulder, CO, No. 79-1742, August 1979.
10. R.E. Skelton, "Observability Measures and Performance Sensitivity in the Model Reduction Problem", Int'l. Journal of Control, Vol. 29, No. 4, 1979, pp. 541-556.
11. R.E. Skelton and P.C. Hughes, "Flexible Spacecraft Model Reduction and Control Design by Modal Cost Analysis", ASME Journal of Dynamic Systems, Measurement and Control, Vol. 102, September 1980, pp. 151-158.
12. G.C. Newton, L.A. Gould and J.F. Kaiser, Analytical Design of Linear Feedback Controls (Wiley, New York, 1957).
13. G.D. Martin and A.E. Bryson, Jr., "Attitude Control of a Flexible Spacecraft", J. Guidance and Control, Vol. 3, No. 1, Jan-Feb 1980, pp. 37-41.
14. T.L. Johnson, "Minimum-Variance Fixed-Form Compensation of Linear Systems", Proc. 17th Conf. on Decision and Control, San Diego, CA, January 1979.

15. W.S. Levine, T.L. Johnson and M. Athans, "Optimal Limited State Variable Feedback Controllers for Linear Systems", IEEE Trans. Autom. Control, Vol. AC-16, December 1971, pp. 785-793.
16. D.C. Hyland, "Optimality Conditions for Fixed-Order Dynamic Compensation of Flexible Spacecraft with Uncertain Parameters", No. 82-0312, AIAA Aerospace Sciences Meeting, January 1982.
17. D.C. Hyland, "Mean-Square Optimal, Fixed-Order Compensation - Beyond Spillover Suppression", No. 82-1403, AIAA Astrodynamics Conf., August 1982.

This Page Intentionally Left Blank

STABLE FEEDBACK CONTROL OF DISTRIBUTED PARAMETER SYSTEMS: TIME AND FREQUENCY DOMAIN CONDITIONS

Mark J. Balas*

Electrical, Computer, and Systems Engineering Department
Rensselaer Polytechnic Institute
Troy, NY 12181

ACKNOWLEDGEMENTS

This research was supported in part by the National Science Foundation under Grant No. ECS-80-16173 and the National Aeronautics and Space Administration under Grant No. NAG-1-171. Any opinions, findings and conclusions or recommendations expressed in this publication are those of the author and do not necessarily reflect the views of NSF or NASA. Also, we wish to thank Dr. Richard Gran (Grumman Aerospace Corp.) for many helpful discussions on these ideas.

ABSTRACT

Large space structures, or any mechanically flexible structures, are inherently distributed parameter systems (DPS) whose dynamics are modeled by partial, rather than ordinary, differential equations. Such DPS are described by operator equations on an infinite-dimensional Hilbert (or Banach) space. However, any feedback controller for such a DPS must be a finite-dimensional (and discrete-time) system in order to be implemented with on-line digital computers and a finite (small) number of actuators and sensors. There are many ways to synthesize such controllers; we will emphasize the Galerkin or finite-element approach.

Although the overall performance of finite-dimensional controllers is important, the first consideration is their stability in closed-loop with the actual DPS. The analysis of DPS makes use of the theory of semigroups on the infinite-dimensional state space. We will present stability bounds in both the time and frequency domains for infinite-dimensional systems. Presently, the frequency-domain approach appears to yield more easily tested stability conditions than the time-domain approach; however, we will show some relationships between these two methods and emphasize the role played by the DPS semigroup and its properties. It seems to us, that such stability conditions are essential for the planning and successful operation of complex systems like large aerospace structures.

1.0 INTRODUCTION

Almost every engineering system will exhibit some distributed parameter behavior if one looks at its dynamics in great detail. Consequently, the dynamical behavior of such a distributed parameter system (DPS) would need to be modeled by partial, rather than ordinary, differential equations to be correctly represented. Of course, in many cases, such detail is not necessary for the successful

*Associate Professor

operation of the system, and a lumped parameter (ordinary differential equation) model is satisfactory. Nevertheless, a large number of current and newly proposed systems, such as industrial processes and mechanically flexible spacecraft and satellites, are so thoroughly distributed parameter in nature that it is impossible to ignore this in modeling and control.

There are many new problems (and some compounding of old ones) in feedback control of DPS. The main questions which concern us are (1) how to synthesize finite-dimensional controllers which can be implemented by a small number of actuators and sensors and on-line computers of limited word-length; (2) how to assess the stability and performance of these controllers in closed-loop with the actual DPS which is infinite-dimensional. Presently, a great deal of thought has gone into DPS control because of the proposed construction and operation on-orbit of large flexible spacecraft and satellites in the near future. Quite a large number of control schemes have been considered for these large space structures (e.g. see the survey [1]) and new ones (or major revisions of the old ones) are being developed almost daily. This kind of activity has been helpful, we believe, because it has called the control systems community's attention to systems whose high performance and reliability is essential for successful operation and has focused it on some of the important "gaps" between control theory and engineering practice. To be sure other applications, e.g. Tokomak fusion reactors and large-scale electric power distribution networks, are having a similar effect.

In past work, we have been strongly in favor of a more practical theory of DPS control which incorporates some of the natural system constraints and uses ideas in infinite-dimensions that appeal to the intuition and experience of the modern control engineer. We have taken some (although not necessarily the only) definitive steps in that direction [2]. In this paper, we intend to continue in that spirit and focus on the stability question of finite-dimensional controllers in infinite-dimensional DPS. Our analysis here will emphasize stability results in both the time and frequency domains and some of the relationships between these results. The unifying concepts of operator equations on Hilbert spaces and the C_0 -semigroup for DPS will be stressed; however, the resulting stability tests will only involve data which, it is reasonable to assume, would be available or could be estimated.

This infinite-dimensional approach can be used effectively in large-scale finite-dimensional systems, as well. One very important consideration in large-scale or DPS is to avoid a dependence on precise knowledge of (a) the total system dimension and (b) the full system parameters, especially those residual parameters not used in the synthesis of the controller. Using an infinite-dimensional approach obviates (a), and for (b) we shall only need to be able to estimate the norms of certain of the residual data.

In previous work, we have emphasized the internal or time-domain viewpoint of exponential stability of the closed-loop system, i.e. the effect of impulsive disturbances on the state decay exponentially to zero. However, another viewpoint is the external or frequency-domain view which describes the effect of persistent disturbances on the system outputs. Here our main results in the frequency domain give conditions under which the closed-loop system is bounded input-bounded output stable in the L^2 sense (L^2 -BIBO stable).

This means any persistent L^2 -disturbance, which is bounded, can only produce L^2 -outputs which are also bounded. While the former looks at the DPS from a state-space viewpoint, the latter looks at it from an input-output standpoint. Both approaches have their strengths and weaknesses, and they are interrelated, as we shall point out later.

In lumped parameter systems, the BIBO approach is very popular (e.g. see [3]-[7]) where it appears to lead to easily verified stability tests. For infinite-dimensional systems, see [8]-[9]. These ideas were applied to modal control of large space structures in [10]. There is also some use of positivity concepts for structures [11]; these yield special conditions under which the closed-loop system is "dissipative" and hence BIBO stable. Much is made of the "robustness" of the BIBO designs, i.e. their placidity in the presence of uncertain system parameters. However, it should be pointed out that the BIBO approach involves one of several very useful perturbation methods and has no intrinsic robustness properties; robustness under uncertainty can be assessed with all perturbation techniques with varying degrees of difficulty. The relative ease accomplished with BIBO methods is what recommends them in lumped parameter systems and suggests their utility for DPS, as well.

In Sec. 2.0, the general DPS mathematical framework of this paper is presented. Basic ideas of reduced-order modeling and control appear in Sec. 3.0 and the concepts of stability for DPS appear in Sec. 4.0. Our main results on time-domain (exponential) stability tests for the closed-loop appear in Sec. 5.0 and the new results on frequency-domain (BIBO) stability are in Sec. 6.0. Our conclusions form Sec. 7.0.

2.0 DPS DESCRIPTIONS

We will consider linear distributed parameter systems (DPS) with the following form:

$$\begin{cases} \frac{\partial v(t)}{\partial t} = Av(t) + Bf(t) + \Gamma f_D(t) \\ y(t) = Cv(t); v(0) = v_0 \end{cases} \quad (2.1)$$

The system state $v(t)$ will lie in a Hilbert space H with inner product denoted by (\cdot, \cdot) and corresponding norm denoted by $\|\cdot\|$. The operator A is an unbounded, closed, time-invariant, linear differential operator whose domain $D(A)$ is dense in H ; furthermore, A generates a C_0 -semigroup $U(t)$. This semigroup is the analogue of the matrix exponential e^{At} for finite-dimensional systems. The input operators B and C are both finite rank M and P respectively. The external disturbances on the system are represented by the persistent term $\Gamma f_D(t)$, where Γ has rank M_D , and the impulsive term v_0 . This is becoming a standard representation for many DPS applications involving interior control and measurement.

From the Hille-Yoshida Theorem (e.g. [12] or [13]), the operator A generates a C_0 -semigroup $U(t)$ satisfying:

$$\|U(t)\| \leq Ke^{-\sigma t} \quad (2.2)$$

where $K \geq 1$ and σ is real, when

$$\|(R(\lambda, A))^n\| \leq \frac{K}{(\lambda + \sigma)^n}; \quad n=1, 2, \dots \quad (2.3)$$

for all real $\lambda > -\sigma$ in the resolvent set of A . The operator $R(\lambda, A) = (\lambda I - A)^{-1}$ is the resolvent operator for A ; by definition, it is a bounded linear operator for each λ in the resolvent set of A . In the special case, where A is dissipative, i.e.

$$\begin{cases} (Av, v) + \sigma(v, v) \leq 0 \\ (A^*v, v) + \sigma(v, v) \leq 0 \end{cases} \quad (2.4)$$

for all v in $D(A)$ or $D(A^*)$ where A^* is the adjoint of A , the constant $K=1$ in (2.2); see [13] Theo. 3.2.

When $\sigma > 0$ in (2.2), A generates an exponentially stable semigroup $U(t)$ whose stability margin is σ . The pair of operators (A, B) is exponentially stabilizable when there is a (bounded) linear gain operator $G: H \rightarrow R^M$ such that the operator $A + BG$ generates an exponentially stable semigroup. There are other types of mathematical stability and stabilizability defined for DPS; some of these ideas will be discussed in Sec. 4.0.

When (A, B) and (A^*, C^*) are exponentially stabilizable, and there are no persistent disturbances (i.e., $f_D(t) \equiv 0$), it has been shown in [2] that the infinite-dimensional controller:

$$\begin{cases} f(t) = G \hat{v}(t) \\ \frac{\partial \hat{v}(t)}{\partial t} = L \hat{v}(t) + K y(t) \\ \hat{v}(0) = 0 \end{cases} \quad (2.5)$$

where $L \equiv A + BG - KC$ with domain $D(L) = D(A)$, exists, and, in closed-loop with (2.1), it produces an exponentially stable system. The gain operators G & K exist and stabilize the operators $A + BG$ and $A - KC$. This controller is mathematically interesting but not very useful from an engineering standpoint since (2.5) cannot be implemented with a finite-dimensional system. In the next section, the concepts of model reduction and reduced-order control are reviewed from [2].

Before closing this section, we want to point out that without any loss of generality we can and will assume in (2.1):

$$\Gamma = B \quad (2.6)$$

This is possible because $F(t) \equiv Bf(t) + \Gamma f_D(t)$ can be rewritten:

$$F(t) = \tilde{B}(\tilde{f}(t) + \tilde{f}_D(t)) \quad (2.7)$$

where $\tilde{B} \equiv [B\Gamma]$, $\tilde{f}(t) \equiv \begin{bmatrix} I_M \\ 0 \end{bmatrix} f(t)$, and $\tilde{f}_D(t) \equiv \begin{bmatrix} 0 \\ I_{M_D} \end{bmatrix} f_D(t)$. Therefore, we will

assume (2.6) and, henceforth, (2.1) will be given by:

$$\begin{cases} \frac{\partial v(t)}{\partial t} = A v(t) + B(f(t) + f_D(t)) \\ y(t) = C v(t); v(0) = v_0 \end{cases} \quad (2.8)$$

where now the rank M of B reflects the total number of actuators and disturbance inputs. This representation will be very convenient later.

3.0 MODEL REDUCTION AND FINITE-DIMENSIONAL DPS CONTROL

In order to produce finite-dimensional controllers for the DPS (2.8), we must make a lumped parameter approximation of it. This is done when numerical methods such as finite elements or finite differences are used to discretize the spacial variables. In general, such an approximation or reduced-order model (ROM) is a (not necessarily orthogonal) projection of (2.8) onto an appropriate finite-dimensional subspace H_N of H ; usually, we will assume $H_N \subset D(A)$. The ROM subspace H_N has dimension N and its projection is denoted by P_N ; the residual subspace H_R associated with H_N completes the decomposition $H = H_N \oplus H_R$, and its projection is denoted by P_R . The total DPS state v can be written:

$$v = v_N + v_R \quad (3.1)$$

where $v_N = P_N v$ and $v_R = P_R v$. The choice of the subspaces H_N and H_R is usually dictated by the physical application and/or the numerical procedures available for integrating the DPS. When feedback control is the ultimate purpose of the model reduction, certain choices of subspaces will yield advantages.

A modal subspace H_N consists of linear combinations of a finite number of modes or eigenfunctions of the operator A . Modal subspaces have very special properties in control applications, e.g., $A_{NR} = 0$ and $A_{RN} = 0$ in (3.2) later.

However, since most engineering applications are too complex for the exact modes to be known, these subspaces are more conceptually, rather than practically, useful. The Galerkin (or finite element) method is the most often used approach.

The projection of the DPS (2.8) onto the subspaces H_N and H_R decomposes the system into the following:

$$\left\{ \begin{array}{l} \frac{\partial v_N}{\partial t} = A_N v_N + A_{NR} v_R + B_N (f + f_D) \\ \frac{\partial v_R}{\partial t} = A_{RN} v_N + A_R v_R + B_R (f + f_D) \\ y = C_N v_N + C_R v_R \end{array} \right. \quad (3.2a)$$

$$\left\{ \begin{array}{l} \frac{\partial v_R}{\partial t} = A_{RN} v_N + A_R v_R + B_R (f + f_D) \end{array} \right. \quad (3.2b)$$

$$y = C_N v_N + C_R v_R \quad (3.2c)$$

where $A_N = P_N A P_N$, $A_{NR} = P_N A P_R$, etc. The terms $A_{NR} v_R$ and $A_{RN} v_R$ are called modeling error and the terms $B_R (f + f_D)$ and $C_R v_R$ are called control and observation spill-over, respectively [2]. The reduced-order model (ROM) is obtained from (3.2) by ignoring the residuals:

$$\left\{ \begin{array}{l} \frac{\partial v_N}{\partial t} = A_N v_N + B_N f \\ y = C_N v_N \end{array} \right. \quad (3.3)$$

in any choice of model reduction scheme it makes no sense if the residuals are unstable; therefore, we will assume that A_R generates a C_0 -semigroup $U_R(t)$ with the property:

$$\|U_R(t)\| \leq K_R e^{-\sigma_R t}, \quad t \geq 0 \quad (2.4)$$

with $K_R \geq 1$ and $\sigma_R > 0$. Such a condition is naturally satisfied in practice, as long as one is careful of the selection of H_N and H_R ; in theory, one would obtain K_R and σ_R from the Hille-Yosida or dissipativity tests (2.3)-(2.4).

In order to control the DPS (2.8), a finite-dimensional controller is generated from the ROM (3.3):

$$\left\{ \begin{array}{l} f = G_N \hat{v}_N \\ \frac{\partial \hat{v}_N}{\partial t} = A_N \hat{v}_N + B_N f + K_N (y - \hat{y}) \\ \hat{y} = C_N \hat{v}_N; \quad \hat{v}_N(0) = 0 \end{array} \right. \quad (3.5)$$

This is the most obvious candidate for a feedback controller; however, there are many ways in which (3.5) can be modified and improved, as pointed out in [2]. Nonetheless, (3.5) is a good starting point for the controller synthesis; it is, in fact, what most control system designers do with both large-scale and distributed parameter systems. The conditions under which a reasonable controller design can take place are essentially that (A_N, B_N, C_N) be controllable and observable in the finite-dimensional sense. Such conditions indicate the minimum number of control devices necessary for the task and also the possible locations for these devices.

Another approach is to obtain a finite-dimensional controller by performing a model reduction on the infinite-dimensional controller (2.5). But this yields [2] a controller whose form is the same as (3.5); hence, our later analysis will be unchanged.

4.0 STABILITY AND STABILIZABILITY CONCEPTS FOR DPS

In infinite-dimensional spaces there are many ways to define the concepts of stability. In this section we shall emphasize the two most useful ones for engineering systems: exponential stability and L^2 -BIBO.

4.1 Exponential Stability

The linear DPS (2.8) is said to be exponentially stabilizable when there exists a full-state feedback law:

$$f(t) = G v(t) \quad (4.1)$$

with $G: H \rightarrow R^M$ a linear finite-rank gain operator such that (2.8) becomes:

$$\begin{cases} \frac{\partial v(t)}{\partial t} = A_0 v(t) + B f_D(t) \\ y(t) = C v(t); v(0) = v_0 \end{cases} \quad (4.2)$$

with $A_0 \equiv A + BG$ generating a C_0 -semigroup $U_0(t)$ which is exponentially stable, i.e.

$$\|U_0(t)\| \leq K_0 e^{-\sigma_0 t}, \quad t \geq 0 \quad (4.3)$$

with constants $K_0 \geq 1$ and $\sigma_0 > 0$. This is a time-domain or state-space concept which says that, in the absence of any persistent disturbances (i.e. $f_D(t) \equiv 0$) the effects of all impulsive disturbances decay to zero exponentially, i.e.

$$\|v(t)\| \leq K_0 e^{-\sigma_0 t} \rightarrow 0 \text{ as } t \rightarrow \infty \quad (4.4)$$

The rate of convergence or stability margin is σ_0 in (4.3).

There are other types of stabilizability for (2.8); these depend on the different types of convergence possible in infinite-dimensional spaces. For example, (2.8) is strongly stabilizable when (4.1) yields an A_0 which generates $U_0(t)$ such that $v(t)$ converges strongly to zero (when $f_D(t) \equiv 0$), i.e.

$$\lim_{t \rightarrow \infty} \|U_0(t)v_0\| = 0 \quad (4.5)$$

for all v_0 in H . Alternatively, (2.8) is weakly stabilizable when (4.1) causes $v(t)$ to converge weakly to zero, i.e.

$$\lim_{t \rightarrow \infty} (U_0(t)v_0, v) = 0 \quad (4.6)$$

for all v_0 and v in H . In these last two types of mathematical stabilizability, no rate of convergence is available; consequently, they are not of much practical interest for engineering systems. Therefore, we will emphasize the exponential stability of (4.3) with its stability margin σ_0 , which becomes essential, as we shall see later. When H is finite-dimensional, all of the above stability concepts are equivalent.

Note that the feedback law (4.1) is only of theoretical interest. It cannot be implemented in practice since it requires instantaneous knowledge of the infinite-dimensional state $v(t)$; except for a few very special gain operators G , this is never practical. The actual control law must be generated by a finite-dimensional system (3.5); for this we need the concept of stabilizing subspaces.

We will say (A,B) in (2.8) has a pair of stabilizing subspaces H_N and H_R if, in addition to the model reduction requirements of Sec. 3.0, they also satisfy:

$A_0 = A + BG$ exponentially stable with a desired stability margin σ_0 for some $G: H \rightarrow R^M$ such that:

$$G = GP_N = G_N \quad (4.7)$$

Note that (4.7) says that $G_R = GP_R = 0$, i.e., A_0 is stabilized by a gain that is restricted to the finite-dimensional subspace H_N . This situation often occurs when modal reducing subspaces are used in "parabolic" or "hyperbolic" problems, but it can also occur in other model reduction schemes for DPS. It means that all but a finite number of the states of the system have the desired stability margin σ_0 and those that do not may be stabilized by the gains (4.7). Furthermore, using (4.7), we obtain:

$$A_0 = \begin{bmatrix} A_N + B_N G_N & A_{NR} \\ A_{RN} + B_R G_N & A_R \end{bmatrix} \quad (4.8)$$

From (4.8), it is easy to see that, if (A_N, B_N) is controllable and $\|A_{NR}\|$ is small, then the model reduction subspaces H_N and H_R are stabilizing subspaces. Furthermore, it seems highly unlikely that a finite-dimensional controller (3.5) can ever stabilize (exponentially) an infinite-dimensional DPS without the existence of stabilizing subspaces.

The stabilizing subspace idea was used in [14] to unify stability and controller synthesis for discrete and continuous-time DPS. As we shall see, it is also useful for interrelating time and frequency domain stability bounds.

4.2 L^2 -Bounded Input Bounded Output Stability

In the previous subsection, stability is treated as an internal or state space

property of the DPS. Alternatively, the stability of (4.2) may be looked at from an external or input-output viewpoint, i.e. what is the behavior of the output $y(t)$ for a given disturbance input $f_D(t)$. The concepts of L^p -bounded input, bounded output (L^p -BIBO) stability have been used for both lumped and distributed parameter systems; see e.g. [7] Chapt. 5, [8], [9], or [15] Chapt. 6. Following [9], we shall say (4.2) is L^p -BIBO stable for $1 < p < \infty$ when, for $v_0 = 0$, we have (a) if $f_D(\cdot)$ is in $L^p(\mathbb{R}, \mathbb{R}^M)$, then $y(\cdot)$ is in $L^p(\mathbb{R}, \mathbb{R}^P)$ and (b) there exists a constant $M_0 < \infty$ such that

$$\|y(\cdot)\|_p \leq M_0 \|f_D(\cdot)\|_p \quad (4.9)$$

where, for any positive integer q , $L^p(\mathbb{R}, \mathbb{R}^q) \equiv \{g(\cdot) \mid g: \mathbb{R} \rightarrow \mathbb{R}^q \text{ and } \int_{-\infty}^{\infty} \|g(t)\|^p dt < \infty\}$

with $\|g(\cdot)\|_p \equiv \left(\int_{-\infty}^{\infty} \|g(t)\|^p dt \right)^{1/p}$ for $1 \leq p < \infty$ for $L^\infty(\mathbb{R}, \mathbb{R}^q) \equiv \{g(\cdot) \mid g: \mathbb{R} \rightarrow \mathbb{R}^q \text{ and } \sup_{t \in \mathbb{R}} \|g(t)\| < \infty\}$ with $\|g(\cdot)\|_\infty \equiv \sup_{t \in \mathbb{R}} \|g(t)\|$. These L^p spaces are Banach

with the given norms $\|\cdot\|_p$ and the \mathbb{R}^q norm taken to be $\|g(t)\| \equiv (g^T(t)g(t))^{1/2}$; when $p=2$, L^2 is a Hilbert space.

In much of the finite-dimensional control literature, bounded input, bounded output stability is a fundamental concept; see e.g. [16] Chapt. 4. The version that is often seen is L^∞ -BIBO stability where a bounded disturbance produces a bounded output when the initial condition is zero. It is shown in [16], Theo. 3 p 197, that exponential stability of A_0 implies L^∞ -BIBO stability; the proof is for finite-dimensions but it extends directly to infinite-dimensions. In fact, for finite-dimensions, the two concepts are equivalent when (A, B, C) is controllable and observable.

However, in more recent literature, e.g. [3]-[11], L^2 -BIBO stability is much more popular. The main reason for this is the Fourier-Plancherel Theorem which says that the Fourier transform:

$$\hat{g}(\omega) \equiv \frac{1}{\sqrt{2\pi}} \int_{-\infty}^{\infty} g(t) e^{-j\omega t} dt \quad (4.10)$$

is a unitary operator on L^2 , i.e.

$$\|\hat{g}(\omega)\|_2 = \|g(t)\|_2 \quad (4.11)$$

where the integral in (4.10) is taken in the sense of "limit in the mean", i.e. it is taken over the bounded interval $[-N, N]$ and converges to (4.10) in the L^2 -norm as $N \rightarrow \infty$. The proof of this result (sometimes known as Parseval's Theorem) is given in [17] p 259 or [7] App B.2. Furthermore, the inverse Fourier transform is given by:

$$g(t) \equiv \frac{1}{\sqrt{2\pi}} \int_{-\infty}^{\infty} \hat{g}(\omega) e^{j\omega t} d\omega \quad (4.12)$$

This provides a way to transform from time to frequency domain and return without changing the L^2 -norm; hence, we have the following result:

Theorem 1: The DPS (4.2) is L^2 -BIBO stable if

$$\sup_{-\infty < \omega < \infty} ||T_o(\omega)|| \leq M_o < \infty \quad (4.13)$$

where

$$\hat{y}(\omega) = T_o(\omega) \hat{f}_D(\omega) \quad (4.14)$$

with $T_o(\omega)$ the $P \times M$ transfer matrix for (4.2) and M_o is the same constant as in (4.9) when $p=2$.

Proof: Let $f_D(\cdot)$ be in $L^2(\mathbb{R}, \mathbb{R}^M)$. Consider, from (4.11) and (4.14), that

$$||y(\cdot)||_2^2 = ||\hat{y}(\cdot)||_2^2 = \int_{-\infty}^{\infty} ||T_o(\omega) \hat{f}_D(\omega)||^2 d\omega \leq \int_{-\infty}^{\infty} ||T_o(\omega)||^2 ||\hat{f}_D(\omega)||^2 d\omega \quad (4.15)$$

Use (4.13) in (4.15) to obtain:

$$||y(\cdot)||_2^2 \leq M_o^2 \int_{-\infty}^{\infty} ||f_D(\omega)||^2 d\omega = M_o^2 \int_{-\infty}^{\infty} ||\hat{f}_D(\omega)||_2^2 d\omega = M_o^2 ||\hat{f}_D(\cdot)||_2^2$$

and the desired result follows. #

Therefore, the sufficient condition (4.13) for L^2 -BIBO stability is

$$||T_o(\omega)|| \leq M_o \text{ for all real } \omega \quad (4.16)$$

where

$$||T_o(\omega)|| \equiv \lambda_{\max}^{1/2}(T_o^*(\omega) T_o(\omega)) \quad (4.17)$$

and $\lambda_{\max}(Q)$ is the largest eigenvalue of the Hermetian matrix Q and $T_o^*(\omega)$ is the conjugate transpose (or adjoint) of the matrix $T_o(\omega)$ for each ω . The singular values of a matrix L are the square-roots of the eigenvalues of the Hermetian matrix L^*L (see, e.g. [3]), and they can be efficiently numerically calculated. Therefore, (4.16)-(4.17) can be written:

$$||T_o(\omega)|| \equiv \overline{sv}(T_o(\omega)) \leq M_o \text{ for all real } \omega \quad (4.18)$$

where $\overline{\text{sv}}(Q)$ indicates the largest singular value of Q . This makes the determination of L^2 -BIBO stability a simple matter even for DPS; so, (4.18) is a frequency domain condition for stability of (4.2).

We can obtain the transfer matrix $T_o(\omega)$ for (4.2) from

$$T_o(\omega) = C R(j\omega, A_o) B \quad (4.19)$$

where

$$R(\lambda, A_o) = (\lambda I - A_o)^{-1} \quad (4.20)$$

is the resolvent operator for A_o which is a bounded linear operator on H for each λ in the resolvent set

$\rho(A_o) \equiv \{\lambda \in \mathbb{C} \mid R(\lambda, A_o) \text{ is bounded operator on } H\}$. The spectrum of A_o is given by $\sigma(A_o) = \rho(A_o)^c$; in infinite-dimensional spaces it can be quite complicated since A_o is an unbounded operator, in general.

Furthermore, the resolvent operator is the Laplace transform of the C_o -semigroup $U_o(t)$ generated by A_o ([17] p 482):

$$R(\lambda, A_o) = \int_0^{\infty} U_o(t) e^{-\lambda t} dt, \quad \text{Re } \lambda > 0 \quad (4.21)$$

This leads to a relationship between exponential and L^2 -BIBO stability:

Theorem 2: If the DPS (4.2) is exponentially stable, then $j\omega$ is in $\rho(A_o)$ and

$$\|R(j\omega, A_o)\| \leq \frac{K_o}{\sigma_o}, \quad \text{for all real } \omega \quad (4.22)$$

where the constants (K_o, σ_o) are obtained from (4.3) and, from (4.22), the DPS is L^2 -BIBO with M_o in (4.9) given by

$$M_o = \|C\| \|B\| K_o / \sigma_o \quad (4.23)$$

Proof: Take $\lambda = \varepsilon + j\omega$, with $\varepsilon > 0$, and λ is in $\rho(A_o)$ by the Hille-Yosida

Theo. From (4.21), we obtain:

$$\begin{aligned} \|R(\varepsilon + j\omega, A_o)\| &\leq \int_0^{\infty} \|U_o(t)\| e^{-\varepsilon t} e^{-j\omega t} dt \\ &\leq K_o \int_0^{\infty} e^{-(\sigma_o + \varepsilon)t} dt \leq \frac{K_o}{\varepsilon + \sigma_o} \end{aligned}$$

Now, let $\epsilon \rightarrow 0$, to obtain (4.22). From (4.19), since B & C are bounded linear operators, we have

$$\begin{aligned} ||T_o(\omega)|| &\leq ||C|| ||B|| ||R(j\omega, A_o)|| \\ &\leq ||C|| ||B|| K_o/\sigma_o \end{aligned}$$

By (4.16) and Theo. 1, we have the desired result. #

See also the inequality (1.39) in [17] p 485. It is not clear under what conditions the converse of Theo. 2 holds for DPS.

Later, we shall need to consider L^2 -BIBO stability for feedback forms, i.e.,

$$H(\omega) = (I - Q(\omega))^{-1} \tag{4.24}$$

where $Q(\omega)$ is a bounded linear operator for each real ω on an appropriate Hilbert space. Stability of $H(\omega)$ in the L^2 -BIBO sense translates into $H(\omega)$ causal and bounded. However, we shall not need to worry about causality ([7] or [8]) because our control systems will be designed to be causal in the time-domain; hence, our analysis of stability will only need to verify the boundedness of $H(\omega)$. Almost all results in BIBO stability make use of the following result (sometimes known as the Small Gain Theorem):

Theorem 3: If $Q(\omega):H \rightarrow H$ is a bounded linear operator on the normed space H for each real ω and

$$||Q(\omega)|| < 1, \text{ for all real } \omega, \tag{4.25}$$

where

$$||Q|| \equiv \inf \{M \mid ||Qv|| \leq M ||v|| \text{ for all } v \text{ in } H\} \tag{4.26}$$

then $H(\omega) \equiv (I - Q(\omega))^{-1}$ is also a bounded linear operator on H for each real ω and

$$||H(\omega)|| \leq [1 - ||Q(\omega)||]^{-1} \tag{4.27}$$

The proof of this result can be obtained from [17] p 30. It uses the Neumann series:

$$(I + Q)^{-1} = \sum_{k=0}^{\infty} Q^k \tag{4.28}$$

which is absolutely convergent when (4.25) is satisfied; (4.27) follows also from (4.28) when $Q(\omega)$ is an $N \times N$ matrix (i.e. $\dim H = N$), then (4.25) becomes:

$$\overline{sv} Q(\omega) < 1, \text{ for all real } \omega \tag{4.28}$$

4.3 Robustness of Stability to Regular Perturbations

Theo. 3 is used in much of the literature to study the effect of regular perturbations on L^2 -BIBO stability. Consider

$$Q(\omega) = Q_o(\omega) + \Delta Q(\omega) \quad (4.29)$$

where $(I-Q_o(\omega))^{-1}$ is known to be bounded, then $(I-Q(\omega))^{-1}$ is also bounded from Theo. 3 when the parameter uncertainty $\Delta Q(\omega)$ satisfies:

$$\|\Delta Q(\omega)\| < [\|(I-Q_o(\omega))^{-1}\|]^{-1} \quad (4.30a)$$

or, for matrices,

$$\overline{\text{sv}}(\Delta Q(\omega)) < \underline{\text{sv}}(I-Q_o(\omega)) \quad (4.30b)$$

for all real ω , where $\underline{\text{sv}}(\cdot)$ denotes the smallest singular value and $\overline{\text{sv}}(\cdot)$ the largest one. The inequality (4.30b) follows from (4.30a), the definition of singular values, and the property [3] that

$$\overline{\text{sv}}[(I-Q)^{-1}] = \frac{1}{\underline{\text{sv}}(I-Q)} \quad (4.31)$$

In lumped parameter systems, (4.30b) is particularly easy to evaluate; hence, the popularity of this approach for robust control design under parameter uncertainty. However, for DPS, the effect of parameter uncertainty or other perturbations on L^2 -BIBO stability can be assessed with (4.30a). Loosely stated: (4.30) is "gain stabilization" of the feedback system.

The corresponding situation with robustness of exponential stability is given by the well-known result:

Theorem 4: Let \tilde{A}_o generate the C_o -semigroup $\tilde{U}_o(t)$ satisfying the exponential stability property:

$$\|\tilde{U}_o(t)\| \leq \tilde{K}_o e^{-\tilde{\sigma}_o t}, \quad t \geq 0 \quad (4.32)$$

where $\tilde{K}_o \geq 1$ and $\tilde{\sigma}_o > 0$. Then the perturbed operator:

$$\tilde{A}_c = \tilde{A}_o + \tilde{\Delta A} \quad (4.33)$$

where $\tilde{\Delta A}$ is a bounded operator, generates the C_o -semigroup $\tilde{U}_c(t)$ satisfying:

$$\|\tilde{U}_c(t)\| \leq \tilde{K}_c e^{-\tilde{\sigma}_c t}, \quad t \geq 0 \quad (4.34)$$

where

$$\begin{cases} \tilde{K}_c = \tilde{K}_o \\ \tilde{\sigma}_c = \tilde{\sigma}_o - \tilde{K}_o \|\tilde{\Delta A}\| \end{cases} \quad (4.35a)$$

$$(4.35b)$$

with the constants $(\tilde{K}_0, \tilde{\sigma}_0)$ given in (4.32). The perturbed system (4.33) is exponentially stable if

$$\|\tilde{\Delta}A\| < \tilde{\sigma}_0 / \tilde{K}_0 \quad (4.36)$$

The proof of this theorem is given in [12] p 210; it is a direct consequence of the well-known Gronwall Inequality. To us, Theo. 4 seems to be one of the essential tools for establishing closed-loop stability of DPS with finite-dimensional controllers, e.g. [2]. In the next two sections, we shall use Theos. 3 and 4 to establish and interrelate some closed-loop stability results for DPS.

5.0 CLOSED-LOOP STABILITY FOR DPS: TIME DOMAIN CONDITIONS

In Sec. 3.0, model reduction is used to obtain a finite-dimensional controller (3.5) for the infinite-dimensional DPS (2.8). In this section, we consider the closed-loop stability of the DPS with the controller (2.8); this stability is not always guaranteed as various computer simulations and laboratory experiments with flexible structures have demonstrated [1]. We want to use Theo. 4, of course, but the main difficulty is to obtain \tilde{K}_0 and $\tilde{\sigma}_0$ in (4.32); our stability lemma in this section gives some reasonable bounds for this data.

We make the following assumptions:

- (a) the ROM (A_N, B_N, C_N) in (3.3) is controllable and observable;
- (b) the estimator gain K_N in (3.5) is chosen so that the spectrum of $A_N - K_N C_N$ is to the left of a vertical line through $(-\sigma_N, 0)$ in the complex plane; i.e. $A_N - K_N C_N$ generates the matrix exponential $U_N(t)$ satisfying:

$$\|U_N(t)\| \leq \tilde{K}_N e^{-\sigma_N t}, \quad t \geq 0 \quad (5.1)$$

where $\tilde{K}_N \geq 1$ and $\sigma_N > 0$.

- (c) the residual subsystem satisfies (2.4);
- (d) the subspaces H_N and H_R used in the model reduction procedure are stabilizing subspaces for (A, B) , as described in Sec. 4.0; hence, A_0 generates the C_0 -semigroup $U_0(t)$ satisfying (4.3);
- (e) $\sigma_0 < \sigma_N$ by the choice of K_N in (3.5);
- (f) $f_D(t) \equiv 0$, i.e. no persistent disturbances.

The controller (3.5) can be designed by standard finite-dimensional techniques.

Let $e_N = \hat{v}_N - v_N$ and obtain, from (2.8) and (3.5):

$$\left\{ \begin{array}{l} f(t) = Gv_N(t) = Gv_N(t) + G_N e_N(t) \\ \frac{\partial e_N(t)}{\partial t} = (A_N - K_N C_N) e_N(t) + (K_N C_R - A_{NR}) P_R v(t) \end{array} \right. \quad (5.2a)$$

$$\left\{ \begin{array}{l} \frac{\partial v(t)}{\partial t} = A_o v(t) + B G_N e_N(t) \\ \frac{\partial e_N(t)}{\partial t} = (K_N C_R - A_{NR}) v(t) + (A_N - K_N C_N) e_N(t) \end{array} \right. \quad (5.2b)$$

Note that we may omit P_R from (5.2b) since it is already incorporated into C_R and A_{NR} . The closed-loop system (2.8) and (3.5) can be written (from (5.2)):

$$\left\{ \begin{array}{l} \frac{\partial v(t)}{\partial t} = A_o v(t) + B G_N e_N(t) \\ \frac{\partial e_N(t)}{\partial t} = (K_N C_R - A_{NR}) v(t) + (A_N - K_N C_N) e_N(t) \end{array} \right. \quad (5.3)$$

We have the following closed-loop stability result:

Theorem 5: If assumptions (a)-(f) are satisfied, then the gain K_N may be chosen so that the finite-dimensional controller (3.5) produces an exponentially stable closed-loop system (5.3) when $\|K_N C_R - A_{NR}\|$ is sufficiently small.

The proof of Theo. 5 is obtained directly by taking $A_{11} = A_o$, $A_{12} = B G_N$, $A_{21} = K_N C_R - A_{NR}$, and $A_{22} = A_N - K_N C_N$ in the following stability lemma whose proof uses Theo. 4 and appears in [2]:

Lemma 1:

$$\text{Consider } \frac{\partial \omega}{\partial t} = \tilde{A}_c \omega = \begin{bmatrix} A_{11} & A_{12} \\ A_{21} & A_{22} \end{bmatrix} \omega \quad (5.4)$$

where A_{ij} are bounded for $i \neq j$ and A_{ii} generates the C_o -semigroup $U_i(t)$ with the growth property:

$$\|U_i(t)\| \leq K_i e^{-\sigma_i t}, \quad t \geq 0 \quad (5.5)$$

for $i=1,2$. Assume $\sigma_1 \neq \sigma_2$. Then \tilde{A}_c generates the C_o -semigroup $\tilde{U}_c(t)$ with growth property:

$$\|\tilde{U}_c(t)\| \leq \tilde{K}_c e^{-\tilde{\sigma}_c t}, \quad t \geq 0 \quad (5.6)$$

where, for exponential stability,

$$\tilde{\sigma}_c = \tilde{\sigma}_o - \tilde{K}_c \|A_{21}\| > 0 \quad (5.7)$$

with

$$\left\{ \begin{array}{l} \tilde{\sigma}_o = \min(\sigma_1, \sigma_2) \end{array} \right. \quad (5.8a)$$

$$\left\{ \begin{array}{l} \tilde{K}_c = K_1 K_2 (1 + \psi + \psi^2)^{1/2} \leq K_1 K_2 (1 + \psi) \end{array} \right. \quad (5.8b)$$

and

$$\psi = \frac{||A_{12}||}{|\sigma_1 - \sigma_2|} \text{ where } ||\omega|| \equiv (||\omega_1||^2 + ||\omega_2||^2)^{1/2}.$$

The dual result with A_{12} and A_{21} interchanged in (5.7) is true, also. The inequality in (5.8b) follows from $(1+a+a^2) \leq (1+a)^2$ when $a > 0$.

Due to assumption (e) and (5.8a), we have

$$\tilde{\sigma}_o = \sigma_o \quad (5.9)$$

and the exponential stability bound of Theo. 5 becomes:

$$||K_{NR} C_R - A_{NR}|| < \sigma_o / \tilde{K}_c \quad (5.10)$$

with \tilde{K}_c given by (5.8b) and

$$\left\{ \begin{array}{l} \psi = ||BG_N|| \cdot (\sigma_N - \sigma_o)^{-1} \\ K_1 K_2 = \tilde{K}_c K_o \end{array} \right. \quad (5.11)$$

where (\tilde{K}_N, σ_N) and (K_o, σ_o) are given in (5.1) and (4.3), respectively. These constants can either be obtained from the finite-dimensional controller design or from the stabilizing subspace calculations of Sec. 4.0. The stability test (5.10) involves the norm

$$||K_{NR} C_R - A_{NR}|| \leq ||K_N|| ||C_R|| + ||A_{NR}|| \quad (5.11)$$

Hence, with only a knowledge of the norms of C_R and A_{NR} , we can assure closed-loop exponential stability when:

$$||K_N|| ||C_R|| + ||A_{NR}|| < \sigma_o / \tilde{K}_c \quad (5.12)$$

Note that \tilde{K}_c involves the norm

$$||BG_N|| \leq ||B|| ||G_N|| \quad (5.13)$$

6.0 CLOSED-LOOP STABILITY FOR DPS: FREQUENCY DOMAIN CONDITIONS

In Sec. 5.0, the internal stability of the closed-loop system was guaranteed by a test of the form (5.12) involving the norms of the residual data. In this section, we consider the closed-loop stability from an external standpoint and use Theo. 3. We assume here (a)-(e) of Sec. 5.0 and also (g) $v_o \equiv 0$ in (2.8), i.e. no impulsive disturbances. The finite-dimensional controller (3.5) remains unchanged.

The closed-loop system consisting of (2.8) and (3.5) may be written:

$$\left\{ \begin{array}{l} \frac{\partial v(t)}{\partial t} = A_o v(t) + B G_N e_N(t) + B f_D(t) \end{array} \right. \quad (6.1a)$$

$$\left\{ \begin{array}{l} \frac{\partial e_N(t)}{\partial t} = (K_{NR} C_N - A_{NR}) v(t) + (A_N - K_{NN} C_N) e_N(t) - B_N f_D(t) \end{array} \right. \quad (6.1b)$$

$$\left\{ \begin{array}{l} y(t) = C v(t) \end{array} \right. \quad (6.1c)$$

The initial conditions are (g) and

$$e_N(o) = \hat{v}_N(o) - v_N(o) = -P_N v_o = 0 \quad (6.2)$$

Note that the term $B_N f_D$ appears in (6.1b) because the controller does not know the persistent disturbance; this seems to be the most realistic (and the most difficult) situation to analyze. From (6.1a) and (g), by taking Fourier transforms we have:

$$\left\{ \begin{array}{l} \hat{v}(\omega) = R(j\omega, A_o) B [G_N \hat{e}_N(\omega) + \hat{f}_D(\omega)] \end{array} \right. \quad (6.3a)$$

$$\left\{ \begin{array}{l} \hat{y}(\omega) = C \hat{v}(\omega) \end{array} \right. \quad (6.3b)$$

where $R(j\omega, A_o) = (j\omega - A_o)^{-1}$. Also, (6.1b) and (6.2) yields:

$$\hat{e}_N(\omega) = R_N(\omega) [\Delta_{NR} \hat{v}(\omega) - B_N \hat{f}_D(\omega)] \quad (6.4)$$

where

$$\left\{ \begin{array}{l} R_N(\omega) \equiv R(j\omega, A_N - K_{NN} C_N) \end{array} \right. \quad (6.5a)$$

$$\left\{ \begin{array}{l} R(\lambda, A_N - K_{NN} C_N) \equiv [\lambda I_N - (A_N - K_{NN} C_N)]^{-1} \end{array} \right. \quad (6.5b)$$

$$\left\{ \begin{array}{l} \Delta_{NR} \equiv K_{NR} C_N - A_{NR} \end{array} \right. \quad (6.5c)$$

This is illustrated in Fig. 1 which suggests defining

$$\hat{E}(\omega) \equiv G_N \hat{e}_N(\omega) + \hat{f}_D(\omega) \quad (6.6)$$

From (6.3) and (6.6), we have

$$\begin{cases} \hat{v}(\omega) = R(j\omega, A_o) B \hat{E}(\omega) & (6.7a) \\ \hat{y}(\omega) = T_o(\omega) \hat{E}(\omega) & (6.7b) \end{cases}$$

where

$$T_o(\omega) \equiv C R(j\omega, A_o) B \quad (6.8)$$

Also, from (6.4) and (6.7a) in (6.6), we obtain:

$$\hat{E}(\omega) = \hat{f}_D^E(\omega) + G_N L(\omega) \hat{E}(\omega) \quad (6.9)$$

where

$$L(\omega) \equiv R_N(\omega) \Delta_{NR} R(j\omega, A_o) B \quad (6.10)$$

and the equivalent disturbance $f_D^E(\omega)$ is

$$\hat{f}_D^E(\omega) \equiv (I_M - G_N R_N(\omega) B_N) \hat{f}_D(\omega) \quad (6.11)$$

Therefore, from (6.9),

$$\hat{E}(\omega) = S(\omega) \hat{f}_D^E(\omega) \quad (6.12)$$

where

$$S(\omega) \equiv (I_M - G_N L(\omega))^{-1} \quad (6.13)$$

which is the inverse of the return difference operator $I_M - G_N L(\omega)$. Furthermore, from (6.7b) and (6.12), we have the closed-loop input-output relationship:

$$\hat{y}(\omega) = T_c(\omega) \hat{f}_D^E(\omega) \quad (6.14)$$

where the $P \times M$ closed-loop transfer matrix is

$$T_c(\omega) \equiv T_o(\omega) S(\omega) \quad (6.15)$$

whenever $S(\omega)$ exists.

Note that, even in the most ideal case when $\Delta_{NR}=0$, (6.14) becomes:

$$\hat{y}_o(\omega) = T_o(\omega) \hat{f}_D^E(\omega) \quad (6.16)$$

with $T_o(\omega)$ given by (6.8) and $\hat{f}_D^E(\omega)$ given by (6.11). This is not surprising because there is still a term due to the unknown disturbance $f_D(t)$ entering the

state-estimator error equation (6.1b). If this disturbance were completely known, then a counteracting term could be added to the controller (3.5), and (6.11) would reduce to $\hat{f}_D^E(\omega) = \hat{f}_D(\omega)$. However, in most practical problems, the disturbance would not be completely known; hence, we must have (6.11). It is clear that, if $f_D(t)$ is an L^2 -bounded disturbance, then so is the equivalent disturbance $f_D^E(t)$; this can be obtained from (4.11) and the fact that (using Theo. 2):

$$\|R_N(\omega)\| \leq \tilde{K}_N/\sigma_N \text{ for all real } \omega \quad (6.17)$$

where (\tilde{K}_N, σ_N) are given in (5.1).

This leads to our main result for DPS stability in the frequency domain:

Theorem 6: If the assumptions (a)-(e) in Sec. 5.0 and (g) in Sec. 6.0 are satisfied and if

$$\|K_N C_R - A_{NR}\| < \frac{\sigma_N \sigma_o}{\tilde{K}_N K_o \|B\| \|G_N\|} \quad (6.18)$$

where (\tilde{K}_N, σ_N) are given in (5.1) and (K_o, σ_o) are given in (4.3), then the finite-dimensional controller (3.5) produces an L^2 -BIBO stable closed-loop system (6.1).

Proof: From the discussion preceding the statement of this theorem, we need only show that the operator $S(\omega)$ in (6.13) exists and is bounded uniformly for all real ω . Then, by Theo. 1 and the condition (4.16), the desired result will follow.

However, by Theo. 3, we need only show that

$$\|G_N L(\omega)\| < 1 \text{ for all real } \omega \quad (6.19)$$

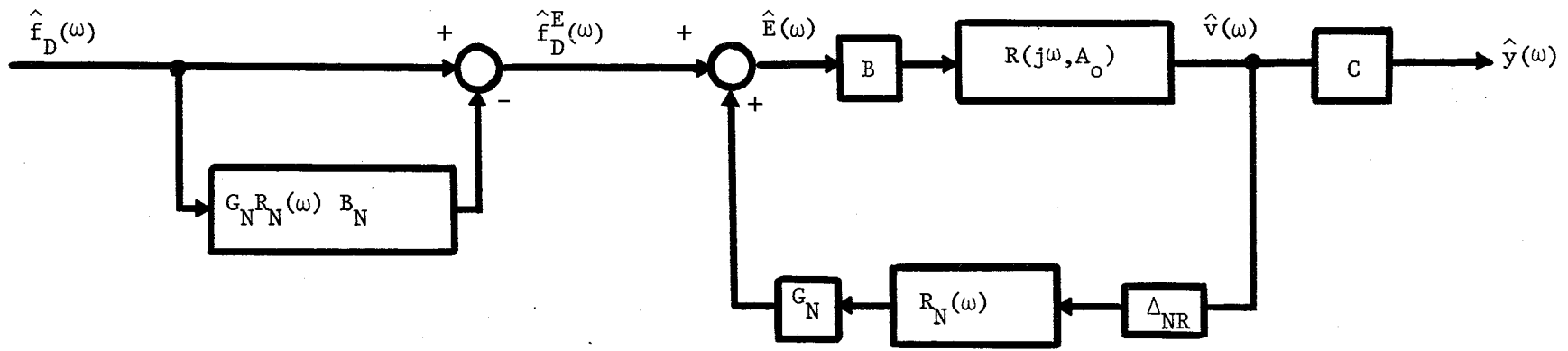
in order that $S(\omega)$ exists and is bounded. But, from Theo. 2, we have

$$\|R(j\omega, A_o)\| \leq \frac{K_o}{\sigma_o} \quad (6.20)$$

because A_o generates an exponentially stable semigroup due to assumptions (c) and (d). Also, from assumptions (a) and (b), (6.17) is satisfied. Note that the spectra of A_o and $A_N - K_N C_N$ are in the open left-half of the complex plane; hence $j\omega$ is in the resolvent set of both operators. Therefore,

$$\|G_N L(\omega)\| \leq \|G_N\| \frac{\tilde{K}_N}{\sigma_N} \|\Delta_{NR}\| \frac{K_o}{\sigma_o} \|B\| < 1 \text{ by (6.18) and}$$

the desired result holds. #



$$\hat{E}(\omega) = \hat{f}_D^E(\omega) + G_N L(\omega) \hat{E}(\omega)$$

FIGURE 1: CLOSED-LOOP STABILITY FOR DPS IN THE FREQUENCY DOMAIN

Of course, when (5.10) holds, the closed-loop system is exponentially stable by Theo. 5, and, consequently by Theo. 2, it is also L^2 -BIBO stable. However, we would like to compare (5.10) with (6.20) to see if the condition for Theo. 6 is easier to satisfy than that for Theo. 5. The answer is: yes, if we bound K_c in (5.10) by

$$\tilde{K}_c \leq \tilde{K}_{N_0} K_o \left(1 + \frac{\|B\| \|G_N\|}{\sigma_N - \sigma_o} \right) \quad (6.21)$$

which is obtained from (5.8b), (5.11), and (5.13). Then (5.10) is satisfied when

$$\|K_{N_0} C_R - A_{NR}\| \leq \frac{\sigma_o}{\tilde{K}_{N_0} K_o \left(1 + \frac{\|B\| \|G_N\|}{\sigma_N - \sigma_o} \right)} \quad (6.22)$$

Now, the right-hand side of (6.22) is less than or equal to the right-hand side of (6.18), i.e. from assumption (e) we have:

$$\frac{\sigma_N}{\alpha} \geq \frac{\sigma_N - \sigma_o}{\alpha} \geq \frac{\sigma_N - \sigma_o}{\alpha + (\sigma_N - \sigma_o)} = \frac{1}{1 + \frac{\alpha}{(\sigma_N - \sigma_o)}} \quad (6.23)$$

where $\alpha \equiv \|B\| \|G_N\|$ and, therefore,

$$\frac{\sigma_o \sigma_N}{\tilde{K}_{N_0} K_o \alpha} \geq \frac{\sigma_o}{\tilde{K}_{N_0} K_o \left(1 + \frac{\alpha}{\sigma_N - \sigma_o} \right)} \quad (6.24)$$

This says that, when (6.21) is used in (5.10), the resulting condition (6.22) for exponential stability is more stringent than the condition (6.20) for L^2 -BIBO stability of the closed-loop DPS.

7.0 CONCLUSIONS

Our main results Theos. 5 and 6, presented in Sec. 5.0 and 6.0, give tests for exponential stability (time-domain) and L^2 -BIBO stability (frequency domain) of closed-loop DPS with finite-dimensional controllers. For the time-domain test, an internal view of the system is taken and exponential decay of the effects of any impulsive disturbance on the full infinite-dimensional state is required. However, for the frequency domain test, an external view is taken and bounded input-bounded output behavior in the L^2 -sense is expected for any square-integrable persistent disturbance. The time-domain result is a consequence of regular perturbation of the C_0 -semigroup generated by the system. The frequency domain result is obtained via the Fourier-Plancherel (or Parseval) Theorem for Fourier transforms and a version of the Small Gain Theorem; in this case, the

system resolvent operator, which is the Laplace transform of the semigroup, becomes the important concept.

It was expected that L^2 -BIBO stability would yield a less stringent test since it is weaker for DPS than exponential stability (see Theo. 2). This was shown to be true for some choices of bounds on the data used for Theo. 5; however, it may not always be so. It should be noted that both approaches are regular perturbation methods where a nominally stable system (e.g., the closed-loop DPS with $A_{NR}=0$ and $C_R=0$) is perturbed by a bounded term; bounds on the size of this term, for which stability is maintained, produce the closed-loop stability tests.

The stability results presented here for the time and frequency domain are related by:

- (a) the C_0 -semigroup of the system and its Laplace transform, the resolvent operator;
- (b) regular perturbation theory;
- (c) the concept of stabilizing subspaces for DPS.

It seems to us that, without the property (c), a DPS would have little or no chance of being stabilized (either exponentially or L^2 -BIBO) by a finite-dimensional controller.

Finally, we note that the controller design was not considered the focus of this paper. The designs can all be based on finite-dimensional reduced-order models; hence, many time or frequency domain techniques are available. Furthermore, to be implementable with a digital computer, the controller (3.5) should be discrete (rather than continuous) time. However, the main conclusions, with which we hope the reader will agree, are that closed-loop stability analysis should be an intrinsic part of any attempt to produce finite-dimensional, practical controllers for infinite-dimensional DPS, and that such analysis can be carried out with perturbation techniques in many disguises.

REFERENCES

1. M. Balas, "Trends in Large Space Structure Control Theory: Fondest Hopes, Wildest Dreams", IEEE Trans. Autom. Contr. AC-27, 522-535, 1982.
2. M. Balas, "Toward A More Practical Control Theory For Distributed Parameter Systems", Control & Dynamic Systems: Advances in Theory and Appl., Vol. 18, C.T. Leondes, ed., Academic Press, NY, 1982.
3. M. Safanov, Stability Robustness of Multivariable Systems, MIT Press, Cambridge, Mass, 1980.
4. J. Doyle and G. Stein, "Multivariable Feedback Design: Concepts for a Classical/Modern Synthesis", IEEE Trans. Autom. Contr. AC-26, 4-16, 1981.
5. J. Doyle, "Robustness of Multiloop Linear Feedback Systems", Proc. 17th IEEE Control and Decision Conf., San Diego, CA, 1979.

6. A. MacFarlane, "Return Difference and Return-Ratio Matrices and Their Use in the Analysis and Design of Multivariable Feedback Control Systems", Proc. IEE Vol. 117, 2037-2049, 1970.
7. C. Desoer and M. Vidyasagar, Feedback Systems: Input/Output Properties, Academic Press, NY, 1980.
8. M. Damborg and A. Naylor, "Fundamental Structure of Input-Output Stability For Feedback Systems", IEEE Trans. Sys. Sci. & Cybernetics, Vol. SSC-6, 92-96, 1970.
9. J.C. Willems, "A Survey of Stability of Distributed Parameter Systems", Control of Distributed Parameter Systems: Joint Autom. Contr. Conf., Am. Soc. of Mech. Engrs., NY, 1969.
10. R. Kosut, "Stability and Robustness of Control Systems For Large Space Structures", Proc. AIAA/VPI Symp. on Dynamics and Control of Large Flexible Spacecraft, Blacksburg, Va., 1981.
11. R. Benhabib, R. Iwens, and R. Jackson, "Stability of Distributed Control for Large Flexible Structures Using Positivity Concepts", Proc. AIAA Guidance and Control Conf., Boulder, CO., 1979.
12. R. Curtain and A. Pritchard, Functional Analysis in Modern Applied Mathematics, Academic Press, NY, 1977.
13. J. Walker, Dynamical Systems and Evolution Equations: Theory and Applications, Plenum Press, NY, 1980.
14. M. Balas, "Stabilizing Subspaces and Linear Distributed Parameter Systems: Discrete and Continuous-Time Control", Proc. of 15th Asilomar Conf. on Circuits, Systems, and Computers, Pacific Grove, CA, 1981.
15. M. Vidyasagar, Nonlinear Systems Analysis, Prentice-Hall, NJ, 1978.
16. R. Brockett, Finite-Dimensional Linear Systems, J. Wiley & Sons, NY, 1969.
17. T. Kato, Perturbation Theory for Linear Operators, Springer, NY, 1966.

This Page Intentionally Left Blank

APPROXIMATION OF THE OPTIMAL COMPENSATOR FOR A LARGE SPACE STRUCTURE*,**

Michael K. Mackay

University of California, Los Angeles
Los Angeles, CA 90024

ABSTRACT

This paper considers the approximation of the optimal compensator for a Large Space Structure. The compensator is based upon a solution to the Linear Stochastic Quadratic Regulator problem. Colocation of sensors and actuators is assumed. A small gain analytical solution for the optimal compensator is obtained for a single input/single output system, i.e., certain terms in the compensator can be neglected for sufficiently small gain. The compensator is calculated in terms of the kernel to a Volterra integral operator using a Neumann series. The calculation of the compensator is based upon the C_0 semigroup for the infinite dimensional system. A finite dimensional approximation of the compensator is, therefore, obtained through analysis of the infinite dimensional compensator which is a compact operator.

1.0 INTRODUCTION

One of the distinguishing properties of a Large Space Structure (LSS) is that it is a distributed parameter system and, hence, an infinite dimensional mathematical model is required for its description. In most applications, active control of shape, attitude, and structural vibrations will be necessary. For such problems, formulation of the control problem as a steady-state (infinite time) linear quadratic regulator is natural. The main advantage for considering the infinite time case is, of course, that the optimal control gain is time invariant. Implementation of the optimal feedback control will generally require an estimate of the system state. For the stochastic problem, the optimal state estimate is provided by an infinite dimensional Kalman filter. However, it is at this point where a significant gap exists between theory and practice in that implementation of an infinite dimensional filter is not generally possible.

The most popular solution to this dilemma at the present time seems to be reduced order modeling of the system, see for example [1],[2],[3], and [4]. Usually, a modal representation of the system is assumed. The basic idea is then to evaluate various computable criteria representing the significance of various modes and then select some finite subset of modes to represent the dominant dynamics of the system. A linear quadratic regulator (controller/estimator combination) for this finite dimensional model is then designed using standard methods. The stability of the system using the resulting compensator is usually checked by computing the eigenvalues of the closed loop system using a high order "truth model" to represent the LSS dynamics, where the truth model is of finite order, but of much higher order than the compensator.

* Research supported in part under Grant No. 78-3550, AFOSR, USAF, Applied Math Division.

** Paper has been revised (8/6/82) from version distributed at workshop (7/15/82).

There are two basic problems with the above approach. The first is that the approximation is performed upon the system rather than the compensator. In effect, the truncation of an infinite number of modes is tantamount to "approximating" an unbounded, infinite dimensional operator by one that is bounded and finite dimensional. Thus, the infinite dimensionality of the problem is never used in designing the compensator. The second problem is that the stability of the closed loop system is also checked against a finite order model and the closed loop stability of the actual infinite dimensional system is inferred essentially on faith.

To avoid these pitfalls essentially requires that we have a partial differential equation (PDE) to represent the system. For complicated structures this may be asking too much. Hence, the method of reduced order modeling may be as viable an approach as any in those cases. However, we can, and should, study the problem of approximating the optimal compensator for appropriate systems where the PDE is known, since we may gain insight into the approximation problem that would apply to more general and more complicated systems.

This paper considers the compensator design and approximation for a class of systems representative of large space structures. An analytical solution for the compensator is obtained using the infinite dimensional model of the system. A finite dimensional approximation of the compensator is then derived based upon analysis of the infinite dimensional compensator.

2.0 SYSTEM MODEL

We will consider the following system

$$M\ddot{w}(t) + A_0 w(t) = bu(t) + bn_d(t) \quad (2.1)$$

$$y(t) = [b, \dot{w}(t)] + e(t) \quad (2.2)$$

(2.1) is the inhomogeneous equation of motion of an undamped oscillator and (2.2) is the system measurement equation. $w(t)$ is an element of a separable Hilbert space H and represents the small displacements of the system (translation and rotational) relative to its equilibrium position. The operator M contains the mass and inertia properties of the system. M maps H to H , is linear bounded, self-adjoint, and positive definite. A_0 represents the stiffness of the structure and maps $\mathcal{D}(A_0)$, the domain of A_0 which is dense in H , to H . A_0 is linear, self-adjoint, closed (or can be closed) and generally unbounded. We assume there exists $\epsilon > 0$ such that

$$[A_0 w, w] \geq \epsilon \|w\|^2, \quad w \in \mathcal{D}(A_0)$$

The spatial domain of A_0 , Ω , is bounded and, thus, the resolvent of A_0 is compact for each λ in the resolvent set of A_0 . Since A_0 is closed and has a compact resolvent, its eigenvalues are isolated (countable), have finite multiplicities, and have infinity as the only limit point ([5], p.187). In addition, the modes $\{\phi_k, k=1,2,\dots\}$ of A_0 are orthogonal and form a basis in H .

A single white noise disturbance $n_d(t)$ is present with a spatial force distribution defined by $b \in H$. The support of b is assumed to be small compared to

the measure of Ω , so that $bn_d(t)$ represents a physical realization of a point disturbance. A single control $u(t)$ and rate sensor $y(t)$ are colocated at the sight of the disturbance. The measurement error $e(t)$ is a white noise process uncorrelated with $n_d(t)$. $u(t)$, $n_d(t)$, $y(t)$, and $e(t)$ are all elements of \mathbb{R} for each $t \in [0, \infty)$. Note also that the control, measurement, and disturbance are all compact, since they are each finite in number.

In order to utilize semigroup theory, (2.1) and (2.2) will be put in first order form. Let $x_1(t) = w(t)$ and $x_2(t) = \dot{w}(t)$ then, the system (2.1) and (2.2) can be written as

$$\dot{x}(t) = Ax(t) + Bu(t) + Fn_d(t) \quad (2.3)$$

$$y(t) = Cx(t) + e(t) \quad (2.4)$$

where

$$x(t) = \begin{bmatrix} x_1(t) \\ x_2(t) \end{bmatrix} \quad A = \begin{bmatrix} 0 & I \\ -M^{-1}A_0 & 0 \end{bmatrix}$$

$$B = F = \begin{bmatrix} 0 \\ M^{-1}b \end{bmatrix} \quad C = [0, (M^{-1}b)^*]$$

Note that $\mathcal{D}(A) = \mathcal{D}(A_0) \times V$, where $V = \{w \mid A_0^{1/2} w \in H\}$. Note also that A will have a compact resolvent since A_0 does.

As a function space, it is natural to use the energy space $E = V \times H$ defined by the inner product

$$[x, z]_E = [A_0^{1/2} x_1, A_0^{1/2} z_1] + [Mx_2, z_2], \quad x, z \in E \quad (2.5)$$

It is easy to verify that $A = -A^*$ under the inner product (2.5). Hence, by [6, Corollary 4.3.1], A generates a norm preserving, strongly continuous group, $T(t)$.

The semigroup can be represented using the modes of $M^{-1}A_0$. The modes ϕ_k are orthogonal under the inner product $[M \cdot, \cdot]$ and are complete in H . Using the ϕ_k 's, a set of basis vectors in E can be defined by $\phi_{1k} = [\phi_k, 0]^T$, $\phi_{2k} = [0, \phi_k]^T$, $k=1, 2, \dots$. The set $\{\phi_{1k}, \phi_{2k}, k=1, 2, \dots\}$ is complete in E and orthogonal under $[\cdot, \cdot]_E$. Thus, any $x \in E$ can be written as

$$x = \sum_{k=1}^{\infty} x_{1k} \phi_{1k} + x_{2k} \phi_{2k}$$

where $[\phi_{1k}, x]_E = \omega_k^2 x_{1k}$, $[\phi_{2k}, x]_E = x_{2k}$.

A representation for the semigroup, can be obtained from the homogeneous solution to (2.3). Writing (2.3) as

$$\dot{x} - Ax = \sum_{k=1}^{\infty} (\dot{x}_{1k} - x_{2k}) \phi_{1k} + (\dot{x}_{2k} + \omega_k^2 x_{1k}) \phi_{2k} = 0$$

we see that x_{1k} and x_{2k} solve

$$\begin{bmatrix} \dot{x}_{1k} \\ \dot{x}_{2k} \end{bmatrix} = \begin{bmatrix} 0 & 1 \\ -\omega_k^2 & 0 \end{bmatrix} \begin{bmatrix} x_{1k} \\ x_{2k} \end{bmatrix}$$

for each k . Thus the semigroup can be expressed as

$$\begin{aligned} x(t) &= T(t) x(0) \\ &= \sum_{k=1}^{\infty} \left\{ \begin{bmatrix} x_{1k}(0) \cos \omega_k t + \frac{x_{2k}(0)}{\omega_k} \sin \omega_k t \\ -\omega_k x_{1k}(0) \sin \omega_k t + x_{2k}(0) \cos \omega_k t \end{bmatrix} \phi_{1k} \right. \\ &\quad \left. + \begin{bmatrix} x_{1k}(0) \sin \omega_k t + \frac{x_{2k}(0)}{\omega_k} \cos \omega_k t \\ -x_{1k}(0) \cos \omega_k t + x_{2k}(0) \sin \omega_k t \end{bmatrix} \phi_{2k} \right\} \end{aligned} \quad (2.6)$$

3.0 STOCHASTIC CONTROL PROBLEM

Given the system (2.3) and (2.4), we want to find a control $u(t)$ to minimize

$$J[u] = \lim_{T \rightarrow \infty} \frac{1}{T} E \left\{ \int_0^T [\gamma^2 |B^*x(t)|^2 + |u(t)|^2] dt \right\} \quad (3.1)$$

where $\gamma > 0$ and $E\{\cdot\}$ denotes expected value. Let the noise covariances be given by $E n_d(t) n_d^*(t) = \sigma_d^2 I$ and $E e(t) e^*(t) = \sigma_s^2$. For (A, B) controllable*, the minimum of (3.1) is attained for

$$u_0(t) = -B^* P_c \hat{x}(t) \quad (3.2)$$

where $\hat{x}(t)$ satisfies

$$\dot{\hat{x}}(t) = A\hat{x}(t) + B u_0(t) + P_f B^* [y(t) + B\hat{x}(t)], \quad \hat{x}(0) = 0 \quad (3.3)$$

and P_c and P_f satisfy, respectively,

$$\begin{aligned} [P_c x, Ax] + [Ax, P_c x] + \gamma^2 [B^* x, B^* x] \\ - [B^* P_c x, B^* P_c x] = 0, \quad x \in \mathcal{D}(A) \end{aligned} \quad (3.4)$$

and

$$\begin{aligned} [P_f x, A^* x] + [A^* x, P_f x] + \sigma_d^2 [B^* x, B^* x] \\ - \frac{1}{2} \frac{\sigma_s^2}{\sigma_s} [B^* P_f x, B^* P_f x] = 0, \quad x \in \mathcal{D}(A^*) \end{aligned} \quad (3.5)$$

* Approximately controllable, see [6, Theorem 4.9.2].

It is easily verified by direct substitution that under the energy inner product

$$P_c = \gamma I \quad \text{and} \quad P_f = \frac{\sigma_s}{\sigma_d} I$$

thus (3.2) and (3.3) become

$$u_o(t) = -\gamma B^* \hat{x}(t) \quad (3.6)$$

$$\dot{\hat{x}}(t) = A\hat{x}(t) + Bu_o(t) + \frac{\sigma_s}{\sigma_d} B[y(t) - B^*\hat{x}(t)], \quad \hat{x}(0) = 0 \quad (3.7)$$

The corresponding minimal cost is

$$J[u_o] = \gamma \left(\frac{\sigma_s}{\sigma_d} \right) \|b\|^2 \left(\gamma + \frac{\sigma_s}{\sigma_d} \right)$$

Remark 3.1. The above solution requires that the steady-state Riccati equations (3.4) and (3.5) have unique positive definite solutions and that $\hat{x}(t)$ be asymptotically stationary. Regarding (3.4) and (3.5), since we have analytical solutions, the only concern is uniqueness and this is guaranteed by (A,B) controllability [8]. The asymptotic stationarity of $\hat{x}(t)$ follows easily through application of [6, Theorem 6.7.1].

Remark 3.2. For more general problems, where for example we replace B in (3.1) with another operator R, which is Hilbert-Schmidt, exponential stabilizability of the system is sufficient to guarantee solutions to the infinite time, stochastic regulator (ITSR) problem [6, Theorem 6.9.1]. However, when compact controls are employed, as is the case here, the system cannot be given a uniform exponential decay rate* unless the open loop system is already uniformly exponentially stable. Note that, here, the open loop system (2.3) is unitary, i.e., $\|T(t)\| = 1$. Hence, the closed loop system can only be strongly stable**.

Remark 3.2. The existence of solutions to the ITSR problem for systems that are only strongly stabilizable is largely an open problem. Recent results concerning strong stability and the steady-state Riccati equation are given in [8], but the sufficient conditions for existence are quite strong, requiring in particular $\|R^*x\| \leq M_1 \|B^*x\|$ for the control problem and $\|F^*x\| \leq M_2 \|Cx\|$ for the filtering problem, where M_1 and M_2 are constants***. One possible physical interpretation of these requirements is that we only attach a performance penalty to those points where we have located actuators and that we locate a sensor at each disturbance source.

* A semigroup $T(t)$ is uniformly exponentially stable if $\exists \omega > 0, M \geq 1 \exists$
 $\|T(t)\| \leq Me^{-\omega t}, t > 0$.

** A semigroup is strongly stable if $\|T(t)x\| \rightarrow 0$ as $t \rightarrow \infty, x \in E$.

***R is the state weighting operator, F is the disturbance input operator, and C is the observation operator.

4.0 OPTIMAL COMPENSATOR

Let $T(t)$ be the C_0 semigroup generated by A . Then, the solution to (3.7) is given by

$$\hat{x}(t) = \int_0^t T(t-\tau) \left\{ Bu(\tau) + \frac{\sigma_s}{\sigma_d} B[y(\tau) - B^* \hat{x}(\tau)] \right\} d\tau \quad (4.1)$$

Using (3.6), we can rewrite (4.1) as

$$\begin{aligned} u(t) &= - \int_0^t B^* T(t-\tau) B \left\{ \gamma u(\tau) + \frac{\sigma_s}{\sigma_d} [\gamma y(\tau) - B^* \hat{x}(\tau)] \right\} d\tau \\ &= - \int_0^t B^* T(t-\tau) B \left\{ \left(\gamma + \frac{\sigma_s}{\sigma_d} \right) u(\tau) + \frac{\gamma \sigma_s}{\sigma_d} y(\tau) \right\} d\tau \end{aligned}$$

Therefore

$$u(t) + k_u \int_0^t B^* T(t-\tau) Bu(\tau) d\tau = -k_y \int_0^t B^* T(t-\tau) By(\tau) d\tau \quad (4.2)$$

where $k_u = \gamma + \sigma_s/\sigma_d$, $k_y = \gamma\sigma_s/\sigma_d$. Observe that (4.2) is a Volterra equation. Define the Volterra operator L as

$$Lf = h ; \int_0^t B^* T(t-\tau) Bf(\tau) d\tau = h(t)$$

Then (4.2) can be written as

$$u + k_u Lu = -k_y Ly \quad (4.3)$$

Solving for u we obtain the optimal compensator in abstract form

$$\begin{aligned} u_c &= -k_y [1 + k_u L]^{-1} Ly \\ &= -k_y [1 + K] Ly \end{aligned} \quad (4.4)$$

where K is also a Volterra operator of the form

$$Kf = h ; \int_0^t K(t,\tau) f(\tau) d\tau = h$$

From [6, p.102-103], $K(t,\tau)$ can be computed iteratively and is given by

$$K(t,\tau) = \sum_{n=1}^{\infty} (-1)^{n+1} g_n(t,\tau) \quad (4.5)$$

where

$$g_n(t,\tau) = g_n(t-\tau) = \int_{\tau}^t g(t-\sigma) g_{n-1}(\sigma-\tau) d\sigma \quad (4.6)$$

$$g_1(t-\tau) = g(t-\tau) = B^* T(t-\tau) B \quad (4.7)$$

Noting that

$$L^n f = \int_0^t g_n(t-\tau) f(\tau) d\tau$$

(4.4) can also be written as

$$\begin{aligned} u_c &= -k_y \left\{ 1 - k_u + k_u^2 L^2 - k_u^3 L^3 + \dots \right\} L y \\ &= -k_y \left\{ \sum_{n=1}^{\infty} (-k_u)^{n-1} L^n \right\} y \end{aligned} \quad (4.8)$$

Since $B^* T(t-\tau) B$ is uniformly continuous and (4.3) is a Volterra equation, the iteration defined by (4.5)-(4.7) and, hence, the series (4.8) converge for $t \in [0, T], \tau \leq t, T < \infty$, [6]. The series (4.8) is sometimes called a Neumann series, [9]. Thus, the optimal compensator is of the form

$$u(t) = -k_y \int_0^t g_0(t-\tau) y(\tau) d\tau \quad (4.9)$$

where the kernel $g_0(t-\tau)$ is given by the bracketed term in (4.8). Note that (4.8) utilizes the infinite dimension system model via (4.7) which is given in terms of the open loop semigroup operator, $T(t)$, and we have a representation for $T(t)$, (2.6), using the modes of $M^{-1}A_0$. In particular, expanding (4.7) on the orthonormal basis for E , as defined in Section 2, gives

$$g(t-\tau) = B^* T(t-\tau) B = \sum_{k=1}^{\infty} b_k^2 \cos \omega_k(t-\tau)$$

where $b_k = [M(M^{-1}b), \phi_{2k}] = [b, \phi_k]$.

Properties of $g(\sigma)$

- i) $g(\sigma) \rightarrow 0$ as $\sigma \rightarrow \infty$
- ii) $g(\sigma)$ is uniformly continuous
- iii) $g(\sigma)$ is compact for each $t \geq 0$.

Condition i) follows since $g(\sigma) = B^* S(\sigma) B$ and $S(\sigma)$ is the C_0 semigroup generated by $A - k_u B B^*$ which is strongly stable. Note that $S(\sigma)$ is also a contraction, i.e., $\|S(\sigma)\| \leq 1$. The second condition results from the strong continuity of $S(\sigma)$. For condition iii), $g(\sigma)$ is compact since B is compact and $S(\sigma)$ is a bounded operator.

5.0 SMALL GAIN APPROXIMATION TO OPTIMAL COMPENSATOR

Using the procedure outlined in Section 4.0, four complete iterations and a partial fifth iteration were performed. This yielded an approximation for the kernel of the optimal filter given by

$$\begin{aligned}
 g_o(\sigma) \approx & \sum_{k=1}^{\infty} b_k^2 \cos \omega_k \sigma \left[1 - \xi_{ck} \sigma + \frac{1}{2} (\xi_{ck} \sigma)^2 - \frac{1}{3!} (\xi_{ck} \sigma)^3 + \frac{1}{4} (\xi_{ck} \sigma)^4 \right] \\
 & - \sum_{k=1}^{\infty} \xi_{ck} b_k^2 \frac{\sin \omega_k \sigma}{\omega_k} \left[1 - \xi_{ck} \sigma + \frac{1}{2} (\xi_{ck} \sigma)^2 - \frac{1}{3!} (\xi_{ck} \sigma)^3 \right] \\
 & - \sum_{k=1}^{\infty} \sum_{\substack{j=1 \\ k \neq j}}^{\infty} \left\{ \Omega_{kj} \frac{b_k^2 \sin \omega_k \sigma}{\omega_k} \left[1 - \xi_{ck} \sigma + \frac{1}{2} (\xi_{ck} \sigma)^2 \right] + \Omega_{jk} \frac{b_j^2 \sin \omega_j \sigma}{\omega_j} \right. \\
 & \left. \cdot \left[1 - \xi_{cj} \sigma + \frac{1}{2} (\xi_{cj} \sigma)^2 \right] \right\} + k_u^2 O_4(k_u; \frac{1}{\omega_k}; \sigma) \tag{5.1}
 \end{aligned}$$

where

$$\xi_{ck} = k_u b_k^2 / 2, \quad \Omega_{kj} = \omega_k^2 b_j^2 / (\omega_k^2 - \omega_j^2), \quad \sigma = t - \tau$$

The remainder term $k_u^2 O_4(k_u; \frac{1}{\omega_k}; \sigma)$ is given in the appendix and is composed of terms of second order or greater in k_u .

It is apparent that the terms in the square brackets in (5.1) are the first few terms of the Taylor series expansion for $\exp(-\xi_{ck} t)$. Thus, the limiting form of the kernel is

$$g_o(\sigma) = \hat{g}_o(\sigma) + k_u^2 O(k_u; \frac{1}{\omega_k}; \sigma) \tag{5.2}$$

where

$$\hat{g}_o(\sigma) = \sum_{k=1}^{\infty} g_{1k}(\sigma) - k_u \sum_{k=1}^{\infty} \sum_{\substack{j=1 \\ k \neq j}}^{\infty} g_{2kj}(\sigma) \tag{5.3}$$

$$g_{1k}(\sigma) = b_k^2 e^{-\xi_{ck} \sigma} \left[\cos \omega_k \sigma - \xi_{ck} \frac{\sin \omega_k \sigma}{\omega_k} \right]$$

$$g_{2kj}(\sigma) = \Omega_{kj} b_k^2 e^{-\xi_{ck} \sigma} \left(\frac{\sin \omega_k \sigma}{\omega_k} \right) + \Omega_{jk} b_j^2 e^{-\xi_{cj} \sigma} \left(\frac{\sin \omega_j \sigma}{\omega_j} \right) \tag{5.5}$$

Note that the component filters $g_{1k}(\sigma)$ have second order dynamics while the filters $g_{2kj}(\sigma)$ have fourth order dynamics. Also, all the parameters in $g_{1k}(\sigma)$ are

related to the k th open loop mode, while $g_{2kj}(\sigma)$ is related to the cross-coupling between the k th and j th modes. Due to the presence of the factors $1/\omega_k$ and $1/\omega_j$ in $g_{2kj}(\sigma)$, the cross-coupling terms are attenuated relative to the "diagonal" terms $g_{1k}(t-\tau)$ as ω_k and ω_j become large. Thus, at high frequencies the dominant filter dynamics are due to the diagonal terms $g_{1k}(\sigma)$. Since the iteration converges and since $g_o(\sigma)$ and $\hat{g}_o(\sigma)$ are continuous in σ , $k_u^2 |0(k_u; 1/\omega_k; \sigma)|$ is continuous in σ . Also $k_u^2 |0(k_u; 1/\omega_k; \sigma)| \rightarrow 0$ as $k_u \rightarrow 0$ for each $\sigma \in [0, T]$. Therefore, for any $\epsilon > 0$, we can find k_u sufficiently small such that

$$\max_{0 < t < T} |k_u^2 |0(k_u; \frac{1}{\omega_k}; \sigma)| < \epsilon$$

The argument $1/\omega_k$ is used to indicate that $|0(k_u; 1/\omega_k; \sigma)| \rightarrow 0$ as $\omega_k \rightarrow \infty$. Therefore, assuming k_u is small, the approximate optimal control is given by

$$\begin{aligned} \hat{u}(t) &= -k_y \int_0^t \hat{g}_o(t-\tau) y(\tau) d\tau \\ &= -k_y \sum_{k=1}^{\infty} \int_0^t g_{1k}(t-\tau) y(\tau) d\tau + k_y k_u \sum_{k=1}^{\infty} \sum_{\substack{j=1 \\ k \neq j}}^{\infty} \int_0^t g_{2kj}(t-\tau) y(\tau) d\tau \end{aligned} \quad (5.6)$$

Since k_y and k_u are both small, as crude first approximation, the double summation in (5.6) could be neglected. In this case, the filter takes a particularly simple form, namely,

$$\hat{u}(t) = \sum_{k=1}^{\infty} \hat{u}_k(t) \quad (5.7)$$

where

$$\hat{u}_k(t) = -k_y \int_0^t g_{1k}(t-\tau) y(\tau) d\tau$$

Here, the basic structure of the compensator is an infinite bank of second order filters, each operating on the sensor output and the control is simply the sum of their outputs. The component filters $g_{1k}(t-\tau)$ in this case have a rather special property. Letting $G_{1k}(s)$ denote the Laplace Transform of $g_{1k}(t-\tau)$, we have

$$G_{1k}(s) = \frac{b_k^2 s^2}{s^2 + 2\xi_{ck} s + \xi_{ck}^2 + \omega_k^2}$$

Such a filter is strictly positive real, [11], [12]. Note that the phase shift of the filter never exceeds $\pm\pi/2$. According to [13], strictly positive real filters have robust stability properties in the sense that they will stabilize any

positive real system (in an input/output sense). The system considered here is positive real since it is an undamped oscillator. Note that any finite sum of positive real filters is also positive real. Therefore, we can truncate the summation (5.7) at any finite number of terms and the compensator will still stabilize the system. It would be expected that the more terms retained in the summation the closer the resulting performance would be to the optimal performance.

Returning to the filter defined by (5.6) another approximation will be obtained. First, consider the Laplace Transform of $k_u g_{2kj}(t)$ given by

$$k_u G_{2kj}(s) = k_u \left[\frac{b_k^2 \Omega_{kj}}{(s + \xi_{ck})^2 + \omega_j^2} + \frac{b_j^2 \Omega_{jk}}{(s + \xi_{cj})^2 + \omega_k^2} \right]$$

Using the definitions of ξ_{ck} , Ω_{kj} , etc, this becomes

$$k_u G_{2kj}(s) = k_u \frac{b_k^2 b_j^2 \left\{ (\omega_k^2 - \omega_j^2) s^2 + 2k_u (\omega_k^2 b_j^2 - \omega_j^2 b_k^2) + k_u^2 (\omega_k^2 b_j^4 - \omega_j^2 b_k^4) / 4 \right\}}{(\omega_k^2 - \omega_j^2) \left[\left(s + \frac{k_u b_k^2}{2} \right)^2 + \omega_k^2 \right] \left[\left(s + \frac{k_u b_j^2}{2} \right)^2 + \omega_j^2 \right]}$$

Dropping all terms second order or greater in k_u gives

$$k_u G_{2kj}(s) \approx k_u \frac{b_k^2 b_j^2 s^2}{(s^2 + k_u b_k^2 s + \omega_k^2) (s^2 + k_u b_j^2 s + \omega_j^2)} \approx k_u G_{1k}(s) G_{1j}(s) \quad (5.8)$$

where $G_{1k}(s)$ is the Laplace Transform of $g_{1k}(t)$ (neglecting ξ_{ck}^2 , ξ_{cs}^2 in the denominator). Thus the Laplace Transform of the compensator is

$$G_o(s) = -k_y \sum_{k=1}^{\infty} \frac{b_k^2 s}{s^2 + k_u b_k^2 s + \omega_k^2} + k_u k_y \sum_{k=1}^{\infty} \sum_{\substack{j=1 \\ k \neq j}}^{\infty} \frac{b_k^2 b_j^2 s^2}{(s^2 + k_u b_k^2 s + \omega_k^2) (s^2 + k_u b_j^2 s + \omega_j^2)} \quad (5.9)$$

In the time domain, the approximation to the optimal control is now given by

$$\hat{u}(t) = -k_y \sum_{k=1}^{\infty} \int_0^t g_{1k}(t-\tau) y(\tau) d\tau + k_y k_u \sum_{k=1}^{\infty} \sum_{\substack{j=1 \\ k \neq j}}^{\infty} \int_0^t \left\{ \int_{\tau}^t g_{1k}(t-\sigma) g_{1j}(\sigma-\tau) d\sigma \right\} y(\tau) d\tau \quad (5.10)$$

This representation is interesting in that the basic building blocks of the filter are the positive real component filter $g_{1k}(t-\tau)$. Note, however, that the convolutions

$$g_{3kj}(t, \tau) = \int_{\tau}^t g_{1k}(t-\sigma) g_{1j}(\sigma-\tau) d\sigma$$

or, equivalently, the products

$$G_{3kj}(s) = G_{1k}(s) G_{1j}(s)$$

are not positive real. However, since the diagonal terms dominate at high frequencies, the high frequency component filters approach a positive real form. Since we would expect a close (finite dimensional) approximation to the optimal filter to stabilize the system, it is interesting that the limiting structure is positive real, i.e., a structure that is compatible with truncation.

6.0 CONCLUSIONS

It has been shown that the optimal compensator can be represented in terms of a kernel of an integral operator. The results demonstrate that the integral representation provides considerable insight into the structure of the compensator. This is due to the compensator being compact and, hence, something that is inherently approximatable by a finite dimensional operator, i.e., the compensator parameters go to zero as $k \rightarrow \infty$. For the system considered here, the optimal filter can be constructed of basic building blocks which are second order positive real filters. The first (low gain) approximation is a diagonal array of these component filters and there is a one to one correspondence with the open loop modes. The second (low gain) approximation adds in the cross-coupling effects in the form of fourth order filters which are convolutions between the various component filters taken two at a time. At high frequencies, the dynamics of the compensator approach the diagonal form of the first approximation which should have advantages when the filter dynamics are truncated in order to obtain a finite dimensional approximation for the compensator. The results also seem to suggest that higher gains will require increasingly higher order convolutions of the component filters.

ACKNOWLEDGEMENT

The author would like to thank Professor A.V. Balakrishnan for suggesting the research problem considered here and for many useful discussions relating to this work.

APPENDIX

The following defines $O_4(k_u; t)$, the remainder term for the optimal compensator, after four complete iterations and part of a fifth iteration:

$$\begin{aligned}
O_4(k_u; \frac{1}{\omega_k}; t) = & \left\{ \sum_{k=1}^{\infty} \frac{b_k^6 t \sin \omega_k t}{8\omega_k} \left[1 - \xi_{ck} t + \frac{1}{2}(\xi_{ck} t)^2 \right] \right. \\
& + \sum_{k \neq j} \sum \left[\frac{\Omega_{kj} b_k^2 \sin \omega_k t}{\omega_k} \left(c_1(k, j) + \frac{tb_k^4}{8}(1 - \xi_{ck} t) \right) + \frac{\Omega_{jk} b_j^2 \sin \omega_j t}{\omega_j} \right. \\
& \cdot \left. \left(c_1(j, k) + \frac{tb_j^4}{8}(1 - \xi_{ck} t) \right) \right] + \sum_{k \neq j} b_k^2 b_j^2 [(c_2(k, j) + k_u c_3(k, j) t) \cos \omega_k t \\
& + (c_2(j, k) + k_u c_3(j, k) t) \cos \omega_j t] - \sum_{k \neq j \neq i} b_k^2 b_j^2 b_i^2 [(c_4(k, j, i) + k_u c_5(k, j, i) t) \\
& \cdot \cos \omega_k t + (c_4(j, k, i) + k_u c_5(j, k, i) t) \cos \omega_j t + (c_4(i, j, k) + k_u c_5(i, j, k)) \cos \omega_i t] \\
& + k_u \left\{ \sum_{k=1}^{\infty} \frac{b_k^8 t \cos \omega_k t}{8\omega_k} - \frac{b_k^2 \sin \omega_k t}{12\omega_k^2} - \sum_{k \neq j \neq i} b_k^2 b_j^2 b_i^2 [c_6(k, j, i) \sin \omega_k t \right. \\
& + c_6(j, k, i) \sin \omega_j t + c_6(i, j, k) \sin \omega_i t] - \sum_{k \neq j \neq i \neq l} b_k^2 b_j^2 b_i^2 b_l^2 [c_7(k, j, i, l) \sin \omega_k t \\
& + c_7(j, k, i, l) \sin \omega_j t + c_7(i, j, k, l) \sin \omega_i t + c_7(l, j, i, k) \sin \omega_l t] \left. \right\}
\end{aligned}$$

where

$$c_1(k, j) = \frac{2}{(\omega_k^2 - \omega_j^2)^2} \left[b_j^4 \omega_k^2 + \frac{\omega_j^4 b_k^4}{\omega_k^2} - \frac{3b_j^2 b_k^2 \omega_j^2}{\omega_k^2} \right] - \frac{2}{\omega_k^2 - \omega_j^2} \left[\frac{(\omega_k^2 - 2\omega_j^2) b_k^4}{\omega_k^2} + \frac{3b_j^2}{4} \right] + \frac{3b_k^4}{4\omega_k^3}$$

$$c_2(k, j) = \frac{3}{2(\omega_k^2 - \omega_j^2)^2} (\omega_j^2 b_k^2 - \omega_k^2 b_j^2)$$

$$c_3(k, j) = \frac{1}{(\omega_k^2 - \omega_j^2)^2} \left[2(\omega_k^2 - 2\omega_j^2) b_k^4 + \frac{\omega_k^2 b_k^2 b_j^2}{2} \right] - \frac{3b_k^4}{\omega_k^2 - \omega_j^2}$$

$$c_4(k, j) = \frac{\omega_k^2 b_k^2}{(\omega_j^2 - \omega_k^2)(\omega_i^2 - \omega_k^2)}, \quad c_5(k, j, i) = \frac{\omega_k^2 b_k^2}{(\omega_i^2 - \omega_k^2)(\omega_j^2 - \omega_i^2)}$$

$$c_6(k, j, i) = \frac{1}{(\omega_j^2 - \omega_k^2)(\omega_i^2 - \omega_k^2)} \left[4\omega_k^3 b_i^2 + \frac{2(\omega_k^3(\omega_i^2 + \omega_j^2) - 2\omega_k \omega_j^2 \omega_i^2) b_k^2}{(\omega_j^2 - \omega_k^2)} + \omega_k b_k^2 \right]$$

$$c_7(k, j, i, \ell) = \frac{\omega_k^3}{(\omega_i^2 - \omega_k^2)(\omega_j^2 - \omega_k^2)(\omega_\ell^2 - \omega_k^2)}$$

$$\xi_{ck} = k_u b_k^2 / 2, \quad \xi_{kj} = \omega_k^2 b_j^2 / \omega_k^2 - \omega_j^2$$

REFERENCES

1. Larson, V., Likins, P., and Marsh, E., "Optimal Estimation and Attitude Control of a Solar Electric Propulsion Spacecraft," IEEE Trans. Aerosp. Electron. Syst., Vol AES-13, Jan 1977, pp 35-47.
2. Skelton, R.E., "On Cost-Sensitivity Controller Design Methods for Uncertain Dynamic Systems," J. of Astronautical Sciences," Vol. XXVII, No.2, Apr-Jun 1979, pp 181-205.
3. Skelton, R.E., "Cost Decomposition of Linear Systems with Application to Model Reduction," Int. J. Control, Vol. 32, No. 6, 1980, pp 1031-1055.
4. Hablani, H., "Dynamics and Control of a Large Two-Dimensional Flexible Spacecraft," Purdue Res. Foundation, School of Aeronautics and Astronautics, Contract No. 955369, August 1980.
6. Kato, T., Perturbation Theory for Linear Operators, Springer-Verlag, New York, 1966.
6. Balakrishnan, A.V., "Applied Functional Analysis," Second Edition, Springer-Verlag, New York, 1981.
7. Gibson, J.S., "A Note on Stabilization of Infinite Dimensional Linear Oscillators by Compact Linear Feedback," SIAM J. Control and Optimization, Vol. 18, No. 3, May 1980.
8. Balakrishnan, A.V., "Strong Stability and the Steady-State Riccati Equation," Appl. Math. Optim. 7, 1981, pp 335-345.
9. Courant, R., and Hilbert, D., Methods of Mathematical Physics, Vol. I, Interscience, New York, 1953.
10. Anderson, B.D.O., "A System Theory Criterion for Positive Real Matrices," SIAM Journal on Control, Vol. 5, No. 2, May 1967, pp 171-182.
11. Anderson, B.D.O., "A Simplified View of Hyperstability," IEEE Trans. Auto. Control, Vol. AC-13, No. 3, June 1968, pp 292-294.
12. Benhabib, R.J., Iwens, R.P., and Jackson, R.L., "Stability of Large Space Structure Control Systems Using Positivity Concepts," J. Guidance and Control, Vol. 4, No. 5, Sept-Oct, 1981.

This Page Intentionally Left Blank

ANALYSIS OF STRUCTURAL PERTURBATIONS IN SYSTEMS VIA COST DECOMPOSITION METHODS

Robert E. Skelton

School of Aeronautics and Astronautics, Purdue University
West Lafayette, IN 47907

Abstract

It has long been common practice to analyze linear dynamic systems by decomposing the total response in terms of individual contributions which are easier to analyze. Examples of this philosophy include the expansion of transfer functions using: (i) the superposition principle, (ii) residue theory and partial fraction expansions, (iii) Markov parameters, Hankel matrices, and (iv) regular and singular perturbations. This paper summarizes a new and different kind of expansion designed to decompose the norm of the response vector rather than the response vector itself. This is referred to as "cost-decomposition" of the system. The notable advantages of this type of decomposition are: (a) easy application to multi-input, multi-output systems, (b) natural compatibility with Linear Quadratic Gaussian Theory, (c) applicability to the analysis of more general types of structural perturbations involving inputs, outputs, states, parameters. Property (c) makes the method suitable for problems in model reduction, measurement/actuator selections, and sensitivity analysis.

1.0 Introduction

For many reasons it is convenient and often necessary to characterize dynamic system behavior in terms of an expansion of the system response into terms which are individually easier to analyze than the total response. For example, it is common practice in the study of linear systems to take advantage of the superposition principle to separately analyze the effect of each input u_j on each output y_i of the system,

$$y_i(s) = \sum_{j=1}^m G_{ij}(s) u_j(s) \quad (1.1)$$

or to analyze the contribution of each mode of the system by using the partial fraction expansion

$$y(s) = G(s) u(s) = \sum_{i=1}^n \frac{R_i}{s - \lambda_i} u(s) \quad (1.2)$$

In lieu of poles and residues the expansion can take on many other forms including the use of Markov parameters, Hankel matrices, and various other moments. In time domain analysis, $y(t)$ may be expanded in the power series form

$$y(t) = \sum_{n=0}^{\infty} \epsilon^n y_n(t) \quad (1.3)$$

where ϵ is a small parameter in the system and $y_n(t)$, $n = 0, 1, \dots$, constitute the n^{th} order approximations of $y(t)$ in perturbation analysis. The regular and singular perturbation analysis (1.3) has been developed extensively in both open-loop and closed-loop problems embracing both linear and nonlinear systems [1]-[2]. In the presence of structural perturbations in the state (singular perturbations) the expansions of the form (3) can be readily employed to predict the perturbed behavior, whereas (1.2) is useful only if the structural perturbations occur in *modal* coordinates. Other types of structural perturbations occur if the number of inputs or outputs change. The effects of these input or output perturbations can be approximated by expansion (1.1) or (1.3).

The purpose of this paper is to investigate a different kind of expansion of the response y in the analysis of dynamic systems subject to all types of structural perturbations; state, input, output. This expansion is called a "cost decomposition" since it involves expansion of a *scalar* function of the output y , denoted by the inner product

$$V \triangleq \langle y, y \rangle = \sum_{i=1}^n V_i \quad (1.4)$$

where V_i are the "component costs" denoting the contribution of the i^{th} system "component" in the overall performance metric V . The motivation for the decomposition of the scalar (1.4) is that

- (a) the overall system performance metric is often characterized in a quadratic form and the expansion (1.4) allows one to determine the relative significance of the components of the system. This relative significance is easily established by comparing the scalars $V_1 \geq V_2 \geq \dots$, etc.

(b) the component costs V_i provide information which can be used to advantage in these problems:

1. Model Reduction
2. Construction of Reduced Controllers
3. Construction of Reduced Estimators
4. Sensor/Actuator Selection
5. Parameter Sensitivity Analysis (determining "critical" parameters)

This paper shows how to exploit cost decomposition methods (4) to generate suboptimal solutions to problems 1-4.

The paper is organized as follows. Section 2.0 describes cost decomposition procedures for determining "component costs," "input costs," and "output costs." Section 3.0 applies these ideas to model reduction. Section 4.0 applies these ideas to controller reduction. Section 5.0 applies these ideas to sensor/actuator selection. Some concluding remarks appear in Section 6.0.

All of the ideas in this paper can be (some have been) extended to time-varying plants with finite time performance metrics. However, in the interest of brevity only the stationary, infinite time results will be presented.

2.0 Cost-Decomposition

Consider the linear system

$$\begin{aligned} \dot{x} &= Ax + Dw & x \in R^{n_x}, \quad w \in R^{n_w} \\ y &= Cx & y \in R^{n_y} \end{aligned} \quad (2.1)$$

where the matrix pair (A,D) is controllable and the matrix pair (A,C) is observable. The input $w(t)$ is a zero-mean white noise with intensity $W(Ew(t))=0, Ew(t)w^T(\tau) = W\delta(t-\tau)$. The model (2.1) exists for the purpose of accurately describing the outputs, y_1, \dots, y_{n_y} . Therefore, a suitable measure by which to quantize the performance of (2.1) is

$$V \triangleq \lim_{t \rightarrow \infty} E \|y\|_Q^2, \quad \|y\|_Q^2 \triangleq y^T Q y \quad (2.2)$$

The matrix Q weights the outputs according to their importance in the performance criteria.

It is of interest to know how sub-state $x_i \in R^{n_i}$ contributes to the cost function V .

The "component costs" V_i associated with components $x_i, i=1, \dots, n$ of the state vector must represent the contribution of x_i in V in such a way that the sum of all the "component costs" V_i equals the total system cost V .

$$V = \sum_{i=1}^n V_i, \quad n_x = \sum_{i=1}^n n_i \quad (2.3)$$

For linear systems (2.1) with quadratic costs (2.2) this V_i qualifies as a component cost definition,

$$V_i \triangleq \lim_{t \rightarrow \infty} E \left(\frac{\partial \|y\|_Q^2}{\partial x_i} x_i \right) \quad (2.4)$$

This definition of component cost V_i reduces to the calculation [4]

$$V_i = \text{tr}[XC^TQC]_{ii}, \quad [XC^TQC]_{ii} \in R^{n_i \times n_i} \quad (2.5a)$$

$$0 = XA^T + AX + DWD^T \quad (2.5b)$$

where the "cost decomposition" property (2.3) holds.

It will also be of interest in Section 5 to know how each input w_i and each out y_i contribute to the cost function V .

The input costs V_i^I ("output costs" V_i^O) associated with $w_i, i=1, \dots, n_w (y_i, i=1, \dots, n_y)$ must represent the contribution of $w_i (y_i)$ in V in such a way that the sum of the "input-costs" V_i^I ("output costs" V_i^O) equals the total system cost V .

$$V = \sum_{i=1}^{n_w} V_i^I \quad (2.6)$$

$$V = \sum_{i=1}^{n_y} V_i^O \quad (2.7)$$

For linear systems (2.1) with quadratic costs (2.2) this $V_i^I(V_i^O)$ qualifies as an "input cost," "output cost" definition,

$$V_i^I \triangleq \lim_{t \rightarrow \infty} E \left(\frac{\partial \|y\|_Q^2}{\partial w_i} w_i \right) \quad (2.8)$$

$$V_i^O \triangleq \lim_{t \rightarrow \infty} E \left(\frac{\partial \|y\|_Q^2}{\partial y_i} y_i \right) \quad (2.9)$$

These definitions reduce to the calculations

$$V_i^I = \text{tr}[D^T K D W]_{ii} \quad (2.10a)$$

$$0 = K A + A^T K + C^T Q C \quad , \quad (2.10b)$$

$$V_i^O = [C X C^T Q]_{ii} \quad (2.11a)$$

$$0 = X A^T + A X + D W D^T \quad . \quad (2.11b)$$

where the cost-decomposition properties (2.6), (2.7) of V_i^I and V_i^O hold.

The component cost V_i , the input cost V_i^I , and the output cost V_i^O quantize the "value" of the state x_i , the input w_i , or the output y_i while all components, inputs, and outputs are in-place and interacting. Indeed, the very definition of a dynamic system is described in terms of "interconnected components casually related in time." It is only natural, then to describe the total system behavior in terms of the contributions from each of the individual components. Component Cost Analysis (CCA) serves this purpose and, as such, it should be interpreted as a *diagnostic* tool to gain insight into system behavior.

If $V_i > V_j$ for all $j \neq i$, then the i^{th} component is the critical performance limiting component. This component might be redesigned to be less dominant in the system performance. Such a "cost-balancing" strategy for system design is under consideration. The critical components from CCA also suggest which components should be made more reliable for minimizing the performance degradation in the presence of the "most-likely" component failure.

The next Section 3.0 will exploit (2.5) in its application to the model reduction problem.

3.0 Application of CCA to Model Reduction

In Section 2.0 it was shown that V_i represents the *in situ* value of x_i in the cost V . Component costs (2.5) may be computed in physical or any other coordinates. If a component x_i is *deleted* from (2.1), the cost V will *not* generally be perturbed by amount V_i . It will be of interest, therefore, to know in what coordinates the cost perturbation is V_i . In other words, when do the V_i satisfy the "cost-superposition" property

$$V_R = \sum_{i=1}^r V_i \quad (3.1)$$

where V_R is the value of V with $n-r$ components *deleted* from the system (2.1).

Definition 1:

Components x_i , $i=1, \dots, n$ which satisfy the cost-superposition property (3.1) for all $1 \leq r \leq n$ are said to be "cost-decoupled components."

Cost-decoupled components are of obvious interest in model reduction problems since the exact perturbation of V resulting from the truncation of $n-r$ components can be predicted *a priori*. There are many cost-decoupled components. Three different choices will be discussed in what follows.

3.1 Modal Cost Analysis

A "component" x_i is called a "coordinate" when $n_i=1$. Let A be diagonal in (2.1). Then x_i , $n_i=1$, $i=1, \dots, n$ are *modal* coordinates. The corresponding component cost analysis (2.5) is then referred to as Modal Cost Analysis (MCA) and the following results are known [3]-[6].

Theorem 1:

If A is diagonal in (2.5) and if either (i), (ii), or (iii) hold

- (i) $d_i^* W d_j = 0$, $i \neq j$, $D^* = [d_1, \dots, d_{n_x}]$
- (ii) $c_i^* Q c_j = 0$, $i \neq j$, $C = [c_1, \dots, c_{n_x}]$
- (iii) $-\text{Re } \lambda_i / \text{Im } \lambda_i < \epsilon$, ϵ arbitrarily small > 0

then

$$V_i = \frac{\|c_i\|_Q^2 \|d_i\|_W^2}{-\text{Re } \lambda_i} \quad (3.2)$$

Theorem 2: Modal Cost Analysis of Lightly Damped Systems

If the system of interest is described by the modal coordinates of a matrix-second order system

$$\ddot{n}_i + 2\zeta_i \omega_i \dot{n}_i + \omega_i^2 n_i = d_i^T W \quad , \quad i=1, \dots, N \quad (3.3)$$

$$y = \sum_{i=1}^N (p_i n_i + p_i' \dot{n}_i)$$

then the modal costs associated with the overall cost (2.2) are

$$V_i = \frac{(\|p_i\|_Q^2 + \omega_i^2 \|p_i'\|_Q^2) \|d_i\|_W^2}{\zeta_i \omega_i^3} \quad , \quad i=1, \dots, N \quad (3.4)$$

where the equality holds in (3.4) if (1) $d_i^T W d_j = 0$, $i \neq j$, or if (ii) $p_i^T Q p_j + p_i'^T Q p_j' = 0$, $i \neq j$, or (iii) in the limit as $\zeta_i \rightarrow 0$.

The formulas (3.2) or (3.4) are useful in determining critical modes of the special class of systems satisfying either (i), (ii), or (iii). Otherwise, numerical solutions of (2.5) are required to compute the modal costs. Both coordinates described by Theorems 1 and 2 are "cost-decoupled" in the sense of Def. 1. As a result, those r modes which should be deleted in order to minimize the cost perturbation

$$\Delta V = V - V_R \quad (3.5)$$

are indicated by the r smallest values of the modal costs V_i .

The use of Modal Cost Analysis for reduced order modeling of large space structures is discussed in [7], [8]. The use of Modal Cost Analysis for diagnosing matrix-second-order systems is presented in [9]. It is clear from (3.2) and (3.4) that the modal cost V_i is the product of three properties of a mode: the weighted observability $\|c_i\|_Q^2$, the weighted disturbability $\|d_i\|_W^2$, and the time constant $-1/\text{Re } \lambda_i$.

3.2 Cost-Equivalent Realizations

Another important set of coordinates which possess the cost-superposition property (3.1) is presented in this section. In this set of coordinates, derived in [10], the matrix $X C^T Q C$ is diagonal. Hence, in these coordinates

$$X C^T Q C = \begin{bmatrix} V_1 & & 0 \\ & \ddots & \\ 0 & & V_{n_x} \end{bmatrix} \quad (3.6)$$

Theorem 3: Coordinates which satisfy (3.6) are "cost-decoupled" in the sense of definition 1.

Now in order to reduce the model (2.1) so as to make the smallest possible perturbation in the cost V , one can rely on Theorem 3 to obtain the following result, [4].

Theorem 4:

Suppose the coordinates of (2.1) are arranged so that (3.6) holds with $V_1 \geq V_2 \geq \dots \geq V_{n_x}$. The reduced model of order r which minimizes (3.5) is obtained by deleting the last $n_x - r$ states in (2.1), and the resulting cost perturbation is equal to

$$\Delta V = \sum_{i=r+1}^{n_x} V_i \quad (3.7)$$

Assume that C in (2.1) has rank $[C] = n_y$, and that $Q > 0$, $W > 0$. Then, by assumption of controllability of (A,D) , (2.5b) has a positive definite solution $X > 0$. The assumption of stable A is added to ensure that X is bounded from above. (However, CCA is not limited to the analysis of stable systems, [12]). Under these conditions, the matrix $XCTQC$ in (3.6) has rank n_y . Hence, $n_x - n_y$ of the v_i in (3.6) are zero. This leads to the following result, [10].

Corollary to Theorem 4:

Let

$$\begin{aligned} \dot{x}_R &= A_R x_R + D_r w & x_R \in R^r \\ y_R &= C_R x_R \end{aligned} \quad (3.8)$$

represent the reduced order model obtained by truncating the last $n_x - r$ states of (2.1). Then if A_R is stable, (3.8) is a "cost-equivalent" realization of (2.1) (in the sense that $\Delta V = 0$) if $r \geq n_y$.

It remains to be shown whether A_R is stable. For this task a particular set of coordinates are described which yield (3.6). Define Ω by the Cholesky square root of X° ,

$$X^\circ = \Omega \Omega^T \quad (3.9)$$

and θ as the orthonormal matrix of eigenvectors of $\Omega^T C^\circ T Q C^\circ \Omega$. Hence, the transformation of the original states x° having parameters $\{A^\circ, C^\circ, D^\circ, X^\circ\}$ by $x^\circ = \Omega \theta x$ yields

$$X = \Omega^{-1} X^\circ \Omega^{-T} = I \quad (3.10)$$

$$C^T Q C = \theta^T \Omega^T C^\circ T Q C^\circ \Omega \theta = \begin{bmatrix} v_1 & & \\ & \ddots & \\ & & v_{n_x} \end{bmatrix} \quad (3.11)$$

$$v_1 \geq v_2 \geq \dots \geq v_{n_x}$$

Hence, (3.6) is satisfied and the states x_i qualify as cost-decoupled coordinates. In these coordinates the last $n_x - r$ states are deleted to form the reduced order model (3.8). The following is known concerning the cost-decoupled coordinates described by (3.10), (3.11) and the resulting reduced order model (3.8) of order r .

Theorem 5:

The cost-decoupled coordinates described by (3.10), (3.11), and the reduced model (3.8) have the following properties [12].

- (a) $v_i \geq 0$ for all $i=1, \dots, n$
- (b) $\text{Re} \lambda_i[A_R] \leq 0$ if $r \geq n_y$
- (c) $\text{Re} \lambda_i[A_R] < 0 \iff (A_R, D_R)$ controllable
- (d) $\Delta V = \sum_{i=r+1}^{n_x} v_i$
- (e) ΔV is minimized by (3.8) for any given r
- (f) $\Delta V = 0$ if $r \geq n_y$ and (c) holds
- (g) $\lim_{t \rightarrow \infty} E y(t) y^T(t) = \lim_{t \rightarrow \infty} E y_R(t) y_R^T(t)$.

Property (f) gives the conditions under which (3.8) is a "cost-equivalent realization" (CER) of (2.1). This result shows that Kalman's minimal realization is not necessarily minimal with respect to cost functions. That is, if the pair (A,D) is controllable and (A,C) is disturbable then (2.1) is minimal in the sense of Kalman. However, (3.8) can be a lower order equivalent realization of (2.1) in the sense of equivalent cost $V = V_R$. According to the examples given in [4], the order of CER (3.8) is usually $r = n_y$. There is a known exception, however.

Theorem 6 [12]:

The CER is of order $r > n_y$ if the first Markov parameter of (2.1) is zero ($CD=0$).

A "stochastic equivalent realization" (SER) is defined in [13] as any realization which matches the first two moments of the output $y(t)$:

$$E y(t) = E y_R(t) \quad , \quad E y(t) y^T(t) = E y_R(t) y_R^T(t). \quad (3.12)$$

The CER has been compared to the SER of Anderson. The significant results are these.

Theorem 7:

Let

$$G(s) = C(sI-A)^{-1}D \quad (3.13)$$

describe the transfer matrix for (2.1) and let

$$G_R(s) = C_R(sI-A_R)^{-1}D_R \quad (3.14)$$

describe the transfer matrix for (3.8). Eq. (3.8) describes an SER of (2.1) if $G(s)$ can be factored into the form

$$G(s) = G_R(s) U(s) \quad (3.15)$$

where $U(s)$ describes an "all-pass" network

$$U(j\omega) W U^*(j\omega) = W \quad (3.16)$$

and any SER is also a CER. For all single-input single-output systems the minimal order SER and CER are the same.

The SER can be of lower order than Kalman's minimal realization, and the CER can be of lower order than the SER (except for single-input, single-output systems). The price paid for this advantage is that the CER matches only the cost ($V = V_R$) and steady state covariance (property (g) of Theorem 5), whereas the SER matches the cost ($V = V_R$) and the covariance for all time (3.12).

The weighting matrix Q in (2.2) often contains some arbitrariness. It is appropriate to ask, therefore, whether the component cost V_i is highly sensitive to the choice of Q or the choice of C in (2.1), (2.2). This sensitivity result is summarized as follows.

Theorem 8:

There is no choice of coordinates which yields a smaller value of the sensitivity $\left| \left| \frac{\partial V_i}{\partial C^T Q C} \right| \right|$, than the cost-decoupled coordinates satisfying (3.10), (3.11).

Proof:

The proof relies on a result from [14] which states that

$$\left| \left| \frac{\partial \lambda_i}{\partial \psi} \right| \right| \geq 1$$

if λ_i is an eigenvalue of ψ and that

$$\left| \left| \frac{\partial \lambda_i}{\partial \psi} \right| \right| = 1$$

if $\psi = \psi^T$. The proof is concluded by noting from (3.11) that V_i is the i^{th} eigenvalue of $C^T Q C$ and that $C^T Q C$ is symmetric.

It may be observed that the entire set of cost decoupled coordinates as defined by (3.6) does not have the minimum sensitivity result of Theorem 8, since (a) V_i is an eigenvalue of $X C^T Q C$ in general, and (b) V_i is an eigenvalue of $X C^T Q C$ which is not generally symmetric, as it is with the choice of (3.10), (3.11).

The cost-decoupled coordinates defined by (3.10), (3.11) are not unique when $n_v \triangleq \text{rank } [C] < n$. In this (usual) case there is some degree of flexibility in the choice of $n-k$ coordinates. The coordinates are arranged in [15] to place the states x_i , $i > k$ in order of their degree of observability in y . (It has already been established from Theorem 4 that the CER truncates some observable subspaces.) The details are described in [15], and the resulting form of the modified cost-decoupled coordinates is

$$\begin{pmatrix} \dot{x}_1 \\ \dot{x}_2 \\ \vdots \\ \dot{x}_p \end{pmatrix} = \begin{bmatrix} A_{11} & A_{12} & 0 & \dots & 0 \\ A_{21} & A_{22} & A_{23} & & 0 \\ & \ddots & \ddots & \ddots & \vdots \\ & & & A_{p-1,p} & \\ A_{p1} & A_{p2} & A_{p3} & & A_{pp} \end{bmatrix} \begin{pmatrix} x_1 \\ x_2 \\ \vdots \\ x_p \end{pmatrix} + \begin{pmatrix} D_1 \\ D_2 \\ \vdots \\ D_p \end{pmatrix} w \quad (3.17)$$

$$y = [C_1 \quad 0 \quad 0 \quad 0] x$$

where $A_{11} \in \mathbb{R}^{n_y \times n_y}$, and

$$\|A_{12}\| \geq \|A_{23}\| \geq \dots \geq \|A_{p-1,p}\| \quad (3.18)$$

The representation (3.17) is similar in structure to the Generalized Hessenberg Representation (GHR) of [16] with these notable *differences*:

- (i) C_1 in (3.17) is not identity
- (ii) the transformations leading to (3.17) involve the matrices Ω, θ in (3.10), (3.11), as described in [15].

Thus, if a CER is desired of any specified order $r \geq n_y$, the choice for $r = n_y$ does *not* involve the modified representation (3.17), whereas for the choice $r > n_y$ the representation (3.17) is useful. In this later case, the CER will have one property in *addition* to cost equivalence ($V = V_R$): it will retain those substates $\{x_i, i > k\}$ which, among the zero cost states ($V_i = 0$), are most observable in the sense of (3.18).

4.0 Controller Reduction

Controller reduction using Component Cost Analysis (CCA) is based upon participation of the optimal controller states in the cost function

$$V = \lim_{t \rightarrow \infty} E(\|y\|_Q^2 + \|u\|_R^2) \quad (4.1)$$

The optimal controller for

$$\begin{aligned} \dot{\hat{x}} &= A\hat{x} + Bu + Dw \\ y &= Cx \\ z &= Mx + v, \quad Ev = 0, \quad Ev(t)^T(\tau) = V\delta(t-\tau) \end{aligned} \quad (4.2)$$

is described by

$$\begin{aligned} \dot{\hat{x}} &= (A + BG - FM)\hat{x} + Fz \\ u &= G\hat{x} \end{aligned} \quad (4.3a)$$

where

$$G = -R^{-1}B^TK, \quad 0 = KA + A^TK - KBR^{-1}B^TK + C^TQC, \quad (4.3b)$$

$$F = PM^TV^{-1}, \quad 0 = PA^T + AP - PM^TV^{-1}MP + DWD^T. \quad (4.3c)$$

Now delete a subset of the states of (4.2) to obtain the reduced controller of dimension r

$$\begin{aligned} \dot{\hat{x}}_R &= (A + BG - FM)_R \hat{x}_R + F_R z, \quad (A + BG - FM)_R = (A_R + B_R G_R - F_R M_R) \\ u_R &= G_R \hat{x}_R \end{aligned} \quad (4.4)$$

where matrices with subscript R have a specified set of rows and/or columns deleted, corresponding to the deleted states, \hat{x}_i . To determine the participation of \hat{x}_i in (4.3a) consider that the plant (2.1) and the controller (4.3) together form the closed loop optimal system with cost V given by

$$V = V_y + V_u \quad (4.5a)$$

$$V_y \triangleq \lim_{t \rightarrow \infty} E \| |y| |^2_Q = \lim_{t \rightarrow \infty} E \| |Cx| |^2_Q = \text{tr}[XC^TQC] \quad (4.5b)$$

$$V_u \triangleq \lim_{t \rightarrow \infty} E \| |u| |^2_R = \lim_{t \rightarrow \infty} E \| |G\hat{x}| |^2_R = \text{tr}[\hat{X}G^TRG], \quad (4.5c)$$

where \hat{X} satisfies

$$0 = \hat{X}(A+BG)^T + (A+BG)\hat{X} + FVF^T \quad (4.5d)$$

Since only controller states \hat{x}_i (and not plant states x_i) are considered for truncation in the controller reduction problem, the controller-cost decoupled (CCD) coordinates are defined as follows.

Definition 2:

Controller-cost-decoupled (CCD) coordinates are defined by the cost-superposition property (3.1) for the system

$$\begin{aligned} \dot{\hat{x}} &= (A+BG)\hat{x} + Fv \\ u &= G\hat{x} \end{aligned} \quad (4.6)$$

As a result of this definition, (4.5c), (4.5d), and (4.6) reveal that CCD coordinates have the property

$$[\hat{X}G^TRG] = \begin{bmatrix} v_1 & & & \\ & \ddots & & \\ & & v_{m_1} & \\ & & & \ddots \\ & & & & 0 \end{bmatrix}, \quad m_1 \triangleq \text{rank } G \quad (4.7)$$

The coordinates satisfying (4.7) are not unique and for reasons similar to Section 3, (4.7) will be satisfied by the choice

$$\hat{X} = I \quad (4.8)$$

$$G^TRG = \begin{bmatrix} v_1 & & & \\ & \ddots & & \\ & & v_{m_1} & \\ & & & \ddots \\ & & & & 0 \end{bmatrix}, \quad v_1 \geq v_2 \geq \dots \geq v_{m_1} \quad (4.9)$$

Hence, these properties hold for the CCD coordinates of (4.6).

Theorem 9:

(a) *The reduced order system of order r*

$$\begin{aligned} \dot{\hat{x}}_R &= (A_R+B_RG_R)\hat{x}_R + F_Rv \\ u_R &= G_R\hat{x}_R \end{aligned} \quad (4.10)$$

is a cost-equivalent realization of (4.6) ($V_u \triangleq \lim_{t \rightarrow \infty} E \| |u| |^2_R = \lim_{t \rightarrow \infty} E \| |u_R| |^2_R = V_{u_R}$, where V_u is calculated from (4.6) and V_{u_R} from (4.10)), if $r \geq m_1$ and $(A_R+B_RG_R)$ is stable.

In addition, (4.6) and (4.10) have these properties:

- (b) $v_i(\hat{x}) \geq 0$
- (c) $\text{Re} \lambda_i[A_R+B_RG_R] \leq 0$ if $r \geq m_1$
- (d) $\text{Re} \lambda_i[A_R+B_RG_R] < 0 \iff (A_R+B_RG_R, F_R)$ is controllable

- (e) $\Delta V_u \triangleq V_u - V_{u_R}$ is minimized by (4.10) for any given r .
- (f) $\lim_{t \rightarrow \infty} E u(t) u^T(t) = \lim_{t \rightarrow \infty} E u_R(t) u_R^T(t)$ if (d) holds. (In this case the reduced system (4.10) is called an Energy Equivalent of (4.6).)
- (g) If the first Markov parameter of (4.6) is zero ($GF = 0$), property (f) holds only if $r > m_1$.
- (h) $\left| \frac{\partial V_i(\hat{x})}{\partial G^T R G} \right|$ is minimized by the choice of coordinates (4.8), (4.9).

Proof:

By the substitution of

$$\begin{array}{lcl}
 A & \rightarrow & A+BG \\
 D & \rightarrow & F \\
 C & \rightarrow & G \\
 x & \rightarrow & \hat{x} \\
 Q & \rightarrow & R \\
 y & \rightarrow & u
 \end{array} \tag{4.11}$$

all of the results of Section 3 as applied to (2.1) and (3.8) now apply to (4.6) and (4.10). Hence, Theorems 5, 6, and 8 readily yield the above results (a)-(h) by use of the dual (4.11).

The next logical step is to put (4.10) in the modified controller cost-decoupled coordinates suggested by (3.17). These details need not be repeated since the dual (4.11) has been established. The modified controller-cost-decoupled coordinates to be used, therefore, employ the Hessenberg-type structure (3.17) applied to (4.10).

The important conclusion concerning component cost analysis is applied to open or closed loop systems is this: even though a realization (A,D,C) may be minimal in the sense of Kalman, there may still be states x_i in the realization which do not contribute to the cost function V . The theory of cost equivalent realizations (CERs) identifies those states.

5.0 Input/Output Perturbations

The input (output) costs $V_i^I (V_i^O)$ of Section 2 describe the contribution of the i^{th} input w_i (the i^{th} output y_i) in the performance matrix (2.2). The following are properties of V_i^I and V_i^O .

Theorem 10: Input/Output Cost Analysis [17], [18]

For the system described by (2.1), (2.2) with input (output) costs $V_i^I (V_i^O)$ given by (2.9)-(2.11):

1. $V = \sum_{i=1}^{n_w} V_i^I = \sum_{i=1}^{n_y} V_i^O$
2. $V_i^I \geq 0$ if $W_{ij} \geq 0$ for all $j=1, \dots, m$
3. $V_i^O \geq 0$ if $Q_{ij} \geq 0$ for all $j=1, \dots, k$
4. $V_i^I > 0$ if (A,C) is observable and (2) holds.
5. $V_i^O > 0$ if (A,D) is controllable and (3) holds.
6. The input cost V_i^I and the output cost V_i^O are invariant under state transformation.
7. The actual perturbation of the cost V due to the deletion of w_i is

$$\Delta V_i^I = 2V_i^I - d_i^* K d_i W_{ii}$$

and $\Delta V_i^I = V_i^I$ if W is diagonal.

8. The actual perturbation of the cost V due to the deletion of y_i is

$$\Delta V_i^O = 2V_i^O - c_i^* X c_i Q_{ii}$$

and $\Delta V_i^O = V_i^O$ if Q is diagonal.

Theorem 10 suggests the solution to the following input (output) selecting problem.

The Input (output) Selection Problem:

From an admissible set of m inputs (k outputs) in (2.1) find the set of $\bar{m} < m$ inputs ($\bar{k} < k$ outputs) which cause the smallest perturbation in the cost V in (2.2).

The solution to this problem is obtained by the deletion of those $m - \bar{m}$ inputs ($k - \bar{k}$ outputs) having the smallest V_i^I, V_i^O in Theorem 10. In [17] it was shown that this approach turns out to be identical to the results of the integer programming approach [19] for solving the output selection problem.

The *closed-loop* application of the input/output cost analysis for actuator/sensor selection is treated in [18], [20], and in the interest of brevity these results are not summarized here. The distinctions to be noted, however, are that the closed loop ICA/OCA algorithm is *iterative*, unlike the open-loop version suggested by Theorem 10. The required iteration is due to the fact that the selection of inputs and outputs changes the closed-loop plant matrix, unlike the open loop version (2.1), (2.2). Further research is required to describe bounds on cost perturbations in the closed-loop situation.

6.0 Conclusions

Concepts of cost-decomposition are described to treat problems where structural perturbations in inputs, outputs, and states may occur.

The input-cost analysis (ICA) and output cost analysis (OCA) determine the inputs/outputs making the largest contribution in a quadratic cost function of the outputs. The component cost analysis (CCA) determines the states making the largest contribution in a quadratic cost function of the outputs. In this setting it is shown that even though a realization (A,B,C) may be minimal in the sense of Kalman, it may contain states which make no contribution to the quadratic cost function of the outputs. A theory of cost-equivalent realization (CER) is developed to find and delete those innocuous states making no contribution. In the open-loop the CER theory is used for model reduction. In the closed-loop the CER theory is used for controller reduction.

References

- [1] Saksena, V.P., and Kokotovic, P.V., "Singular Perturbations in Control Theory", Bibliography prepared for IFAC Workshop on Singular Perturbations and Robustness of Control Systems, Ohrid, Yugoslavia, July 1982.
- [2] Kokotovic, P.V., O'Malley, R.E., Jr., and Sannuti, P., "Singular Perturbations and Order Reductions in Control Theory - An Overview", Automatica 12, pp. 123-132, 1976.
- [3] Skelton, R.E., "Cost Decomposition of Linear Systems with Application to Model Reduction", Int. J. Control, vol. 32, no. 6, pp. 1031-1055, 1980.
- [4] Skelton, R.E., and Yousuff, A., "Component Analysis of Large Scale Systems", Control and Dynamic Systems, Academic Press, vol. 18, 1982, ed. C.T. Leondes.
- [5] Skelton, R.E., and Gregory, C.Z., "Measurement Feedback and Model Reduction by Modal Cost Analysis", JACC, Denver, 1979.
- [6] Skelton, R.E., "Cost Sensitive Model Reduction for Control Design", AIAA Guidance and Control Conf., Palo Alto, Ca. 1978.
- [7] Skelton, R.E., "Control Design of Flexible Spacecraft", Agardograph No. 251 Theory and Applications of Optimal Control in Aerospace Systems, ed. I.P. Kant, 1981. Distributed by NASA Langley Va. 23365, attn: Report Distribution and Storage Unit.
- [8] Skelton, R.E., Hughes, P.C., and Hablani, H., "Order Reduction for Models of Space Structures Using Modal Cost Analysis", AIAA J. Guidance and Control, to appear 1982.
- [9] Skelton, R.E., and Hughes, P.C., "Modal Cost Analysis for Linear Matrix-Second-Order Systems", J. Dynamic Systems, Measurement, and Control, Sept. 1980, vol. 102.
- [10] Skelton, R.E., "Component Cost Analysis of Linear Systems", IEEE ISCAS Proceedings, April 1981, Chicago.
- [11] Skelton, R.E., "Partial Realizations of Linear Stochastic Time-Varying Systems", 1980 Allerton Conf. on Computing and Control, Monticello, Ill.
- [12] Yousuff, A., and Skelton, R.E., "Cost Equivalent Realizations of Stochastic Processes".
- [13] Anderson, B.D.O., "The Inverse Problem of Stationary Covariance Generation", J. Stat. Phys., vol. 1, no. 1, 1969.
- [14] Skelton, R.E., "Root Sensitivity in Linear Systems Analysis and Design", submitted for publication.
- [15] Yousuff, A., and Skelton, R.E., "Controller Reduction by Component Cost Analysis", submitted for publication.
- [16] Tse, E.C.Y., Medanic, J.W., and Perkins, W.R., "Generalized Hessenberg Transformations for Reduced Order Modeling of Large Scale Systems", Int. J. Control, vol. 27, no. 4, 1978.

- [17] Chiu, Di., and Skelton, R.E., "Selecting Measurements and Controls in LQG Problems", IEEE CDC, Dec. 1981, San Diego.
- [18] Chiu, Di., "Optimal Sensor/Actuator Selection Number, and Placement for Linear Stochastic Systems", Purdue University Technical Report prepared under Contract No. 955369 for the Jet Propulsion Lab., May 1981.
- [19] Chen, W.H., and Seinfeld, J.H., "Optimal Location of Process Measurements", Int. J. Control, 1975, vol. 21, no. 6.
- [20] Skelton, R.E., and DeLorenzo, M., "Selection of Sensors and Actuators in an LQG Program", to appear J. Large Scale Systems.

This Page Intentionally Left Blank

FINITE DIFFERENCE NUMERICAL METHODS FOR BOUNDARY CONTROL PROBLEMS GOVERNED BY HYPERBOLIC PARTIAL DIFFERENTIAL EQUATIONS*

Goong Chen, Quan Zheng, Matthew Coleman, and Sunethra Weerakoon, Department of
Mathematics, Pennsylvania State University
University Park, PA 16802

ABSTRACT

This paper briefly reviews convergent finite difference schemes for hyperbolic initial boundary value problems and their applications to boundary control systems of hyperbolic type which arise in the modelling of vibrations. We show how these difference schemes are combined with the primal and the dual approaches to compute the optimal control in the unconstrained case, as well as the case when the control is subject to inequality constraints. Some of our preliminary numerical results are also presented.

§1. Introduction

Many problems in controlled vibration can be modelled by a first order hyperbolic partial differential system of the following type

$$(1.1) \quad \begin{cases} \frac{\partial}{\partial t} y(x,t) = A \frac{\partial}{\partial x} y(x,t) + By(t) + f(x,t), & 0 \leq x \leq 1, 0 \leq t \leq T, \\ y(x,0) = y_0(x), & 0 \leq x \leq 1, \end{cases}$$

where the state $y(x,t) = (y_1(x,t), \dots, y_n(x,t))^{\text{Tr}}$ is a vector function of (x,t) and without loss of generality it is assumed that A is a constant diagonal matrix of the form

$$(1.2) \quad A = \begin{bmatrix} A^- & 0 \\ 0 & A^+ \end{bmatrix}_{n \times n}, \quad A^- = \begin{bmatrix} a_1 & & & 0 \\ & a_2 & & \\ & & \ddots & \\ & & & a_\ell \\ 0 & & & & & \end{bmatrix}_{\ell \times \ell}, \quad A^+ = \begin{bmatrix} a_{\ell+1} & & & \\ & \ddots & & \\ & & \ddots & \\ 0 & & & a_n \end{bmatrix}_{(n-\ell) \times (n-\ell)}$$

$$a_1 \leq a_2 \leq \dots \leq a_\ell < 0 \leq a_{\ell+1} \leq \dots \leq a_n.$$

$B = [b_{jk}]$ is an $n \times n$ constant matrix. Associated with the decomposition of A ,

* Supported in part by National Science Foundation Grant MCS 81-01892

FINITE DIFFERENCE NUMERICAL METHODS FOR BOUNDARY CONTROL PROBLEMS

B can be written as

$$B = \begin{bmatrix} B_-^- & B_+^- \\ B_-^+ & B_+^+ \end{bmatrix}.$$

The boundary conditions and control are

$$(1.3) \quad y^-(0,t) = S_1 y^+(0,t), \quad y^+(1,t) = S_2 y^-(1,t) + Cu(t), \quad u \equiv \text{control},$$

where $y^- = (y_1, \dots, y_\ell)^{\text{Tr}}$ and $y^+ = (y_{\ell+1}, \dots, y_n)^{\text{Tr}}$ are defined according to the partition of \bar{y} and S_1, S_2 and C are constant matrices of size $\ell \times (n-\ell)$, $(n-\ell) \times \ell$, $(n-\ell) \times m$, respectively. We wish to minimize a quadratic cost

$$(1.4) \quad J(y,u) \equiv \int_0^T [\int_0^1 \langle y(x,t), W(x)y(x,t) \rangle dx + \langle u(t), N(t)u(t) \rangle] dt,$$

where the matrix N is positive definite, and W is positive semi-definite. The above cost is associated with the vibration energy and the control cost of the system. Quadratic regulator problems of this and similar type have been considered in [1], [4], wherein the main emphasis is on the synthesis of optimal controls and existence proofs of solutions of Riccati equations.

Numerical analysis of optimal control problems governed by ordinary differential equations has been very well studied. Nevertheless, for control systems governed by hyperbolic partial differential equations, there has been, to our knowledge, very little systematic investigation on the numerical methods for such problems. In this presentation we wish to make a preliminary study of this topic.

§2. Smoothness of State and Control

Before one conducts any numerical study, it is important to know the answers to the following basic questions.

- (Q1) In what sense is the partial differential equation (1.1), (1.3) well-posed?
- (Q2) Does the optimal regulator (1.4) subject to (1.1) and (1.3) have a unique optimal control \hat{u} ?
- (Q3) How smooth is the control \hat{u} and the corresponding state \hat{y} ?

(Q1) can be answered in terms of the following theorem [2, Theorem 2.3]

Theorem 2.1

For any $f \in L^2((0,1) \times (0,T))$, $y_0 \in L^2(0,1)$ and $u \in L^2(0,T)$, the solution y of (1.1), (1.3) exists uniquely in $L^2((0,1) \times (0,T))$. Furthermore, there exists $K > 0$, independent of f , y_0 and y , such that

$$(2.1) \quad \|y\|_{L^2((0,1) \times (0,T))}^2 \leq K (\|y_0\|_{L^2(0,1)}^2 + \|u\|_{L^2(0,T)}^2 + \|f\|_{L^2((0,1) \times (0,T))}^2). \quad \square$$

FINITE DIFFERENCE NUMERICAL METHODS FOR BOUNDARY CONTROL PROBLEMS

Using Theorem 2.1, Duhamel's formula and the standard primal theory (cf. [5], e.g.), we easily answer (Q2) in

Theorem 2.2

Assume that $f \in L^2((0,1) \times (0,T))$, $y_0 \in L^2(0,1)$. Then the optimal regulator problem (1.4), (1.1) and (1.3) has a unique optimal control \hat{u} . \square

In fact, [2, Theorem 2.3] gives an \acute{a} priori bound which is even stronger than (2.1) and can probably be used to prove existence of optimal controls on $[0, \infty)$.

Theorems 2.1 and 2.2 only guarantee the minimal regularity of the optimal \hat{u} and the corresponding state \hat{y} . Assume that the inhomogeneous forcing term f in (1.1) is C^0 continuous in $[0,1] \times [0,T]$. One can solve (1.1) by the method of characteristics. In fact, the k -th component y_k of y satisfies a first order linear ordinary differential equation

$$(2.2) \quad \frac{d}{dt} y_k(x_k(t), t) = \sum_{j=1}^n b_{jk} y_j(x_k(t), t) + f_k(x_k(t), t), \quad k=1, 2, \dots, n,$$

along the characteristic curve $x = x_k(t)$, along which is satisfied

$$(2.3) \quad \frac{d}{dt} x_k(t) = -a_k, \quad k=1, 2, \dots, n,$$

where f_k in (2.2) is the k -th component of f .

Assume now that the initial condition y_0 is piecewise smooth on $[0,1]$ and u is also piecewise smooth on $[0,T]$. One can solve y by converting (2.3) into a system of integral equations. Such a system has a solution y (as the fixed point of an integral operator) which is easily seen to be also piecewise smooth in $[0,1] \times [0,T]$. Since y depends linearly on f, y_0 and u , we write

$$(2.4) \quad y = L(f, y_0, u),$$

where L is an integral operator. Substituting (2.4) into (1.4) and minimizing with respect to u , we get another new integral equation for \hat{u} . This equation has a unique solution \hat{u} which is easily seen to be piecewise smooth on $[0,T]$. Thus we state

Theorem 2.3

Assume that $f \in C^0([0,1] \times [0,T])$ and y_0 is piecewise smooth on $[0,1]$. Then the optimal control \hat{u} of (1.4) is piecewise smooth on $[0,T]$. \square

In Theorem 2.3, even if y_0 is assumed to be in $C^\infty([0,1])$, the smoothness of

of \hat{u} will not necessarily be improved to $C^0([0,1])$. For \hat{u} to be $C^0([0,T])$, compatibility conditions at $(x,t) = (0,0)$ and $(x,t) = (1,0)$ must be met: necessarily,

$$(2.5) \quad y_0^-(0) = S_1 y_0^+(0), \quad y_0^+(1) = S_2 y_0^-(1) + C\hat{u}(0).$$

For \hat{u} to be $C^1([0,T])$, one must further have $y_0 \in C^1([0,1])$ and

$$(2.6) \quad \begin{aligned} A^- \frac{dy_0^-}{dx}(0) + B_-^- y_0^-(0) + B_+^- y_0^+(0) + f^-(0,0) &= S_1 [A^+ \frac{dy_0^+}{dx}(0) + B_-^+ y_0^-(0) + B_+^+ y_0^+(0) \\ &\quad + f^+(0,0)] \\ A^+ \frac{dy_0^+}{dx}(1) + B_-^+ y_0^-(1) + B_+^+ y_0^+(1) + f^+(1,0) &= S_2 [A^- \frac{dy_0^-}{dx}(1) + B_-^- y_0^-(1) + B_+^- y_0^+(1) \\ &\quad + f^-(1,0)] + C \frac{d\hat{u}}{dt}(0). \end{aligned}$$

In practice, we find that $\hat{u} \in C^0([0,T])$ is probably the best we can get. Thus if (2.5) is satisfied, the corresponding state \hat{y} will be $C^0([0,1] \times [0,T])$ smooth, but not $C^1([0,1] \times [0,T])$. Thus, discontinuities of first order partial derivatives of y will propagate along characteristics (2.3).

§3. Finite Difference Approximations

The main objective of this section is to introduce several commonly used stable finite difference schemes and different ways of defining boundary conditions.

In computing the optimal control and the governing partial differential equation, one introduces a time-step $k > 0$, a spatial mesh width $h > 0$ by dividing the $[0,1]$ interval into $N = \frac{1}{h}$ segments, then approximates the partial differential equation (1.1) by a consistent single or multi-step difference scheme

$$(3.1) \quad \begin{cases} (I + Q_0)w_\nu(t+k) = (I + Q_1)w_\nu(t) + kf_\nu(t), & t = \mu k, \mu = 0, 1, 2, \dots, \frac{T}{k}; \\ w(x_\nu, 0) = w_0(x_\nu), & \nu = -r+1, -r+2, \dots, N+p-1, \quad \nu = -r+1, -r+2, \dots, N+p-1; \end{cases}$$

where the notations [2,3]

$$x_\nu = \nu h$$

$$w_\nu(t) = w(x_\nu, t), \quad f_\nu(t) = f(x_\nu, t),$$

$$Q_i \equiv \sum_{j=-r}^p A_j^i E^j, \quad i=0,1; \quad A_j^i \equiv A_j^i(h,k) \text{ are constant } n \times n \text{ matrices;}$$

FINITE DIFFERENCE NUMERICAL METHODS FOR BOUNDARY CONTROL PROBLEMS

$Ew_\nu \equiv w_{\nu+1}$, i.e., E is the right translation operator;

are adopted. The initial condition w_0 in (3.1.2) is determined by (3.1.2) and the equation (1.1), and the boundary conditions (1.3) are discretized into

$$(3.2) \quad \begin{aligned} w_\mu(t+k) &= R^{(\mu)} w_1(t), & \mu &= -r+1, \dots, 0, \\ w_\mu(t+k) &= R^{(\mu)} w_{N-1}(t), & \mu &= N, N+1, \dots, N+p-1, \end{aligned}$$

where

$$R^{(\mu)} = \sum_{j=0}^q C_j^{(\mu)} E^j.$$

We define the central, forward and backward difference operators, respectively, as

$$D_0 \equiv \frac{1}{2h} (E - E^{-1}), \quad D_+ \equiv \frac{1}{h} (E - E^0), \quad D_- \equiv \frac{1}{h} (E^0 - E^{-1}).$$

The most often used finite difference schemes are listed below:

(L-W) Lax-Wendroff:

$$y(x, t+k) = y(x, t) + k(AD_0 + B)y(x, t) + \frac{k^2}{2} A^2 D_+ D_- y(x, t) + kf(x, t);$$

(L.F.) Leap Frog:

$$y(x, t+k) = y(x, t-k) + k(2AD_0 + B)y(x, t) + kf(x, t);$$

(C-N) Crank-Nicolson:

$$\left(I - \frac{k}{2} AD_0\right)y(x, t+k) = \left(I + \frac{k}{2} AD_0 + kB\right)y(x, t) + kf(x, t);$$

for $x = h, 2h, \dots, (N-1)h$.

Note that although L.F. is a multi-step scheme, it can be written as a single step scheme (3.1) by doing as in [3, p. 62]. All the above three schemes are accurate of order (2.2) [3, pp. 54, 62]. In addition, the L-W scheme is dissipative of order 4 [3, p. 62]. The L. F. and C-N schemes are non-dissipative, but they can be made dissipative by adding some small "higher order" terms.

The stability theory of difference schemes for purely initial value problems is very well understood. The question of stability can usually be answered by the standard Fourier transform technique. For initial-boundary value problems, however, their stability theory is not as well developed as its counterpart for purely initial value problems. The difficulty lies in the fact that boundary discretizations also affect the overall stability in a very important way — a boundary discretization may be stable for one scheme but may not be stable for another. To determine the stability of the overall finite difference scheme, one must analyze the eigenvalues of the resolvent operator induced by the difference schemes as in [2]. Following [2], assume that $f \equiv 0$ in (1.1) and let

FINITE DIFFERENCE NUMERICAL METHODS FOR BOUNDARY CONTROL PROBLEMS

$$(3.3) \quad (hD_+)^j w_0^+(t) = 0, \quad (hD_-)^j w_N^-(t) = 0, \quad j = \text{a natural number},$$

$$(3.4) \quad w_0^+(t+k) = w_0^+(t) + kA_+^D w_0^+(t), \quad w_N^-(t+k) = w_N^-(t) + kA_-^D w_N^-(t),$$

$$(3.5) \quad w_0^+(t+k) + w_1^+(t+k) - kA_+^D w_0^+(t+k) = w_0^+(t) + w_1^+(t) + kA_+^D w_0^+(t), \\ w_N^-(t+k) + w_{N-1}^-(t+k) - kA_-^D w_N^-(t+k) = w_N^-(t) + w_{N-1}^-(t) + kA_-^D w_N^-(t),$$

$$(3.6) \quad (\bar{\Delta}_+)^j w_0^+ = 0, \quad (\bar{\Delta}_-)^j w_N^- = 0, \quad j = \text{a natural number},$$

$$(\bar{\Delta}_+ u_v(t) \equiv u_{v+1}(t-k) - u_v(t), \quad \bar{\Delta}_- u_v(t) \equiv u_{v-1}(t-k) - u_v(t)).$$

In [2, p. 671], it is suggested* that the above boundary discretizations, along with (1.3), when combined with the L-W, L.F. or C-N schemes on the interior nodes, yields stable approximations with no exponentially growing eigensolutions** in the following cases:

Boundary discretization	Approximations with no exponentially growing eigensolutions
(3.3), $j = 1$	L-W; C-N for N even
(3.3), $j = 2$	C-N for N even
(3.3), $j = 3$	L-W; C-N for N even
(3.4)	L-W; L.F.***; C-N***
(3.5)	L-W for N odd; L.F.***, C-N***
(3.6)	L.F. for N even; C-N for N even

It is also pointed out in [2] that, e.g., for L-W, using (1.3) and (3.3) with $j = 2$ or 3 , the finite difference scheme is stable but has exponentially growing eigensolutions. However, such exponential solutions can be avoided by adding two more dissipative boundary conditions

$$(1-h^2 D_+^2) w_0^-(t) = w_0^+(t), \quad (1-h^2 D_-^2) w_N^+(t) = w_N^-(t).$$

A standard consequence here is that stability plus consistency yields convergence (for $T < \infty$). This is mentioned in [2] without proof. Meanwhile, it

*: This is justified for a specific (but quite standard) example only. Its general validity remains to be investigated.

** : Those eigensolutions generate large errors as $T \rightarrow \infty$.

*** : The stability eigenvalue analysis was carried out by computer calculations (instead of a rigorous proof).

should also be mentioned that although the accuracy of any of L-W, L.F. and C-N on the interior nodes is (2,2), the overall accuracy (i.e., taking into account of the boundary discretization) still needs careful analysis. Rates of convergence are then determined by the accuracy of the overall finite difference scheme.

§4. Computational Approaches to the Quadratic Regulator Problem (I): Primal and Dual Methods for the Unconstrained Case

Once a finite difference scheme is chosen, it is a rather straightforward matter to compute the optimal control \hat{u} and the corresponding state. We first replace the quadratic cost integral (1.4) by a suitable quadrature

$$(4.1) \quad J_{hk}(w, u) \equiv \sum_{\substack{0 \leq i \leq N \\ 0 \leq j \leq \frac{T}{k}}} H_{ij} \langle w_i(jk), W_i w_i(jk) \rangle_1 + \sum_{0 \leq \ell \leq \frac{T}{k}} H_\ell \langle u(\ell k), N_\ell u(\ell k) \rangle_2,$$

where $\langle \cdot, \cdot \rangle_1$ and $\langle \cdot, \cdot \rangle_2$ are inner products in appropriate Euclidean spaces, and $\{H_{ij}, H_\ell\}$ are weights of quadrature. For simplicity, we assume that $r = 1$ and $p = 1$ in (3.1).

Since it is a common practice in the method of finite differences to choose equal grids in the space variable and in the time variable, one is forced to do the same for the quadrature in (4.1). This has the disadvantage of decreasing the accuracy of the entire problem since such quadrature accuracy is limited only to $O(h+k)$. We are still trying to improve the accuracy for (4.1).

We now use (3.1) and (3.2) to represent w as

$$(4.2) \quad w_\nu(t) = \sum_{0 \leq j \leq \frac{t}{k}} \alpha_{\nu j} u(jk) + F_\nu(t), \quad \nu=0,1,\dots,N-1,N; \quad t=\mu k \text{ for } \mu=0,1,2,\dots,\frac{T}{k},$$

where $F_\nu(t)$ denote the sum of all inhomogeneous terms depending on the initial condition y_0 and the inhomogeneous term f in (1.1), and the coefficients $\alpha_{\nu j}$ are determined iteratively from the related coefficients in (3.1) and (3.2). For explicit schemes ($Q_0 \equiv 0$) such as L-W and L.F., the iterative computations of $\alpha_{\nu j}$ can be directly carried out on a computer. For the C-N scheme which is implicit, an additional matrix inversion $(I+Q_0)^{-1}(I+Q_1)$ is needed at each time step in the iterative computations of $\alpha_{\nu j}$.

Now, we substitute (4.2) into (4.1). This yields a quadratic expression J_{hk} depending on $u(0), u(k), u(2k), \dots, u(T)$ only:

$$(4.3) \quad J_{hk} = \frac{1}{2} \sum_{j,\ell=0}^{T/k} \langle u(jk), D_{j\ell} u(\ell k) \rangle + \sum_{j=0}^{T/k} \langle \gamma_j, u(jk) \rangle + \zeta.$$

To compute the optimal discrete control $\hat{u}(0), \hat{u}(k), \dots, \hat{u}(T)$, we set

$$\frac{\partial}{\partial u(jk)} J_{hk} \Big|_{\hat{u}(jk)} = 0, \quad j=0,1,\dots,\frac{T}{k},$$

this gives a linear matrix equation

$$M_{hk} \hat{u}_{hk} = \theta_{hk}, \quad \hat{u}_{hk}^{Tr} = (\hat{u}(0), \hat{u}(k), \dots, \hat{u}(T)),$$

where M_h is a full $(\frac{T}{k} + 1) \times (\frac{T}{k} \times 1)$ stiffness matrix, and θ_h is a $(\frac{T}{k} + 1)$ vector depending on the initial condition y_0 and inhomogeneous forcing term f only. Thus

$$(4.4) \quad \hat{u}_{hk} = M_{hk}^{-1} \theta_{hk}.$$

We state the following theorem without proof.

Theorem 4.1

Assume that the scheme (3.1) and (3.2) be convergent. Let $f \in C^0([0,1] \times [0,T])$ and let y_0 be piecewise continuous on $[0,1]$. Then \hat{u}_{hk} as obtained in (4.3) converges to \hat{u} , the unique optimal control of (1.4), (1.1), (1.2), in $L^2(0,T)$. \square

Next, we discuss the duality approach: we consider the max-min problem

$$(4.5) \quad \max_p \min_{w,u} [J_{hk}(w,u) + \sum_{\substack{1 \leq j \leq \frac{T}{k} \\ 0 \leq v \leq N}} \langle p_v(jk), \text{CONSTRAINT} \rangle],$$

where

$$(4.6) \quad \text{CONSTRAINT} = \begin{cases} (3.1.1) & \text{if } (x_v, t) = (vh, jk) \text{ is an interior node,} \\ (3.2.1) \text{ or } (3.2.2) & \text{if } (x_v, t) = (vh, jk) \text{ is a boundary node,} \end{cases}$$

and

$$(4.7) \quad p_v(jk) = p(vh, jk), \quad -1 \leq v \leq N+1, \quad 1 \leq j \leq \frac{T}{k},$$

are the discrete dual variables defined at each nodal point.

Problem (4.5) is equivalent to the primal problem (4.1), (3.1) and (3.2).

In (4.5), for each given $\{p_v(jk)\}$, we first minimize with respect to w_v and $u(jk)$, obtaining minimizing solutions

$$(4.8) \quad \hat{w}_{v,p} = \mathbb{E}_v^1(p), \quad 0 \leq v \leq N,$$

$$(4.9) \quad \hat{u}_{j,p} = \mathbb{E}_j^2(p), \quad 0 \leq j \leq \frac{T}{k},$$

where in the above, $\{\mathbb{E}_v^1\}$ and $\{\mathbb{E}_j^2\}$ are affine linear operators of the discrete dual variable p . The relation j (4.9) is explicit, but (4.8) is usually implicit unless the matrix W in (1.4) is positive definite.

Substituting (4.8) and (4.9) into (4.5) for all the w, u , we obtain a new quadratic functional $I_{hk}(p)$ of the dual variable. We maximize $I_{hk}(p)$ with respect to p and obtain \hat{p} , which is unique provided that W is positive definite. From (4.9) and (4.8), we obtain the discrete optimal control

$$(4.10) \quad \hat{u}(jk) = \mathbb{E}_j^2(\hat{p})$$

and the corresponding discrete state

$$(4.11) \quad \hat{w}_v = \mathbb{E}_v^1(\hat{p}).$$

§5. Computational Approaches to the Quadratic Regulator Problem (II): Quadratic Programming Methods for the Constrained Case

Suppose that the class of admissible controls is constrained by linear inequalities

$$(5.1) \quad \begin{cases} Ku(t) \leq g(t), \\ u(t) \geq 0, \end{cases} \quad 0 \leq t \leq T,$$

where K is a constant $s \times m$ matrix and g is a continuous s -vector valued function on $[0, T]$; (5.1) is meant in the sense of componentwise inequalities. We assume that there exists at least one control $u(t)$ satisfying (5.1).

After discretizations, (5.1) becomes

$$(5.2) \quad \begin{cases} Ku(jk) \leq g(jk) \\ u(jk) \geq 0 \end{cases}, \quad 0 \leq j \leq \frac{T}{k},$$

Thus, from (4.3), we are faced with a discrete quadratic programming problem

$$(5.3) \quad \begin{cases} \min_u \frac{1}{2} \sum_{j, \ell=0}^{T/k} \langle u(jk), D_{j\ell} u(\ell k) \rangle + \sum_{j=0}^{T/k} \langle \gamma_j, u(jk) \rangle + \zeta \\ u(jk) \text{ subject to (5.2) for } 0 \leq j \leq \frac{T}{k}. \end{cases}$$

We wish to use the simplex method of P. Wolfe [6] to solve (5.3). Let $\hat{u}(jk)$ ($0 \leq j \leq T/k$) be the unique minimizing solution of (5.3). From the Kuhn-Tucker conditions, there exists a (discrete) dual variable $\hat{\lambda} = \{\hat{\lambda}(jk) | \hat{\lambda}(jk) \in \mathbb{R}^s, 0 \leq j \leq T/k\}$ such that the following relations hold simultaneously:

FINITE DIFFERENCE NUMERICAL METHODS FOR BOUNDARY CONTROL PROBLEMS

(5.4) (primal feasibility) $K\hat{u}(jk) \leq g(jk), \hat{u}(jk) \geq 0$

(5.5) (dual feasibility) $\sum_{\ell=0}^{T/k} D_{j\ell} \hat{u}(\ell k) + \gamma_j + K^{Tr} \hat{\lambda}(jk) \geq 0, \hat{\lambda}(jk) \geq 0,$
 $\forall j : 0 \leq j \leq \frac{T}{k},$

(5.6) (complementary slackness) $\hat{\lambda}_{i_1}(jk) [K\hat{u}(jk) - g(jk)]_{i_1} = 0, \forall i_1 : 0 \leq i_1 \leq s,$
 $[\sum_{\ell=0}^{T/k} D_{j\ell} \hat{u}(\ell k) + \gamma_j + K^{Tr} \hat{\lambda}(jk)]_{i_2} \hat{u}_{i_2}(jk) = 0,$
 $\forall i_2 : 0 \leq i_2 \leq m,$

where the subscripts i_1 and i_2 denote, respectively, the i_1 -th and i_2 -th component of each vector.

Now define the slack variables

(5.7) $\hat{\xi}(jk) = g(jk) - K\hat{u}(jk) \in \mathbb{R}^s$

(5.8) $\hat{\eta}(jk) = \sum_{j=0}^{T/k} D_{j\ell} \hat{u}(\ell k) + \gamma_j + K^{Tr} \hat{\lambda}(jk) \in \mathbb{R}^m$

for all $j = 0 \leq j \leq \frac{T}{k}$. In the new variables ξ, η , the complementary slackness conditions (5.6) become

(5.9) $\hat{\lambda}_{i_1}(jk) \hat{\xi}_{i_1}(jk) = 0, \quad 0 \leq i_1 \leq s,$

(5.10) $\hat{\eta}_{i_2}(jk) \hat{u}_{i_2}(jk) = 0, \quad 0 \leq i_2 \leq m.$

The problem now becomes one of finding a feasible solution $(\hat{u}, \hat{\lambda}, \hat{\xi}, \hat{\eta})$ of the following system:

(5.11)
$$\left\{ \begin{array}{l} Ku(jk) + \xi(jk) = g(jk) \\ \sum D_{j\ell} u(\ell k) + K^{Tr} \lambda(jk) - \eta(jk) = -\gamma_j \\ u(jk) \geq 0 \\ \lambda(jk) \geq 0 \\ \xi(jk) \geq 0 \\ \eta(jk) \geq 0 \\ \lambda_{i_1}(jk) \xi_{i_1}(jk) = 0 \end{array} \right.$$

$$\begin{cases} u_{i_2(jk)} \eta_{i_2(jk)} = 0 \\ \forall j = 0 \leq j \leq \frac{T}{k}, \forall i_1 : 0 \leq i_1 \leq s, \forall i_2 : 0 \leq i_2 \leq m, \end{cases}$$

which is a linear programming phase I problem.

One then proceeds to solve (5.11) by the simplex technique with the restricted-entry rule.

§6. Example: a Regulator Problem Governed by the One-Dimensional Wave Equation

Consider a quadratic regulator problem governed by the one-dimensional wave equation:

$$(6.1) \quad \min \int_0^T \int_0^1 \left[\frac{\partial z^2}{\partial x^2}(x,t) + \frac{\partial z^2}{\partial t^2}(x,t) \right] dx dt + \rho \int_0^T u^2(t) dt,$$

subject to

$$(6.2) \quad \begin{cases} \frac{\partial^2 z}{\partial t^2}(x,t) - \frac{\partial^2 z}{\partial x^2}(x,t) = 0, & 0 \leq x \leq 1, 0 \leq t \leq T, \\ z(x,0) = \alpha(x), \quad \frac{\partial z}{\partial t}(x,0) = \beta(x), & 0 \leq x \leq 1, \text{ (initial conditions)} \\ z(0,t) = 0, \quad \frac{\partial z}{\partial x}(1,t) = u(t), & 0 \leq t \leq T, \text{ (boundary condition and control)}. \end{cases}$$

The quadratic index (6.1) is associated with the vibration energy and control cost, which are to be minimized.

Letting

$$(6.3) \quad y_1 = \frac{1}{\sqrt{2}} \left(-\frac{\partial z}{\partial x} + \frac{\partial z}{\partial t} \right), \quad y_2 = \frac{1}{\sqrt{2}} \left(\frac{\partial z}{\partial x} + \frac{\partial z}{\partial t} \right),$$

we transform (6.2) into a first order hyperbolic equation

$$(6.4) \quad \begin{cases} \frac{\partial}{\partial t} \begin{bmatrix} y_1(x,t) \\ y_2(x,t) \end{bmatrix} = \begin{bmatrix} -1 & 0 \\ 0 & 1 \end{bmatrix} \frac{\partial}{\partial x} \begin{bmatrix} y_1(x,t) \\ y_2(x,t) \end{bmatrix}, & 0 \leq x \leq 1, 0 \leq t \leq T, \\ \begin{bmatrix} y_1(x,0) \\ y_2(x,0) \end{bmatrix} = \begin{bmatrix} h_1(x) \\ h_2(x) \end{bmatrix}, & 0 \leq x \leq 1, (h_1 = \frac{1}{\sqrt{2}}(-\alpha' + \beta), h_2 = \frac{1}{\sqrt{2}}(\alpha' + \beta)), \\ y_1(0,t) + y_2(0,t) = 0, \quad y_2(1,t) - y_1(1,t) = \sqrt{2} u(t), \end{cases}$$

with cost index

$$(6.5) \quad \int_0^T \int_0^1 [y_1^2(x,t) + y_2^2(x,t)] dx dt + \rho \int_0^1 u^2(t) dt.$$

The new form of the problem agrees with (1.1), (1.3) and (1.4) in §1.

Let $T = 1$ and $h_2(x) = 0$ in (6.4) and (6.5). Using the method of characteristics, we find that the optimal control is

$$\hat{u}(t) = \frac{-\sqrt{2}(1-t) \cdot h_1(1-t)}{\rho + 2(1-t)}, \quad 0 < t \leq 1,$$

and the corresponding state is

$$\hat{y}_1(x,t) = \begin{cases} 0 & t > x, \\ h_1(x-t), & \text{if } t < x, \end{cases}$$

$$\hat{y}_2(x,t) = \begin{cases} 0, & t + x - 1 < 0, \\ h_1(2-x-t) + \sqrt{2} \hat{u}(t+x-1), & \text{if } t + x - 1 > 0, \end{cases}$$

for $(x,t) \in (0,1) \times (0,1)$.

We have computed a set of examples using the primal method. The Lax-Wendroff scheme is adopted, with boundary discretization (3.4). The number ρ is set to 1 in (6.5).

In Figures 1, 2 and 3, $h_1(x) = \sin \pi x$ is used; the compatibility condition (2.5) is satisfied, so the optimal control \hat{u} is $C^1([0,T])$. The corresponding state \hat{y} is $C^0([0,1] \times [0,1])$.

In Figures 4, 5 and 6, $h_1(x) = 1$ ($0 \leq x < 0.5$) and $h_1(x) = -1$ ($0.5 < x \leq 1$) is used; none of the compatibility conditions (2.5) and (2.6) are satisfied. The optimal control \hat{u} and state \hat{y} are both discontinuous, but are piecewise smooth.

In each of the above two cases, the numerical results show good agreement with the exact solutions.

We have also computed two examples using the dual method, with the leap frog scheme and boundary discretization (3.4); $h_1(x) = \sin(\pi x)$ and $h_1(x) = \sin \frac{\pi}{2} x$ are used. The numerical results for \hat{u} are shown in Figure 7 and Figure 8, respectively. At this stage, numerical results are still not very satisfactory and the computer program is currently being improved.

For the constrained case studied in (§5), we have computed two examples with the same Lax-Wendroff scheme and boundary discretization (3.4) as in the primal method. Figure 9 is the numerical solution for $h_1(x) = \sin \pi x$, with

control constrained by $-0.3 \leq u(t) \leq 0$ ($0 \leq t \leq 1$). Figure 10 is the numerical solution for $h_1(x) = 1$ ($0 \leq x < 0.5$) and -1 ($0.5 < x \leq 1.0$), with constraint $-0.3 \leq u(t) \leq 0$. For these two examples, no exact solutions are known which can be used for comparison. We have managed to test the optimality of these numerical solutions through other means and have found that they are indeed very satisfactory.

§7. Concluding Remarks

Although the order of convergence of our numerical results has not been tested, we believe that for $C^1([0, T])$ optimal controls and $C^1([0, 1] \times [0, T])$ states, the rate is $O(h+k)$. As indicated in §2, the control and the state in general do not have such smoothness. Thus, the rates of convergence can be expected to be quite slow for hyperbolic control problems. If we know a priori where the locations of discontinuities of \hat{u} and \hat{y} are, then using high accuracy difference schemes can usually increase the rate of convergence.

In using the dual method, the preliminary calculations for (4.8), (4.9) and the subsequent programming work are much larger in amount than the total work in the primal method. Consequently, errors tend to occur more often and are harder to correct, and computation costs are much higher. It seems to us that the primal method is more preferable.

In applications, only feedback controls are used. To obtain such closed loop controls, one must solve or compute the (nonlinear hyperbolic) Riccati partial differential equation first. Unfortunately, work in this area is incomplete [1]. This remains challenging research work for control theorists in the future.

REFERENCES

- [1] H. L. Koh, Structure of Riccati equation solutions in optimal boundary control of hyperbolic equations with quadratic cost functionals, Math. Res. Center Technical Summary Rep. #1642, Univ. of Wisconsin, Madison, June 1976.
- [2] H. O. Kreiss, B. Gustafsson, A. Sundström, Stability theory of difference approximations for mixed initial boundary value problems (II), Math. Comp. 26 (1972), 649-686.
- [3] H. O. Kreiss, Numerical Methods for Solving Time-Dependent Problems for Partial Differential Equations, Univ. of Montreal Press, Montreal, Quebec, Canada, 1978.
- [4] D. L. Russell, Quadratic performance criteria in boundary control of linear symmetric hyperbolic systems, SIAM J. Control 11 (1973), 475-509.
- [5] D. L. Russell, Mathematics of Finite Dimensional Control Systems, Theory and Design, Marcel Dekker, New York, 1979.

- [6] P. Wolfe, The simplex method for quadratic programming, *Econometrica*, 27 (1959), pp. 382-398.

APPENDIX: Preliminary Computational Results

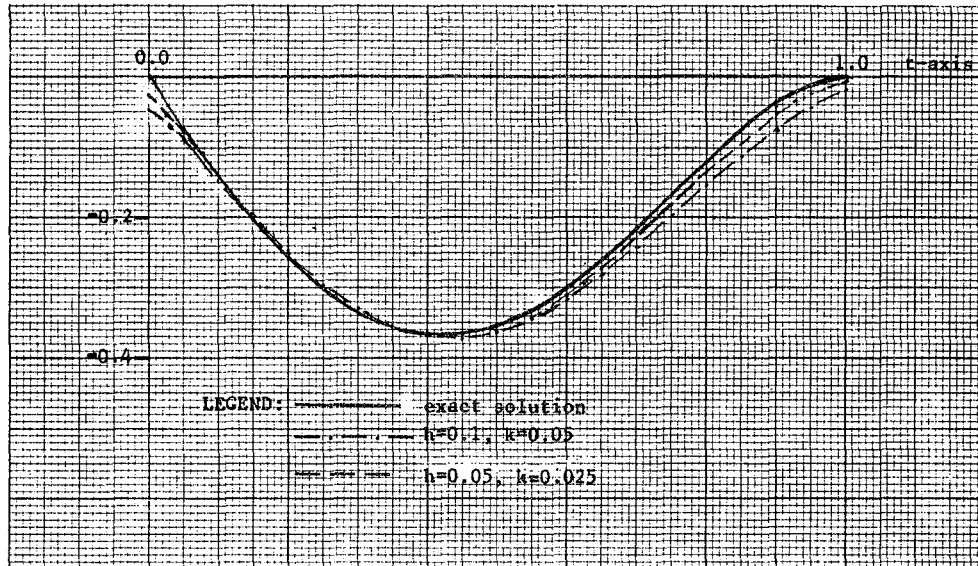


Figure 1: Optimal Control U

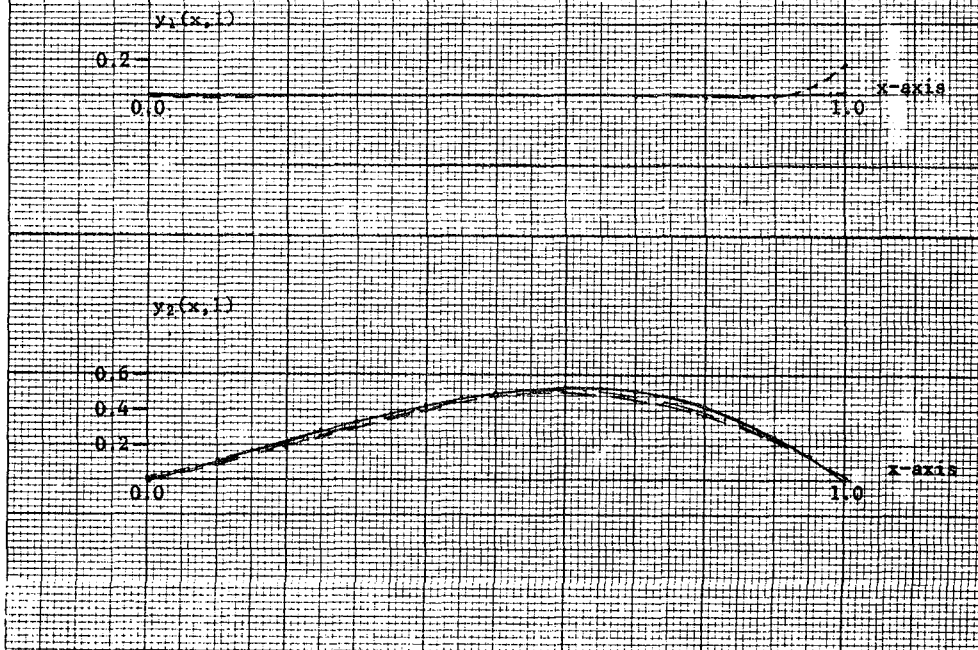
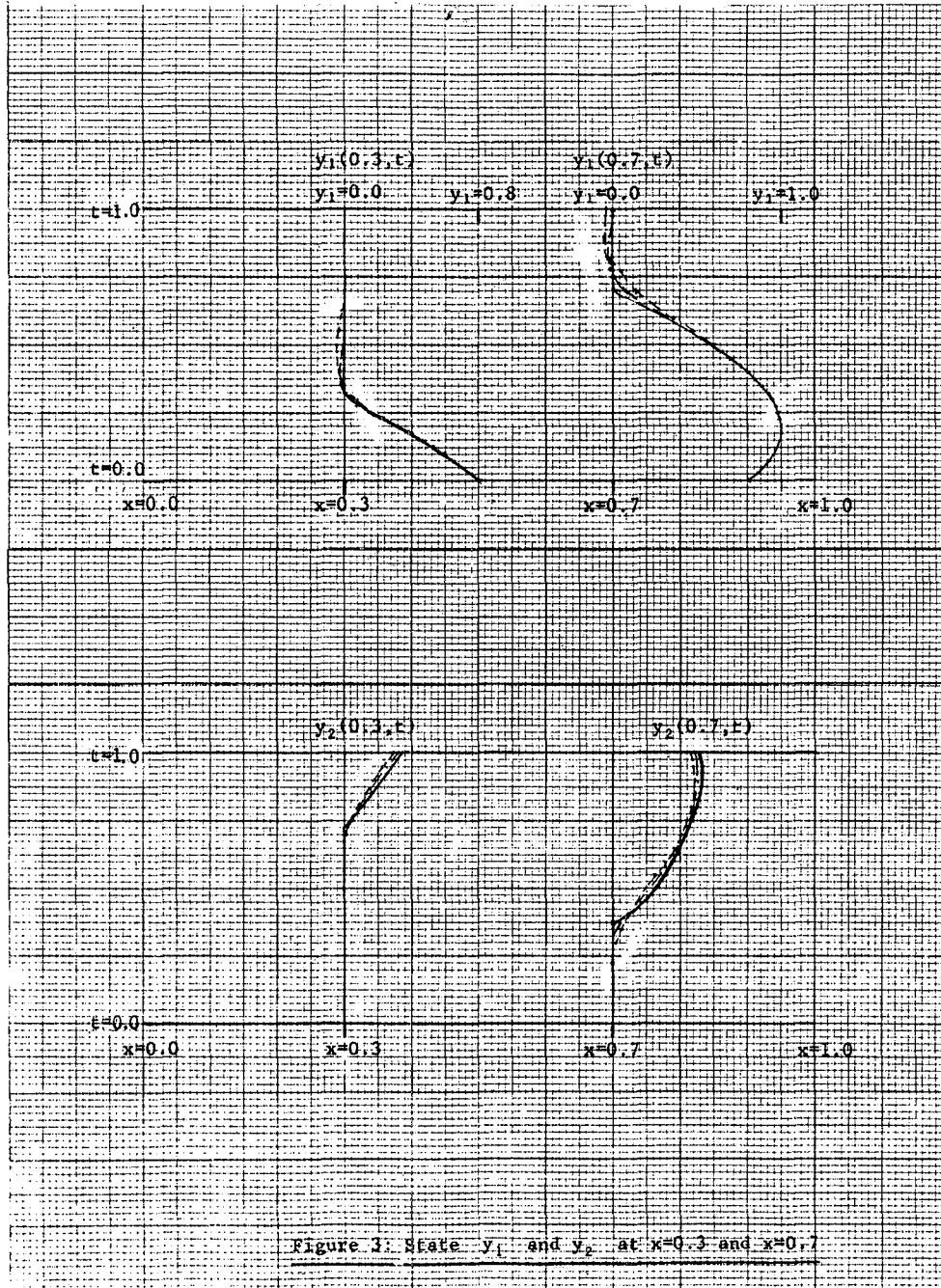
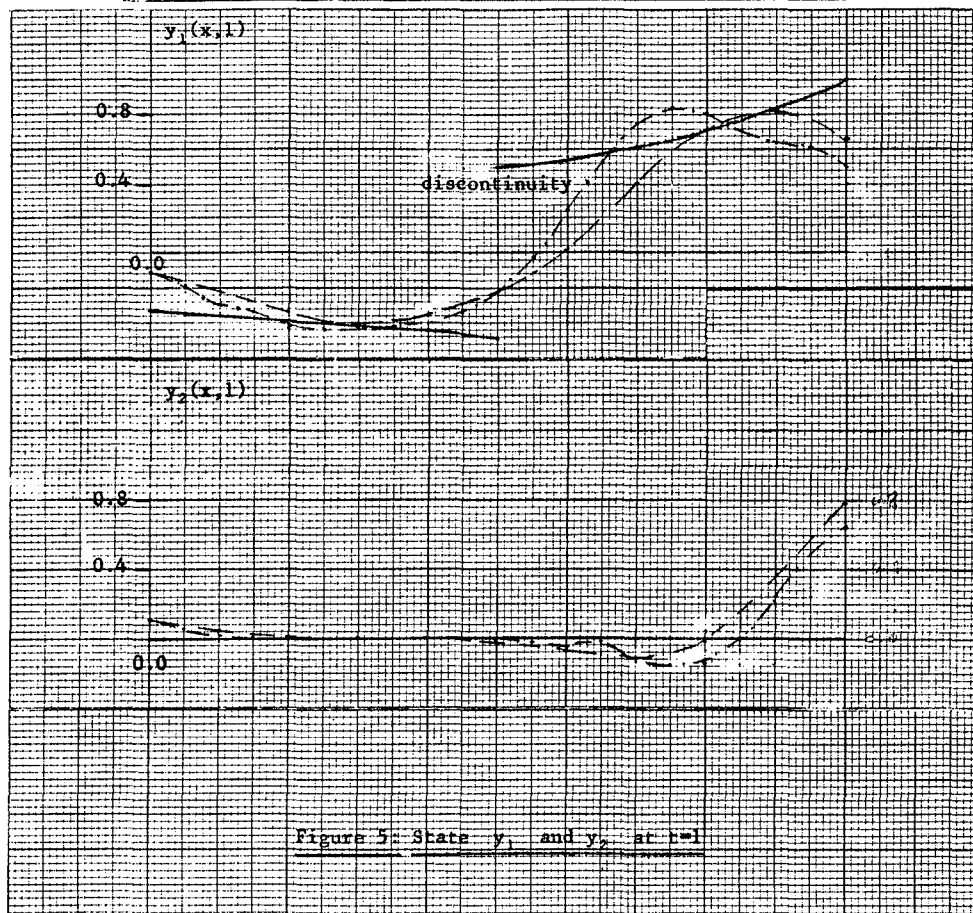
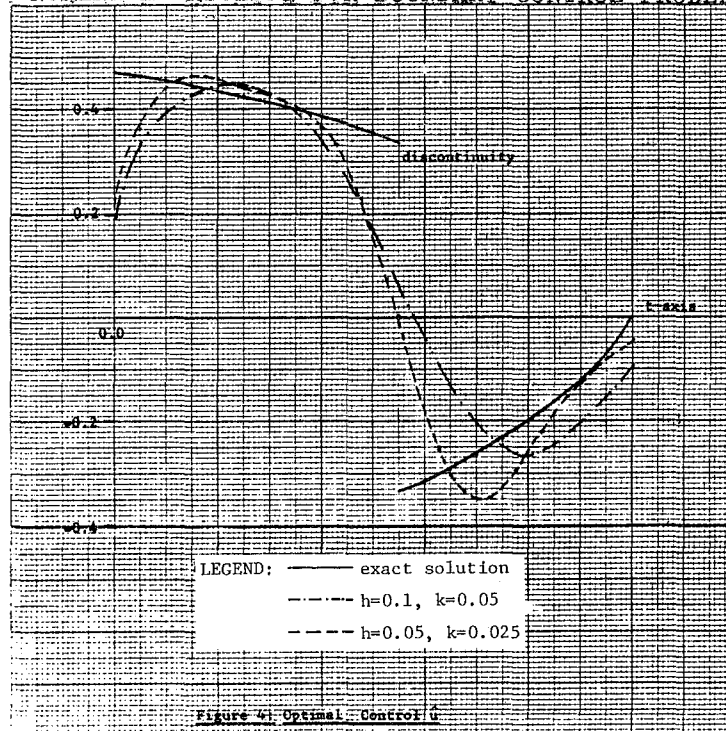
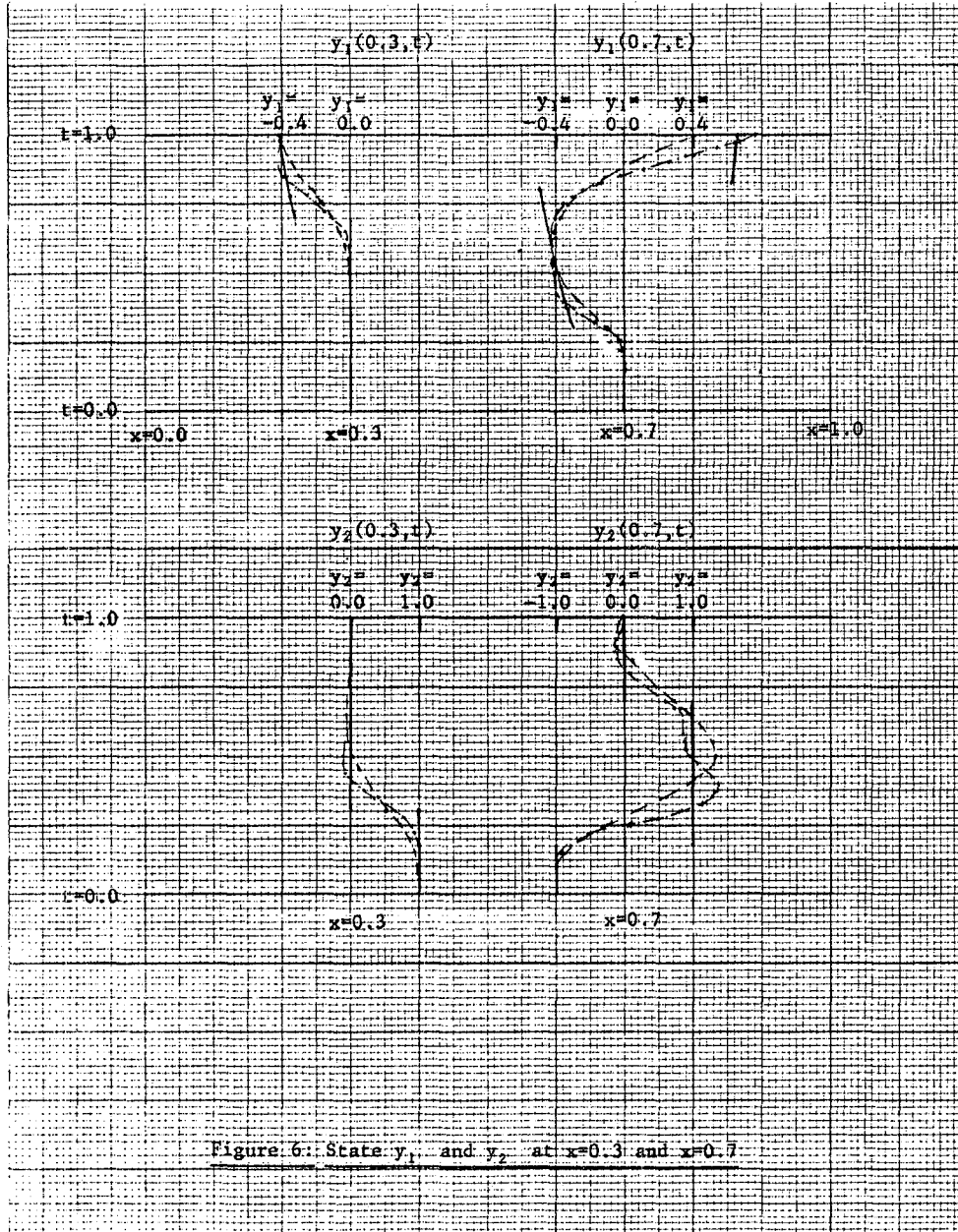


Figure 2: State y_1 and y_2 at $t=1$



FINITE DIFFERENCE NUMERICAL METHODS FOR BOUNDARY CONTROL PROBLEMS





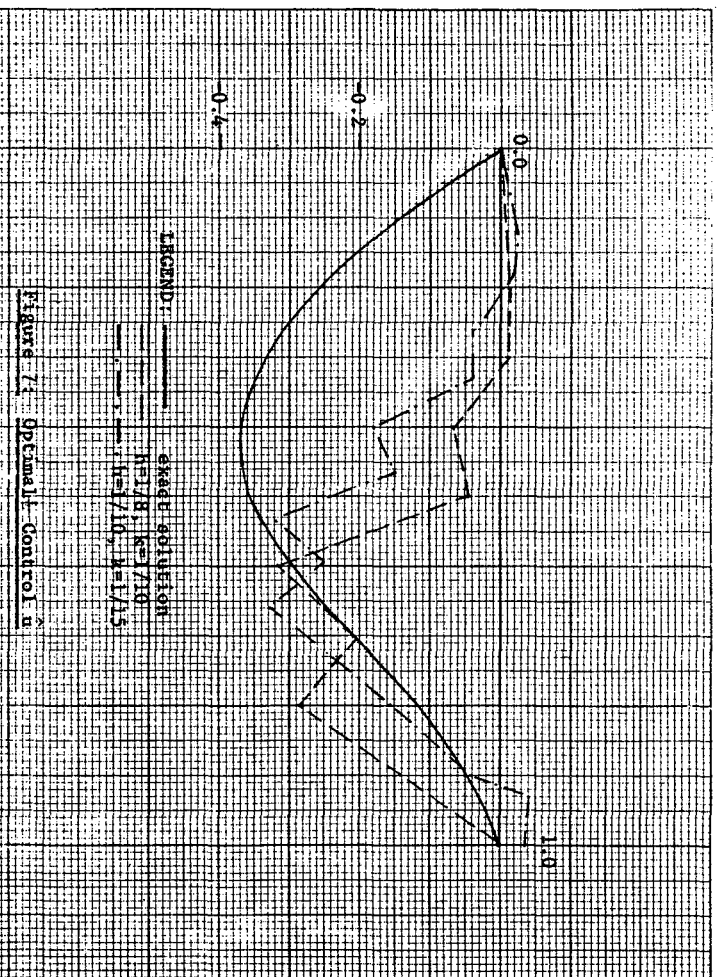


Figure 7: Optimal Control u

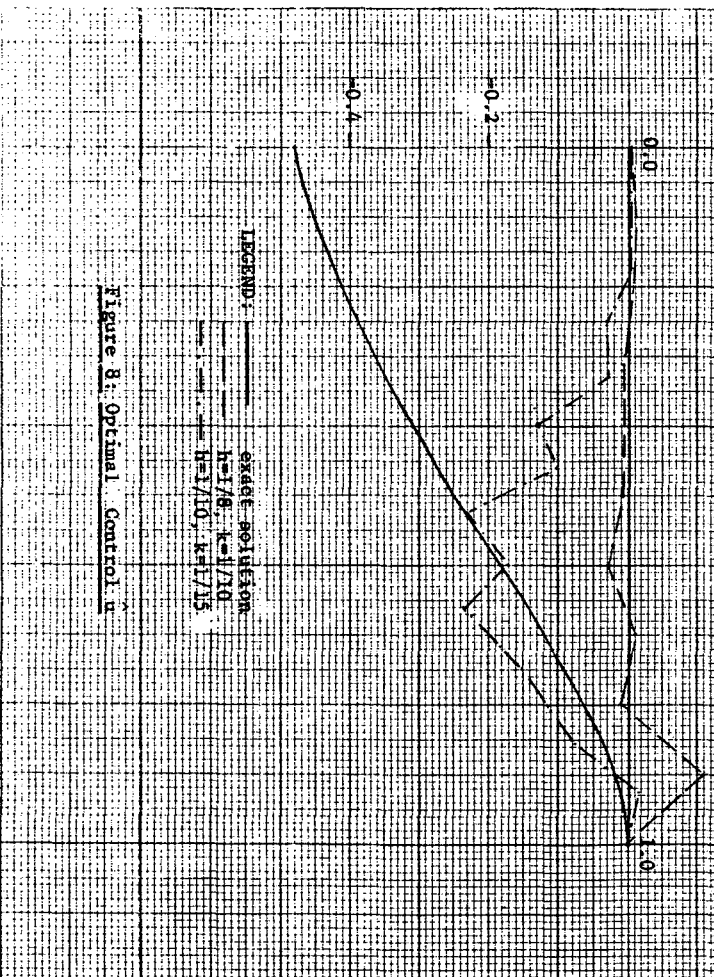
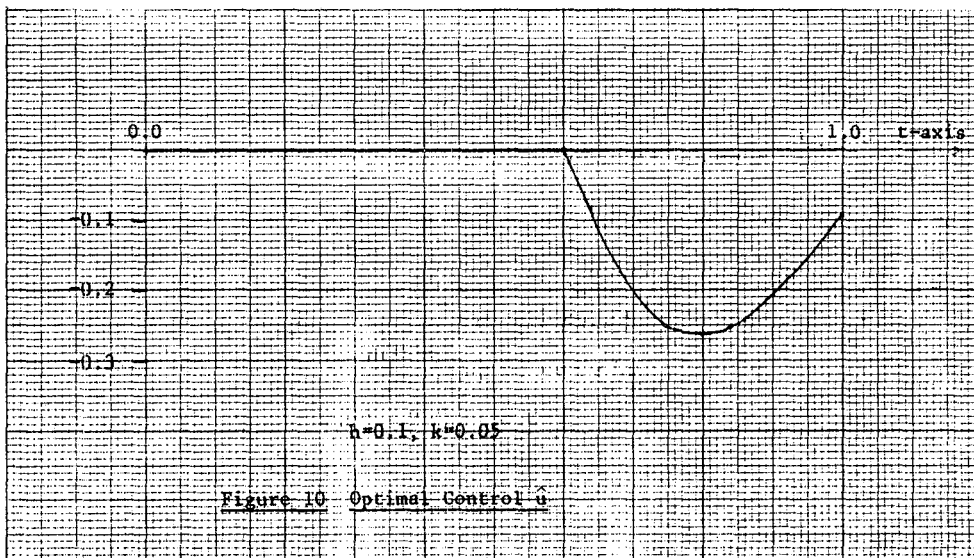
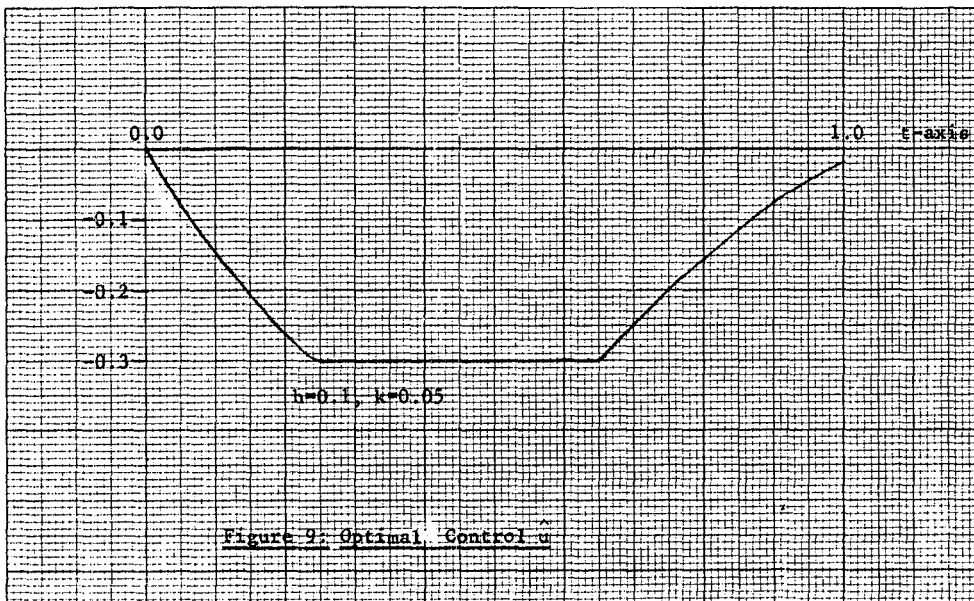


Figure 8: Optimal Control u

FINITE DIFFERENCE NUMERICAL METHODS FOR BOUNDARY CONTROL PROBLEMS



This Page Intentionally Left Blank

SESSION VI: DISCUSSION - LSS APPLICATIONS OF DISTRIBUTED SYSTEM THEORY

Moderator: **R.S. Gran**, Grumman Aerospace Corporation
Panel Members: **J.S. Gibson**, University of California, Los Angeles, **V. Komkov**,
West Virginia University, **D.L. Russell**, University of Wisconsin,
and **D.C. Washburn**, A.F. Weapons Lab

SYNOPSIS*

R. S. GRAN: The title of this session is LSS Applications of Distributed System Theory, and we are to discuss what the role of this theory is in future large space structure (LSS) designs. The theme for the discussion is set by addressing the question: Is the LSS finite or infinite? That question has been addressed a lot today and yesterday. How can we treat it as an infinite system? If we treat it as an infinite system, can we say something that we cannot say if we treat it as a finite system?

D. C. WASHBURN: The Air Force Weapons Laboratory (AFWL) interests in large space structures are a little different than those of NASA. AFWL is interested in high-energy laser applications in space. The systems have very large deformable mirrors that are controlled with perhaps thousands of actuators. The laser looks a lot like a rocket engine as far as vibrations go. There are isolation mechanisms which kill many of the vibrations. The coolant flow is probably the single largest source of vibration to the forward structure where the mirrors are located. Another significant source of vibration to the structure is introduced through controlling the mirrors to shape the wavefront. The control performance requirements for the optics are extremely tight, much tighter than anything mentioned yesterday.

Everybody seems to be using NASTRAN modeling to define the models, which are then truncated for designing the controller. The design is then patched up to take care of the "spillover" problem. The idea of this conference was to bring together the partial-differential-equations (PDE) and finite-element people to discuss other approaches.

Finite-element and PDE models are both approximate and it is not necessary to argue over whether the system is really finite or infinite. Clearly, only so many modes are of interest in the final design. It seems that the finite-element approach has been thoroughly investigated. The point I would like to make is that there should be a little more investigation of PDE modeling. Not because it is going to be better or worse, but because it has not been investigated very deeply. It may give us some new insight or have other attributes to offer.

*This synopsis attempts to capture the main points discussed but has not been reviewed or endorsed by the speakers.

Some research at JPL using a PDE model to design an infinite-dimensional controller, which was then truncated for implementation, showed that it automatically took care of the spillover problem. The point is that you are truncating at a different point in the problem. Truncating in the finite-element approach, in which you throw away modes, implies throwing away a whole different kind of information. You might expect different results with PDE and possibly more robustness. That was a simple example but it provided an initial indication of the PDE methods' potential.

The bottom line is that it seems to me that a certain percentage of our effort ought to go into investigating all avenues, including applications of approximate PDE models to controller design.

G. IANCULESCU, JPL: The finite-element method has some advantages over the PDE approach, but it cannot be used for parametric studies. In controller design, we really do not want to solve only one problem, but a class of problems with various applications toward various designs. That is not easy with a finite-element model because you have to arrange for new data sets and new models for each application. The PDE method can result in analytical solution to perform parametric studies.

A lot of very useful work on PDE control exists, especially regarding necessary conditions for optimality, existence of solutions, and uniqueness. One can use these techniques on the PDE solution, then apply some approximation to implement the control law. Mathematicians know so much more about PDE theory than has been used thus far in designing large space structures. More research is needed to explore these types of things.

L. S. WEISSTEIN, Lockheed Missiles and Space Co.: Most of the comments made here come to the same conclusion: the models in general are pretty crummy. There are mathematical engineering works that have addressed modeling of lattice structures with the complexities of large space platforms, large antenna booms, and parabolic dishes. The basic two approaches that are used are the discrete-field method and the continuum modeling technique. In certain classes of problems, it is possible to obtain analytical closed-form solutions.

J. N. JUANG, Martin Marietta Aerospace: Our experience would indicate that you can achieve about the same accuracy with finite-element and PDE models and the solution should be about the same.

V. KOMKOV: I am concerned about how badly both finite-element and continuum models generally represent the real physical systems. It seems that people really pay no attention to the physics of the problem and check all the assumptions made.

A second concern is that the models must include damping because the effects can be very serious.

A third criticism is that millions of dollars are spent on experiments before an adequate theoretical basis has been established. Good experimental data can tell you why an experiment is being performed and what is expected to be proved or disproved by the experiment.

It is surprising that so little attention is given at this workshop to adaptive control. It is an important subject in the control of large space structures.

Finally, we should ask the question: Do we always really need to suppress vibrations in large space structures? In some cases, it may not be necessary to suppress vibrations to achieve the mission objectives.

B. R. HANKS, Langley: I generally agree with the comment that most of the time the errors in modeling are directly related to the failure of the structure to obey the assumptions used. Simple structures can be modeled well by either PDE or finite-element methods, but the difficult problem comes from trying to model a real vehicle such as Voyager, for example. PDE's are regularly used in structures to do parametric studies, and I would think that controls people would do the same. When you get ready to design or analyze a complicated system that is to fly, then you should turn to the finite-element approach. Nonlinearities, joints, and damping present the real difficulties in complicated systems.

D. ELDRED, JPL: It is disturbing the way people neglect damping in large space structure models. Damping is very important, and I do not see a lot of effort on modeling damping effects or using parameter identification techniques to estimate damping coefficients.

DISCUSSION: A discussion followed among the audience, Eldred, Gran, and Gibson concerning adaptive control and identifying damping parameters. A question was raised as to whether damping uncertainties would be of much importance if adaptive control was used. One response was essentially that it is important to know quite a bit about the space structure characteristics, including damping, in order to design an effective adaptive controller. Part of the reason that you do not hear much about adaptive control is that it is highly nonlinear and difficult to design.

A specific question from the audience was addressed to Gibson on the use of the semigroup framework in parameter estimation and adaptive control. Would it be possible to use very sophisticated off-line estimation algorithms based on semigroup theory to determine changes in the space structure characteristics, and then change the control gains in a linear optimal control law? The control would still be linear and the adaptation would be in the form of a moving window around the Riccati equation. Gibson responded that he thought it would be possible and that he is beginning to study parameter estimation in the semigroup context. The semigroup theory is quite useful in providing convergence results. If you look at the adaptive control literature, all of the global stability results that are available for adaptive control schemes generally rely on knowing the structure, and the dimension of the system. That translates into having to know something about the structure of the semigroup when the system is infinite-dimensional. Gibson thought that the semigroup theory will be useful certainly in off-line parameter estimation and expected that it will be useful in on-line adaptive parameter estimation and control.

D. L. RUSSELL: There are several reasons why PDE models are needed. First of all, PDE's are free from an arbitrary dimensionality imposed through discretization. We need to recognize that discretization is an error that we impose,

externally, into our model, and to the extent that we can avoid in analysis, we certainly should.

PDE models are also free from the qualitative differences that arise when we try to decide what sort of elements to use, whether we are going to use piecewise linear elements or cubic splines or what have you. They are not, of course, free from all sorts of qualitative differences. If you look at all the models that are available for modeling beams -- the Euler beam, the Bernoulli beam, and the Timoshenko beam -- certainly there are plenty of qualitative differences among these. To the extent possible, we should not compound that with the kinds of differences that arise through the discretization procedures, even though, in the end, you are going to have to discretize.

The third point, a very serious one, is that the control properties may be radically different for a distributed system from those that are exhibited by any finite-dimensional system of ordinary differential equations. Prime examples are the hyperbolic systems in which all finite-dimensional models are, in principle, controllable in an arbitrarily short length of time, whereas the infinite-dimensional models, at least for point control as distinct from distributed control, require a certain minimum time before control can be carried out. If you go to the parabolic systems, there are very severe limitations with regard to the smoothness of final states that actually can be achieved with controls, none of which show up in discrete models. Indeed, I am not sure -- just based on discrete models -- whether the fundamental differences between hyperbolic and parabolic systems could be formulated and perceived, in the exactness that we have them, based on partial differential equations.

The fourth point, of particular relevance here, is that the control based on finite-dimensional approximation may take advantage of what I would call "accidental" relationships between coefficients. Accidental, in the sense that they are a consequence of the particular discretization, or particular dimension chosen, or whatever. And if the control law takes advantage of these more or less accidental variations and coefficients, we may very well arrive at a false conclusion and lack of robustness, and so on, simply because those relationships will not hold if you change the dimension a little bit or change the type of discretization. So, while we have granted that, in the end, the finite-dimensional models must be used, nevertheless the control law itself should, if at all possible, be formulated in such a way that it is relatively free from the effects of discretization.

The fifth point is that partial differential equations are very intimately related to conservation laws and, in most cases, the parallel conservation laws should be taken advantage of when discrete models are employed. The discrete models should be as close as possible to the kind of things we would do if we were going to develop a partial differential equation for the same system.

There is another important point to make here: in early 20th-Century physics, the idea of a thought experiment was very important, and it is certainly still important. One conceived an experiment in one's mind, which was not actually to be carried out, but which clarified the mental processes that were being applied to the problem at hand. A partial differential equation model can be thought of as a gedankenexperiment in that sense. What we have sitting out

there in the world are distributed processes, distributed plants for which no finite-dimensional model is going to be completely accurate. Now the point with a partial differential equation is that it is a relatively manageable conceptual model that has some of the same properties. Also, it is such that no finite-dimensional approximation is going to be completely accurate in describing its behavior. If we seriously expect to control these very complex objects in the real world with relatively simple control strategies, those same strategies ought to work, mathematically, in handling partial differential equations, whose relationship to finite-dimensional systems is much better understood than is the relationship between physically distributed processes and finite-dimensional systems. So, there is this thought-experiment side to partial differential equations, which, in fact, I think is one of the stronger points.

The seventh point is the relative manipulative simplicity of partial differential equations. We all know that one of the reasons for the success of the calculus is that it is a lot easier to do calculus than it is to do the parallel discrete mathematics. Part of the thinking process is manipulative and being able to work with equations. It is difficult to work with the vast mass of equations that result from finite-element methods, valuable though they are in numerical procedures. It is unimaginable that they could be used very effectively in conceptual studies, which are very important. Can you imagine Maxwell's equations being developed from the beginning in terms of three-dimensional cubic splines or something of that sort? There are very important general principles in control theory of distributed systems that simply are not going to emerge or become apparent unless continuous models are used.

A final point that should be made is that PDE's are not sacred in any respect. You must consider what you need based on the physical system. For example, to obtain structural damping in a linear oscillatory system, in which the rate of attenuation is proportional to the magnitude of the frequency, one has to put in nonlocal operators, not differential operators, in order to realize that type of behavior of the spectrum. Right away you are dealing with a class of objects that no longer is, strictly speaking, in the set of partial differential equations.

L. MEIROVITCH, Virginia Polytechnic Institute and State University (VPI): I fully agree with Professor Russell. Many of the problems now in control theory are caused by trying to apply finite-dimensional control theory to infinite-dimensional systems. People like to talk about large structures; in fact, they quote that future spacecraft will be the size of Manhattan, and by that they automatically shift attention to size rather than order. When we are talking about large structures, we should think in terms of large-order systems, not in terms of physical dimensions. What is really needed is a control theory which will close the gap between the finite-dimensional modern control theory and the infinite-dimensional systems that we really have.

R. S. GRAN: This discussion is reminiscent of the fight not too long ago between classical and modern control engineers. As we know, some of the recent research on robustness has helped fill the gap between the two. Actually the gap was more perceived than real. The research provided the understanding to remove the perceptual problems. When we consider the large space structure problem, we should really work on filling the gap, real or perceived, between finite-element and continuum-model approaches.

J. S. GIBSON: In modeling large space structures, we have been discussing primarily two methods: finite-dimensional discrete models and PDE models. Those are not the only possibilities. It is not true that if you want to use an infinite-dimensional model that it must be PDE. For example, if you want a model that has the same damping ratio for every mode of a beam or plate, there are no PDE models that can provide that. However, semigroup theory would handle that case. Those of us who advocate treating the problem in the infinite-dimensional context, using semigroup theory, are not necessarily talking about PDE's. Semigroup theory includes both finite-dimensional and infinite-dimensional situations.

D. C. WASHBURN: I don't think the discussion should center around the difference between PDE and finite-element modeling. We should be looking at whether we are going to make approximations along modal lines or along some other lines. Using PDE you can make approximation in other ways.

R. S. GRAN: One class of engineers that are not really represented at this workshop are those on the firing line to design and build the space systems that actually fly. Those people have been designing systems for years, very successfully, and they would not know a PDE if they tripped over it. What do we tell those people about why they should use PDE models? (There were no direct responses to this question.)

Comments and Questions from the Audience

R. P. IWENS, TRW: It seems the consensus of the panel is that we should be looking more at partial differential equations. I would like to ask the people who advocate the use of partial differential equations, how do we model the structure flexibility in the Voyager? We may learn a lot from the theory by studying control of simple structures using partial differential equations, but the question still remains: if we look at real structures, how are we going to model something as complex as the Voyager with PDE's?

V. KOMKOV: Well, it has been done recently. There's a group at the University of Iowa that have taken some extremely complex, very large structures and developed a combined finite-element and PDE model. Of course, it is a computer algorithm in which they worked for a long time, but it can be done.

G. RODRIGUEZ, JPL: There is no alternative to the partial differential equation approach, in that the finite-element model is itself based on partial differential equations. To obtain a finite-element model we partition the structure into a number of segments, subassemblies, or substructures, and within each subassembly we assume a simple, partial differential equation. It could be a beam, it could be a plate, membrane, whatever. But nonetheless, there is a partial differential equation model. For complicated structures, this process results in a very complicated set of partial differential equations coupled by inter-element or interface conditions. We have been very successful in implementing approximate solutions to these complicated equations to the extent that finite-element techniques, which involve approximating the solutions by interpolating polynomials, have been very successfully developed and implemented in computer programs such as NASTRAN. So the mechanism to obtain the eigenvalues and eigenfunctions of that complicated partial differential equation model has been

automated, and that is what was used in the Voyager spacecraft and is used in many other spacecraft. There is the possibility of going beyond the computation of eigenvalues and eigenfunctions and determine control and estimation gains directly by means of the finite element method. In other words, we would start with the complicated partial differential equation model, which we do not even have to write, just as we do not have to write the model for NASTRAN. We just assume that it exists, and proceed to use the approximating polynomials, to solve not only for the eigenvalues, but to solve also for the control gains and the feedback matrices. So I think that the issue is not really whether there is an option to the partial differential equation -- there really is not. The question is whether we can develop numerical algorithms or numerical techniques, approximation techniques, to compute directly more than the eigenvalues and the eigenfunctions of a complicated structure.

L. MEIROVITCH, VPI: There is a method that is called Component-Mode, which was developed by Professor Walter G. Hurty from UCLA, that can be regarded as envisioning the spacecraft as a collection of PDE's, each member being represented by a set of so-called modes, which could be obtained by solving a partial differential equation for each of the members.

A. N. MEYSTEL, University of Florida: I would prefer to have as complex a model as possible. There is no rush during design, and it is possible to have a very complex model of the system being designed with all the partial differential equations necessary to describe the system. Then the control person can try this model and find out which simplified models can be built for control.

B. R. HANKS, Langley: I want to reiterate in a slightly different way what I said earlier. I think the argument between finite-element models and partial differential equation models is academic because the real errors come about due to the structure not obeying any sort of equation.

For example, on Voyager, the problems were that the joints have motion and that pieces on the arm move about, rattle, and cause all sorts of problems that are not modeled in anybody's model. The error in truncating one model versus truncating another model is not going to be anything like what it is in the real structure. So use whichever one is necessary and actually design something, but you can not guarantee stability in any case until you put it in hardware and fly. Take something like the Voyager and extend it to 30 times its size. The little arms out there that did not have to be controlled in the Voyager case will have to be controlled. So we do have that problem to work with, and component-mode synthesis, everything we have available to use will not solve the problem by itself.

This Page Intentionally Left Blank

ALGORITHMS FOR ESTIMATION IN DISTRIBUTED MODELS WITH APPLICATIONS TO LARGE SPACE STRUCTURES

H.T. Banks

Lefschetz Center for Dynamical Systems, Division of Applied Mathematics
Brown University
Providence, RI 02912

ABSTRACT

We discuss theoretical and computational results for spline based approximation schemes used in parameter estimation algorithms for distributed systems. Specific applications include beam-like structures described by the Euler-Bernoulli and Timoshenko theories and antenna surfaces such as that in the deployable Maypole Hoop/Column model.

INTRODUCTION

With the use of composite materials in large space structures and the exotic shapes and configurations for antennae, space stations, etc., the need for analysis with distributed system models to describe complex structures in changing environments has become evident. The expected fatigue, degradation, and changes in material properties due to ageing and environmental stress increase the importance of parameter and state estimation techniques for such models. We report here on our investigations of methods for parameter estimation. The ideas involve spline based approximation schemes to reduce the distributed system problem to approximate finite dimensional state system problems where existing algorithms can be employed. Our goals have been to guarantee convergence of our methods and to test their numerical feasibility. As we shall outline, the methods can be successfully used with both static and dynamic systems data.

DYNAMIC MODEL PARAMETER ESTIMATION

We present a brief summary of our joint efforts with J.M. Crowley (U.S. Air Force Academy) reported in more detail in [1], [2], [3]. We consider the following problem: In a dynamical model (e.g. Euler-Bernoulli or Timoshenko theories) for elastic structures, estimate parameters (such as flexural rigidity, shear rigidity, structural damping, loading, etc.) in the model from observations of the system.

Theory

For convergence results, we have developed a semigroup approximation framework for these higher order models that is related to that given for second order distributed systems in [4],[5]. A rather concise series of steps can be used to describe these efforts.

- (i) We write the system (partial differential equation with boundary and initial data) to be investigated as an abstract evolution equation

$$(S) \quad \begin{aligned} \dot{z}(t) &= A(q)z(t) \\ z(0) &= z_0 \end{aligned}$$

in an appropriately chosen Hilbert space. Here the operator A (and possibly the initial data z_0) depend on the vector of parameters q to be estimated, for example, by a least-squares fit to the observation data.

- (ii) We choose approximation subspaces Z^N to Z and operators $A^N = P^N A P^N$, where P^N is the orthogonal projection of Z onto Z^N . This gives rise to an approximating system

$$(S_N) \quad \begin{aligned} \dot{z}^N(t) &= A^N(q)z^N(t) \\ z^N(0) &= P^N z_0 \end{aligned}$$

in a finite dimensional space Z^N . (We have found it very profitable to use linear spans of spline basis elements - linear, cubic, quintic - for these subspaces.) An associated sequence ($N = 1, 2, \dots$) of estimation problems for (S_N) is solved, yielding approximate parameter estimates \bar{q}^N .

- (iii) A convergence theory for $\bar{q}^N \rightarrow \bar{q}, \bar{q}$ a solution of the estimation problem for (S) , is obtained by employing general linear semigroup approximation results (the Trotter-Kato theorem) along with fundamental estimates on how Z^N and A^N approximate Z and A respectively (i.e. how (S_N) approximates (S)). (In our efforts these estimates are obtained from basic approximation theorems in spline analysis - e.g. [6],[7].)

We note that while most of our efforts in problems for elastic structures have dealt with estimation of constant parameters, our theoretical ideas (as well as the associated computational packages) are readily extended to treat problems with spatially varying coefficients. Our initial computational findings for these more difficult problems indicate that the resulting algorithms are very efficient.

Implementation

In practice we have used the spline approximation schemes with a standard package (IMSL-ZXSSQ) for the Levenberg-Marquardt finite dimensional optimization technique. The resulting algorithms have proved (as predicted by the theory) quite efficient in our program of extensive numerical testing. We have developed and tested algorithms based on quintic, cubic, and linear spline generated subspaces (the choices we used in each example depending to some extent on the particular system, the desired accuracy, and the amount of computational effort we were willing to expend).

In our testing of the algorithms we have focused on dynamic beam models. Our emphasis here has been largely motivated by the interest of engineers at NASA and elsewhere in the analysis of large complex structures through the use of equivalent simple continuum models (e.g. see [8],[9],[10]).

Examples

We have developed the theory and carried out numerical testing for a number of situations including the following.

(A) Viscoelastic models (the Euler-Bernoulli theory): Equations such as

$$m \frac{\partial^2 u}{\partial t^2} + \frac{\partial^2}{\partial x^2} \left(EI \frac{\partial^2 u}{\partial x^2} + cI \frac{\partial^3 u}{\partial x^2 \partial t} \right) + \gamma \frac{\partial u}{\partial t} = f$$

with various types of boundary conditions (combinations of fixed, simple and free) have been investigated and parameters such as $\frac{EI}{m}$ (flexural rigidity), $\frac{cI}{m}$ (structural damping), and $\frac{\gamma}{m}$ (viscous damping) have been successfully estimated. Schemes with quintic and cubic spline elements were employed.

(B) Models with shear and rotatory inertia (the Timoshenko theory): Equations studied include those for the transverse displacement y and angle ψ of cross sectional rotation

$$\frac{\partial^2 y}{\partial t^2} = \alpha \left(\frac{\partial^2 y}{\partial x^2} - \frac{\partial \psi}{\partial x} \right) + f$$

$$\frac{\partial^2 \psi}{\partial t^2} = \beta \left(\frac{\partial y}{\partial x} - \psi \right) + \gamma \frac{\partial^2 \psi}{\partial x^2}$$

with $\alpha = k'AG/m$, $\beta = \alpha A/I$, $\gamma = EA/m$ (E, G, I, k', A represent the usual Young's modulus, shear modulus, moment of inertia, shear coefficient, and cross sectional area respectively) among the parameters estimated. For a fixed end beam, cubic elements were employed while both cubic and linear element schemes were tested for the cantilever beam.

STATIC MODEL PARAMETER ESTIMATION

Our efforts on static estimation have involved at various stages joint efforts with P. Daniel (Southern Methodist University), E. Armstrong (NASA Langley), and R. Teglus (ICASE, NASA Langley). In this case the semigroup formulation for the theory underlying our algorithms is not needed. Instead we use a weak or variational equation formulation

$$\langle A_0(q)u-f, v \rangle = 0$$

of the equation of state in a Hilbert space. However the general steps (i)-(iii) outlined above in the dynamic case are again followed. In this case we also use spline subspaces (linear and cubic elements) for the approximations, combining standard spline theory estimates with variational inequalities to obtain the convergence theory of (iii).

In our implementation we have again used spline schemes with the Levenberg-Marquardt to generate and test our algorithms. We are presently still testing the methods on examples, but our initial computational findings are very promising.

Examples

We have developed the theory and are testing our algorithms on a distributed model for the antenna surface in the deployable Maypole Hoop/Column configuration under development by the Harris Corp. Our investigations have focused on the variational form state equation

$$\int_0^{2\pi} \int_{R_1}^{R_2} \{E \nabla u \cdot \nabla v - fv\} r dr d\theta = 0$$

where u is the vertical displacement (from hoop level $u=0$), $E = E(r, \theta)$ is the stiffness (elastic) coefficient, and f represents the applied distributed load (e.g. through the control stringers and catenary cord elements). In a simplified 1-dimensional test example (for which the convergence theory is rather easily obtained) where we assume angular symmetry, we have employed with success both cubic and linear element approximation schemes. Convergence

results in the 2-dimensional model can be obtained but require somewhat more effort than in the 1-dimensional case. We are currently in the process of numerically testing the algorithms for this more general model.

ACKNOWLEDGEMENTS

Work supported in part by the Air Force Office of Scientific Research under contract AFOSR 81-0198, in part by the U.S. Army Research Office under contract ARO-DAAG 29-79-C-0161 and in part by NASA grant NASA-NAG 1-258.

REFERENCES

1. Banks, H.T., and Crowley, J.M., Parameter estimation for distributed systems arising in elasticity, LCDS Report #81-24, Brown University, November 1981.
2. Crowley, J.M., Numerical methods of parameter identification for problems arising in elasticity, Ph.D. Thesis, Brown University, May 1982.
3. Banks, H.T., and Crowley, J.M., Parameter estimation in Timoshenko beam models, LCDS Report #82-14, Brown University, June 1982.
4. Banks, H.T., and Kunisch, K., An approximation theory for nonlinear partial differential equations with applications to identification and control, LCDS Tech. Rep. 81-7, Brown Univ., 1981; SIAM J. Control and Optimization, to appear.
5. Banks, H.T., Crowley, J.M., and Kunisch, K., Cubic spline approximation techniques for parameter estimation in distributed systems, LCDS Tech. Rep. 81-25, Brown Univ., 1981; IEEE Trans. Auto Control, to appear.
6. Prenter, P.M., Splines and Variational Methods, J. Wiley, New York, 1975.
7. Schultz, M.H., Spline Analysis, Prentice-Hall, Englewood Cliffs, N.J., 1973.
8. Sun, C.T., Kim, B.J., and Bogdanoff, J.A., On the derivation of equivalent simple models for beam-and plate-like structures in dynamic analysis, Proc. AIAA Dynamics Specialists Conf., Atlanta, April 6-8, 1981, pp. 523-532.
9. Chen, C.C., and Sun, C.T., Transient analysis of large frame structures by simple models, J. Astronautical Sci., to appear.
10. Juang, J.N., and Sun, C.T., System identification of large flexible structures by using simple continuum models, to appear.

This Page Intentionally Left Blank

IDENTIFICATION OF LARGE FLEXIBLE STRUCTURES MASS/STIFFNESS AND DAMPING FROM ON-ORBIT EXPERIMENTS⁺⁺

S.L. Hendricks*, S. Rajaram**, M.P. Kamat†, and J.L. Junkins†, Engineering
Science and Mechanics, Virginia Polytechnic Institute and State University
Blacksburg, VA 24061

Abstract

Two methods for identifying the mass, damping and stiffness matrices of a linear vibrating system are presented. Both methods require the measurement of acceleration, velocity and displacement at various locations of the system. In the first method, the response of the system subjected to known forces is used while the second method employs the free vibration data. The unknown parameters are recovered through the standard least squares procedure. Numerical results are presented for several examples.

Introduction

Many proposed space missions for the coming decades involve large space structures (LSS). Typical applications are large communication antenna, manned orbiting stations, astronomical telescopes and solar power stations. All these structures need to be actively controlled to realize their mission objectives. A fundamental problem, which poses a significant obstacle to realizing the missions for LSS is that the mass, damping and stiffness characteristics will not be accurately known a priori. The structures are made flexible to meet the weight constraints and hence fully erected or deployed ground vibration tests are not generally possible. The use of composite materials results in uncertain time variations of the structural parameters. Further variations result from vehicle re-configuration, thermal environment and fuel consumption. Active control of LSS necessitates an accurate estimate of the parameters so that control laws can be tuned on-orbit to permit less control effort to be expended.

The LSS are described by partial differential equations and are associated with infinite number of modes of vibration. Usually a finite element method is used to obtain a finite dimensional model for LSS. Accordingly, two approaches

⁺⁺Submitted to AIAA Journal of Guidance and Control.

* Assistant Professor.

**Graduate Research Assistant.

† Professor.

to the identification problem can be found in the literature. One approach (Ref. 1-5) is to identify the discrete or lumped parameter model of the system. The other approach (Refs. 6-9) is to identify the distributed model i.e., the partial differential equation along with the boundary conditions. In this paper we adopt the first approach. Here, we first formulate a forced response problem to identify the mass, damping and stiffness matrices. The free response problem based on this formulation degenerates to the method discussed in Ref. (1). The methods proposed in this paper require the measurements of acceleration, velocity and displacement at various locations of the system. The unknown parameters are recovered through a standard least squares procedure¹⁰. Numerical examples to illustrate the concepts are also presented.

Forced Vibration Method

Consider a LSS whose dynamics is governed by the following linear matrix differential equation

$$M\ddot{x} + C\dot{x} + Kx = F \quad (1)$$

where

- x : $n \times 1$ configuration vector of physical displacement
- M : $n \times n$ symmetric positive definite mass matrix
- K : $n \times n$ symmetric, positive semi-definite stiffness matrix
- C : $n \times n$ symmetric, positive semi-definite damping matrix
- F : $n \times 1$ force vector

Equation (1) can be rewritten as

$$\begin{bmatrix} \ddot{x}^T & \dot{x}^T & x^T \end{bmatrix} \begin{bmatrix} M \\ C \\ K \end{bmatrix} = F^T \quad (2)$$

T: transpose

Now we consider a measurement process wherein the position, velocity, acceleration and the forces are measured at discrete instants (t_1, t_2, \dots, t_m). Also, we consider the worst case in which the a priori M, C and K matrices are felt unreliable and we seek to establish best estimates of all elements of M, C and K . Upon writing m equations identical to Eqn. (2), one for each measurement time, the resulting m matrix equations can be recollected in the following form

$$AP = U \quad (3)$$

where A is a $m \times 3n$ matrix whose j^{th} row contains measurements of the system response at time t_j .

$$j^{\text{th}} \text{ row of } A = [\ddot{x}^T(t_j) \quad \dot{x}^T(t_j) \quad x^T(t_j)] \quad (4)$$

U is a $m \times n$ matrix containing the forcing functions

$$j^{\text{th}} \text{ row of } U = [F^T(t_j)] \quad (5)$$

P is a $3n \times n$ matrix containing the unknown mass, damping and stiffness parameters.

$$P = \begin{bmatrix} M \\ C \\ K \end{bmatrix} \quad (6)$$

Letting $\{ \}_i$ denote the i^{th} column of a rectangular matrix, Eq. (3) can be written as

$$A\{P\}_i = \{U\}_i \quad i = 1, 2, \dots, n \quad (7)$$

Since the number of elements in $\{P\}_i$ is $3n$, if $m > 3n$, then Eqs. (7) overdetermine $\{P\}_i$. The only requirement is that the A matrix has full rank. Assume that the least squares solution minimizes the residual sum square error

$$\psi_i = \frac{1}{2} \{R\}_i^T \{R\}_i \quad (8)$$

where

$$\{R\}_i = \{U\}_i - A\{P\}_i \quad (9)$$

Then we can write

$$\{P\}_i = L\{U\}_i \quad i = 1, 2, \dots, n \quad (10)$$

where the least square operator

$$L = (A^T A)^{-1} A^T \quad (11)$$

Notice that L is invariant so that it can be calculated once and re-used n times to calculate the n columns of P. Obviously the method is straight forward. However it requires a large number of sensors. Also the number of forces must be equal to the order of the system.

Now consider partitioning the configuration space so that equations of motion are

$$\begin{bmatrix} M_{11} & M_{12} \\ M_{12}^T & M_{22} \end{bmatrix} \begin{Bmatrix} \ddot{x}_1 \\ \ddot{x}_2 \end{Bmatrix} + \begin{bmatrix} C_{11} & C_{12} \\ C_{12}^T & C_{22} \end{bmatrix} \begin{Bmatrix} \dot{x}_1 \\ \dot{x}_2 \end{Bmatrix} + \begin{bmatrix} K_{11} & K_{12} \\ K_{12}^T & K_{22} \end{bmatrix} \begin{Bmatrix} x_1 \\ x_2 \end{Bmatrix} = \begin{Bmatrix} F_1 \\ 0 \end{Bmatrix} \quad (12)$$

x_1 and x_2 are $(n_1 \times 1)$ and $(n_2 \times 1)$ vectors respectively. Note $n_1 + n_2 = n$. The degrees of freedom in x_1 are excited directly through the external forces. x_2 refers to the degrees of freedom that are excited through the coupling terms. The question is whether we can obtain all the parameters by using forces less than the number of degrees of freedom. Equation (12) can be written as

$$\begin{bmatrix} \ddot{x}_1^T & \dot{x}_1^T & x_1^T & \ddot{x}_2^T & \dot{x}_2^T & x_2^T \end{bmatrix} \begin{bmatrix} M_{11} \\ C_{11} \\ K_{11} \\ M_{12} \\ C_{12} \\ K_{12} \end{bmatrix} = [F_1^T] \quad (13)$$

One can easily observe that \ddot{x}_2 is a linear combination of $\ddot{x}_1, \dot{x}_1, x_1, \dot{x}_2$ and x_2 . Hence the A matrix is rank deficient and the least squares process fails. This difficulty can be overcome if we assume that the matrix M_{12} is known a priori. Then the A matrix can be formed such that

j^{th} row of A =

$$[\ddot{x}_1^T(t_j) \quad \dot{x}_1^T(t_j) \quad x_1^T(t_j) \quad \dot{x}_2^T(t_j) \quad x_2^T(t_j)] \quad (14)$$

Also, j^{th} row of U matrix =

$$[F_1^T(t_j) - \ddot{x}_2^T(t_j) M_{12}^T] \quad (15)$$

The P matrix is given as

$$P = \begin{bmatrix} M_{11} \\ C_{11} \\ K_{11} \\ C_{12}^T \\ K_{12}^T \end{bmatrix} \quad (16)$$

We can solve for P as before. The matrices M_{22}, C_{22} and K_{22} are obtained in

where M , C and K are as defined earlier. G is the gyroscopic matrix and H is the circulatory matrix. G and H are skew symmetric. Premultiplying Eq. (25) by M^{-1}

$$\ddot{\underline{x}} + M^{-1}(G + C)\dot{\underline{x}} + M^{-1}(K + H)\underline{x} = \underline{0} \quad (26)$$

Equation (26) can be written as

$$\begin{bmatrix} \dot{\underline{x}}^T & \underline{x}^T \end{bmatrix} \begin{bmatrix} (G + C)^T M^{-T} \\ (K + H)^T M^{-T} \end{bmatrix} = -\ddot{\underline{x}}^T \quad (27)$$

Thus we can solve for $M^{-1}(G + C)$ and $M^{-1}(K + H)$. The eigenvalue problem is solved from a single matrix D given as¹¹

$$D = \begin{bmatrix} M^{-1}(G + C) & -M^{-1}(K + H) \\ I & 0 \end{bmatrix}$$

The free response data can therefore be used to determine the eigenvalues and eigenvectors of a general dynamic system

Numerical Examples

Example 1: Figure (1) shows a five degree of freedom mass-spring damper system. The system matrices are

$$M = \text{diag}[m_1 \quad m_2 \quad m_3 \quad m_4 \quad m_5]$$

$$K = \begin{bmatrix} k_1+k_2 & -k_2 & 0 & 0 & 0 \\ -k_2 & k_2+k_3 & -k_3 & 0 & 0 \\ 0 & -k_3 & k_3+k_4 & -k_4 & 0 \\ 0 & 0 & -k_4 & k_4+k_5 & -k_5 \\ 0 & 0 & 0 & -k_5 & k_5 \end{bmatrix}$$

$$C = \begin{bmatrix} c_1+c_2 & -c_2 & 0 & 0 & 0 \\ -c_2 & c_2+c_3 & -c_3 & 0 & 0 \\ 0 & -c_3 & c_3+c_4 & -c_4 & 0 \\ 0 & 0 & -c_4 & c_4+c_5 & -c_5 \\ 0 & 0 & 0 & -c_5 & c_5 \end{bmatrix}$$

the following manner. The estimated C_{12} and K_{12} are substituted into the matrix Eq. (12) to form

$$[B] \begin{bmatrix} M_{22} \\ C_{22} \\ K_{22} \end{bmatrix} = -[V] \begin{bmatrix} M_{12} \\ C_{12} \\ K_{12} \end{bmatrix} \quad (17)$$

B and V are constructed from the measurements as

$$j^{\text{th}} \text{ row of } B = [\ddot{x}_2^T(t_j) \quad \dot{x}_2^T(t_j) \quad x_2^T(t_j)] \quad (18)$$

$$j^{\text{th}} \text{ row of } V = [\ddot{x}_1^T(t_j) \quad \dot{x}_1^T(t_j) \quad x_1^T(t_j)] \quad (19)$$

The linear system of Eqns. (17) can be solved through least squares to get M_{22} , C_{22} and K_{22} . Usually the mass matrix is diagonal and hence M_{12} is zero.

Free Vibration Method

Consider the free vibration problem for an undamped system

$$M\ddot{x} + Kx = 0 \quad (20)$$

Since M is positive definite M^{-1} exists

$$\ddot{x} + M^{-1}Kx = 0 \quad (21)$$

Equation (21) can be rewritten as

$$x^T [M^{-1}K] = -\ddot{x}^T \quad (22)$$

Let $D = M^{-1}K$. As before we can solve for D by least squares method. The A matrix in this case is formed such that

$$j^{\text{th}} \text{ row of } A = x^T(t_j) \quad (23)$$

$$\text{Also, } j^{\text{th}} \text{ row of } U = -\ddot{x}^T(t_j) \quad (24)$$

Notice that all modes should participate in the free response. Otherwise A matrix becomes rank deficient. Also, note that $M^{-1}K$ is the eigenvalue matrix for the system. Hence the system eigenvalues and eigenvectors can be obtained from D. Even for low dimensioned systems failure to excite a particular mode obviously means that the corresponding eigenvalues and eigenvectors cannot be obtained. Broad-band random initial excitation at several stations is recommended in Ref. (2). In case we need to estimate M and K explicitly, we should have apriori knowledge of the mass matrix.

Now we can generalize the free vibration method. Consider a general dynamic system expressed as¹¹

$$M\ddot{x}(t) + (G+C)\dot{x}(t) + (K+H)x(t) = 0 \quad (25)$$

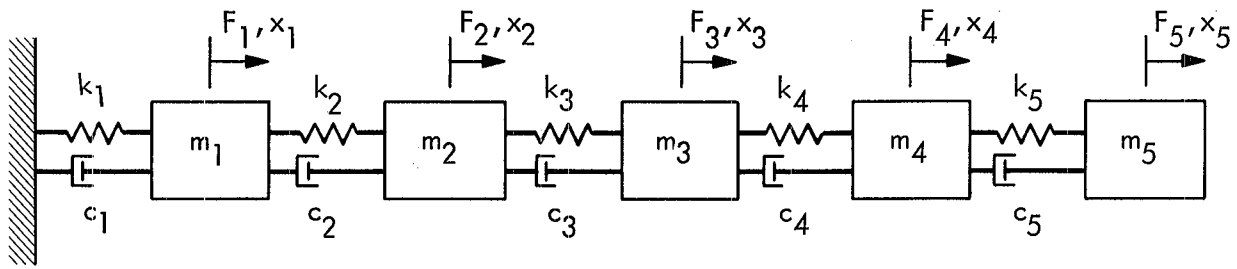


Figure 1. Mass Spring Damper System.

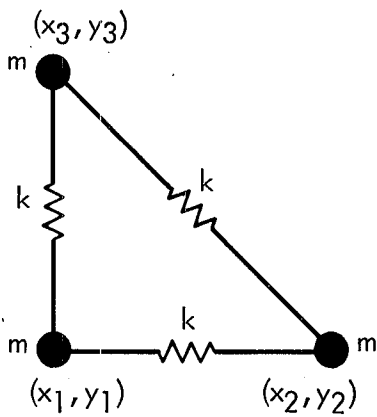


Figure 2. Triangular Plane Truss.

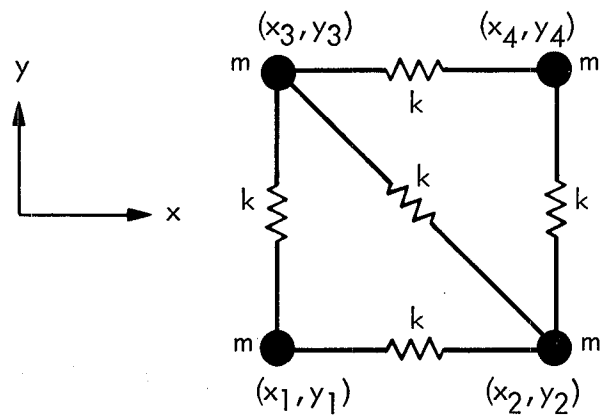


Figure 3. Four Mass Plane Truss.

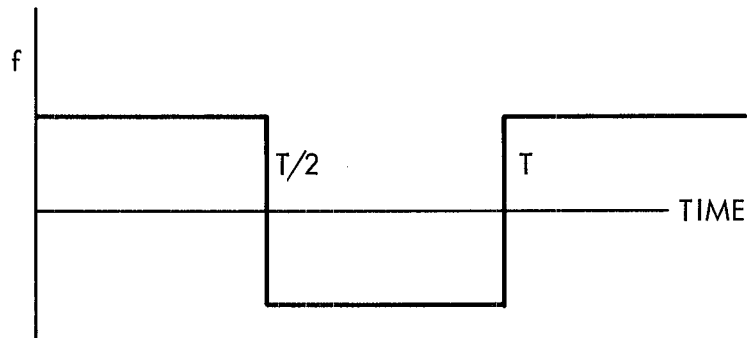


Figure 4. Forcing Function.

The following sets of forcing functions are used

	Set 1	Set 2
F_1	$\cos t$	t
F_2	$\cos 2t$	t^2
F_3	$\cos 3t$	$\cos t$
F_4	$\cos 4t$	$\cos 2t$
F_5	$\cos 5t$	$\cos 3t$

For simulation we assumed

$$m_1 = m_2 = m_3 = m_4 = m_5 = 100 \text{ kg}$$

$$k_1 = k_2 = k_3 = k_4 = k_5 = 36 \text{ N/m}$$

$$c_1 = c_2 = c_3 = c_4 = c_5 = 1.2 \text{ N}\cdot\text{sec/m}$$

All the parameters are recovered very well for both the sets of excitation.

Example 2: A triangular plane truss (Fig. 2) is used as a second example. The masses and spring constants are assumed to be the same. The equation of motion for small displacements takes the form

$$M\ddot{x} + Kx = F$$

where

$$x^T = [x_1 \ y_1 \ x_2 \ y_2 \ x_3 \ y_3],$$

$$F^T = [F_1 \ F_2 \ F_3 \ F_4 \ F_5 \ F_6]$$

$$M = mI$$

$$K = k/2 \begin{bmatrix} 2 & 0 & -2 & 0 & 0 & 0 \\ 0 & 1 & 0 & 0 & 0 & -2 \\ -2 & 0 & 3 & -1 & -1 & 1 \\ 0 & 0 & -1 & 1 & 1 & -1 \\ 0 & 0 & -1 & 1 & 1 & -1 \\ 0 & -2 & 1 & -1 & -1 & 3 \end{bmatrix}$$

After considerable effort, the following forcing functions proved to be useful to recover the parameters.

$$F_1 = \sin t$$

$$F_2 = \cos t$$

$$F_3 = \sin 0.2t$$

$$F_4 = 1 + (\sin 3t)^2$$

$$F_5 = \cos 5t$$

$$F_6 = \cos 6t$$

Simple harmonic functions such as $\sin t, \sin 2t, \dots, \sin 6t$ are not useful.

Example 3: A four mass five spring planar truss as shown in Fig. 3 is used as the third example. Assuming small deflection, the mass and stiffness matrices are given as

$$M = mI$$

$$K = k/2 \begin{bmatrix} 2 & 0 & -2 & 0 & 0 & 0 & 0 & 0 \\ 0 & 2 & 0 & 0 & 0 & -2 & 0 & 0 \\ -2 & 0 & 3 & -1 & -1 & 1 & 0 & 0 \\ 0 & 0 & -1 & 3 & 1 & -1 & 0 & -2 \\ 0 & 0 & -1 & 1 & 3 & -1 & -2 & 0 \\ 0 & -2 & 1 & -1 & -1 & 3 & 0 & 0 \\ 0 & 0 & 0 & 0 & -2 & 0 & 2 & 0 \\ 0 & 0 & 0 & -2 & 0 & 0 & 0 & 2 \end{bmatrix}$$

$$\tilde{x}^T = [x_1 \ y_1 \ x_2 \ y_2 \ x_3 \ y_3 \ x_4 \ y_4]$$

$$\tilde{F}^T = [F_1 \ F_2 \ F_3 \ F_4 \ F_5 \ F_6 \ F_7 \ F_8]$$

Simple harmonic functions as forces are not suitable to recover all the parameters. Hence we decided to use square-wave type excitation as shown in Fig. 4. Eight forcing functions of different period 'T' are used. The amplitude of the forces, f is made equal to 0.078 N. Defining $\omega_i = 2\pi/T_i$, $i = 1, 2, \dots, 8$, we set $\omega_i = (i + 1)/2$. All the parameters (for zero measurement noise) were recovered to their exact values. The important factor appears to be the type of excitation.

The free vibration method worked very well with Example 1.

Conclusions

Two methods are presented to identify the vibration parameters of a linear system. The forced vibration method recovers all the parameters of the system. Further research is needed to determine the optimal excitation of the structure to maximize observability and computability of the system parameters.

References

1. S. R. Ibrahim and E. C. Mikulcik, "A Time Domain Modal Vibration Test Technique," *The Shock and Vibration Bulletin*, Bulletin 43, Part 4, June 1973.
2. S. R. Ibrahim and E. C. Mikulcik, "A Method for the Direct-Identification of Vibration Parameters from the Free Response," *The Shock and Vibration Bulletin*, Bulletin 47, Part 4, 1977.
3. R. J. Benhabib and F. C. Tung, "Large Space Structures Control: System Identification Versus Direct Adaptive Control," *Joint Automatic Control Conference*, San Francisco, California, August, 1980.
4. F. E. Thau and R. C. Montgomery, "Adaptive/Learning Control of Large Space Structures: System Identification Techniques," *Joint Automatic Control Conference* San Francisco, California, August, 1980.
5. Gervasio Prado and R. K. Pearson, "Efficient Techniques for System Identification of Large Space Structures," *Joint Automatic Control Conference*, San Francisco, California, August, 1980.
6. O. B. Dale and R. Cohen, "Multiparameter Identification in Linear Continuous Vibratory Systems," *Journal of Dynamic Systems, Measurement and Control*, March 1971, pp. 45-52.
7. G. R. Spalding, "Distributed System Identification: A Green's Function Approach," *Journal of Dynamic Systems, Measurement and Control*, June 1976, pp. 146-151.
8. Polis, M. P., Goodson, R. E., and Wozny, M. J., "On Parameter Identification for Distributed Systems Using Galerkin's Criterion," *Automatica*, Vol. 9, pp. 53-64, 1973.
9. Connie Weeks, "The Control and Estimation of Large Space Structures," *Joint Automatic Control Conference*, San Francisco, California, August 1980.
10. J. L. Junkins, Optimal Estimation of Dynamical Systems, Sijthoff-Noordhoff Co., Alphen aan den Rijn, The Netherlands/Rockville, Maryland, 1978.
11. L. Meirovitch, Computational Methods in Structural Dynamics, Sijthoff-Noordhoff Co., Alphen aan den Rijn, The Netherlands/ Rockville, Maryland, 1980.

JOINT STATE AND PARAMETER ESTIMATION

N. Carmichael, University of Warwick, Coventry, U.K. CV4 7AL
M.D. Quinn, Sheffield City Polytechnic, Sheffield, U.K. S1 1WB

ABSTRACT

Recent results are described concerning the problem of state reconstruction for a class of nonlinear distributed systems. The methods are then applied to the problem of joint state and parameter estimation. An example with the wave equation is presented.

1. INTRODUCTION

An observed semi-linear system of evolution equations can be described by

$$\left. \begin{aligned} \dot{z} &= Az + f(z), & z(0) &= z_0 \\ y &= Cz \end{aligned} \right\} \quad (1)$$

where z denotes the system state lying in an appropriate Banach space, z_0 is the initial state, A is a linear operator, f is a non-linear operator, y denotes the output and C is a linear output operator. The objective is to consider the state reconstruction problem for infinite dimensional systems of this form. There is a substantial theory already available for state reconstruction in linear systems described by

$$\left. \begin{aligned} \dot{z} &= Az \\ y &= Cz \end{aligned} \right\} \quad (2)$$

In this paper we use the results from linear theory together with suitable fixed-point theorems to find a solution to the state reconstruction problem for (1). We apply these results to the joint state and parameter estimation problem where the parameters are assumed to be constants, and the system has nonlinearities in both state and parameter. (see [1], [3])

2. STATE RECONSTRUCTION

Consider the linear system (2) and assume that A generates a strongly continuous semigroup $S(t)$. Then (2) is said to be initially observable if the map from the initial state to the output trajectory

$$H : z_0 \rightarrow CS(\cdot)z_0$$

is injective, i.e. $\text{Ker } H = \{0\}$. The system (2) is said to be continuously initially observable if $\text{Ker } H = \{0\}$ and $\text{Range } H$ is closed. This latter definition means that we are able to reconstruct the initial state z_0 given the output trajectory

$y(\cdot)$. That is to say we may construct a linear bounded inverse of H , denoted H^{-1} , which has as its domain space the chosen space of output trajectories (this space is usually larger than the range of H). Of course, as elsewhere in partial differential equations much depends on the particular function spaces used.

We proceed formally by writing down the mild solution of system (1)

$$z(t) = S(t)z_0 + \int_0^t S(t-s)f(z(s)) ds \quad (3)$$

$$y(t) = CS(t)z_0 + C \int_0^t S(t-s)f(z(s)) ds \quad (4)$$

Then the map H is defined by

$$H z_0 = y(\cdot) - C \int_0^\cdot S(\cdot-s)f(z(s)) ds \quad (5)$$

therefore

$$z_0 = H^{-1}(y(\cdot) - C \int_0^\cdot S(\cdot-s)f(z(s)) ds) \quad (6)$$

Now substituting (6) into (3) we obtain

$$z(t) = S(t)H^{-1}(y(\cdot) - C \int_0^\cdot S(\cdot-s)f(z(s))ds) + \int_0^t S(t-s)f(z(s))ds \quad (7)$$

$$(c) \quad B_a = \{z \in L^r(0, t_1; Z_1) : \|z\|_{L^r(0, t_1; Z_1)} \leq a\}$$

and

$$(Rc_1 + c_2) \alpha (\|z\|, \|\hat{z}\|) \leq K \leq 1$$

for $z, \hat{z} \in B_a$; and where R is defined by

$$\left\| \int_0^{\cdot} S(\cdot - \tau) f(z(\tau)) d\tau \right\|_{\mathcal{Y}} \leq R \|z\|_{L^s(0, t_1; Z_2)}$$

(\mathcal{Y} denotes the space in which the output trajectories lie)

then: the state of the system described by (1) can be reconstructed given an observation, $y(\cdot)$, satisfying

$$\|y(\cdot)\|_{\mathcal{Y}} \leq \frac{(1-K)a}{c_2 \|H^{-1}\|} \mathcal{L}(\mathcal{Y}, Z)$$

Proof

See [1].

3. JOINT STATE AND PARAMETER ESTIMATION

Consider a nonlinear system of the form

$$\left. \begin{aligned} \dot{z} &= g(z, \alpha, t), \quad z(0) = z_0 \\ y &= h(z, \alpha, t) \end{aligned} \right\} \quad (8)$$

where z is the state, y is the output and α is a vector of, a priori unknown, parameters. Taking a local approximation of these equations about an initial guess $(\bar{z}(\cdot), \bar{\alpha})$ we assume that we can obtain a system

$$\left. \begin{aligned} \dot{z} &= Az + A_1 \alpha + f(z, \alpha) \\ y &= Cz \end{aligned} \right\} \quad (9)$$

where A, A_1, C are time-independent linear operators.

The right-hand side of (7) defines a map Φ operating on the space of trajectories $z(\cdot)$. A fixed point of this map Φ will be consistent both with the state equations (3) and the output equation $y = Cz$ (since of z^* is such that $z^* = \Phi z^*$ then $Cz^* = C\Phi z^* = y$). Thus we have reduced the reconstruction problem to finding fixed points of the nonlinear map Φ . In general, the results obtained are local, both in the space of trajectories and in time.

There are several fixed-point theorems available for use (see [1], [3]) but here we state a theorem using a local version of the contraction mapping theorem.

Theorem

Suppose that A generates a strongly continuous semigroup $S(t)$ and that the linear system (2) is continuously initially observable. Let Z, Z_1, Z_2 be Banach spaces and

$$p, r, q, s, a, c_1, c_2, K, R \in \mathbb{R}^+ \text{ with } r \geq 1, p \geq q \geq 1, \frac{1}{r} = \frac{1}{q} + \frac{1}{s} - 1, s \geq 1.$$

Assume

$$(a) \quad S(t) \in \mathcal{L}(Z_1, Z) \cap \mathcal{L}(Z_2, Z)$$

with

$$\|S(t)z\|_Z \leq g_1(t) \|z\|_{Z_1}, \quad \|g_1\|_{L^r(0, t_1)} = c_1 < \infty$$

$$\|S(t)z\|_Z \leq g_2(t) \|z\|_{Z_2}, \quad \|g_2\|_{L^p(0, t_1)} = c_2 < \infty$$

(b) for some $\alpha : \mathbb{R}^+ \times \mathbb{R}^+ \rightarrow \mathbb{R}^+$ which is continuous and symmetric with $\alpha(\theta, 0) \rightarrow 0$ as $\theta \rightarrow 0$ we have

$f : L^r(0, t_1; Z_1) \rightarrow L^s(0, t_1; Z_2)$ satisfying

$$\|f(z) - f(\hat{z})\|_{L^s(0, t_1; Z_2)} \leq \alpha(\|z\|, \|\hat{z}\|) \|z - \hat{z}\|$$

the norms on the right-hand side computed in $L^r(0, t_1, Z_1)$.

In practice, however, we may have a time varying linear part, a non-linear part in the output equation and known functions in both the state and output equations. All these factors entail modifications to the detail, but not necessarily the essence, of the present approach.

Assume that the parameters are constant and finite-dimensional so that $\dot{\alpha} = 0$ and $\alpha \in \mathbb{R}^P$. Let $\begin{bmatrix} z \\ \alpha \end{bmatrix}$ denote the augmented state

and so the system is described by

$$\frac{d}{dt} \begin{bmatrix} z \\ \alpha \end{bmatrix} = \begin{bmatrix} A & A_1 \\ 0 & 0 \end{bmatrix} \begin{bmatrix} z \\ \alpha \end{bmatrix} + \begin{bmatrix} f(z, \alpha) \\ 0 \end{bmatrix}, \quad \begin{bmatrix} z \\ \alpha \end{bmatrix}(0) = \begin{bmatrix} z_0 \\ \alpha \end{bmatrix} \quad (10)$$

$$y = [c, 0] \begin{bmatrix} z \\ \alpha \end{bmatrix} \quad (11)$$

The joint state and parameter estimation problem is to reconstruct the state $z(t)$ ($t \geq 0$) and the parameters α , given $y(\cdot)$ on $[0, t_1]$.

This has now been reduced to the state estimation (for the augmented state) case of Section 2. To apply the result of Section 2 we require that the linear part of (10), (11) be continuously observable.

Lemma

Suppose that the pair (A, C) is continuously initially observable and that the linear part of (10), (11) describes a well-defined dynamical system. If the map

$$\begin{bmatrix} A & A_1 \\ C & 0 \end{bmatrix} \quad \text{is injective}$$

then the linear part of (10), (11) is continuously initially observable.

Proof

Consider the linear part

$$\dot{z} = Az + A_1 \alpha \quad (12)$$

$$y = Cz$$

and the corresponding initial state-to-output map given by

$$y(t) = CS(t)z_0 + C \int_0^t S(t-s) A_1 \alpha \, ds \quad (13)$$

Denote the right hand side of (13) by $F\left(\begin{bmatrix} z_0 \\ \alpha \end{bmatrix}\right)$, a linear

map acting on the augmented initial state, and suppose that $y(t) \equiv 0$ for all $t \in [0, t_1]$. Then for $z_0 \in D(A)$ (the

domain of A) differentiation yields

$$CS(t) (Az_0 + A_1 \alpha) = 0 \quad (14)$$

and so, since (A, C) is initially observable,

$$Az_0 + A_1 \alpha = 0.$$

Let $t = 0$ then $Cz_0 = 0$. Hence $Cz_0 = Az_0 + A_1 \alpha_0 = 0$

which, by the injectivity assumption, is only possible when $z_0 = 0$, $\alpha = 0$. Therefore the map defined by (13)

is injective and so the linear part of the augmented system is initially observable. Since we have assumed that (A, C) is continuously initially observable and the parameter-space is finite dimensional then, by (13), the range of F is closed. Hence the linear augmented system is continuously initially observable. ■

The theorem of Section 2 can now be applied with the additional assumption that

$$\text{Ker} \begin{bmatrix} A & A_1 \\ C & 0 \end{bmatrix} = \{0\}.$$

This will provide (at least in the contraction mapping case) both conditions for the existence of a fixed point and an algorithm (successive approximation) for finding it.

Further development of this method will consider the case when the original system (A,C) is only initially observable and also the case when the parameter-space is not finite dimensional (e.g. spatially varying parameters).

4. EXAMPLE

Here we apply the results of the preceding sections to the observed one-dimensional wave equation

$$\begin{aligned} w_{tt} &= w_{xx} + \alpha w \\ w(0,t) &= w(1,t) = 0 \end{aligned} \tag{15}$$

where $\alpha \in \mathbb{R}$ is the unknown parameter, and the observation is

$$y(\cdot) = \int_0^1 c(x) w(x, \cdot) dx = \langle c, w \rangle$$

Taking initial guesses for state and parameter as \bar{w} , $\bar{\alpha}$ respectively (\bar{w} does not depend on t , $\bar{w}(0) = \bar{w}(1) = 0$ and $\bar{\alpha} = 0$ for simplicity) we then make the usual local approximation $w = \bar{w} + w'$, $\alpha = \bar{\alpha} + \alpha'$ to obtain

$$w'_{tt} = w'_{xx} + \bar{w}\alpha' + \bar{w}_{xx} + \alpha'w' \tag{16}$$

with $w'(0,t) = w'(1,t) = 0$

The observation is now given by

$$y(\cdot) = \langle c, w'(\cdot) \rangle_{L^2(0,1)} + \langle c, \bar{w} \rangle_{L^2(0,1)} \tag{17}$$

Substituting $z = \begin{bmatrix} w' \\ w'_t \end{bmatrix}$, in the usual way, we obtain a

system in the form

$$\begin{aligned}\dot{z} &= Az + A_1 \alpha + f(z, \alpha) + u \\ y &= Cz + v\end{aligned}$$

where u, v are known inputs

A standard result shows that (A, C) is continuously initially observable if y , the space of output trajectories, consists of functions of the form

$$y(t) = \sum_{n=1}^{\infty} (a_n \cos n\pi t + b_n \sin n\pi t)$$

normed by

$$\|y\|_{\mathcal{Y}}^2 = \sum_{n=1}^{\infty} \frac{n^2 \pi^2 (a_n^2 + b_n^2)}{c_n^2}$$

Now, using the lemma in Section 3, continuous initial observability for the linear part of the augmented system obtained if

$$\sum_{n=1}^{\infty} \frac{c_n \bar{w}_n}{n^2} \neq 0 \quad \text{for } \bar{w}_n = \langle \bar{w}, \phi_n \rangle_{L^2(0,1)}$$

where $\phi_n = \sqrt{2} \sin n\pi x$. Hence we may apply the theorem of

Section 2 (suitably modified to account for the known inputs u and v) to jointly identify initial state and parameters. In the present example we have $\alpha(\theta_1, \theta_2) = c(\theta_1 + \theta_2)$ for part (b)

of the theorem, where c is some constant. The principles illustrated here can be extended to create joint and parameter estimators for other hyperbolic-type equations.

5. REFERENCES

1. Carmichael, N., Pritchard, A.J., and Quinn, M.D., State estimation for nonlinear systems, accepted for publication in Applied Mathematics and Optimization.
2. Ichikawa, A., and Pritchard, A.J., Existence, uniqueness and stability of non-linear evolution equations, J. Math. Anal. Appl., Vol 68, 1979, pp. 454-476.
3. Carmichael, N., Pritchard, A.J., and Quinn, M.D., Nonlinear control and estimation: an approach via fixed point theorems and degree theory, Proceedings of Graz 1981 Symposium.

This Page Intentionally Left Blank

PARAMETER ESTIMATION IN TRUSS BEAMS USING TIMOSHENKO BEAM MODEL WITH DAMPING

C.T. Sun,

School of Aeronautics and Astronautics, Purdue University, West Lafayette, IN 47907

J.N. Juang*

Guidance and Control Section, Martin Marietta Aerospace, Denver, CO 80201

ABSTRACT

Truss beams with members having viscous damping are modeled with a Timoshenko beam. Procedures for deriving the equivalent bending rigidity, transverse shear rigidity, and damping are presented. Explicit expressions for these equivalent beam properties are obtained for a specific truss beam. The beam model thus established is then used to investigate the effect of damping in free vibration. Finally, the beam is employed in the estimation of structural parameters in a simply-supported truss beam using a random search algorithm.

INTRODUCTION

Many methods currently employed for the dynamic analysis of structures such as the finite element method are adequate and accurate. However, as the system becomes large, direct application of the finite element method is found to be computationally expensive and its accuracy degenerates. Moreover, as each individual structural component is taken into account in the formulation, the number of structural parameters is large which makes the system identification very difficult.

In view of the fact that many large space structures, although large in size and complex in detail, often appear grossly as a beam, plate, or thin shell, some researchers have derived equivalent continuum models for dynamic analyses [1-3]. These simple continuum models have proven to be quite accurate in predicting natural frequencies and mode shapes for a significant number of modes. Since these equivalent continuum models have few structural parameters, they are particularly useful in system identification problems [4].

* Now with NASA Langley Research Center, Hampton, Virginia 23665

Structural damping plays an important role in the prediction of spacecraft structural responses and loads [5] which are needed in the structural and control design. As the aerodynamic damping is absent in the space environment, damping in a spacecraft results from the deformation in each structural member and joint. The contribution to the overall structural damping from each member with known damping properties can be theoretically estimated. In this paper, procedures are presented for deriving the gross damping properties for the simple beam model which is used to represent beam-like trusses. The beam model with damping thus constructed is then used to study the effect of damping in free vibration of a simply-supported truss beam. Finally, this model is employed in the estimation of structural parameters of the truss beam by using a random search algorithm.

BEAM MODEL WITH DAMPING

Detailed procedures for deriving the equivalent beam rigidities from a truss beam were given by [1]. Among the three beam models, shear beam, Bernoulli-Euler beam, and Timoshenko beam, the Timoshenko beam theory was found to be most accurate and most suitable to represent general trusses. In this study, the Timoshenko beam model is used.

For simplicity, consider a beam which is symmetric with respect to the mid-plane so that the extension is not coupled with the flexural deformation. The shear force Q and bending moment M are related to the transverse displacement w and the rotation ψ as

$$\begin{Bmatrix} Q \\ M \end{Bmatrix} = \begin{bmatrix} \overline{GA} & \eta_{23} \\ \eta_{23} & \overline{EI} \end{bmatrix} \begin{Bmatrix} w_{,x} + \psi \\ \psi_{,x} \end{Bmatrix} \quad (1)$$

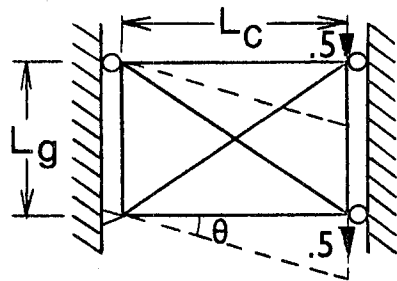
where \overline{GA} is the transverse shear rigidity, \overline{EI} the bending rigidity, and η_{23} is the bending-shear coupling coefficient.

The displacement-equations of motion are [1]

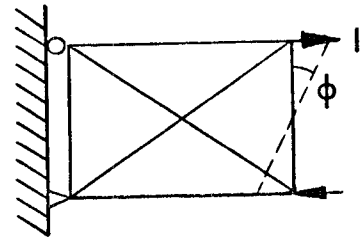
$$\begin{aligned} \overline{EI} \psi_{,xx} - \overline{GA}(w_{,x} + \psi) &= \overline{\rho I} \ddot{\psi} \\ \overline{GA}(w_{,xx} + \psi_{,x}) &= \overline{m} \ddot{w} - q \end{aligned} \quad (2)$$

where $\overline{\rho I}$ is rotatory inertia, \overline{m} is mass per unit length, and q is transverse load per unit length.

The bending rigidity \overline{EI} and shear rigidity \overline{GA} are obtained from a typical substructure by applying a bending moment and shear force, respectively, as shown in Fig. 1. They are expressed as [1]



Substructure in Shear



Substructure in Bending

Fig 1 Substructure in transverse shear and bending deformations.

$$\begin{aligned} \overline{EI} &= \frac{L_g L_c}{\phi} \\ \overline{GA} &= \frac{1}{\theta} \end{aligned} \quad (3)$$

The deformations ϕ , and θ , can be calculated analytically or numerically using the matrix method. From the solutions for the substructure, we also obtain the uniaxial strains in the truss members as

$$\begin{Bmatrix} \epsilon_1 \\ \epsilon_2 \\ \vdots \\ \epsilon_6 \end{Bmatrix} = \begin{Bmatrix} a_1 \\ a_2 \\ \vdots \\ a_6 \end{Bmatrix} \psi, x \quad (4)$$

for the bending deformation, and

$$\begin{Bmatrix} \epsilon_1 \\ \epsilon_2 \\ \vdots \\ \epsilon_6 \end{Bmatrix} = \begin{Bmatrix} b_1 \\ b_2 \\ \vdots \\ b_6 \end{Bmatrix} (w, x + \psi) \quad (5)$$

for the transverse shear deformation. In Eqs. (4-5), the rotation gradient ψ, x and the transverse shear strain $w, x + \psi$ are approximated by

$$\psi_{,x} = \phi/L_c \quad (6)$$

and

$$w_{,x} + \psi = \theta \quad (7)$$

respectively.

Consider truss member i for which the stress-strain relation is given by

$$\sigma_i = E_i \epsilon_i + d_i \dot{\epsilon}_i \quad (8)$$

in which the viscous damping is included. In Eq. (8), σ is the normal stress, E is the Young's modulus, ϵ is the normal strain, d is the damping coefficient, and a subscript i denotes member i .

It is assumed that the damping is small so that the damping force is much smaller than the elastic force. As a result of this assumption, the elastic relations given by Eqs. (4-5) are taken also for nonvanishing strain rates, i.e.,

$$\dot{\epsilon}_i = a_i \dot{\psi}_{,x} \quad (9)$$

$$\dot{\epsilon}_i = b_i (\dot{w}_{,x} + \dot{\psi}) \quad (10)$$

The resulting damping forces in the truss members computed according to Eqs. (8-10) are then added to the elastic forces. Equation (1) then takes the new form

$$\begin{Bmatrix} Q \\ M \end{Bmatrix} = \begin{bmatrix} \overline{GA} & \eta_{23} \\ \eta_{23} & \overline{EI} \end{bmatrix} \begin{Bmatrix} w_{,x} + \psi \\ \psi_{,x} \end{Bmatrix} + \begin{bmatrix} C_{22} & C_{23} \\ C_{32} & C_{33} \end{bmatrix} \begin{Bmatrix} \dot{w}_{,x} + \dot{\psi} \\ \dot{\psi}_{,x} \end{Bmatrix} \quad (11)$$

where the equivalent global damping coefficient C_{ij} are functions of the damping coefficients and elastic properties of the ij truss members.

As an illustration, consider the substructure shown in Fig. 1 with

$$A_1 = A_2, \quad A_3 = A_4, \quad A_5 = A_6$$

$$d_1 = d_2, \quad d_3 = d_4, \quad d_5 = d_6$$

and that all the members have the same elastic constants. The simple bending and transverse shear deformations yield the following axial strains in the truss members as

$$\begin{Bmatrix} \epsilon_1 \\ \epsilon_2 \\ \epsilon_3 \\ \epsilon_4 \\ \epsilon_5 \\ \epsilon_6 \end{Bmatrix} = \begin{Bmatrix} \frac{1}{2} L_g \\ -\frac{1}{2} L_g \\ 0 \\ 0 \\ 0 \\ 0 \end{Bmatrix} \psi, x \quad (12)$$

$$\begin{Bmatrix} \epsilon_1 \\ \epsilon_2 \\ \epsilon_3 \\ \epsilon_4 \\ \epsilon_5 \\ \epsilon_6 \end{Bmatrix} = \begin{Bmatrix} 0 \\ 0 \\ L_g L_c / (L_g^2 + L_c^2) \\ -L_g L_c / (L_g^2 + L_c^2) \\ 0 \\ 0 \end{Bmatrix} (w, x + \psi) \quad (13)$$

From the above relations, we obtain the equivalent elastic transverse shear force and bending moment:

$$\begin{Bmatrix} Q \\ M \end{Bmatrix}_{\text{elastic}} = \begin{bmatrix} \frac{2 L_g^2 L_c}{(L_g^2 + L_c^2)^{3/2}} EA_3 & 0 \\ 0 & \frac{1}{2} L_g^2 A_1 E \end{bmatrix} \begin{Bmatrix} w, x + \psi \\ \psi, x \end{Bmatrix} \quad (14)$$

for which we have

$$\overline{GA} = \frac{2 L_g^2 L_c}{(L_g^2 + L_c^2)^{3/2}} EA_3 \quad (15)$$

$$\overline{EI} = \frac{1}{2} L_g^2 A_1 E \quad (16)$$

The additional transverse force and bending moment due to damping are calculated using Eqs. (12-13). We obtain

$$\begin{Bmatrix} Q \\ M \end{Bmatrix}_{\text{damping}} = \begin{bmatrix} \frac{2 L_g^2 L_c}{(L_g^2 + L_c^2)^{3/2}} A_3 d_3 & 0 \\ 0 & \frac{1}{2} L_g^2 A_1 d_1 \end{bmatrix} \begin{Bmatrix} \dot{w}_{,x} + \dot{\psi} \\ \dot{\psi}_{,x} \end{Bmatrix} \quad (17)$$

Thus, the equivalent global damping coefficients for the beam model are

$$\begin{aligned} C_{22} &= \frac{2 L_g^2 L_c}{(L_g^2 + L_c^2)^{3/2}} A_3 d_3 \\ C_{33} &= \frac{1}{2} L_g^2 A_1 d_1 \\ C_{23} &= C_{32} = 0 \end{aligned} \quad (18)$$

Combining Eqs. (14) and (17), we obtain

$$\begin{aligned} Q &= \overline{GA} (w_{,x} + \psi) + C_{22} (\dot{w}_{,x} + \dot{\psi}) \\ M &= \overline{EI} \psi_{,x} + C_{33} \dot{\psi}_{,x} \end{aligned} \quad (19)$$

The corresponding displacement-equations of motion are

$$\begin{aligned} (\overline{EI} \psi_{,x})_{,x} - \overline{GA}(w_{,x} + \psi) + (C_{33} \dot{\psi}_{,x})_{,x} \\ - C_{22}(\dot{w}_{,x} + \dot{\psi}) = \overline{\rho I} \ddot{\psi} \end{aligned} \quad (20)$$

$$[\overline{GA}(w_{,x} + \psi)]_{,x} + [C_{22}(\dot{w}_{,x} + \dot{\psi})]_{,x} = \overline{m} \ddot{w} - q \quad (21)$$

PARAMETER ESTIMATION - RANDOM SEARCH METHOD

The Timoshenko beam equations, Eqs. (20-21), and the measurement equation can be expressed in the form

$$\begin{aligned} \ddot{z} &= Dz + Kz + Bu, \quad x \in \Omega, \quad t \in T \\ y &= Cz \end{aligned} \quad (22)$$

where $z = (z_1, z_2)^T = (w, \psi)^T$ is the distributed state vector, $u = (\bar{m}^{-1}q, 0)$ is a ρ -vector control input, $t \in T (= (t_0, t_f))$ is time, x is the spatial coordinate in domain Ω , D and K are linear matrix differential operators in Ω given by

$$D = \begin{bmatrix} \beta_4 D^2 & \beta_4 D \\ -\beta_5 D & \beta_6 D^2 - \beta_5 \end{bmatrix}, \quad D = \partial/\partial x \quad (23)$$

$$K = \begin{bmatrix} \beta_1 D^2 & \beta_1 D \\ -\beta_2 D & \beta_3 D^2 - \beta_2 \end{bmatrix} \quad (24)$$

in which

$$\begin{aligned} \beta &\triangleq (\beta_1, \beta_2, \beta_3, \beta_4, \beta_5, \beta_6)^T \\ &= (\overline{GA}/\bar{m}, \overline{GA}/\rho I, \overline{EI}/\rho I, C_{22}/\bar{m}, C_{22}/\rho I, C_{33}/\rho I)^T \end{aligned}$$

is a vector of all the parameters in the simple continuum model, and B and C are finite-dimensional influence matrix functions or integral operators.

Of practical interest are the following boundary conditions:

(1) Fixed-Fixed Beam:

$$z(0, t) = z(\ell, t) = 0 \quad (25)$$

(2) Simply Supported Beam:

$$\Gamma z(0, t) = \Gamma z(\ell, t) = 0 \quad (26)$$

where

$$\Gamma = \begin{bmatrix} 1 & 0 \\ 0 & D \end{bmatrix}$$

(3) Cantilever Beam:

$$z(l, t) = rz(0, t) = 0 \quad (27)$$

where

$$\Gamma = \begin{bmatrix} 1 & -1 \\ 0 & D \end{bmatrix} \quad (28)$$

The output error is given by

$$e(t) = y(t) - \hat{y}(t) = (y_1 - \hat{y}_1, \dots, y_m - \hat{y}_m) \quad (29)$$

where \hat{y} is the actual measurement vector.

The error cost function is defined by

$$J(\beta) = \frac{1}{2t_f} \int_0^{t_f} e^T R e dt \quad (30)$$

in which R is a positive definite weighting matrix. The objective of updating the simple model is to adjust β so that $J(\beta)$ achieves the minimum.

The estimation procedure of the random search method has been successfully employed for parameter estimation for the Timoshenko beam model without damping [4]. The procedure is briefly outlined as follows. We start with an initial estimate of parameter β obtained from the simple model. Then, an iterative process follows to match the test data by updating the analytical model. Specifically, at the i th iteration, the parameter vector $\beta|_i$ is given by

$$\beta|_i = \beta|_{i-1} + \Delta\beta; \beta|_{i-1} = (\beta_1, \beta_2, \dots, \beta_6)_{i-1} \quad (31)$$

where the increment $\Delta\beta$ is given by

$$\Delta\beta \triangleq (\pm \alpha_1 \beta_1, \pm \alpha_2 \beta_2, \dots, \pm \alpha_6 \beta_6)^T \quad (32)$$

in which α_i ($=N(\sigma, \gamma)$) is a Gaussian distributed random number with mean σ and standard deviation γ which are determined by the accuracy requirement

of parameter estimation. For example, the $(1+0.25)\%$ error limit can be provided by selecting $\sigma = 0.01$ and $\gamma = 0.0025$. The values of α_i ($i = 1-6$) are fixed for each iteration. The constant α_i should be carefully chosen as this scheme may diverge if α_i are too large. On the other hand, if α_i are too small, then β would converge to true values very slowly. Note that the plus and minus signs in $\Delta\beta$ result in 2^6 trial samples of $\beta|_i$.

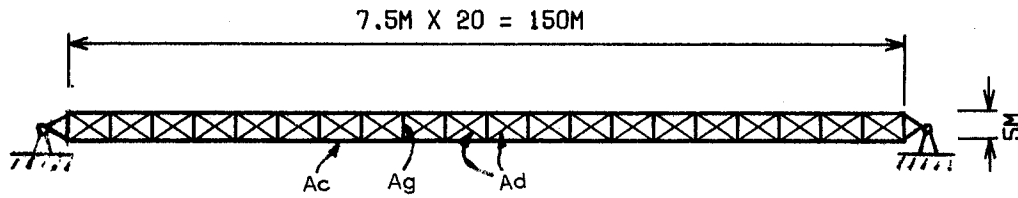
For each iteration, the following steps are carried out.

- Step 1: Compute Gaussian distributed random numbers α_j
- Step 2: Discretize the continuum model (22) with given parameters $\beta|_i$ to obtain a finite dimensional model including all the chosen natural modes.
- Step 3: Compute cost function $J(\beta|_i)$ (see Eq. (30)) by integrating the square of the measurement error between the analytical model and the actual system.
- Step 4: Go back to step 2 with different β resulting from the different plus and minus combinations in Eq. (32) until 2^6 trial samples of $\beta|_i$ run out.
- Step 5: Obtain the direction $\Delta\beta_S$ of the smallest $J_S(\beta|_i)$ in the group of 2^6 cost function $J(\beta|_i)$. If $J_S(\beta|_i) > J_S(\beta|_{i-1})$, go to step 8.
- Step 6: Perform a one-dimensional minimization of $J(\beta)$ along the direction $\Delta\beta_S$ until the slope of the cost function $J(\beta)$ changes sign.
- Step 7: Update $\beta|_i$ at which cost function $J(\beta)$ is minimum and return to Step 1.
- Step 8: Minimization is completed.

EXAMPLE

Consider a simply-supported truss beam for which the dimension and properties of the truss members are given in Fig. 2. In this figure, A_c , A_g , and A_d indicate the member cross-sectional areas, E is the modulus of elasticity, and ρ is the mass density. The damping coefficients will be assumed as variables.

The equivalent bending and transverse shear rigidities for the Timoshenko beam model are computed from Eqs. (15-16), and the equivalent mass \bar{m} and rotatory inertia $\bar{\rho I}$ are obtained using the procedure suggested by [1]. We have



$$\begin{aligned}
 E &= 71.7 \times 10^9 \text{ [N/m}^2\text{]} & , & \quad \rho = 2768 \text{ [kg/m}^3\text{]} \\
 A_c &= 80 \times 10^{-6} \text{ [m}^2\text{]} & , & \quad A_g = 60 \times 10^{-6} \text{ [m}^2\text{]} \\
 A_d &= 40 \times 10^{-6} \text{ [m}^2\text{]}
 \end{aligned}$$

Fig. 2 Simply-supported truss beam.

$$\begin{aligned}
 \overline{GA} &= 1.468 \times 10^6 \text{ N} \\
 \overline{EI} &= 7.17 \times 10^7 \text{ N-m}^2 \\
 \overline{m} &= 0.875 \text{ N-sec}^2/\text{m}^2 \\
 \overline{\rho I} &= 3.55 \text{ N-sec}^2
 \end{aligned} \tag{33}$$

Damped Free Vibration

Free vibration ($q=0$) of the simply-supported Timoshenko beam can be studied using Eqs. (20-21) or Eq. (22) with the boundary conditions, Eq. (26). The frequency equation is obtained as

$$\lambda^4 + h_3 \lambda^3 + h_2 \lambda^2 + h_1 \lambda + h_0 = 0 \tag{34}$$

where

$$h_0 = \beta_1 \beta_3 \omega_r^2 ; \quad \omega_r^2 = (r\pi/l)^2, \quad r = 1, 2, \dots$$

$$h_1 = (\beta_1 \beta_6 + \beta_3 \beta_4) \omega_r^2$$

$$h_2 = (\beta_1 + \beta_3) \omega_r + \beta_2 + \beta_4 \beta_6 \omega_r^2$$

$$h_3 = (\beta_4 + \beta_6) \omega_r + \beta_5$$

The biquadratic equation, Eq. (34), can be solved numerically yielding an infinite number of solutions λ in the form

$$\lambda_r^{(1)} = -\eta_r^{(1)} \pm i \omega_r^{(1)} ; \quad i = \sqrt{-1} \quad (35)$$

$$\lambda_r^{(2)} = -\eta_r^{(2)} \pm i \omega_r^{(2)} \quad (36)$$

where η_r and ω_r are positive quantities. The two roots $\lambda_r^{(1)}$ and $\lambda_r^{(2)}$ represent two different branches of deformation with one frequency $\omega_r^{(2)}$ much larger than $\omega_r^{(1)}$. The branch with the lower frequency is of practical interest and henceforth will be taken for further discussions.

Corresponding each eigenvalue λ_r , we obtain the mode shape of deflection as

$$\begin{aligned} w &= W_r e^{\lambda_r t} \sin(r\pi x/\ell) \\ \psi &= \Psi_r e^{\lambda_r t} \cos(r\pi x/\ell) \end{aligned} \quad (37)$$

where the amplitudes W and Ψ are related by

$$\Psi_r = W_r [-\lambda_r^2 - (\beta_1 + \beta_4 \lambda_r) (r\pi/\ell)^2] / (\beta_1 + \beta_4 \lambda_r) (r\pi/\ell) \quad (38)$$

For the following three sets of damping coefficients,

$$C_{22} = 0 \quad \text{N-sec} , \quad C_{33} = 4 \times 10^4 \quad \text{N-m}^2\text{-sec}$$

$$C_{22} = 200 \quad \text{N-sec} , \quad C_{33} = 0 \quad \text{N-m}^2\text{-sec}$$

$$C_{22} = 100 \quad \text{N-sec} , \quad C_{33} = 4 \times 10^4 \quad \text{N-m}^2\text{-sec}$$

the frequencies of the lowest branch and the corresponding damping ratios are presented in Table 1. Only the modes of odd numbers are listed.

The numerical results shown in Table 1 reveal an interesting damping characteristic in Timoshenko beam, i.e., the amount of damping due to bending increases initially as the frequency increases, but decreases after the eleventh mode. On the other hand, the amount of damping due to the transverse shear deformation is larger for higher modes. For the lower modes, the transverse shear damping is negligible as the bending deformation dominates in the lower mode vibration. When both bending and transverse shear dampings are present, the former is dominant in the lower

Table 1 Natural Frequencies and Damping Ratios

Damping	$C_{33} = 4 \times 10^4, C_{22} = 0$		$C_{33} = 0, C_{22} = 200$		$C_{33} = 4 \times 10^4, C_{22} = 100$	
Freq. Mode	Frequency (rad/sec)	Damping Ratio(%)	Frequency (rad/sec)	Damping Ratio(%)	Frequency (rad/sec)	Damping Ratio(%)
1	3.691	0.094	3.691	0.00051	3.691	0.094
3	30.66	0.673	30.66	0.032	30.66	0.689
5	74.99	1.303	74.99	0.169	74.99	1.388
7	127.4	1.699	127.4	0.422	127.4	1.910
9	182.8	1.869	182.6	0.753	182.7	2.246
11	239.0	1.891	238.6	1.126	239.0	2.458
13	295.0	1.834	294.4	1.519	295.0	2.599
15	322.9	1.789	349.8	1.918	350.4	2.707
17	406.0	1.626	404.7	2.318	406.0	2.801
19	460.8	1.512	459.2	2.716	433.0	2.845

modes and the latter is dominant in the higher modes as revealed by the results for the third set of damping coefficients.

Since a truss beam has been shown to behave like a Timoshenko beam [1], its motion at higher modes is dominated by transverse shear deformations. Thus, there may exist a lower bound frequency which could give rise to enough damping ratio specified by the control designer. Moreover, the control and observation spillover may be overcome by the material damping and no complicated control compensations are needed. In that case, control designs based upon discrete models without residual modes may be justified.

Parameter Estimation

In the undamped or purely elastic case, the truss beam (see Fig. 2) can be analyzed by using the finite element method to model each individual truss member as a rod element. The solution thus obtained can be regarded as the "exact solution" except for very high modes. This exact solution can be used as a basis for estimating the accuracy of the simple continuum model. For the simply-supported beam shown in Fig. 2, the first five undamped natural frequencies obtained from the finite element program SAPIV and from the Timoshenko beam model are presented in Table 2. The corresponding modal displacements at the mid-span are also given in this table. It is evident that the simple model yields excellent frequency and displacement predictions. It is reasonable to say that the simple model provides a good initial estimate of the structural properties of the actual system.

Table 2 Actual and Updated Simple Model Solutions for the Truss Beam

Mode	Finite Element		Simple Model		Updated Simple Model	
	Frequency (rad/sec)	Modal Displ.	Frequency (rad/sec)	Modal Displ.	Frequency (rad/sec)	Modal Displ.
1	3.684	0.124	3.564	0.121	3.692	0.121
2	14.32	0.0	13.84	0.0	14.32	0.0
3	30.84	-0.123	29.75	-0.121	30.75	-0.121
4	51.87	0.0	49.95	0.0	51.69	0.0
5	76.30	0.123	73.20	0.121	76.08	0.121

When damping is present, we will still take the finite element solution as the actual solution and the simple model (with damping) will be updated using the random search algorithm described in the previous section. A single noise-free displacement sensor and a force actuator are chosen and co-located at the center of the span for input and output measurements.

For a unit impulse applied at the mid-span, the response of displacement at the mid-span can be written in the form

$$y = \sum_{j=1}^n \hat{\phi}_j^2 e^{\eta_j t} (\sin \omega_j t) / \omega_j \quad (39)$$

where $\eta_j + i\omega_j = \lambda_j$, $i = \sqrt{-1}$, $\hat{\phi}_j$ is the transverse modal displacement at the mid-span of the beam corresponding to the eigenvalue λ_j , and n is the total mode number to be included in the simulation.

The cost function $J(\beta)$ given by Eq. (30) with R chosen as a unity matrix is obtained by exciting both the actual system and the simple model with the same impulse input. For the purpose of simulation, the full-scale finite element modeling of the actual truss beam (without damping) is regarded as the actual system. In updating the simple model, only the bending rigidity EI and the transverse shear rigidity \overline{GA} are varied while the damping coefficients, $C_{22} = 100$ $C_{33} = 4 \times 10^4$, are kept constant. By using the random search algorithm, the bending and transverse rigidities which minimize the cost function are found to be

$$EI = 7.7 \times 10^7 \text{ N-m}^2$$

$$\overline{GA} = 1.499 \times 10^6 \text{ N}$$

The natural frequencies and modal displacements for the first five modes calculated using these updated beam rigidities are shown in the last column in Table 2. It is evident that these frequencies of the updated simple model are all within 0.3% of the actual solutions. The mode shapes remain unchanged since they do not depend on the bending and shear rigidities which are represented by the parameters β_1 , β_2 , and β_3 .

It is noted that in the updating process, the bending rigidity is modified more than the transverse shear rigidity. However, one should expect a greater modification on the transverse shear rigidity when more higher modes are included.

CONCLUDING REMARKS

In this paper, a simple Timoshenko beam model is developed for representing truss beams. Viscous damping in truss members is included in the formulation. This model makes it feasible to perform the control analysis by either using partial differential equations or systems of ordinary differential equations obtained from the discretization of the simple model.

The simple model thus constructed is shown to yield quite accurate predictions in natural frequencies and mode shapes. Moreover, with much fewer parameters than the finite element model, it also provides an efficient way for performing system identification when actual measurements on the system are available. This feature of the simple model is particularly attractive if in-flight tests are to be implemented and results used for updating the structural model.

The random search algorithms used in this study is efficient when the number of parameters to be identified is small. The Newton-Raphson method [6] will be employed and compared with the random search method in a future report.

REFERENCES

1. Sun, C.T., Kim, B.J., and Bogdanoff, J.L., "On the Derivation of Equivalent Simple Models for Beam- and Plate-Like Structures in Dynamic Analysis," Proceedings AIAA Specialists Conference, Atlanta, Georgia, April 6-8, 1981, pp. 523-532.
2. Chen, C.C., and Sun, C.T., "Transient Analysis of Large Frame Structures by Simple Models," Proceedings of Symposium on Engineering Science and Mechanics, National Cheng Kung University/American Astronautical Society, Dec. 28-31, 1981, also to appear in J. Astronautical Sciences.
3. Noor, A.K. and Anderson, C.M., "Analysis of Beam-Like Lattice Trusses," Comp. Meth. Appl. Mech. Engrg. Vol. 20, 1979, pp. 53-70.

4. Juang, J.N. and Sun, C.T., "System Identification of Large Flexible Structures by Using Simple Continuum Models," to appear in J. Astronautical Sciences.
5. Kana, D.D., and Huzar, S., "Synthesis of Shuttle Vehicle Damping Using Substructure Test Results," J. Spacecraft and Rockets, Vol. 10, No. 12, 1973, pp. 790-797.
6. Balakrishnan, A.V., "Modeling and Identification Theory: A Flight Control Application," Theory and Applications of Variable Structure Systems, Academic Press, New York, 1972.

This Page Intentionally Left Blank

A FUNCTION SPACE APPROACH TO STATE AND MODEL ERROR ESTIMATION FOR ELLIPTIC SYSTEMS

G. Rodriguez

Jet Propulsion Laboratory
California Institute of Technology
Pasadena, CA 91109

ABSTRACT

An approach is advanced for the concurrent estimation of the state and of the model errors of a system described by elliptic equations. The estimates are obtained by a deterministic least-squares approach that seeks to minimize a quadratic functional of the model errors, or equivalently, to find the vector of smallest norm subject to linear constraints in a suitably defined function space. The minimum norm solution can be obtained by solving either a Fredholm integral equation of the second kind for the case with continuously distributed data or a related matrix equation for the problem with discretely located measurements. Solution of either one of these equations is obtained in a batch-processing mode in which all of the data is processed simultaneously or, in certain restricted geometries, in a spatially scanning mode in which the data is processed recursively. After the methods for computation of the optimal estimates are developed, an analysis of the second-order statistics of the estimates and of the corresponding estimation error is conducted. Based on this analysis, explicit expressions for the mean-square estimation error associated with both the state and model error estimates are then developed. While this paper focuses on theoretical developments, applications arising in the area of large structure static shape determination are contained in a closely related paper [1] also included in these proceedings.

I. INTRODUCTION

Objectives

The main objectives of the paper are: 1) to outline an approach to estimate the state of a system modeled by means of single or multiple elliptic partial differential equations or, for complex structures, by fine-resolution piecewise-continuum models, and 2) to advance a closely related approach to estimate the errors inherent in such models.

Mathematical Statement of State and Model Error Estimation Problems

A general statement of the estimation problems is provided by the following equations:

$$\text{System Model} \quad Au = f, \quad (1)$$

$$\text{Observations} \quad y = Hu + n, \quad (2)$$

$$\text{Boundary Conditions} \quad Bu = 0, \quad (3)$$

where u and y are respectively the state and observations, and A is an elliptic differential operator defined over the spatial domain Ω . As outlined in Ref. [1], the operator A could represent symbolically a large number of interconnected partial differential equations defined over a multiplicity of sub-domains that together make up the overall structural domain Ω . Such fine-resolution piecewise-continuum models would be appropriate for complex structures that cannot be modeled completely by a single partial differential equation. The boundary conditions $Bu = 0$ are specified at the boundary of the domain, where B is a differential operator that characterizes the geometric and natural boundary conditions applicable to the system model. The range of the operator H could be finite-dimensional, corresponding to the case of discretely located observations.

The traditional state estimation problem consists of estimating the state u of the system from the observations y . A related estimation problem, and one that is less commonly addressed, is that of estimating the model errors f and n , which reflect the combined effect of a large number of uncertainties and error sources. In many cases, these two terms cannot be fully determined in advance of the model's application. The traditional 'white-noise' model does not always lead to useful results. Consequently, estimation is the only viable means to establish knowledge of the model errors.

Specific cases in which the problem of model error estimation occurs include: determining the quasi-static gravity loads in a ground antenna, estimating internal disturbances (forces and moments) due to attitude and shape control actuators, and evaluating the lumped effect of nonlinear terms, governing nonlinear elastic behavior, which have been neglected by the approximate linear model in (1).

The estimation approach advanced here provides a solution to both of the foregoing problems simultaneously, in that the same computations required to determine the state estimates can be used (with minor modifications) to determine the corresponding model error estimates.

Least-Squares Approach to Estimation

The method of least-squares seeks to minimize the following quadratic functional of the model errors:

$$J(f) = \int_{\Omega} (n^2 + f^2) d\Omega, \quad (4)$$

subject to the constraints imposed by the state equations (1) and (2). The solution of this problem provides an optimal pair $e_o = [f_o, n_o]$, consisting of a process error estimate f_o and a corresponding observation error estimate n_o , that is the least-squares estimate of the actual model errors $e = [f, n]$. The state estimate, satisfying $Au_o = f_o$, also arises from the least-squares formulation. In Ref. [2], a similar least-squares formulation has been used to develop a combined state and model error estimation approach for time-dependent causal systems. The aim of this paper is to extend these results to infinite-dimensional elliptic systems.

Elliptic Models for Estimator Design

Central to the shape determination schemes under development here is the selection of a mathematical model to represent the elastic behavior of the structure. Three classes of models, useful at three distinct stages of the design process, that are applicable to this selection are: 1) single partial-differential-equation models defined over a single domain for development of initial physical insight and understanding, 2) multiple PDE models defined over multiple spatial domains for more in-depth parametric studies and estimator design, and 3) piecewise-continuum models, defined over a possibly fine structural-element grid (exact finite-elements), for detailed design and evaluation. A more complete description of these models with typical examples are provided in Ref. [1].

The Observation Model

To complete a description of the models used for estimator design, it is of interest to make a few brief comments about the observation equation (2). This equation is characterized by the operator H defining the state-to-observations map. By appropriate definition of this operator, it is possible to encompass within the observation model, a wide range of data collection strategies of practical interest.

TYPE OF MEASUREMENT	STATE-TO-OBSERVATION MAP
(a) Full Domain	$Hu = u(x) \quad x \in \Omega$
(b) Boundary	$Hu = u(x) \quad x \in \Gamma(T)$ (5)
(c) Discrete	$Hu = [u(x_1), \dots, u(x_N)]$

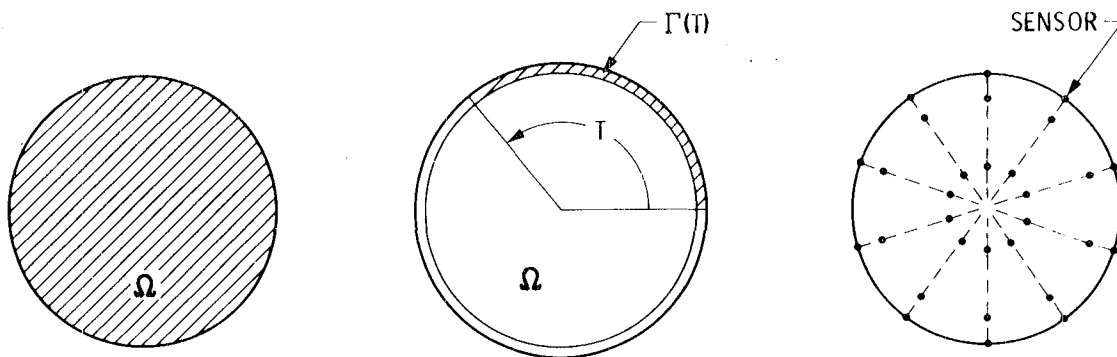


Fig. 1 Illustration of Sensing Strategies

Some typical distributed sensing strategies are illustrated in Fig.1. Out of the three types of measurement strategies shown above, perhaps most commonly encountered in practice is the one corresponding to discretely distributed sensing. Consequently, the estimation methodology advanced here will ultimately be implemented for this case. However, investigation of the schemes involving sensing either at the boundary or within the entire spatial domain is also of interest at times (in this paper), because such an investigation can lead to valuable insight and understanding about the estimation problem and its corresponding solution.

The function space approach to estimation advanced below encompasses within the same general framework all of the three cases, provided that an appropriate interpretation of H is used. Other schemes, such as those based on spatial-slope data (as opposed to the deflection measurements discussed so far) can also be investigated within the same formulation or, at most, with possible minor modifications.

2. OUTLINE OF FUNCTION SPACE APPROACH TO ESTIMATION

One of the major objectives of the paper is to advance a function space approach to estimation for elliptic systems that extends results reported previously [2], applicable primarily to time-evolving causal systems. Because of its length, it is convenient to partition the presentation of the approach into the following major pivotal steps (see illustration in Fig. 2):

1. Showing that the least-squares estimation problem is equivalent to that of finding a vector of smallest norm subject to linear constraints (Sec. 3).
2. Establishing that the optimal estimate (of smallest norm) can be determined in terms of the generalized inverse of the operator characterizing the linear constraints (Sec. 3).
3. Computing the generalized inverse above from the solution of a Fredholm integral equation of the second kind, for the case with continuously distributed measurements, and from the solution of a closely related matrix equation, for discretely distributed data (Sec. 3).
4. Specifying a number of alternative methods (direct matrix inversion, eigenfunction expansions, etc.) for solving either the integral equation or the related matrix equation. These methods can be classified into the two broad categories of batch solutions (Sec. 4), in which all of the data is processed simultaneously, and scanning algorithms (Sec. 5), in which the data is processed recursively.
5. Developing a statistical analysis that results on explicit formulas for the second-order statistics of the important variables (state and model-error estimates, estimation error, etc.) in the problem formulation (Secs. 6-7).

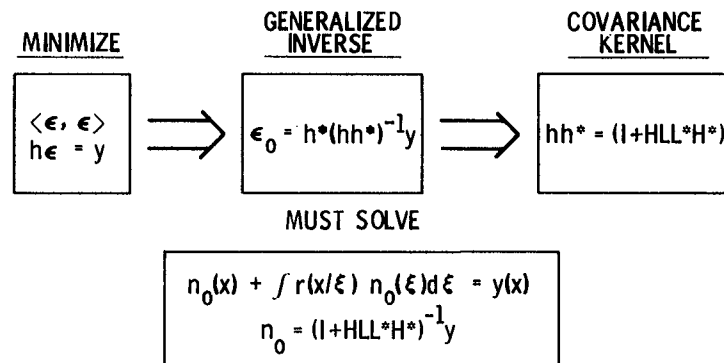


Fig. 2 Illustration of Function Space Approach to Estimation

3. MINIMUM NORM PROBLEM, GENERALIZED INVERSE AND FREDHOLM EQUATION

To develop the estimation approach, it is convenient to first introduce notation necessary to define suitable function spaces for the estimation problem. Let H_1 , H_2 and H_3 denote respectively the function spaces to which the process error f , the state u , and the observations y (and the observation error n) belong. For example, $H_1=H_2=H_3=L_2(\Omega)$ would be appropriate for the problem with continuously distributed data, while $H_1=H_2=L_2(\Omega)$ and $H_3=R^N$ would be applicable to the situation with discrete measurements. The model error ε is then defined to be the pair $\varepsilon = [f, n]$ belonging to the Cartesian product space [3] $H_1 \times H_3$. This space is endowed with the inner product $\langle \varepsilon_1, \varepsilon_2 \rangle = (f_1, f_2)_1 + (n_1, n_2)_3$, where $\varepsilon_1 = [f_1, n_1]$ and $\varepsilon_2 = [f_2, n_2]$ are two arbitrary vectors in the space, and $(\cdot, \cdot)_i$ is the inner product in $H_i(\Omega)$.

Based on these definitions, the optimization problem can be recast as follows:

$$\text{minimize} \quad \langle \varepsilon, \varepsilon \rangle, \quad (6)$$

$$\text{subject to} \quad h\varepsilon = y, \quad (7)$$

where $h = [HL \ I]$ is a linear operator mapping $H_1 \times H_3 \rightarrow H_3$ that characterizes the linear constraints under which the optimization problem must be solved. This operator h is defined in terms of the integral operator L specified by

$$Lf = \int_{\Omega} \mathcal{G}(x/\xi) f(\xi) d\xi, \quad (8)$$

where \mathcal{G} is the Green's function for A in (1). If A is symmetric, as is the case in most elastic models representing practical structures, then $\mathcal{G}(x/\xi) = \mathcal{G}(\xi/x)$ is also symmetric, and the corresponding operator $L=L^*$ is self-adjoint with respect to the inner product $(\cdot, \cdot)_2$.

The model error estimates $\varepsilon_0 = [f_0, n_0]$ are the solutions of this minimum norm problem. The unique element of smallest norm is given by [3]:

$$\varepsilon_0 = h^*(hh^*)^{-1} y, \quad (9)$$

where h^* mapping $H_3 \rightarrow H_1 \times H_3$ is the operator adjoint to h with respect to the inner product $\langle \cdot, \cdot \rangle$. Since $hh^* = [I + HLL^*H^*]$, the model error estimates (and the corresponding state estimate) can be expressed as

$$f_0 = L^* H^* [I + HLL^* H^*]^{-1} y, \quad (10)$$

$$n_0 = [I + HLL^* H^*]^{-1} y, \quad (11)$$

$$u_0 = LL^* H^* [I + HLL^* H^*]^{-1} y, \quad (12)$$

where the state estimate u_0 specified by (12) has been obtained by substitution of (10) into (8).

The above are the most general equations to be presented here for evaluation of the model error and state estimates. The key computation required by these equations is the inversion of the operator $[I + HLL^* H^*]$. Because this inversion takes place in the Hilbert space H_3 , the computations required to conduct the inversion depend on the measurement scheme under investigation (see Fig. 1). For continuously distributed measurements, as in Figs. 1(a) and 1(b), the inversion of $[I + HLL^* H^*]$ can be achieved by solving a Fredholm integral equation of the second kind. With discretely located data as in Fig. 1(c), $[I + HLL^* H^*]$ is a matrix whose dimensions are equal to the number of data points.

Inversion of $[I + HLL^* H^*]$ with Continuously Distributed Data

This case corresponds to that of Fig. 1(a) and assumes that H in (1) is the identity. With this assumption, a direct computation of LL^* using (8) leads to the following Fredholm integral equation of the second kind:

$$n_0(x) + \int_{\Omega} r(x/\xi) n_0(\xi) d\xi = y(x) \quad \text{for } x \text{ in } \Omega, \quad (13)$$

specified in terms of its kernel $r(x/\xi)$ given by

$$r(x/\xi) = \int_{\Omega} \mathcal{G}(x/\eta) \mathcal{G}(\eta/\xi) d\eta. \quad (14)$$

Because the kernel is the one key element characterizing the integral equation, it is of interest to explore some of its major properties. First, observe that $r(x/\xi)$ is a Green's function for A^*A , i.e.,

$$A_x^* A_x r(x/\xi) = \delta(x-\xi), \quad (15)$$

where δ is the impulsive 'delta' function, and the subscript x in A_x implies that the spatial differentiations embedded in A are conducted with respect to x (as opposed to being performed with respect to ξ). This result can be obtained readily by operating on (14) with $A_x^* A$ and using twice the condition $A \mathcal{G} = \delta$, which follows from the observation that \mathcal{G} is a Green's function for A . This result implies that $r(x/\xi)$ can be computed directly using (15), without necessarily solving first for an approximation to \mathcal{G} and then using (14) to approximate r . Such a direct method could potentially be more accurate as discussed further in Ref. [1].

Another important property of $r(x/\xi)$ is its interpretation as the covariance $E[u(x)u(\xi)]$ of the state u , under the assumption (used only infrequently in this paper) that the actual errors $\varepsilon = [f,n]$ in (1) and (2) are spatially distributed white noise. This property will be investigated further as an integral part of the statistical analysis provided in Sec. 7.

The immediate aim here, however, is to first state the matrix equation related to (13) that must be solved for the case with discretely located data.

Inversion of $[I + (HL)(HL)^*]$ with Discretely Spaced Data

This case corresponds to Fig. 1(c) where the data is collected only at a finite number of spatial locations distributed throughout the domain. The matrix equation analogous to (13) that must be solved for this case is

$$n_0^k + \sum_{m=1}^N r(x_k/\xi_m)n_0^m = y^k, \quad k = 1, \dots, N, \quad (16)$$

where n_0^k denotes the value of the observation error estimate at the location x_k , and where N denotes the number of spatial measurements. Note that in both (13) and (16) the kernel $r(x/\xi)$ plays a key role in characterizing the equation to be solved. For the problem with continuously distributed data in Fig. 3(a), the kernel $r(x/\xi)$ is defined over the square region $[x,\xi] \in \Omega \times \Omega$. For the case with discrete data in Fig. 3(b), the kernel $r(x/\xi)$ needs to be evaluated only over a finite-dimensional grid to specify the matrix equation that needs to be solved. In both of these cases A^*Ar has a singularity along the diagonal as indicated by Eq. (15).

In the foregoing, it has been established that, depending on the type of data available, inversion of $[I + HLL^*H^*]$ can be achieved by either solving a Fredholm integral equation or a related matrix equation. A number of potential batch and recursive processing methods to conduct this computation are developed in the following two sections.

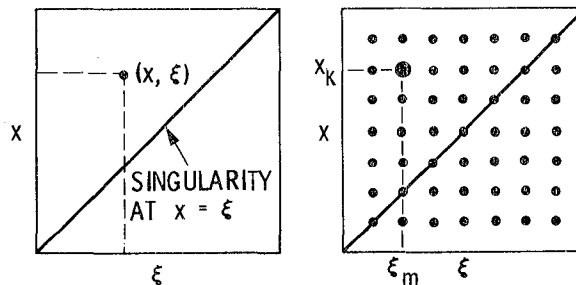


Fig. 3 Domains of Definition of State Covariance Kernel

4. BATCH SOLUTIONS

The aim of this section is to convert equations (10)-(12), which are based on a somewhat abstract operator notation, into a more explicit form that more directly represents the computations that must be performed in a batch-processing estimation mode. The following three major batch-processing alternatives are explored:

- o Direct inversion of the matrix $(I+HLL^*H^*)$, a solution primarily applicable to the discrete-data case and only applicable as an approximation to the continuous-data problem
- o Expansion of the estimates in terms of the eigenfunctions ϕ_k of $R = HLL^*H^*$ defined by $R\phi_k = \lambda_k^2 \phi_k$ with λ_k^2 being the eigenvalues
- o Solutions based on the Fredholm resolvent G of R defined by $(I+R)^{-1} = (I-G)$

Estimates Based on Inversion of $(I+HLL^*H^*)$ Matrix for Discrete Data Problem

This approach involves a direct solution to the matrix equation in (16) which results initially in a set of observation error estimates $n_o = [n_o^1, \dots, n_o^N]$. Then, to complete the estimation process involving also the state estimate u_o and the process error estimate f_o , Eqs. (10) and (12) are converted into

$$f_o(x) = \sum_{k=1}^N \mathcal{G}(x_k/x) n_o^k, \quad (17)$$

$$u_o(x) = \sum_{k=1}^N r(x_k/x) n_o^k, \quad (18)$$

where \mathcal{G} and r are as before the Green's function for A in (1) and the state covariance kernel in (14).

The computations required by this sequence of equations can be summarized as follows. First, the value of the kernel $r(x_k/\xi_m)$ must be determined at the grid points in Fig. 3(b) corresponding to the discrete spatial locations x_k and ξ_m where the measurements are being taken. For complicated structures, obtaining the kernels r and \mathcal{G} requires a non-trivial computation that is best achieved by using the finite-element method [1]. After r and \mathcal{G} are determined, the matrix inversion required to solve (16) must be conducted to arrive at the observation error estimates n_o . Finally, f_o and u_o are determined by (17) and (18) based on the kernels \mathcal{G} and r . Note that if knowledge of f_o and u_o is required at a point x where a measurement is not available, then the kernels $\mathcal{G}(x_k/x)$ and $r(x_k/x)$ must also be evaluated at that point in conducting the computations in (17) and (18).

One of the main advantages of the above approach is the conceptual simplicity of the required computations. However, in situations with many discrete measurements, the required matrix inversion may limit the

applicability of the method (although this limitation may be alleviated somewhat by performing the inversion in an off-line processing mode).

While the approach is most useful for the discrete-data problem, it can also be viewed as an approximate method to solve the case with continuously distributed data. With continuous data, HLL^*H^* is an integral operator and the equation that must be solved is an integral equation. An approximate solution to this equation could consist of first discretizing the integral equation to obtain a corresponding matrix equation and then solving the matrix equation.

Although the approach is computationally convenient, it generally does not lead to much insight and understanding about the problem of inverting $(I+HLL^*H^*)$ and of interpreting the resulting state and model error estimates. A more thorough understanding of the inversion problem is best obtained by investigating the two methods outlined below.

Eigenfunction Expansions for the State and Model Error Estimates

This approach is generally applicable to both the continuous and discrete problems, although minor differences may exist between the two problems. For both of these cases, the eigenvectors $R = HLL^*H^*$ are defined as the nontrivial solutions of

$$R \phi_k = \lambda_k^2 \phi_k, \quad (19)$$

where λ_k^2 are the corresponding eigenvalues. For the discrete-data problem, R is a matrix, and there is a finite number of finite-dimensional eigenvectors ϕ_k .

For the continuous-data problem, R is an integral operator (that in most practical cases satisfies the property of compactness [3]) with an infinite number of function-space eigenvectors ϕ_k . With R compact, the corresponding eigenvalues $\lambda_k^2 \rightarrow 0$ as $k \rightarrow \infty$. Note finally, as a point of interest, that in cases with H in (2) equal to the identity and $L=L^*$ self-adjoint, then λ_k in (19) are also the eigenvectors of L and $L \phi_k = \lambda_k \phi_k$.

In terms of ϕ_k , the process error and state estimates can be expressed as

$$f_o = \sum_k f_o^k \phi_k, \quad (20)$$

$$u_o = \sum_k u_o^k \phi_k, \quad (21)$$

where the 'modal' coefficients f_o^k and u_o^k are given by

$$u_o^k = \frac{\lambda_k^2}{1 + \lambda_k^2} \hat{y}_k, \quad f_o^k = \frac{\lambda_k}{1 + \lambda_k^2} \hat{y}_k, \quad (22)$$

and $\hat{y}_k = (\phi_k, y)_3$ represents the corresponding modal coefficient of the data y .

Note that while (20) and (21) constitute expansions for f_o and u_o , no attempt has been made so far to obtain a similar expansion for the related observation error estimate n_o . In general, such an expansion is not possible because (in somewhat imprecise mathematical terms) n_o can exhibit a 'wild' spatial behavior that cannot adequately be represented by nicely behaved functions ϕ_k . To illustrate the possible pitfalls, consider

$$n_o = \sum_k \hat{n}_o^k \phi_k, \quad (23)$$

an equation that in the same spirit as (20) and (21) attempts to expand n_o in terms of the eigenvectors ϕ_k . Routine manipulations based on the integral equation (13) can be used to show that

$$\hat{n}_o^k = \frac{1}{1 + \lambda_k^2} \hat{y}_k, \quad (24)$$

where, as before, \hat{y}_k is the modal coefficient of the data y .

This equation can be used to show the problems inherent with the attempted expansion. Recall first that for typical cases $\lambda_k^2 \rightarrow 0$ as $k \rightarrow \infty$, and the coefficient $1/(1 + \lambda_k^2)$ in (24) approaches unity. This implies that unless $\hat{y}_k \rightarrow 0$ sufficiently fast (which would be the case if the data y is well-behaved), then \hat{n}_o^k may be such that the corresponding expansion (23) does not converge. Consequently, the expansion (23) must be used with care because its validity is guaranteed only in cases where the data y is well-behaved. Note parenthetically that in the discrete-data case, the number of eigenvalues is finite and the above convergence problem does not occur.

One way to avoid the convergence problem is to express n_o as

$$n_o = y - u_o, \quad (25)$$

where the state estimate u_o can be obtained from (21). This expression, which does not involve a direct expansion of n_o as in (23), provides a more reliable means to compute the observation error estimate n_o .

Expressions for the Estimates Based on the Fredholm Resolvent

It has been established in the previous section that inversion of the operator $(I + R)$ is equivalent to the solution of the Fredholm integral equation (13). If the Fredholm resolvent G defined by $(I+R)^{-1} = (I-G)$ is introduced in conducting this inversion, then the solution to the integral equation is:

$$n_0(x) = y(x) - \int_{\Omega} g(x/\xi)y(\xi)d\xi, \quad (26)$$

an equation that determines the observation error estimate in terms of the data y and of the yet to be determined Fredholm resolvent kernel g . If for the moment it is assumed that g is available (see below for methods that can be used for its computation), then (26) is all that is needed to compute the observation error estimates. The related estimates f_0 and u_0 can be computed by means of

$$f_0(x) = \int_{\Omega} \mathcal{G}(x/\xi)n_0(\xi)d\xi, \quad (27)$$

$$u_0(x) = \int_{\Omega} r(x/\xi)n_0(\xi)d\xi, \quad (28)$$

which are the continuous-data versions of the discrete-data equations (17) and (18).

A useful alternative method for computation of u_0 (for the case where $H=I$) is to use

$$u_0(x) = \int_{\Omega} g(x/\xi)y(\xi)d\xi, \quad (29)$$

an equation that can be readily established by the following sequence of mathematical steps: $u_0 = LL^*H^*(I+HLL^*H^*)^{-1}y = LL^*(I+LL^*)^{-1}y = R(I+R)^{-1}y = Gy$. Because it provides a direct solution for the state estimate u_0 in terms of the data, this equation provides a preferable alternative to the indirect computation of u_0 using (26) and (28). However, as noted above, (29) is limited to cases where the observations are available throughout the entire spatial domain.

An important element of the expressions outlined above is the Fredholm resolvent which must be determined before computations based on (26) can be carried out. Some remarks about how to achieve this computation are outlined below. Note first that $(I+R)^{-1}=(I-G)$ implies that $R=G+RG$ which in terms of the corresponding integral operator kernels r and g becomes

$$r(x/\xi) = g(x/\xi) + \int_{\Omega} r(x/\eta)g(\eta/\xi)d\eta. \quad (30)$$

This represents an integral equation for the unknown resolvent kernel g with the known state covariance kernel r given by (14). One approach to its solution is to obtain an expansion in terms of the eigenfunctions ϕ_k of R in (19). To this end, it is useful to first recall the following Mercer expansion [3] for the kernel r

$$r(x/\xi) = \sum_k \lambda_k^2 \phi_k(x) \phi_k(\xi), \quad (31)$$

which can be obtained routinely from the integral representation for r in (14) or, equivalently, from the boundary-value problem in (15). Substitution of (31) in (30) leads to the following expansion for the Fredholm resolvent kernel g

$$g(x/\xi) = \sum_k \frac{\lambda_k^2}{1+\lambda_k^2} \phi_k(x) \phi_k(\xi). \quad (32)$$

This summation constitutes the desired solution g of (30). Note that the summation is very well-behaved because as $k \rightarrow \infty, \lambda_k^2 \rightarrow 0$ and consequently $\lambda_k^2/(1+\lambda_k^2) \rightarrow 0$.

The above method of solution applies primarily in cases where all of the data is processed simultaneously in a batch-processing mode. In the following section, an alternative (sequential) method for computation of the Fredholm resolvent will be used to develop, in certain restricted geometries and coordinate systems, a class of scanning algorithms where recursive processing of the data is used to generate the desired state and model error estimates.

5. SCANNING SOLUTIONS FOR CIRCULAR REGIONS

The scanning algorithms developed here provide an interesting alternative to the batch solutions just presented because of two fundamental reasons: 1) they have the potential for avoiding inversion of large-dimension matrices, as is necessary if many measurements are available, and 2) they solve the problem of how to process additional data (for instance, the $N+1$ measurement) after estimates based on a fixed data-set with N measurements have been determined. Additional motivation for investigating the scanning solutions, of course, is due to the possibility of gaining further insight into the estimation problems which constitute the central theme of this paper.

Definition of Simple PDE Model to Illustrate the Scanning Solutions

Consider a simple PDE model consisting of $\nabla^2 u = f$ defined over the circular region $\Omega = \{(p, \theta): 0 \leq p \leq P, 0 \leq \theta \leq 2\pi\}$ with the free-boundary condition $\partial u(R, \theta)/\partial r = 0$ at the edge of the region and the internal condition $u(0, \theta) = 0$ at the origin. The observation equation, illustrated in Fig. 1,

$$y(\theta) = u(p, \theta) + n(\theta), \quad 0 \leq \theta \leq T, \quad (33)$$

is based on the assumption that data is available only over the circular arc $\Gamma(T) = \{(p, \theta): p=R, 0 \leq \theta \leq T\}$. Partial boundary data (as opposed to data over the entire circumference) is assumed because the estimation problem will be solved first with a fixed and prescribed data interval $0 \leq \theta \leq T$. Then, the scanning algorithms will be developed by examining the dependence of the fixed-interval solution on incremental changes of the upper limit of observation T .

The Fredholm Integral Equation With Partial Boundary Data

It has been shown that the integral equation (13) is central to the estimation schemes under development in this paper. For the particular example involving the circular region described above, this equation assumes the following form:

$$n_o(T; \theta) + \int_0^T r(R, \theta; R, \psi) n_o(T; \psi) d\psi = y(\theta) \text{ for } 0 \leq \theta \leq T, \quad (34)$$

where the dependence of the observation error estimate n_o on T has been indicated by the explicit notation $n_o(T; \theta)$. As before, one of the key features of this integral equation is the kernel $r(R, \theta; R, \psi)$ which for this particular problem has the following interesting properties.

Stationarity and Periodicity of the State Covariance Kernel

For the example under study here, the partial differential equation for the state covariance kernel becomes

$$\nabla^2 \nabla^2 r(p, \theta; q, \psi) = p^{-1} \delta(p-q) \delta(\theta - \psi), \quad (35)$$

where $\nabla^2 = \partial^2 / \partial p^2 + p^{-1} \partial / \partial \theta + p^{-2} \partial^2 / \partial \theta^2$ is the Laplacian operator in polar coordinates. In order to compute r , this equation must be solved with both r and $\nabla^2 r$ simultaneously satisfying the free boundary conditions and the internal conditions specified for the original problem in the previous subsection. Note parenthetically that the kernel $r(p, \theta; q, \psi)$ corresponds to the solution of (35) evaluated at an arbitrary point with polar coordinates (p, θ) under the assumption that the forcing term represented by a 'delta' function is applied at the noncoincident point (q, ψ) . The solution of (35) is very conveniently obtained using a trigonometric expansion along the θ direction. Use of such an expansion for $r(p, \theta; q, \psi)$ and evaluation along the radial boundary $p=q=R$ results in the following expression

$$r(R, \theta; R, \psi) = \frac{R^3}{2\pi} \sum_k \frac{\cos k(\theta - \psi)}{k^2(k+1)}. \quad (36)$$

This provides a trigonometric expansion for the kernel involved in the integral equation (34). Inspection of the above expansion reveals that the kernel r is stationary, periodic and irrational as discussed in more detail below.

The kernel r is azimuthally stationary in the sense that it is a function of the difference $\beta = \theta - \psi$ of its two azimuthal arguments θ and ψ . Hence, the simplified notation $r_0(\beta) = r(R, \theta; R, \psi)$ can be used, and the resulting function $r_0(\beta)$ investigated. Note from (36) that when $r_0(\beta)$ is viewed as a function of β , it can be interpreted as a correlation function with symmetry $r_0(\beta) = r_0(-\beta)$ about the origin $\beta = 0$, and with its maximum value $r_0(0)$ being achieved at $\beta = 0$. The kernel $r_0(\beta)$ is the correlation $r_0(\beta) = E [u(R, \theta)u(R, \theta + \beta)]$ of the boundary values $u(R, \theta)$ and $u(R, \theta + \beta)$ of the displacement u , under the assumption that the actual process error is spatially distributed white noise (see Sec. 7 of this paper for a more complete discussion of this interpretation).

Stationarity of the kernel $r_0(\beta)$ is closely related to the circular symmetry and homogeneity of the model equations and of the circular domain. Usually, kernels that possess this property lead to special cases of the integral equation (34) that are easier to solve than the general case in which stationarity of the kernel does not exist. One of the interesting areas requiring further investigation involves the development of solutions to (34) that make optimum use of the stationarity of the kernel. However, these solutions are not yet available. The scanning algorithms to be developed in a subsequent subsection do not make use of this property. Consequently, such algorithms may not be the most efficient solutions in cases where stationarity holds. On the other hand, however, their range of applicability is much broader since they apply to general types of kernels without being constrained to integral equations where the stationarity condition is satisfied.

An additional property of the kernel $r_0(\beta)$ is that it is irrational, in the usual sense that its double-sided Laplace transform $r_0(s) = \int_{-\infty}^{\infty} \exp(-s\beta)r_0(\beta)d\beta$ is not a ratio of finite-order polynomials in s . This property is a direct consequence of the infinite dimensionality of the mapping $u = HLf$ from $f(\cdot, \cdot) \rightarrow u(R, \cdot)$. The main implication of this property is that the scanning solutions to be developed will necessarily involve infinite-dimensional models (which in the end may nonetheless have to be approximated by finite-dimensional computations).

The final major condition of the kernel is its azimuthal periodicity $r_0(\beta) = r_0(\beta + 2\pi)$. This property will turn out to have an important impact on the resulting scanning algorithms.

A more detailed investigation of the foregoing stationarity, periodicity, and irrationality properties of the kernel $r_0(\beta)$, as well as the development of corresponding estimation schemes that make optimum use of these properties, is currently under way but definitive results are not yet available. For now, the paper turns to the development of scanning solutions where such properties are not fully exploited, with the understanding that the more refined schemes are yet to come.

A Partial Differential Equation for the Fredholm Resolvent

In the particular example under consideration here, the integral equation (30) for the Fredholm resolvent g becomes

$$r_0(\theta - \psi) = g(T; \theta, \psi) + \int_0^T r_0(\theta - \eta) g(T; \eta, \psi) d\eta, \quad (37)$$

where the notation $g(T; \theta, \psi)$ indicates explicitly the dependence of g on the upper limit of observation T . The immediate aim here is to use (37) to develop the celebrated [4] Krein-Bellman equation

$$\partial g(T; \theta, \psi) / \partial T + g(T; \theta, T) g(T; T, \psi) = 0, \quad (38)$$

by means of the following sequence of manipulations. Differentiation of (37) with respect to T leads to

$$0 = \frac{\partial g}{\partial T}(T; \theta, \psi) + \int_0^T r_0(\theta - \eta) \frac{\partial g}{\partial T}(T; \eta, \psi) d\eta + r_0(\theta - T) g(T; T, \psi). \quad (39)$$

Evaluation of (37) at $\psi = T$ implies that the last term in (39) is given by

$$r_0(\theta - T) g(T; T, \psi) = g(T; \theta, T) g(T; T, \psi) + \int_0^T r_0(\theta - \eta) g(T; \eta, T) g(T; T, \psi) d\eta, \quad (40)$$

and substitution of (40) in (39) leads to

$$0 = Q(T; \theta, \psi) + \int_0^T r_0(\theta - \eta) Q(T; \eta, \psi) d\eta, \quad (41)$$

where $Q(T; \theta, \psi) = \partial g(T; \theta, \psi) / \partial T + g(T; \theta, T) g(T; T, \psi)$. Since $(I+R)$ is nonsingular, (41) implies that $Q=0$ thereby establishing the identity (38). This is the central result needed to establish the Gohberg-Krein factorization for this problem as outlined below.

Gohberg-Krein Factorization

The factorization states that

$$(I + HLL^*H^*)^{-1} = (I - \mathcal{L}^*H^*) (I - H\mathcal{L}), \quad (42)$$

where $H\mathcal{L}$ and \mathcal{L}^*H^* are the mutually adjoint operators

$$H\mathcal{L}y = \int_0^t g(t;t,\tau)y(\tau)d\tau, \quad (43)$$

$$\mathcal{L}^*H^*e = \int_t^T g(t;\tau,t)e(\tau)d\tau, \quad (44)$$

This result can be established by first computing $\mathcal{L}^*H^*H\mathcal{L}$ from (43) and (44) and then using (38) to obtain the identity

$$G = H\mathcal{L} + \mathcal{L}^*H^* - \mathcal{L}^*H^*H\mathcal{L}, \quad (45)$$

that relates the Fredholm resolvent G and the Volterra operators $H\mathcal{L}$ and \mathcal{L}^*H^* . This equation implies that $[I + H\mathcal{L}\mathcal{L}^*H^*]^{-1} = (I - G) = I - H\mathcal{L} - \mathcal{L}^*H^* + \mathcal{L}^*H^*H\mathcal{L} = (I - \mathcal{L}^*H^*)(I - H\mathcal{L})$, which is the desired result.

The State and Model Error Estimates

A direct implication of (42) is that the model error estimate $\varepsilon_0 = [f_0, n_0]$ can be expressed as

$$\varepsilon_0 = h^*(I - \mathcal{L}^*H^*)(I - H\mathcal{L})y, \quad (46)$$

or more explicitly as $n_0 = (I - \mathcal{L}^*H^*)(I - H\mathcal{L})y$ and $f_0 = L^*H^*n_0$. This equation defines n_0 (and f_0 as well) in terms of a linear transformation operating on the data y . This overall transformation can be viewed as the product of the two terms $(I - \mathcal{L}^*H^*)$ and $(I - H\mathcal{L})$ which specify a two-stage scheme for processing of the data y . The first stage, corresponding to $(I - H\mathcal{L})$, leads to a 'filtered' estimate $H\mathcal{L}y$ together with a residual (innovations) process $e = (I - H\mathcal{L})y$. The residual process e is then operated upon by the second factor $(I - \mathcal{L}^*H^*)$ to obtain the desired observation error $n_0 = (I - \mathcal{L}^*H^*)e$. The process error f_0 and the state estimates u_0 corresponding to n_0 can be obtained by means of the equations (10) and (12).

An illustration of the foregoing two-stage process defined by the consecutive transformations $(I - H\mathcal{L})$ and $(I - \mathcal{L}^*H^*)$ in (46) is shown in Fig. 4. The sketch on the left corresponds to the operator $(I - H\mathcal{L})$, whereas the one on the right illustrates its adjoint $(I - \mathcal{L}^*H^*)$. The clockwise operation on the left leads first to an estimate $H\mathcal{L}y$ and then to an innovations process $e = (I - H\mathcal{L})y$. The innovations process e is obtained by subtracting the observed-state estimate (in this particular case, the value of the state estimate at the boundary) from the boundary data y . The innovations process e , defined by $e = (I - H\mathcal{L})y$, is then used in the counter-clockwise stage, illustrated on the right-side sketch, to obtain the desired observation error estimate n_0 .

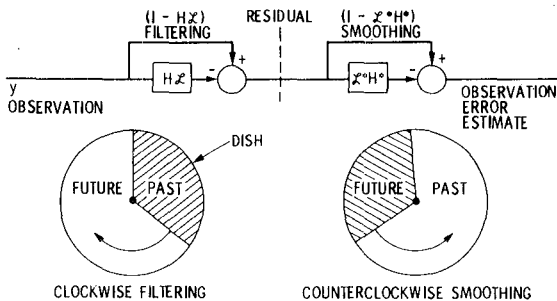


Figure 4. Scanning Solutions Based on Azimuthal Sweeps

Computation of Volterra Kernels

The one missing ingredient in the forward-backward azimuthal sweep just described is the specification of the kernels $g(t;t,\tau)$ and $g(t;\tau,t)$ in $H\mathcal{L}$ and \mathcal{L}^*H^* in (43) and (44). For causal time-evolving systems, it is known [2] that the kernels can be computed as $g(t;t,\tau) = H\Phi(t,\tau)\hat{p}(\tau)H^*$ and $g(t;\tau,t) = H\hat{p}(t)\Phi^T(\tau,t)H^*$, where Φ is the transition matrix for a Kalman filter, and \hat{p} is the solution to the related Riccati equation. Unfortunately, such general results for computation of the kernels are not yet available for the class of elliptic systems under investigation here, where the causal structure generated by the azimuthal sweep is introduced somewhat artificially. Analysis to date indicates that, contrary to the time-evolving causal case, the kernels cannot be generated by means of a simple Kalman filter (even one of infinite dimensionality). The main reason for this lack of simplicity is the periodicity of the kernel $r_0(\beta)$ in (36). However, the kernels $g(t;t,\tau)$ and $g(t;\tau,t)$ in (43) and (44) are well-defined functions of the running variable τ and the upper limit of observation t . Hence, even though they most likely cannot be generated by means of straight-forward Kalman filtering, alternative methods for their computation should be effective. Such methods are currently under investigation.

6. RELATIONSHIPS BETWEEN ACTUAL AND ESTIMATED ERRORS

One of the key results of the previous sections is that in equation (9), $\varepsilon_0 = h^*(hh^*)^{-1}y$, which relates the model error estimates ε_0 to the available data y . By substitution of (7) in (9), it is possible to go one step beyond and obtain the following relationship between the actual and estimated errors:

$$\varepsilon_0 = W\varepsilon, \tag{47}$$

where $W = h^*(hh^*)^{-1}h$ is a linear transformation whose mathematical properties are important to understand.

Result 6.1 W is a self-adjoint projection operator. This result can be established readily by the following sequence of statements $W^2 = [h^*(hh^*)^{-1}h][h^*(hh^*)^{-1}h] = h^*(hh^*)^{-1}h = W$. Hence, $W^2 = W$ and W is a projection operator. Self-adjointness of W can be established by inspection of the definition $W = h^*(hh^*)^{-1}h$.

Result 6.2 $(I-W)$ is a self-adjoint projection operator. Note that $(I-W)^2 = (I-2W+W^2) = (I-W)$, thereby establishing the result.

Define now the model-error estimation error $\epsilon_p = \epsilon - \epsilon_o$ as the difference between actual and estimated errors. Since $\epsilon_o = W\epsilon$, then $\epsilon_p = \epsilon - W\epsilon$ and

$$\epsilon_p = (I-W)\epsilon, \tag{48}$$

an equation that relates the model-error estimation error and the actual error ϵ .

Result 6.3 ϵ_o and ϵ_p are orthogonal complements. This result follows immediately from $\langle \epsilon_o, \epsilon_p \rangle = \langle W\epsilon, (I-W)\epsilon \rangle = \langle \epsilon, (W-W^2)\epsilon \rangle = 0$. This last result is extremely interesting because it establishes a decomposition of the actual error vector ϵ as a sum of orthogonal complements which can be interpreted geometrically as outlined below.

Geometrical Interpretation

The horizontal axis in the figure denotes conceptually the process error f , while the vertical axis corresponds to the observation error n . These two variables comprise the two-component model error vector $\epsilon = [f, n]$. Consequently, an arbitrary error vector can be represented as a point on the two-dimensional surface shown in the figure. Those pairs $\epsilon = [f, n]$ which satisfy the system model equation (7) define conceptually a straight-line segment characterized by the relation $h\epsilon = y$. The observation y is represented as a single point appearing at a prescribed location along the vertical axis. The minimum norm problem in (6) and (7) can be thought of as that of finding the shortest vector ϵ_o from the origin to the straight-line segment $h\epsilon = y$. The corresponding minimum distance $\langle \epsilon_o, \epsilon_o \rangle^{1/2}$ equals the norm of the minimum error vector $\epsilon_o = [f_o, n_o]$ representing the model error estimates. By simple geometry (see Fig. 5), the shortest vector ϵ_o joining a point and a straight line is orthogonal to the line. This also implies that an arbitrary actual error vector ϵ (one that satisfies $h\epsilon = y$, but whose norm may not be minimum) can be decomposed as the sum of the minimal error vector ϵ_o and its orthogonal complement ϵ_p , i.e.,

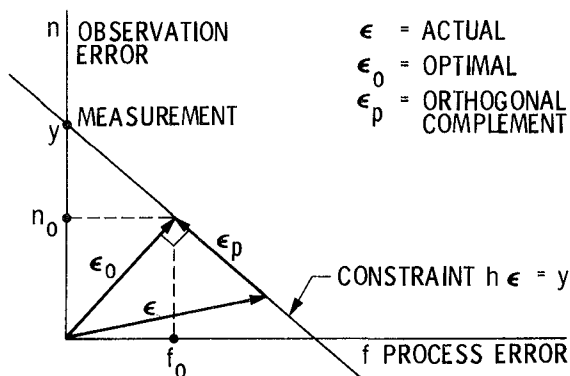


Fig. 5 The Actual Error Vector as a Sum of Orthogonal Complements

$$\varepsilon = \varepsilon_0 + \varepsilon_p, \quad (49)$$

where $\langle \varepsilon_0, \varepsilon_p \rangle = 0$. The square of the 'length' of the vector ε of non-minimum norm can be expressed as

$$\langle \varepsilon, \varepsilon \rangle = \langle \varepsilon_0, \varepsilon_0 \rangle + \langle \varepsilon_p, \varepsilon_p \rangle, \quad (50)$$

an equation that can be interpreted as a mathematical statement of the ancient geometrical theorem that the square of the length of the hypotenuse of a right triangle equals the sum of the squares of its sides.

Result 6.4 Azimuthal factorization of W in circular regions. The objective here is to show that, in cases where the Gohberg-Krein factorization (42) holds, W can be factored as the product $W = w^* w$ of the yet to be defined operator w and its adjoint w^* .

To establish this result, it is convenient to begin by recalling that by definition $W = h^*(hh^*)^{-1}h = h^*(I + HLL^*H^*)^{-1}h$. Use of the Gohberg-Krein factorization in this equation implies that

$$W = w^* w, \quad (51)$$

where w is the operator $w = (I - H\mathcal{L})h$. A block diagram illustrating this factorization is shown in Fig. 6. The diagram shows the two major stages w and w^* that together constitute the overall transformation $W = w^* w$. The first stage $w = (I - H\mathcal{L})h$, shown on the left portion of the diagram, maps the actual error vector $\varepsilon = [f, n]$ into the residual process $e = w\varepsilon$. This first stage characterized by w involves first the generation of the data y by means of the equation $y = h\varepsilon = HLf + n$ followed by the use of this data to generate the residual process $e = (I - H\mathcal{L})y$. The second stage, represented by the operator w^* , operates on the residual process in order to obtain the model error estimates $\varepsilon_0 = w^* e$. Because w and w^* are mutually adjoint, the first and second stages can be viewed as being mirror images of each other, with respect to the dotted vertical line in the diagram representing the innovations process.

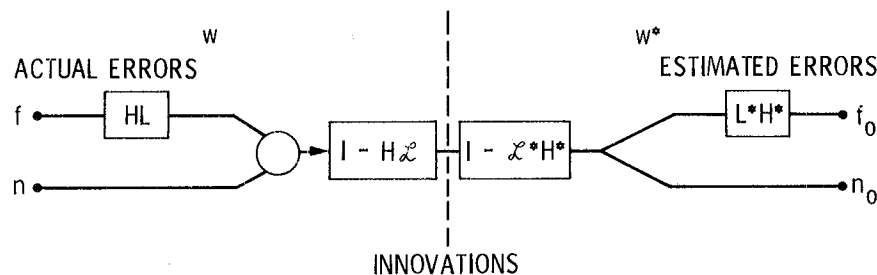


Fig. 6 Factorization of W

Another very interesting result is that if the above two-stage process is reversed, and w^* is performed before w , then the identify transformation results.

Result 6.5 $ww^* = I$. This identity can be established by the following sequence of operations $ww^* = (I-H\mathcal{L})hh^*(I-\mathcal{L}^*H^*) = (I-H\mathcal{L})(I+HLL^*H^*) (I-\mathcal{L}^*H^*) = I$.

Result 6.6 The 'lengths' of the minimal error vector and of the innovations process are equal. This result follows from $\langle \varepsilon_0, \varepsilon_0 \rangle = \langle we, we \rangle = (e, w^* we)_3$ which implies that

$$\langle \varepsilon_0, \varepsilon_0 \rangle = (e, e)_3. \quad (52)$$

Both of these last two results are intimately related to the 'whiteness' of the innovations process in cases where the actual errors ε are assumed to be spatially distributed white-noise, as will be discussed in more detail in Sec. 7.

An Eigenfunction Expansion for W

Although an eigenfunction expansion is possible in both the continuous and discrete cases, only the continuous-data problem is discussed here, because the notation is much simpler for this problem. For the continuous-data problem, the transformation W can be viewed as a mapping from the product space $L_2(\Omega) \times L_2(\Omega)$ into itself. The transformation can be more explicitly characterized by the following set of equations

$$f_0(x) = \int_{\Omega} W_{11}(x/\xi) f(\xi) d\xi + \int_{\Omega} W_{21}(x/\xi) n(\xi) d\xi, \quad (53)$$

$$n_0(x) = \int_{\Omega} W_{21}(x/\xi) f(\xi) d\xi + n(x) - \int_{\Omega} W_{22}(x/\xi) n(\xi) d\xi, \quad (54)$$

where W_{ij} are integral operator kernels that characterize the transformation. By means of routine manipulations, it can be shown that these kernels can be expressed as

$$W_{11}(x/\xi) = W_{22}(x/\xi) = \sum_k \frac{\lambda_k^2}{1+\lambda_k^2} \phi_k(x) \phi_k(\xi), \quad (55)$$

$$W_{12}(x/\xi) = W_{21}(x/\xi) = \sum_k \frac{\lambda_k}{1+\lambda_k^2} \phi_k(x) \phi_k(\xi), \quad (56)$$

in terms of the eigenfunctions ϕ_k of the operator R in (19).

Reorientation

This concludes the development of a number of important relationships between actual and estimated errors. In the following section, these relationships will be shown to be fundamental to the study of a probabilistic interpretation of the deterministic least-squares estimates previously described.

7. COVARIANCE ANALYSIS WITH WHITE-NOISE MODEL ERRORS

The estimation approach presented so far is based on the principle of least-squares, which involves the deterministic minimization of a quadratic functional of the model errors. This deterministic approach does not require that probabilistic notions be introduced in order to derive the state and model error estimates. Equations (10)-(12) can be viewed as establishing a totally deterministic rule by which the data may be processed to obtain the desired estimates. Here, the objective is to explore a probabilistic interpretation of the estimates. This is done under the assumption, not previously used in the paper, that the actual errors possess the properties of a yet to be defined spatially distributed white-noise process.

The specific objectives of the section are:

- o to investigate the second-order statistical properties (the covariance primarily, since all processes are zero-mean) of the state and model error estimates u_0 and ε_0 and of the corresponding state estimation error $u_p = u - u_0$ and model-error estimation error $\varepsilon_p = \varepsilon - \varepsilon_0$.
- o To obtain explicit expressions for the covariance of the estimation errors u_p and ε_p and to obtain related expressions for the mean-square estimation errors $E(u_p, u_p)$ and $E(\varepsilon_p, \varepsilon_p)$.
- o To show that the state and model error estimates u_0 and ε_0 can be interpreted probabilistically as the conditional expectations $\varepsilon_0 = E(\varepsilon/y)$ and $u_0 = E(u/y)$.

Since these results are based on the assumption that the actual errors ε are spatially distributed white-noise, it is of interest to first make somewhat more precise the notion of such a process.

Definition of a Spatially Distributed White-Noise Process

Intuitively (see [3] for a more precise definition), a spatially distributed white-noise process f is characterized by an impulsive 'delta-function' covariance, i.e.,

$$E[f(x)f(\xi)] = \delta(x-\xi). \quad (57)$$

This definition, which is in the same spirit as that used for time-dependent causal systems, implies that the values $f(x)$ and $f(\xi)$ of the process at the two distinct points x and ξ are totally uncorrelated. The definition also reflects the fact that, if the points x and ξ are coincident, the correlation becomes infinite. Based on this definition, it is possible to state that, if $\varepsilon=[f,n]$ are assumed to be white-noise, then the corresponding covariance is

$$E[\varepsilon(x)\varepsilon^T(\xi)] = U\delta(x-\xi), \quad (58)$$

where U is an appropriately dimensioned unit matrix that accounts for the possibility that $\varepsilon(x)$ may be a vector of a finite number of dimensions.

The foregoing is only a formal definition of the covariance of spatially distributed white-noise, because it attempts to define in a pointwise sense a quantity (the spatial covariance) that cannot be defined precisely in this sense. A somewhat more rigorous notion is that of a covariance operator for a white-noise process as defined below.

Definition of the Covariance Operator of a White-Noise Process

In approximate terms, the covariance operator is the 'integrated' version of the covariance function in (57). For example, the covariance operator $E[\varepsilon\varepsilon^*]$ for the process ε is defined to be that integral operator whose kernel is the covariance function in (58). Since the covariance function of white-noise is impulsive, the corresponding covariance operator is the identity. This can be observed from the following sequence of operations: $E[\varepsilon\varepsilon^*]v = \int_{\Omega} E[\varepsilon(x)\varepsilon(\xi)]v(\xi)d\xi = v$, which is valid for all admissible functions v . Consequently, the covariance operator $E(\varepsilon\varepsilon^*)$ of ε satisfies the condition

$$E(\varepsilon\varepsilon^*)=I, \quad (59)$$

where I is the appropriately dimensioned identity operator. Eq. (59), which can be viewed as the integrated version of (58), represents the key assumption needed to compute the corresponding covariances of the estimates and of the related estimation errors.

The Covariance Operator $E[uu^*]$ of the State u . The following sequence of steps $E[uu^*] = E[Lff^*L^*] = LE[ff^*]L^* = LL^*$ imply that

$$E[uu^*] = LL^*. \quad (60)$$

Note that the kernel of LL^* is $r(x/\xi)$ implying that

$$E[u(x)u(\xi)] = r(x/\xi), \quad (61)$$

which justifies the earlier interpretation of r as the state covariance kernel.

The Covariance Operator $E[yy^*]$ of the Data y . This operator is given by

$$E[yy^*] = I + HLL^*H^*, \quad (62)$$

as can be established by $E[yy^*] = E[h\varepsilon\varepsilon^*h^*] = hE[\varepsilon\varepsilon^*]h^* = hh^* = I + HLL^*H^*$.

The Covariance Operators $E[\varepsilon_0\varepsilon_0^*]$ and $E[\varepsilon_p\varepsilon_p^*]$ of ε_0 and ε_p .
The following sequence of steps $E[\varepsilon_0\varepsilon_0^*] = E[W\varepsilon\varepsilon^*W^*] = WE[\varepsilon\varepsilon^*]W^* = W^2 = W$ and $E[\varepsilon_p\varepsilon_p^*] = E[(I-W)\varepsilon\varepsilon^*(I-W)] = (I-W)E[\varepsilon\varepsilon^*](I-W) = (I-W)$ imply that

$$E[\varepsilon_0\varepsilon_0^*] = W, \quad (63)$$

$$E[\varepsilon_p\varepsilon_p^*] = I - W, \quad (64)$$

where W is the projection operator defined in (47) that relates the actual and estimated errors ε and ε_0 .

Whiteness of the Innovations Process. This result

$$E(ee^*) = I, \quad (65)$$

valid in cases where the Gohberg-Krein factorization holds, follows from the following sequence of steps $E(ee^*) = E[w\varepsilon\varepsilon^*w^*] = ww^* = I$.

The Covariance Operator $E[u_p u_p^*]$ of the State Estimation Error u_p . The state estimation error u_p is defined as the difference $u_p = u - u_0$ of the actual and estimated state u and u_0 . Since $u = Lf$ and $u_0 = Lf_0$, then $u_p = L(f - f_0) = Lf_p$, where f_p is the process-error estimation error that together with n_p forms the two-component model-error estimation error $\varepsilon_p = [f_p, n_p]$. Hence, $E[u_p u_p^*] = LE[f_p f_p^*]L^*$ and

$$E[u_p u_p^*] = L[I - L^*H^*(I + HLL^*H^*)^{-1}HL]L^*, \quad (66)$$

where $E[f_p f_p^*]$ has been computed by taking that component of $E[\varepsilon_p \varepsilon_p^*]$ in (64) that corresponds to $E[f_p f_p^*]$.

An alternative expression for $E[u_p u_p^*]$ can be found by rearranging (66) to obtain

$$E[u_p u_p^*] = L(I + L^* H^* H L)^{-1} L^* \quad (67)$$

Note that (66) requires inversion of the operator $(I + H L L^* H^*)$, whereas (67) involves inversion of the related but distinctly different operator $(I + L^* H^* H L)$. The availability of the two options in (66) and (67) provides the possibility of using whichever option turns out to be simplest in a given situation.

The Mean-Square State Estimation Error $E(u_p, u_p)$. The mean-square state estimation error, defined as $E(u_p, u_p)$, is related to the trace of the covariance operator $E[u_p u_p^*]$ by means of the following identity

$$E(u_p, u_p) = \text{Tr } E[u_p u_p^*], \quad (68)$$

where the trace Tr of an operator is defined in the sense of Ref. [3]. Substitution of (67) in (68) leads to the following expression for the mean-square state estimation error

$$E(u_p, u_p) = \text{Tr} [L(I + L^* H^* H L)^{-1} L^*] \quad (69)$$

An alternative expression for $E(u_p, u_p)$, of course, can be obtained by substitution of (66) in (68).

An eigenfunction expansion can also be found for $E(u_p, u_p)$ in terms of the orthonormal basis ϕ_k in (19). For simplicity, the assumption is made that $H = H^* = I$, corresponding to the case with observations over the entire domain. For this case, it can readily be shown that

$$E(u_p, u_p) = \sum_k \lambda_k^2 / (1 + \lambda_k^2), \quad (70)$$

where λ_k^2 are the eigenvalues of $R = LL^*$.

The Mean-Square Model-Error Estimation Error $E\langle \varepsilon_p, \varepsilon_p \rangle$. Since $E\langle \varepsilon_p, \varepsilon_p \rangle = \text{Tr} E[\varepsilon_p \varepsilon_p^*]$, Eq. (64) implies that

$$E\langle \varepsilon_p, \varepsilon_p \rangle = \text{Tr}(I - W), \quad (71)$$

or, in terms of the components f_p and n_p of ε_p ,

$$E\langle \varepsilon_p, \varepsilon_p \rangle = E(f_p, f_p) + E(n_p, n_p), \quad (72)$$

$$E(f_p, f_p) = \text{Tr}[I - L^* H^* (I + HLL^* H^*)^{-1} HL], \quad (73)$$

$$E(n_p, n_p) = \text{Tr}[I - (I + HLL^* H^*)^{-1}], \quad (74)$$

The last two terms $E(f_p, f_p)$ and $E(n_p, n_p)$ are the mean-square estimation errors inherent in the process-error and observation-error estimates. Note parenthetically that by use of the identity $(I + HLL^* H^*)^{-1} = I - G$, where G is the Fredholm resolvent in (26), the condition (74) can be converted to

$$E(n_p, n_p) = \text{Tr}[G] = \int_{\Omega} \text{Tr}[g(x/x)] dx \quad (75)$$

an equation which is somewhat more convenient than (74).

Eigenfunction expansions for $E(f_p, f_p)$ and $E(n_p, n_p)$ can also be found as

$$E(f_p, f_p) = \sum_k 1/(1 + \lambda_k^2), \quad (76)$$

$$E(n_p, n_p) = \sum_k \lambda_k^2 / (1 + \lambda_k^2), \quad (77)$$

where, for simplicity, it has been assumed that $H = H^* = I$ in (73) and (74).

Unboundedness of the Process-Error Mean-Square Estimation Error

Under the assumption used in this section that the actual errors ε are white-noise and that the corresponding covariance operator $E[\varepsilon \varepsilon^*]$ is the identity as in (59), the mean-square estimation error $E(f_p, f_p)$ of the process error becomes unbounded. This unboundedness can be ascertained by inspection of the right-hand side of (76). By an argument similar to the one used to analyze the summation in (23), it can be established that the term $1/(1 + \lambda_k^2) \rightarrow 1$ as $k \rightarrow \infty$. This implies that the summation in (76) does not converge, and, in fact, becomes unbounded.

This lack of convergence is due to the fact that the process-error estimation error $f_p = f - f_0$ is a spatially distributed process that for large k retains many of the spatial characteristics of the white-noise process f . This similarity between f and f_p at large k can follow from the fact that

f_0 is a 'smoothed' estimate in the sense that it is dominated primarily by the spatial characteristics associated with small values of k . Since f_0 is being subtracted from f to obtain f_p , the resulting process $f_p = f - f_0$ will tend to be dominated at large k by the spatial characteristics of the initial white-noise process f .

Although it should be kept in mind at all times, the problem of unboundedness of $E(f_p, f_p)$ is not as serious as it may seem initially, since the white-noise assumption used for f is never satisfied in practice. In physical situations, the actual errors are never white and the corresponding model error estimates f_0 and the process error estimation error f_p are well-behaved. The white-noise assumption (59) is a mathematical fiction that generally is useful because it leads to a relatively simple 'a priori' covariance analysis as represented by (60)-(77). However, the results obtained by such an analysis should be used only if they make sense and should be discarded otherwise. The unboundedness of $E(f_p, f_p)$ is therefore a property that is primarily of mathematical interest but that can be ignored in practice because the assumptions under which the lack of boundedness occurs are seldom satisfied.

The State and Model-Error Estimates as Conditional Expectations

The aim here is to reinterpret the state and model-error estimates u_0 and ε_0 in (9) and (12) as the conditional expectations $\varepsilon_0 = E(\varepsilon/y)$ and $u_0 = E(u/y)$. To this end, consider the general formula [3] for the conditional expectation of u given y :

$$E(u/y) = E(uy^*) [E(yy^*)]^{-1}y, \quad (78)$$

expressed in terms of the 'cross-covariance' operator $E[uy^*]$ and the 'auto-covariance' operator $E[yy^*]$. Direct computation of these two operators leads to $E[uy^*] = LL^*H^*$ and $E[yy^*] = I + HLL^*H^*$. These last two equations imply that

$$u_0 = E(u/y) = LL^*H^* [I + HLL^*H^*]^{-1}y, \quad (79)$$

an equation that has previously been recorded as (12), but that can now be used to observe the equivalence of u_0 and $E(u/y)$.

Similar arguments can be used to show that

$$E(\varepsilon/y) = E(\varepsilon y^*) [E(yy^*)]^{-1}y, \quad (80)$$

where $E(\varepsilon y^*) = E(\varepsilon \varepsilon^* h^*) = h^*$ and $E(yy^*) = E(h \varepsilon \varepsilon^* h^*) = h h^*$. Consequently,

$$\varepsilon_0 = E(\varepsilon/y) = h^* (h h^*)^{-1}y, \quad (81)$$

an equation previously recorded as (9) but that now makes explicit the equivalence of ε_0 and $E(\varepsilon/y)$.

The above equivalence has been established using a somewhat indirect approach where the deterministic solutions ε_0 and u_0 in (9)-(12) were first obtained using a least-squares formulation. The deterministic solutions were then re-interpreted probabilistically as the conditional expectations $E(\varepsilon/y)$ and $E(u/y)$ in (79) and (81). An alternative and more direct approach to establish that $\varepsilon_0 = E(\varepsilon/y)$ and $u_0 = E(u/y)$ would be to introduce a probabilistic framework with u , ε and y assumed to be random-fields from the outset, and then to use a direct computation of the conditional expectations to arrive at (79) and (81). Such an approach is currently under investigation and will be reported on elsewhere by the author.

8. CONCLUDING REMARKS

This paper has advanced an approach to the concurrent estimation of the state and of the model errors for a system described by elliptic equations. The approach is based on the principle of least-squares that seeks to find the model error vector with smallest norm subject to linear constraints in a suitably defined function space. Solution of the optimization problem leads to state and model error estimates that can be computed either in a batch-processing mode where all of the data is processed simultaneously or in a scanning mode where the data is processed recursively. A probabilistic interpretation of the deterministic least-squares solutions makes possible an 'a priori' covariance analysis of the estimation error associated with the estimates. The covariance analysis also provides formulas to evaluate the mean-square estimation error corresponding to both the state and the model error estimates.

REFERENCES

1. Rodriguez, G. and R. Scheid, State and Model Error Estimation for Elliptic Systems: Applications to Large Antenna Static Shape Determination, Proceedings of Workshop on Applications of Distributed System Theory to the Control of Large Space Structures, July 14-16, 1982, Jet Propulsion Laboratory, Pasadena, California.
2. Rodriguez, G., A Function Space Approach to Smoothing with Application to Model Error Estimation for Flexible Spacecraft Control, 20th IEEE Conference on Decision and Control, San Diego, California, December 1981.
3. Balakrishnan, A. V., Applied Functional Analysis, Springer-Verlag, 1976.
4. Bellman, R. E., Functional Equations in the Theory of Dynamic Programming-VI: A Partial Differential Equation for the Fredholm Resolvent, Proc. Amer. Math. Soc 8 (1957), pp. 435-440.

ACKNOWLEDGEMENT

The research described in this paper was carried out at the Jet Propulsion Laboratory, California Institute of Technology, under contract with the National Aeronautics and Space Administration.

This Page Intentionally Left Blank

STATE AND MODEL ERROR ESTIMATION FOR ELLIPTIC SYSTEMS: APPLICATIONS TO LARGE ANTENNA STATIC SHAPE DETERMINATION

G. Rodriguez and R.E. Scheid, Jr.

Jet Propulsion Laboratory, California Institute of Technology
Pasadena, CA 91109

ABSTRACT

This paper outlines the application of the estimation approaches of Ref. [1] to the problem of static shape determination for large antenna systems. The problem consists of estimating the shape of an antenna surface from measurements of its static deflection. The estimation schemes are based on any one of the modeling options of a single PDE for early insight and understanding, coarse-resolution multiple-PDE models for parametric studies and fine-resolution piecewise-continuum models for detailed design. For any one of these three models, estimator design can be developed using an infinite-dimensional approach, where the necessary finite-element truncation and approximation is conducted after the analytical design has taken place, or it can be based on a finite-dimensional approach, where the model is truncated before the estimation problem is formulated. One of the main objectives of the paper is to develop both approaches while simultaneously investigating their differences and similarities. Simulation results of an application of the finite-dimensional approach to a large parabolic reflector are presented. Similar large antenna simulations for the infinite-dimensional approach are currently being carried out.

1. INTRODUCTION

The problem of static shape determination consists of finding the shape of an antenna surface from multi-point spatially distributed measurements of the structural deflections, as illustrated in Fig. 1(a). A large flexible antenna will be perturbed from a nominal shape by disturbances due, for example, to control actuation and external loads. To meet future antenna performance requirements, it will be necessary to determine these deflections quite accurately, and in some cases, to apply control forces and/or moments to restore the desired antenna shape. The estimation methods described here would constitute a fundamental element of such a combined shape determination and control capability.

Current methods for antenna calibration entail a painstaking survey of the entire surface of the structure, usually accomplished by a technician armed with a theodolite as in Fig. 1(b). Once the survey is complete, a least-squares fit of the data to the parameters of a paraboloid is performed. The entire process can take on the order of days and is clearly inadequate for systems requiring real-time autonomous operation.

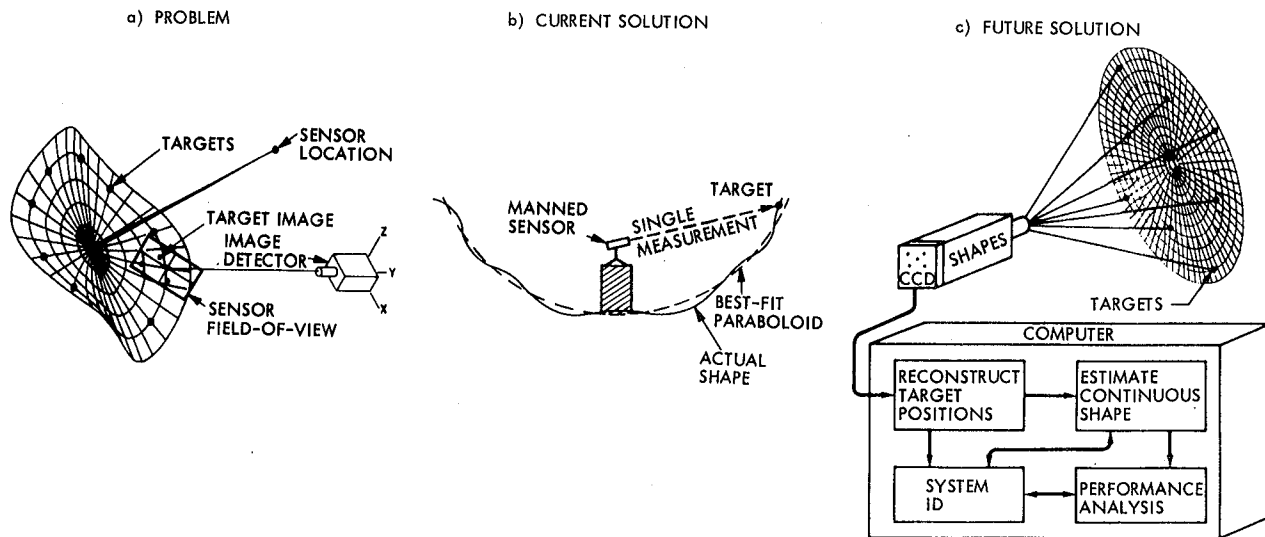


Fig. 1. Static Shape Determination Problem

An improved solution to the shape determination problem is provided by an integrated system in Fig. 1(c), currently under development at JPL, that combines the two mutually complementary technologies of electro-optical sensing for shape determination and estimation/identification methodology for processing of the sensor data. Sensing is provided by SHAPES [2], a sensor capable of the real-time, simultaneous measurement of the three-dimensional deflections of about 50 points on a structure at a sampling rate of 10 hz. While Fig. 1(c) illustrates the full system capability for static and dynamic shape estimation and for parameter identification, this paper focuses primarily on the static shape estimation algorithms as described below.

2. ELLIPTIC MODELS FOR SHAPE ESTIMATOR DESIGN

Central to the shape determination schemes under development here is the selection of a mathematical model to represent the elastic behavior of the structure. The following types of models (Fig. 2) are useful at three distinct stages of the design process: 1) single PDE models defined over a single domain for development of initial physical insight and understanding, 2) coarse-resolution multiple-PDE models for parametric studies and design and 3) fine-resolution piecewise-continuum models, defined over a possibly fine structural-element grid, for detailed design and evaluation.

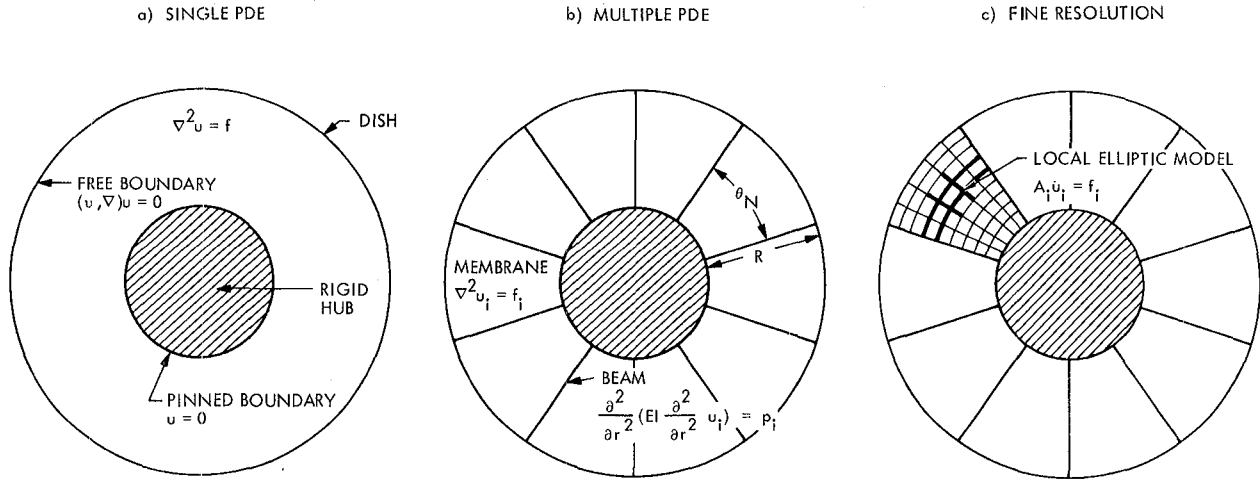


Fig. 2. Models for Estimator Design

Single PDE Models

Such models are most useful in the early stages of a design, when one of the main objectives is to create physical understanding and insight about the design problem. An example of such a model, one that would be applicable as a simple approximation to a parabolic antenna system, is illustrated in Fig. 2(a). This model has been used to develop the scanning solutions for data-processing outlined in [1]. The model consists of the following equations for the out-of-plane displacement of a membrane in tension:

$$\nabla \cdot (T\nabla u) = f, \quad \int_0^R \int_0^{2\pi} frd\theta dr = 0, \quad (1)$$

$$y(\theta) = u(R, \theta) + n(\theta), \quad \text{for } 0 \leq \theta \leq 2\pi, \quad (2)$$

defined over a circle of radius R in terms of the polar coordinates r and θ . The symbol T denotes the membrane tension for unit area. The free-boundary condition $(\mathbf{v} \cdot \nabla)u = 0$ is assumed at the outer boundary, where \mathbf{v} denotes the corresponding unit normal. The "internal" condition $u(0, \theta) = 0$ is assumed to hold at the origin $r = 0$ to account for the fact that the sensor is assumed to measure the relative displacement between the boundary and the origin. The observation equation (2), in this particular case, assumes that the data is available continuously at the boundary of the domain. This assumption, however, is not a major restriction, as other types of observations (such as discrete measurements along the boundary) can be encompassed with a similar formulation as described in Ref. [1].

An alternative approach to describing the model, which will be useful later in applying the finite-element method, is based on the following variational formulation. The potential energy $a(u,u)$ associated with the model is $a(u,u) = (1/2) \int_{\Omega} T \nabla u \cdot \nabla u \, d\Omega$. A variational (weak) solution to (1) is obtained by solving the following minimization problem

$$\min J(u) = a(u,u) - (u, f), \quad \text{for } u \text{ in } V, \quad (3)$$

where V , commonly referred to as the space of admissible functions, consists of those functions which possess square-integrable first-order spatial derivatives and which satisfy the geometric boundary conditions $u(0, \theta) = 0$ of the problem. The boundary condition $(\nu \cdot \nabla u) = 0$ at the circumference of the domain emerges as a natural condition by solving the minimization problem in (3). Ref. [3] contains a more precise statement of the above variational formulation.

Closely related to the minimization problem in (3) is the principle of virtual work stating that

$$2 a(u, v) = (v, f), \quad \text{for } v \text{ in } V, \quad (4)$$

which is obtained readily from (3) as a necessary condition for minimization.

The value of introducing the variational model-statements in (3) and (4) is that they can be readily extended to describe complicated multiple-PDE models. While in the simple case of a single equation, it is equally convenient to write either the explicit form (1) or the variational forms (3) and (4), in more complicated cases described below, the variational formulation results in a somewhat simpler statement of the model.

Coarse-Resolution Multiple-PDE Models

These models involve first subdividing a structure into a few major substructures, describing each substructure by means of a simple set of partial differential equations, and then specifying appropriate continuity conditions at the interfaces between substructures. The models that result from this process are specified in terms of a few coupled partial differential equations together with the corresponding boundary and interface conditions.

An example of such a model is illustrated in Fig. 2(b). The structure consists of an antenna dish with a prescribed number N of ribs emerging from a central rigid hub. The ribs provide the necessary tension to support a membrane-like mesh. In the interest of obtaining a relatively simple model, the antenna dish is assumed to be flat, and only the out-of-plane deflection is considered. Additional simplifying assumptions are that the mesh can be described by the equations for a membrane in tension and that

the deflection of each rib is governed by a simple beam-equation model. The out-of-plane deflection of the dish is described by the composite N-vector $u(r, \theta) = [u_1(r, \theta), \dots, u_N(r, \theta)]$, where $u_1(r, \theta)$ is the displacement of the dish within each subdomain. In terms of this displacement field, the total potential energy can be expressed as:

$$a(u, u) = \frac{1}{2} \int_0^R \int_0^{\theta_N} T \nabla u(r, \theta) \cdot \nabla u(r, \theta) r d\theta dr + \frac{1}{2} \int_0^R EI [\partial^2 u(r, \theta_N) / \partial r^2]^2 dr, \quad (5)$$

where $\nabla u = [\nabla u_1, \dots, \nabla u_N]$, and T and EI are respectively the membrane-tension and beam-stiffness coefficients.

The variational principles in (3) and (4) above apply to the multiple PDE models once the potential energy (and the corresponding space V of admissible functions) has been specified. For the example in Fig. 2(b), the potential energy is given by (5). The related admissible space V consists of those displacements that are sufficiently differentiable so that the potential energy (5) is well-defined and that, in addition, satisfy the following geometric boundary and interface conditions. The inner-boundary geometric conditions $u(0, \theta_N) = \partial u(0, \theta_N) / \partial r = 0$ for the rib elements correspond to the assumption that the ribs are pinned at the hub. For the mesh elements, the inner-boundary condition $u(0, \theta) = 0$ corresponds to a similar assumption. The natural boundary conditions for the ribs $\partial^2 u(R, \theta_N) / \partial r^2 = \partial^3 u(R, \theta_N) / \partial r^3 = 0$ and for the mesh $\partial u(R, \theta) / \partial r = 0$ for $0 \leq \theta \leq \theta_N$ emerge from the variational formulation.

To complete a specification of the admissible displacements, it is necessary to determine interface conditions. These conditions, based on the assumption that the displacement field is continuous at the interfaces between rib and mesh elements, can be stated as $u_i(r, \theta_N) = u_{i+1}(r, 0)$ for $0 \leq r \leq R$ or in the more convenient matrix form

$$u(r, \theta_N) = C u(r, 0), C = \begin{bmatrix} 0 & 1 & 0 & \dots & \dots & 0 \\ 0 & 0 & 1 & 0 & \dots & 0 \\ \cdot & & & & & \cdot \\ \cdot & & & & & \cdot \\ \cdot & & & & & \cdot \\ 0 & 0 & \dots & \dots & \dots & 1 \\ 1 & 0 & \dots & \dots & \dots & 0 \end{bmatrix}. \quad (6)$$

It is of interest to note that C is a periodic matrix with all of its eigenvalues equally spaced on the unit circle, a property that can be used very efficiently to analyze the model by means of cyclic symmetry as outlined in Ref. [4].

A more explicit form, analogous to (1), of the above coarse-resolution multiple-PDE model can be obtained by a set of analytical manipulations (closely related to integration-by-parts). Use of the divergence theorem and of the geometric boundary conditions (6) in (4) results in

$$\begin{aligned} & \int_0^R \int_0^{\theta_N} \left\{ f(r, \theta) - \nabla \cdot [T \nabla u(r, \theta)] \right\} \cdot v(r, \theta) r d\theta dr + \\ & \int_0^{\theta_N} T [\partial u(r, \theta) / \partial r] \cdot v(r, \theta) r d\theta + \int_0^R EI [\partial^2 u(r, \theta_N) / \partial r^2] \\ & [\partial^2 v(r, \theta_N) / \partial r^2] dr + \int_0^R T r^{-1} [\partial u(r, \theta_N) / \partial \theta \cdot v(r, \theta_N) \\ & - \partial u(r, 0) / \partial \theta \cdot v(r, 0)] dr = 0, \end{aligned} \quad (7)$$

which must be valid for all admissible virtual displacements v . This condition, after two integrations by parts in the third term and use of the geometric constraints (6) in the last term, results in the following more explicit set of equations describing the model:

$$\nabla \cdot (T \nabla u) = f, \quad (8)$$

$$\frac{\partial^2}{\partial r^2} \left[EI \frac{\partial^2 u}{\partial r^2} (r, \theta_N) \right] = \frac{T}{r} \frac{\partial}{\partial \theta} [C u(r, 0) - u(r, \theta_N)], \quad (9)$$

together with the natural boundary conditions $\partial u(R, \theta) / \partial r = \partial^2 u(R, \theta_N) / \partial r^2 = \partial^3 u(R, \theta_N) / \partial r^3 = 0$. As expected, this set of equations are in the general form of (1), with perhaps the exception of (9) which requires further investigation.

Equation (9) is an interface condition reflecting the forces that the mesh membrane applies at each of the beam elements. Some physical insight can be gained by transforming (9) into the following scalar notation:

$$\frac{\partial^2}{\partial r^2} [EI \frac{\partial^2}{\partial r^2} u_i(r, \theta_N)] = \frac{T}{r} [\frac{\partial}{\partial \theta} u_{i+1}(r, 0) - \frac{\partial}{\partial \theta} u_i(r, \theta_N)] \quad (10)$$

in terms of the scalar displacements u_i of the individual rib elements. Note that the term on the right reflects the forces that the adjacent membrane elements apply on the i^{th} rib element. This force is dependent on the difference in the circumferential slope (the partial derivative of the displacement with respect to θ) of the membrane deflection at the interface. A different way to interpret this equation is based on the observation that a rib deflection, as represented by the left side of (10), would cause a "jump" discontinuity in the circumferential slope of the membrane.

The foregoing equations represent the sought-after multiple-PDE model for the structure. While the model as developed here involves only out-of-plane deflections, a similar approach can also be used for the in-plane deflections as described in more detail in Ref. [4].

Some remarks are appropriate about the potential uses and limitations of such coarse-resolution models. Because of their relative simplicity, the models are usually a very coarse approximation to the actual structure. For instance, the dish has been assumed to be flat, whereas, in more complete models, the parabolic dish geometry has to be taken into account. Also, the ribs have been modeled as simple beam elements, while, in reality, each rib is in itself a complicated structure (of variable cross-section and curved geometry) that would require a more complete model for its full description. Because of these and other limitations (such as the use of a linear elastic model to approximate the actual nonlinear mesh behavior), it is necessary to use caution in applying these models.

Most of the applications of the piecewise-continuum models result from their ability to describe many of the basic features of the actual structure, while still retaining a relative simplicity. Since the models typically involve only a few parameters, they can be quite useful in conducting parametric design studies. For example, they can be used to establish the sensitivity of estimator performance to changes in the structural stiffness properties. For the same reasons, the models can also be used in non-modal parameter-identification approaches to estimate such parameters as the average mesh tension T that, in a global somewhat approximate sense, characterize the stiffness properties of the structure.

In summary, while the coarse-resolution multiple PDE models can be useful in many cases, their inherent limitations must be understood in order for the models to be applied correctly. In cases where more resolution is required, the models described below have a better potential (by no means always achieved) for characterizing accurately the behavior of complicated structures.

Fine-Resolution Multiple PDE Models

Development of these models begins by first partitioning a structure into a possibly large number of elements, as in the finite-element approach to structural modeling. After this element grid has been specified, the deflection within each of its elements is described by the relatively simple PDE's used in the traditional elements (beams, plates, membranes, etc.) in structural analysis. To complete the model, interface conditions reflecting continuity of the displacement field and possibly some of its spatial derivatives are then specified. An illustration of the grid for representing an antenna-reflector model is contained in Fig. 2(c).

A fine-resolution piecewise-continuum model would be obtained as follows. The structural deflection within each element would, as in the previous model, be described by the symbol $u_i(x_i)$, where x_i are the local spatial coordinates within each grid element Ω_i . The total potential energy of the system can be expressed as:

$$a(u,u) = \frac{1}{2} \sum_i \int_{\Omega_i} c_i [D_i u_i \cdot D_i u_i] d\Omega_i, \quad (11)$$

where D_i are appropriately defined partial differential operators, and c_i are constants characterizing the elastic properties of each element. Note that while the local element stiffness has been characterized by a single scalar (for the sake of simplicity), the formulation can be extended readily to cases where the stiffness properties are specified by several scalars.

This definition of the potential energy is the key step required to apply either one of the variational principles in (3) and (4) to the fine-resolution PDE models. The corresponding space V of admissible displacements is, as before, based on the peculiarities of the problem under investigation. In general terms, however, the displacements in this space are selected so that the potential energy makes sense and so that the geometric boundary conditions (and also the inter-element conditions) are satisfied.

Fine-Resolution Matrix Differential Operator Models

A more explicit matrix-differential-operator model, similar to that in Eq. (8), can be developed for complicated structures requiring a fine-resolution grid description as in Fig. 2(c). To this end, consider the identity

$$\int_{\Omega_i} c_i [D_i u_i \cdot D_i u_i] d\Omega_i = \int_{\Gamma_i} [u_i \cdot B_i u_i] d\Gamma_i - \int_{\Omega_i} [u_i \cdot D_i^* c_i D_i u_i] d\Omega_i, \quad (12)$$

where B_i denotes a matrix differential operator defined over the boundary Γ_i of Ω_i , and D_i^* is for formal adjoint of D_i . For specific cases of practical interest, this identity can be obtained readily by a process analogous to integration-by-parts, as in the case of Eq. (8). Use of (12) in (11) implies that $Au = f$, where u is the composite vector $u = [u_1, \dots, u_N]$, and A is a matrix-differential operator whose diagonal elements are $D_i^* c_i D_i$ in (12). In some cases, it is convenient to replace this model $Au = f$ with the more general model

$$Au = Bf, \tag{13}$$

where the operator B has been added to reflect the fact that the forcing term $f = [f_1, \dots, f_N]$ may not be applied at all elements Ω_i .

The operator A in (13) may appropriately be referred to as the "stiffness operator" because it is a generalization of the traditional stiffness matrix of structural mechanics. This equation must be satisfied together with a set of inter-element conditions (emerging as natural conditions from the first term on the right side of (12)), which reflect the continuity of the quantity $B_i u_i$ at the interelement boundaries Γ_i .

Discussion

The piecewise-continuum models just described simultaneously retain both the conceptual completeness of partial differential equations and the versatility of the finite-element approach to modeling of complicated structures. Retention of the infinite-dimensionality of the continuum models implies that the model has the potential for describing many of the important physical characteristics (which may be important to estimation accuracy) of the structure. For example, in the antenna shape determination problem, it is necessary to have an accurate description of the antenna deflection inside each grid element in order for the shape estimates to be consistent with the relatively short wavelength (4 cm for a typical electrical operating frequency of 2.5 Ghz) of intended operations. The ability to retain such resolution makes the model potentially more accurate, although finer resolution does not necessarily imply improved accuracy. It is quite possible that the additional information being retained by the fine-resolution model is corrupted by inevitable model errors. However, in spite of these errors, the models can still be quite useful if they retain qualitatively the significant effects of the structure response.

One of the main objectives of developing such models of course is to conduct the shape estimator designs. As will be discussed in Sec. 3, this design can be based on the abstract-operator model in (13), without having to convert this model into scalar PDE notation. Obtaining such a scalar model would be impossible for structures of even reasonable complexity, because of the large number of coupled differential equations, inter-element boundary conditions and coordinate transformations which would be involved.

However, before introducing the design approach based on the operator models (to be done in Sec. 3), it is of interest to develop first a finite-dimensional version of (13) as described below.

Finite-Dimensional Models

An alternative to the above infinite-dimensional models is obtained by solving approximately the minimization problem (3) by means of the finite-element method [5]. The finite-element solution is obtained by solving (3) within an approximation subspace V^N typically consisting of piecewise polynomial functions defined over a finite-element structural grid. Every function u within this subspace V^N can be expressed as

$$u = \sum_k x^k \phi_k, \quad (14)$$

where ϕ_k is a piecewise-polynomial basis, and x^k are the corresponding coefficients. Substitution of (14) in (3) and performance of the indicated minimization results in

$$KX = F, \quad (15)$$

where K is a stiffness matrix whose general element $K^{km} = 2a(\phi_k, \phi_m)$; F is a vector whose elements $F_k = (\phi_k, f)$, and X is a vector formed by the coefficients x^k in (14).

Orientation

One of the central themes of this paper is to understand the relationship between the following two approaches to estimator design:

- an approach where an infinite-dimensional model is retained as long as possible throughout the design process while delaying the necessary truncation until the analytical design has taken place.
- a finite-dimensional design approach where the structural model is first truncated and the subsequent estimator design is based on the approximate model.

Although in the first approach the design is obtained first and then truncated, in the second approach these two steps of design and approximation are reversed. A development of the two approaches, together with illustrative examples and applications, is contained in the next three sections of the paper.

3. INFINITE-DIMENSIONAL APPROACH TO ESTIMATION

The infinite-dimensional approach to estimator design begins from the basic goal of minimizing the following quadratic functional of the model errors:

$$\min J(f) = (y - Hu, y - Hu)_3 + (f, f)_2, \quad (16)$$

where the inner product notation is defined in Ref. [1]. The optimization problem must be solved subject to the constraints specified by the model equations $Au = Bf$ in (13), emerging from a single PDE, a coarse-resolution multiple PDE model, or a fine-resolution piecewise-continuum model. These constraint equations must be satisfied together with interelement conditions, similar to (9) above, reflecting continuity of the displacements and possibly a finite number of its spatial derivatives. The observation equation is again specified by $y = Hu + n$.

Application of a calculus of variations approach [3] leads to the following boundary-value problem

$$Au_0 = BB^*\lambda, \quad (17)$$

$$A^*\lambda = H^*(y - Hu_0), \quad (18)$$

whose solution is specified in terms of the optimal estimates u_0 and the adjoint variables λ . The corresponding model error estimates f_0 and n_0 are provided by

$$f_0 = B^*\lambda, \quad (19)$$

$$n_0 = y - Hu_0, \quad (20)$$

in terms of the previously determined variables u_0 and λ .

The above is a boundary-value problem of the type traditionally encountered [3] in solving optimal control and estimation problems with quadratic criteria. Its solution leads to the state and model error estimates u_0 and $\epsilon_0 = [f_0, n_0]$. This boundary-value problem provides an equivalent alternative to the integral equation approach of Ref. [1] for computation of the optimal estimates.

Equivalence of Boundary-Value Problem and Fredholm Integral Equation

To show the equivalence, first solve (18) for λ to obtain $\lambda = L^*H^*n_0$, where L^* is the integral operator whose kernel is the Green's function for A^* . Substitution of this equation in (17) implies that $u_0 = LBB^*L^*H^*n_0$, and use of this in the observation equation $y = Hu_0 + n_0$ leads to

$$(I + HLBB^*L^*H^*)n_0 = y, \quad (21)$$

which, upon setting $B = I$, can be recognized as the integral equation in [1].

An Alternative Form for the Boundary-Value Problem

An alternative form of the above boundary-value problem is obtained, in cases where $B = I$, by eliminating the adjoint variables λ in (17) and (18). First, operate on (17) by A^* to obtain the intermediate equation $A^*Au_0 = A^*\lambda$. Then, use this in (18) to arrive at $(A^*A + H^*H)u_0 = H^*y$, which implies that

$$u_0 = (A^*A + H^*H)^{-1} H^*y. \quad (22)$$

It is of interest to explore the relationship between this state-estimate solution and that obtained in [1]. Recall that in [1] u_0 has been specified as

$$u_0 = LL^*H^*(I + HLL^*H^*)^{-1} y. \quad (23)$$

Since both (22) and (23) determine u_0 in terms of the data y , these equations together imply the interesting identity:

$$(A^*A + H^*H)^{-1} H^* = LL^*H^*(I + HLL^*H^*)^{-1}. \quad (24)$$

Solution of Boundary-Value Problem by Finite-Element Method

The finite-element method [6] is applied here to obtain an approximate solution to the boundary-value problem in (17) and (18) that characterizes the optimal estimates. While the general methodology of finite-element analysis can be applied in a number of ways to this problem, an approach involving the consecutive solution of (18) and (17) is perhaps the most appropriate.

Consider first the following minimization problem whose solution corresponds to that of (18):

$$\min J(\lambda) = a(\lambda, \lambda) - (H\lambda, n_o)_3, \quad (25)$$

where $a(\lambda, \lambda)$ is the potential energy. To obtain an exact variational (weak) solution to this problem requires that the minimization in (25) be conducted in a space V of admissible functions. A finite-element approximate solution, however, is obtained by conducting the minimization in an approximation subspace V_1^N . The functions in V_1^N can be expressed as

$$\lambda = \sum_k \lambda^k \phi_k, \quad (26)$$

where ϕ_k form a piecewise polynomial basis in V_1^N , and λ_k are the corresponding coefficients. Substitution of (26) in (25) leads to

$$\Lambda = K_1^{-1} H_1^T n_o, \quad (27)$$

where $\Lambda = [\lambda^1, \dots, \lambda^N]$ is the vector of nodal-point adjoint variables, and $H_1 = [H\phi_1, \dots, H\phi_N]$ is a "modified" observation matrix. A stiffness matrix K_1 with a general element $K_1^{km} = 2a(\phi_k, \phi_m)$, has been assembled using the approximation subspace V_1^N .

This equation determines the values of the adjoint variables at the nodal coordinates, whereas the closely related Eq. (26) provides the necessary interpolation inside the elements themselves. Consequently, (26) and (27) together provide the sought-after solution of (18), and there remains only the task of solving (17) in order to compute the state estimates u_o .

The variational form of (17) is

$$\min J(u_o) = a(u_o, u_o) - (Bu_o, B\lambda), \quad (28)$$

where the minimization takes place in an approximation subspace V_2^N that, in general, may be distinctly different from the subspace V_1^N used to solve (25). The functions in V_2^N can be expressed as

$$u_o = \sum_k x_o^k \psi_k, \quad (29)$$

where ψ_k is a piecewise polynomial basis in V_2^N , and x^k are the corresponding coefficients which form the composite nodal-point state estimates $X_o = [x_o^1, \dots, x_o^N]$. Substitution of (29) in (28) results in

$$X_o = K_2^{-1} C_2 \Lambda, \quad (30)$$

where the stiffness matrix K_2 and the related matrix C_2 are specified in terms of their general elements $K_2^{km} = 2a(\psi_k, \psi_m)$ and $C_2^{km} = (B\psi_k, B\phi_k)$. Eqs. (27) and (30), when used in the observation equation $y = Hu_o + n_o = H_2 X_o + n_o$, imply

$$(I + H_2 K_2^{-1} C_2 K_1^{-1} H_1^T) n_o = y, \quad (31)$$

where $H_2 = [H\psi_1, \dots, H\psi_N]$. This equation determines the observation estimates n_o from the data y , while the related nodal coordinate state estimates are determined from (27) and (30). The interpolation formulas (26) and (29) provide the value of the estimates in that part of the spatial domain within the individual finite elements.

Illustrative Example

Consider the following example illustrated in Fig. 3:

$$d^2 u(\xi)/d\xi^2 = f(\xi), \quad y_k = u(\xi_k) + n_k, \quad (32)$$

with the boundary conditions $u(0) = u(\ell) = 0$, where ℓ is the length of the structure. The objective of the estimation process is to minimize the functional

$$J(f) = \sigma^2 \sum_{k=1}^M n_k^2 + \int_0^1 f^2(\xi) d\xi, \quad (33)$$

which is a special case of (16) above. Note that for completeness a weighting coefficient σ has been introduced that can be varied as a parameter in the estimator design.

The boundary-value problem, analogous to (17) and (18), whose solution determines the optimal estimates is

$$d^2 u_o(\xi)/d\xi^2 = \lambda, \quad 0 \leq \xi \leq \ell, \quad (33)$$

$$d^2 \lambda(\xi)/d\xi^2 = 0, \quad \xi_k^+ \leq \xi \leq \xi_{k+1}^-, \quad (34)$$

$$d\lambda(\xi_k^+)/d\xi - d\lambda(\xi_k^-)/d\xi = y_k - u_0(\xi_k), \quad (35)$$

with the boundary conditions $u(0) = u(l) = \lambda(0) = \lambda(l) = 0$. The symbols $d\lambda(\xi_k^+)/d\xi$ and $d\lambda(\xi_k^-)/d\xi$ denote the upper and lower limits of the slope $d\lambda/d\xi$ at the measurement location ξ_k .

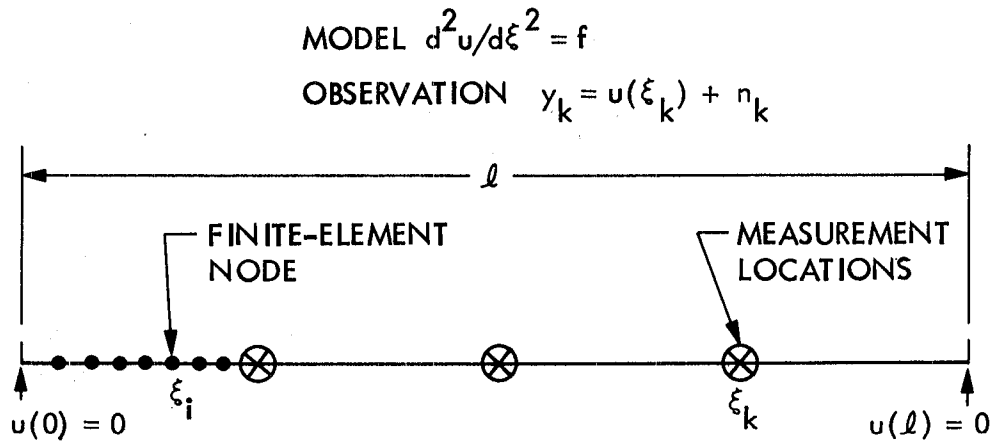


Fig. 3. Example to Illustrate Estimation Approaches

To obtain the solution of this problem by means of the finite-element method, it is necessary to first convert the problem statement to variational form as in (25). Consider the following minimization problem

$$\min J(\lambda) = a(\lambda, \lambda) - \sum_{k=1}^M \lambda^k n_o^k, \quad (36)$$

$$a(\lambda, \lambda) = \frac{1}{2} \sum_k \int_{\Omega_k} [d\lambda/d\xi]^2 d\xi, \quad (31)$$

The vector X_0 in (30) for this example is $X_0 = [x^1, \theta^1, \dots, x^N, \theta^N]$ consisting of the nodal deflections x^i and the corresponding nodal slopes θ^i . The vector Λ on the right side of (40) consists of the previously determined values of the adjoint variables at the nodal points.

The solution for the nodal-point state estimates X_0 then proceeds as follows. Eqs. (39) and (42) specify the necessary ingredients to form the matrix $(I + H_2 K_2^{-1} C_2 K_1^{-1} H_1^T)$ in (31), from which the nodal-point observation error estimate n_0 is evaluated in terms of the data y . Once n_0 is determined, Eq. (30) provides the desired nodal-point state estimate X_0 .

Simulation Results for Illustrative Example

Assume that the model in Fig. 3 is being perturbed from its nominal shape by a force of unit amplitude. The actual deflection, illustrated in Fig. 4(a), due to this forcing function is described by the formula $u(\xi) = (1/8)\ell^2 - (1/2)[\xi - (1/2)\ell]^2$. A total of three equally spaced measurements at the locations $(1/4)\ell$, $(1/2)\ell$ and $(3/4)\ell$ produce the data $y_1 = y_3 = 3\ell^2/32$ and $y_2 = \ell^2/8$ to be used for estimation.

Fig. 4(a) shows a comparison between the actual deflection and the related estimates for three distinct values of the coefficients σ in (33). Note that as the weighting on the observation error is increased (by selecting larger values of σ), estimates that are closer to the actual deflection result. The reason for this improvement is that the forcing function of $f = -1$ represents a relatively large process error, whereas the observation error has been assumed to be zero. Consequently, estimator designs based on a large weighting for the observation error are more consistent with the relatively high degree of confidence that can be placed on the measurements. Note also that because of the piecewise-cubic interpolation in Eq. (41) the estimated displacement can, by appropriate selection of σ , be made quite close to the actual displacement.

Fig. 4(b) shows a comparison between the actual process error f and the corresponding estimate f_0 for the same three distinct values of the weighting coefficient σ . The actual error f is a force of unit magnitude, whereas $f_0 = \lambda$ is an estimate based on the piecewise-linear approximation (38). Note that the best process-error estimate is achieved for the case where the weighting coefficient in (33) is large, so that the estimates are more heavily dependent on the data than they are on the model equations (32). Note also that close to the ends of the domain, the boundary conditions $\lambda(0) = \lambda(\ell) = 0$ cause the process-error estimate $f_0 = \lambda$ to differ substantially in a point-wise sense from the actual process error. This discrepancy at the boundaries can be easily reduced by use of additional measurements close to the edges of the domain.

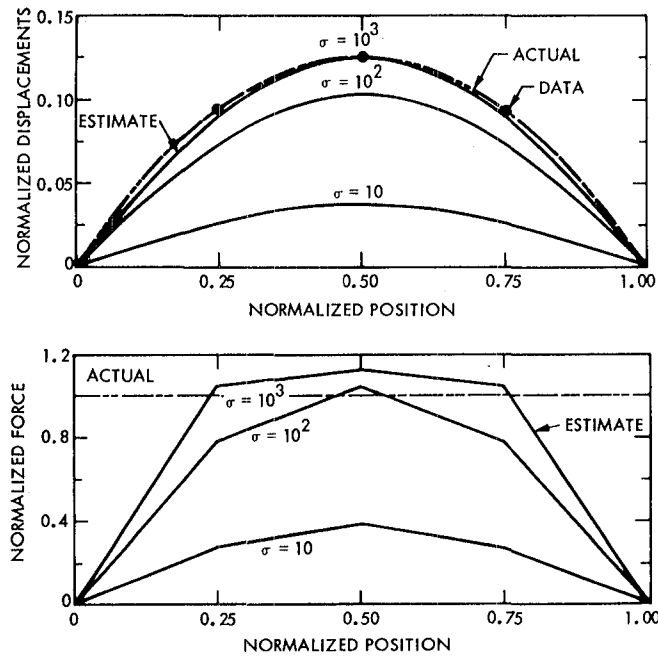


Fig. 4. Comparison Between Actual and Estimated Deflections and Forces

Discussion

While for the simple example above, solution of (17) and (18) by means of the finite-element method can be readily achieved, obtaining similar solutions for structures of even relatively moderate complexity is a nontrivial undertaking. A key challenge is that there is currently no widely available automated means to assemble the matrices K_2 and C_2 in (30), for the approximation subspaces that are specifically tailored to the solution of the boundary-value problem (17) and (18). Current finite-element codes assemble a stiffness matrix based on an approximation subspace that is consistent with obtaining accurate eigenvalues and eigenfunctions. The approximations used to compute eigenvalues, however, may or may not be appropriate for the estimation (and the control) problem. The appropriate choices for approximation subspaces must depend on the properties of the solution as outlined below.

Examine the boundary value problem derived from (17) and (18) with $B = I$:

$$\begin{bmatrix} I & A \\ A^* & H^*H \end{bmatrix} \begin{pmatrix} \lambda \\ u \end{pmatrix} = \begin{pmatrix} 0 \\ H^*y \end{pmatrix}. \quad (42)$$

Let u_k and λ_k be the solutions of the corresponding systems

$$\begin{bmatrix} I & A \\ A^* & 0 \end{bmatrix} \begin{pmatrix} \lambda_k \\ u_k \end{pmatrix} = \begin{pmatrix} 0 \\ H^*e_k \end{pmatrix}, \quad (43)$$

where, as in the illustrative example,

$$H^*e_k = \delta(x - \xi_k). \quad (44)$$

Then, by the principle of superposition the solution of (42) can be expressed as

$$u = \sum_k \alpha_k u_k, \quad \lambda = \sum_k \alpha_k \lambda_k, \quad (45)$$

where the coefficients α_k are determined by the system (21).

From (43), (44) and (45), it follows that the solution to the estimation problem is a superposition of fundamental solutions (Green functions) derived by considering the response to an impulse force at each of the measurement points. Thus, for the antenna models considered here, logarithmic singularities will be present in the impulse forces if measurements are to be taken on the mesh. Standard modal approximations cannot adequately cope with this difficulty when it is a physically significant feature of the estimation problem.

The infinite-dimensional approach provides the framework by which finite-element approximations that are consistent with good estimation and control accuracy can be systematically specified. In spite of its potential, however, application of this approach to complicated structures is not readily achieved now and may only be possible in the future if software that automates the required computations becomes available.

4. ESTIMATOR DESIGNS BASED ON FINITE-DIMENSIONAL MODELS

Since in this approach the system model is first truncated to a finite number of dimensions, the least-squares method for estimation has to be modified somewhat in order to apply to the finite-dimensional model (15). The key modification involves the least-squares criterion (16), which for finite-dimensional models becomes an ordinary function (as opposed to a functional for the infinite-dimensional problem). The least-squares function applicable to the finite-dimensional model (15) is

$$\min J(F) = (Y - HX)^T (Y - HX) + F^T F, \quad (46)$$

where F and X are constrained by (15). The finite-dimensional approach to estimator design is based on minimizing (46) subject to these constraints. The observation equation corresponding to this model is assumed to be $Y = HX + N$, where as before Y is the data, N is the observation error, and H is the observation matrix.

Application of a variational approach to (46) leads to the following solutions for the state and model error estimates X_o and $\epsilon_o = [F_o, N_o]$:

$$X_o = K^{-2} H^T [I + HK^{-2} H^T]^{-1} Y, \quad \epsilon_o = h^T (hh^T)^{-1} Y, \quad (47)$$

where $h = [HK^{-1} \mid I]$, or in more explicit notation,

$$F_o = K^{-1} H^T [I + HK^{-2} H^T]^{-1} Y, \quad N_o = [I + HK^{-2} H^T]^{-1} Y. \quad (48)$$

These equations, involving finite-dimensional matrices, are analogous to the linear operator formulas presented in Ref. [1] for the infinite-dimensional problem. For instance, Eq. (10) in Ref. [1] states that the observation error estimate n_o is specified by $n_o = (I + HLL^*H^*)^{-1} \bar{y}$ in terms of the data y . The similarity between this equation and (48) can be ascertained by inspection. Similar analogies can be drawn between (47) - (48) and the infinite-dimensional solutions. The main difference between the two sets of equations is that (47) and (50) involve matrices, whereas [1] contains their infinite-dimensional counterparts.

These are also close similarities between Eqs. (47) and (48) specifying the estimates based on a finite-dimensional model and (27), (30) and (31) which apply to the infinite-dimensional approach. The main difference

between the two sets of equations is that the stiffness matrices in (31) are formed using an approximation subspace that is consistent with the estimation problem, whereas the stiffness matrix in (47) and (48) was determined prior to the problem formulation.

Adjoint Variable Approach

An alternative method for solving the constrained minimization problem in (46) involves adjoining the constraints (15) to (46) by means of a set of adjoint variables Λ to obtain

$$\min J(F, X, \Lambda) = (Y - HX)^T (Y - HX) + F^T F + \Lambda^T (KX - F). \quad (49)$$

Use of the adjoint variables converts the original constrained minimization problem to one involving no constraints. A set of conditions for optimality for this problem is

$$KX_0 = \Lambda, \quad (50)$$

$$K\Lambda = H^T(Y - HX_0), \quad (51)$$

whose solution results in the nodal-point state estimate X_0 . The related nodal-point model error estimates are specified by $F_0 = \Lambda$ and $N_0 = Y - HX_0$.

To show equivalence of (50) and (51) with (47) first solve (51) for Λ in terms of N_0 as $\Lambda = K^{-1}H^T N_0$. Substitution of this equation in (50) leads to $X_0 = K^{-2}H^T N_0$. Since $Y = HX_0 + N_0$, then $[I + HK^{-2}H^T]N_0 = Y$, an equation previously recorded in (48).

If a different set of manipulations is applied to (50) and (51), a distinctly different set of equations results. Multiplication of (50) by K and substitution in (51) imply that

$$(K^2 + H^T H)X_0 = H^T Y, \quad (52)$$

an equation that can be used as an alternative to (47) in solving for the nodal-point state estimates X_0 in terms of the data Y . Solution of (52) requires, however, inversion of the matrix $(K^2 + H^T H)$ whose dimensions are equal to the total number of degrees of freedom in the finite-element model. The inversion of $(I + HK^{-2}H^T)$ required by (47) is typically easier to carry out because this matrix has dimensions equal to the number of data points, and this number is usually smaller than the number of nodes. Eq. (47), on the other hand, is not totally free from inversion of matrices of large dimension because of the need to invert the stiffness matrix K in forming the matrix $(I + HK^{-2}H^T)$. Note parenthetically the similarities between the matrix equation Eq. (52) and the previously developed operator equation (22).

A final alternative to (47) in solving the minimization problem (46) is to observe that (50) and (51) can be rearranged as

$$\begin{bmatrix} K & & -I \\ & & \\ & & \\ H^T & & K \end{bmatrix} \begin{bmatrix} X_0 \\ & \\ & \\ \Lambda \end{bmatrix} = \begin{bmatrix} 0 \\ & \\ & \\ H^T \end{bmatrix} Y. \quad (53)$$

Upon inversion of the matrix on the left side of this equation, it is possible to solve simultaneously for the nodal-point state estimates and the corresponding adjoint variables. However, an undesirable feature of (53) is that it involves inversion of a matrix of dimensions equal to twice the number of degrees-of-freedom in the finite-element model. An additional possibly undesirable feature of (53) is that the matrix that must be inverted is not symmetrical, whereas both (47) and (52) involve inversion of symmetric matrices.

Interpolation Within Finite-Elements

The foregoing provides the values of the estimates X_0 only at the finite number of nodal points. Interpolation in regions inside the finite-elements is provided by Eq. (14), which has been used originally to form the stiffness matrix K in (15) associated with the finite-dimensional model.

Covariance Analysis with White-Noise Model Errors

An "a priori" covariance analysis of the estimation errors inherent in the state and model error estimates (47) above can be conducted in the same spirit as that of Secs. 6-7 of Ref. [1]. The analysis is based on the assumption, not used in the deterministic least-squares approach applied to arrive at (47), that the actual errors $\epsilon = [F, N]$ are white-noise with a unit covariance-matrix. In other words, it is assumed that $E(\epsilon\epsilon^T) = I$, where I is the appropriately dimensioned unit matrix.

It is convenient to first review the relationships between actual and estimated errors developed in Sec. 6 of Ref. [1] as they apply to the finite-dimensional problem in this section. Note that (47) implies that $\epsilon_0 = W\epsilon$ and $\epsilon_p = (I - W)\epsilon$, where W is the matrix $W = h^T(hh^T)^{-1}h$. As in [1], W and $(I - W)$ are projection matrices in the sense that $W^2 = W$ and $(I - W)^2 = (I - W)$. This implies that the optimal error estimates ϵ_0 and the model error estimation error $\epsilon_p = \epsilon - \epsilon_0$ are orthogonal complements since $\epsilon_0^T \epsilon_p = 0$. The orthogonality of ϵ_0 and ϵ_p implies that the square of the norm $\epsilon^T \epsilon$ of a model error vector ϵ of nonminimum norm can be expressed as $\epsilon^T \epsilon = \epsilon_0^T \epsilon_0 + \epsilon_p^T \epsilon_p$, a relationship that has been illustrated graphically in Fig. 5 of Ref. [1]. These are the key relationship required to conduct the covariance analysis of the estimation errors.

The covariance matrix of the model-error estimation error $\epsilon_p = \epsilon - \epsilon_0$ is given by

$$E[\varepsilon_p \varepsilon_p^T] = E[(I - W)\varepsilon\varepsilon^T(I - W)] = (I - W), \quad (54)$$

or in more explicit notation

$$\begin{bmatrix} E[F_p F_p^T] & E[F_p N_p^T] \\ \vdots & \vdots \\ E[N_p F_p^T] & E[N_p N_p^T] \end{bmatrix} = \begin{bmatrix} I - K^{-1}H^T(I + HK^{-2}H^T)^{-1}HK^{-1} & -K^{-1}H^T(I + HK^{-2}H^T)^{-1} \\ \vdots & \vdots \\ -(I + HK^{-2}H^T)^{-1}HK^{-1} & I - (I + HK^{-2}H^T)^{-1} \end{bmatrix}. \quad (55)$$

The diagonal terms in this last equation imply that

$$E\|F - F_o\|^2 = \text{Tr}[I - K^{-1}H^T(I + HK^{-2}H^T)^{-1}HK^{-1}], \quad (56)$$

$$E\|N - N_o\|^2 = \text{Tr}[I - (I + HK^{-2}H^T)^{-1}], \quad (57)$$

which correspond respectively to the mean-square estimation error of the process-error estimate F_o and the observation error estimate. Use of the identity $[I - K^{-1}H^T(I + HK^{-2}H^T)^{-1}HK^{-1}] = [I + K^{-1}H^T H K^{-1}]^{-1}$ in (56) results in the following more convenient expression for $E\|F - F_o\|^2$:

$$E\|F - F_o\|^2 = \text{Tr}(I + K^{-1}H^T H K^{-1})^{-1} \quad (58)$$

To evaluate the state estimation error $X_o = X - X_o$, note first that $KX = F$ and $KX_o = F_o$ imply that $KX_p = F_p$ and $X_p = K^{-1}F_p$. Hence, $E[X_p X_p^T] = K^{-1}E[F_p F_p^T]K^{-1}$ which together with (58) leads to

$$E\|X - X_o\|^2 = \text{Tr}[K^{-1}(I + K^{-1}H^T H K^{-1})^{-1}K^{-1}]. \quad (59)$$

Note the similarity between (59) and its infinite-dimensional counterpart (67) of Ref. [1].

Illustrative Example

Consider again the example in Fig. 3. By application of the finite-element method, it is possible to arrive at the model $KX = F$, where $X = [x^1, \dots, x^N]$ is a vector of nodal deflections; K is a stiffness matrix given in (39); and $F = [F_1, \dots, F_N]$ is a vector of applied forces. This truncated model can be obtained readily by a process quite similar to that used in arriving at Eq. (39). The interpolation inside elements is provided by the following linear interpolation, $u(\xi) = x^i + (\xi - \xi_i)(x^{i+1} - x^i)/\Delta$, for $\xi_i^+ \leq \xi \leq \xi_{i+1}^-$, which is identical to the one used in (38). The estimation problem to be solved consists of obtaining an estimate of

the static deflection and of the applied force from the three equally spaced measurements of the deflection.

Fig. 5 shows a comparison between the deflection estimates obtained from the two approaches. The key difference between the estimation approaches becomes apparent upon inspection of Figs. 5(a) and 5(b). In Fig. 5(a), the estimated deflection is obtained by first solving for the nodal-point deflection estimates and then using a piecewise-linear interpolation to arrive at the estimates within the finite-element. On the other hand, Fig. 5(b) is based on a piecewise cubic approximation within each element. Whether the loss accuracy inherent in the lower-order approximation in Fig. 5(a) can be overcome by use of a finer subdivision of the domain is an option that should be investigated for each particular problem. For this example, the intuitive notion has been verified that increasing the number of nodes in the finite-dimensional approach results in estimated solutions that become closer to those obtained with the infinite-dimensional technique. This has been done by computing the root-mean-square (RMS) value of the estimation error associated with the infinite-dimensional and finite-dimensional solutions. The infinite-dimensional solution results in an RMS estimation error of 1.2 mm, whereas the finite-dimensional approach with 4 finite elements has an error of 5.9 mm. Increasing the number of elements to 12 results in an estimation error of 1.5 mm, which compares quite favorably with that obtained using the infinite-dimensional method.

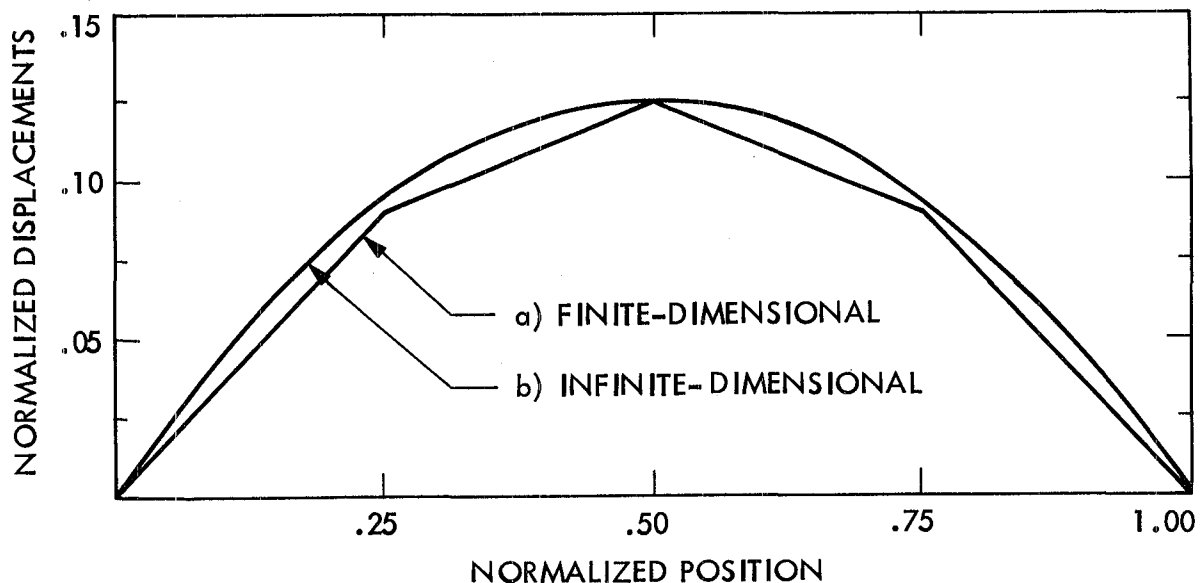


Fig. 5. Comparison of Estimated Solutions With Four Finite Elements

Discussion

The key feature of the finite-dimensional approach to estimator design is that it is based on a model that has been truncated without taking into account the subsequent problem to which the model is to be applied. For

example, Eq. (15), which constitutes the finite-element model, was developed before the estimation problem in (46) was formulated. Selection of the grid size as well as the order of the interpolating polynomials in the approximation subspace has been made without prior knowledge of the estimation problem (46). In the case of the illustrative example, the piecewise-linear interpolation (38) is not necessarily optimal in solving the estimation problem, whereas it may be completely satisfactory to obtain a characterization of the structural static response. Note also that because the finite-dimensional approach uses a truncated model (15) as its basic premise, the corresponding estimation problem (46) must also be finite-dimensional. This finite-dimensional problem (46) is not necessarily the most appropriate estimation problem that can be solved to obtain the best static shape estimates for a given structure. The one ingredient missing in (46) that is important to the problem of static shape estimation is the ability to account for the behavior of the structure within each finite-element. The quadratic functional in (16), on the other hand, is a more complete criterion because through its last term $(f, f)_2$ and by use of the infinite-dimensional model (13), it is able to account for this behavior.

In some cases, the difference between the two approaches can be reduced where it is feasible to select a sufficiently fine finite-element grid in forming the finite-dimensional model (15). In other words, the two approaches can probably be made to yield substantially the same results. However, even if in the end the finite-dimensional formulas (47) are used, it is convenient to keep in mind the approximations inherent in those formulas.

5. APPLICATION TO A LARGE ANTENNA MODEL

Simulations are currently being conducted to apply the foregoing estimation methodology to the problem of large antenna static shape determination. While both approaches are under development, most of the numerical work to date has focused initially on the finite-dimensional approach.

The model used for simulation is that of a 55-m diameter parabolic reflector formed by a total of 48 rib elements emerging from a common central hub. A membrane-like mesh is supported in tension by the rib elements. Such reflectors have been under recent intensive investigations for potential communication, radiometry and radio-astronomy missions as well as for possible shuttle-attached flight experiments. The finite-element model used in the simulations is that of Ref. [7].

The simulations involved reconstructing the antenna surface from a set of discrete measurements as shown in Fig. 6. In each simulation, a deformation of a nominal antenna shape was produced by a linear combination of the first 18 modes provided by a finite-element model of the antenna, as illustrated in Fig. 6(a). The estimator performance in a batch mode was then investigated for several sensor-placement configurations. Fig. 6(b) shows an illustration of the estimator performance for a case where a total of 12 discrete measurements of the deflection around the circumference of the reflector are available for estimation. Parenthetically, it should be pointed out that a parallel investigation (based on methods similar to the ones outlined in this paper) of the problem of figure control has also been

under way. Illustrations of figure control performance with a total of eight actuators mounted at the central hub is shown in Fig. 6(c). Most of the estimation results presented here and in Ref. [1] have a parallel (dual) interpretation in terms of figure control.

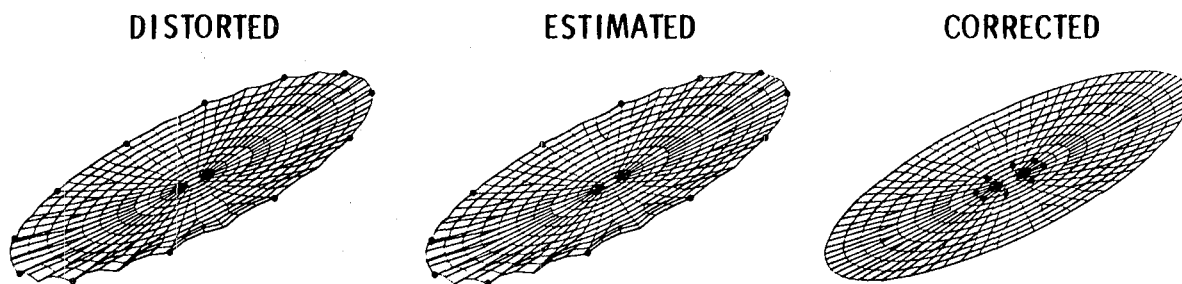


Fig. 6. Shape Estimation and Control Performance for 55-m Diameter Antenna Model

One of the uses that can be made of the "a priori" covariance analysis of the previous section is to analyze the problem of sensor placement. For example, Fig. 7 illustrates the sensitivity of the mean-square state estimation error as given by Eq. (59) to small repositionings of a set of 12 sensors mounted on the circumference of the dish. Note that the estimation error is significantly reduced by a 5° rotation in 8 of the targets at the boundary or by selecting a nonuniform placement. The reason for this sensitivity is the presence of spatial correlations in the displacement at the boundary of the type discussed in detail in Sec. 5 of Ref. [1]. Sensitivity to sensor placement is one of the areas currently under intensive investigation as will be discussed in more detail in a forthcoming publication [7].

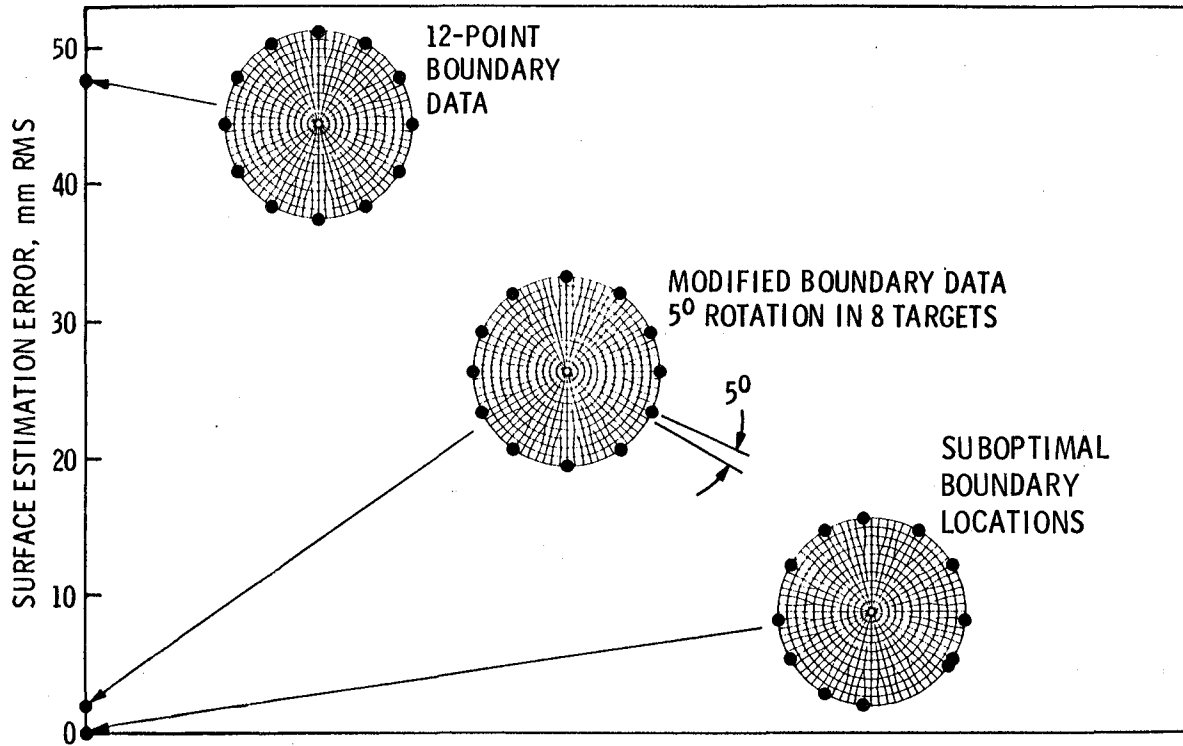


Fig. 7. Estimation Error Sensitivity to Sensor Placement

6. SUMMARY AND CONCLUDING REMARKS

The paper provides a complement to Ref. [1] by describing in detail how the general state and model error estimation methodology can be applied to specific structures. For structures modeled by a single PDE, multiple PDE's or a fine-resolution piecewise-continuum model, two approaches for estimator design have been developed. The first approach involves the solution by means of the finite-element method of the boundary-value problem associated with the optimal estimates. The second approach is based on obtaining a finite-element model first and then conducting the estimator design based on the truncated model. The similarities and differences between the two approaches have been outlined in a general framework and with a simple illustrative example. Simulation results of the application of the finite-dimensional approach to the problem of static shape determination of a large antenna model have been presented. While the analytical foundation for both approaches has been established, large-scale numerical simulations for the infinite-dimensional approach are still under development.

ACKNOWLEDGEMENTS

The research described in this paper was carried out at the Jet Propulsion Laboratory, California Institute of Technology, under contract with the National Aeronautics and Space Administration.

M. Milman and J. M. Cameron of JPL conducted the simulations in Sec. 6.

REFERENCES

1. Rodriguez, G., "A Function Space Approach to State and Model Error Estimation for Elliptic Systems," Workshop on Applications of Distributed System Theory to the Control of Large Space Structures, JPL, July 14-16, 1982.
2. McLaughlan, J. M., "Spatial, High-Accuracy, Position-Encoding Sensor (SHAPES) for Large Space System Control Applications," Large Space Systems Technology Technical Review, Langley Research Center, Nov. 16-19, 1981 (NASA CP 2215).
3. Lions, J. L., Optimal Control of Systems Governed by Partial Differential Equations, Springer-Verlag, 1981.
4. M. Hamidi, G. Rodriguez and D. B. Schaechter, "Distributed System Modeling of a Large Space Antenna," Workshop on Applications of Distributed System Theory to the Control of Large Space Structures, JPL, July 14-16, 1982.
5. Strang, G. and G. J. Fix, An Analysis of the Finite Element Method, Prentice Hall, Inc., 1973.
6. El Raheb, M., "Analytical Performance Prediction for Large Antennas," Large Space System Technology Technical Review, Langley Research Center, Nov. 16-19, 1981 (NASA CP 2215).
7. Milman, M. H., J. M. Cameron and G. Rodriguez, "Static Shape Determination for Large Structures," to be presented at 4th VPISU/AIAA Symposium on Dynamics and Control of Large Structures, Blacksburg, Virginia, June 6-8, 1983.

This Page Intentionally Left Blank

SESSION VIII: DISCUSSION — FUTURE RESEARCH OPPORTUNITIES

Moderator: **H.A. Rediess**, Milco International, Inc.

Panel Members: **A.V. Balakrishnan**, University of California, Los Angeles, **J.A. Breakwell**, Lockheed Missiles and Space Company, **A.E. Bryson, Jr.**, Stanford University, **P.C. Hughes**, University of Toronto, and **W.E. Vander Velde**, Massachusetts Institute of Technology

SYNOPSIS*

The intent in this session was to provide views on the state of distributed control systems' theory and application and to draw together a collection of suggested research opportunities to present to NASA. Each panel member gave an opening statement, then a general discussion with the audience followed. Rediess concluded the session by stating a synthesized set of recommendations.

H. A. REDIESS: In Holt Ashley's talk last night, there was one particular law of Augustine's that he presented, the one about it taking one-third more time to complete a task than is estimated at any point in time in the project. I think there is a corollary to that of sorts: "Project managers always freeze the control system design before the controls engineer feels it is ready to be frozen." In spite of that, the systems usually work reasonably well. There are often minor, sometimes even major, problems that are found in ground testing, in closed-loop tests, in vibration tests, or on into flight testing. But quite often the design flaws that are found later have to be fixed with notch filters or other type of changes in the compensation. And this goes all the way up into the flight-test phase of the program. Changes late in the development process are usually very expensive, particularly if we are talking about reverification of the software. Many times, the changes that one would like to make because of problems found well down into the process do not get made because it is just too costly or too time-consuming. An interesting point about many of these problems is that they are generally not a surprise to the control engineer. The problems often arise in areas where he knew that he was using an outdated model. Sometimes the structural model is several iterations back in the configuration by the time that the controls person gets it for his analysis and design work. Another possibility is that the controls design engineer has had to accept a compromise solution in his design, one that he does not particularly like because of constraints that are beyond his control or because he has literally run out of time or resources to iterate further.

That brings me to my point. In considering partial differential equations (PDE's), ordinary differential equations, or other theory in this workshop, it seems to me that the primary thing we are talking about is providing a set of tools which designers/analysts can use to achieve a better design at the point where the project manager freezes it. I mean better in several ways, certainly

*This synopsis attempts to capture the main points discussed but has not been reviewed or endorsed by the speakers.

in terms of just being able to achieve a higher degree of confidence in the design when it goes into flight. If PDE models can provide a better physical understanding of the process, as suggested by Professor Russell, they might help us to recognize essential differences of the control process in the early conceptual design phase of the problem in which you would like to do some parametric studies and interact with other disciplines.

If PDE approaches can provide a better, more structured approach to establishing or developing robustness in the system, they might give us much better confidence that the final system will perform in the presence of component uncertainties and variations. And if we are really fortunate and come up with a totally different design approach that is in some way better through PDE's, as suggested by Colonel Washburn, we might be able to simplify the design process greatly. It seems like there are several good theoretical concepts in the community that have promise. Most of these will not probably lead to practical tools, but maybe a few will. That is the nature of research.

A. V. BALAKRISHNAN: I formally suggest that some part of the effort of large space systems research be directed toward the use of continuum models. To me this is almost an obvious statement, but after listening to some renowned experts here, who apparently do not recommend this point of view, I will add some reasons why this direction may not be totally useless.

In the continuum-model approach, the structure is modeled by a partial differential equation, and the crucial fact is that the optimal controller design is based on the PDE model. Then that optimal system is approximated. This, of course, is in contrast to discretizing the system first by truncating at the modal level or at the finite-element level, and then designing a control system for that truncated model. Everybody knows how to develop designs, at least in theory, based on this second approach. However, in doing so, you are subject to what I would like to suggest are serious drawbacks. The truncation in the second approach is natural if you are considering the calculations of the open-loop response. But if optimal control is your design objective then it is not necessary to solve those equations characterizing the open-loop response. One can go directly to calculating the control gains. Discretizing first can obscure fundamental phenomena as referred to earlier, such as the impossibility of guaranteeing a stability margin unless the system is already exponentially stable. But I think the most compelling reason is that of robustness which, in the light of discussions here, is clearly one of the important issues in the control of large space structures. It is generally agreed that there are always uncertainties in the model. The remedy suggested is that we have on-line identification to update the parameters. In that case, we are then talking about an identification phase and then the controller based on the identification. It is here that the problem of modeling becomes crucial. The one advantage that the PDE model has is that of simplicity. This simplicity is more than a qualitative simplicity. It is reflected in the fact that if you estimate parameters of the PDE model rather than all the modes and the modal frequencies, it is far more efficient. Furthermore, we do have now considerable experience on such on-line identification. So the point is that if robustness is a main criterion, then the description of the system itself should be simple enough, because the larger the number of parameters you have to estimate, as is well known, the more the error you introduce. Moreover, you only need to

estimate those parameters that affect the control gain, nothing else. I think we can perhaps substantiate this claim theoretically, but I know that will not satisfy many of you, so we should also try to satisfy this in practice.

And so I think that some part of the large-space-structures effort should be directed toward the use of continuum models. I do not mean merely the token support to universities with graduate students doing the work, but I mean a real substantial practical model, the results of which would be acceptable.

J. A. BREAKWELL: I would like to advocate two small fields that I have brushed up against. It is fairly clear that there is an immense collection of tools assembled to attack the problem and I think that it is about time we used some of them. The ACOSS program is a good example of the customer providing a real model and requirements to the controls community and asking them to solve the problem. That is a very good idea and NASA would do well to follow suit. I also advocate small experiments, which are becoming more feasible because they are becoming cheaper. The reason that I advocate actually getting your hands dirty is that a lot of the problems that are anticipated might turn out to be not such bad problems after all, but you might find other problems that are more important. In the former category, I think there are several paper tigers that, once you have a specific example in mind, tend not to be quite as big a problem as you might imagine. Global stability is the first thing that comes to mind. Robustness is another popular subject right now which you may find is not as much of a problem when you go to experimentation.

To tell, in general, what kind of mode you want to keep and what you do not want to keep in model reduction is a rather difficult question. But when you have the modes in hand and you can put your fingers on them, I think you could tell quite easily. So those are the category of problems that might go away once you start doing experimental work. There will also be other problems that come up. There are two that I have seen and would really like to see attacked. The first is the selection of the weighting matrices, or, for filters, the covariance matrices. There is not much that has been said about this, but the assumption of a white-noise covariance in a truncated system is a fiction. I would like somebody to develop a rather good theoretical test procedure for developing covariance inputs to the filter.

The second unexpected problem I have seen is large variations in the low frequency modes. In laboratory experiments, you will see rather large variations in the position of the very low frequency modes well within your filter bandwidth, as much as you will see perturbations in the first unmodeled modes (spillover). That is a problem that I have not seen addressed theoretically.

Having taken a very pragmatic approach to some of the things I advocate, I would now like to turn to partial differential equations. There may be times when it is appropriate to use partial differential equations to model large systems, sometimes not. That is not the question. The partial differential equation, the sophisticated mathematics that we have seen in the last couple of days, provides a much more convenient formulation of the problem. It allows a much more direct attack to the control problem and to the modeling problem. It takes away the burden of the notation, the infinite number of subscripts that we are saddled with in the discrete approach, and allows you to think about the

problem. It is entirely conceivable to me that there may never be a successful application directly of this theory. But still, if any breakthroughs in basic control theory, which later will be passed along to the engineers, are to be made, they must be made there. There is no chance that the old calculus of variations, or the Weiner approach, is going to yield very much more in the way of new useful theoretical approaches. I say that we must not let the control theory stagnate.

A. E. BRYSON, JR.: Well, I very much like the ideas expressed the first day by Dick Gran and Peter Hughes. I have been advocating ideas similar to those. There is a finite bandwidth for any system that you are trying to design. The idea of having an infinitely wide bandwidth is sort of ridiculous. When you do decide what the disturbances are and what your criteria are you can pretty well establish the closed-loop bandwidth required, and any structural mode that has a frequency of say 10 times that does not have anything to do with the problem. I like Dick Gran's idea of the unstably interacting modes. That is a very nice concept and very easy to understand. The ideas of Skelton, Gran, and others of leaving out terms that do not have much to do with the problem, such as small residues or well-damped or very high frequencies, is also very important. I think we have made a beginning, but only a beginning, on the problem of robust control synthesis. The first thing you have to realize is that robustness has a trade-off with performance. If you want to have a system that is robust over a wide range of some parameter, you are not going to have as good a performance at the nominal value of that parameter. We have a program at Stanford now that was put together by Leroy Lee, a young man from Boeing who came to study with us, that I think is a very important forward step in this direction. The idea is to use multiple performance indices. If you have parameters that vary over a wide range, you minimize a sum of quadratic performance indices evaluated for the different values of those parameters. To do that you have to use a non-linear programming technique for the parameters and feedback gains. With this technique you can get output feedback or low-order compensator designs for rather high-order systems very rapidly and efficiently. In cases where a robust controller design gives poor system performance, you are going to have to go to adaptive control, which involves some kind of identification, to get better performance. One of the first steps toward actually doing this with a piece of hardware was presented in the paper by Eldred and Schaechter yesterday, which I thought was a very interesting paper. But this is only a beginning. They were identifying one frequency and the problem has three frequencies. The problem also has mode shapes which affect the modal control distribution matrices. So we have got some way to go yet. Finally, I certainly agree with Breakwell that ground experiments can give us a lot of information cost-effectively as compared to putting things up in orbit. We ought to explore that much harder than we have. Vacuum chambers could be used perhaps to get rid of the damping due to the air. Large enough experiments should be used so that we do not have big scaling effects, which are very hard to extrapolate.

P. C. HUGHES: I think one possibly can identify four times when partial differential equations are appropriate to use. The first one is when you are dealing strictly symbolically with the equation. We saw that in the very first paper by L. Meirovitch, the last paper by G. Rodriguez, and many papers in between. It is just as easy to write down the differential operator as it is to write down a matrix. If you feel more comfortable with PDE's, or if it gives you an

analytic result that you are aiming for, then I certainly would have no objections to such a thing.

The second case is where the system is very simple. In those cases, you can write down partial differential equations that are relatively tractable and even get solutions to them.

Then a third possible case I can see is when one has a fairly complicated structure, but one wants to do some feasibility and parametric studies. This has been mentioned by other people and we have seen examples of it at this workshop - for example, a large antenna reflector, which contains a lot of ribs and mesh. If you neglect a number of things, you can get an approximate partial differential equation, which has some characteristics that are nicer than a finite-element model. Namely, the PDE model usually has two or three very simple parameters, which makes it very nice for parametric studies. But, it is usually a rough approximation, unless it is made more exact for the first two or three modes by comparison to some more accurate model.

The fourth case is where one has dense periodic structures, such as the example presented by J. N. Juang this morning, where you have a truss which has hundreds or thousands of little tiny members all in a periodic lattice. You can smear that into a continuum, with very little loss in accuracy.

These are four cases for which I personally feel that partial differential equations are quite reasonable. The thing that I am trying to speak out against particularly is a feeling expressed by some people that partial differential equations are more advanced than discrete models, or that they are automatically more accurate, or that they will disclose all sorts of extremely important new phenomena that discrete models will not.

There are a couple of more comments on control of large space structures that I would like to make. I would draw an analogy with cancer research, but not in the way you might think. In spite of all the significant research being reported on in hundreds and hundreds of papers every year, there does not seem to be a tremendous amount of progress. I think the reason for that, in part, may be that the progress is not necessarily in the right direction, although that is very hard to judge. Another reason that I think we may not be making as much progress is that the problem keeps getting harder, because we keep making it harder. Holt Ashley referred to it several times last night in his talk, and several other people have mentioned it at this workshop. I would like to mention some specific examples of where we are making the problem too hard.

The first one is disturbance models, which are not mentioned very often in technical papers. The control system in the first instance is supposed to control against the disturbance. In fact, the disturbances in space tend to be quasi-steady. Solar radiation pressure and gravity gradient disturbances, for example, tend to have a frequency content with a period of one orbit. So what is causing the disturbance? In most cases, the control system itself. What happens in space is that the rigid-body modes are the things that are unstable. They are very gently perturbed by quasi-steady forces, and, in an attempt to control them, we unwittingly or unintentionally excite the spacecraft structural modes. Therefore, our aim should be to control rigid modes, without exciting the structural modes.

Another way we make things hard for ourselves is that we ignore the inherent stability of the system. Everybody is very fuzzy about damping. I would say half of the control papers assume zero damping. We tend to ignore simple passive solutions like passive damping. Composite materials provide a tremendous opportunity to design passive damping into the system.

Lastly, we make things difficult with our actuator schemes that tend to excite the system more than they really should. If the disturbances are really so low in magnitude, and are so nearly constant, then the ideal actuator would be one with a very low force and very nearly constant. I will give you a very specific example of that. Suppose you are north/south station-keeping one of these satellites. The major force on the satellite is due to the moon. The magnitude of the force is very, very gentle but acts continuously over a long period of time. The ideal control system would be an actuator force acting constantly with that very low force to exactly counteract the force of the moon. We do not do that. We wait until the motion builds up and then we fire at a node of the orbit with a big bang and get everything all shaken up.

I would like to make specific recommendations. Firstly -- and this is the wrong group to mention this to because it is not primarily a structural dynamics audience -- we have to get good damping models. Secondly, we should instrument all possible satellites to get information on structural modeling, particularly damping information. Thirdly, we should continue, and intensify, ground experiments, particularly the ones that have the rigid-body modes. And lastly, we have to develop some very benign variable-force, linear actuators.

W. E. VANDER VELDE: My first area will be the issue of dealing with unreliability in these control systems. Of the thirty some papers that were presented in this workshop, only one dealt even with one small aspect of that problem. Maybe that was justified because the principal focus of this workshop was on distributed system issues. But this was also essentially true of the other workshops that have taken place during the course of this summer. I think this really is a true indication of the amount of research support that is being given to the question, as it applies specifically to large space structure control. There is some work going on related to fault-tolerant computers, and in the past there has been a reasonable amount of research support for failure detection and isolation as it applied in the context of aircraft flight control systems. But the large space structure control problem really is different. Take failure detection just as one part of what one needs to do; the same problems of inadequate modeling that make control difficult make failure detection difficult also. In fact, modeling inadequacy is even a more serious problem in failure detection than it is in designing a control system.

The number of components in these large space structure controls is simply overwhelming and assures that we will suffer failures. It is clear that we have to do something about it. This whole area is one that ought to be emphasized much more in NASA's research planning. The other area that seems to me important and probably insufficiently addressed at the moment is the question of system identification after deployment in orbit. That strikes me as a very difficult problem.

For some cases, it may not be necessary. However, there will be mission situations wherein the a priori information that we have obtained may not be

adequate. I envision an initial period in orbit during which the system is exercised in one way or another for system identification which would allow us to tune up our knowledge of the system dynamic parameters.

The first step in addressing it would be to determine the most efficient way to parametrize the system. It is at that step that continuum modeling may have a role to play. It strikes me that, however the parametrization is done, there may well be thousands of parameters to fully characterize the system dynamics at all the sensor and actuator locations. It may be almost an unfeasible problem to solve. At the beginning of the mission, the spacecraft would only have minimal capability because it would not be controlled very well due to model uncertainties. Most of the onboard data-processing resources, or the telemetry resources, may be available for the identification problem during that period, and later on, of course, they can serve what is ultimately a more useful function. I would like to suggest that, in addition to that initial period of full-up identification, there be a second mode of identification to periodically monitor the dynamic performance of the system throughout the mission. It would have to be done with an approach which is far less demanding on computational resources. The idea would be to do a test which would indicate when something had gone wrong, perhaps identifying what parameter had changed enough to require a new system identification test. This approach is very much like the component-failure detection problem. In effect, you are identifying that a particular component sensor or an actuator has changed its performance characteristics significantly.

Comments and Questions from the Audience

D. C. WASHBURN, Air Force Weapons Laboratory (AFWL): Dr. Breakwell has recommended that NASA perhaps go the DARPA route of creating a model and distributing it to the community for control of large space structure research. I think that is a good idea, and I am planning to do a similar thing for AFWL problems. I would recommend that they create a PDE model so that people can treat it with several approaches, including NASTRAN. The current DARPA model absolutely forces modal control, because that is the only thing it provides.

I would like to add another area where PDE's might be useful: that of controller design. I certainly do not advocate that an exact PDE model be built for any structure. But just from a strictly philosophical point of view, our controllers are extremely simple and involve 10, 20 states, or whatever. The controllers finally designed are generally very simple and, philosophically, it might be appropriate to base those on a simple model which is an approximate PDE.

In the case of AFWL large space structures with large beam expanders for space laser applications, there are very real disturbances that are not just created by the controller. I think in most applications you have disturbances induced by slewing. For AFWL applications, slew-induced disturbances will be severe. There is also broadband coolant-induced jitter on the secondary mirror, which will feed into the primary structure. It will go out to 200 Hz practically flat. So you will have continual excitation of modes up to at least 200 Hz. The whole thing is hooked to a rocket engine, called a laser, sitting back behind it, which is shaking everything pretty violently. So, at least for

some applications there are genuine broadband disturbances that you are just going to have to deal with.

This is the first time I have come in contact with this group, but it is almost unbelievable that nobody has sat down and taken the simplest possible example, and worked through and designed a controller based on PDE theory, and then designed a modal controller and compared results either analytically by simulation or experimentally. We are all offering opinions as to the merits and drawbacks of each method, but we have not even worked through this simple example to provide a common basis for comparison. I recommend that NASA undertake such a task.

Question from the Audience -- Would Dr. Hughes expand on his reasons not to use PDE? I think he said that when the structure is simple, then the PDE's are okay, but when the structure is complex, then PDE's are not useful. There are two parts to my question:

- a) What do you mean by complex? Do you mean a large number of PDE's, or a large number of boundary conditions that need to be matched? Why is the system being complex a reason not to use the PDE model per se? Is it numerical algorithm problems?
- 2) Can you give me an example of a project or some reference in the literature in which PDE overkill has occurred?

P. C. HUGHES: Well, there are several sources of complexity: one is complex boundaries; a second one is a large number of individual structural members; and a third one is where you have spatially varying inertia or stiffness properties that lead to variable coefficients. If you put all these complexities together, which is the case in most structures, you find that you have a real mess on your hands, and I for one would not use partial differential equations to get what might be called the most exact model. If you want to do some simple approximations and get an approximate model for some feasibility studies or perhaps some simple parametric variations, that is different. After you have got these partial differential equations, how are you going to solve them? Are you going to use hundreds of hyperbolic sines and cosines, or what are you going to do with them? Your second question was, have I an example of overkill? No. The people that advocate them are smart enough not to use them in cases where I would not use them.

A. V. BALAKRISHNAN: May I point out that in control system theory we do not solve PDE equations. That is a common misunderstanding. We do not solve partial differential equations in control systems design, any more than we do ordinary differential equations.

A. N. MEYSTEEL, University of Florida: I would like to attract attention to one of the problems that has not yet been mentioned. All of our control systems work well for stabilization, but any slewing will create something unexpected and all these stabilizers will be ruined. Any slewing of position of an antenna in space, especially quick changes, will require a type of controller that we are now not thinking about.

Now let us consider another matter. The door of the shuttle, as we all know, warped due to thermal gradients. The same will happen to large space structures. Some parts are in the sun, and some parts are shadowed. These temperature fields will create something unexpected and difficult to model. I believe that we are dealing with a future set of systems in which it will be impossible to determine the parameters with the accuracy required to meet the performance objectives. It may be necessary to use a new class of systems, called intelligent control systems, which are not only self-organizing but also involve special modeling of unpredictability of behavior. There are several groups in the United States, including the University of Florida, who are working in this direction.

A. N. MADIWALE, MIT Lincoln Laboratory: I would like to recommend an emphasis on a particular topic. It is generally acknowledged that there are going to be large uncertainties in the modeling process. There should be more effort on stochastic models and designs that account for uncertainties.

R. R. STRUNCE, Charles Stark Draper Laboratory, Inc. (CSDL): There are some very important lessons to be learned from history. The concept of feedback, for example, was motivated by a real problem. That was to design low-output distortion for transmission-line amplifiers. It was the extensive interaction between laboratory experiments and theoretical development that resulted in the Bode frequency response diagrams and the Regeneration Theory by Nyquist for example. If we are going to resolve some of these large space structure problems, we will need that same type of natural interaction between laboratory experiments and the theoretical development. Take, for example, the Explorer I. It is intuitively obvious to the most casual observer that it is a relatively rigid body. Yet those four very flimsy antennas destabilized that vehicle and resulted in a plethora of structural dynamic interaction research. I think that some of these very large space structures may be headed for some unforeseen problems that could result in catastrophic failures. This particular community must seek out those people who hold the purse-strings within DoD and NASA and educate them as to the necessity for an evolution of integrated experimental and theoretical development to give us the necessary knowledge to bring these large space structures to fruition.

Comment from the Audience -- At this workshop, it has been tacitly assumed that you will eventually discretize to implement any control that you generate with a PDE analysis or some other distributed system analysis. That seems to be based on the assumption that the processing will be digital. The evolution of high-speed digital processing has been overtaken by developments in optical processing which are not digital or discrete in time at all. Is it not possible that the estimators and, perhaps, some other parts of the control might remain in the continuous domain and be implemented by analog processing?

H. A. REDIESS: The question of real-time processing was brought up earlier by Gupta. It certainly is true that there are some new optical processing techniques that perform vector/matrix operation directly in real-time, which will make certain types of modern control theory computations very attractive.

A. E. BRYSON, JR.: In Breakwell's thesis, he took the partial differential equation approach to design a controller for the simple beam equation. His full-state feedback solution amounts to an integral of a gain kernel against a

deflection as a function of distance along the beam, plus another integral of a gain and the velocities times the velocities along the beam. So the problem becomes one of finding the gain kernel as a function of the distance along the beam. You can imagine performing this integration optically with a TV camera and an optical integration device. However, if you compare it with taking a few finite elements, it is pretty easy to convince yourself that you are not going to get a significant improvement going into this integral, with a nice smooth kernel, compared to one with a few discrete elements.

W. E. VANDER VELDE: One application that might be a good experiment of continuous modeling would be the electrostatically-shaped mesh antenna that we heard about Thursday morning. That is a case in which the geometry might be simple enough so that a PDE description would be tractable. And, in fact, you could approximate a distributed force on that antenna quite closely.

H. A. REDIESS: It would be difficult, if not impossible, to draw a consensus viewpoint from a group of such a diverse nature. I will attempt to synthesize what appear to be the most generally endorsed recommendations for future research resulting from this workshop:

- 1) Develop control law design and analysis methodology for continuum and piecewise-continuum models for large space structures. Additional research is needed to mature the continuum model methodology to a point where it can be applied effectively on realistic configurations.
- 2) Conduct or sponsor a comparative study of controllers designed using continuum and finite-element models. Use a simplified model of a realistic structure that could be tested in a laboratory. Compare the results of both designs with experimental data obtained by a third party.
- 3) NASA should create one or preferably more "benchmark" generic models representative of configurations for potential future NASA missions that can be used to develop and evaluate system identification and control law methodologies. Both continuum and finite-element models should be constructed for each "benchmark" configuration.
- 4) Develop and validate system identification techniques suitable for identifying a large space structure in the initial phase of operation and for continuous monitoring during the entire mission to detect changes. Both continuum and finite-element model approaches should be investigated.
- 5) Conduct and/or sponsor experiments for system identification and control law methodology development and evaluation. Use simple laboratory experiments to evaluate identification techniques and control laws. Consider larger-scale experiments in a vacuum chamber to minimize the effects of air on damping. Use all possible space flights as experiments to increase knowledge of structural dynamics in space, e.g., instrument satellites or the Shuttle Remote Manipulator System to measure damping. Proceed with space shuttle flight experiments with flexible structures.

- 6) Develop adaptive and/or reconfigurable control laws for large space structures to compensate for model errors, spacecraft configuration changes, or system failures.

This Page Intentionally Left Blank

This Page Intentionally Left Blank

This Page Intentionally Left Blank

TECHNICAL EVALUATION REPORT OF THE WORKSHOP ON APPLICATIONS OF DISTRIBUTED SYSTEM THEORY TO THE CONTROL OF LARGE SPACE STRUCTURES*

July 14-16, 1982

Jet Propulsion Laboratory
California Institute of Technology
Pasadena, CA 91109

INTRODUCTION

The ability to stabilize and control large structures in space is vital to establishing efficient earth-orbiting systems of the size required for many of the future applications and science missions. Large space systems' configurations with low mass densities are more accurately modeled as a continuously distributed mass over the entire structural area (distributed parameter system or continuum model) rather than a sequence of finite mass elements coupled together (lumped parameter system or finite-element model). By far, the most effort put forth in studying these challenging control problems to date has been based on the finite-element model, which can be addressed using ordinary differential equations control theory. Substantial theory now exists to treat distributed parameter systems and some effort is directed towards control of large space structures. This approach involves formulation of the problem in partial differential equations and results in solutions in infinite-dimensional Hilbert space which must be approximated. Fewer control analysts are familiar and comfortable with the distributed parameter systems approach; hence, it has not been explored to the same degree as the finite-element approach.

The term distributed systems was used in two different senses at the workshop. One sense was control theory for distributed parameter system modeling as discussed above. The second sense was control theory for systems requiring spatially distributed multipoint sensing and actuation. Many large-space-structure configurations being considered will require multisensors and actuators distributed in some fashion throughout the structure. One must consider the spatial distribution of sensors and actuators whether treating the problem from the finite-elements or continuum model approach.

The main objectives of the workshop were:

- to provide a forum for exchanging ideas and exploring the application of the control theory for distributed systems to the control of large flexible multibody spacecraft; and

*Prepared by Milco International, Inc., Avionics and Software Division.

- to identify the important unsolved problems of current interest leading to possible future collaborative NASA/university/industry efforts.

The workshop was organized with several sessions addressing the major technical issues through invited and contributed papers by leading researchers, panel discussions and a final wrap-up session to extract the key unsolved problems and recommendations for future research. The workshop agenda is presented in Appendix A. The list of attendees and participants is presented in Appendix B.

The purpose of this report is to present a technical evaluation of the workshop that synthesizes the most important results, conclusions and recommendations for future research. The future research recommendations are presented in the next section followed by the technical evaluation.

FUTURE RESEARCH RECOMMENDATIONS

The major recommendations presented here are believed to represent a consensus view from the workshop and draw heavily on the results of the wrap-up panel discussion. One should not conclude, nor is there any intent to imply, that all participants of the workshop or the wrap-up panel discussion endorsed these recommendations. However, the recommendations listed under the heading of "Major" were those summarized at the end of the wrap-up panel discussion and were generally endorsed by the workshop participants.

Several additional recommendations that were made by various participants are listed under the heading of "Other Recommendations." Some of those do not address directly the theme of the Workshop, but do apply to large space systems and were felt to be of sufficient importance to include.

Major Recommendations for Areas of Future Research

1. Control law design and analysis methodology for continuum and piecewise continuum models for large space structures.

Rationale: Proponents of the continuum model approach believe that it will provide a better physical insight to the control problem and solution since it is based on physical laws governing structural dynamics rather than a functional representation of the dynamics that may obscure some fundamental properties of the problem, e.g., stability and robustness. It may be a better way to assure robustness of the controller design because it does not arbitrarily limit the number of modes included as in the finite-element approach. Furthermore, the proponents state that the mathematical formulation of the model and control problem is simpler, even for piecewise continuum models in which there are combinations of distributed and lumped parameters. Additional research is needed to mature the continuum model methodology to the point where it can be applied effectively on realistic configurations.

2. Comparative study of controllers designed using continuum and finite-element models.

- Use a simplified model of a realistic structure that could be tested in a laboratory.
- Have each controller designed by experts in the corresponding method.
- Compare results of both with experimental data obtained by a third party.
- Assess results based on controller performance robustness, plant identifiability, computational efficiency and other appropriate measures.

Rationale: A well-structured study of this nature is needed to assess the relative advantages and disadvantages of each approach. Many claims and concerns are voiced at workshops and conferences about both approaches without appropriate comparative data to substantiate the positions voiced.

3. NASA should create one or preferably more "benchmark" generic models representative of configurations for potential future NASA missions that can be used to develop and evaluate systems identification and control law methodologies.

- Both continuum and finite-element models should be constructed for "benchmark" configuration.

Rationale: There are currently no realistic models available for potential NASA missions that are developed in sufficient detail to use in advanced identification and control theory for both continuum and finite-element models. The DARPA ACOSS models are finite-element models and preclude the continuum model approach. If such models were developed and distributed to universities and industry as well as NASA centers, a large amount of research would be focused on NASA's type of problems.

4. Systems identification research for large space structures.

- Apply to realistic type configurations (NASA benchmarks, for example).
- Consider both continuum and finite element model approaches.
- Obtain experimental space flight data to assess methods.
- Develop techniques suitable for identifying a space structure in the initial phase of operation and for monitoring it during the remainder of the mission to detect changes.

Rationale: It will not be possible to obtain valid experimental test data on the ground for large, flexible space-structures. It is highly likely that modeling errors of a structure to be deployed in space will be sufficiently large to seriously affect the controller performance. Appropriate systems identification techniques must be developed and assessed with whatever limited flight data that are available before they are needed in an actual mission. (See Appendix C for an expanded statement on systems identification research by Professor W.E. Vander Velde of the Massachusetts Institute of Technology (MIT).

5. Experiments for systems identification and control law methodology development and evaluation.

- Simple laboratory experiments to evaluate identification techniques and control laws.
- Consider larger-scale experiments in a vacuum chamber to minimize the effects of air on damping.
- Use all possible space flights as experiments to increase knowledge of structural dynamics in space, e.g., instrument satellites to measure damping.
- Consider using the space shuttle Remote Manipulator System (RMS) in an on-orbit experiment to compare predicted dynamic characteristics to flight data.
- Proceed with space shuttle flight experiments with flexible structures (i.e., MAST, SAFE, DAFE, and SADE) to obtain structural dynamics data and experience with stabilization and control.

Rationale: Experimentation is the surest way to develop confidence in design and analysis methodologies. Simple laboratory experiments can be very useful in understanding the control problem. Some anticipated problems turn out not to be problems at all and other new problems may arise that were not anticipated. It is extremely important to determine the damping of structures in space because of the effect on the controller design. Tests in a vacuum chamber may help get some initial data. Ultimately, it is necessary to obtain space flight data. Both continuum and finite-element models should be used in the analyses, controller designs and systems identification methods associated with the flight experiments.

6. Adaptive and/or reconfigurable control laws.

- Adaptive control laws to compensate for model errors, spacecraft configuration changes or system failures.
- Reconfigurable control laws to compensate for spacecraft configuration changes or system failures.

Rationale: Certain large structures considered for space, such as a modular space platform, would have major configurational changes over its lifetime. Modules will be transported to space via multiple shuttle flights, then assembled in space. Once a basic platform is assembled, other masses may be attached periodically, such as the shuttle docking with the platform, attaching an Orbital Transfer Vehicle (OTV), adding or subtracting fuel, adding or subtracting experiments and/or satellites. The inertial characteristics and dynamics would vary widely with these changes. Control laws that self-adapt or that reconfigure (either automatically or through manual software changes) should be investigated that could cope with these wide variations. A second motivation is to compensate for failures in the control system. There are likely to be a large number of components in a large space structure control system. If a component fails, or if a fault occurs in software that can affect the controller performance, it may be possible to reconfigure the remaining healthy

elements of the system to maintain adequate, though nonoptimal, control until the faulty elements can be corrected. An alternate approach and further discussion of reliability issues are presented in the next recommendation.

7. Control system fault tolerance research.

- Choice of number, location and control laws to accommodate likely faults over the expected operational lifetime (including effects of periodic component repair or replacement).
- Systems performance and fault monitoring (hardware and software), failure detection and isolation (FDI), fault-tolerant processing and data distribution and control law reconfiguration.

Rationale: The control and stabilization system for large space structures is likely to have several hundreds of components dispersed over the structure and linked together by some form of data distribution networks. Even with extremely reliable components, there are bound to be numerous component failures or even software faults that have the same effect as a hardware failure over the lifetime of the spacecraft. The system must have the capability of accommodating these faults in some manner. (See Appendix D for an expanded statement of reliability issues by Professor W.E. Vander Velde of MIT.)

Other Recommendations

1. Finite-dimensional compensator design methodology

- Model order reduction
- Reduced order compensator design
- Robustness techniques with truncated modes
- Direct digital design and implementation
- Fixed-form, low-order compensator design via nonlinear programming

2. Sensor and actuator technology

- Very low frequency
- Very broad bandwidth
- Proportional actuator from very small to large forces (benign actuators)
- Long life, low mass, and low power

3. Real-time processor control laws

- Need 10 to 100 million-operation-per-second capability
- High reliability
- Software languages, verification, validation, and fault tolerance

4. Hardware-in-the-loop simulation
 - Digital, analog or hybrid
 - Partial or complete system
5. Modeling accuracy for large space structures
 - Upper atmosphere model
 - Disturbance model
6. Rendezvous and docking control and guidance
7. Control laws for very large amplitudes due to slewing or major disturbance.
8. On-orbit vibration tests of operational spacecraft to determine model characteristics similar to ground vibration tests on aircraft.
9. Systematic method for selecting the weighting matrices in estimation and filtering problems.

TECHNICAL EVALUATION OF WORKSHOP

The workshop must be considered an unqualified success. There were over 150 attendees and participants (see Appendix B) who included most of the key researchers in the U.S. concerned with this subject. In general, the technical papers were of excellent quality and pertinent to the theme. Structuring the workshop to have discussion panels each day was an important factor to achieving lively participation of the audience in discussions.

The workshop was designed to stimulate a strong exchange of views between two segments of the control research community: those supporting the use of finite-element models and those supporting the use of continuum models. It was very effective in doing just that. Strong viewpoints were expressed on the advantages and disadvantages of both approaches. It appeared to bring out all the major issues associated with applications of distributed system theory to the control of large space structures. The workshop was also very effective in surfacing important unsolved problems worthy of future research.

A very stimulating and entertaining after-dinner talk was given by Professor Holt Ashley of Stanford University. He drew heavily on his experience in aircraft structural dynamics and aeroelasticity to project what he believes are the key factors to address in large, flexible space-structures.

The following sections discuss each session of the workshop in sequence. The final section gives some general observations and comments developed over the three-day workshop.

Session I: Modeling and Control

This session addressed the fundamental questions of mathematical modeling of large space structures for control purposes. The papers were largely tutorial in nature and identified what the authors believed to be the major features of each modeling and control law design approach.

Meirovitch's paper recommends the independent modal-space control (IMSC) method, which was illustrated for control of distributed and discretized structure models. Several advantages are listed for the IMSC approach as compared to coupled controls, including lower control energy and provable robustness. Robustness was only discussed in terms of spillover modes and not with respect to uncertainties of changes in the overall structure or controller. It would be of interest for the IMSC method to be applied to a more realistic example.

Hughes' paper presents strong arguments against the "Infinite Modes Assertion" as being the true characterization of structures, in terms of both its importance and the assertion itself. It is a very readable exposition on what the author believes are absurd assertions made by certain control theorists and applied mathematicians: that physical structures actually have an infinite number of modes. Much of the argument centers around the concept of a mathematical model vs. the real physical structure. The main point is that models based on partial differential equations or ordinary differential equations are both mathematical approximations to the real structure and either is only as good an approximation as is shown to be useful in a practical application. The paper expresses the viewpoint that a modal representation with relatively few modes is the most effective method for realistic large space structures. A very effective criterion for selecting the modes to include in an analysis of control design problems was presented. The paper, however, does not seem to recognize that a continuum model may be a better mathematical model of the physical system than a finite-element model for certain situations. The author did acknowledge that point in a later panel discussion.

Gran's paper presents an interesting middle ground position between the continuum and finite-element model enthusiasts. The paper advocates designing large space structures using finite element methods and verifying the design's robustness using a continuum model. The paper presents a concept of stable and unstable interactive modes that is very important in selecting which modes should be retained in a truncated model. A pole-zero set near the $j\omega$ -axis in the complex plane is unstably interacting if the zero is above the pole. The paper states that stably interacting modes with small contribution to the cost may be discarded, but beware of unstably interacting modes because of potential robustness problems. Several other practical suggestions and guidelines are presented for designing satellite control systems in a systematic way.

The final paper of the session by Hamidi, Rodriguez and Schaechter presents a solid case for modeling complex large space structures as coupled rigid and flexible bodies using discrete models for the rigid bodies and continuum models for the flexible bodies. Contrary to statements by other participants that one could not use a continuum model for complex spacecraft, this paper shows that a

very simple and compact mathematical model can be constructed. The model retains sufficient dynamics, provides good physical insight to the problem, and is suitable for parametric studies. The technique was illustrated by modeling a 55-meter wrap-rib antenna with an L-shape boom connecting the dish to the feed. The model was in good agreement with a finite element model and required very little computational effort.

A participant from the audience, Larry Weisstein, supported the idea of continuum models for even complex space structures. He referred to his masters thesis*, which presents a continuum modeling approach for lattice-type structures that are very common elements in space systems. The reference also includes an extensive bibliography of continuum models for space structures.

Session II: Control and Stabilization

Session II consisted of eight papers presenting a series of examples of modeling and/or control for a variety of configurations. Rather than reviewing each paper individually, some of the major points made are highlighted here.

Bryson's paper makes a simple, but potentially very important, point. If a flexible structure has a plane of symmetry, it may be possible to split the control problem into two uncoupled sets. The example used resulted in a greatly simplified task of synthesizing the active control logic.

The paper by Hamidi and Manshadi addresses developing a control law that optimizes the overall performance objective of a large space antenna, that is, the resulting RF pattern, rather than an intermediate objective of controlling dish shape and feed position. By including an RF electromagnetic model as well as the structural model in the design loop, the control of the relative feed/dish motion can be synthesized to maximize the peak electric field.

Considerable discussion was generated over Henderson's presentation of the ACOSS** Model #2. Most participants were generally familiar with ACOSS and endorsed the idea of such models. Several requests were made about how to acquire the model. Interested parties can contact Timothy C. Henderson at the Charles Stark Draper Laboratory (CSDL). The discussions led to recommendations that NASA develop similar Benchmark models for its potential missions.

Two realistic examples of distributed control of large space antennas (hoop/column and wrap-rib) were presented in the final paper of this session by Cameron, Hamidi, Lin and Wang. They found that distributed sensing and control provides significant performance improvement. The study also indicates that, for the linear optimal controller, system parameter errors could result

*Weisstein, Larry S., Continuum Models for Repetitive Beamlike Lattice Structures, masters thesis, George Washington University, Washington, D.C., 1982.

**ACOSS stands for Active Control of Space Structures, which is a DARPA-sponsored program.

in significant performance degradation and even instability. The paper recommends the use of in-flight systems identification for certain critical model parameters.

Session III: Discussion - LSS Control Problems

The panel discussion was aimed at further definition of the control problems of large space structures. The moderator was R.R. Strunce of CSDL and the panel members were: J. Sesak of General Dynamics, N.K. Gupta of Integrated Systems, and A.F. Tolivar of the Jet Propulsion Laboratory (JPL). The panel and participants from the audience focused primarily on what they believed to be the major technology needs and recommended research. The following are what appeared to be the most important comments:

- The control theory and control law design methodology have not yet been developed to the stage where one could design with confidence a stabilization and control system for a large, flexible space-structure to meet both the performance and robustness requirements. There are still issues of modeling, model order reduction, robustness of stability, and systems identification. It will be necessary to demonstrate the technology, probably in the flight environment, to assure confidence in the methods.

- There are very little experimental data for identification and control of large, flexible space-structures. The data available are for simple experiments which are not very representative of a real space structure. It is extremely important to obtain better experimental data from more realistic ground tests and on-orbit flight tests.

- The robustness problem has not been solved when one considers the total problem including actuator and sensor dynamics and realistic parameter uncertainties. The problem of uncertainty management through systems identification techniques and/or adaptive control should be given more attention.

- There is a real need for research to develop actuator and sensor technology for low frequency operations that are appropriate for space applications. Actuators will be needed with force ranges from very small to very large.

- Many of the control concepts being studied for large-scale systems would challenge the real-time processing technology. Better analytical/numerical techniques, as well as much higher processing capacity devices, must be developed. It may be necessary to have computational capability of from 10 to 100 million operations per second. It is not clear that VHSIC (Very-High-Speed Integrated Circuits) will even solve this problem.

- More attention must be paid to the question of assuring adequate performance of a stabilization and control system in the presence of component failures. Systems must be made fault-tolerant to some level.

Session IV: Distributed Control

Session IV continued addressing the issues involved in control and stabilization of large space structures.

The paper by Vander Velde is an excellent treatment of a very important practical aspect of distributed control of large space structures, that of selecting the sensor set (number and location) considering possible failures. A methodology is presented that would assist the designer in the process of selecting the sensor set that maximizes the degree of observability over the operating lifetime of the system accounting for the likelihood of failures. The sensor set that one selects considering the possibility of component failures can be quite different from that one would select considering only optimizing performance. The author has treated the companion topic for actuators in a separate paper presented elsewhere. A discussion of reliability issues by Vander Velde is presented in Appendix D of this report.

J.A. Breakwell's paper presents a strong case for using laboratory experiments for gaining a better understanding of the control problem with flexible structures. Through his experiment with TOYSAT, Breakwell found that some problems he anticipated from theory never materialized, but new ones arose. The TOYSAT experiment was designed to test hypotheses concerning the application of optimal control theory to flexible spacecraft. Breakwell suggests that with the relatively low cost of microcomputers, almost anyone can afford to conduct simple laboratory experiments that can be very useful.

The last paper of this session, by Schaechter and Eldred, also addresses laboratory experimentation for verification of control laws. Two major points demonstrated are that model parameter errors can cause an optimal control design to drive a system unstable and that adaptive control can stabilize a system with an uncertain model. The experiment proved useful in validating the analytical techniques.

Two special kinds of flexible space structures were analyzed by J.V. Breakwell: orbiting chains and rings. Another special case, vibration control of a tethered satellite, was discussed in the paper by Xu et al.

Session V: Control Theory for Distributed Systems

Nine papers were presented in this session which reviewed and treated primarily control theory of distributed parameter systems and approximation methods to achieve finite-dimensional controllers. This session and the following discussion panel stimulated a lively discussion of the pros and cons of partial differential equation (PDE) control theory for large, flexible space-structures.

An excellent review of the control theory of hyperbolic systems was given by Russell. The paper covers important questions of controllability, stabilization, robustness, canonical forms and eigenvalue placement. The paper presents a very promising method for canonical compensation for hyperbolic systems.

Gibson's paper illustrates how conceptually easy it is to treat continuum systems in infinite-dimensional space rather than being more complex as some have suggested. Once the infinite-dimensional compensator is designed conceptually, then a finite-dimensional approximation is made. This approach provides more insight into the nature of the control problem than the finite-element approach. A simple example is presented to illustrate the method. It now needs to be applied to a model more representative of real space structures.

The paper by Hyland and Madiwale presents a new look at a fixed order controller design method which allows for incorporating system parameter uncertainties directly in the design process. It is based on a finite-dimensional (modal truncation) model. Explicit optimality conditions are derived for minimum data/maximum entropy stochastic model of the system parameter uncertainties. A major feature of this approach seemed to be the ability to directly secure robust stability and mean-square performance optimality.

Mackay's paper solves for the optimal compensator of a distributed parameter system in terms of the kernel of a Volterra integral operator. A finite-dimensional approximation to the optimal compensator is thus obtained.

The paper by Chen et al. addresses the very important and little-studied problem of numerical methods for solution of control systems governed by hyperbolic PDE. The discussion that followed the paper recognized the importance of the problem, not only for PDE, but also for finite-element control laws because of the high dimensionality. There was substantial support expressed for much more research in numerical techniques.

The two main results of Balas' paper are stability criteria in both the time and frequency domains for closed-loop distributed parameter systems with finite-dimensional controllers. The stability analysis of the system uses the theory of semigroups on the infinite-dimensional state space. The criteria is not constrained by the controller design approach, e.g., finite-dimensional reduced-order models. The author stresses the point that closed-loop stability analysis must be a part of any attempt to produce finite-dimensional controllers for infinite-dimensional systems.

Skelton* was unable to attend the workshop and present his paper. Peter Hughes graciously offered to summarize the main points of Skelton's "Analysis of Structural Perturbations via Cost Decomposition Methods," since he was a close associate and familiar with Skelton's work. The paper presents a method of analysis of linear dynamical systems by decomposition of some functional expansion of the system such that it is possible to measure the contribution of each component to the cost function. It would be effective, for example, in model order reduction of a modal representation of a large space structure or in constructing a reduced-order controller from an optimal regulator design. The discussion of this method generally concluded that it was very effective. One cautionary note was raised with respect to what Gran termed "unstably interacting" modes. The cost decomposition method might indicate that such a mode could be discarded, because of insignificant contribution to the cost with nominal system parameters, but a small change in some parameter could lead to the control system driving that mode unstable.

*Skelton's paper was in Session VII, not V, but is discussed here because it fits this topic better.

Session VI: Discussion - LSS Applications of Distributed System Theory

The panel discussion was aimed at identifying the role that the control theory for distributed systems can play in the control of large space structures. The moderator was R.S. Gran of Grumman Aerospace and the panel members were: D.C. Washburn of the Air Force Weapons Labs (AFWL), V. Komkov of West Virginia University, D.L. Russell of the University of Wisconsin and J.S. Gibson of the University of California, Los Angeles (UCLA). The following are what appeared to be the most important comments:

- In selecting a model to represent a large space structure one must consider what the purpose is of the model. One may want a different model for design and analysis than for real-time control. All mathematical models are approximations. A major objective of research is to attempt to determine what are the best models for various purposes. Considerable research has been conducted on finite-element models. More research is needed on PDE modeling to determine where and for what purposes they are most useful.

- Truncating a PDE model before solving the control problem may be throwing away important information and obscuring some of the fundamental properties of the problem. If the PDE control problem is solved and then approximated, one might expect something different, e.g., robustness may be achieved more easily.

- If a PDE model or a compound PDE/ODE model best describes the physical laws of the structural dynamics, and one chooses to use some form of a functional expansion or finite-element model, then one may lose the physical insight into the control problem. Fundamental phenomena may be lost and the control properties may be very different. Once a controller is designed, the closed-loop performance should be analyzed using the best physical law model and should assure that assumptions have not been violated.

- There is a real need to estimate better the damping in large space structures and include realistic damping in controller designs.

- Structural dynamicists regularly use PDE models to do parameter studies of relatively simple structures. Finite-element models are used in the final design of complicated systems such as, for example, Voyager. When the hardware is built, vibration testing is conducted to verify the dynamics and update the controller, if necessary. Predicting the damping is particularly difficult for real, complex systems because of joints and nonlinearities. The argument between finite element and continuum models may be academic because the real errors come about due to the structure not obeying any sort of equation.

- PDE models can be very useful in "thought experiments" which can help clarify the mental processes that one would apply to the analysis or control of a distributed parameter system. They help in the thinking process before doing massive number crunching on a computer.

Session VII: Estimation/Identification

The last session of formal papers dealt with the questions of systems identification, parameter estimation and model error estimation. There were five papers presented on these subjects and all but one addressed continuum models.

The importance of this subject was emphasized several times during the workshop. A statement of systems identification in large space structure control by Vander Velde is included in Appendix C. A consensus of the workshop participants appeared to support the need for increased research to assure that techniques are adequately developed and tested before a large structure is deployed in space.

The paper by Hendricks et al. presents a simple study of two methods (forced and free vibrations) and a standard least-squares numerical procedure to extract damping and stiffness parameters for a lumped parameter model. A more interesting study would have been to include unmodeled effects (spillover) and measurement noise.

Banks' paper presents a good theoretical discussion of spline-based approximation schemes for parameter estimation algorithms for distributed parameter systems. Several numerical examples have been conducted to show the effectiveness of the schemes although these were not reviewed in much detail at the workshop. The technique now needs to be tried on a more realistic model of a space structure.

One of the most impressive papers of this session, and possibly the entire workshop, was the Juang and Sun paper, "Parameter Estimation in Truss Beams Using Timoshenko Beam Model with Damping." Simple continuum models to represent large truss beams and truss platforms are formed, then discretized for use in a least square identification problem. This results in a greatly reduced number of parameters that have to be identified over using a truncated finite-element model of the entire structure. A numerical example for a truss beam shows excellent comparison between the actual model and the simple continuum model.

The final paper of the workshop by Rodriguez formulates a model error estimation technique for elliptic systems with a specific application to a large space antenna static shape determination. The simple geometric shape of the antenna allowed a simple PDE formulation and sequential solutions which are combinations of "forward" filtering and "backward" smoothing. The paper shows how conceptually simple the PDE formulation is.

Session VIII: Discussion - Future Research Opportunities

The wrap-up panel discussed the state of distributed system theory and applications to the control of large space structures and identified potential research opportunities for NASA consideration. It also provided a forum for all participants to comment on the workshop topics and contribute to recommendations.

The moderator was H.A. Rediess of Milco and the panel members were: A.V. Balakrishnan of UCLA, A.E. Bryson, Jr., of Stanford, J.A. Breakwell of LMSC, P.C. Hughes of the University of Toronto, and W.E. Vander Velde of MIT. Some of the discussion and conclusions reached were reiterations of comments made during the first two panel discussions. At the conclusion of the panel, Rediess summarized the major recommendations to NASA, which are listed in the section on future research recommendations and are not repeated here. The following are what appeared to be the most important comments:

- On the central question of the workshop on the use of continuum models vs. finite-element models, there were three principal questions--

1. Most practical large space structure configurations are too complicated to model as a distributed parameter system and it is best to use a finite-element one.
2. Practical large space structures cannot only be modeled as distributed parameter systems (or in combination with lumped parameter elements) but also the PDE control theory results in a simpler formulation, potentially better control laws and better physical insight into the problem.
3. Finite-element models have proven to be effective in designing spacecraft whereas continuum models have not yet been proven to be as useful. Research should continue on the continuum model approach because if there is to be a major advancement in control theory, it most likely will come from that approach.

- On the question of bandwidth and controller complexity, there were two distinctly different viewpoints expressed--

1. There is only a limited bandwidth that needs to be considered in any real system; hence, a reduced order model is sufficient. Linear Quadratic Gaussian (LQG) design is always too complex. A reduced-order controller or a fixed, low order compensator is a better approach.
2. A truncated model with limited bandwidth may throw away important information needed for robustness considerations and obscure certain fundamental characteristics of the system. It is preferable to design a controller based on infinite-dimensional LQG to assure performance and robustness, and then to discretize for implementation.

- PDE estimation and control theory is at the state of development when it should be tested on major, realistic space-structure problems and compared to the finite-element approach. The comparison should include experimental evaluation, if possible.

- The problem of assuring robustness in the controller design, whether based on continuum or finite-element models, is still a major concern and needs much more study. Several participants believed PDE is the best approach for treating robustness.

- Simple laboratory experiments are now affordable and can be very useful in understanding the control problem and model order reduction.

- Systems identification for large space structures in orbit is going to be a very difficult task. Because of modeling uncertainties, it will be necessary to identify key parameters in space when the structure is first deployed in order to "tune up" the control laws before the system goes into operation. Another kind of identification will be needed to monitor the system's characteristics throughout the mission lifetime to detect changes that could cause control system instabilities (see Appendix C).

- Reliability issues for large space structure distributed control and stabilization systems have not been adequately addressed in considering control law design. Such systems are expected to have hundreds of components, and failures are likely to occur. Controller designs that account for potential failures may be quite different from those that assume no failures (see Appendix D).

- The space environment is, for the most part, very benign, and natural disturbances tend to be quasi-static within a period of one orbit. The major disturbances that excite structural modes tend to be man-made: impulsive actuators, slewing, orbit changes, docking, mass changes and astronaut operations.

- One of the most important technology developments needed for large space structure control is an accurate method to predict and model damping. Passive damping should not be ignored in design of a large space structure.

General Observations of the Reviewer

During the course of the workshop, and in preparing this evaluation report, the reviewer developed the following general observations about the state of distributed system theory and applications to control of large space structures:

- Deficiencies in control theory are probably not critical in the development of near-term space structures. However, advances in control theory and technology have the potential of providing design methods and control laws which could result in more efficient large space systems in the future and may be necessary for structures exceeding a few hundred meters in dimension.

- One should not argue that distributed parameter control theory is better or worse than lumped parameter control theory but rather think of them as complementary methodologies. They are both tools which the designer/analyst should use where they are most useful. It appears that distributed parameter control theory may be very useful in the early conceptual analysis and investigating control law concepts. It appears that finite-element models may be a most effective way to design and analyze the extremely complicated final space system to be deployed. Where appropriate, one should use a compound model of finite-elements and distributed parameter.

In view of the fact that distributed parameter system control theory has not been developed to anywhere near the same level as lumped parameter system control technology, it seems wise to accelerate research in the applications of distributed parameter control for large space structures.

APPENDIX A - WORKSHOP AGENDA

WEDNESDAY, JULY 14

8:00 a.m. Registration

Welcome to JPL - General C.H. Terhune, Jr.
Acting Director, Jet Propulsion Laboratory

Introduction to Workshop - H.A. Rediess, Milco International, Inc.

NASA LSS Missions and Control Requirements - A.F. Tolivar, Jet
Propulsion Laboratory

Break

10:00 - SESSION I: MODELING AND CONTROL

12:00 noon CHAIRMAN: P.K.C. Wang, University of California, Los Angeles

Modeling and Control of Distributed Structures
L. Meirovitch, Virginia Polytechnic Institute and State
University

Space Structure Vibration Modes: How Many Exist? Which Ones
Are Important?

P.C. Hughes, University of Toronto

Control of Flexible Structures: A Systematic Overview of the
Problem

R.S. Gran, Grumman Aerospace Corporation

Distributed System Modeling of a Large Space Antenna

M. Hamidi, G. Rodriguez, and D.B. Schaechter, Jet Propulsion
Laboratory

12:00 noon Lunch

1:00 - SESSION II: CONTROL AND STABILIZATION

4:00 p.m. CHAIRMAN: R.R. Strunce, Charles Stark Draper Laboratories, Inc.

Modeling of Flexible Structures for Active Control

A.E. Bryson, Jr., Stanford University

Vibration Suppression in Large Space Structures

T.K. Caughey and C.J. Goh, California Institute of Technology

Control of Antenna-Feed Attitude and Reflector Vibrations in Large
Spaceborne Antennas by Mechanical Decoupling and Movable Dampers

P.K.C. Wang, Jet Propulsion Laboratory; and E.C. Hong and J.C.
Sarina, University of California, Los Angeles

A Closed-Loop Principal Component Analysis of a Tetrahedral Truss
E.A. Jonckheere, University of Southern California

Control of Large Space Antennas Based on Electromagnetic -
Structural Models
M. Hamidi and F. Manshadi, Jet Propulsion Laboratory

Break

Active Control of Space Structures (ACOSS) Model 2
T.C. Henderson, Charles Stark Draper Laboratories, Inc.

Travelling Wave Effects in Large Space Structures
A. von Flotow, Stanford University

Distributed Control of Large Space Antennas
J. Cameron, M. Hamidi, Y.H. Lin, and S.J. Wang, Jet Propulsion
Laboratory

Break

4:45 - SESSION III: DISCUSSION - LSS CONTROL PROBLEMS
6:00 p.m. Participants: R.R. Strunce, Charles Stark Draper Laboratories,
Inc., Moderator; J. Sesak, General Dynamics; N.K. Gupta, Inte-
grated Systems, Inc.; and A.F. Tolivar, Jet Propulsion
Laboratory

THURSDAY, JULY 15, 1982

8:00 a.m. - SESSION IV: DISTRIBUTED CONTROL
11:20 a.m. CHAIRMAN: A.F. Tolivar, Jet Propulsion Laboratory

Number and Placement of Control System Sensors Considering
Possible Failures
W.E. Vander Velde, and C.R. Carignan, Massachusetts Institute
of Technology

The TOYSAT Structural Control Experiment
J.A. Breakwell and G.J. Chambers, Lockheed Missiles and Space
Company

Large Space Structure Model Reduction and Control System Design
Based upon Actuator and Sensor Influence Functions
Y. Yam, J.H. Lang, T.L. Johnson, S. Shih, and D.H. Staelin,
Massachusetts Institute of Technology

A Design Procedure for Active Control of Beam Vibrations
S.L. Dickerson and G. Jarocki, Georgia Institute of Technology

On Vibration Control of Tethered Satellite Systems
D.M. Xu and A.K. Misra, McGill University; and V.J. Modi,
University of British Columbia

Break

Orbiting Chains and Rings
J.V. Breakwell, Stanford University

Hardware Verification of Distributed/Adaptive Control
D. Eldred and D.B. Schaechter, Jet Propulsion Laboratory

Lunch

12:30 p.m. - SESSION V: CONTROL THEORY FOR DISTRIBUTED SYSTEMS
3:20 p.m. CHAIRMAN: Lt. Col. D.C. Washburn, Kirtland Air Force Base

Some Remarks on the Current Status of the Control Theory of
Single Space Dimension Hyperbolic Systems
D.L. Russell, University of Wisconsin

Approximation in Control of Flexible Structures, Theory and
Applications
J.S. Gibson, University of California, Los Angeles

Simultaneous Control and Optimization for Elastic Systems
V. Komkov, West Virginia University

Robust Control of Higher Order Systems Using Positivity
R.J. Benhabib and R.P. Iwens, TRW Space Technology Group

Fixed-Order Dynamic Compensation through Optimal Projection
D.C. Hyland and A.N. Madiwale, Massachusetts Institute of
Technology Lincoln Laboratory

Approximation of the Optimal Compensator for a Large Space
Structure
M.K. Mackay, University of California, Los Angeles

Finite Difference Numerical Methods for Boundary Control Problems
Governed by Hyperbolic Partial Differential Equations
G. Chen, Q. Zheng, M. Coleman and S. Weerakoon, Pennsylvania
State University

*Stable Feedback Control of Distributed Parameter Systems: Time
and Frequency Domain Conditions
M.J. Balas, Rensselaer Polytechnic Institute

*Analysis of Structural Perturbations in Systems via Cost
Decomposition Methods
R.E. Skelton, Purdue University

Break

*These papers were presented in Session VII but the subjects are more suitable
for Session V.

SESSION VI: DISCUSSION - LSS APPLICATIONS OF DISTRIBUTED SYSTEM
THEORY

Participants: R.S. Gran, Grumman Aerospace Corporation,
Moderator; D.C. Washburn, Air Force Weapons Laboratory; V.
Komkov, West Virginia University; D.L. Russell, University of
Wisconsin; and J.S. Gibson, University of California, Los
Angeles

6:30 p.m. - SOCIAL HOUR AND BANQUET (Pasadena Holiday Inn)
9:30 p.m. Speaker: H. Ashley, Stanford University

FRIDAY, JULY 16, 1982

8:00 a.m. - SESSION VII: ESTIMATION/IDENTIFICATION
11:30 a.m. CHAIRMAN: L.W. Taylor, Jr., Langley Research Center

Algorithms for Estimation in Distributed Models with Applications
to Large Space Structures
H.T. Banks, Brown University

Identification of Large Flexible Structures Mass/Stiffness and
Damping from On-Orbit Experiments
S.L. Hendricks, S. Rajaram, M.P. Kamat and J.L. Junkins, Virginia
Polytechnic Institute and State University

Break

Joint State and Parameter Estimation
N. Carmichael, University of Warwick, and M.D. Quinn, Sheffield
City Polytechnic, United Kingdom

Parameter Estimation in Truss Beams Using Timoshenko Beam Model
with Damping
C.T. Sun, Purdue University; and J.N. Juang, Martin Marietta
Aerospace

A Function Space Approach to State and Model Error Estimation
for Elliptic Systems
G. Rodriguez, Jet Propulsion Laboratory

Lunch

1:00 p.m. - SESSION VIII: DISCUSSION - FUTURE RESEARCH OPPORTUNITIES
3:00 p.m. Participants: H.A. Rediess, Milco International, Inc.,
Moderator; A.V. Balakrishnan, University of California, Los
Angeles; A.E. Bryson, Jr., Stanford University; J.A. Breakwell,
Lockheed Missiles and Space Company; P.C. Hughes, University
of Toronto; and W.E. Vander Velde, Massachusetts Institute of
Technology

APPENDIX B
WORKSHOP ON APPLICATIONS OF DISTRIBUTED SYSTEM THEORY
TO THE CONTROL OF LARGE SPACE STRUCTURES

ATTENDEES/PARTICIPANTS

- | | |
|--|---|
| ⁺ A.K. Agrawal
JPL M/S 130-117 | D. Bernard (Stanford University)
778 Moreno Ave.
Palo Alto, CA 94303 |
| [†] J.L. Allen
Office of Director for Projects
LaRC | S. Bickerstaff
Riverside Research Institute
1701 N. Ft. Myer Dr., #700
Arlington, VA 22202 |
| H. Ashley
School of Aero & Astro
Stanford University
Stanford, CA 94305 | ⁺ R.A. Boundy
JPL M/S 157-205 |
| ⁺ W. E. Bachman
JPL M/S 198-112D | ⁺ D. Bousallis
JPL M/S 198-326 |
| A.V. Balakrishnan
System Science Dept.
UCLA
Los Angeles, CA 90024 | J.A. Breakwell
LMSC
3251 Hanover St.
Palo Alto, CA 94304 |
| M.J. Balas
ESCE Department
Rensselaer Polytechnic Institute
Troy, N.Y. 12181 | J.V. Breakwell
School of Aero & Astro
Stanford University
Stanford, CA 94305 |
| H.T. Banks
Applied Math Dept.
Brown University
Providence, RI 02912 | T. Brennan
Aerospace Corporation
2350 El Segundo Blvd.
El Segundo, CA 90245 |
| S. Beach (Lockheed, Palo Alto)
P.O. Box 504
Sunnyvale, CA 94086 | ⁺ G.M. Burdick
JPL M/S 198-112A |
| ⁺ M. Belhadeh
JPL M/S 264-519 | G. Butson
Kirtland AFB
New Mexico 87117 |
| ⁺ C.E. Bell
JPL M/S 198-326 | A.E. Bryson, Jr.
School of Aero & Astro
Stanford University
Stanford, CA 94305 |
| R.J. Benhabib
TRW, Defense & Space Systems Group
1 Space Park Blvd.
Redondo Beach, CA 90278 | |
| ⁺ Affiliated with Jet Propulsion Laboratory, California Institute of Technology
4800 Oak Grove Drive, Pasadena, CA 91109 | |
| [†] Affiliated with NASA Langley Research Center, Hampton, VA 23665 | |

<p>+ J.M. Cameron JPL M/S 198-326</p> <p>C.R. Carignan (MIT) 550 Memorial Dr., #21A Cambridge, MA 02139</p> <p>+ G.L. Carlisle JPL M/S T-1201</p> <p>T. Caughey Caltech M/S 104-44 1201 East California Blvd. Pasadena, CA 91125</p> <p>S. Chang System Science Department School of Engineering & Applied Science UCLA Los Angeles, CA 90024</p> <p>C. Chen Hughes Aircraft Co. Bldg. 512 M/S V362 P.O. Box 92919 Los Angeles, CA 90009</p> <p>G. Chen Department of Mathematics Pennsylvania State University University Park, PA 16802</p> <p>+ J.C. Chen JPL M/S 157-316</p> <p>+ J.L. Chodas JPL M/S 198-326</p> <p>+ P.W. Chodas JPL M/S 264-686</p> <p>J. Cisneros System Science Department UCLA Los Angeles, CA 90024</p> <p>+ K.C. Coon JPL M/S 180-701</p> <p>+ Affiliated with Jet Propulsion Laboratory, California Institute of Technology 4800 Oak Grove Drive, Pasadena, CA 91109</p>	<p>P.G. Coxson (University of Delaware) 10537 DuBarry St. Bellflower, CA 90706</p> <p>J. Dahlgren RTE-6 NASA Hdq. Washington, D.C. 20546</p> <p>P.L. Daniel Department of Mathematics Southern Methodist University Dallas, TX 75275</p> <p>A. Das (Virginia Tech.) Edwards Air Force Base CA 93523</p> <p>A. DeVilliers Riverside Research Institute 1701 N. Ft. Myer Dr., #700 Arlington, VA 22202</p> <p>S. Dickerson Mechanical Engineering Georgia Institute of Technology Atlanta, GA 30332</p> <p>G. Doane III Control Dynamics Co. 221 East Side Square Huntsville, AL 35801</p> <p>R.S. Edmunds c/o D. Brickner Sperry Flight Systems P.O. Box 9200 Albuquerque, N.M. 87117</p> <p>+ D.B. Eldred JPL M/S 198-326</p> <p>J. Etter (Kirtland AFB, AFWL/DARPA) 972 Antelope Ave. N.E. Albuquerque, N.M. 87122</p> <p>+ R.E. Freeland JPL M/S 157-410</p>
---	--

+ J.A. Garba
JPL M/S 157-316

J.S. Gibson
School of Engineering & Applied Science
UCLA
Los Angeles, CA 90024

J. Gillis
System Science Department
UCLA
Los Angeles, CA 90024

J. Gliniak (Ames Research Center)
500 West Middlefield Rd. #83
Mountain View, CA 94043

C.J. Goh
Caltech M/S 104-44
1201 East California Blvd.
Pasadena, CA 91125

R. Gran
Grumman Aerospace Corporation
Res. Dept. A08-35
Bethpage, N.Y. 11714

+ S.H. Graff
JPL M/S 198-326

N.K. Gupta
Integrated Systems
151 University Ave., #400
Palo Alto, CA 94301

+ M. Hamidi
JPL M/S 198-326

+ B.R. Hanks
LaRC M/S 230

+ J.E. Harris
LaRC M/S 158

+ S.A. Hayati
JPL M/S T-1201

T.C. Henderson
C.S. Draper Laboratories
555 Technology Square
Cambridge, MA 02139

J.L. Hendricks
Virginia Polytechnic Institute &
State University
Blacksburg, VA 24061

E. Hong (UCLA)
3185 Sepulveda Blvd., #1
Los Angeles, CA 90034

+ H.H. Horiuchi
JPL M/S 198-112A

+ E.K. Huckins
LaRC M/S 158

P.C. Hughes (University of Toronto)
4295 Dufferin St.
Toronto, Ontario, CANADA M3H 5T6

+ G.D. Ianculescu
JPL M/S 198-326

D.J. Inman
Department of Mech. & Aero Engr.
State University of New York at
Buffalo
Buffalo, N.Y. 14260

R. Iwens
TRW Defense & Space Systems Group
1 Space Park Blvd.
Redondo Beach, CA 90278

+ M.H. Jahanshahi
JPL M/S T-1201

+ G.I. Jaivin
JPL M/S T-1201

E.A. Jonckheere, PE 528
Electrical Engineering Systems
University of Southern California
University Park
Los Angeles, CA 90007

+ V. Jamnejad
JPL M/S 161-213

+ J.N. Juang (as of 10/82)
LaRC M/S 230

+ Affiliated with Jet Propulsion Laboratory, California Institute of Technology
4800 Oak Grove Drive, Pasadena, CA 91109

+ Affiliated with NASA Langley Research Center, Hampton, VA 23665

- + E.P. Kan
JPL M/S T-1201
- + S. Kerridge
JPL M/S 156-220
- + R.W. Key
JPL M/S 198-326
- + T. Kia
JPL M/S T-1201
- W. Kilmer
ECE, EBE
University of Massachusetts at Amherst
Amherst, MA 01003
- V. Komkov (West Virginia University)
1238 Van Voorhis - A5
Morgantown, W. VA 26505
- J. Kovarna
University of New Mexico
NMERI/Campus P.O. Box 25
Albuquerque, N.M. 87131
- + G. Kuo
JPL M/S 157-316
- + G.C. Lagomarsini
JPL M/S 198-326
- + J.Y. Lai
JPL M/S T-1201
- T. Larson (Hughes Aircraft Co.)
412 Palos Verdes Blvd.
Redondo Beach, CA 90277
- A. Laub
University of Southern California
University Park
Los Angeles, CA 90007
- + W. Lautz
JPL
- W.H. Lee
Alphatech
3 New England Exec. Park
Burlington, MA 01803
- + Affiliated with Jet Propulsion Laboratory, California Institute of Technology
4800 Oak Grove Drive, Pasadena, CA 91109
- + Affiliated with NASA Langley Research Center, Hampton, VA 23665
- + A. Leibold
JPL M/S 264-647
- L. Lemke
NASA Ames Research
M/S 244-7
Moffett Field, CA 94035
- † E.B. Lightner
LaRC M/S 158
- + H.S. Lin
JPL M/S 198-326
- + Y.H. Lin
JPL M/S 198-326
- + J.M. Longuski
JPL M/S T-1201
- J. Maatuk
Seven Engineering
2925 4th Street
Santa Monica, CA 90405
- + G.A. Macala
JPL M/S 198-326
- M.K. Mackay (TRW/UCLA)
P.O. Box 434
Hermosa Beach, CA 90254
- A.N. Madiwale
Control Systems Engr. Group
MIT-Lincoln Laboratory
244 Wood Street
Lexington, MA 02173
- + G. K. Man
JPL M/S 198-326
- + F. Manshadi
JPL M/S 198-326
- + B.R. Markiewicz
JPL M/S T-1201
- + J.R. Matijevic
JPL M/S T-1201

+K. D. Mease
JPL M/S 264-686

J. Meier
Aerojet Liquid Rocket
P.O. Box 13222
Sacramento, CA 95813

L. Meirovitch
Virginia Polytechnic Institute
& State University
Blacksburg, VA 24061

+E. Mettler
JPL M/S T-1201

A.M. Meystel
Department of Electrical Engineering
137 Larson Hall
University of Florida
Gainesville, Florida 32611

+M.M. Milman
JPL M/S 198-326

A.K. Misra
Department of Mechanical Engineering
McGill University
Montreal, Quebec, Canada H3A 2K6

M.I. Miyagi
Hughes Aircraft Co.
P.O. Box 92919
Los Angeles, CA 90009

+M. Namiri
JPL M/S 198-326

N.C. Nguyen
LMSC
P.O. Box 504
Sunnyvale, CA

R. Oglevie
Mail Code SK39
Rockwell International - Space
Operations/Integration & Satellite
Systems Division
12214 Lakewood Blvd.
Downey, CA 90241

+H. Ohtakay
JPL M/S 198-326

+M.F. Pompa
JPL M/S 125-224

R. Preston
AFRPL/DYA
Edwards Air Force Base
CA 93523

R. Quartararo (Rockwell Int'l.)
21 Fox Hill
Irvine, CA 92714

M.D. Quinn
Department of Mathematics
Sheffield City Polytechnic
England

S. Rahmani
(Rockwell Int'l.)
7672 Tracy Lane
La Palma, CA 90623

H.A. Rediess (Milco Inc.)
2036 Lakewinds Fr.
Reston, VA 22091

E. Reich
Aerojet Liquid Rocket
P.O. Box 13222
Sacramento, CA 95813

+G. Rodriguez
JPL M/S 198-326

D.L. Russell
Department of Mathematics
University of Wisconsin
Madison, WI 53706

†R.A. Russell
LaRC M/S 158

G. Ruzicka
System Science Department
UCLA
Los Angeles, CA 90024

+Affiliated with Jet Propulsion Laboratory, California Institute of Technology
4800 Oak Grove Drive, Pasadena, CA 91109

†Affiliated with NASA Langley Research Center, Hampton, VA 23665

A. Schumitzky Department of Mathematics University of Southern California University Park Los Angeles, CA 90007	G.T. Tseng Aerospace Corporation 2350 El Segundo Blvd. El Segundo, CA 90245
+ J.R. Scull JPL M/S 180-604	+ F. Udvardia JPL
R.P. Sena Aerospace Corporation 2350 El Segundo Blvd. El Segundo, CA 90245	W.E. Vander Velde Department of Aero and Astro Room 33-109 Massachusetts Institute of Technology Cambridge, MA 02139
J. Sesak Mail Zone 21-9530 General Dynamics-Convair Division P.O. Box 80847 San Diego, CA 92138	J. Velman Hughes Aircraft Co. P.O. Box 92919 Los Angeles, CA 90009
+ C.F. Shih JPL M/S 157-316	A. von Flotow Department of Aero and Astro Stanford University Stanford, CA 94305
R.R. Strunce C.S. Draper Laboratories 555 Technology Square Cambridge, MA 02139	+ B.K. Wada JPL M/S 157-507
A.R. Stubberud (UC Irvine) 19532 Sierra Sota Rd. Irvine, CA 92715	P.K.C. Wang System Science Department School of Engineering & Applied Science UCLA Los Angeles, CA 90024
J. Sun Stanford University P.O. Box 11555 Stanford, CA 94305	+ S.J. Wang JPL M/S 198-326
+ S.Z. Szirmay JPL M/S 198-326	D.C. Washburn (Kirtland AFB, AFWL/ARAA) 2207 22nd Dr. Albuquerque, N.M. 87116
+ L.W. Taylor, Jr. LaRC M/S 161	C.J. Weeks Engineering Quadrangle Princeton University Princeton, N.J. 08544
+ A.F. Tolivar JPL M/S 198-326	
B.L. Triezenberg (Hughes Aircraft Co.) 349 Virginia #2 El Segundo, CA 90245	L. Weisstein (IMSC) 130 Oakdale Dr. Redwood City, CA 94062
+ Affiliated with Jet Propulsion Laboratory, California Institute of Technology 4800 Oak Grove Drive, Pasadena, CA 91109	
+ Affiliated with NASA Langley Research Center, Hampton, VA 23665	

P. Welch (HR Textron)
11748 Skypark Blvd. #150
Irvine, CA 92714

+L.K. White
JPL M/S 264-686

+E.C. Wong
JPL M/S 198-326

+L.J. Wood
JPL M/S 264-686

Y. Yam
Massachusetts Institute of Technology
Room 516B Ashdown House
305 Memorial Drive
Cambridge, MA 02139

J. Yocum (Hughes Aircraft Co.)
28717 Shire Oaks Dr.
Rancho Palos Verdes, CA 90274

+M.A. Zak
JPL M/S 157-316

+Affiliated with Jet Propulsion Laboratory, California Institute of Technology
4800 Oak Grove Drive, Pasadena, CA 91109

APPENDIX C - STATEMENT ON SYSTEM IDENTIFICATION IN
LARGE SPACE STRUCTURE (LSS) CONTROL

W.E. VANDER VELDE, MIT

One of the most unsettling aspects of the prospect of controlling flexible structures in space is the fact that many configurations will not permit experimental tests on the ground to verify or improve the models of their dynamic properties. In some mission situations, then, depending on the bandwidth of the controlled system necessary to meet the performance specifications, it is virtually certain that the modeling errors upon initial deployment of the assembly in space will be great enough to preclude the successful operation of the required control system. In that case, there will have to be an initial period of operation under the control of a more tolerant system during which the dynamics of the structure are identified.

It is suggested that dynamic model identification in the large space structure (LSS) context be visualized as having two modes.

1. Complete system identification during the initial phase of operation.
2. Dynamic model monitoring during the remainder of the mission period with selected parameters updated as necessary.

The first mode of initial system identification is a massive undertaking whose purpose is to estimate the large number of parameters necessary to define the dynamic model required for the control function. Because only elementary control can be exercised during this period, and special test inputs may be necessary to enhance the identifiability of system parameters, the system will not be able to perform its primary mission(s) during this time. Thus a large part of the system's data processing capability can be devoted to the identification function in this initial phase. Later, when the system is in full operation, the data processors will be devoted largely to mission requirements such as sensor signal processing and thus the need for the second mode of dynamics monitoring which must be designed to place only a small demand on the data processor.

A considerable amount of research has been done on the mode 1 type of problem--complete system identification--but the LSS identification task is far more demanding in that such a large number of parameters will have to be identified. It is not clear that this task is computationally feasible; specific research should be directed at the LSS identification problem with the objective of formulating an approach with the best possible computational efficiency. The mode 2 task of monitoring the dynamics and improving the estimates of selected parameters as necessary is a new concept which deserves research support.

APPENDIX D - STATEMENT ON RELIABILITY ISSUES IN
LARGE SPACE STRUCTURE (LSS) CONTROL

W.E. VANDER VELDE, MIT

One aspect of active control of large space structures that is receiving too little attention is the importance of the unreliability of control system components. This is not to say that unreliable components, according to our best standards, will be utilized. Rather, it is the sheer number of these components, notably sensors and actuators, which will likely be required to effect good control over the structure which assures that we will have to deal with failures. As one example, if the system has a total of 400 sensors and actuators, each with a mean time to failure of 100,000 hours (optimistic by today's standards), one may expect to experience a component failure about every 10 days on average. Obviously, the system must be designed to accommodate these failures and continue to function.

There are several aspects to the overall problem of designing a control system for fault tolerance. The most important of these are:

1. Choose the number of sensors and actuators to be incorporated in the system, and decide to place them on the structure, with recognition of the fact that many of them are likely to fail during the mission period.
2. Incorporate a fault-monitoring function in the control system to detect the events of a component failure and isolate the faulty component.
3. Utilize a fault-tolerant signal transmission and data processing system to implement the controller and fault-monitoring functions.
4. Implement a method of reconfiguring the control system, upon isolation of a component failure, so as to function without the faulty component.
5. Devise means for evaluating the likely performance of a proposed system configuration including its failure accommodating functions.

Some research has been performed on all of these subjects, but most of it was in the context of other applications than LSS control. Some current research is being funded on fault-tolerant computers, item 3 above, but very little support is being given to work on the other items. Failure detection and isolation (FDI), item 2 above, has been developed largely in the context of aircraft flight control systems. But the LSS application is different. The same characteristics that make control of LSS difficult, such as high dimensionality and inadequate modeling, also make FDI difficult. But given that component failures are virtually certain to occur, these aspects of dealing with component unreliability should be given high priority in NASA planning for research.

End of Document